

# **Preparation, characterization and thermophysical investigations on thorium- based nuclear fuels and related systems**

*By*

**DHEERAJ JAIN**

**CHEM 01 2012 04014**

**Bhabha Atomic Research Centre, Mumbai**

*A thesis submitted to the  
Board of Studies in Chemical Sciences  
In partial fulfilment of requirements  
for the degree of*

**DOCTOR OF PHILOSOPHY**

*of*

**HOMI BHABHA NATIONAL INSTITUTE**

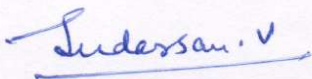
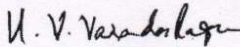
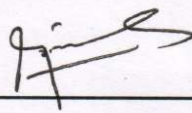
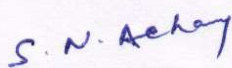


**August 2020**

# Homi Bhabha National Institute

## Recommendations of the Viva Voce Committee

As members of the Viva-Voce Committee, we certify that we have read the dissertation prepared by **Shri Dheeraj Jain** entitled, “**Preparation, characterization and thermophysical investigations on thorium-based nuclear fuels and related systems**” and recommend that it may be accepted as fulfilling the thesis requirement for the award of Degree of Doctor of Philosophy.

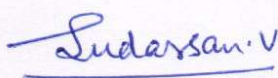
Chairman	Prof. S. K. Mukerjee		28.01.2021
Guide / Convener	Prof. A. K. Tyagi		28.01.2021
Co-Guide	Prof. V. Sudarsan		28.01.2021
Examiner	Prof. U. V. Varadaraju		28.01.2021
Member	Prof. S. C. Parida		28.01.2021
Member	Prof. S. N. Achary		28.01.2021
Technology Adviser	Dr. Manidipa Basu		28.01.2021

Final approval and acceptance of this thesis is contingent upon the candidate's submission of the final copies of the thesis to HBNI.

We hereby certify that we have read this thesis prepared under our direction and recommend that it may be accepted as fulfilling the thesis requirement.

Date: 28.01.2021

Place: BARC, Mumbai



(V. Sudarsan)

Co-guide



(A.K. Tyagi)

Guide

## STATEMENT BY AUTHOR

This dissertation has been submitted in partial fulfilment of requirements for an advanced degree at Homi Bhabha National Institute (HBNI) and is deposited in the library to be made available to borrowers under the rules of HBNI.

Brief quotations from this dissertation are allowable without special permission, provided that accurate acknowledgement of the source is made. Requests for permission for extended quotation from or reproduction of this manuscript in whole or in part may be granted by the Competent Authority of HBNI when in his or her judgement the proposed use of the material is in the interest of scholarship. In all other instances, however, permission must be obtained from the author.



**Dheeraj Jain**

# DECLARATION

I, hereby declare that the investigation presented in the thesis has been carried out by me. The work is original and has not been submitted earlier as a whole or in part for a degree / diploma at this or any other Institution / University.



**Dheeraj Jain**

# List of publications arising from the thesis

## Journals

### a. Published:

1. On the origin of exothermic DSC peak prior to glycine-nitrate gel combustion during ThO<sub>2</sub> synthesis

**Dheeraj Jain**, V. Sudarsan, A.K. Tyagi

*Thermochim. Acta* 674 (2019), 76–81.

2. Effect of local ordering around Th<sup>4+</sup> ions in glycine-nitrate precursor gel on the powder characteristic of gel-combusted ThO<sub>2</sub>

**Dheeraj Jain**, V. Sudarsan, A.K. Patra, P.U. Sastry, A.K. Tyagi

*J. Nucl. Mater.* 527 (2019) 151826.

3. Effect of structural phase transitions on high temperature thermal conductivity of nuclear-grade uranium

**Dheeraj Jain**, J. Nuwad, V. Sudarsan, A.K. Tyagi

*J. Alloys Compd.* 831 (2020) 154706.

### b. Communicated:

1. Desintering in solution combustion synthesized nanocrystalline ThO<sub>2</sub>: A comparison of glycine-nitrate and citrate-nitrate synthesis routes

**Dheeraj Jain**, V. Sudarsan, A.K. Tyagi

(Communicated to *J. Nucl. Mater.*)

## Book/Book Chapter

1. Thorium-based fuels for advanced nuclear reactors: thermophysical, thermochemical and thermodynamic properties

**Dheeraj Jain**, D. Das, B.N. Jagatap

Thorium-Energy for Future (Eds.: A.K. Nayak, B. Sehgal) Springer (2019).

## Conference/Symposium

1. Role of thermal analysis in probing combustion synthesis of thoria: A case study with glycine-nitrate and citrate-nitrate routes

**Dheeraj Jain**, V. Sudarsan, A.K. Tyagi

*Proceedings of 22nd DAE-BRNS Symposium on Thermal Analysis (2020)* 135-136.

2. Thermophysical properties of nuclear materials

**Dheeraj Jain**, V. Sudarsan, A.K. Tyagi

*Proceedings of 8th National Conference on Thermophysical Properties (NCTP-2015), Jaipur (2015).*

3. Application of Temperature Modulated DSC for rapid and reliable heat capacity measurement of nuclear fuels: A case study on Thorium metal and Th-U alloys

**Dheeraj Jain**, M.T. Saify, S.K. Jha, C.G.S. Pillai

*Proceedings of 18th International symposium on Thermal Analysis (THERMANS-2012) (2012)* p. 86-88.

## Bulletin Articles

1. Thorium-based metallic alloys as nuclear fuels: present status, potential advantages and challenges

**Dheeraj Jain**, V. Sudarsan, A.K. Tyagi

*SMC Bulletin, Society for Materials Chemistry*, Volume 4, Issue No.: 1 (2013) 27-40.

2. Thermophysical characterization of Thorium and Uranium based metallic fuels and alloys

**Dheeraj Jain**, C.G.S. Pillai

*ITAS Bulletin, Indian Thermal Analysis Society* Volume 4 (2011) 10-22.



**Dheeraj Jain**

**Dedicated to**

**My Parents**

*Smt. Manorama Jain and Shri Suresh Chandra Jain*

**&**

**My Teacher**

**Prof. Raj Kumar Bansal**

*Former Head, Department of Chemistry,*

*University of Rajasthan, Jaipur*

## ACKNOWLEDGEMENTS

At the outset, I would like to place my deepest acknowledgement to my guide, **Prof. A.K. Tyagi** for allowing me to work as one of his Ph.D. students and guiding me at each stage of research work, presented in this thesis. His energy and optimism with valuable suggestions and advices have bettered my efforts in pursuing the presented work and taking up the future directions in my career.

I feel immensely blessed to have **Prof. V. Sudarsan** as my co-guide. His involvement in carrying out many of the experiments and continued guidance in interpreting the results has made me learn new things almost each day of interaction with him. Apart from being my co-guide, he has been a mentor for me, shaping the way to pick up the problems and plan the experiments. I would like to thank him for all his guidance.

I would like to thank members of the doctoral committee: **Prof. S.K. Mukerjee, Prof. S.C. Parida, Dr. S.N. Achary** and **Dr. (Ms.) Manidipa Basu** for providing useful suggestions in each of the progress review meetings. I also thank **Dr. R. Mishra** and **Dr. (Smt.) Vinita Grover Gupta** for sparing their valuable time in attending all progress review meetings and providing encouraging suggestions.

I place my sincere gratitude to my former colleagues and mentors **Dr. C.G.S. Pillai** and **Dr. D. Das** for assigning me to work in the area of thorium-based nuclear materials and guiding me during my formative years in BARC.

I wholeheartedly thank the following collaborators, who have contributed to the completion of the work presented here: **Shri J. Nuwad** for SEM-EDS measurements; **Dr. A.K. Patra** and **Dr. P.U. Sastry** for SAXS measurements; **Shri Raj Kumar, Dr. S.K. Satpati, Dr. (Smt.) S.B. Roy, Shri M.L. Sahu, Shri M.T. Saify** and **Shri S.K. Jha** for providing thorium and uranium metals.

I place my sincere acknowledgements to **Dr. Rakesh Shukla, Dr. A.V.R. Reddy, Dr. R. Kameswaran, Shri. K. Venketesh, Dr. V.S. Tripathi, Dr. P.S. Dhani, Dr. S. Panja** and **Shri B.B. Kalekar** for their help and cooperation in allowing me access some of their experimental facilities as well as analysis support. I also thank **Shri Dasari Rao** for helping me in day-to-day laboratory work.

I place my sincere gratitude to former heads of Chemistry Division: **Dr. V.K. Jain** and **Dr. (Smt.) K.I. Priyadarsini** for their support in each stage of work. I wish to place my deepest acknowledgement to former directors of Chemistry Group: **Dr. T. Mukherjee, Dr. S.K. Sarkar, Dr. B.N. Jagatap** and former associate director **Dr. P.D. Naik** for encouraging me during this work.

I would also like to thank **Drs. A.K. Tripathi, R.K. Vatsa, P.A. Hassan** for their encouraging support. I also thank my colleagues **Shri N. Manoj, Shri R.K. Mishra, Shri R. Manimaran, Dr. (Smt.) Seemita Banerjee, Dr. (Smt.) P. Ruz, Shri Asheesh Kumar** and the youngest **Sourav Majumder** for all their support.

I place my heartfelt gratitude to my family friends **Aishwarya, Soumitra, Sangita, Raju, Chhavi** and **Shankar** for the best of the support they have always extended.

Before I conclude, I wish to say that I am indebted to **Prof. R.K. Bansal** (Former Head, Department of Chemistry, University of Rajasthan, Jaipur), to whom I dedicate this thesis. I also thank **Prof. (Smt.) Neelima Gupta**, Department of Chemistry, UoR, Jaipur.

Completion of this work has only been possible with the blessings and wishes of **my parents, parent-in-laws, my sister Sama, my brother Neeraj** and **all family members**. The ones who knit the entire supporting framework for me are my wife **Renu**, daughter **Ridhi** and son **Samyak**. *My heart feels heavy while attempting to thank them.*

**Dheeraj Jain**

## CONTENTS

TOPIC	Page No.
<b>SYNOPSIS.....</b>	<b>I - XII</b>
<b>LIST OF FIGURES.....</b>	<b>XIII - XXIII</b>
<b>LIST OF TABLES.....</b>	<b>XXIV - XXV</b>
<b>CHAPTER-1: Introduction.....</b>	<b>1-37</b>
1.1. Nuclear energy program in India.....	1
1.2. Thorium in Indian nuclear energy program.....	4
1.3. Metallic fuelled nuclear reactor systems.....	8
1.3.1. Advantages of metallic nuclear fuels.....	10
1.3.2. Challenges / limitations of metallic nuclear fuels.....	12
1.3.3. Thorium-based metallic fuels and Indian program.....	13
1.3.4. Advantages of thorium-based metallic fuels over uranium-based metallic fuels.....	14
1.3.5. Limitation of thorium-based metallic alloys.....	17
1.3.6. Review of existing literature on thorium-based metallic alloy fuels.....	20
1.3.7. Thermophysical properties of thorium-based metallic alloys.....	26
1.4. Nanocrystalline thoria.....	28
1.5. Scope of the present thesis.....	36
<b>CHAPTER-2: Experimental section.....</b>	<b>38-76</b>
2.1. Introduction.....	38
2.2. Materials.....	38

2.3. Methods.....	39
2.3.1. Preparative methods.....	39
2.3.1.1. Metal and alloy handling.....	39
2.3.1.2. Thorium metal-pre-sintering.....	41
2.3.1.3. Metal cutting.....	43
2.3.1.4. Arc melting method.....	43
2.3.1.4.1. Advantages of DC arc melting method.....	47
2.3.1.4.2. Limitations of DC arc melting method.....	47
2.3.1.5. Solution combustion method.....	48
2.3.1.5.1. Advantages of solution combustion synthesis.....	51
2.3.1.5.2. Limitations of solution combustion synthesis.....	51
2.3.2. Characterization techniques.....	52
2.3.2.1. Elemental (C, N, O) analysis.....	53
2.3.2.2. Powder X-ray diffraction technique (XRD).....	54
2.3.2.3. Scanning electron microscopy (SEM).....	57
2.3.2.4. Energy dispersive X-ray spectroscopy (EDS).....	59
2.3.2.5. Raman spectroscopy.....	60
2.3.2.6. Fourier transform infra-red (FT-IR) spectroscopy.....	62
2.3.2.7. Small angle X-ray scattering (SAXS).....	63
2.3.2.8. Thermo-gravimetry.....	64
2.3.2.9. Differential scanning calorimetry (DSC).....	65
2.3.2.10. Thermo mechanical analysis (TMA).....	68
2.3.2.11. Laser flash technique.....	71

<b>CHAPTER 3: Thermophysical studies on reactor-grade uranium and thorium metals.....</b>	<b>77-120</b>
3.1. Introduction.....	77
3.2. Experimental.....	79
3.3. Results and Discussion.....	81
3.3.1. Impurity analysis.....	81
3.3.2. Structural characterization.....	83
3.3.3. Surface morphology and Raman Spectroscopy analysis.....	86
3.3.4. Thermal diffusivity of thorium and uranium.....	88
3.3.5. Linear thermal expansion of thorium and uranium.....	95
3.3.6. Specific heat capacity of thorium and uranium.....	105
3.3.7. Thermal conductivity of thorium and uranium.....	109
3.3.8. Uncertainty analysis for thermal conductivity of uranium and thorium.....	115
3.4. Conclusions.....	119
<b>CHAPTER-4: Thermophysical studies on thorium-uranium (Th-U) binary metallic alloys.....</b>	<b>121-147</b>
4.1. Introduction.....	121
4.2. Experimental.....	123
4.3. Results and discussion.....	125
4.3.1. Impurity analysis.....	125
4.3.2. Phase analysis of Th-10U and Th-20U alloys (XRD results).....	128
4.3.3. Microstructural characterization (SEM studies).....	132
4.3.4. Thermal diffusivity of Th-U binary alloys.....	134

4.3.5. Bulk thermal expansion of Th-U binary alloys.....	136
4.3.6. Specific heat of Th-U binary alloys.....	142
4.3.7. Thermal conductivity of Th-U binary alloys.....	143
4.4. Conclusions.....	146
<b>CHAPTER-5: Thermophysical studies on thorium-uranium-zirconium (Th-U-Zr) ternary metallic alloys.....</b>	<b>148-170</b>
5.1. Introduction.....	148
5.2. Experimental.....	150
5.3. Results and discussion.....	151
5.3.1. Phase characterization of ternary alloys.....	151
5.3.2. Thermal diffusivity of Th-U-Zr ternary alloys.....	160
5.3.3. Linear thermal expansion of Th-U-Zr ternary alloys.....	164
5.3.4. Thermal conductivity of Th-U-Zr ternary alloys.....	168
5.4. Conclusions.....	170
<b>CHAPTER-6: Combustion synthesis of nanocrystalline ThO<sub>2</sub>: Probing synthesis mechanism by thermal analysis.....</b>	<b>171-222</b>
6.1. Introduction.....	171
6.2. Experimental.....	172
6.3. Results and discussion.....	174
6.3.1. Mechanism of glycine-nitrate combustion synthesis of nanocrystalline ThO <sub>2</sub> .....	176
6.3.1.1. Probing glycine-nitrate combustion by thermal analysis (DSC results).....	176
6.3.1.2. Visual evolution of glycine-Th(IV)-nitrate gel during	

	combustion process.....	180
6.3.1.3.	Thermo gravimetric analysis (TGA) of glycine-Th(IV)-nitrate gel.....	181
6.3.1.4.	X-Ray diffraction studies on glycine-Th(IV)-nitrate gel and ThO <sub>2</sub> powders.....	183
6.3.1.5.	FT-IR and Raman spectroscopy studies on aqueous gel and ThO <sub>2</sub> powders.....	185
6.3.1.6.	Discussion (Glycine-nitrate solution combustion synthesis of ThO <sub>2</sub> ).....	187
6.3.2.	Mechanism of citrate-nitrate combustion synthesis of nanocrystalline ThO <sub>2</sub> .....	191
6.3.2.1.	Probing citrate-nitrate combustion by thermal analysis (DSC results).....	191
6.3.2.2.	X-ray diffraction studies on citrate-Th(IV)-nitrate gel and ThO <sub>2</sub> powders.....	197
6.3.2.3.	Raman Spectroscopic studies on citrate-Th(IV)-nitrate system.....	198
6.3.2.4.	Citrate-nitrate solution combustion synthesis of ThO <sub>2</sub> : mechanistic aspects.....	200
6.3.3.	Role of fuel to oxidant ratio on the mechanism of glycine-Th(IV)-nitrate combustion synthesis of ThO <sub>2</sub> .....	204
6.3.3.1.	Powder properties of combustion synthesized nanocrystalline ThO <sub>2</sub> .....	204
6.3.3.2.	Thermal analysis of glycine-Th(IV)-nitrate gels with different F:O values.....	206

6.3.3.3. Small angle X-ray scattering (SAXS) on aqueous gels and as-combusted ThO <sub>2</sub> .....	210
6.3.3.4. Role of F:O on mechanism of glycine-Th(IV)-nitrate combustion.....	214
6.3.3.5. Supporting evidence for mechanism of glycine-nitrate combustion (FT-IR).....	217
6.4. Conclusions.....	220
<b>CHAPTER-7: Desintering in combustion synthesized ThO<sub>2</sub>: A comparison of glycine-nitrate and citrate-nitrate route...</b>	<b>223-249</b>
7.1. Introduction.....	223
7.2. Experimental.....	225
7.3. Results and discussion.....	227
7.3.1. Powder properties of gn-ThO <sub>2</sub> and cn-ThO <sub>2</sub> powders.....	227
7.3.2. Sintering behavior of gn-ThO <sub>2</sub> and cn-ThO <sub>2</sub> powder compacts....	233
7.3.3. Morphology of gn-ThO <sub>2</sub> and cn-ThO <sub>2</sub> powders and sintered pellets.....	239
7.3.4. Discussion (Desintering of nanocrystalline ThO <sub>2</sub> ).....	241
7.3.5. Supporting evidence to proposed origin of desintering in ThO <sub>2</sub> (FT-IR results).....	247
7.4. Conclusions.....	249
<b>CHAPTER-8: Conclusion and future scope.....</b>	<b>250-254</b>
<b>REFERENCES.....</b>	<b>255-284</b>

## LIST OF FIGURES

Figure No.	Figure caption	Page No.
Fig. 2.1	(a) Photograph of inert atmosphere glove box for handling uranium and thorium-based alloys, (b) Gas purification panel used for metal fuel handling	40
Fig. 2.2	Vacuum sintering furnace for metal powder compacts	42
Fig. 2.3	Metal cutting by diamond impregnated blade. Th-U alloys cut into small pieces	43
Fig. 2.4	Photograph of Arc melting setup. Insets show copper anode cup (right frame) and as-melted alloy button (left frame)	44
Fig. 2.5	Schematic of laser flash experiment and typical time dependent rear surface temperature profile of the sample	72
Fig. 3.1	Graphical comparison of reported thermal conductivity data for uranium	78
Fig. 3.2	EDS spectra recorded on (a) polished thorium and (b) polished uranium metal. Insets show the SEM micrographs over which the EDS spectra were recorded	83
Fig. 3.3	Room temperature XRD pattern recorded over polished pellet of (a) thorium metal and (b) uranium metal. Black curves show experimental data while blue lines are peak positions corresponding to reported XRD patterns of FCC thorium [166] and orthorhombic uranium [167]. Insets show the presence of weak reflections due to impurity phases. Peaks marked with ‘*’ and ‘o’ symbols represent ThO <sub>2</sub> and UO <sub>2</sub> / UO / UC phases	85

- Fig. 3.4 (a) SEM micrograph of thorium metal power compact (fractured surface), (b) arc-melted and polished thorium metal pellet surface, (c) arc-melted and polished uranium metal pellet, (d) EDS spectra of arc-melted thorium pellet showing distinct oxygen-rich regions ( $\text{ThO}_2$  inclusions), (e) Raman spectrum recorded over arc-melted thorium pellet. Optical micrograph of  $\text{ThO}_2$  inclusion is shown in inset of Fig. 3.4(e) 87
- Fig. 3.5 X-ray elemental mapping results performed over thorium metal surface. Presence of  $\text{ThO}_2$  inclusions is clearly seen from elemental mapping results 88
- Fig. 3.6 (a) Thermal diffusivity of thorium and uranium as a function of temperature. Solid dots represent average value of four laser shots on each temperature, while plus symbols show as-measured individual data. Open dots are values recommended by Touloukian et al., [150]; (b) thermal diffusivity results on Inconel-600 reference material obtained under identical experimental conditions. Inset shows percentage error in diffusivity measurements 89
- Fig. 3.7 (a) Linear thermal expansion of polycrystalline thorium and uranium metal as a function of temperature. For uranium, both phase transitions, namely  $\alpha \rightarrow \beta$  and  $\beta \rightarrow \gamma$  are observed during heating as well as cooling cycles; (b) Linear thermal expansion of sapphire reference measured under identical experimental conditions. Inset shows percentage deviation in measured expansion of sapphire from NIST recommended values 96

Fig. 3.8	Effect of thermal cycling on linear thermal expansion of polycrystalline uranium; Inset shows the linear dilation curves for thorium metal over three consecutive thermal cycles	99
Fig. 3.9	Comparison of linear thermal dilation behavior of polycrystalline samples of uranium and thorium with literature data on single crystal uranium [189] and polycrystalline thorium [152]	101
Fig. 3.10	Bulk density of thorium and uranium metal obtained from measured linear thermal expansion data during heating cycle. IAEA recommended values are also plotted along [175]	103
Fig. 3.11	(a) Representative heat flow curve obtained on thorium metal after a temperature modulated DSC experiment, (b) Specific heat of sapphire measured under identical experimental conditions along with the NIST recommended $C_p$ data. Inset shows percentage deviation in measured $C_p$ from recommended values	106
Fig. 3.12	Isobaric specific heat of (a) thorium and (b) uranium as a function of temperature; Black data points show literature reported values. Pink colour data show experimental $C_p$ obtained from TMDSC measurements (298 K - 773 K)	108
Fig. 3.13	Thermal Conductivity of nuclear-grade thorium and uranium as a function of temperature. Plus symbols indicate the estimated average error in thermal conductivity measurements	110
Fig. 3.14	Comparison of temperature dependence of thermal conductivity of thorium and uranium studied in present investigation with available literature data	112

Fig. 3.15	Effect of thermal cycling on thermal diffusivity of uranium; a comparison with literature reported values is also shown along	114
Fig. 4.1	EDS curve recorded on surface cleaned Th-20U alloy. Inset shows the electron micrograph, over which EDS curve was recorded	128
Fig. 4.2	XRD patterns recorded on thorium, uranium, Th-10U and Th-20 U alloy. Black curves show the measured diffraction data. Red and blue lines show reported peak positions for orthorhombic uranium [167] and FCC thorium [201]	129
Fig. 4.3	Thorium-Uranium phase diagram [Bull. Alloy Phase Diagr. 6 (5) (1985) 443-445, © Springer; Reproduced with kind permission of Springer Science & Business Media; Licence number: 4897030537802]	130
Fig. 4.4	Back scattered electron (BSE) micrographs of (a) Th-10U alloy, (b) Th-20U alloy (c) thorium metal and (d) uranium metal	132
Fig. 4.5	Thermal diffusivities of Th-10U, Th-20U alloys and constituent metals as a function of temperature. Filled circles represent the average value of multiple laser shots while plus symbols show individual data points. Thermal diffusivities of both alloys calculated from weighted average rule are also plotted (open circle symbols)	134
Fig. 4.6	Linear dilation of Th-10U alloy, Th-20U alloy, thorium and uranium as a function of temperature. Dilation estimated from weighted average rule is also shown	137

Fig. 4.7	Temperature dependent bulk density of Th-10U and Th-20U alloys (wt. %) in comparison to that of thorium and uranium metals. Alloy densities estimated from weighted average rule are also shown	141
Fig. 4.8	Specific heat ( $C_p$ ) of Th-10U, Th-20U alloys, thorium and uranium metals. Reported $C_p$ data on thorium and uranium are also plotted. $C_p$ of alloys estimated from weighted average rule using reported $C_p$ of constituent metals is also shown	143
Fig. 4.9	Thermal conductivity of Th-10U, Th-20U (wt. %) alloys as a function of temperature. Thermal conductivities of thorium and uranium metals (from chapter-3) and reported data on U-14 wt. % Zr alloy [155] and U-11.4 wt. % Zr alloy [204] are also shown for comparison	144
Fig. 5.1	Optical micrographs of as-melted Th-7U-3Zr and Th-3U-7Zr (wt. %) alloys. Representative back scattered electron (BSE) images of thorium and uranium metals used for preparation of ternary alloys are also shown	152
Fig. 5.2	Ambient temperature XRD patterns of Th-3U-7Zr and Th-7U-3Zr alloys and constituent elements (Th, U and Zr). Reported diffraction peak positions for ambient temperature allotropes of Th [167], U [201] and Zr [213] also indicated. Symbols have following meaning: $\bullet$ ( $U_3O_8$ ); $\square$ ( $(U_{0.67}Zr_{0.33})O_{2.33}$ ); $\circ$ ( $ThO_2$ ); $\blacktriangle$ ( $(Th_{0.33}Zr_{0.67})$ )	153

Fig. 5.3	Raman spectra corresponding to different regions of Th-3U-7Zr ternary alloy (polished surface); recorded at ambient temperature. Different regions in optical micrographs of alloy, over which Raman spectra were acquired, are shown in the inset	156
Fig. 5.4	SEM micrographs of (a, c) Th-7U-3Zr and (b, d) Th-3U-7Zr alloys	158
Fig. 5.5	Results of elemental mapping analysis on Th-7U-3Zr alloy	159
Fig. 5.6	EDS patterns recorded from different regions of Th-7U-3Zr alloy, as marked in the electron micrograph image	160
Fig. 5.7	Thermal diffusivities of Th-3U-7Zr and Th-7U-3Zr alloys measured over three thermal cycles (298 K → 1273 K → 298 K)	161
Fig. 5.8	Thermal diffusivities of Th-3U-7Zr and Th-7U-3Zr alloys (298 K - 1273 K). Thermal diffusivities of thorium, uranium, Th-10U alloy measured during present investigations and reported diffusivity data of zirconium [150] are also plotted	163
Fig. 5.9	Linear thermal expansion of Th-3U-7Zr, Th-7U-3Zr ternary alloys and constituent metals (thorium, uranium and zirconium) (308 K – 1373 K)	164
Fig. 5.10	Variation of density as a function of temperature for Th-3U-7Zr, Th-7U-3Zr alloys along with that of Th and U metals. Inset shows the temperature dependent density for zirconium	167
Fig. 5.11	Temperature dependent thermal conductivity of Th-3U-7Zr and Th-7U-3Zr alloys, constituent metals (Th, U, Zr) and ThO <sub>2</sub> [224]	169

Fig. 6.1	DSC thermograms of stoichiometric glycine-Th(IV)-nitrate and citric acid-Th(IV)-nitrate aqueous gels. Inset shows thermograms recorded on DSC residues	175
Fig. 6.2	DSC thermograms recorded on stoichiometric glycine-Th(IV)-nitrate aqueous gel during consecutive heating cycles. Inset shows the cooling cycle thermograms	177
Fig. 6.3	DSC thermograms of glycine-Th(IV)-nitrate gels with varying F:O values. Insets show expanded view of thermograms in lower temperature region	178
Fig. 6.4	DSC thermograms of starting materials ( $\text{Th}(\text{NO}_3)_4 \cdot 5\text{H}_2\text{O}$ and glycine) in comparison to that of stoichiometric glycine-Th(IV)-nitrate aqueous gel	179
Fig. 6.5	Photographs of glycine-Th(IV)-nitrate gel and residue obtained during DSC thermal cycling experiments (a) Transparent gel at 373 K, (b) porous yellowish-brown solid obtained after first heating up to 498 K, (c) further swollen porous solid obtained after 3 <sup>rd</sup> heating up to 498 K and, (d) as-combusted product popped out of sample pan	180
Fig. 6.6	Variation of weight of residue as a function of temperature obtained for off-line TG experiment on stoichiometric glycine-Th(IV)-nitrate gel	182
Fig. 6.7	Powder XRD patterns of as-prepared glycine-Th(IV)-nitrate gel, gel heated to 373 K and 460 K along with as-combusted product. Inset shows XRD pattern of as-prepared gel dried at ambient temperature inside a desiccator	184

Fig. 6.8	(a) FT-IR patterns of glycine, $\text{Th}(\text{NO}_3)_4 \cdot 5\text{H}_2\text{O}$ , glycine-Th(IV)-nitrate gel and as-combusted $\text{ThO}_2$ , (b) Corresponding patterns of gel heated at different temperatures	185
Fig. 6.9	Raman spectrum of as-prepared glycine-Th(IV)-nitrate gel	187
Fig. 6.10	Estimation of pH of vapours evolved during heating of glycine-Th(IV)-nitrate gel. Gel was heated inside quartz tube and vapours were carried up to pH paper by argon gas flow	188
Fig. 6.11	DSC thermograms recorded on stoichiometric citrate-Th(IV)-nitrate gels during consecutive heating cycles	192
Fig. 6.12	DSC thermograms of citrate-nitrate gels ( $0.75 \leq \text{F}:\text{O} \leq 1.25$ ). Inset shows expanded view of thermograms over 475 K to 630 K	193
Fig. 6.13	DSC thermograms of anhydrous citric acid ( $\text{C}_6\text{H}_8\text{O}_7$ ), $(\text{Th}(\text{NO}_3)_4 \cdot 5\text{H}_2\text{O})$ and citrate-Th(IV)-nitrate gel ( $\text{F}:\text{O} = 1.0$ ) in flowing oxygen atmosphere	194
Fig. 6.14	Variation of autoignition temperature with fuel to oxidant ratio. Corresponding variation for high temperature exothermic peaks (620 K – 660 K) is shown in the inset	195
Fig. 6.15	Enthalpy associated with high temperature DSC exotherm(s) in citrate-Th(IV)-nitrate gels as a function of F:O. Corresponding variation in enthalpy of autoignition process is shown in the inset	196
Fig. 6.16	Powder XRD patterns corresponding to as-prepared stoichiometric ( $\text{F}:\text{O} = 1.0$ ) citrate-Th(IV)-nitrate gel, as-combusted $\text{ThO}_2$ powder and 723 K calcined powder	197

Fig. 6.17	Ambient temperature Raman Spectra of thorium nitrate (solid), citric acid (solid) and stoichiometric citrate-Th(IV)-nitrate aqueous solution	198
Fig. 6.18	Ambient temperature Raman spectra of as-combusted citrate-Th(IV)-nitrate gel (F:O = 1.0), calcined ThO <sub>2</sub> powder and sintered ThO <sub>2</sub>	199
Fig. 6.19	Variation of average crystallite size with fuel to oxidant ratio for nanocrystalline ThO <sub>2</sub> synthesized from glycine-Th(IV)-nitrate and citrate-Th(IV)-nitrate combustion. Inset shows XRD patterns recorded on few representative samples (F:O = 0.75, 0.90, 1.00, 1.25)	205
Fig. 6.20	Width (FWHM) of the first order Raman peak ( $\sim 458 \text{ cm}^{-1}$ ) recorded on ThO <sub>2</sub> powders (calcined at 723 K) prepared by citrate-nitrate and glycine-nitrate combustion. Inset shows representative Raman spectra	206
Fig. 6.21	DSC thermograms of glycine-Th(IV)-nitrate gels with different fuel-to-oxidant ratios	207
Fig. 6.22	Photograph of as-combusted powders with varying F:O ( $0.65 \leq \text{F:O} \leq 1.25$ )	209
Fig. 6.23	Small angle X-ray scattering (SAXS) profiles of three gel samples (S1-S3; F:O = 0.75, 0.90, 1.00) and solid crystals obtained from glycine-rich gel (S4; F:O = 1.25). Inset shows powder XRD pattern of crystal grown in fuel-rich solution (F:O = 1.25)	210

Fig. 6.24	SAXS profiles of as-combusted ThO <sub>2</sub> powders (S1-S4; F:O = 0.75, 0.90, 1.00, 1.25). Symbols are experimental data whereas solid lines are fits	211
Fig. 6.25	Crystallite size distribution for as-combusted ThO <sub>2</sub> powders (a) smaller crystallites and (b) larger crystallites. (S1-S4; F:O = 0.75, 0.90, 1.00, 1.25)	213
Fig. 6.26	FT-IR spectra of glycine-Th(IV)-nitrate aqueous gels for different F:O values: (a) higher wave number range and (b) lower wave number range	218
Fig. 7.1	Flow sheet for ThO <sub>2</sub> pellet processing	227
Fig. 7.2	Powder XRD pattern of citrate-Th(IV)-nitrate as-combusted product (F:O = 1.10), calcined ThO <sub>2</sub> powder and silicon standard. Inset shows the Williamson-Hall plot for calcined ThO <sub>2</sub> powder	228
Fig. 7.3	Section of powder XRD patterns recorded on (a) calcined gn-ThO <sub>2</sub> and (b) calcined cn-ThO <sub>2</sub> for studied fuel to oxidant ratios. Inset in each figure shows XRD trace of as-combusted powders	229
Fig. 7.4	(a) Equal amounts of as-combusted cn-ThO <sub>2</sub> (TC7; F:O = 1.05) and gn-ThO <sub>2</sub> (TG5; F:O = 1.00); (b) corresponding powders after air calcination at 973 K for 5 h	233
Fig. 7.5	Linear shrinkage behavior of (a) gn-ThO <sub>2</sub> and (b) cn-ThO <sub>2</sub> compacts under non-isothermal constant rate heating program. Inset shows the nature of curve before the onset of rapid sintering	234
Fig. 7.6	Linear shrinkage behavior of (a) gn-ThO <sub>2</sub> and (b) cn-ThO <sub>2</sub> compacts during isothermal heating cycle (1773 K for 1 h)	238

- Fig. 7.7 SEM micrographs recorded on (i) calcined powders (a) gn-ThO<sub>2</sub> (F:O = 0.9) (b) cn-ThO<sub>2</sub> (F:O = 0.9) (ii) sintered pellet surface (c) gn-ThO<sub>2</sub>, (d) cn-ThO<sub>2</sub>, (iii) fractured pellet surface (e) gn-ThO<sub>2</sub>, (f) cn-ThO<sub>2</sub> 240
- Fig. 7.8 SEM micrographs recorded on fractured pellet surface of (a) gn-ThO<sub>2</sub> and (b) cn-ThO<sub>2</sub> at higher magnification. Pore sizes are also indicated in the micrographs 241
- Fig. 7.8 (c) Schematic illustration of various mass transport mechanisms that take place during sintering process. Inset shows the dihedral angle ( $\phi$ ) between coexisting phases (solid-solid interface and solid-vapour interface) that govern the mass transport 244
- Fig. 7.9 FT-IR Spectra of gn-ThO<sub>2</sub> and cn-ThO<sub>2</sub> powders: (a) air calcined at 973 K and (b) sintered at 1773K. For both samples F:O ratio is 1.20 247

## LIST OF TABLES

<b>Table No.:</b>	<b>Table caption</b>	<b>Page No.</b>
Table 1.1:	Properties of thorium, uranium and plutonium metals	15
Table 3.1:	Table 3.1. Details of uranium sample purity and method used for thermal conductivity determination for literature data plotted in Fig. 3.1	79
Table 3.2:	Carbon, oxygen and nitrogen content of thorium and uranium metals	82
Table 3.3:	Effects of impurities (C, N, O) on thermal diffusivity of thorium and uranium	93
Table 3.4:	Average coefficient of linear thermal expansion for uranium and thorium	104
Table 3.5:	Non-metallic impurities in thorium used for $C_p$ measurements	107
Table 3.6:	Non-metallic impurities in uranium used for $C_p$ measurements	107
Table 4.1:	Carbon, oxygen and nitrogen contents in binary alloys (Th-10U, Th-20U) and constituent metals (Th and U)	125
Table 4.2:	Average coefficient of linear thermal expansion (CTE) for Th-10U and Th-20U binary alloys and constituent metals (Th and U) in different temperature intervals	137
Table 5.1:	Average coefficient of linear thermal expansion for Th-3U-7Zr, Th-7U-3Zr ternary alloys and constituent metals (Th, U and Zr) in different temperature intervals	165
Table 6.1:	Peak temperatures and enthalpy values obtained from analysis of DSC thermograms recorded on glycine-thorium nitrate aqueous gels	208

Table 6.2:	Crystallite size of as-combusted ThO <sub>2</sub> powders evaluated from SAXS data. Symbol 'r' and 'R' represent radius of smaller and larger crystallites, respectively	214
Table 7.1:	Powder properties of gn-ThO <sub>2</sub> powders (973 K calcined samples)	230
Table 7.2:	Powder properties of cn-ThO <sub>2</sub> powders (973 K calcined samples)	230
Table 7.3:	Details of sintering parameters for gn-ThO <sub>2</sub> compacts	235
Table 7.4:	Details of sintering parameters for cn-ThO <sub>2</sub> compacts	236

# CHAPTER 1

## Introduction

---

### 1.1. Nuclear energy program in India

Thorium (atomic number  $Z = 90$ ) and uranium ( $Z = 92$ ) are the only two naturally occurring reasonably abundant actinide elements on earth. Discovered in the year 1828 and 1789 by Sir Jön's Jacob Berzelius and Martin Klaproth, respectively, thorium and uranium take 41<sup>st</sup> and 48<sup>th</sup> position in the most abundant elements in earth's crust with Th/U ratio generally accepted between 3 to 4 [1]. Quite interestingly, radioactive nature of thorium and uranium was identified long after their discovery in 1898 (independently by Gerhard Schmidt and Marie Curie) and in 1896 (by A.H. Becquerel), respectively. While natural uranium consists of three isotopes namely  $^{234}\text{U}$  (traces),  $^{235}\text{U}$  (~0.7%) and  $^{238}\text{U}$  (~99.3%), natural thorium almost exclusively exists as  $^{232}\text{Th}$  isotope. These elements were used in various applications / products, which included (i) uranium in ceramic glazes (as colouring agent), glass tinting agent, gyroscope wheel, catalysis, radiation shielding, X-ray target, and military armours / ammunition [2] and (ii) thorium in gas mantles, toothpaste, magnesium-based alloys, tungsten-based filaments for electric bulbs and welding / arcing electrodes, catalysis, dental filling, etc. [3-5]. However, the discovery of nuclear fission of uranium (in nitrate salt) in December 1938 by Otto Hahn and Fritz Strassmann [6] and its immediate follow up developments brought these two elements to the category of precious energy materials. Nuclear fission was such an important discovery that it took only less than three years to understand the fission process in detail with its underlying physics and led to the first ever demonstration of controlled self-sustaining fission chain reaction in a man-made experiment named Chicago Pile (CP-1) Test in December 1942 [7]. Rapid worldwide research and development led to comprehensive understanding of nuclear properties of uranium, thorium

and plutonium (man-made actinide) isotopes. Potential of thorium as a unique nuclear material for electricity generation had been identified during the first two decades of nuclear technology development after the discovery of nuclear fission [8, 9]. Distinct advantages of  $^{232}\text{Th}$  as a fertile nuclei and  $^{233}\text{U}$  as fissile nuclei (produced from  $^{232}\text{Th}$  by neutron-capture transmutation process:  $^{232}\text{Th} + {}^1_0\text{n} \rightarrow {}^{233}\text{Th} \rightarrow \beta^- + {}^{233}\text{Pa} \rightarrow \beta^- + {}^{233}\text{U}$ ) over other fissile isotopes (naturally occurring  $^{235}\text{U}$  and man-made  $^{239}\text{Pu}$ ) and fertile isotopes (naturally occurring  $^{238}\text{U}$ ) were well established. Potential role of thorium as an unlimited and sustainable source of clean nuclear energy had been identified and it was hoped that large-scale deployment of thorium for nuclear energy generation would not take more than a few decades. Foundation of India's nuclear energy program was also laid quite early; immediately after becoming an independent nation, by Dr. Homi Jahangir Bhabha; the architect of Indian nuclear program [10]. Recognising the essential and critical role of nuclear energy in the energy and national security of India, and with true assessment of country's own nuclear resources, Dr. Bhabha conceived a three-stage nuclear power program, which aims to ultimately utilise the vast and easily available thorium resources in India [11]. The three-stage program is based on effective utilisation of India's limited uranium resources in heavy water moderated natural uranium (in the form of  $\text{UO}_2$ ) fuelled reactors (PHWRs) in the first stage. These reactors produce electricity and gradually build-up artificial fissile inventory in the forms of plutonium ( $^{239}\text{Pu}$ ) by neutron capture reaction of fertile  $^{238}\text{U}$  isotope followed by two successive beta decays ( $^{238}\text{U} + {}^1_0\text{n} \rightarrow {}^{239}\text{U} \rightarrow \beta^- + {}^{239}\text{Np} \rightarrow \beta^- + {}^{239}\text{Pu}$ ). Higher long lived isotopes of plutonium ( $^{240}\text{Pu}$ ,  $^{241}\text{Pu}$ ,  $^{242}\text{Pu}$ , etc.) may also be formed during fuel irradiation in PHWRs by successive neutron capture reactions of  $^{239}\text{Pu}$ . Plutonium inventory so generated would serve as the driver fissile element for electricity production in the second stage of nuclear energy program by burning it in liquid metal cooled fast breeder reactors (FBRs). Additional plutonium inventory would also be generated using the leftover uranium (depleted

uranium; containing  $< 0.3\%$   $^{235}\text{U}$ ) from the first stage thermal reactors as fertile material. Reactors in the second stage are envisaged to not only generate large amount of nuclear electricity and sustain on themselves for their fuel requirements but also breed extra fuel for additional FBRs. During the second stage, it is also envisaged to introduce thorium in the blanket region of FBRs so that a sustained build-up of future fissile inventory in the form of  $^{233}\text{U}$  can be initiated. Nuclear properties of  $^{232}\text{Th}$  and  $^{233}\text{U}$  indicate that they are by far the best fertile and fissile radionuclide pair over a wide range of neutron energy spectrum from thermal to fast region [12]. With sustained build-up of  $^{233}\text{U}$  from second stage FBRs, the third stage of India's nuclear energy program is based on reactors generating nuclear electricity predominantly from the fission of  $^{233}\text{U}$ ; in combination with  $^{232}\text{Th}$  being used as fertile nuclei. It is envisaged that the  $^{232}\text{Th}$ - $^{233}\text{U}$  fuel cycle would become a source of practically unlimited amount of energy by utilising the vast indigenous thorium reserves. A unique attribute of India's three stage nuclear program is complete closure of the nuclear fuel cycle that is achieved by reprocessing the spent nuclear fuel and retrieving the fissile and fertile fuel inventories for fuel re-fabrication [13, 14]. Spent fuel is the fuel irradiated in a nuclear reactor to the limit of economically viable energy extraction. Several valuable radioisotopes (fission products and / or their activation / decay products), such as  $^{137}\text{Cs}$ ,  $^{90}\text{Sr}$ ,  $^{106}\text{Ru}$ ,  $^{99}\text{Mo}$ , etc., which are useful in medical, healthcare and industrial applications, are extracted from the nuclear waste during fuel reprocessing. Increasing worldwide demand of these radioisotopes makes closed fuel cycle option a lot more economically advantageous (also known as wealth-from-waste strategy). Long-lived transuranic elements (TRU); also known as minor actinides (MAs), such as americium (Am), neptunium (Np) and curium (Cm) can also be separated (known as partitioning) from spent fuel during reprocessing [15]. These MAs can be utilized in nuclear reactors for energy production (transmutation) [16]. In this way, only a very small and easily manageable short-lived radioactive waste is left out, which

can be safely stored under surveillance for practically manageable duration (up to few hundred years), instead of several tens of thousands of years when minor actinides (MAs) are not separated but left inside the nuclear waste (or spent fuel). On average, 90 - 95% of the starting fuel inventory can be retrieved through spent fuel reprocessing and it is therefore the only way to utilise precious nuclear fuel resources in an environmentally benign manner. Inherent advantages of closed fuel cycle concept make India's three stage nuclear energy program unique and sustainable in the long term. India now stands as one of the few nations that have mastered the closure of uranium-based nuclear fuel cycles both, for thermal and fast neutron spectrum reactors. With currently operational nineteen pressurised heavy water reactors (PHWRs) and four light water reactors (LWRs), a rapid expansion of first stage of nuclear program is underway. This includes seven new thermal reactors under construction and more than ten reactors being approved [17]. Development of second stage reactors is also continuing wherein feasibility of closure of the fast reactor fuel cycle has been demonstrated with continuing operation of world's only uranium-plutonium mixed carbide fuelled Fast Breeder Test Reactor (FBTR) for more than three decades [18] and successfully reprocessing its spent fuel. For demonstration of industrial scale electricity production from fast breeder systems, construction of U-Pu mixed oxide (MOX) fuelled 500 MWe Prototype Fast Breeder Reactor (PFBR) has also been completed, which is being commissioned at present [19, 20]. Design and development of next stage of commercial fast breeder reactors (600 MWe FBR) is also underway. With the progress made so far, entering the industrial scale operation of the second stage is awaiting the penultimate step of PFBR commissioning.

## **1.2. Thorium in Indian nuclear energy program**

From the inception of atomic energy program in India, thorium is envisaged to be the ultimate source of fission-based nuclear electricity [21-24]. While construction of thorium-

based commercial nuclear reactors will take place few decades later from now, research and development efforts on thorium-based fuel cycle technologies are being pursued continuously [25, 26]. Neutron irradiation of thoria pellets in Indian research reactors (In J-rod positions of CIRUS, regular fuel assembly position of Dhruva, blanket region of FBTR) and commercial PHWRs (for neutron flux flattening and  $^{233}\text{U}$  production) [27, 28] has been ongoing since early eighties. Post irradiation examination and reprocessing of irradiated thoria fuel bundles have also been carried out [29]. All these efforts have led to detailed understanding of thorium fuel cycle and development of innovative reactor systems. Design and development of 300 MWe Advanced Heavy Water Reactor (AHWR) and AHWR-LEU (LEU = low enriched uranium) are unique examples of thorium-based nuclear energy systems [30, 31]. As technology demonstrators, these reactors are designed to produce significant fraction of fission energy from utilization of thorium and, with advanced passive safety features, they pave the way for their construction in populous region with minimum exclusion zone requirements [32]. Several engineering-scale experimental demonstration facilities and the AHWR-critical facility ( $100\text{ W}_{\text{th}}$ ) [33] have been in continued operation for physics validation of AHWR, lattice code analyses, testing of control and instrumentation systems, and advanced materials development. Two recent books on development of thorium-based nuclear materials and energy systems amply articulate the current status and future directions of Indian program in this regard [25, 26]. It has been demonstrated that thorium-based fuels are advantageous for safe, sustained and proliferation-resistant nuclear energy systems in the long term. It has also been understood that technological solutions to the challenges associated with the material and radiological aspects of thorium fuel cycle would have to be obtained for large-scale thorium utilization. One of these challenge stems from highly refractory nature of bulk thorium dioxide ( $\text{ThO}_2$ ) that has the highest melting point of all known oxides ( $\sim 3663\text{ K}$ ) [33a, 33b]. It makes fabrication of thoria-based nuclear fuels (front

end process) an energy intensive process and also renders difficulties in dissolution of spent thorium-based fuels in nitric acid ( $\text{HNO}_3$ ) medium (back end process) unless fluoride ions are added. Addition of corrosive fluorides limits the operational lifespan of process structural materials (dissolution vessel, tubing, pipes, etc.) and increase the waste loading capacity due to incorporation of metal ions from these structural materials. A radiological concern pertaining to thorium-based spent fuels is higher radiation dose arising from high energy gamma radiation emitting radionuclides ( $^{208}\text{Tl}$ ;  $E_\gamma =$  up to  $\sim 2.6$  MeV and,  $^{212}\text{Bi}$ ;  $E_\gamma =$  up to  $\sim 1.8$  MeV), which are generated in the decay series of  $^{232}\text{U}$  ( $t_{1/2} = 76.3$  years) [34].  $^{232}\text{U}$  is invariably produced during reactor irradiation of thorium-based fuels. If  $^{208}\text{Tl}$  and  $^{212}\text{Bi}$  concentrations (in spent fuel / reprocessing solutions) exceeds the limit that can be handled in glove box / fume hood, extensive shielding is required for handling (reprocessing) these fuels. This makes the reprocessing of thorium-based fuels technologically challenging. Interestingly, with more impetus being given to the security and safeguarding of nuclear materials worldwide, this challenge is now being viewed as an inherent advantage. Higher radiological shielding requirements for thorium-based spent fuels impart proliferation-resistant attribute to these fuels. In other words, it is very difficult to divert them for weapon applications. A critical view to the non-proliferative advantage of thorium-based fuels [34a] as compared to those based on uranium is based on the possibility that weapon-grade  $^{233}\text{U}$  can still be obtained by chemical reprocessing of irradiated  $^{232}\text{Th}$ . Neutron irradiation of thorium produces some amount of  $^{232}\text{U}$  along with  $^{233}\text{U}$ .  $^{232}\text{U}$  decays ( $t_{1/2} \sim 76.3$  years)) to highly radiotoxic and short-lived daughter nuclei ( $^{208}\text{Tl}$ ;  $E_\gamma \sim 2.6$  MeV and  $^{212}\text{Bi}$ ;  $E_\gamma \sim 0.72$  MeV). Therefore, small concentrations ( $\geq 500$  ppm) of  $^{232}\text{U}$  in reprocessed uranium necessitate extensive radiation shielding requirements for uranium extraction and fuel re-fabrication and thus bring proliferation resistant attribute. Short irradiation of thorium in research reactors can minimize  $^{232}\text{U}$  build up in spent fuel and therefore relatively ease out

the spent fuel handling to obtain weapon grade  $^{233}\text{U}$ . Weapon-grade  $^{233}\text{U}$  can also be obtained via chemical separation of intermediate isotope protactinium ( $^{233}\text{Pa}$ ;  $t_{1/2} \sim 26.95$  days) from irradiated thorium-based fuels via aqueous or non-aqueous routes.  $^{233}\text{Pa}$  transmutes to pure  $^{233}\text{U}$  upon beta decay, which can be used for weapon application. The critical view cautioning thorium fuel irradiation for wilful accumulation of  $^{233}\text{U}$  has indeed highlighted the technological challenges associated with both handling short irradiated thorium fuel as well as chemical separation of  $^{233}\text{Pa}$  [34a]. However, it has perhaps purposefully undermined the fact that possibility of accumulating weapon grade fissile  $^{233}\text{U}$  stockpile from unsafeguarded irradiation facilities (e.g., research reactors) is far more difficult and challenging than obtaining weapon-grade  $^{239}\text{Pu}$  from well established uranium fuel cycle. It should also be kept in view that due to technological and process challenges associated with thorium fuel cycle, large-scale utilization of thorium for nuclear electricity production is certainly a better proliferation resistant option. From scientific and technological perspective, it is believed that challenges associated with thorium fuel cycle will be met with development of improved materials and better shielding methodologies. Currently, India is at the forefront of developing thorium-based nuclear technologies worldwide.

While significant progress has been made on thorium-based materials and related fuel cycle technologies [25, 26, 30], it is essential to develop other fuel forms based on thorium for advanced nuclear energy systems. These include thorium-based (i) metallic alloys for advanced breeder reactors [35], (ii) halide (fluoride) salts for molten salt reactors (MSR) [36], (iii) innovative hydride fuels [37, 38], (iv) ceramic-metal composites (cermet) [39] and ceramic-ceramic (cercer) composites or inert matrix fuels (IMF) for accelerator driven sub-critical reactor systems [40], (v) oxide fuels with novel microstructures for improved irradiation performance [41], (vi) nitride and carbide fuels, etc. Many of these fuel forms are

potential options for thorium utilization in the generation-IV nuclear reactor systems [42, 43]. A timely assessment of these fuels forms is the need of hour for development of fission-based future nuclear energy systems. The present work is an initial research on two of the above mentioned fuel systems namely, thorium-based metallic alloys and nanocrystalline thoria ceramics. Preparation, characterization and thermophysical properties evaluation of thorium-based metallic alloys and, formation mechanism as well as sintering behaviour of nanocrystalline thorium dioxide ( $\text{ThO}_2$ ) have been studied during the course of this work. Following sections of this chapter briefly summarise the rationale of studies on these two fuel types and also review the literature information on them.

### 1.3. Metallic fuelled nuclear reactor systems

Globally, nuclear technology development started with metals as the preferred fuel form. This was the obvious choice for simple reasons like, well-known physico-chemical behavior of metals and alloys, ease of fabrication, simple and compact core design and production of artificial fissile inventory ( $^{239}\text{Pu}$  /  $^{233}\text{U}$ ) from neutron capture induced transmutation of naturally abundant fertile actinides ( $^{238}\text{U}$  /  $^{232}\text{Th}$ ) [44, 45]. Experimental Breeder Reactor-I (EBR-I) was the first ever metal fuelled, liquid metal cooled fast reactor in the world, which produced nuclear electricity for lighting application for the very first time. EBR-I demonstrated the concept of breeding, which is the capability of a reactor system to generate more fissile material than it consumes for its operation) [46]. EBR-I was followed by Experimental Breeder Reactor-II (EBR-II), which provided extensive experience on the performance potential of a variety of metallic fuels (uranium metal, U-Fs alloys, U-Zr alloys, U-Pu-Zr alloys, etc.) and demonstrated inherently safe irradiation of metallic alloy fuels up to very high burn-ups (up to 19 atom %) [44, 47]. Here, 'Fs' refers to fissium, which is a mixture of Mo, Rh, Ru, Pd, Zr and Nb. U-5Fs alloy corresponds to composition obtained by

electro-refining of irradiated uranium and contains 95 U - 2.4 Mo - 1.9 Ru - 0.3 Rh - 0.2 Pd - 0.1 Zr - 0.1 Nb (all in wt.%). Several other metal / alloy fuelled reactors like Fast Flux Test Facility (FFTF), Fermi nuclear power station, Dounreay fast reactor (DFR), etc. also demonstrated power production with excellent fuel performance and provided sufficient evidence that metal fuelled reactors are among the best options for safe and rapid expansion of nuclear power. During late 1960s, global interest shifted towards oxide fuels for both thermal and fast reactors. This was mainly driven by very high temperature stability of isotropic single-phase cubic oxides ( $\text{UO}_2$ ,  $\text{ThO}_2$ ,  $\text{PuO}_2$ ,  $\text{U}_{1-x}\text{Pu}_x\text{O}_2$ ,  $\text{Th}_{1-x}\text{U}_x\text{O}_2$ ,  $\text{Th}_{1-x}\text{Pu}_x\text{O}_2$ ) and ease of large-scale oxide fuel fabrication under ambient atmosphere conditions. Still extensive research and irradiation tests continued on metallic fuels, which established their high burn-up capability (10 - 20 at. %) with inherent safety features. It must be noted that burn-up in metallic fuels has been mainly limited due to fuel-clad interaction (FCMI: fuel clad mechanical interaction and, FCCI: fuel clad chemical interaction), irradiation induced damages and thermal effects (irradiation creep, thermal creep, radiation embrittlement, etc.) that deteriorate clad properties [48] and other structural materials, but not the fuel. In spite of shift of global interest towards development of light water thermal reactors (BWRs, PWRs, HWRs) for electricity production, several countries like Russia (BN-series reactors), France (Rapsodie, Phoenix, Super-Phoenix), Japan (Monju) and India (FBTR, PFBR) continued to develop fast reactors; primarily fuelled with U-Pu-based ceramics (mixed oxide, mixed carbide). Use of ceramic fuels in fast reactors also affected large-scale development of metallic fuelled reactors. In spite of already demonstrated excellent performance and safety potential of metallic fuels, commercial metal fuelled fast breeder reactors are yet to come. It is also important to mention that all along the development of nuclear technologies till date, a large number of metallic fuelled research reactors (metal fuel with aluminium alloy clad) continue to be the safe, proven and efficient means of transmutation of fertile actinides into

fissile ones as well as large-scale isotope production for wide variety of applications. A renaissance, however, is around for past few years on re-development of metal fuelled fast reactors, mainly driven by their (i) inherent capability to provide excellent breeding performance, (ii) proven and safe fuel performance during normal and transient conditions, (iii) compact core design for small modular reactors (SMRs) and (iv) capability to transmute long-lived minor actinides (MAs). Liquid sodium cooled, metal fuelled fast breeder reactors are also being developed as one of the generation-IV nuclear reactor systems [49]. Another concept in metallic fuelled fast reactor design is that of travelling wave reactor (TWR), which works on *in situ* breeding of subcritical fuel (depleted uranium, natural uranium, LEU) into a new critical fuel so that a breed and burn wave propagates in the reactor system. In these reactor systems, slightly higher enrichment in the starting reactor core can lead to once through utilisation of metallic fuelled fast reactors up to very high burn ups (~50 atom %), which has never been achieved till date [48]. Another innovative design includes use of fine UO<sub>2</sub> particles (fuel) dispersed in low melting (~363 K) eutectic alloy (52.5% Bi + 32% Pb + 15.5% Sn), which has density (~10200 kg.m<sup>-3</sup>) comparable to solid UO<sub>2</sub> fuel (~ 10960 kg.m<sup>-3</sup>) [50]. It offers advantages in terms of simplified core design, possibility of Th-U mixed oxide utilization as fuel in the molten eutectic alloy, excellent heat transfer from fuel particles to coolant via liquid metal eutectic medium, homogenous suspension of fuel particles in the eutectic liquid, non-pyrophoric Pb-based molten medium, etc. Similar to these examples, ongoing programs worldwide clearly indicate the inevitability of early development of metal fuelled commercial nuclear power reactors for faster and safer expansion of nuclear energy.

### 1.3.1. Advantages of metallic nuclear fuels

Metallic fuels provide following main advantages: With the highest fissile atom densities possible with any fuel form, metallic fuels enable design of compact reactor cores and highest

possible conversion factors. Conversion factor is defined as ratio of fissile material created to fissile material consumed either by fission or neutron absorption. For conversion factor greater than one, reactor is called a breeder since net additional fissile fuel inventory is generated during the fuel irradiation cycle. For fast reactors, metallic fuels provide the hardest possible neutron spectrum since lighter constituents (low Z elements) in the form of oxygen (oxide fuel), nitrogen (nitride fuel), carbon (carbide fuel), halogen (molten salt fuel), hydrogen (hydride fuel), etc., which reduce neutron energy within the fuel, are absent. Highest thermal conductivity of metals and alloys impart superior heat transfer characteristics to the fuel, which is one of the most essential requirements for efficient heat extraction and safe fuel performance. Lower specific heats of metals and alloys among all the possible fuel forms (metallic, ceramics, molten salts, hydrides, etc.) are a safety related advantage. It results into lower stored energy within the fuel for management under transient / accident conditions. Ductile and malleable nature of metals and alloys ease the fuel fabrication in different shapes (rods, pellets, plates, tubes, etc.). Chemical state of irradiated metallic / alloy fuel (spent fuel) is dominated by fission products and unutilized fuel mostly in the form of metals, alloys and inter-metallic compounds, except only the fission gases (Xe, Kr) and volatile compounds (such as iodine, bromine, caesium iodide, etc.). Management of metallic spent fuel is simple and straightforward either for reprocessing (via pyro-metallurgy or aqueous reprocessing) or safe storage (as dense spent fuel in shielded and safeguarded facilities). Non-aqueous reprocessing of metallic fuels by electro-metallurgy in molten halide (mostly alkali chlorides) salts also generates lesser nuclear waste as compared to aqueous reprocessing. Due to high radioactivity of spent metallic fuel (as well as reprocessed fuel), pyrochemical reprocessing needs to be done remotely under inert atmospheres, which brings-in proliferation-resistant advantage to metallic fuels. During electro-refining of metallic spent fuels, long-lived higher actinides (MAs) are retained with reprocessed fuel and can be

efficiently incinerated in reactors for energy production. MA incineration also reduces the duration for long-term safe storage of nuclear waste from tens of thousands of years to few hundreds of years. All these advantages make metallic fuels a promising option for fast as well as thermal reactors.

### 1.3.2. Challenges / limitations of metallic nuclear fuels

Metallic fuels however have certain inherent challenges / limitations associated with them, which are mentioned now. Fabrication of metallic fuels needs to be carried out under inert atmospheres since actinide metals (U, Pu, Th) are highly reactive. In case of powder handling, maintaining strict inert conditions (Argon) is essential due to their pyrophoric nature in air / moisture. Operating fuel temperature (centreline temperature) of metallic fuels is lower than that of ceramic fuels, which is limited due to lower melting temperatures of constituent elements, particularly uranium (~1404 K) and plutonium (~915 K). Zirconium is usually added to increase alloys' solidus temperature. Metallic alloy fuels are usually multi-phase composites as compared to isotropic cubic single-phase ceramic fuels. As compared to ceramics, metallic fuels show higher thermal expansion and swelling during in-pile irradiation. Particularly, uranium and plutonium-based metallic fuels show high anisotropic swelling due to composite (multi-phase) nature of fuel and multiple allotropic phase transformations in both uranium (three allotropic phases) and plutonium (seven allotropic phases). Higher densities of uranium (~19050 kg.m<sup>-3</sup>) and plutonium (~19860 kg.m<sup>-3</sup>) also provides lesser volume within the fuel lattice for fission production accommodation and fission gas retention, which also contributes to fuel's swelling behavior. As a result, fission gas released from metallic fuels need to be retained inside the fuel pin by providing a larger plenum volume, which makes fuel pin design relatively complex. Higher swelling makes fuel-clad contact more probable, which results into fuel clad mechanical interactions (FCMI)

and fuel clad chemical interaction (FCCI). Both FCMI and FCCI may cause clad breach by mechanical failure or eutectic formation between components of fuel and clad, respectively. Development of high performance cladding materials (HT9, D9, ODS steel, etc.) have led to better control over the occurrence of FCMI and FCCI in fast reactors [51].

### 1.3.3. Thorium-based metallic fuels and Indian program

The second stage of Indian nuclear power program is based on liquid sodium cooled fast breeder reactors. Along with the ongoing commissioning of industrial scale technology demonstration of indigenous fast breeder technology (PFBR), design of 600 MWe U-Pu mixed oxide (MOX) fuelled fast breeder reactor (FBR) is underway [19]. This will be followed by setting up metallic fuelled fast reactors [18], basic physics and core design for which are presently underway [52, 53]. Candidate fuels for these metal fuelled reactors include U-Zr binary and U-Pu-Zr ternary alloys. Various lab-scale as well as engineering-scale facilities are being setup to establish different aspects of fast reactor metal fuel cycle. The choice of uranium and plutonium-based alloys (U-Zr, U-Pu-Zr, etc.) in the first phase of metal fuelled reactor development program is obvious since significant experience exists on these alloys under fast neutron spectrum irradiation conditions. These alloys are also being irradiated in FBTR [54]. However, a long term strategy calls for development of alternative fuel options that include the inherent advantages of metallic fuels and also addresses the challenges that are associated with U-Zr and U-Pu-Zr alloys. For India's three stage program with thorium being the ultimate nuclear energy resource, development of thorium-based metallic alloy fuels is a much needed requirement from the perspective of their qualification for future fast reactors as well as thermal breeders. Candidate alloys which can be used as nuclear fuels include Th-U (using  $^{235}\text{U}$  or  $^{233}\text{U}$  isotopes), Th-Pu binary alloys as well as Th-Pu-Zr and Th-U-Zr and Th-MA-Zr alloys (MA = minor actinides) [35]. While advantages of

thorium-based metallic alloy fuels have been documented in reports published during first three decades of nuclear technology development, detailed assessment of properties of these alloys is limited as compared to U-Zr and U-Pu-Zr alloys. Before reviewing the existing literature on thorium-based metallic alloy fuels, a brief summary of their advantages over uranium-based metallic fuels is provided.

#### 1.3.4. Advantages of thorium-based metallic fuels over uranium-based metallic fuels

Table 1.1 presents some of the properties of metallic thorium in comparison to uranium and plutonium metals [12]. Based on these properties, advantages of thorium-based metallic alloys over uranium-based alloys are briefly mentioned now.

- Higher melting point of thorium ( $\sim 2025$  K) as compared to uranium ( $\sim 1404$  K) provides better thermo-chemical stability to thorium-based alloys. Also, these alloys can be irradiated with higher centerline temperatures so that thermal efficiency can be improved and higher burnups can be achieved. Due to higher melting temperature of thorium, solidus temperatures of Th-based alloys (Th-U, Th-U-Pu, Th-Pu, Th-U-Zr) are sufficiently high for their use in fast spectrum reactors with average outlet coolant temperature of 923 K [55]. This is an important advantage over U-based alloys, where solidus temperature drops down significantly to cause fuel melting under typical fast reactor conditions.
- Thorium has much higher thermal conductivity ( $\sim 48$  W.m<sup>-1</sup>K<sup>-1</sup> at 298 K) as compared to uranium ( $\sim 27$  W.m<sup>-1</sup>K<sup>-1</sup> at 298 K). Thermal conductivity of thorium increases with increasing temperature as in case of uranium. This is very important advantages in terms of efficient extraction of fission heat during fuel irradiation.

**Table 1.1. Properties of thorium, uranium and plutonium metals**

Property	Thorium	Uranium	Plutonium
<b>Structure</b>	FCC (RT-1673 K)  BCC (1673-T <sub>m</sub> )	Orthorhombic (RT-952 K)  Tetragonal (952-1045 K)  FCC (1045 K – T <sub>m</sub> )	Six allotropes up to melting  (Monoclinic at RT)
<b>Lattice parameter (Å)</b> (for RT phase)	5.07	a = 2.85, b = 5.87,  c = 4.95	a = 6.18, b = 4.82  c = 10.9, β = 101.8°
<b>Melting point (K)</b>	2025	1404	913
<b>Boiling Point (K)</b>	5060	4405	3508
<b>Theoretical density</b> (kg.m <sup>-3</sup> at 298 K)	11680	19050	19860
<b>Specific Heat</b> (J.mol <sup>-1</sup> .K <sup>-1</sup> at 298 K)	26.2	27.7	35.5
<b>Thermal conductivity</b> (W.m <sup>-1</sup> .K <sup>-1</sup> at 773K)	43.1	30	30
<b>Coefficient of thermal expansion</b> (× 10 <sup>6</sup> / K)	11.9 (30-600 K)	14.2 (30-600 K)	56 (α-phase)

➤ Lower thermal expansion coefficient of thorium ( $\sim 11.9 \times 10^{-6} / \text{K}$ ; 298 - 600 K) as compared to uranium ( $\sim 14.2 \times 10^{-6} / \text{K}$ ; 298 - 600 K) indicates lesser expansion-induced swelling behavior, which delays fuel clad interaction.

- Lower specific heat and higher thermal conductivity of thorium as compared to uranium indicate lower stored energy inside thorium-based fuels, and therefore safer fuel performance during off-normal events such as under cooling (LOCA) or transients.
- Isotropic crystal structure of thorium (FCC up to 1723 K; BCC up to melting temperature) indicate thorium-rich fuel matrix to remain in FCC phase during normal irradiation conditions. This would lead to lower anisotropic expansion of thorium-based alloys during irradiation and / or thermal cycling. On the other hand, uranium has three allotropic transformations from ambient to melting temperature, which would results into anisotropic expansion of uranium-rich alloys and cause higher dimensional deformations.
- Thorium has higher creep resistance and better ductility as compared to uranium metal, which are desired attributes towards fabrication and thermal performance of alloy fuels.
- Low density (~11.7 g/cc) isotropic crystal structure of thorium as compared to U (~19.05 g/cc) and Pu (~19.86 g/cc) provides significantly larger lattice space for retention of fission products. This would lead to lower fission product-induced swelling / deformation. Higher solidus temperatures of thorium-based alloys would also benefit in terms of slower diffusion of fission products (volatile / gaseous). Higher fission gas retention and lesser fission gas-induced swelling help in preventing fuel pin failure, which occurs by fuel-clad interaction (FCMI and /or FCCI) during irradiation. Previous in-pile studies on thorium-based alloys have revealed the same.
- Thorium-based alloys are easier to work (hot/cold rolling, swaging, etc.) to form various fuel shapes as compared to uranium-based alloys. This is an advantage in fuel fabrication, particularly when the fuel is required in specific shape/form. Hot rolling of thorium is easier than cold rolling and does not require intermediate annealing. As-cast thorium on the other hand may have large grains, which may lead to crack formation upon cold rolling.

- As compared to ceramic fuel forms of thorium (oxides, carbides, etc.), thorium-based alloys are expected to result into higher breeding gains.
- Th-based alloys are promising options for efficient burning of stock-piled plutonium and transuranic (TRU) inventory without compromising the safety characteristics of fuel [56].
- Inherent advantages of thorium fuel cycle in terms of negative sodium void coefficient and more negative Doppler coefficient are larger with metallic fuel form and offer increased safety attributes to fast reactors [21].
- Like other metallic fuels, thorium-based alloys are also amenable to pyrochemical reprocessing and remote fabrication.

### **1.3.5. Limitation of thorium-based metallic alloys**

Advantages mentioned above indicate superior performance potential of thorium-based metallic alloys fuels over uranium-based alloys. Yet, following aspects can be viewed as scientific and technological challenges, which need to be overcome for large scale utilization of thorium-based metallic alloy fuels:

- Fabrication of thorium-rich alloys by injection-casting route, which is routinely employed for uranium-based metallic fuel pins, is challenging. Due to higher solidus temperatures, conventional casting moulds (fused-quartz, Vycor, etc.) cannot be used. Suitable mould tubes such as graphite coated with suitable protective layer so that molten alloys do not pick up excessive carbon during injection-casting, needs to be developed [55]. Other methods of fuel fabrication such as (i) arc-melting followed by swaging / rolling or (ii) tilt-pour casting, etc. also require optimization for large-scale fuel fabrication.
- Preparation of thorium-based alloys via powder metallurgy is also challenging. It requires preparation and handling of high purity metal powders (Th, U, Pu, Zr, etc.), which are

highly reactive (pyrophoric) and radiological issues during powder handling need to be addressed. Fuel fabrication has to be done under inert atmosphere (argon) with appropriate radiation shielding. Very little experience exists on powder metallurgy of thorium-based alloys. A potential solution to this includes preparation of hydrides using bulk alloys followed by de-hydrating and sintering (preferably vacuum hot pressing) in controlled atmospheres and final alloy shaping [57].

- Unlike established oxide-fuel technology and adequate information on uranium-based metallic fuels, very limited information is available on thorium-based metallic fuels. Data available is either limited to lower burn-ups or detailed post irradiation analyses (PIA) has not been carried out/reported [58].
- Limited solubility of uranium in thorium ( $< 2$  wt.% up to 1273 K) is also a concern [59]. While uranium up to  $\sim 15$  wt. % can be accommodated in thorium matrix in the form of randomly distributed isolated particles / grains and the overall fuel microstructure remains similar to typical dispersion type fuels. However, beyond 15 wt.%, uranium tends to segregate at grain boundaries and further makes continuous network of metallic uranium, which may lead to higher irradiation swelling and dimensional instability [58]. One of the possible solutions is to keep fuel stoichiometry below 15 wt.% uranium so that overall integrity of the fuel is governed by thorium matrix. Another prospect is to optimize alloy microstructure to minimize anisotropic swelling behavior [60].
- It has been reported that only marginal increase in breeding ratio is expected with thorium-based metallic alloys fuels as compared to oxide fuels in fast spectrum reactors [61]. Similar argument of insignificant advantage has been reported for replacing  $\text{ThO}_2$  blanket by thorium metal. In view of limited work on thorium-based alloy fuels, more studies are required to address this concern.

- Issues of higher fission gas-induced swelling are reported for thorium-based alloys irradiated to high burn-ups. Thermal expansion coefficients as high as  $\sim 25 \times 10^{-6} / \text{K}$  have been reported for Th-11 wt.% U alloys [62]. It has however not been made clear if observed extent of swelling is of the same order as that in U-Zr or U-Pu-Zr alloys or lesser. Thermo-physical studies on metallic alloys must be carried out under highly inert atmospheres and detailed investigations on Th-U binary alloys and SIMFUELS are needed to confirm if alloy oxidation had a role in such large expansion behavior. The term SIMFUEL refers to fuels prepared by incorporating inactive fission products in fresh fuel to simulate the chemical state of irradiated fuel for a given burn-up.
- Due to large difference in melting points and densities of thorium in comparison with uranium / plutonium, and limited solubility of U or Pu in Th [63], preparation of single phase and homogenous thorium-based alloys is challenging.
- Similar to the back-end of thoria-based oxide fuels, reprocessing of thorium-based metallic alloy spent fuels would require extensive radiological shielding. At the same time, their reprocessing by pyro-metallurgical route in molten alkali halide salts is easier than aqueous reprocessing and difficulties associated with dissolution of spent thoria fuel are also not present. More recently, zone-refining methods has also been proposed as clean and effective route for thorium-based metallic fuel reprocessing [64].

Considering the inherent advantages and challenges associated with thorium-based metallic alloy fuels; as discussed above, and in view of India's three stage nuclear energy program centred on large-scale thorium utilization in the long term, it is worthwhile that an indigenous research database is created on potential thorium-based metallic alloys. The first step of this program would majorly be a responsibility of basic researchers working in the area of materials' research to develop methodologies for preparation of these alloys and characterize

them for their physico-chemical properties relevant to their assessment as potential nuclear fuels. Simultaneously, reactor physics aspects need to be studied for conceptual core design and optimization of neutronic parameters for fast and thermal spectrum reactors.

### 1.3.6. Review of existing literature on thorium-based metallic alloy fuels

Majority of work related to development of thorium-based metallic alloy nuclear fuels is reported in first three decades of nuclear technology development. It seems that the major objective to study these alloys then was to understand the breeding performance of  $^{233}\text{U}$  from  $^{232}\text{Th}$  in metallic matrix. Alloys of thorium with fissile actinides ( $^{235}\text{U}$  /  $^{239}\text{Pu}$ ) have been tested in several experimental facilities / power reactors to understand their in-pile performance [12]. These alloys have been investigated as potential fuel for both thermal and fast reactors. This information can be fruitfully used for comparative assessment of indigenous database. A brief summary of the available information is presented now.

Earliest works on Th-U binary alloys (1-2 wt.% highly enriched uranium (HEU)) could be traced back to 1952, when these alloys; in the form of aluminum clad plate type fuels were irradiated in high power research reactor (MTR) up to an integrated neutron flux of  $2.6 \times 10^{21}$  n/cm<sup>2</sup>, corresponding to ~1 at.% burn-up [65] to produce  $^{233}\text{U}$  for defence applications. Post irradiation analysis (PIA) results reported on these alloys indicate dimensional integrity (of core as well as clad) and excellent radiation stability. Irradiated fuel core was found to be hardened as compared to fresh fuel. Further studies also indicated better radiation stability of Th-U binary alloys (up to 10 wt. % U) as compared to uranium-based alloys [66]. Engineering-scale irradiation testing of Th-U, U-Zr and U-Mo binary alloys up to ~850 MWd / MTU burn-up also indicated promising potential of Th-U and U-Mo alloys as nuclear fuels [67]. Olsen et al. [68] have studied corrosion behavior of Th-M alloys (M = Cr, Nb, Zr, Ti;

doping  $\leq 6$  wt.%) in distilled water at  $\sim 368$  K for 30 days and reported notable variation in the extent of corrosion as a function of alloys' metallurgical processing (cold-rolling) history. Origin of such variation in alloys' corrosion behavior is not known so far. With the objective of improved irradiation performance, Farkas et al., [69] developed Th-U binary alloys with varying microstructures using a variety of processing techniques (melting, hot/cold working, heat treatment, etc.) and reported that arc-melted alloys exhibit ideally suited morphology with small uranium particles uniformly dispersed in thorium matrix. They also reported effect of increasing uranium content on work hardening and recrystallization behavior of these binary alloys. In order to stabilize FCC gamma-phase of uranium for improving the irradiation performance and high temperature stability of Th-U binary alloy fuels, doping with metals such as Zr, Nb and Mo has also been reported. Effect of Mo and Nb towards gamma-phase stabilization and that of Zr for improving the water corrosion resistance has also been discussed [69]. Cole et al., [70] studied the effect of alloying (Nb, Mo, Al, Be, C) on physical, mechanical and structural properties of Th-5U and Th-10U (wt.%) alloys and reported significant enhancement in high temperature tensile strength and stress-rupture strength upon alloying, with the most pronounced effect shown by Zr incorporation (2-5 wt.%). Their results indicated improved resistance of doped Th-U alloys to radiation-induced swelling at high temperatures (up to 1073 K), which was attributed to both, formation of solid-solution phases and dispersion strengthening of fuel. Irradiation performance of few of these alloys at 1073 K and higher target burn-ups (up to 30,000 MWd/t) has also been reported [70]. Neutron irradiation behavior of a number of Th-  $x$  wt.% U alloys ( $0 \leq x \leq 31$ ), prepared / processed by different methods (rolling, swaging, chill-casting, etc.) has been studied by Kittel et al., [71] at various irradiation temperatures (318 – 1273 K) and target burn-ups (0.3 – 10 atom %). They reported significantly lesser irradiation-induced swelling for Th-U alloys compared to uranium-based alloys under identical irradiation conditions. This

has been attributed to lower alloy density, isotropic crystal structure of thorium metal and dispersion-type morphology of Th-U alloys consisting of uniform distribution of uranium phase in bulk thorium matrix. It is also reported that fission recoils are more likely to escape from small uranium particles (which show anisotropic swelling) into thorium matrix and immobilize there. Similar behavior can also be expected for Th-<sup>233</sup>U, Th-Pu and Th-U-Zr alloy fuels. Bement et al., [72] have reported burn-up and specific power calculations on thorium metal and Th-5.4 wt.% U alloy. In a review on Th-U binary alloys for their use in sodium cooled Unclad Metal Breeder Reactor (UMBR) program, Copeland [62] summarized and compared different methods of alloy preparation, mechanical properties of un-irradiated as well as irradiated alloys, thermo-physical and thermodynamic properties, and irradiation performance, etc.. Th-20% U alloy composition was proposed as safe fuel option for ~4.3 atom % burn-up with isotropic swelling behavior up to ~923 K operating temperature. He also emphasized the need for extensive research, especially on high temperature properties of these alloys and compatibility with molten metal coolants.

Preparation, characterization and phase diagram studies on binary (Th-U, Th-Pu, U-Pu) and ternary (Th-U-Pu) systems, as reported by Blumenthal et al., [63] indicate that Th-U-Pu ternary alloys consist of co-existing FCC-thorium and multiple U-Pu phases. They identified two alloy compositions namely, 80Th-10U-10Pu and 70Th-20U-10Pu (wt.%) as prospective fast reactor fuels and reported their mechanical, thermal & thermophysical properties as well as irradiation performance [55]. Their results indicate excellent performance of ternary alloy fuels with un-altered fuel microstructure up to 5.6 at.% burn-up, with ~7.3% irradiation-induced swelling per atom % burn-up and safe release of ~70% of the total fission gases into the plenum volume of test fuel pins. Suitability of biphasic Th-U-Pu ternary alloys consisting of (U-Pu) phases dispersed in (Th-Pu) solid-solution matrix as a fast reactor fuel has also

been reported up to ~923 K, which is typical operating temperature of liquid metal cooled fast reactors. Results reported on thermal cycling of Th-U-Pu alloys (723-1073 K; molten NaK; > 100 cycles) also indicated significantly smaller variations in alloy density and dimensions as compared to uranium-based alloys (U-Pu-Zr, U-Pu-Ti, etc.) [55].

Limited literature is available on reprocessing aspects of irradiated thorium-based alloy fuels. Use of vacuum induction drip melting method under remote handling conditions has been reported for reprocessing of thorium-alloy fuels [73]. Separation of uranium and fission products from thorium present in irradiated U-Th-Mg alloys via pyro-metallurgy route was studied by Chiotti et al., [74], who determined solubility of uranium in Th-Mg alloys (Th-55Mg, Th-65Mg, Th-84Mg, Mg; in wt. %) and explored removal of fission products from Th-Mg alloys. They also reported purification of thorium from magnesium by vacuum distillation or precipitation of thorium as ThH<sub>2</sub> at ambient pressures and high temperatures. Hensen [75] reported electro-refining of Th-U alloys in a fused salt medium (using impure thorium or uranium metal as anode) to obtain pure Th / U metals and separated electro-refined metal / alloy from cathode by vacuum distillation. Thermo-chemical modeling has also been reported for reprocessing Th-U-Pu-Zr metallic fuels via pyrochemical electro-refining, which indicate possibility of thorium being retained in the anode basket along with zirconium and noble metals while U, Pu, MAs and rare-earth fission products co-deposited in molten cadmium cathode [12]. For extraction of thorium metal from thorium-based spent fuels (metallic / ceramic), electrochemical reduction of Th(IV) in molten chloride salts using bismuth electrodes has been recently reported [76]. Apart from these few reports, information on reprocessing of thorium-based metallic fuels is quite limited.

Potential of thorium-based metallic alloys had also been studied for light water reactors (LWRs) [77]. As compared to ThO<sub>2</sub>-fueled LWBR and UO<sub>2</sub>-fueled PWR, use of metallic thorium alloys has been attributed with several benefits along with uranium resource conservation. It has also been suggested that metallic thorium fuels would have better compatibility with water coolant, which is quite poor for uranium metal. In another study, Correa et al., [78] based on calculation of average fuel-rod temperature and energy stored within a fuel, reported that energy stored in metallic thorium fuel would be significantly less than UO<sub>2</sub> fuels due to the lower specific heat of thorium. Further, the stored energy would dissipate faster from metallic thorium fuels during LOCA conditions due to higher thermal conductivity of thorium, which is a significant safety advantage. Potential of thorium-based metal fuels has also been claimed for accelerator driven sub-critical (ADSS) systems, wherein thorium-based metallic (or nitride) fuel forms are suggested to be more suitable for efficient actinide incineration [12] apart from inherent advantages like minimized TRU production, limited reactivity variation during repeated cycling and <sup>233</sup>U breeding.

In recent years, development of metallic fuelled fast reactors is gaining momentum. As a result of this, there has been a renewed interest in thorium-based metallic alloy fuels. Recent reports have emphasized the importance of early development of thorium-based binary (Th-U, Th-Pu), ternary (Th-U-Zr, Th-Pu-Zr) and quaternary (Th-Pu-MA-Zr) alloy fuels. Recent computational results [64] suggest that compared to uranium-based fuels, thorium-based metallic fuels can bring a paradigm shift in nuclear technology with respect to sustainability and renewability of the fuels. It has been reported that use of thorium-based metallic fuels in fast spectrum reactors would lead to (i) minimum production of Pu and TRUs, (ii) efficient burning of existing Pu/ TRU stockpiles, (iii) stable fuel irradiation over longer durations (iv) simpler fuel reprocessing by remotely operated zone refining method and (v) inherently

proliferation-resistant spent fuel. A new Pb-<sup>7</sup>Li or Pb-cooled, metal fuelled (Th-U, Th-Pu or Th-TRU alloys) fast reactor (400 MW<sub>th</sub>) has also been proposed in this report, which is designed to burn higher actinides and produce nearly comparable amount of <sup>233</sup>U during a decade of operation. Few other studies have reported the use of computational thermodynamics for better understanding of phase equilibrium in thorium-based alloys and evaluation of their thermodynamic properties [79]. Actinide incineration in Th-TRU-Zr and U-TRU-Zr alloy fuels (up to 30 atom % TRU) has been simulated by Ghayeb et al., [80] using theoretical methods and various fuel performance codes (MCNP 5, ORIGIN 2.2, MONTEBURNS 2.0) and superior performance of thorium-based alloys has been reported in terms of higher actinide burn-ups, generation of proliferation-resistant spent fuel and depletion of plutonium isotopes. Studies indicated higher isotopic destruction achievable with thorium-based alloy fuels (-1.0384 g / MWd) as compared to uranium-based alloys (-0.3206 g / MWd). Th-U-Zr ternary alloys have been investigated for effective power flattening feasibility in liquid metal cooled large scale CANDLE (*Constant Axial shape of Neutron flux, nuclide densities and power shape During Life of Energy production*) burning reactors [81]. These results suggest (i) flattened power density profiles for these reactors by uniform addition of thorium in the inner core region and (ii) a significant drop in the radial peaking factor from ~1.87 (for U-10Zr alloy fuel) to ~1.44 (for mixed core consisting of Th-U-10Zr in the inner region and U-10Zr in the outer region). Higher average discharge burn-up and lower fuel requirements are also proposed as additional incentives of mixed alloy-based core designs of CANDLE reactors. Thorium and uranium-based alloys are ideal starting materials for preparation of their hydrides. These hydrides are being developed as a new class of nuclear fuels for TRIGA reactor concept (Training, Research, Isotopes, General Atomics) and other hydride fuelled reactors [82, 83]. Fabrication and neutron irradiation behavior of hydrides of Th-U-Zr alloys has also been reported [84].

Some of the most recent reports on thorium-based metallic alloys include preparation, characterization, microstructural and thermodynamic studies on Th- $x$  wt. % U binary alloys ( $x = 0.03, 0.30, 0.52$ ) [85-88] as well as molybdenum doped Th-30 wt. % U binary alloys. The latter composition was developed with the objective of stabilizing the FCC gamma-phase of uranium, which can be randomly dispersed in bulk thorium matrix [89]. A unique concept for thorium utilisation in PWRs is recently reported, which includes a seed uranium alloy (or oxide) fuel surrounded by a bi-metallic cladding comprising of thorium metal bonded to zirconium alloy, wherein thorium metal is in contact with seed fuel and acts as breeding blanket for each individual fuel element [90]. Such fuel design utilises the established performance of zirconium-based cladding with pressurized water on the coolant side and thorium metal breeder layer on the fuel side. Recently reported neutronic studies on thorium-based metallic alloys in ASTRID-type fast reactors indicate the suitability of alloys as an alternative fuel in the reference core design (U-Pu MOX or U-Pu-Zr alloy) with superior performance potential [91]. First principle computational methods are also emerging as an attractive research tool for investigations of structural, elastic, thermal and thermodynamic properties of thorium-based metallic alloys [92].

### **1.3.7. Thermophysical properties of thorium-based metallic alloys**

During neutron irradiation, physico-chemical scenario inside a nuclear fuel evolves dynamically. The fuel undergoes thermo-mechanical, thermo-chemical changes and radiation induced structural variations. Chemical state of nuclear fuel also changes with increasing burn-up and temperature since both, fission product concentration as well as interaction among them evolves continuously. For safe and economically viable fuel utilization, heat produced inside the fuel as a result of fission and radioactive decay of fission products should be efficiently removed by the coolant, which is primarily governed by thermal conductivity

of fuel and clad. Also, fuel should remain intact within the clad boundary with mechanical and chemical integrity of the fuel-clad system maintained throughout its in-pile residence time. This is dependent upon thermal expansion and swelling behavior of fuel. During off-normal conditions such as loss of coolant accident (LOCA), decay heat should be efficiently removed and the stored energy within the fuel should be minimum possible. This again is governed by thermal conductivity (heat removal) and specific heat (stored energy) of the fuel and clad. From this discussion, it is evident that information on thermophysical properties of nuclear fuel, cladding and other structural materials is one of the primary requirements for assessment of fuel performance during normal operating as well as off-normal accidental situations using suitable fuel performance codes [93, 94]. The main thermophysical properties that are of use to nuclear scientists and engineers are bulk thermal expansion coefficient, specific heat capacity and thermal conductivity of fuels as a function of temperature from ambient to fuel melting temperatures.

Although several reports detail preparation, microstructure evaluation, mechanical properties and irradiation performance of thorium-based metallic alloys [55, 60, 85-89, 95], information on their thermophysical properties as a function of temperature is very limited [55, 60, 69, 86, 96]. Values reported in various compilations are either restricted to constituent metals [12] or are reported for select temperatures for few alloy compositions [55]. Generation of reliable indigenous database on thermophysical properties of these alloy systems is therefore absolutely essential for their possible utilization as nuclear fuels.

Above mentioned reports also indicate that thorium-based metallic alloys have notably superior properties as compared to uranium-based alloys and are promising fuel options for advanced nuclear reactors, both operating with thermal and fast neutron spectrum. These

alloy fuels can be safely used at higher coolant temperatures also. It has also been suggested that these alloys can be used as alternative fuels with self-sustained mode of operation of future reactors, where burnt  $^{233}\text{U}$  could be replaced by in-situ bred  $^{233}\text{U}$  from fertile  $^{232}\text{Th}$  for a long duration [97]. It can be summed up that potential of thorium-based metallic alloy fuels has rather been overlooked for large-scale utilization. It is needed to carry out detailed indigenous evaluation of these alloy fuels with the objective of their utilization in future reactor systems. Chapters 3, 4 and 5 of this thesis discuss the work carried out in this direction. Findings of the present studies will be quite useful for understanding the variation in thermophysical properties of thorium-based alloys fuels as a function of temperature and composition.

#### 1.4. Nanocrystalline thoria

In the preceding section (section 1.3) of this chapter, potential of thorium-based metallic alloys as candidate fuels for future nuclear reactor systems was discussed. At present, thorium utilization in Indian nuclear power program is mainly in the form of ceramic oxide fuels ( $\text{ThO}_2$ ,  $\text{Th}_{1-x}\text{U}_x\text{O}_2$ ,  $\text{Th}_{1-x}\text{Pu}_x\text{O}_2$ , etc.). Apart from oxides, thorium and uranium-based fluoride salts and related fuel cycle technologies are also being developed for the Indian molten salt breeder reactor (MSBR) development program [36, 98]. Thoria-based nuclear fuels have advantages over uranium-based fuels in terms of higher thermal conductivity, lower thermal expansion, lower specific heat capacity, higher chemical stability, lower fission gas release behaviour, etc. [25]. These oxides are, therefore, excellent fuel options for safe irradiation up to very high burn-ups up to 50 GWd/tHM [99]. Excellent thermo-chemical stability of thoria also allows safe storage of high burn-up thoria-based spent fuels as such without the need of fuel reprocessing, which is not possible in case of Uranium-based fuels. Recent review on thorium oxide nuclear fuels [99] details the performance of these fuels in

various reactors world over. Irradiation of high density thoria ( $\text{ThO}_2$ ) pellets is continuing in Indian nuclear reactors (research and power reactors) for more than four decades now [27, 28]. Closing of thoria-based fuel cycle has also been demonstrated by chemical reprocessing of irradiated thoria fuel from these reactors [25, 29].  $^{233}\text{U}$  separated from reprocessed thoria has also been fabricated in the form of  $^{233}\text{U}$ -Al alloy fuel with aluminum cladding and is being continuously used in world's only operating  $^{233}\text{U}$ -fuelled research reactor KAMINI [100]. Mixed oxide solid solutions of thorium with uranium / plutonium ( $\text{Th}_{1-x}\text{U}_x\text{O}_2$ ,  $\text{Th}_{1-x}\text{Pu}_x\text{O}_2$ ) are proposed driver fuels for Indian AHWR [30, 31].  $\text{ThO}_2$  powder is one of the starting materials for fabrication of all these fuel forms. Bulk  $\text{ThO}_2$  in large scale is prepared from thermal decomposition of thorium oxalate that is extracted by processing of monazite ore [101]. Apart from its utilization as a fertile nuclear material,  $\text{ThO}_2$  is used in a variety of other applications such as high-temperature refractory oxide ceramic, support material for catalysis, high temperature oxide-ion conductor and oxygen sensors, high temperature transparent oxide ceramics, etc.  $\text{ThO}_2$  (2-4 wt. %) is also used as stabiliser in tungsten electrodes used for TIG (tungsten inert gas) welding and non-consumable arc-melting electrodes to improve the arc starting characteristics, stabilise the arc and extend the electrode life.  $\text{ThO}_2$  in powdered form is used for catalysis application as well as dopant in tungsten electrodes, For all other applications including as nuclear fuel,  $\text{ThO}_2$ -based oxides are mostly required in the form of dense ceramics, which are prepared by conventional powder metallurgy route. For example, high density  $\text{ThO}_2$  (and  $\text{ThO}_2$ -based MOX fuels) pellets are produced by sintering bulk oxide ( $\text{ThO}_2$ ,  $\text{UO}_x$ ,  $\text{PuO}_2$ , etc.) powder compacts at very high temperatures (up to  $\sim 2000$  K). Preparation of thoria-based fuels is therefore an energy intensive process. Sintering of bulk  $\text{ThO}_2$  has also been well investigated [102-105]. Microstructures of ceramics obtained from sintering of bulk (microcrystalline)  $\text{ThO}_2$  powders comprise of large grains (up to several tens of microns) and wide grain size distribution. Such

microstructure usually degrades mechanical strength of sintered pellets (ceramics), which is undesired for nuclear fuel application. Coarse microstructure also makes it difficult to dissolve irradiated ThO<sub>2</sub>-based fuel pellets for chemical reprocessing and necessitates addition of highly corrosive fluoride ions for fuel dissolution. As mentioned earlier, addition of fluorides in reprocessing solutions increase the radioactive waste load fraction and also limits the performance and lifespan of process vessels and related structural materials (tubes, pipes, sensors, etc.). High temperature requirements for sintering bulk ThO<sub>2</sub> and, process difficulties associated with dissolution of spent ThO<sub>2</sub>-based fuels are two major technological challenges associated with the front-end and, back-end of thorium fuel cycle, respectively. One approach to lower the sintering temperature of ThO<sub>2</sub> is by doping with sintering aids, which are usually aliovalent cations such as M<sup>2+</sup> (M = Mg, Ca [106], Ni, Zn, Co, Cu [107]), M<sup>3+</sup> (M = Al) [108], M<sup>5+</sup> (M = Nb, V, Ta) [109], , M<sup>6+</sup> (M = U) [110], etc.. These ions usually create defects in ThO<sub>2</sub> lattice in such a way that cation diffusion is accelerated at lower temperatures and sintering kinetics is improved. However, research community has always been on debate whether chemical doping should be adopted to obtain nuclear-grade dense ThO<sub>2</sub> pellets for neutron irradiation in reactors. Another way to improve the sintering behaviour of ThO<sub>2</sub>-based oxides is to use novel sintering techniques such as microwave sintering, spark plasma sintering [111], flash sintering [112], two-step sintering [113], etc. which can lead to reduced sintering time as well as temperature at the same time provide high density thorium pellets. For large-scale production of nuclear fuel pellets in a cost-effective manner, above mentioned methods too have been a subject of critical discussion since sophisticated equipments are involved. Another alternative route is liquid-phase sintering, in which powders compacts are made with addition of specific impurity phase that remain insoluble in thorium and becomes liquid at sintering temperatures so that inter-grain (particle) contact is improved, which leads to faster diffusion kinetics and as a result accelerated sintering. Liquid phase sintering in

thoria-based oxide fuels has not been reported. The most probable reason could be presence of impurity phase that becomes liquid around sintering temperature (by melting or by reaction with  $\text{ThO}_2$ ), which is not preferred for fuel application.

The most attractive route to improve sintering kinetics of thoria-based high temperature refractory oxides is use of nanocrystalline starting oxide powders. This approach does not require any chemical modification in starting powder(s), used for nuclear fuel application. Nanocrystalline powders having high surface to volume ratio and large specific surface area are ideally suited for rapid solid-state diffusion across the grain/particle surfaces at relatively lower temperatures and have the potential to produce dense ceramics with excellent mechanical properties. Further, sintering can be carried out in conventional furnaces at lower temperatures for shorter duration (i.e., soaking / dwell time at high temperature) thereby resulting into lower energy expenses. Apart from average crystallite size (and size distribution), shape of crystallites (and shape distribution) and surface structure (texture) of particles / grains are also important characteristics of nanocrystalline powders. The latter aspect affects the nature of inter-particle (or inter-grain) contacts that is primarily responsible for initial stage of densification by atomic / ionic diffusion (surface diffusion, grain boundary diffusion, etc.).  $\text{ThO}_2$  nano-powders with minimum surface impurities (carbonaceous or hydroxyl groups at surfaces) and inclusions (carbon, un-reacted salts / compounds, etc.), which can be compacted into dense green pellets with low porosity are ideally required for efficient sintering. It has been reported that nanocrystalline  $\text{ThO}_2$  compacts can be sintering to very high densities ( $\geq 93\%$  of theoretical density) at much lower temperatures ( $\sim 1573$  K) [114], as compared to bulk microcrystalline  $\text{ThO}_2$  compacts, which require heat treatment up to  $\sim 2000$  K [103]. Recent literature also indicates melting of nanocrystalline thoria ( $\sim 4$  nm) at temperatures several hundreds of K below than the melting point ( $\sim 3651$  K) of bulk

thorium dioxide and corresponding formation of metastable liquid phase [114a]. Apart from economic benefits from low temperature sintering of nanocrystalline thoria compacts, another advantage of using these powders as starting material for production of nuclear fuel pellets is that nanocrystalline microstructure can be preserved in sintered ceramic by controlling the sintering conditions. These ceramics consist of efficiently packed and uniformly distributed sub-micron or nano size grains, which impart them excellent mechanical strength. As compared to conventional ceramic fuels, bulk nanocrystalline ceramics offer many advantages such as (i) better fission gas retention capability in small sized isolated closed pores, (ii) better resistance to fuel-clad interactions by efficiently relaxing the interaction stresses (super-plasticity behavior) and (iii) improved tolerance to irradiation induced amorphisation due to nanostructure morphology [41]. These ceramics also show minimum deterioration of thermal behavior due to grain boundary effects (or thermal boundary resistance, also known as Kapitza resistance), if grain size in sintered product can be kept  $>100$  nm. It is important to note that for high burn-up fuel irradiated in LWR environment, pellet microstructures in peripheral region (near clad surface) (also known as High Burn-up Structure (HBS) or rim transformation) are similar to bulk nanocrystalline ceramics. These rim-transformation regions consist of nanocrystalline grains ( $\sim 200$ - $300$  nm) and uniformly distributed isolated closed pores. Most of the fission gases are entrapped in these closed pores [115]. Bulk nanocrystalline thoria is also likely to ease the spent fuel dissolution process, which otherwise is only possible in presence of chemically aggressive species such as fluoride ion in the dissolution reagents, as discussed earlier. Due to small grain morphology of bulk nanocrystalline thoria-based fuels, the surface reactivity with less aggressive reagents like nitric acid is expected to be higher and can be further accelerated if the surface product layer can be continuously removed (without addition of fluorides) so that fresh  $\text{ThO}_2$  surface is available for dissolution. A recent report on sonochemical dissolution of nano-sized thoria

without fluoride ion incorporation is quite encouraging [116], and provides scope for further optimization of nano-scale thoria dissolution for addressing the back end challenge of thoria-based fuel cycle. It is therefore essential to understand the synthesis mechanism, properties and sintering behavior of nanocrystalline thoria-based oxides.

Nanocrystalline thoria can be synthesized in many ways. The central objective should be to obtain thoria phase in as small crystallites as possible and prevent / minimize their aggregation / agglomeration. In-fact, any synthesis route that is capable to produce disordered / amorphous pure thoria phase would be the ideal precursor for obtaining size and shape controlled crystalline thoria powders. From the point of view of large-scale production of nanocrystalline thoria (and thoria-based oxides) and keeping in mind their radioactive nature, the synthesis method should be simple, scalable, highly efficient (~ 100 % product yield) and less energy intensive (preferably ambient temperature process). It should also use commonly and abundantly available starting reagents (such as oxalates, nitrates, etc.), generate minimum amount of non-radioactive and environmentally benign waste / by-products and should provide the end product with minimum impurities or residual reactants. Based on these requirements, the simplest route could be solid-state transformation of commonly available salts (nitrates, oxalates, acetates, carbonates, etc.) of thorium and other actinides by thermal treatment in such a way that the decomposed oxide product is kinetically stabilized in nano-size grains / particles. Formation of nanocrystalline thoria by controlled thermal decomposition of thorium carbonate [117], thorium oxalate [118] and thorium nitrate [119] has indeed been reported. Advantage of this approach is pure product phase with minimum residual impurities. Morphology of oxides is also usually a reflection of starting salt's morphology. However, in large-scale preparation, these powders usually undergo rapid grain coarsening to give wide particle/grain size distribution. Another simple and nearly ambient

temperature method to prepare nanocrystalline thorium-based oxides is precipitation from aqueous solution of Th(IV) (and other dopant) ions. Most of the thorium salts are readily soluble in water and can be precipitated as colloidal / crystalline hydrated hydroxides using alkali solution as precipitating agent. The hydroxide precipitate can be isolated and thermally treated to obtain corresponding oxide. However, this process also is limited by rapid growth of hydroxide precipitates, which results into either bulk oxides or wide particle size distribution. Use of suitable chemical reagents (capping reagents) such as poly-hydroxy alcohols (polyol synthesis) may inhibit the agglomeration and growth of as-formed precipitates. Alternatively, hydrothermal treatment of precipitate has also been reported to yield nanocrystalline (~2.5 - 35 nm) thorium [120]. Synthesis of monodispersed and isotropic nanocrystalline oxides of uranium and thorium (< 10 nm) via non-aqueous surfactant-assisted method has also been reported by Hudry *et al.*, [120a]. Their results indicate metal centre (thorium vs uranium) dependent characteristics (size, shape, morphology) of product oxides as well as their tunability by controlling the nature of actinide precursor and synthesis conditions. Apart from direct thermal decomposition or hydroxide precipitation from aqueous medium, solution combustion synthesis is another simple and scalable route for preparation of nanocrystalline oxides [121, 122]. It essentially involves highly exothermic redox decomposition of a viscous and transparent aqueous gel precursor. Gel precursor is obtained by thermal treatment (< 400 K) of aqueous solution prepared by dissolving metal salt(s); usually nitrates (acting as oxidant) and fuel(s) (acting as reducing agent; mostly a commonly available organic compound like urea, glycine, citric acid, etc.) in minimum volume of water. Once formed, the highly viscous gel remains stable and upon further heating (~400-550 K), it rapidly undergoes combustion with evolution of large volume of gaseous by-products (N<sub>2</sub>, CO<sub>2</sub>, H<sub>2</sub>O, NH<sub>3</sub>, etc.) leaving behind solid residue, which is a mixture of nanocrystalline metal oxide(s) and residual organic /nitrate-based impurities. The nature of chemical

interaction among various species present in the aqueous gel (metal ions, nitrate ions, ligand (fuel) molecules and hydrated protons) forms the chemical basis of combustion and therefore governs the nature of final product. It is therefore apparent that relative concentration of fuel and oxidant (commonly referred as fuel-to-oxidant ratio) would influence the combustion reaction and the product characteristics. Apart from this, other conditions also influence the nature of combustion. These include (i) nature of starting materials, (ii) atmosphere in which combustion is carried out (oxidizing / reducing / inert), (iii) nature (surface heating / volume heating) and rate (slow and fast heating) of heat treatment and (iv) material of construction of the vessel (possible catalytic effect) in which combustion is carried out.

Combustion synthesis of nanocrystalline thoria and thoria-based oxides is reported by several researchers [109, 113, 114, 123-126]. However, most of these studies have focused on synthesis conditions particularly, fuel-to-oxidant ratio (F:O), nature of fuel, heat treatment conditions, effect of calcination on properties of combustion synthesized powders, sintering behavior and properties of sintered ceramics. No emphasis has been given to the mechanism of solution combustion synthesis, which is based on the nature of molecular interaction among the constituent species present in the gel phase. Further, since  $\text{ThO}_2$  powder properties are directly correlated to the nature of decomposition behavior of complexes formed inside these gels, mechanistic insights into combustion process would provide better control of the synthesis parameters, which therefore would enable preparation of  $\text{ThO}_2$  powders with tailored properties. With this objective in mind, mechanism of solution combustion synthesis of nanocrystalline  $\text{ThO}_2$  by two different methods namely, glycine-nitrate route and citrate-nitrate route have been investigated in detail covering a range of fuel-to-oxidant ratios. These results have been presented in chapter-6 of the thesis. For fabrication of dense ceramic pellets as fuel for nuclear reactors, such nanocrystalline  $\text{ThO}_2$  powders need to be sintered into

mechanically strong ceramics having uniform microstructures. Sintering behavior of combustion synthesized nanocrystalline ThO<sub>2</sub> and its correlation with powder properties has been presented in chapter-7. Particularly, origin of desintering effect, which is exclusively observed in ThO<sub>2</sub> synthesized by glycine-nitrate combustion synthesis has been explained in detail.

### 1.5. Scope of the present thesis

- From the reported information, it is clear that thorium-based metallic alloys are excellent candidate nuclear fuels for advanced reactor systems, operating in both thermal and fast neutron spectrum.
- Development of these fuels would require detailed assessment of their physico-chemical properties in the first place. Reported studies on thermophysical properties of these alloys are very limited and generation of indigenous database is essential.
- To address this requirement, nuclear-grade thorium and uranium metals, thorium-uranium (Th-U) binary alloys and thorium-uranium-zirconium (Th-U-Zr) ternary alloys have been investigated in detail covering their preparation, characterization and high temperature thermophysical properties evaluation in chapter-3, 4 and 5.
- Literature review on thoria-based oxide fuel materials also indicates the importance of sinter-active nanocrystalline thoria (ThO<sub>2</sub>) powders for fabrication of thoria-based fuels. Solution combustion synthesis is a promising route for synthesis of nanocrystalline thoria powders. However, mechanism of combustion synthesis of nanocrystalline thoria, based on the nature of chemical interaction between the reactants is not available. Understanding of combustion mechanism is essential to optimize synthesis parameters for obtaining powders with desired properties.

- To address this gap area, mechanism of solution combustion synthesis of nanocrystalline thoria powders via glycine-Th(IV)-nitrate and citrate-Th(IV)-nitrate route has been investigated. Effect of fuel-to-oxidant ratio (F:O) on the nature of molecular interaction in combustion precursor and its influence on powder properties of nanocrystalline thoria has also been discussed in chapter-6.
- Oxide-based nuclear fuel pellets are fabricated by high temperature sintering of powder compacts. For nanocrystalline oxide powders, sintering may be accompanied with loss of bulk density at higher temperatures due to a phenomenon known as desintering. Desintering can cause deterioration in mechanical properties of fuel pellets.
- While desintering is reported for nanocrystalline thoria, its origin is not yet established. Considering the importance of this, sintering behavior of combustion synthesized nanocrystalline thoria powder compacts has been investigated. Origin of desintering that is exclusively observed in glycine-Th(IV)-nitrate combustion synthesized thoria has been explained in terms of density inhomogeneity in powder compacts and powder morphology as discussed in chapter-7.
- Finally, all the findings are summarized in chapter-8.

## References:

- [1] C. Degueudre, M.J. Joyce, “Evidence and uncertainty for uranium and thorium abundance: a review”, *Prog. Nucl. Energy* 124 (2020) 103299.
- [2] L.S. Keith, O.M. Faroon, B.A. Fowler, “Uranium (book chapter); handbook on the toxicology of metals: fourth edition (Eds: G.F. Nordberg, B.A. Fowler, M. Nordberg)”, Elsevier (2015) 1307-1345 (DOI: <https://doi.org/10.1016/C2011-0-07884-5>).
- [3] G. Sadagopan, K.S.V. Nambi, G. Venkataraman, V.K. Shukla, S. Kayasth, “Estimation of thorium in gas mantles to ascertain regulatory compliance”, *Radiat. Prot. Dosim.* 71(1) (1997) 53-56.
- [4] T.E. Leontis, “Properties of magnesium-thorium and magnesium-thorium-cerium alloys”, *J. Min. Metals Mater. Soc.* 4 (3) (1952) 287-294.
- [5] R.A. Glenner, P. Willey, P.S. Sledzik, E.P. Junger, “Dental fillings in civil war skulls: What do they tell us?”, *J. Am. Dent. Assoc.* 127(11) (1996) 1671-1677.
- [6] O. Hahn, F. Strassmann, “Über den nachweis und das verhalten der bei der bestrahlung des urans mittels neutronen entstehenden erdalkalimetalle (English translation: Concerning the existence of alkaline earth metals resulting from neutron irradiation of uranium)”, *Die Naturwissenschaften* 27 (1939) 11-15.
- [7] “The first reactor” The US department of energy report: DOE/NE-0046 (1982) 1-40 (Web-link: <https://www.energy.gov/ne/downloads/first-reactor>).
- [8] R.L. Crowther, “Use of thorium in boiling water reactors”, *J. Nucl. Energy AB* 16(4) (1962) 181-194.
- [9] J.R. Dietrich, “The physics of advanced reactors”, *Brit. J. Appl. Phys.* 7(S5) 302 (1956) S9-S23.
- [10] H.N. Sethna, “India’s atomic energy program: past and future”, *International Atomic Energy Agency (IAEA) Bulletin* 21 (5) (1979) 2-11.

## References

- [11] S. Banerjee, H.P. Gupta, “The evolution of the Indian nuclear power programme”, Prog. Nucl. Energy 101 (2017) 4-18.
- [12] International Atomic Energy Agency “Thorium fuel cycles - potential benefits and challenges”, IAEA-TECDOC-1450, IAEA, Vienna (2005) 1-105.
- [13] P.K. Wattal, “Back end of Indian nuclear fuel cycle - A road to sustainability”, Prog. Nucl. Energy 101 (2017) 133-145.
- [14] R. Natarajan, “Reprocessing of spent nuclear fuel in India: Present challenges and future programme”, Prog. Nucl. Energy 101 (2017) 118-132.
- [15] S.A. Ansari, P. Pathak, P.K. Mohapatra, V.K. Manchanda, “Aqueous partitioning of minor actinides by different processes” Sep. Purif. Rev. 40(1) (2011) 43-76.
- [16] M. Salvatores, “Nuclear fuel cycle strategies including partitioning and transmutation”, Nucl. Eng. Des. 235(7) (2005) 805-816.
- [17] Press Information Bureau, Government of India, “Setting up of ten indigenous nuclear power reactors” (Web-link: <http://pib.nic.in>)
- [18] S.C. Chetal, P. Chellapandi, P. Puthiyavinayagam, S. Raghupathy, V. Balasubramanian, P. Selvaraj, P. Mohanakrishnan, B. Raj, “Current status of fast reactors and future plans in India” Energy. Proced. 7 (2011) 64-73.
- [19] P. Puthiyavinayagam, P. Selvaraj, V. Balasubramanian, S. Raghupathy, K. Velusamy, K. Devan, B.K. Nashine, G.P. Kumar, K.V.S. Kumar, S. Varatharajan, P. Mohanakrishnan, G. Srinivasan, A.K. Bhaduri, “Development of fast breeder reactor technology in India”, Prog. Nucl. Energy 101 (Part A) (2017) 19-42.
- [20] Bharatiya Nabhikiya Vidyut Nigam Limited, Department of Atomic Energy “Present status of 500 MWe Prototype Fast Breeder Reactor (PFBR)”, (Web-link: <http://www.bhavini.nic.in>).

## References

- [21] P. Rodriguez, C.V. Sundaram, "Nuclear and materials aspects of the thorium fuel cycle", *J. Nucl. Mater.* 100 (1981) 227-249.
- [22] R. Ramanna, S.M. Lee, "The thorium cycle for fast breeder reactors", *Pramana* 27(1-2) (1986) 129-137.
- [23] R. Chidambaram, C. Ganguly, "Plutonium and thorium in the Indian nuclear programme", *Curr. Sci. India* 70(1) (1996) 21-35.
- [24] P.K. Vijayan, V. Shivakumar, S. Basu, R.K. Sinha, "Role of thorium in the Indian nuclear power programme", *Prog. Nucl. Energy* 101 (2017) 43-52.
- [25] "Thoria-based nuclear fuels: thermophysical and thermodynamic properties, fabrication, reprocessing, and waste management", (Eds.: D. Das, S.R. Bharadwaj) Springer (2013) (DOI: 10.1007/978-1-4471-5589-8).
- [26] "Thorium-energy for the future", (Eds.: A.K. Nayak, B.R. Sehgal), Springer (2019) (DOI: 10.1007/978-981-13-2658-5).
- [27] S. Mukherji, B.K. Mohan, P.D. Krishnani, V. Jagannathan, S. Ganesan, "Thorium irradiation in Indian PHWRs - applications and limitations of origin code", *Proceedings of First National Conference in Nuclear Reactor Technology* (2002) (Web-link: [https://inis.iaea.org/search/search.aspx?orig\\_q=RN:34011468](https://inis.iaea.org/search/search.aspx?orig_q=RN:34011468)).
- [28] M. Das, "Design and irradiated experience with thorium based fuels in PHWRs" *Annual International Conference - Canadian Nuclear Association* (1992) 10.1-10.
- [29] P.S. Dhama, J.S. Yadav, K. Agarwal, "Power reactor thoria reprocessing facility (PRTRF), Trombay", *Proceedings of the Theme Meeting on the Journey of BARC Safety Council for Strengthening Safety Culture in BARC Facilities* (Eds: V.M. Jolly) (2017) (Web-link: [https://inis.iaea.org/search/search.aspx?orig\\_q=RN:48089837](https://inis.iaea.org/search/search.aspx?orig_q=RN:48089837)).
- [30] R.K. Sinha, A. Kakodkar, "Design and development of the AHWR - the Indian thorium fuelled innovative nuclear reactor" *Nucl. Eng. Des.* 236 (7-8) (2006) 683-700.

## References

- [31] R. Sinha, A. Kakodkar, "India's passive breeder", Nucl. Eng. Int. 55(668) (2010) 30-31.
- [32] A. Kakodkar, "Evolution of nuclear reactor containments in India: Addressing the present day challenges", Nucl. Eng. Des. 269 (2014) 3-22.
- [33] S. Sengupta, S.B. Chafle, S. Mammen, K. Sasidharan, V.K. Raina, "Critical facility for AHWR and PHWRs", Proceedings of International Conference on Peaceful uses of Atomic Energy (2009). V. 1. [33a] C. Ronchi, J.-P. Hiernaut, Experimental measurement of pre-melting and melting of thorium dioxide, J. Alloys Comp. 240 (1-2) (1996) 179-185. [33b] R. Böhler, A. Quaini, L. Capriotti, P. Cakir, O. Beneš, K. Boboridis, A. Guiot, L. Luzzi, R.J.M. Konings, D. Manara, "The solidification behavior of the UO<sub>2</sub>-ThO<sub>2</sub> system in a laser heating study" J. Alloys. Comp. 616 (2014) 5-13.
- [34] D. Greneche, W.J. Szymczak, J.M. Buchheit, M. Delpech, A. Vasile, H. Golfier, "Rethinking the thorium fuel cycle: An industrial point of view", Proceedings of ICAPP (Nice, France), (2007) Paper-7367. [34a] S.F. Ashley, G.T. Park, W.J. Nuttall, C. Boxall, R.W. Grimes, "Thorium fuel has risks", Nature 492 (2012) 31-33.
- [35] D. Jain, V. Sudarsan, A.K. Tyagi, "Thorium-based metallic alloys as nuclear fuels: Present status, potential advantages and challenges", SMC Bulletin (Society for Materials Chemistry, India) 4 (1) (2013) pp. 27-40 (Web-link: <https://www.smcindia.org/smc-bulletin.php>).
- [36] P.K. Vijayan, A. Basak, I.V. Dulera, K.K. Vaze, S. Basu, "Conceptual design of Indian molten salt breeder reactor", Pramana - J. Phys. 85 (2015) 539-554.
- [37] T. Yamamoto, H. Suwarno, H. Kayano, M. Yamawaki, "Development of new reactor fuel materials: Hydrogen absorption properties of U-Th, U-Th-Zr and U-Th-Ti-Zr alloys", J. Nucl. Sci. Tech. 32(3) (1995) 260-262.

## References

- [38] K.A. Terrani, G.W.C. Silva, C.B. Yeamans, “Fabrication and characterization of uranium thorium zirconium hydride fuels”, *Trans. Am. Nucl. Soc.* 98 (2008) 1060-1061.
- [39] S.M. McDeavitt, T.J. Downar, A.A. Solomon, S.T. Revankar, M.C. Hash, A.S. Hebden, “Thoria-based cermet nuclear fuel: Cermet fabrication and behavior estimates”, *Proc. Int. Conf. Nucl. Eng. (ICONE 4)* (2002) 59-67.
- [40] C. Lombardi, L. Luzzi, E. Padovani, F. Vettrano, “Thoria and inert matrix fuels for a sustainable nuclear power”, *Prog. Nucl. Energy* 50(8) (2008) 944-953.
- [41] J. Spino, H.S. Cruz, R. Jovani-Abril, R. Birtcher, C. Ferrero, “Bulk-nanocrystalline oxide nuclear fuels - An innovative material option for increasing fission gas retention, plasticity and radiation-tolerance”, *J. Nucl. Mater.* 422 (1-3) (2012) 27-44.
- [42] H. György, S. Czifrus, “The utilization of thorium in generation IV reactors”, *Prog. Nucl. Energy* 93 (2016) 306-317.
- [43] D. Heuer, E. Merle-Lucotte, M. Allibert, M. Brovchenko, V. Ghetta, P. Rubiolo, “Towards the thorium fuel cycle with molten salt fast reactors”, *Ann. Nucl. Energy* 64 (2014) 421-429.
- [44] G.L. Hofman, L.C. Walters, T.H. Bauer, “Metallic fast reactor fuels”, *Prog. Nucl. Energy* 31(1-2) (1997) 83-110.
- [45] W.J. Carmack, D.L. Porter, Y.I. Chang, S.L. Hayes, M.K. Meyer, D.E. Burkes, C.B. Lee, T. Mizuno, F. Delage, J. Somers, “Metallic fuels for advanced reactors”, *J. Nucl. Mater.* 392 (2) (2009) 139-150.
- [46] Idaho National Laboratory, “Experimental breeder reactor-I (EBR-I) (Web-link: <https://inl.gov/experimental-breeder-reactor-i/>).
- [47] L.C. Walters, “Thirty years of fuels and materials information from EBR-II”, *J. Nucl. Mater.* 270(1) (1999) 39-48.

## References

- [48] K. D. Weaver, J. Gilleland, C. Whitmer, G. Zimmerman, “High burn-up fuels for fast reactors: past experience and novel applications”, International Congress on Advances in Nuclear Power Plants (ICAPP 2009) (2009) 795.
- [49] G. Locatelli, M. Mancini, N. Todeschini, “Generation IV nuclear reactors: Current status and future prospects”, *Energ. Policy* 61 (2013) 1503-1520.
- [50] Z.S. Takibaev, “Fast homogeneous nuclear reactor”, *Atom. Energy* 100 (2006) 154-156.
- [51] T. Jayakumar, M.D. Mathew, K. Laha, R. Sandhya, “Materials development for fast reactor applications”, *Nucl. Eng. Des.* 265 (2013) 1175-1180.
- [52] A. Riyas, P. Mohanakrishnan, “Studies on physics parameters of metal (U-Pu-Zr) fuelled FBR cores”, *Ann. Nucl. Energy* 35(1) (2008) 87-92.
- [53] P. Chellapandi, V. Balasubramaniyan, P. Puthiyavinayagam, R. Sundararajan, M. Kanakkil, P. Selvaraj, P.R. Vasudeva Rao, “Design of 500 MWe metal fuel demonstration fast reactor”, *Proc. Int. Conf. Nucl. Eng.* (2014) (DOI: <https://doi.org/10.1115/ICONE22-30727>).
- [54] Indira Gandhi Centre for Atomic Research, “Fast Breeder Test Reactor”, (Web-link: <http://www.igcar.gov.in/rfg/fbtrhist.html>).
- [55] B. Blumenthal, J.E. Sanecki, D.E. Busch, D.R. O’Boyle, “Thorium-uranium-plutonium alloys as potential fast power reactor fuels; part-II: Properties and irradiation behavior of thorium-uranium-plutonium alloys”, ANL-7259, Argonne National laboratory, Illinois (October 1969).
- [56] S.Z. Ghayeb, “Investigations of thorium-based fuels to improve actinide burning rate in S-PRISM reactor”, M.Sc. Thesis, The Pennsylvania State University (2008) (Web-link: <https://etda.libraries.psu.edu/catalog/9160>).

## References

- [57] R.G. Wymer, D.A. Douglas Jr., "Status and progress report for thorium fuel cycle development for period ending December 31, 1964", Report no.: ORNL-3831, Oak Ridge National laboratory, Tennessee (May 1966).
- [58] "Fast spectrum reactors", (Eds.: A.E. Waltar, D. Todd, P.V. Tsvetkov) Springer (2011) (ISBN 978-1-4419-9572-8).
- [59] D.E. Peterson, "The (Th-U) Thorium-uranium system", Bull. Alloy Phase Diagr. 6 (5) (1985) 443-445.
- [60] S. Peterson, R.E. Adams, D.A. Douglas Jr., "Properties of thorium, its alloys and its compounds", Report no.: ORNL-TM-1144, Oak Ridge National laboratory, Tennessee (June 1965).
- [61] D.R. Marr, D.A. Cantley, J.C. Chandler, D.C. McCurry, R.P. Omberg, "Performance of thorium fuelled fast breeders", Report no.: HEDL-SA-1327-FP, Hanford Engineering Development Laboratory, Richland, USA (October 1977).
- [62] G.L. Copeland, "Evaluation of thorium-uranium alloys for the unclad metal breeder reactor", Report no.: ORNL-4557, Oak Ridge National Laboratory, Tennessee (June 1970).
- [63] B. Blumenthal, J.E. Sanecki, D.E. Busch, "Thorium-uranium-plutonium alloys as potential fast power reactor fuels; part-I: Thorium-uranium-plutonium phase diagram", Report no.: ANL-7258, Argonne National Laboratory, Illinois (September 1968).
- [64] C.S. Holden, "Rapid computational path for sustainable and renewable nuclear energy using metallic thorium fuels", Proceedings of 2<sup>nd</sup> Thorium energy conference (ThEC-2010), Mountain View CA (2010).
- [65] R.M. Carroll, "The effects of reactor irradiation on thorium-uranium alloy fuel plates", Report no.: ORNL-1938, Oak Ridge National Laboratory, Tennessee (August 1955).

## References

- [66] B.R. Hayward, P. Corzine, "Thorium uranium fuel elements for SRE", Proc. 2<sup>nd</sup> UN Int. Conf. Peaceful uses of Atom. Energy, Geneva (October 1958).
- [67] J.L. Ballif, B.R. Hayward, J.W. Walter, "Engineering evaluation of a mixed alloy fuel element irradiated at elevated temperatures in SRE", Technical report no.: NAA-SR-3888, Atomics International Division, North American Aviation Incorporation, California, USA (June 1960).
- [68] A.R. Olsen, "Thorium and thorium alloys: Preliminary corrosion tests", Report no.: ORNL-1066, Oak Ridge National Laboratory, Tennessee (November 1951).
- [69] M.S. Farkas, A.A. Bauer, R.F. Dickerson, "Development of thorium-uranium-base fuel alloys," Report no.: BMI-1428, Battelle Memorial Institute, Columbus, Ohio (March 1960).
- [70] R.H. Cole, L.E. Wilkinson, "Development of high strength ternary and quaternary thorium-uranium base alloys", Technical report no.: ATL-A-128, Advanced Technology Laboratory, California (1961).
- [71] J.H. Kittel, J.A. Horak, W.F. Murphy, S.H. Paine, "Effect of irradiation on thorium and thorium-uranium alloys", Technical report no.: ANL-5674, Argonne National laboratory, Illinois, USA (April 1963).
- [72] A.L. Bement, "Burn-up and specific power calculations for the thermal neutron irradiation on thorium-uranium alloys", Technical report no: HW-56631, General Electric Co. Hanford Atomic Products Operation, Richland, Washington (1958).
- [73] F.W. Dodge, E.W. Murbach, L.A. Hanson, "Low decontamination reprocessing of thorium-uranium alloys by induction drip melting", Nucl. Sci. Eng. 6 (6) (1959) 533-536.
- [74] P. Chiotti, A.F. Voigt, "Pyrometallurgical processing", Technical report: A/CONF.15/P/517; ISC-1018, Ames Laboratory, Iowa (October 1958).

## References

- [75] W.N. Hensen, "Electrolysis of thorium and uranium", US-Patent no.: US 2951793 (1960).
- [76] S. Jiang, K. Liu, Y. Liu, T. Yin, Z. Chai, W. Shi, "Electrochemical behavior of Th(IV) on the bismuth electrode in LiCl–KCl eutectic", *J. Nucl. Mater.* 523 (2019) 268-275.
- [77] G.B. Zorzoli, "Use of metallic thorium for LWBRs and LWRs", *Nucl. Tech.* 20 (1973) 109-113.
- [78] F. Correa, D.J. Driscoll, D.D. Lanning, "An evaluation of tight pitch PWR cores", technical report no.: MIT-EL-79-022, Massachusetts Institute of Technology, Cambridge, Massachusetts (1979).
- [79] Z.S. Li, X.J. Liu, C.P. Wang, "Thermodynamic modelling of the Th-U, Th-Zr and Th-U-Zr systems", *J. Alloy Compd.* 473 (2009) 193-198.
- [80] S.Z. Ghrayeb, K.N. Ivanov, S.H. Levine, E.P. Loewen, "Burn-up performance of sodium-cooled fast reactors utilizing thorium-based fuels", *Nucl. Tech.* 176 (2011) 188-194.
- [81] T. Okawa, H. Sekimoto, S. Nakayama, "Design study on power flattening to sodium cooled large scale CANDLE burning reactor with using thorium fuel", *Proc. 18<sup>th</sup> Int. Conf. Nucl. Eng., ICONE18, China, (2010).*
- [82] M.T. Simnad, "The U-ZrH<sub>x</sub> alloy: Its properties and use in TRIGA fuel", *Nucl. Engg. Des.* 64 (1981) 403-422.
- [83] K. Konashi, B.A. Pudjanto, T. Terai, M. Yamawaki, "Thermodynamic stability of ThZr<sub>2</sub>H<sub>x</sub> at high temperature", *J. Phys. Chem. Solids* 66 (2–4) (2005) 625-628.
- [84] T. Yamamoto, H. Suwarno, F. Ono, H. Kayano, M. Yamawaki, "Preparation, analysis and irradiation of hydride Th-U-Zr alloy samples for a new fuel", *J. Alloy Compd.* 271-273 (1998) 702-706.

- [85] S. Das, R. Kumar, S.B. Roy, A.K. Suri, "Development study on metallic thorium and uranium-thorium alloy", BARC Newsletter-Founder's Day Special issue (2011) 72-76.
- [86] S. Das, R. Kumar, S. Kaity, S. Neogy, K.N. Hareendran, S.B. Roy, G.K. Dey, B.S.S. Daniel, G.P. Chaudhari, "Characterization of microstructural, mechanical and thermal properties and ageing study of Th-3 wt.% U alloy" Nucl. Eng. Des. 282 (2015) 116-125.
- [87] S. Das, S. Kaity, R. Kumar, J. Banerjee, S.B. Roy, G.P. Chaudhari, B.S.S. Daniel, "Characterization of microstructural, mechanical and thermophysical properties of Th-52 U alloy", J. Nucl. Mater. 480 (2016) 223-234.
- [88] S. Das, S.B. Roy, G.P. Chaudhari, B.S.S. Daniel, "Microstructural evolution of as-cast Th-U alloys", Prog. Nucl. Energy 88 (2016) 285-296.
- [89] R. Kumar, S. Das, S.B. Roy, R. Agarwal, J. Banerjee, S.K. Satpati, "Effect of Mo addition on the microstructural evolution and  $\gamma$ -U stability in Th-U alloys", J. Nucl. Mater. 539 (2020) 152317.
- [90] S. Vaidyanathan, "Thorium utilization in pressurized water reactors using bimetallic thorium-zirconium alloy cladding", Nucl. Tech. (2020) (DOI: <https://doi.org/10.1080/00295450.2019.1706377>).
- [91] D. Escorcia-Ortiz, J. François, C. Martín-del-Campo, "Comparative study of the neutronic performance of thorium-based metallic fuel and MOX fuel in an ASTRID-like fast reactor core", Nucl. Eng. Des. 347 (2019) 122-131.
- [92] J.K. Startt, C.S. Deo, "First principles study of the structure and elastic properties of thorium metal", MRS Adv. 1 (35) (2016) 2447-2452.
- [93] A. Karahan, J. Buongiorno, "A new code for predicting the thermo-mechanical and irradiation behavior of metallic fuels in sodium fast reactors", J. Nucl. Mater. 396 (2010) 283-293.

## References

- [94] K. Lassmann, "TRANSURANUS: a fuel rod analysis code ready for use", *J. Nucl. Mater.* 188 (1992) 295-302.
- [95] J.P. Hamond, "Physical, mechanical and irradiation properties of thorium and thorium alloys", ORNL-4218, Oak Ridge National Laboratory, USA (1968) 29-30.
- [96] J.K. Fink, M.G. Chasanov, L. Leibowitz, "Thermophysical properties of thorium and uranium systems for use in reactor safety analysis", Report no.: ANL-CEN-RSD-77-1, Argonne National Laboratory (1977) 11-12.
- [97] M. Lung, "A present review of the thorium nuclear fuel cycles", European commission report no.: EUR-17771-EN, (1997).
- [98] S. Kolay, S. Phapale, R. Dawar, M. Jafar, S. N. Achary, A. K. Tyagi, R. Mishra, M. Basu, "Phase characterization and thermal study of SrF<sub>2</sub> and NdF<sub>3</sub> doped fluoride salt containing 78 mol % LiF - 20 mol % ThF<sub>4</sub> - 2 mol % UF<sub>4</sub>", *J. Radioanal. Nucl. Chem.* 314 (2) (2017) 1267-1271.
- [99] M. Verwerft, B. Boer, "Thorium oxide nuclear fuels", *Comprehensive nuclear materials* (Second edition) 5 (2020) 139-168 (DOI: <https://doi.org/10.1016/B978-0-12-803581-8.11770-9>).
- [100] S. Usha, R.R. Ramanarayanan, P. Mohanakrishnan, R.P. Kapoor, "Research reactor KAMINI", *Nucl. Eng. Des.* 236 (7-8) (2006) 872-880.
- [101] T.K. Mukherjee, "Processing of Indian monazite for the recovery of thorium and uranium values", *Proceedings of International Conference on Characterisation and Quality Control of Nuclear Fuels* (Eds.: C. Ganguly, R.N. Jayaraj) Allied Publishers Pvt. Ltd. (2002) 187-195.
- [102] J.R. Johnson, C.E. Curtis, "Note on sintering of ThO<sub>2</sub>", *J. Am. Ceram. Soc.* 37(12) (1954) 611.

## References

- [103] T.R.G. Kutty, K.B. Khan, P.V. Hegde, J. Banerjee, A.K. Sengupta, S. Majumdar, H.S. Kamath, "Development of a master sintering curve for ThO<sub>2</sub>", *J. Nucl. Mater.* 327(2-3) (2004) 211-219.
- [104] P. Balakrishna, B.P. Varma, T.S. Krishnan, T.R.R. Mohan, P. Ramakrishnan, "Thorium oxide: Calcination, compaction and sintering", *J. Nucl. Mater.* 160(1) (1988) 88-94.
- [105] N. Clavier, R. Podor, L. Deliere, J. Ravoux, N. Dacheux, "Combining in situ HT-ESEM observations and dilatometry: An original and fast way to the sintering map of ThO<sub>2</sub>", *Mater. Chem. Phys.* 137(3) (2013) 742-749.
- [106] K. Ananthasivan, S. Balakrishnan, S. Anthonysamy, R. Divakar, E. Mohandas, V. Ganesan, "Synthesis and sintering of nanocrystalline thoria doped with CaO and MgO derived through oxalate-deagglomeration", *J. Nucl. Mater.* 434 (1-3) (2013) 223-229.
- [107] G.P. Halbfinger, M. Kolodney, "Activated Sintering of ThO<sub>2</sub> and ThO<sub>2</sub>-Y<sub>2</sub>O<sub>3</sub> with NiO", *J. Am. Ceram. Soc.* 55(10) (1972) 519-524.
- [108] A. Baena, T. Cardinaels, J. Vleugels, K. Binnemans, M. Verwerft, "Activated sintering of ThO<sub>2</sub> with Al<sub>2</sub>O<sub>3</sub> under reducing and oxidizing conditions", *J. Nucl. Mater.* 470 (2016) 34-43.
- [109] K. Ananthasivan, S. Anthonysamy, C. Sudha, A.L.E. Terrance, P.R. Vasudeva Rao, "Thoria doped with cations of group VB-synthesis and sintering", *J. Nucl. Mater.* 300(2-3) (2002) 217-229.
- [110] T.R.G. Kutty, P.V. Hegde, K.B. Khan, T. Jarvis, A.K. Sengupta, S. Majumdar, H.S. Kamath, "Characterization and densification studies on ThO<sub>2</sub>-UO<sub>2</sub> pellets derived from ThO<sub>2</sub> and U<sub>3</sub>O<sub>8</sub> powders", *J. Nucl. Mater.* 335 (3) (2004) 462-470.
- [111] V. Tyrpekl, M. Cologna, D. Robba, J. Somers, "Sintering behaviour of nanocrystalline ThO<sub>2</sub> powder using spark plasma sintering", *J. Eur. Ceram. Soc.* 36(3) (2016) 767-772.

- [112] W. Straka, S. Amoah, J. Schwartz, “Densification of thoria through flash sintering”, *MRS Commun.* 7(3) (2017) 677-682.
- [113] D. Sanjay Kumar, K. Ananthasivan, R.V. Krishnan, S. Amirthapandian, A. Dasgupta, “Studies on the synthesis of nanocrystalline  $Y_2O_3$  and  $ThO_2$  through volume combustion and their sintering”, *J. Nucl. Mater.* 479 (2016) 585-592.
- [114] R.D. Purohit, S. Saha, A.K. Tyagi, “Nanocrystalline thoria powders via glycine-nitrate combustion” *J. Nucl. Mater.* 288 (1) (2001) 7-10. [114a] F. Cappia, D. Hudry, E. Courtois, A. Janßen, L. Luzzi, R.J.M. Konings, D. Manara, High-temperature and melting behavior of nanocrystalline refractory compounds: an experimental approach applied to thorium dioxide, *Mater. Res. Express* 1 (2014) 0250341-12.
- [115] J. Spino, K. Vennix, M. Coquerelle, “Detailed characterisation of the rim microstructure in PWR fuels in the burn-up range 40–67 GWd/tM”, *J. Nucl. Mater.* 231 (3) (1996) 179-190.
- [116] L. Bonato, M. Viot, X. Le Goff, P. Moisy, S.I. Nikitenko, “Sonochemical dissolution of nanoscale  $ThO_2$  and partial conversion into a thorium peroxo sulphate”, *Ultrason. Sonochem.* 69 (2020) 105235.
- [117] S. Dash, A. Singh, P.K. Ajikumar, H. Subramanian, M. Rajalakshmi, A.K. Tyagi, A.K. Arora, S.V. Narasimhan, B. Raj, “Synthesis and characterization of nanocrystalline thoria obtained from thermally decomposed thorium carbonate”, *J. Nucl. Mater.* 303 (2–3) (2002) 156-168.
- [118] S. Dash, R. Krishnan, M. Kamruddin, A.K. Tyagi, B. Raj, “Temperature programmed decomposition of thorium oxalate hexahydrate”, *J. Nucl. Mater.* 295(2-3) (2001) 281-289.

## References

- [119] S. Dash, M. Kamruddin, P.K. Ajikumar, A.K. Tyagi, B. Raj, S. Bera, S.V. Narasimhan, “Temperature programmed decomposition of thorium nitrate pentahydrate”, *J. Nucl. Mater.* 278 (2–3) (2000) 173-185.
- [120] T.V. Plakhova, A.Y. Romanchuk, D.V. Likhosherstova, A.E. Baranchikov, P.V. Dorovatovskii, R.D. Svetogorov, T.B. Shatalova, T.B. Egorova, A.L. Trigub, K.O. Kvashnina, V.K. Ivanov, S.N. Kalmykov, “Size effects in nanocrystalline thoria”, *J. Phys. Chem. C* 123 (37) (2019) 23167-23176. [120a] D. Hudry, C. Apostolidis, O. Walter, T. Gouder, E. Courtois, C. Kübel, D. Meyer, Controlled Synthesis of Thorium and Uranium Oxide Nanocrystals, *Chem. Eur. J.*, 19 (2013) 5297-5305.
- [121] F. Deganello, A.K. Tyagi, “Solution combustion synthesis, energy and environment: Best parameters for better materials”, *Prog. Cryst. Growth Char.* 64 (2018) 23-61.
- [122] A. Varma, A.S. Mukasyan, A.S. Rogachev, K.V. Manukyan, “Solution combustion synthesis of nanoscale materials”, *Chem. Rev.* 116 (2016) 14493-14586.
- [123] V. Chandramouli, S. Anthonysamy, P.R. Vasudeva Rao, “Combustion synthesis of thoria - A feasibility study”, *J. Nucl. Mater.* 265(3) (1999) 255-261.
- [124] S. Anthonysamy, K. Ananthasivan, V. Chandramouli, I. Kaliappan, P.R. Vasudeva Rao, “Combustion synthesis of urania-thoria solid solutions”, *J. Nucl. Mater.* 278(2) (2000) 346-357.
- [125] D. Sanjay Kumar, K. Ananthasivan, S. Amirthapandian, A. Dasgupta, G. Jogeswara Rao, “Citrate gel-combustion synthesis and sintering of nanocrystalline ThO<sub>2</sub> powders”, *J. Nucl. Mater.* 497 (2017) 16-29.
- [126] R.D. Purohit, S. Saha, A.K. Tyagi, “Combustion synthesis of 5 and 10 mol% YO<sub>1.5</sub> doped ThO<sub>2</sub> powders”, *J. Nucl. Mater.* 323 (1) (2003) 36-40.

- [127] K.C. Patil, M.S. Hegde, T. Rattan, S.T. Aruna, "Chemistry of nanocrystalline oxide materials combustion synthesis, properties and applications", World Scientific Publications (2008) (DOI: <https://doi.org/10.1142/6754>).
- [128] F.-T Li, J. Ran, M. Jaroniec, S.Z. Qiao, "Solution combustion synthesis of metal oxide nanomaterials for energy storage and conversion", *Nanoscale* 7(42) (2015) 17590-17610.
- [129] A. Kumar, E.E. Wolf, A.S. Mukasyan, "Solution combustion synthesis of metal nanopowders: nickel-reaction pathways", *AIChE J.* 57(8) (2011) 2207-2214.
- [130] A. Kumar, E.E. Wolf, A.S. Mukasyan, "Solution combustion synthesis of metal nanopowders: Copper and copper / nickel alloys", *AIChE J.* 57(12) (2011) 3473-3479.
- [131] S. Zhang, Z.A. Munir, "The combustion synthesis of refractory nitrides: Part II the synthesis of niobium nitride", *J. Mater. Sci.* 26 (1991) 3380–3385.
- [132] "Nitride ceramics: Combustion synthesis, properties, and applications", (Eds.: A.A. Gromov, L.N. Chukhlomina) Wiley-VCH Verlag GmbH (2015) (DOI:10.1002/9783527684533).
- [133] H.V. Kirakosyan, K.T. Nazaretyan, R.A. Mnatsakanyan, S.V. Aydinyan, S.L. Kharatyan, "Solution combustion synthesis of nanostructured molybdenum carbide", *J. Nanopart. Res.* 20 (2018) 214.
- [134] N.A. Marand, S.M. Masoudpanah, M. Sh. Bafghi, "Solution combustion synthesis of nickel sulfide composite powders", *Ceram. Int.* 44 (14) (2018) 17277-17282.
- [135] K. Rajeshwar, N.R. De Tacconi, "Solution combustion synthesis of oxide semiconductors for solar energy conversion and environmental remediation", *Chem. Soc. Rev.* 38 (7) (2009) 1984-1998.

- [136] K.C. Thomas, J.R. Kale, R.G. Dalavi, K. Venkatesh, R. Kameswaran, A.V.R. Reddy  
"Development of an IR-based carbon analyser for uranium metal", BARC Newsletter  
311 (2009) 2-6 (Web-link: <http://barc.gov.in/publications/nl/2009/200912.pdf/>)
- [137] B.D. Cullity, "Elements of X-ray diffraction", Addison-Wesley Publishing Company  
Inc. (1956).
- [138] R. Tilley, "Crystals and crystal structures", John Wiley & Sons, Ltd. (2006) (ISBN-13  
978-0-470-01820-0).
- [139] E. Smith, G. Dent, "Modern Raman spectroscopy - A practical approach", John Wiley  
& Sons, Ltd. (2006) (ISBN 0-471-49794-0).
- [140] M. Roessle, D.I. Svergun, "Small angle X-ray scattering", In "Encyclopaedia of  
biophysics" (Eds.: G.C.K. Roberts) Springer, Berlin, Heidelberg (2013) (DOI:  
[https://doi.org/10.1007/978-3-642-16712-6\\_284](https://doi.org/10.1007/978-3-642-16712-6_284)).
- [141] P.W. Schmidt, R. Height, "Slit height corrections in small angle X-ray scattering", Acta  
Crystallogr. 13 (1960) 480-483.
- [142] G. Höhne, W.F. Hemminger, H.J. Flammersheim, "Differential scanning calorimetry",  
Springer-Verlag. (2003) (ISBN 978-3-540-00467-7).
- [143] M. Reading, A. Luget, R. Wilson, "Modulated differential scanning calorimetry",  
Thermochim. Acta 238(C) (1994) 295-307.
- [144] J.E.K. Schawe, T. Hutter, C. Heitz, I. Alig, D. Lellinger, "Stochastic temperature  
modulation: A new technique in temperature-modulated DSC", Thermochim. Acta 446  
(2006) 147-155.
- [145] N. Manoj, D. Jain, J.K. Gautam, K.C. Thomas, V. Sudarsan, C.G.S. Pillai, R.K. Vatsa,  
A.K. Tyagi, "A simple, reliable and cost-effective, high temperature dilatometer for  
bulk thermal expansion studies on solids", Measurement 92 (2016) 318-325.

## References

- [146] W.J. Parker, R.J. Jenkins, C.P. Butler, G.L. Abbott, “Flash method of determining thermal diffusivity, heat capacity, and thermal conductivity”, *J. Appl. Phys.* 32 (1961) 1679-1684.
- [147] H.S. Carslaw, J.C. Jaeger, “Conduction of heat in solids”, 2nd edition, Oxford University Press, New York, (1959).
- [148] D. Jain, D. Das, B.N. Jagatap, “Thorium-based fuels for advanced nuclear reactors: Thermophysical, thermochemical and thermodynamic properties”, in A.K. Nayak, B.R. Sehgal (Eds.), *Thorium—Energy for the Future*, Springer (2019) (ISBN 978-981-13-2658-5) 257-275.
- [149] Y.S. Touloukian, R.W. Powell, C.Y. Ho, P.G. Klemens, “Thermophysical properties of matter - The TPRC data series. Volume 1. Thermal conductivity - metallic elements and alloys”, (1970) 429-440; 381-384.
- [150] Y.S. Touloukian, R.W. Powell, C.Y. Ho, M.C. Nicolaou, “Thermophysical properties of matter - The TPRC data series. Volume 10. Thermal diffusivity”, (1974) 205-208.
- [151] Y.S. Touloukian, E.H. Buyco, “Thermophysical properties of matter - The TPRC data series. Volume 4. Specific heat - metallic elements and alloys”, (1971) 268-270.
- [152] Y.S. Touloukian, R.K. Kirby, R.E. Taylor, P.D. Desai, “Thermophysical properties of matter - The TPRC data series. Volume 12. Thermal expansion metallic elements and alloys”, (1975) 365-372.
- [153] H.G. Schettler, J.J. Martin, F.A. Schmidt, G.C. Danielson, “Thermal conductivity of high purity thorium”, *Phys. Rev.* 187 (3) (1969) 801-804.
- [154] T.A. Sandenaw, “Thermal conductivity of uranium: Effects of purity and microstructure”, Report no.: LA-6092-MS, United States (1975) 1-8.
- [155] Y. Takahashi, M. Yamawaki, K. Yamamoto, “Thermophysical properties of uranium-zirconium alloys”, *J. Nucl. Mater.* 154 (1988) 141-144.

## References

- [156] R.W. Logan, D.H. Wood, "Thermal expansion of rolled and extruded uranium", *J. Less-Common Met.* 90 (1983) 233-241.
- [157] J. Nakamura, Y. Takahashi, S. Izumi, M. Kanno, "Heat capacity of metallic uranium and thorium from 80 to 1000 K", *J. Nucl. Mater.* 88 (1980) 64-72.
- [158] M. Boivineau, H. Colin, J.M. Vermeulen, Th. Thévenin, "Thermophysical properties of solid and liquid thorium", *Int. J. Thermophys.* 17(5) (1996) 1001-1010.
- [159] S. Zhou, R. Jacobs, W. Xie, E. Tea, C. Hin, D. Morgan, "Combined ab-initio and empirical model of the thermal conductivity of uranium, uranium-zirconium, and uranium-molybdenum", *Phys. Rev. Mater.* 2 (2018) 083401-1-21.
- [160] Y. Li, A. Chernatynskiy, J.R. Kennedy, S.B. Sinnott, S.R. Phillpot, Lattice expansion by intrinsic defects in uranium by molecular dynamics simulation, *J. Nucl. Mater.* 475 (2016) 6-18.
- [161] K.D. Joshi, S.C. Gupta, S. Banerjee, "Ab-initio theoretical analysis of thermal expansivity, thermal vibrations and melting of thorium", *Phil. Mag.* 88 (27) (2008) 3145-3152.
- [162] S. Jaroszewicz, H.O. Mosca, J.E. Garcés, "The temperature behaviour of the elastic and thermodynamic properties of fcc thorium", *J. Nucl. Mater.* 429(1-3) (2012) 136-142.
- [163] L. Kývala, D. Legut, "Lattice dynamics and thermal properties of thorium metal and thorium monocarbide" *Phys. Rev. B* 101 (2020) 075117.
- [164] P.L. Vijay, J.C. Sehra, C.V. Sundaram, K.R. Gurumurthy, R.V. Raghavan, "Studies on the preparation of thorium metal sponge from thorium oxalate", *BARC Report no.:* 969 (1978) 1-11.
- [165] M.D. Smith, R.W.K. Honeycombe, "The effect of oxygen, carbon and nitrogen on the properties of sintered thorium", *J. Nucl. Mater.* 4 (1959) 345-355.

- [166] Inorganic Crystal Structure Database (ICSD FIZ Karlsruhe GmbH, Version 4.4.0 (2020); collection code: 653236); from: J. Bohet, W. Müller, “Preparation and structure studies of “Van Arkel” protactinium”, *J. Less-Common Met.* 57 (2) (1978) 185-1995.
- [167] International Centre for Diffraction Data (ICDD Database; JCPDF card no.: 720659).
- [168] Inorganic Crystal Structure Database (ICSD FIZ Karlsruhe GmbH, Version 4.4.0 (2020) collection code: 253564) from: V.K. Tripathi, R. Nagarajan, “Sol–gel synthesis of high-purity actinide oxide ThO<sub>2</sub> and its solid solutions with technologically important tin and zinc ions” *Inorg. Chem.* 55 (24) (2016) 12798-12806.
- [169] Inorganic Crystal Structure Database (ICSD FIZ Karlsruhe GmbH, Version 4.4.0 (2020) collection code: 35204); from: S.A. Barrett, A.J. Jacobson, B.C. Tofield, B.E.F. Fender, “The preparation and structure of barium uranium oxide BaUO<sub>3+x</sub>”, *Acta Crystallogr. B* 38 (1982) 2775-2781. [169a] S. Ellison, A. Williams, *Eurachem / CITAC guide: Quantifying Uncertainty in Analytical Measurement* (2012) ISBN 978-0-948926-30-3 (Web-link: [www.eurachem.org](http://www.eurachem.org)).
- [170] Inorganic Crystal Structure Database (ICSD FIZ Karlsruhe GmbH, Version 4.4.0 (2020) collection code: 24223); from: R.E. Rundle, N.C. Baenziger, A.S. Wilson, R.A. McDonald, “The structures of the carbides, nitrides and oxides of uranium”, *J. Am. Chem. Soc.* 70 (1948) 99-105.
- [171] Inorganic Crystal Structure Database (ICSD FIZ Karlsruhe GmbH, Version 4.4.0 (2020) collection code: 26476); from: A.E. Austin, “Carbon positions in uranium carbides”, *Acta Crystallogr.* 12 (1959) 159-161.
- [172] “Augmented uranium metal production facility”, *BARC Newsletter* 200 (2000) 15-18 (Web-link: <http://barc.gov.in/publications/nl/2000/200009.pdf>).
- [173] G.C. Allen, P.M. Tucker, “Surface oxidation of uranium metal as studied by X-ray photoelectron spectroscopy”, *J. Chem. Soc. Dalton* 5 (1973) 470-474.

- [174] R. Rao, R.K. Bhagat, N.P. Salke, A. Kumar, "Raman spectroscopic investigation of thorium dioxide-uranium dioxide ( $\text{ThO}_2\text{-UO}_2$ ) fuel materials", *Appl. Spectrosc.* 68(1) (2014) 44-48.
- [175] "Thermophysical properties of materials for nuclear engineering: A tutorial and collection of data", (IAEA-THPH), International Atomic Energy Agency, Vienna (2008).
- [176] I.F. Barwood, B.R. Butcher, "The  $\alpha \rightarrow \beta$  phase transformation in uranium", *J. Nucl. Mater.* 8 (1963) 232-240.
- [177] C. Yoo, H. Cynn, P. Söderlind, "Phase diagram of uranium at high pressures and temperatures", *Phys. Rev. B* 57 (1998) 10359-10362.
- [178] P. Zhou, X. Wang, H. Yang, X. Fu, "Effect of vacuum heat treatment on oxidation of uranium surfaces", *Rare Metal Mat. Eng.* 37 (2008) 94-97.
- [179] G. Erez, U. Even, "The Wiedemann-Franz ratio of metallic uranium at elevated temperatures", *J. Appl. Phys.* 37 (1966) 4633-4644.
- [180] S. Nasu, S. Fukushima, T. Ohmichi, T. Kikuchi, "Thermal diffusivity of uranium by laser pulse method from 20° to 850°C", *Jap. J. Appl. Phys.* 7 (1968) 682.
- [181] D. Jain, C.G.S. Pillai, B.S. Rao, R.V. Kulkarni, E. Ramdasan and K.C. Sahoo, "Thermal diffusivity and thermal conductivity studies on thoria-lanthana solid solutions up to 10 mol. %  $\text{LaO}_{1.5}$ ", *J. Nucl. Mater.* 353 (2006) 35-41.
- [182] S.S. Parker, J.T. White, P. Hosemann, A.T. Nelson, "Thermophysical properties of thorium mononitride from 298 to 1700 K", *J. Nucl. Mater.* 526 (2019) 151760.
- [183] H. He, J. Majewski, D.D. Allred, P. Wang, X. Wen, K.D. Rector, "Formation of solid thorium monoxide at near-ambient conditions as observed by neutron reflectometry and interpreted by screened hybrid functional calculations", *J. Nucl. Mater.* 487 (2017) 288-296.

## References

- [184] B.R. Butcher, A.H. Rowe, "Phase transformation in uranium", *Nature* (1953) 817.
- [185] H.H. Klpefer, P. Chiotti, "Characteristics of the solid state transformations in uranium", USAEC Report no.: ISC-893 (1957) 1-113.
- [186] W.S. Blackburn, " $\alpha$ - $\beta$  Thermal cycling of uranium", *J. Nucl. Mater.* 2 (1960) 191.
- [187] J.J. Stobo, "Alpha beta cycling of uranium", *J. Nucl. Mater.* 2 (1960) 97-109.
- [188] L.T. Lloyd, "Thermal expansion of alpha-uranium single crystals", *J. Nucl. Mater.* 3 (1961) 67-71.
- [189] L.T. Lloyd, C.S. Barrett, "Thermal expansion of alpha uranium", *J. Nucl. Mater.* 18 (1966) 55-59.
- [190] E.S. Fisher, "Preparation of alpha uranium single crystals by a grain-coarsening method", *J. Metals* 9 (1957) 882-888.
- [191] D.C. Wallace, "Specific heat of thorium at high temperatures", *Phys. Rev.* 120 (1) (1960) 84-88.
- [192] E.A. Mit'kina, "Experimental determination of the true specific heats of uranium, thorium, and other metals", *Sov. Atom Energy* 7 (2) (1959) 163-165.
- [193] F.L. Oetting, D.T. Peterson, "Heat capacity of well characterized thorium metal from 298 to 700 K", *J. Less-Common Met.* 128 (1987) 231-239.
- [194] D.C. Ginnings, R.J. Corruccini, "Heat capacities at high temperatures of uranium, uranium trichloride, and uranium tetrachloride, *J. Res. Nat. Bur. Stand.* 39 (1947) 309-316.
- [195] F.K. Oetting, M.H. Rand, R.J. Ackermann, "The chemical thermodynamics of actinide elements and compounds, Part 1, The actinide elements", International Atomic Energy Agency (IAEA), Vienna (1976).
- [196] A.L. Loeb, "Thermal conductivity: VIII, A theory of thermal conductivity of porous materials", *J. Am. Ceram. Soc.* 37 (1954) 96-99.

## References

- [197] S. Kaity, J. Banerjee, M.R. Nair, K. Ravi, S. Dash, T.R.G. Kutty, A. Kumar, R.P. Singh, "Microstructural and thermophysical properties of U-6 wt.% Zr alloy for fast reactor application", *J. Nucl. Mater.* 427 (2012) 1-11.
- [198] C. Hin, "Thermal conductivity of metallic uranium", NEUP 14-6767 (2018) (Web-link: <https://www.osti.gov/servlets/purl/1433931>).
- [199] M. Floyd, B. Bromley, J. Pencer, "A Canadian perspective on progress in thorium fuel science and technology", *CNL Nucl. Rev.* 6 (1) (2017) 1-17.
- [200] S. Thakur, P.S.R. Krishna, A.B. Shinde, R. Kumar, S.B. Roy, "Quantitative analysis of thorium phase in Th-U alloys using diffraction studies", *AIP Conf. Proc.* 1832 (2017) 060012.
- [201] P. Chiotti, "High temperature crystal structure of thorium", *J. Electrochem. Soc.* (1955) 567-570.
- [202] G.G. Bente, "A Physical Metallurgical Study of Thorium-Rich Thorium-Uranium Alloys", Report no.: NAA-SR-2069 (1958).
- [203] G.H. Bannister, R.C. Burnett, J.R. Murray, "Ageing and hot hardness characteristics of certain thorium alloys", *J. Nucl. Mater.* 2(1) (1960) 51-61.
- [204] "Chemical technology division annual technical report for 1986," ANL-87-19, Argonne National Laboratory (1987) 122.
- [205] V. Crewe, S. Lawroski, "Reactor development program progress report", Argonne National Laboratory, ANL-7230, Lemont, IL, USA (1966).
- [206] O. Beneš D. Manara R.J.M. Konings, "Thermodynamic assessment of the Th-U-Pu system", *J. Nucl. Mater.* 449 (1-3) (2014) 15-22.
- [207] S. Kneppel, "Aqueous corrosion of thorium alloys and zircaloy-clad thorium alloys", NMI-1226, United States Atomic Energy Commission (1960) 1-49 (Web-link: <https://play.google.com/books/reader?id=OGCWvHY4xRwC&hl=en&pg=GBS.PA1>)

## References

- [208] D.S. Evans, G.V. Raynor, "The solubility of zirconium in  $\alpha$ -thorium", *J. Nucl. Mater.* 4 (1) (1961) 66-69.
- [209] R.I. Sheldon, D.E. Peterson, "The (U-Zr) Uranium-zirconium system", *Bull. Alloy Phase Diagr.* 10 (2) (1989) 165-171.
- [210] O.N. Carlson, "Some studies on the uranium-thorium-zirconium ternary alloy system", AECD-3206, United States Atomic Energy Commission (1950) 1-72.
- [211] J.W. Goffard, R.K. Marshall, "Irradiation behavior of Zircaloy-2 clad thorium-uranium-zirconium alloy fuel elements Interim report 1", BNWL-479, Pacific Northwest Laboratory, United States Atomic Energy Commission (1967).
- [212] T. Okawa, S. Nakayama, H. Sekimoto, "Design study on power flattening to sodium cooled large-scale CANDLE burning reactor with using thorium fuel", *Energ. Convers. Manage.* 53 (1) (2012) 182-188.
- [213] Inorganic crystal Structure Database (ICSD FIZ Karlsruhe GmbH, Version 4.4.0 (2020) collection code: 164572) from: A.I. Kolesnikov, A.M. Balagurov, I.O. Bashkin, A.V. Belushkin, E.G. Ponyatovsky, M. Prager, "Neutron scattering studies of ordered gamma -ZrD", *J. Phys. Condens-Mat.* 6 (43) (1994) 8977-8988.
- [214] Inorganic crystal Structure Database (ICSD FIZ Karlsruhe GmbH, Version 4.4.0 (2020) collection code: 16559) from: B.O. Loopstra, "Neutron diffraction investigation of  $U_3O_8$ ", *Acta Crystallogr.* 17 (1964) 651-654.
- [215] Inorganic crystal Structure Database (ICSD FIZ Karlsruhe GmbH, Version 4.4.0 (2020) collection code: 246035) from: S.K. Sali, N.K. Kulkarni, K. Krishnan, S.N. Achary, A.K. Tyagi, "Oxidation / reduction studies on  $Zr_yU_{1-y}O_{2+x}$  and delineation of a new orthorhombic phase in U-Zr-O system", *J. Solid-State Chem.* 181 (8) (2008) 1859-1866.

## References

- [216] Inorganic crystal Structure Database (ICSD FIZ Karlsruhe GmbH, Version 4.4.0 (2020) collection code: 108756) from: H.L. Luo, J.G. Huber, “Superconductivity in Th-Zr alloys”, *J. Less-Common Met.* 65 (1) (1979) 13-17.
- [217] J.M. Elorrieta, L.J. Bonales, M. Najj, D. Manara, V.G. Baonza, J. Cobos, “Laser-induced oxidation of  $\text{UO}_2$ : A Raman study”, *J. Raman Spectrosc.* 49 (5) (2018) 878-884.
- [218] H. He, D. Shoesmith, “Raman spectroscopic studies of defect structures and phase transition in hyper-stoichiometric  $\text{UO}_{2+x}$ ”, *Phys. Chem. Chem. Phys.* 12 (2010) 8109-8118.
- [219] X. Zhao, D. Vanderbilt, “Phonons and lattice dielectric properties of zirconia”, *Phys. Rev. B* 65 (2002) 075105.
- [220] E. Hashem, A. Seibert, J-F. Vigier, M. Najj, S. Mastromarino, A. Ciccioli, D. Manara, “Solid-liquid equilibria in the  $\text{ThO}_2$ - $\text{ZrO}_2$  system: An experimental study” *J. Nucl. Mater.* 521 (2019) 99-108.
- [221] O.N. Carlson, E.R. Stevens, “A compilation of thorium binary phase diagrams”, USAEC Report (1968) (Web-link: <https://www.osti.gov/servlets/purl/4529064>).
- [222] G.B. Skinner, H.L. Johnston, “Thermal Expansion of zirconium between 298°K and 1600°K”, *J. Chem Phys.* 21 (1953) 1383.
- [223] P.L. Brown, E. Curti, B. Grambow, C. Ekberg, “Chemical thermodynamics of zirconium”, OECD Nuclear energy agency, data bank (Eds.: F.J. Mompean, J. Perrone, M. Illemassene) (2005) (Web-link: <https://www.oecd-nea.org/dbtdb/pubs/vol8-zirconium.pdf>).
- [224] C.G.S. Pillai, P. Raj, “Thermal Conductivity of  $\text{ThO}_2$  and  $\text{Th}_{0.98}\text{U}_{0.02}\text{O}_2$ ”, *J. Nucl. Mater.* 277 (2000) 116-119.

- [225] S.S. Manoharan, K.C. Patil, "Combustion synthesis of metal chromite powders", *J. Am. Ceram. Soc.* 75 (1992) 1012-1015.
- [226] S.R. Jain, K.C. Adiga, V.R. Pai Verneker, "A new approach to thermochemical calculations of condensed fuel-oxidizer mixtures," *Combust. Flame* 40 (6) (1981) 71-79.
- [227] S. Roy, A. Das Sharma, S.N. Roy, H.S. Maiti, "Synthesis of  $\text{YBa}_2\text{Cu}_3\text{O}_{7-x}$  Powder by Autoignition of Citrate-Nitrate Gel", *J. Mater. Res.* 8(11) (1993) 2761-2766.
- [228] M. Gizowska, I. Kobus, K. Perkowski, M. Piatek, G. Konopka, I. Witosławska, M. Osuchowski, "Size and morphology of yttria nanopowders obtained by solution combustion synthesis" *Arch. Metall. Mater.* 63(2) (2018) 743-748.
- [229] G.A.M. Hussein, H.M. Ismail, "Texture assessment of thoria as a final decomposition product of hydrated thorium nitrate and oxycarbonate", *Colloids Surf. A*: 99 (1995) 129-139.
- [230] I.M. Weiss, C. Muth, R. Drumm, H.O.K. Kirchner, "Thermal decomposition of the amino acids glycine, cysteine, aspartic acid, asparagine, glutamic acid, glutamine, arginine and histidine", *BMC Biophys.* 11 (2018) 1-15.
- [231] N. Raje, A.V.R. Reddy, "Mechanistic aspects of thermal decomposition of thorium oxalate hexahydrate: A review", *Thermochim. Acta* 505 (2010) 53-58.
- [232] H. Hayashi, T. Watanabe, "Properties of thoria obtained by thermal decomposition of thorium salts", *Nippon Kagaku Kaishi* 4 (1973) 858-860.
- [233] Y. Saito, "Thermal decomposition of thorium oxalate", *J. Jpn. Soc. Powder Metall.* 17(1971) 235-242.
- [234] M.T. Aybers, "Kinetic study of the thermal decomposition of thorium oxalate dehydrate", *J. Nucl. Mater.* 252 (1998) 28-33.
- [235] D.Y. Chung, E. H. Lee, "Microwave-induced combustion synthesis of  $\text{Ce}_{1-x}\text{Sm}_x\text{O}_{2-x/2}$  powder and its characterization", *J. Alloys Compd.* 374 (2004) 69-73.

## References

- [236] “The Aldrich Library of FT-IR Spectra, Edition-II, Volume-1”, 1 898 A 897-898.
- [237] S. Kumar, A.K. Rai, V.B. Singh, S.B. Rai, “Vibrational spectrum of glycine molecule”, *Spectrochim. Acta A* 61 (2005) 2741-2746.
- [238] J. R. Ferraro, A. Walker, “Comparison of the infrared spectra of the hydrates and anhydrous salts in the systems  $\text{UO}_2(\text{NO}_3)_2$  and  $\text{Th}(\text{NO}_3)_4$ ”, *J. Chem. Phys.* 45 (1966) 550-552.
- [239] J.H-Paredes, D.G-Mitnik, H.E. E-Ponce, M.E. A-Ramos, A.D-Moller, “Band structure, optical properties and infrared spectrum of glycine–sodium nitrate crystal”, *J. Mole. Str.* 875 (2008) 295-301.
- [240] S.L. Estes, M.R. Antonio, L. Soderholm, “Tetravalent Ce in the nitrate-decorated hexanuclear cluster  $[\text{Ce}_6(\mu_3\text{-O})_4(\mu_3\text{-OH})_4]^{12+}$ : A structural end point for ceria nanoparticles, *J. Phys. Chem. C* 120 (2016) 5810-5818.
- [241] M. Rand, L. Fuger, I. Grenthe, V. Neck, D. Rai, “Chemical thermodynamics: Chemical thermodynamics of thorium”, (OECD, NEA-TDB) Vol. 11, Elsevier, Amsterdam (2007).
- [242] C. Hennig, K. Schmeide, V. Brendler, H. Moll, S. Tsushima, A.C. Scheinost, “EXAFS Investigation of U(VI), U(IV), and Th(IV) sulfato complexes in aqueous solution”, *Inorg. Chem.* 46 (2007) 5882-5892.
- [243] J. Rothe, M.A. Denecke, V. Neck, R. Muller, J.I. Kim, XAFS “Investigation of the structure of aqueous thorium(IV) species, colloids, and solid thorium(IV) oxide / hydroxide”, *Inorg. Chem.* 41 (2002) 249-258.
- [244] C. Hennig, S. Takao, K. Takao, S. Weiss, W. Kraus, F. Emmerling, A.C. Scheinosta, “Structure and stability range of a hexanuclear Th(IV)-glycine complex”, *Dalton Trans.* 41 (2012) 12818-12823.

## References

- [245] Y. Hu, K.E. Knope, S. Skanthakumar, L. Soderholm, "Understanding the ligand-directed assembly of a hexanuclear Th<sup>IV</sup> molecular cluster in aqueous solution", *Eur. J. Inorg. Chem.* 24 (2013) 4159-4163.
- [246] M. Nourmand, N. Meissami, "Complex formation between uranium(VI) and thorium (IV) ions with some  $\alpha$ -amino-acids", *J. Chem. Soc. Dalton* 8 (1983) 1529-1533.
- [247] Bismondo, L. Rizzo, G. Tomat, "Thermodynamic properties of actinide complexes. uranyl (VI)- and thorium (IV)-glycine systems", *Inorg. Chim. Acta* 74 (1983) 21-24.
- [248] B.G. Oliver, A.R. Davis, "The structure of aqueous thorium nitrate solution by laser Raman spectroscopy", *J. Inorg. Nucl. Chem.* 34 (1972) 2851-2860.
- [249] Z. Huang, X. Chen, Y. Li, J. Chen, J. Lin, J. Wang, J. Lei, R. Chen, "Quantitative determination of citric acid in seminal plasma by using Raman spectroscopy", *Appl. Spectrosc.* 67 (7) (2013) 757-760.
- [250] A.K. Arora, M. Rajalakshmi, T.R. Ravindran, V. Sivasubramanian, "Raman spectroscopy of optical phonon confinement in nanostructured materials", *J. Raman Spectrosc.* 38 (2007) 604-617.
- [251] D. Langmuir, J.S. Herman, "The mobility of thorium in natural waters at low temperatures", *Geochim. Cosmochim. Ac.* 44 (1980) 1753-1766.
- [252] M. Bobtelsky, B. Graus, "Thorium citrate complexes, their composition, structure and behavior", *J. Am. Chem. Soc.* 76 (6) (1954,) 1536-1539.
- [253] G.R. Choppin, H.N. Erten, Y. Xia, "Variation of stability constants of thorium citrate complexes with ionic strength", *Radiochim. Acta* 74 (1996) 123-127.
- [254] D.P. Raymond, J.R. Duffield, D.R. Williams, "Complexation of plutonium and thorium in aqueous environments", *Inorg. Chim. Acta* 140 (1987) 309-313.
- [255] M.M. Barbooti, D.A. Al-Sammerrai, "Thermal decomposition of citric acid", *Thermochim. Acta* 98 (1986) 119-126.

## References

- [256] D. Hennings, W. Mayr, "Thermal decomposition of (BaTi) citrates into barium titanate", *J. Solid State Chem.* 26 (1978) 329-338.
- [257] N.S. Gajbhiye, S. Prasad, "Thermal decomposition of hexahydrated nickel iron citrate", *Thermochim. Acta* 285 (1996) 325-336.
- [258] J. Tsay, T. Fang, "Effects of molar ratio of citric acid to cations and of pH value on the formation and thermal-decomposition behavior of barium titanium citrate", *J. Am. Ceram. Soc.* 82(6) (1999) 1409-1415.
- [259] A. Marcilla, A. Gómez-Siurana, M. Beltrán, I. Martínez-Castellanos, I. Blasco, D. Berenguer, "TGA-FTIR study of the pyrolysis of sodium citrate and its effect on the pyrolysis of tobacco and tobacco/SBA-15 mixtures under N<sub>2</sub> and air atmospheres", *J. Sci. Food Agr.* 98 (15) (2018) 5916-5931.
- [260] O. Glatter, O. Kratky, "Small angle X-ray scattering", Academic, London (1982).
- [261] A. Guinier, G. Fournet, "Small angle scattering of X-rays", Wiley, New York (1955).
- [262] J. Aitchison, J.A.C. Brown, "The log normal distribution", Cambridge University Press, Cambridge (1957).
- [263] R.D. Purohit, B.P. Sharma, K.T. Pillai, A.K. Tyagi, "Ultrafine ceria powders via glycine-nitrate combustion", *Mater. Res. Bull.* 36 (15) (2001) 2711-2721.
- [264] V.R. Choudhary, A.M. Rajput, B. Prabhakar, A.S. Mamman, "Partial oxidation of methane to CO and H<sub>2</sub> over nickel and/or cobalt containing ZrO<sub>2</sub>, ThO<sub>2</sub>, UO<sub>2</sub>, TiO<sub>2</sub> and SiO<sub>2</sub> catalysts", *Fuel* 77 (15) (1998) 1803-1807.
- [265] V. Múčka, J. Podlaha, R. Silber, "NiO-ThO<sub>2</sub> mixed catalysts in hydrogen peroxide decomposition and influence of ionizing radiation", *Radiat. Phys. Chem.* 59 (5-6) (2000) 467-475.

## References

- [266] P. Balakrishna, B.N. Murty, K.P. Chakraborty, R.N. Jayaraj, C. Ganguly, “Special features in powder preparation, pressing, and sintering of uranium dioxide”, *Mater. Manuf. Process.* 15(5) (2000) 679-693.
- [267] C.S. Morgan, K.H. McCorkle, G.L. Powell, “Sintering and desintering of thoria”, In: Kuczynski G.C. (Eds.) *Sintering and Related Phenomena*. Materials Science Research, Vol. 6, Springer, Boston, MA (1973).
- [268] J.M. Pope, K.C. Radford, “Physical properties of some thoria powders and their influence on sinterability”, *J. Nucl. Mater.* 52 (1974) 241-254.
- [269] Z. Chen, J. Mabon, J. Wen, R. Trice, “Degradation of plasma-sprayed yttria-stabilized zirconia coatings via ingress of vanadium oxide”, *J. Eur. Ceram. Soc.* 29(9) (2009) 1647-1656.
- [270] M.A. Delfrate, J. Lemaitre, V. Buscaglia, M. Leoni, P. Nanni, “Slip casting of submicron BaTiO<sub>3</sub> produced by low-temperature aqueous synthesis”, *J. Eur. Ceram. Soc.* 16(9) (1996) 975-984.
- [271] T.K. Gupta, R.L. Coble, “Sintering of ZnO: II, density decrease and pore growth during the final stage of the process”, *J. Am. Ceram. Soc.* 51 (9) (1968) 525-528.
- [272] C.-H. Chang, J.F. Rufner, K.V. Benthem, R.H.R. Castro, “Design of desintering in tin dioxide nanoparticles”, *Chem. Mater.* 25(21) (2013) 4262-4268.
- [273] P. Duran, J. Tartaj, C. Moure, “Sintering behaviour and microstructural evolution of agglomerated spherical particles of high-purity barium titanate”, *Ceram. Int.* 29(4) (2003) 419-425.
- [274] C.-Y. Tsao, W.-H. Tuan, K.-C. Feng, “De-sintering of Ba<sub>5</sub>Nb<sub>4</sub>O<sub>15</sub> ceramic and its influence on microwave characteristics”, *J. Eur. Ceram. Soc.* 37(4) (2017) 1517-1521.
- [275] Cs. Balázs, F.S. Cinar, O. Addemir, F. Wéber, P. Arató, “Manufacture and examination of C/Si<sub>3</sub>N<sub>4</sub> nanocomposites” *J. Eur. Ceram. Soc.* 24(12) (2004) 3287-3294.

## References

- [276] R. Besler, M.R. da Silva, J.J. do Rosario, M. Dosta, S. Heinrich, R. Janssen, “Sintering simulation of periodic macro porous alumina”, *J. Am. Ceram. Soc.* 98(11) (2015) 3496-3502.
- [277] K. Ananthasivan, S. Anthonysamy, A. Singh, P.R. Vasudeva Rao, “De-agglomeration of thorium oxalate - A method for the synthesis of sinter active thoria”, *J. Nucl. Mater.* 306 (1) (2002) 1-9.
- [278] R.H.R. Castro, “Controlling sintering and grain growth of nanoceramics”, *Cerâmica* 65 (373) (2019) 122-129. **[278a]** Thermodynamics of sintering, R.M. German, *Sintering of advanced materials: Fundamentals and processes* (Ed.: Z.Z. Fang) Woodhead Publishing Ltd. (2010), ISBN 978-1-84569-562-0. **[278b]** G.S. Upadhyaya, *Sintered metallic and ceramic Materials*, John Wiley & Sons Ltd. (1999) ISBN 0-471-98155-9.
- [279] O. Sudre, F.F. Lange, “The effect of inclusions on densification; III, The desintering phenomenon”, *J. Am. Ceram. Soc.* 75 (12) (1992) 3241-3251.
- [280] F. Li, J. Pan, A. Cocks, “Defect healing and cracking in ceramic films during constrained sintering” *J. Am. Ceram. Soc.* 95(12) (2012) 3743-3749.
- [281] S. Knight, R. Korlacki, C. Dugan, J.C. Petrosky, A. Mock, P.A. Dowben, J. Matthew Mann, M.M. Kimani, M. Schubert, “Infrared-active phonon modes in single-crystal thorium dioxide and uranium dioxide”, *J. Appl. Phys.* 127 (2020) 125103.

## CHAPTER 2

### Experimental section

---

#### 1.1. Introduction

This chapter is divided into two sections namely, (i) Materials and (ii) Methods. In the ‘Materials’ section, details of chemicals used during the course of this research work are provided. ‘Methods’ section is sub-divided into two parts namely methods used for (a) material preparation (synthesis methods) and (b) material characterization and thermophysical properties evaluation. A summary of these methods has been provided with their advantages, limitations, and application in the context of presented work.

#### 1.2. Materials

Nuclear-grade natural uranium and thorium metals were obtained from Atomic Fuels Division (AFD) and Uranium Extraction Division (UED) of Bhabha Atomic Research Centre (BARC), Mumbai. Both these Divisions at BARC are engaged in production of uranium and thorium metals as well as nuclear fuels for research reactors in India. Uranium metal was obtained in the form of cylindrical pellets (~15 mm diameter, 5-8 mm thickness). Thorium metal was obtained in two different forms namely (a) tube form (~12 mm outer diameter, ~1 mm thickness) and (b) cylindrical metal powder compacts (~20 mm diameter, 10-15 mm thickness). Zirconium metal rods (> 99.99% purity; ~8 mm outer diameter) were procured from local vendors. These metals were processed by cutting, polishing, pre-sintering, melting, etc. to prepare various alloys. Details of different processing steps are discussed in methods section.

For synthesis of nanocrystalline thorium dioxide ( $\text{ThO}_2$ ) powders, thorium nitrate pentahydrate ( $\text{Th}(\text{NO}_3)_4 \cdot 5\text{H}_2\text{O}$  (minimum assay > 99.5 %) was obtained from Indian Rare Earth Limited (IREL). Being highly hygroscopic in nature, it was stored inside a desiccator maintained at < 10% relative humidity by using activated silica gel and anhydrous calcium chloride desiccants. Prior to use, thorium nitrate was vacuum dried for ~2 h ( $P < 10^{-3}$  Torr). Pentahydrate stoichiometry was confirmed from thermo-gravimetric analysis by decomposing a vacuum dried sample (~250 mg) into  $\text{ThO}_2$  by heating up to 1073 K (heating rate ~ 4 K / min) in static air and weighing the residue. Polycrystalline glycine ( $\text{NH}_2\text{CH}_2\text{COOH}$ ; > 99.5% pure, M/s. Sisco Research Laboratories Pvt. Ltd., Mumbai) was dried in a desiccator (relative humidity  $\leq$  10%) before use. Polycrystalline citric acid monohydrate ( $\text{C}_6\text{H}_8\text{O}_7 \cdot \text{H}_2\text{O}$ , > 99.9% pure, M/s. Chemco Fine Chemicals, Mumbai) was used without further treatment. Deionized water (conductivity ~2  $\mu\text{Sv} / \text{cm}$ ) was used as solvent for preparation of aqueous solutions of thorium nitrate and glycine /citric acid.

All other solvents (hexane, methyl alcohol, acetone, etc.) used were of analytical reagent (AR)-grade. Hexane was purified to remove all traces of moisture by refluxing over sodium metal turnings with the help of water condenser. Benzophenone was used as the indicator for completion of dissolved moisture removal. Dry hexane was collected as distillate and stored over sodium metal turnings for further use.

### **1.3. Methods**

#### **1.3.1. Preparative methods**

##### **1.3.1.1. Metal and alloy handling**

Both, uranium and thorium metals are highly electropositive and reactive towards air, moisture and several gases in nature. Uranium metal in pure form (such as freshly polished

metal) is silvery white with bright metallic lustre. Upon exposure in air, it readily tarnishes into golden yellow color at ambient temperature due to surface oxidation. Thorium metal ingots show stainless steel like lustre in the pure form and tarnish relatively slowly. Freshly polished zirconium metal is stable and remains visibly intact for several days. In powdered form, all these metals are highly reactive and pyrophoric and must be handled under inert atmospheres. Uranium and thorium are also mildly radioactive with long half lives ( $\sim 14.05 \times 10^9$  years for  $^{232}\text{Th}$ ,  $\sim 4.5 \times 10^9$  years for  $^{238}\text{U}$ ,  $\sim 0.704 \times 10^9$  years for  $^{235}\text{U}$ ). Both these elements primarily decay with alpha particle emission (alpha energies (in MeV):  $\sim 4.01$  for  $^{232}\text{Th}$ ,  $\sim 4.397$ ,  $\sim 4.366$ ,  $4.214$  for  $^{235}\text{U}$  and  $\sim 4.198$  for  $^{238}\text{U}$ ). Due to high chemical reactivity and radioactive nature, safe handling of these metals and alloys prepared from them is essential. Keeping this in mind, thorium and uranium metals, and alloys prepared from them were handled inside a leak-tight inert atmosphere (argon) glove box facility, which was set up during the course of this work. Fig. 2.1(a) shows a photograph of the glove box facility.

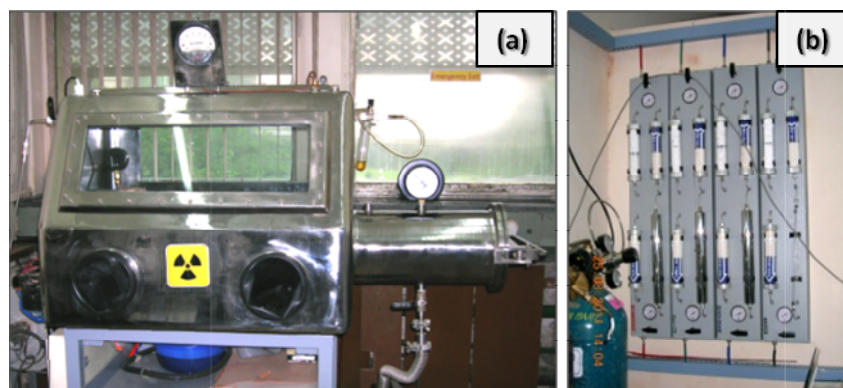


**Fig. 2.1. (a) Photograph of inert atmosphere glove box for handling uranium and thorium-based alloys, (b) Gas purification panel used for metal fuel handling**

The glove box has two compartments namely, sample handling space and sample transfer tunnel. These compartments are separated by a leak-tight stainless steel (SS-316) flange,

which can be opened / closed from inside the glove box. Sample transfer tunnel is connected to vacuum system (for evacuation up to  $10^{-3}$  Torr) and gas-line (for filling the tunnel with inert gas) by independent valves. Tunnel can be filled with inert gas, which can either be sourced from the glove box itself or separately from a gas reservoir. Glove box is filled with high purity argon gas and maintained at slightly higher pressure above ambient (monitored by Magnehelic gauge) to prevent air ingress inside the glove box. Argon gas is passed through gas purification panel (Fig. 2.1(b)) consisting of leak tight columns filled with silica gel, dehydrated calcium chloride and activated charcoal prior to filling inside the glove box. Metal and alloy handling, which include cutting, grinding, surface cleaning, polishing, powder handling, weighing, etc. were carried out inside the glove box.

Metal / alloy ingots were stored by immersing in dry hexane while thorium powder compacts were stored inside argon-filled glass vials. All radioactive samples were stored inside a shielded lead (Pb) cask for minimization of radiation exposure (radiation dose rate  $< 0.1 \mu\text{Sv}\cdot\text{h}^{-1}$ ). For characterization and alloy preparation, uranium and thorium metals were surface cleaned using a diamond coated file under hexane immersion till silvery white lustre appeared. Surface cleaned metal pieces were polished using SiC abrasive paper (600 and 1000 grit) and diamond paste ( $\sim 250 \text{ nm}$  and  $1 \mu\text{m}$ ); ultrasonicated in dry hexane and vacuum-dried.

### **1.3.1.2. Thorium metal-pre-sintering**

For handling of metal powder compacts, a high vacuum sintering facility was set up during the course of this work. Fig. 2.2 shows the photograph of this facility. A one end closed re-crystallized alumina (RCA) sample tube ( $\sim 6 \text{ mm}$  wall thickness) with air-cooled vacuum flange (SS-316) was fabricated for sample heating. Using this flange, sample tube can be

connected to high vacuum system (Model: ED-6, M/s. Hind high vacuum Co. (Pvt.) Ltd., India) using threading arrangement and push-fit (Swagelok) unions. Vacuum system consists of a water-cooled oil diffusion pump (pumping speed =  $135 \text{ l.s}^{-1}$ ) coupled with liquid nitrogen trap and backed by a direct-drive rotary vane pump (pumping speed =  $100 \text{ l.min}^{-1}$ ; 1440 rpm). RCA tube is inserted into a platinum resistive tube furnace (Maximum operating temperature  $\sim 1523 \text{ K}$ ) whose temperature is monitored by S-type thermocouple and controlled with the help of PID controller and thyristor power unit.



**Fig. 2.2. Vacuum sintering furnace for metal powder compacts**

Thorium powder compacts were wrapped in tantalum foil ( $\sim 0.1 \text{ mm}$  thick) and kept inside a tantalum boat. Few pieces of natural uranium metal scrap were also kept in tantalum boat to act as preferential scavenger of air molecules released from RCA tube due to degassing at high temperatures. Using this setup, thorium metal powder compacts were pre-sintered up to  $1400 \text{ K}$  (dynamic vacuum  $\sim 5 \times 10^{-6} \text{ Torr}$ ). Marginal weight gain ( $\sim 0.03 \%$ ) was noted upon pre-sintering of thorium as  $\sim 20 \text{ g}$  scale. Pre-sintered thorium pellets were arc-melted to obtain dense metal ingots.

### 1.3.1.3. Metal cutting

Thorium and uranium metals and their alloys were cut into small pieces using a low-speed metal cutting machine (Model: Metacut DCM, M/s. Metatech Industries, India). Diamond impregnated circular blade mounted on a horizontal metallic shaft was used for cutting purpose. Metal / alloy to be cut are mounted on specimen holder and cutting position is adjusted with the help of micrometer screw attached to it. Specimen holder is lowered so that sample touches diamond cutting blade at marked location. Blade is rotated (100 -1000 RPM) resulting into uniform cutting of specimen. Blade surface is kept lubricated (with distilled water or machine oil) for removal and collection of powdered metal scrap in water/oil bath kept below the rotating blade. For cutting of hard materials like uranium-based alloys, additional load (100 g – 300 g) is applied over the sample holder to speed up cutting. Specimen and cutting blade remain enclosed with Perspex cover to ensure that cut metal pieces fall in lubricant bath when cutting is over. Cutting of uranium and as-cut Th-U alloys are shown in Fig. 2.3.



**Fig. 2.3. Metal cutting by diamond impregnated blade. Th-U alloys cut into small pieces**

### 1.3.1.4. Arc melting method

One of the major challenges in studying alloys based on thorium, uranium and zirconium is to prepare them in homogeneous phase without contamination, which can occur even with

traces of impurities ( $O_2$ ,  $N_2$ ,  $H_2O$ , etc.) present in the atmosphere used for their preparation (vacuum / argon / helium). Uranium and thorium do not dissolve appreciable amounts of oxygen or nitrogen and oxide / nitride phase is readily formed and remain as inclusions in as-prepared alloys. Zirconium dissolves up to  $\sim 40$  atom % oxygen and  $\sim 20$  atom % nitrogen and extreme care must be taken for melting zirconium-based alloys in oxygen free containers. A method that enables fast melting in controlled atmosphere is therefore desired. DC (direct current) arc melting method fulfils these requirements and was used for preparation of thorium and uranium-based metallic alloys.

In this method, reactants (metals, metalloids, alloys) are quickly heated to very high temperatures ( $> 2500$  K) over a span of few seconds. As a result, reactants undergo rapid melting and a homogeneous molten mass is formed. Rapid melting is achieved by DC arc generated between a cathode (usually made of thoriated tungsten in the form of sharp tipped rod) and a water cooled high thermal conductivity metallic anode (usually made of copper). Anode also serves as crucible / container in which melting is carried out. Fig. 2.4 shows the arc melting setup used for alloy preparation during the course of this work. Inset shows the copper cup (anode) used for melting the alloy and as-melted alloy in the shape of a button.



**Fig. 2.4. Photograph of Arc melting setup. Insets show copper anode cup (right frame) and as-melted alloy button (left frame)**

Arc is generated by applying high current-low voltage (~ 65 volts, 300-350 amperes) DC power between cathode (thoriated tungsten) and anode (copper). DC power is applied through multi-strand water cooled copper cables running from the output terminal of power supply to the electrodes of arc melting setup. These electrodes are separated from each other by electrically insulating, optically transparent and high temperature compatible (up to 1200 K) cylindrical quartz tube, which also enables viewing the sample during arc melting. Quartz tube is fixed to water cooled top and bottom plates (made of brass) in a leak-proof manner using neoprene / Viton o-rings. The most crucial component of arc melting setup is ball seal, which is a sphere-shaped leak-tight metallic seal attached to the top metallic plate. Thoriated tungsten cathode is connected to a metal rod (copper) that passes through this ball seal. The ball seal arrangement allows (i) linear motion of cathode, which enables arc generation when two electrodes come in close proximity and (ii) radial motion of cathode so that arc can be uniformly moved over the sample for uniform melting and phase homogenization. Sample to be melted is kept in cleaned copper cup (anode) and the cup is fixed into the bottom plate with O-ring seal. The setup is flushed with inert gas (high purity argon; 100 – 200 ml /min.) with gas inlet from the port available in bottom plate and outlet from the port available in top plate. This ensures that lighter air moves upwards and sample is covered with heavier argon gas. Cathode tip is kept away from the anode by moving the central rod upwards through the ball seal. After flushing argon for 15-20 minutes, water cooling of top and bottom plate, anode cup and DC power cables is enabled. It is essential to ensure inert atmosphere prior to cooling so that moisture inside the arc melting furnace can be minimized. Once water flow is ensured, power supply is activated and cathode tip is carefully lowered to approach the anode surface. Operator must wear welding view glasses during system operation. At close proximity of electrodes (few millimetres), potential gradient is large enough to generate spark, which is instantaneously followed by sustained arc. Cathode is slowly moved over the

sample surface (without touching the sample) so that the uniform melting takes place. In less than a minute (typically few seconds), sample melting is completed and a molten mass contained in copper anode is seen. Arc is uniformly moved over the molten sample to ensure homogenous mixing of constituent reactants. Once melting is completed, DC power is put off to stop the arc. Molten sample quickly solidifies in the form of button (or ingot) and total arc melting process is completed in less than a minute. Cooled sample button is inverted with the help of cathode tip and melting is repeated to obtain uniform distribution of constituents in as-melted alloy. An oxygen scavenger (zirconium metal) is usually melted prior to melting any sample so that oxide layer over the surface of anode cup is removed during zirconium melting and sample with minimum oxygen contamination is obtained. Melting zirconium prior to sample is quite useful for arc melting systems with provision of multiple anode cups so that one cup is used for zirconium melting while the other is charged with the sample. This enables removal of residual oxygen from the furnace environment during zirconium melting and improves the purity of actual alloy sample. For single anode setups, zirconium melting prior to alloy preparation can be avoided if anode surface is thoroughly polished with diamond impregnated cloth and cleaned by ultrasonication. This practice was adopted for alloy preparation during the course of work presented here. Prior to flushing the arc melting setup, argon gas was purified by passing over heated uranium trap ( $\sim 600$  K), which ensured removal of trace oxygen impurities from feed argon. This was confirmed by oxygen partial pressure in purified argon ( $P_{O_2} < 10^{-18}$  atmosphere) evaluated by EMF measurements using gadolinia doped ceria (GDC) oxide ion electrolyte at 1023 K. With all precautions, uranium and thorium-based metallic alloys ( $\sim 10$ -15 gram scale) were prepared with an average increase of  $< 0.03$  wt. %.

#### 1.3.1.4.1. Advantages of DC arc melting method

- Melting is completed in a very short time (typically less than a minute), which minimize sample contamination from impurities present in the cover gas or crucible material.
- Arc melting setup is simple and requires minimum maintenance in terms of routine electrical safety measures and checking of leak proof water and gas tubes.
- This method is suitable for preparation of metal-ceramic composites where metallic phase forms a continuous network in the molten phase.
- Melting can be carried out in oxidising or inert atmospheres and at low pressures (partial evacuation) provided that the arc is sustained through the short duration of operation.
- Since arc melted samples are fast cooled to ambient temperatures, high temperature phases may get quenched. Materials prepared by arc melting can therefore be used to study physico-chemical and structural properties of high temperature metastable phases.
- Method is suitable for preparation of small samples with negligible loss during melting (due to evaporation or sticking with sample crucible), which is an advantage for preparation of precious/rare metal alloys (based on Pt, Au, Rh, Ir, Pd, Ag, etc.).

#### 1.3.1.4.2. Limitations of DC arc melting method

- The method is most effective for small-scale sample preparation. Sample size is limited by the size of anode cup, design of cathode and DC power supply rating. In comparison, large samples can be prepared by vacuum induction melting technique.
- For multi-component alloys, where difference in melting temperature of constituent elements is large, arc melting may cause deviation from intended stoichiometry due to preferential vaporization loss of low melting (or highly vaporizing) constituents.
- Arc melting is not suitable for preparation of ceramics. Either melting temperatures of ceramics are difficult to achieve or arc may not sustain through ceramic phase.

- Care must be taken to ensure that neither the cathode touches the anode / sample nor it is unevenly moved over the melting mass. The former leads to termination of arc and contamination of sample while the later results into inhomogeneous alloy. However, these limitations can be overcome with experimental care.

### 1.3.1.5. Solution combustion method

Solution combustion method is among the most widely used synthesis routes for preparation of nanoscale materials; in particular oxide-based ceramics [127, 128]. However, metals [129], metallic alloys [130], and other class of ceramics such as nitrides / oxynitrides [131, 132], carbides / oxycarbides [133], sulphides / oxysulfides [134], etc. can also be synthesised by this route. It is a simple, scalable and novel method by which fine powders having large specific surface area and active surface / pore structure can be prepared. This method was used for synthesis of nanocrystalline ThO<sub>2</sub> powders studied during the present work, with specific emphasis to understand the mechanism of combustion process and study the sintering behaviour of ThO<sub>2</sub> compacts made from nanocrystalline powders.

The method consists of thermally activated, highly exothermic, redox mediated decomposition (combustion) of a viscous aqueous gel (also referred as combustion precursor). Gel is formed when suitable oxidant(s) (metal salts; preferably nitrates) and reducing agent(s) (referred as fuel; can be organic /inorganic compounds) are dissolved in water and excess solvent is evaporated ( $\leq 400$  K). When the viscous gel is further heated, it undergoes auto-ignition; typically over a temperature range from 400 K to 600 K, and rapidly decomposes into product phase. Decomposition of gel precursor is exothermic in nature and is accompanied with evolution large volume of gaseous by-products (such as H<sub>2</sub>O, N<sub>2</sub>, CO, CO<sub>2</sub>, SO<sub>2</sub>, etc.). Other gases such as NH<sub>3</sub>, NO<sub>x</sub>, HX (X = Halogen), may also evolve depending upon starting reagents as well as the manner in which combustion is carried out.

Precursor heating can be performed over a hot plate (planer heat source) or inside an electrical oven (three dimensional volume heating), which results into combustion occurring in the form of self-propagating self-sustained combustion wave (also known as gel combustion) or volume combustion with explosive reaction, respectively [122]. Another way to heat gel precursor is in a microwave field (uniform bulk heating), which also would affect the nature of combustion process. Manner in which gel precursor is heated, affects the properties of combustion product. Solution combustion synthesis is different from self-propagating high temperature synthesis (SHS) route where combustion is carried out in an all solid-state mixture of fuel and oxidant. Ideally, it is desired to perform combustion in such a way that fuel and oxidant are completely utilised during the reaction. However, in practice, as-combusted products may contain residual impurities in the form of incompletely utilised fuel and / or oxidant species. These impurities are usually removed by calcination / heat treatment of as-combusted products. As-combusted product could also be obtained as disordered or amorphous solid, particularly when either heat evolved during combustion is insufficient to cause rapid crystallization of product phase, or, when large excess of partially utilised fuel embeds poorly ordered particles of product phase. Calcination / heat treatment also helps in improving the crystallinity / structural order in such products. Ideally, for achieving compositional homogeneity of end-product obtained after combustion, transparent gel formation without any precipitation (or colloid formation) is required. Nature, chemical composition and solid-state structure of combustion product depend on synthesis parameters. Simple variations in reaction scheme can lead to wide variations in product quality, which is a unique attribute of solution combustion synthesis. Some of these variations include (1) choice of fuels (urea, amino acids, polyhydroxy carboxylic acids, carbohydrates, hydrazine derivatives, etc.), (2) use of one fuel or a mixture of fuels, (3) choice of oxidants (nitrates, nitrites, halides, acetates, etc.), (4) fuel to oxidant ratio, (5) atmosphere in which combustion

is carried out (inert, oxidising, reducing), (6) Material of construction (MoC) of combustion vessel (glass, steel, etc.), (7) pH of starting solution, etc. Combustion synthesis can also be used to prepare carbon-based nanomaterials by carrying out the combustion reaction of different carbon bearing fuels with ammonium nitrate as oxidant. Many review articles, exclusively dedicated to the subject of solution combustion synthesis [121, 122, 135] are a testimony to the usefulness of this simple synthesis route, which is being practiced by the global research fraternity. While combustion is thermally activated kinetic process, it is governed by the nature of chemical interactions among the constituent species (metal ions, nitrate ions, fuel molecules, solvent molecules, etc.) present in aqueous solution and the gel phase resulting from it. Principles of propellant chemistry for reaction between oxidant and fuel species present in aqueous solution / gel therefore play important role in defining the nature of combustion. Further, being a thermally activated process, it can be effectively studied by thermal methods of analysis.

Nanocrystalline  $\text{ThO}_2$  powders were synthesised by using two commonly available fuels namely glycine (an amino acid) and citric acid (hydroxy polycarboxylic acid). Thorium nitrate pentahydrate ( $\text{Th}(\text{NO}_3)_4 \cdot 5\text{H}_2\text{O}$ ) was used as the source of thorium and oxidant (nitrate ions). Fuel to oxidant ratio for stoichiometric combustion (Fuel to oxidant ratio = 1) was calculated by balancing the oxidizing and reducing valences of different elements (C: +4, H: +1, N: 0, O: -2, Th: +4) based on the oxidation states of various elements in their ideal product state (carbon as  $\text{CO}_2$ , hydrogen as  $\text{H}_2\text{O}$ , nitrogen as  $\text{N}_2$ , oxygen as  $\text{CO}_2$ ,  $\text{H}_2\text{O}$  and Th as  $\text{ThO}_2$ ). Fuel to oxidant ratio (F:O) was varied from 0.65 to 1.25. Aqueous solutions were prepared by dissolving fuel and oxidant in minimum volume of deionised water. Gels were obtained by removal of excess solvent either by mild heating over a water bath ( $\sim 373$  K) or by drying at ambient temperature in a moisture-free environment. Transformation of aqueous

gel precursor into nanocrystalline thoria was probed by thermal analysis using differential scanning calorimetry (DSC) and thermo gravimetric analysis (TGA). Combustion of aqueous gels was performed in glass containers (borosilicate glassware) inside a fume hood by heating the gel precursor over a hot plate. Due care was taken to avoid powder spillage or release of aerosol-induced air-borne particles during the combustion process. As-combusted powders were air calcined and used for detailed characterization and further studies. Specific experimental details of preparation of nanocrystalline thoria powders will be mentioned in the experimental section of chapter-6.

#### **1.3.1.5.1. Advantages of solution combustion synthesis**

While excellent review articles detail the attributes of solution combustion synthesis of nanoscale materials [121, 122, 135], the main advantages are point-wise mentioned below.

- It is a very simple, scalable, fast and energy efficient (occurring near ambient temperature) synthesis route.
- Commonly available and highly cost effective reactants are used.
- It is a highly versatile method with different choice of reactants as well as their stoichiometries.
- Multi-element compounds with excellent compositional homogeneity can be prepared.
- Materials with tailored microstructures can be prepared.
- Metastable and non-stoichiometric compounds can be prepared.
- Combustion synthesised powders usually have high sinterability at lower temperature.

#### **1.3.1.5.2. Limitations of solution combustion synthesis**

Some of the limitations / challenges associated with solution combustion synthesis are as follows:

- Very high temperatures are locally attained in the combusting precursor. This may cause local sintering of as-synthesized particles / grains and product obtained may consist of pre-sintered hard agglomerates.
- Some of the gaseous by-products which may form during combustion (such as CO, NH<sub>3</sub>, NO<sub>x</sub>, SO<sub>2</sub>, etc.) are toxic and therefore should be treated appropriately (oxidised or captured) prior to their release in atmosphere.
- Finding optimum fuel to oxidant ratio that is required for a clean combustion reaction to obtain the product with minimum residual impurities is challenging. Further, it may also change with process variables (nature of reactants, atmosphere, etc.) for same combustion product.
- During sintering, combustion synthesised powders may undergo rapid grains growth, which sometimes result into apparent loss in bulk density; also known as desintering. Desintering deteriorates mechanical strength of sintered ceramic.
- Being highly exothermic in nature, large-scale production of materials by combustion synthesis requires additional safety precautions.

### 1.3.2. Characterization techniques

Elemental analysis techniques (C, N, O determination), powder X-ray diffraction (PXRD), scanning electron microscopy (SEM), energy dispersive spectroscopy (EDS), Raman spectroscopy, Fourier transform infra-red spectroscopy (FT-IR), small angle X-ray scattering (SAXS), thermo-gravimetry (TGA), differential scanning calorimetry (DSC), thermo mechanical analysis (TMA), laser flash technique (LFA), etc. were used for characterisation and thermophysical properties evaluation of materials during the course of work. A brief summary of working principle and experimental details for each of these techniques is described in the following section.

### 1.3.2.1. Elemental (C, N, O) analysis

Non-metallic impurities such as carbon, nitrogen, oxygen, hydrogen, etc., which may be present in metals and alloys, may affect their physico-chemical properties. Their accurate estimation is therefore essential. Total carbon-content in metals (uranium and thorium) and their alloys studied during the present work was measured on an indigenously developed carbon analyzer [136]. Surface cleaned metal / alloy samples (~ 100-150 mg) were combusted at high temperature (~ 923 K) under O<sub>2</sub> gas flow and CO<sub>2</sub> gas produced from oxidation of carbon is quantitatively analyzed using an infra-red (IR) detector. The residue (oxides of thorium and uranium) were analyzed by energy dispersive spectroscopy to check if carbon is still present in the sample. Prior to each specimen, reference measurements were made with known volume of CO<sub>2</sub> gas (purity > 99.9%) injected in the flowing stream of oxygen (purity > 99.99%) to minimize the effect of instrumental drift. Overall performance of carbon-analyzer was checked by decomposing AR-grade calcium carbonate (CaCO<sub>3</sub>) under O<sub>2</sub> gas flow. Results obtained with calcium carbonate indicated ~ 5% accuracy (RSD) over the measurement range from ~10 ppm to 5 wt. %. RSD refers to relative standard deviation.

Oxygen and nitrogen contents in studied metals and alloys were simultaneously measured using a commercial O, N analyzer (Model: TC-300, M/s. LECO Corporation). Samples (~100-150 mg) wrapped in tin metal flux (used as heat booster) were kept inside graphite crucibles and combusted under high purity argon (> 99.99%) gas flow. Oxygen and nitrogen liberated as CO<sub>2</sub> and N<sub>2</sub> gases were quantitatively analyzed by infra-red (IR) detector and thermal conductivity detector (TCD), respectively. Calibration of N, O-analyzer was carried out using metallic standards, which indicated ~ 3% accuracy (RSD) over the measurement range from 2 ppm to 0.2 wt. % and 2 ppm to 0.5 wt. % for oxygen and nitrogen, respectively.

Each metal / alloy was measured in quintuplicate for elemental (C, O and N) determination and average values of these measurements are reported.

### 1.3.2.2. Powder X-ray diffraction technique (XRD)

For materials research, powder X-ray diffraction (XRD) is one of the most essential characterisation techniques. It provides information on (i) nature of solid (crystalline / amorphous), (ii) phase behaviour (single or multi-phase) and phase transformations, (iii) crystal structure (lattice type, unit cell parameters), (iv) texture (preferred orientation of atomic planes), (v) crystallite size (for solids composed of nano-sized grains) and structural strain (deviation from ideal crystal structure), (vi) solid solubility limits and structural behaviour of solid solutions, etc. [137, 138].

In this technique, a solid sample; usually taken in the form of fine powder, is exposed to a beam of monochromatic X-rays. X-rays have wavelengths of the same order as inter-atomic separation in solids (0.5 - 2 Å). Interaction of oscillating electric field of X-rays with atomic electrons in the sample leads to oscillation of electrons about their equilibrium position, which becomes a source of electromagnetic radiation having same frequency as that of the incident X-rays. This phenomenon is known as elastic scattering (or secondary emission) of X-rays, which has angular dependence with respect to the direction of incident X-ray beam for multi-electron elements. Scattered X-rays intensity is proportional to atomic number of scattering element. For crystalline solids, which are formed by long range periodic arrangement of atoms / ions, the structure can be visualised in the form of atoms arranged in parallel planes spaced at certain inter-planar spacing. X-rays scattered (reflected) from such parallel atomic planes interfere constructively whenever the path difference between the X-rays scattered from different atomic planes is an integral multiple of the incident X-ray

wavelength. This condition, which is necessary for constructive interference of specularly reflected X-rays to result into a diffracted X-ray beam is known as Bragg's law (equation-2.1).

$$n\lambda = 2 d_{(hkl)} \sin \theta_{(hkl)} \quad (2.1)$$

Here, 'n' is order of diffraction, 'λ' is wavelength of incident X-ray, 'd<sub>(hkl)</sub>' is inter-planer spacing between crystal planes having miller indices (h k l) and, 'θ<sub>(hkl)</sub>' is the Bragg angle (angle between the incident X-ray and atomic plane) corresponding to (h k l) set of planes.

For polycrystalline solids, which are composed of a large ensemble of small crystallites (few nm to several microns), sample is taken in the form of fine powder consisting of randomly oriented crystallites so that all crystal planes are exposed to incident X-rays at the same time. In case of a powder diffractometer, experiments are performed in two dimensions where incident X-rays, sample and X-ray detector are present in same plane. Sample and detector is rotated within this plane by different angles (for example sample by 'θ' and detector by '2θ', which is known as Bragg-Brentano geometry) while X-ray source is kept at fixed position. Whenever Bragg condition is satisfied for any set of (h k l) planes, diffracted X-rays are detected and a two dimensional plot between diffraction angle (2θ) (x-axis) and X-ray intensity (y-axis) is obtained, which is known as powder diffractogram (or powder XRD pattern). Powder diffractograms of crystalline materials show sharp diffraction peaks while that of amorphous materials show only broad hump(s); which contain information on short range structural order. A powder XRD pattern contains information on crystal structure, phase behaviour, crystallite size, structural strain, etc. Diffraction pattern is analyzed in terms of peak positions (2θ values), peak profile (peak shape, peak broadening), relative peak intensities, etc. Peak positions are compared with reported data to identify the phase. Least

square fitting analysis of peak positions gives information of type of lattice and values of lattice parameters. Ratio of peak intensities for different crystal planes in a powder diffraction pattern in comparison to the ratio expected for randomly oriented polycrystalline sample give information about the texture (preferred orientation of crystal planes). Peak broadening can be used to estimate (i) average crystallite size ( $t$ ) of nanocrystalline solids ( $< 100$  nm) and (ii) average lattice strain ( $\epsilon$ ). Scherrer formula (equation-2.2) or Williamson-Hall plot (equation-2.3) method can be used to determine the crystallite size and lattice strain.

$$t = 0.9\lambda/B.\cos(\theta) \quad (2.2)$$

$$B.\cos(\theta) = \epsilon.\sin(\theta) + k\lambda/t \quad (2.3)$$

$$\text{Where, } B = (B_{\text{sample}}^2 - B_{\text{instrument}}^2)^{1/2} \quad (2.4)$$

Here, ‘ $t$ ’ is average crystallite size ( $\text{\AA}$ ), ‘ $\lambda$ ’ is X-ray wavelength ( $\text{\AA}$ ), ‘ $B$ ’ is net peak broadening (FWHM) due to sample (radians), ‘ $\theta$ ’ is Bragg angle, ‘ $\epsilon$ ’ is the average lattice strain and ‘ $k$ ’ is a constant ( $k$  is assumed to be 0.9 in the present studies). Using Williamson-Hall Plot, effective crystallite size is evaluated from the intercept of linear fit obtained using equation-2.3 while average lattice strain ( $\epsilon$ ) can be estimated from the slope value.

An iterative fitting analysis of relative peak intensities along with peak positions in comparison to a postulated crystal structure is the subject of crystal structure refinement (also known as Rietveld refinement), which enables determination of closest possible match of sample’s crystal structure with postulated structure.

Structural analysis of materials studied during the present work was performed on a powder diffractometer (Model: Smart Lab, M/s Rigaku, Japan) operating at 1.2 kW power. Graphite

monochromated Cu-K $\alpha$  X-Rays ( $\lambda = 1.54186 \text{ \AA}$ ) were used to record diffractograms over  $10^\circ$ - $70^\circ$  with a step size of  $0.02^\circ$ . Diffractometer was calibrated using a silicon standard sample and XRD data were mostly collected over a period of 1h duration. For diffraction experiments, metallic samples were taken in the form of powders (obtained by filing the metal / alloy ingots under inert atmosphere) or polished pellets. Aqueous gels, used for synthesis of nanocrystalline thoria were spread over a glass slide and dried under ambient temperature inside a desiccator prior to the measurements. As-combusted powders were spread over a glass slide using methanol and the same was used for XRD experiments. Unit cell parameters were determined using least-square refinement fitting program. Average crystallite size and lattice strain were calculated using Scherrer formula (equation-2.2) and Williamson-Hall plot (equation-2.3).

### 1.3.2.3. Scanning electron microscopy (SEM)

Scanning electron microscopy is a powerful technique to probe surface morphology, topography and microstructural phase distribution of solids. The sample to be analyzed is placed under a focused and intense beam of high energy electrons (typically accelerated by  $\sim 20 \text{ kV}$  potential). Upon interaction of incident electron beam with sample, several different signals are generated in terms of secondary electrons, back scattered electrons, Auger electrons, characteristic X-rays (emitted from the elements present in the sample) and continuous X-rays (Bremsstrahlung radiation) apart from visible light emission and heat generation. With suitable detection tools, each of these signals can be collected and important information about the characteristics of samples can be obtained. When the incident electron beam scans over the sample surface, the various signals generated from the scanned area can be processed electronically to produce a two dimensional image of the sample surface, known as the electron micrograph image. Secondary electrons emanate out of the sample from very

thin layer (50 – 500 Å) below the surface. Yield of secondary electrons therefore is strongly dependent on its surface morphology. As a result of this, a secondary electron image (SEI) provides information on surface structure, phase morphology, grain boundaries, size and shape (of crystallites, particles and pores), nature of crystallites (dispersed / agglomerated), etc. On the other hand, back-scattered electrons emerge from relatively higher depth (~1-2 µm) below the sample surface and their yield is proportional to the atomic number of elements present in the sample. Back scattered electron image (BEI) therefore provides phase contrast information, which is very important for characterization of composite materials consisting of multiple phases. Combination of SEI and BEI images gives detailed information on phase distribution and morphology of analyzed material. SEM equipments can also be hyphenated with additional analytical tools such as Auger electron spectroscopy (AES), cathodoluminescence (CL) spectroscopy, etc. Using these hyphenated techniques, additional information on chemical state and optical properties of materials can also be obtained simultaneously.

In the present work, surface morphology of thorium and uranium-based materials were analyzed using a tungsten filament-based scanning electron microscope (SEM) (Model: AIS 2100, M/s. Seron Inc., Korea) operated at 20 kV acceleration voltage. Morphologies were analyzed in both secondary electron (SE) and backscattered electron (BE) image modes of operation using Everhart-Thornley detector and solid-state backscattered electron detector (Robinson), respectively. Electrically insulating samples were sputter-coated with gold to avoid surface charging.

#### 1.3.2.4. Energy dispersive X-ray spectroscopy (EDS)

Energy dispersive X-ray spectroscopy (EDS) is very useful elemental analysis technique; usually hyphenated with electron microscopes (SEMs, TEMs). It is based on X-ray fluorescence phenomenon. When high energy electron beam accelerated by applying a voltage (~5-20 kV) interacts with atoms present in the sample, inner shell electrons are ejected to create vacant shells. Radiative de-excitation of electrons from higher energy states to these vacant shells results into emission of characteristic X-rays, which can be detected using suitable X-ray detectors (Solid-state semiconductor detectors). Elemental identification and quantification is based on energy and intensity of emitted X-rays, respectively. Since intensity of characteristic X-rays is proportional to atomic number of elements, this technique is more sensitive for quantification of heavy elements. It is ideal to have flat sample surface for better results. In case of electrically insulating samples, conducting coating (gold) needs to be provided over the sample surface. Main advantages of EDS technique include fast measurements, minimum sample requirement, non-destructive nature of analysis, good sensitivity for most of the elements ( $Z > 11$ ), etc. Major limitations of this technique include poor sensitivity for quantification of lighter elements ( $Z \leq 11$ ) and interference of continuous X-rays (Bremsstrahlung radiation) with low energy X-rays peaks (particularly for low-Z elements).

In the present work, elemental analysis of thorium and uranium-based alloys and constituent metals was performed using an energy dispersive spectrometer (EDS) (Model: INCA E350, M/s. Oxford Instruments, UK), attached to SEM system discussed above. EDS spectra were recorded at 5-20 kV electron acceleration potential using liquid nitrogen cooled Li-doped Silicon (Si(Li)) solid-state semiconductor detector. For elemental quantification purpose, EDS system was calibrated by analyzing high purity electro-polished cobalt and the results

were found to match within  $\pm 4\%$ . For determination of relative concentration of carbon and oxygen in metallic alloys, EDS spectra were recorded at lower accelerating potential (5 kV) to minimize the background radiation.

### 1.3.2.5. Raman spectroscopy

Raman spectroscopy is very useful for structural characterization of solids [139]. In case of oxide ceramics, while X-ray diffraction is mainly sensitive to the metal sub-lattice, information of oxide sub-lattice is usually not obtained in detail. Raman spectroscopy on the other hand is quite sensitive to Metal – oxygen (M-O) vibrations and provides valuable information about the oxide sub-lattice in ceramic oxides. In this technique, a sample (preferably used in flat pellet form) is placed under a focused beam of monochromatic continuous (CW) laser light beam (UV, visible or NIR). When the laser beam (photons) interacts with sample, it may undergo absorption, reflection, transmission or scattering. Most of the scattered light ( $> 99\%$ ) has same frequency as that of the incident light beam. This is known as elastic scattering (or Mie scattering or Rayleigh scattering). However, a very small fraction of scattered light ( $\sim 1$  in  $10^6$  to  $10^8$  photons) has frequencies different from that of the incident light beam. This phenomenon is known as inelastic scattering or Raman scattering. The difference in frequency of Raman scattered light and incident light corresponds to difference in vibrational energy states of material (molecular vibrational states). The extremely lower probability of Raman scattering is the reason why intense laser light is required in Raman spectrometers. Use of laser light coupled with optical microscope assembly allows very high power densities over the sample to easily observe the Raman effect. Primary interaction of laser light brings the molecular system to high-energy states, which are referred as virtual states. The virtual states can be visualized in terms of change in the shape of electron density distribution (polarization) for a given molecular system. If the

frequency of scattered light is less than the incident light, it is known as Stokes Raman scattering while for the opposite case, i.e., when frequency of scattered light is more than the incident light, it is known as anti-Stokes Raman scattering. Stokes or anti-stokes lines originate when the transition leaves the molecule to a higher vibrational energy state than its original state, or to a lower vibrational energy state than its original, respectively. Stokes Raman scattering has higher intensity than anti-Stokes scattering, which is due to higher relative population of the lower vibrational energy states as compared to higher vibrational levels in a given molecular system. Most of the Raman spectrometers measure the Stokes Raman scattering. Raman scattered light contains the information about vibrational behavior of a solid. When the scattered light is dispersed using suitable grating and allowed to fall on sensitive detectors (typically Peltier cooled charge-coupled device (CCD) detectors are used), a Raman spectrum consisting of peaks due to vibrational motion of atoms or molecules as a function of wave number ( $\text{cm}^{-1}$ ) is obtained. Both Raman and infra-red (IR) spectroscopies probe the vibrational motions of atoms and molecules in materials. However, Raman effect is observed when there is a change in shape of electron density distribution due to vibrational motion. On the other hand, IR effect is observed when there is change in dipole moment of the molecular system due to vibrational motion. These two techniques are therefore complementary to each other and provide valuable structural information. An important advantage of Raman spectroscopy is its capability to probe the local structure in a material. Since intense beam of laser light focused with the help of suitable optics can be made to fall on micron (or sub-micron) sized regions of a sample, characterization of structure at grain level is possible, which is a limitation in the case of diffraction techniques, as it provides average structural information recorded on a large sample size.

In the present work, characterization of thoria-based ceramics has been carried out using Raman spectroscopic investigations on a micro-Raman spectrometer (Model: LabRAM HR, M/s. Horiba Jobin-Yvan, France) using 632.8 nm emission line of He-Ne gas laser (Maximum power output ~15 mW). Samples were taken in the form of pellets or polished alloys and laser light was focused over the sample surface using a long working distance optical microscope (Model: Olympus BX-40; 10X and 50 X magnifications). Light scattered from sample was collected in a backscattered geometry and Rayleigh scattered light was filtered with the help of edge filters. Only Raman scattered light along with luminescence radiation (if any) were allowed to reach the holographic grating (600 groves/mm, 1800 groves /mm) for light dispersion. Raman signal was collected on a Peltier cooled CCD detector. Each spectrum was recorded with 2 s scan duration and averaged over 50 repeated scans. Spectral resolution of the system was  $\pm 2 \text{ cm}^{-1}$ . Frequency calibration was carried out by measuring the Raman spectrum of high purity single crystal silicon ( $\sim 520 \text{ cm}^{-1}$ ) prior to each set of experiments.

#### **1.3.2.6. Fourier transform infra-red (FT-IR) spectroscopy**

Similar to Raman spectroscopy, FT-IR spectroscopy is very useful for structural and functional group characterization of materials by probing atomic / molecular vibrations. It is based on change in net dipole moment of a vibrating oscillator upon light absorption in infra-red region of electromagnetic spectrum. When a sample is exposed to infra-red light radiation, some of the radiation whose frequencies match with those of atomic / molecular vibrations is absorbed by the sample. Light transmitted from the sample therefore contains information of absorbed frequencies, which can be analyzed to identify various functional groups and specific atomic / molecular vibrations. Infra-red spectra can be recorded in absorption or transmission mode. Typical IR spectrum shows variation of % transmittance of

IR radiation as a function of wave number ( $\text{cm}^{-1}$ ). Spectrum is usually recorded over 200 to  $4000 \text{ cm}^{-1}$  since most organic and inorganic substances have their absorption spectra in this range. FT-IR spectrometers used for routine sample characterization operate in mid-IR region ( $5000\text{--}400 \text{ cm}^{-1}$ ) and utilize a heated silicon carbide ( $\sim 1200 \text{ K}$ ) IR source (also known as Globar source), which gives IR spectrum closely matching to a blackbody. Commonly, low band gap semiconductors such as HgCdTe are used for detecting the transmitted light.

In the present work, structural characterization of thorium-bearing aqueous gels and nanocrystalline thoria ceramics were carried out by FT-IR spectroscopic analysis performed on Bomem MB 102 infra-red spectrometer with deuterated triglycine sulphate (DTGS) as the detector. Samples were prepared in the form of thin semi-transparent pellets in pre-heated IR-grade KBr matrix (Sample: KBr weight ratio = 1: 100) using a hydraulic press with the help of tungsten carbide (WC) die-plunger. Background subtracted FT-IR spectra were recorded over  $200 - 4000 \text{ cm}^{-1}$  with  $\pm 2 \text{ cm}^{-1}$  spectral resolution.

#### 1.3.2.7. Small angle X-ray scattering (SAXS)

Small-angle X-ray scattering (SAXS) is a useful technique for structural characterization of nanomaterials, macromolecules and materials which show structural ordering at different length scales. It is therefore suitable for characterization of crystalline, semi-crystalline, amorphous and structurally disordered materials [140]. Bragg's law indicate that with decrease in scattering angle ( $\theta$ ), structural information from larger length scales ( $d \sim 1 - 100 \text{ nm}$ ) can be obtained since scattering angle is inversely related to the length scale of ordering in a material. In this technique, a sample (solid, powder, liquid, gel, dispersions, etc.) is exposed to a narrow and highly intense monochromatic X-ray beam and X-rays scattered with very small angles ( $0.1^\circ - 5^\circ$ ) are detected in transmission geometry. Intense and narrow X-ray source is required to measure weak scattering from the sample in immediate vicinity of

incident beam. Detectors with high spatial resolution are desirable for this purpose. For this reason, SAXS measurements can be best performed with intense X-ray beams obtained from synchrotron radiation source. Scattering profile is evaluated to estimate the size distribution of nanoparticles, shape and structure of particles, specific surface area, pore-size distribution, etc. Advantages of SAXS technique is that ease of measurement with minimal sample preparation. Similar to powder XRD, SAXS also probe bulk sample and provides structural information averaged over an ensemble of microscopic particles / molecules / structural moieties. SAXS is a complementary technique to XRD since the former probes the structure at larger length scales while the later does it at a scale of interatomic distances.

In present work, SAXS experiments were performed at ambient temperature on glycine-Th(IV)-nitrate aqueous gels, solid crystals obtained from these gels, and as-combusted nanocrystalline thoria powders. Measurements were performed on a Rigaku small-angle goniometer mounted on rotating anode X-ray generator. Scattered X-ray intensity 'I(q)' was recorded using a scintillation counter by varying the scattering angle '2θ' where 'q' is the scattering vector given by  $\{4\pi.\sin(\theta)/\lambda\}$  and 'λ' is the wavelength of X-rays (Cu-Kα). Measured intensities were corrected for sample absorption and smearing effects of collimating slits [141]. As-measured scattering profiles were evaluated with the help of different structural models for aqueous gels as well as nanocrystalline thoria powders to obtain information on nature of ordering in gels and crystallite size and size distribution in as-combusted powders.

#### **1.3.2.8. Thermo-gravimetry**

Thermo-gravimetry is very useful thermo-analytical technique to probe thermo-chemical behavior of a material, which is accompanied by weight change. In this technique, change in

the weight of a sample subjected to a programmed heating cycle is recorded. The technique is useful to probe variety of physico-chemical transformations such as decomposition, oxidation, reduction / hydrogenation, evaporation, condensation, hygroscopic moisture absorption, etc., provided that the process is accompanied with change in mass of the sample. In the present work, off-line thermo-gravimetry was used for probing the progress of solution combustion synthesis of nanocrystalline thoria powders. Aqueous gel samples prepared by heating the aqueous solutions of thorium nitrate and fuel at 373 K were used as starting material. These gel samples (~200 mg) were taken in small glass vials and heated in a tubular resistive furnace at pre-defined temperatures (at 10 K interval). Vials were removed from the furnace after 15 minutes soaking at each temperature and cooled inside a desiccator maintained at 5 % relative humidity, followed by weight measurement on high precision balance having 0.01 mg readability and 0.015 mg repeatability (model: XP-205, M/s. Mettler-Toledo GmBH, Switzerland). Based on weight change at different soak temperatures, off-line thermo-gravimetric curves were obtained.

#### **1.3.2.9. Differential scanning calorimetry (DSC)**

Differential scanning calorimetry (DSC) is a thermo-analytical technique used for measurement of enthalpy changes in a material that is subjected to programmed thermal cycle (heating / cooling / isothermal hold). In this technique, a sample and a reference material is placed in suitable containers (DSC pans) over a coupled temperature sensor (known as DSC sensor). DSC sensor is kept in a symmetric thermal environment, which is a fast heating / cooling furnace with thermal mass much higher than that of sample. Reference usually taken is an inert material (in the temperature range of investigation) or an empty DSC pan. Under thermal equilibrium, no net heat exchange occurs between the DSC sensor and furnace. Under non-equilibrium conditions, heat exchange is governed by temperature dependent

variation in specific heat of sample and reference. If reference pan is empty and identical to sample pan in terms of size, shape, mass, contact area with the DSC sensor and thermal coupling with furnace, then the heat (enthalpy) exchange is a measure of sample's specific heat. Any physico-chemical transformation that results into liberation (exothermic process) or absorption (endothermic process) of heat, results into variation in sample temperature ( $T_S$ ) while reference temperature ( $T_R$ ) closely follows the furnace temperature. Difference in sample and reference temperatures ( $\Delta T = T_S - T_R$ ) is measured by temperature sensors (thermocouples, thermopiles, etc.) placed at sample and reference position over the DSC sensor. If the equipment is configured to record this differential temperature signal ( $\Delta T$ ) as a function of reference temperature ( $T_R$ ) or furnace temperature ( $T_F$ ), the technique is called differential thermal analysis (DTA). On the other hand, if ' $\Delta T$ ' acts as a feedback signal to regulate the net heat flux in order to keep the differential temperature zero (close to zero) all the time, the technique is known as differential scanning calorimetry (DSC). Differential heat flux can be regulated by two methods. When, heat flux is regulated by thermal environment (furnace temperature regulation), which together heats the sample and reference, the configuration is known as heat flux DSC. Most of the commercial equipments are heat flux DSCs. Alternatively, sample and reference material are kept independently in small heat sources (furnaces) and this assembly is further enclosed with a uniform thermal environment (furnace). In this configuration, differential temperature ( $\Delta T$ ) is nullified by providing electrical power input to sample or reference furnace. This technique is known as power compensated DSC. Since electrical power can be more accurately measured as compared to differential heat flux derived from ' $\Delta T$ ' and thermal resistance ( $R_{th}$ ) of DSC sensor, power compensated DSC is more sensitive than heat flux DSC and provide better results, particularly highly accurate specific heat values. Detailed information on theory, instrumentation and data evaluation methods of DSC technique can be obtained from

monograph written by Honne et al., [142]. DSC is a very sensitive technique to study various thermal events such as melting / freezing, boiling (only to be performed on materials that do not contaminate DSC cell), glass transition, phase transitions, curing of polymers, crystallization kinetics, reaction kinetics, specific heat measurements, etc.

Uniform temperature programs (constant rate of heating, cooling and isotherms) are used in conventional heat flux DSC. A modified method of measurement is temperature modulated DSC [143], in which an oscillating temperature program is superimposed over a constant rate temperature program. Temperature oscillations can be obtained in terms of stepwise heating / cooling (e.g., square-wave), sinusoidal or random multi-frequency variations [144]. The system simultaneously measures the response to constant heating as well as periodic oscillations and the output heat flow behavior is composed of reversing and non-reversing components, which correspond to thermodynamic and kinetic response of the specimen, respectively. Examples of reversing transitions include specific heat variation, melting, glass transition while that of non-reversible transitions are enthalpy relaxation, decomposition, curing, crystallization, etc. Reversing and non-reversing components of heat flow can be resolved by Fourier transformation to separate the overlapping events and also to obtain frequency dependence of melting, glass transition, etc. An important application of modulated DSC is reliable measurement of specific heat of materials in a single experiment. On the other hand, similar measurements by conventional three step method require three different experiments performed under identical conditions.

In this work, a heat-flux DSC (Model: DSC 823<sup>c</sup>, M/s. Mettler-Toledo GmbH, Switzerland) was used for measurement of (i) isobaric specific heat ( $C_p$ ) of thorium-based metallic alloys and (ii) heat flow behavior of aqueous gels used for solution combustion synthesis of

nanocrystalline ThO<sub>2</sub>. DSC instrument was calibrated for temperature, heat flow and time constant using various standard materials (Hg, H<sub>2</sub>O, In, Sn, Pb and Zn). Results showed  $\pm 0.1\%$  temperature accuracy and  $\pm 1\%$  heat flow accuracy over a temperature range from 233 to 823 K. Reference sample was always taken as a sealed empty DSC pan (identical to sample pan) for all measurements. Specific heat measurements were performed in temperature modulated mode over 298 K to 773 K. Modulated temperature program with 2 K / min. underlying heating rate,  $\pm 0.1$  K modulation amplitude and 15-30 s pulse duration interval was used throughout the experiments. Modulated heat flow data was Fourier transformed to obtain reversing and non-reversing heat flow components. Temperature dependence of isobaric specific heat values was obtained using the multi-frequency modulation software package (TOPEM<sup>®</sup>) [144]. Specific heat measurements were performed by keeping the samples in hermitically sealed aluminum crucibles (40  $\mu$ l capacity) under flowing argon atmosphere ( $\sim 60$  ml/min.). Performance of DSC for specific heat ( $C_p$ ) measurements was checked using NIST Sapphire standard reference material (SRM) and results were found within  $\pm 4\%$  of the recommended  $C_p$  values. Heat flow measurements on thorium-bearing aqueous gels were carried out in aluminum / platinum / sapphire crucibles under inert (Argon;  $\sim 60$  ml/min.) as well as oxidizing (O<sub>2</sub>;  $\sim 60$  ml/min.) atmospheres. Heating rate was generally kept at 10 K/min. for most of the heat flow experiments.

#### **1.3.2.10. Thermo mechanical analysis (TMA)**

Thermo mechanical analysis (TMA) is a useful technique to study linear dilation behavior of solids subjected to programmed heating. From linear dilation data, information about solid's bulk thermal expansion behavior, 1<sup>st</sup> order structural phase transitions, glass transition, sintering kinetics, oxidation kinetics, etc. can be obtained. For example, coefficient of linear

thermal expansion (CTE) for a solid can be calculated from temperature dependent linear dilation characteristics as follows:

True coefficient of linear thermal expansion:

$$\alpha_{\text{true}} = \lim_{\Delta T \rightarrow 0} \frac{1}{L_0} \left( \frac{\partial L}{\partial T} \right) \quad (2.5)$$

Average coefficient of linear thermal expansion:

$$[\alpha_{\text{average}}]_{T_1}^{T_2} = \frac{1}{L_0} \left( \frac{\Delta L}{\Delta T} \right), \Delta T = (T_2 - T_1) \quad (2.6)$$

Here, ' $\alpha_{\text{true}}$ ' is instantaneous CTE, ' $\alpha_{\text{average}}$ ', is average CTE, ' $L_0$ ' is sample length at 298 K, ' $(\partial L/\partial T)$ ' is rate of dilation, ' $\Delta L = (L_{T_2} - L_{T_1})$ ' is net dilation in temperature interval  $\Delta T$ .

Similarly, volume expansion coefficient ( $\beta = 1/V_0 \cdot (\partial V/\partial T)$ ) of a solid can also be evaluated using TMA. It can be done either by directly measuring the volume expansion on powders (using volumetric sample holders) or measuring the linear thermal expansion of single crystal solid along three crystallographic axes. For polycrystalline solids consisting of randomly oriented grains, volume expansion coefficient is estimated from linear thermal expansion coefficient using simple relation ( $\beta = 3\alpha$ ). When linear dilation is measured without any external load over the sample, technique is known as dilatometry [145]. On the other hand, when dilation is measured with a pre-defined load over the sample, it is known as thermo mechanical analysis (TMA). The equipment consists of a dilation sensor (linear variable differential transformer (LVDT)), a push-rod that is connected to LVDT at one end and touches the sample surface at the other end and a stable platform over which sample is

placed. Entire assembly is housed in a high temperature furnace with suitable temperature regulation. When sample dimension changes along the push rod direction, a differential voltage signal, which is proportional to the extent of dilation, is generated as LVDT output. This is continuously recorded as a function of time / temperature by suitable electronics. As-measured signal comprises of contributions from dilation of sample, sample holder and push-rod. Sample dilation is calculated by subtracting equipment's baseline behavior (blank) from as-measured dilation using suitable algorithm [145]. Dilatometry and high temperature X-ray diffraction (HT-XRD) are complementary techniques to study thermal expansion behavior of solids. The former probes dimensional changes on bulk scale while the later studies variation in crystal's unit cell parameters as a function of temperature. Apart from thermal expansion, results obtained from both the techniques can be used to estimate defect concentration in solids. TMA is very useful for characterization of nuclear materials (fuel, clad, structural materials, etc.) to understand their deformation behavior as a function of temperature, composition and microstructure.

In present work, TMA technique has been used to evaluate (i) linear thermal expansion behavior of thorium and uranium-based metallic alloys, and (ii) sintering behavior of nanocrystalline thoria compacts using a commercial thermo mechanical analyzer (Model: SETSYS TMA 1600, M/s. Setaram Instrumentation, France). For measurement of thermal expansion, cylindrical samples (diameter ~6 mm; thickness ~4 - 8 mm) were prepared and loaded inside TMA in sandwich configuration between two high density (~96% theoretical density) ThO<sub>2</sub> pellets (diameter ~8 mm, thickness ~3 mm). ThO<sub>2</sub> pellets were used to prevent chemical interaction of metals / alloys with alumina (Al<sub>2</sub>O<sub>3</sub>) sample support and pushrod during the experiments. Linear dilation was measured from 298 K up to 1373 K in both, heating (10 K / min.) and cooling (20 K / min.) cycle under high purity argon gas flow (~100

ml/min.). Argon gas was purified over heated uranium metal turnings (~623 K) prior to use. For thermal expansion studies on U/Th-based alloys, a blank run (298 - 1473 K) under identical conditions was recorded prior to each experiment to maximize the degassing of TMA's ceramic components in heated zone under flowing inert atmosphere. This helped in measurement of reliable expansion data with minimum surface oxidation of alloys. Expansion behavior of ThO<sub>2</sub>-ThO<sub>2</sub> couple was measured and net dilation due to metal/alloy was calculated by subtracting the baseline corrected dilation of ThO<sub>2</sub>-ThO<sub>2</sub> couple from that of ThO<sub>2</sub>-sample-ThO<sub>2</sub> stack. Quality of expansion data was assessed by (i) monitoring the difference in LVDT signal (LVDT<sub>Start</sub> - LVDT<sub>Stop</sub>) during a complete thermal cycle and (ii) measuring the change in sample weight after the experiment. Here, 'LVDT<sub>Start</sub>' and 'LVDT<sub>Stop</sub>' are dilation readings at the start of heating cycle and at the end of cooling cycle, respectively. Performance of TMA was analyzed by measuring the linear thermal expansion of NIST sapphire SRM. Results obtained were within ± 2% of the recommended values. Sintering behavior of nanocrystalline thoria compacts was investigated using TMA. Linear shrinkage curves were recorded by heating the green pellets from 308 K to 1773 K (heating rate = 10 K/minute) followed by isothermal heating at 1773 K for 1 h. Cooling up to 473 K was controlled (20 K/min.) followed by furnace cooling up to ambient temperature. Load over the sample was kept ~1 g to measure true shrinkage behavior. All sintering experiments were performed under high purity helium atmosphere (> 99.99%, flow rate = ~60 ml/min.). Sintered pellets were weighed to calculate the weight change during sintering. Densities of all the samples were evaluated from measured sample weight and geometric volume.

#### **1.3.2.11. Laser flash technique**

Laser flash technique is the most popular method for measurement of thermal diffusivity and specific heat of solids over a wide range of temperature (150 K to 3073 K). It is called flash

technique since a radiation pulse (infra-red laser) is flashed over one of the surface of a sample and temperature response at the opposite surface is recorded as a function of time. Flash method was pioneered by Parker et al., in 1961 [146], wherein two parallel surfaces of a flat sample (cylindrical pellet or square disc) are coated with optically absorbing material like colloidal graphite such that the coating thickness ( $t$ ) is very small as compared to distance ( $L$ ) between two parallel surfaces of the sample (sample thickness). A radiation pulse (Energy =  $Q$ ) obtained from infra-red laser ( $\sim 1064 \mu\text{m}$ ; Nd-YAG / Nd-Glass laser) falls over one of the flat surfaces (front surface) of sample kept under adiabatic environment. It is assumed that pulse energy is readily absorbed in a thin layer ( $x$ ) of sample, which is small compared to sample thickness ( $x \ll L$ ). Colloidal graphite coating facilitates efficient energy absorption. The heat absorbed diffuses through the sample from the thin layer ( $x$ ). It is also assumed that for a thin sample ( $L \sim 1\text{-}3 \text{ mm}$ ), heat diffusion in small time scale ( $< 5 \text{ s}$ ) is predominantly uniaxial in the central region of the sample and is perpendicular to the sample surface. Due to diffusion of heat energy, average temperature at the opposite surface (rear surface) of the sample increases with time until the pulse energy is uniformly distributed throughout the sample. A schematic diagram of flash method and typical temperature response curve of the sample surface with time is shown in Fig. 2.5.

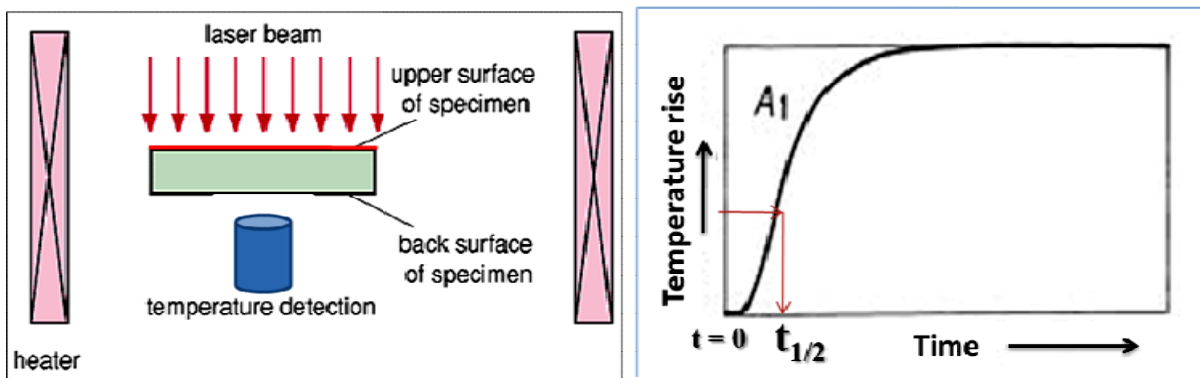


**Fig. 2.5. Schematic of laser flash experiment and typical time dependent rear surface temperature profile of the sample**

Starting time ( $t = 0$ ) corresponds to firing of laser pulse over the sample surface. Laser pulse is significantly short ( $< 1$  ms) as compared to time required for rise of rear surface temperature to a new equilibrium. The shape of this time-temperature curve (measured as voltage-time curve) contains the information related to sample's thermal diffusivity at a certain temperature 'T'. Based on the analytical solution of one dimensional heat flow equation as proposed by Carslaw et al., [147], thermal diffusivity (D) is calculated by following equations (equation-2.7 or equation-2.8):

$$D = 1.38L^2 / \pi^2 \cdot t_{1/2} \quad (2.7)$$

$$D = 0.48L^2 / \pi^2 \cdot t_x \quad (2.8)$$

Here, 'D' is thermal diffusivity, 'L' is sample thickness, ' $t_{1/2}$ ' is time required for rear surface to reach half the maximum rise in temperature and ' $t_x$ ' is time-axis intercept of the time versus temperature curve. It can be seen that measurement of thermal diffusivity is not dependent on the amount of energy absorbed (Q) in the thin layer (x) of sample, which provides experimental flexibility in terms of variable laser power as well as pulse duration. As a result of this, flash method is very useful for thermal diffusivity measurements on a variety of materials. For high diffusivity materials (metals, carbides, diamond, etc.), very short laser pulse (0.3 ms) and lower laser power is sufficient. On the other hand, higher laser power and longer pulses (up to 1 ms) are needed for measurements on highly insulating samples (porous refractory materials, foams, ceramics, etc.). Sample thickness (L), which is included in equation-2.7, is proportional to thermal diffusivity of sample. Thicker samples (~4-5 mm) are therefore preferred for high diffusivity materials (metals, alloys) while thin samples (~1 mm) are ideal for thermally insulating samples (ceramics, foams, etc.). In modern flash equipments, depending on nature of rear surface time-temperature response

curve, dynamic optimization of experimental variables such as laser power, pulse duration, etc. is possible during the experiment. Detectors used are liquid nitrogen cooled (or Peltier cooled) infra-red detectors (InSb, CdTe, etc.) that monitor the intensity of thermal radiation emitted from the rear surface as a function of time. Detector parameters such as exposure area of In-Sb crystal, amplifier gain, data acquisition period, etc. can also be dynamically optimised during an experiment. When measurements are performed on samples equilibrated at different temperatures, temperature dependent thermal diffusivity data can be obtained.

While laser pulse energy ( $Q$ ) is not included in diffusivity calculation (equation-2.7), it can affect the physico-chemical properties of the sample, particularly the thin layer in which pulse energy is absorbed. Laser power therefore cannot be increased arbitrarily. Care must be taken so that incident laser pulse does not ablate the front surface or partially melt it, which would not only damage the sample, but also affect the quality of measurements.

Specific heat measurements by flash method are based on estimation of energy absorbed by the sample ( $Q$ ) under thermal isolation and resulting temperature rise ( $\Delta T$ ) of the rear surface. It is assumed that net rise in rear surface temperature is due to complete absorption of heat pulse ( $Q$ ) within the sample. Specific heat ( $C_p$ ) is evaluated by dividing  $Q$  with  $\Delta T$ . For estimation of  $Q$ , measurements are performed with a sample and a reference under identical experimental conditions. Reference material should be a closest possible match to the sample in terms of nature of reference material and its physico-chemical properties. Thermal diffusivity of reference is measured followed by sample. Since specific heat of reference is known and it is assumed that same amount of heat energy is absorbed by both under identical experimental conditions, rear surface temperature rise (detector signal) of reference and sample can be compared and specific heat can be evaluated using equation-2.9.

$$C_{P-(\text{Sample})} / C_{P-(\text{Reference})} = \Delta T_{(\text{reference})} / \Delta T_{(\text{Sample})} \quad (2.9)$$

Specific heat measurement is an important advantage of laser flash technique. However, care must be taken to measure both, sample and reference under identical conditions. Availability of suitable reference is another challenge. Best possible results on materials with known specific heat indicate up to ~10% deviation from recommended  $C_p$  values. For thermal conductivity measurements, flash technique is an indirect method. Thermal conductivity ( $\lambda$ ) is related to thermal diffusivity ( $D$ ), density ( $\rho$ ) and specific heat ( $C_p$ ) ( $\lambda = D \cdot \rho \cdot C_p$ ). Out of the three properties, two can be measured by flash technique itself and temperature dependence of density for isotropic polycrystalline materials can be evaluated from bulk thermal expansion. Error associated with each measurement contributes to total error associated with thermal conductivity data.

In the present work, thermal diffusivity of thorium and uranium-based metallic alloys was measured using a laser flash apparatus (Model: LFA 427, M/s. Netzsch Geratebau GmbH, Germany). Small samples (~12.5 mm diameter; ~ 4.5 mm thickness) were prepared by machining the metal/alloy ingots and polished to obtain flat discs with circular surfaces. A thin coating of colloidal graphite was sprayed over both circular surfaces. These pellets were loaded inside LFA system using yttria-coated sample holder and measurements were carried out under dynamic vacuum ( $P \leq 2 \times 10^{-6}$  mbar). Heat pulse was provided over sample's front surface by pulsed Nd-YAG laser (maximum 40 J/pulse, pulse duration ~0.4 ms) and time dependent temperature response of sample's rear surface was recorded by liquid nitrogen cooled InSb infra-red detector. Diffusivity values were evaluated by fitting the detector response curve using suitable correction method. Diffusivity was measured over 298 K to 1273 K at 50 - 100 K interval. Four measurements were made at each temperature and data

from acceptable shots were averaged to obtain diffusivity values. Performance of LFA system was checked with Inconel-600 standard reference material (SRM) and results were found within  $\pm 3\%$  of recommended values.

Results obtained on materials studied in the present work using above mentioned experimental techniques are presented in the subsequent chapters of this thesis.

## References:

- [1] C. Degueudre, M.J. Joyce, “Evidence and uncertainty for uranium and thorium abundance: a review”, *Prog. Nucl. Energy* 124 (2020) 103299.
- [2] L.S. Keith, O.M. Faroon, B.A. Fowler, “Uranium (book chapter); handbook on the toxicology of metals: fourth edition (Eds: G.F. Nordberg, B.A. Fowler, M. Nordberg)”, Elsevier (2015) 1307-1345 (DOI: <https://doi.org/10.1016/C2011-0-07884-5>).
- [3] G. Sadagopan, K.S.V. Nambi, G. Venkataraman, V.K. Shukla, S. Kayasth, “Estimation of thorium in gas mantles to ascertain regulatory compliance”, *Radiat. Prot. Dosim.* 71(1) (1997) 53-56.
- [4] T.E. Leontis, “Properties of magnesium-thorium and magnesium-thorium-cerium alloys”, *J. Min. Metals Mater. Soc.* 4 (3) (1952) 287-294.
- [5] R.A. Glenner, P. Willey, P.S. Sledzik, E.P. Junger, “Dental fillings in civil war skulls: What do they tell us?”, *J. Am. Dent. Assoc.* 127(11) (1996) 1671-1677.
- [6] O. Hahn, F. Strassmann, “Über den nachweis und das verhalten der bei der bestrahlung des urans mittels neutronen entstehenden erdalkalimetalle (English translation: Concerning the existence of alkaline earth metals resulting from neutron irradiation of uranium)”, *Die Naturwissenschaften* 27 (1939) 11-15.
- [7] “The first reactor” The US department of energy report: DOE/NE-0046 (1982) 1-40 (Web-link: <https://www.energy.gov/ne/downloads/first-reactor>).
- [8] R.L. Crowther, “Use of thorium in boiling water reactors”, *J. Nucl. Energy AB* 16(4) (1962) 181-194.
- [9] J.R. Dietrich, “The physics of advanced reactors”, *Brit. J. Appl. Phys.* 7(S5) 302 (1956) S9-S23.
- [10] H.N. Sethna, “India’s atomic energy program: past and future”, *International Atomic Energy Agency (IAEA) Bulletin* 21 (5) (1979) 2-11.

## References

- [11] S. Banerjee, H.P. Gupta, “The evolution of the Indian nuclear power programme”, Prog. Nucl. Energy 101 (2017) 4-18.
- [12] International Atomic Energy Agency “Thorium fuel cycles - potential benefits and challenges”, IAEA-TECDOC-1450, IAEA, Vienna (2005) 1-105.
- [13] P.K. Wattal, “Back end of Indian nuclear fuel cycle - A road to sustainability”, Prog. Nucl. Energy 101 (2017) 133-145.
- [14] R. Natarajan, “Reprocessing of spent nuclear fuel in India: Present challenges and future programme”, Prog. Nucl. Energy 101 (2017) 118-132.
- [15] S.A. Ansari, P. Pathak, P.K. Mohapatra, V.K. Manchanda, “Aqueous partitioning of minor actinides by different processes” Sep. Purif. Rev. 40(1) (2011) 43-76.
- [16] M. Salvatores, “Nuclear fuel cycle strategies including partitioning and transmutation”, Nucl. Eng. Des. 235(7) (2005) 805-816.
- [17] Press Information Bureau, Government of India, “Setting up of ten indigenous nuclear power reactors” (Web-link: <http://pib.nic.in>)
- [18] S.C. Chetal, P. Chellapandi, P. Puthiyavinayagam, S. Raghupathy, V. Balasubramanian, P. Selvaraj, P. Mohanakrishnan, B. Raj, “Current status of fast reactors and future plans in India” Energy. Proced. 7 (2011) 64-73.
- [19] P. Puthiyavinayagam, P. Selvaraj, V. Balasubramanian, S. Raghupathy, K. Velusamy, K. Devan, B.K. Nashine, G.P. Kumar, K.V.S. Kumar, S. Varatharajan, P. Mohanakrishnan, G. Srinivasan, A.K. Bhaduri, “Development of fast breeder reactor technology in India”, Prog. Nucl. Energy 101 (Part A) (2017) 19-42.
- [20] Bharatiya Nabhikiya Vidyut Nigam Limited, Department of Atomic Energy “Present status of 500 MWe Prototype Fast Breeder Reactor (PFBR)”, (Web-link: <http://www.bhavini.nic.in>).

## References

- [21] P. Rodriguez, C.V. Sundaram, "Nuclear and materials aspects of the thorium fuel cycle", *J. Nucl. Mater.* 100 (1981) 227-249.
- [22] R. Ramanna, S.M. Lee, "The thorium cycle for fast breeder reactors", *Pramana* 27(1-2) (1986) 129-137.
- [23] R. Chidambaram, C. Ganguly, "Plutonium and thorium in the Indian nuclear programme", *Curr. Sci. India* 70(1) (1996) 21-35.
- [24] P.K. Vijayan, V. Shivakumar, S. Basu, R.K. Sinha, "Role of thorium in the Indian nuclear power programme", *Prog. Nucl. Energy* 101 (2017) 43-52.
- [25] "Thoria-based nuclear fuels: thermophysical and thermodynamic properties, fabrication, reprocessing, and waste management", (Eds.: D. Das, S.R. Bharadwaj) Springer (2013) (DOI: 10.1007/978-1-4471-5589-8).
- [26] "Thorium-energy for the future", (Eds.: A.K. Nayak, B.R. Sehgal), Springer (2019) (DOI: 10.1007/978-981-13-2658-5).
- [27] S. Mukherji, B.K. Mohan, P.D. Krishnani, V. Jagannathan, S. Ganesan, "Thorium irradiation in Indian PHWRs - applications and limitations of origin code", *Proceedings of First National Conference in Nuclear Reactor Technology* (2002) (Web-link: [https://inis.iaea.org/search/search.aspx?orig\\_q=RN:34011468](https://inis.iaea.org/search/search.aspx?orig_q=RN:34011468)).
- [28] M. Das, "Design and irradiated experience with thorium based fuels in PHWRs" *Annual International Conference - Canadian Nuclear Association* (1992) 10.1-10.
- [29] P.S. Dhimi, J.S. Yadav, K. Agarwal, "Power reactor thoria reprocessing facility (PRTRF), Trombay", *Proceedings of the Theme Meeting on the Journey of BARC Safety Council for Strengthening Safety Culture in BARC Facilities* (Eds: V.M. Jolly) (2017) (Web-link: [https://inis.iaea.org/search/search.aspx?orig\\_q=RN:48089837](https://inis.iaea.org/search/search.aspx?orig_q=RN:48089837)).
- [30] R.K. Sinha, A. Kakodkar, "Design and development of the AHWR - the Indian thorium fuelled innovative nuclear reactor" *Nucl. Eng. Des.* 236 (7-8) (2006) 683-700.

- [31] R. Sinha, A. Kakodkar, "India's passive breeder", Nucl. Eng. Int. 55(668) (2010) 30-31.
- [32] A. Kakodkar, "Evolution of nuclear reactor containments in India: Addressing the present day challenges", Nucl. Eng. Des. 269 (2014) 3-22.
- [33] S. Sengupta, S.B. Chafle, S. Mammen, K. Sasidharan, V.K. Raina, "Critical facility for AHWR and PHWRs", Proceedings of International Conference on Peaceful uses of Atomic Energy (2009). V. 1. **[33a]** C. Ronchi, J.-P. Hiernaut, Experimental measurement of pre-melting and melting of thorium dioxide, J. Alloys Comp. 240 (1-2) (1996) 179-185. **[33b]** R. Böhler, A. Quaini, L. Capriotti, P. Cakir, O. Beneš, K. Boboridis, A. Guiot, L. Luzzi, R.J.M. Konings, D. Manara, "The solidification behavior of the UO<sub>2</sub>-ThO<sub>2</sub> system in a laser heating study" J. Alloys. Comp. 616 (2014) 5-13.
- [34] D. Greneche, W.J. Szymczak, J.M. Buchheit, M. Delpech, A. Vasile, H. Golfier, "Rethinking the thorium fuel cycle: An industrial point of view", Proceedings of ICAPP (Nice, France), (2007) Paper-7367. **[34a]** S.F. Ashley, G.T. Park, W.J. Nuttall, C. Boxall, R.W. Grimes, "Thorium fuel has risks", Nature 492 (2012) 31-33.
- [35] D. Jain, V. Sudarsan, A.K. Tyagi, "Thorium-based metallic alloys as nuclear fuels: Present status, potential advantages and challenges", SMC Bulletin (Society for Materials Chemistry, India) 4 (1) (2013) pp. 27-40 (Web-link: <https://www.smcindia.org/smc-bulletin.php>).
- [36] P.K. Vijayan, A. Basak, I.V. Dulera, K.K. Vaze, S. Basu, "Conceptual design of Indian molten salt breeder reactor", Pramana - J. Phys. 85 (2015) 539-554.
- [37] T. Yamamoto, H. Suwarno, H. Kayano, M. Yamawaki, "Development of new reactor fuel materials: Hydrogen absorption properties of U-Th, U-Th-Zr and U-Th-Ti-Zr alloys", J. Nucl. Sci. Tech. 32(3) (1995) 260-262.

## References

- [38] K.A. Terrani, G.W.C. Silva, C.B. Yeamans, “Fabrication and characterization of uranium thorium zirconium hydride fuels”, *Trans. Am. Nucl. Soc.* 98 (2008) 1060-1061.
- [39] S.M. McDeavitt, T.J. Downar, A.A. Solomon, S.T. Revankar, M.C. Hash, A.S. Hebden, “Thoria-based cermet nuclear fuel: Cermet fabrication and behavior estimates”, *Proc. Int. Conf. Nucl. Eng. (ICONE 4)* (2002) 59-67.
- [40] C. Lombardi, L. Luzzi, E. Padovani, F. Vettrano, “Thoria and inert matrix fuels for a sustainable nuclear power”, *Prog. Nucl. Energy* 50(8) (2008) 944-953.
- [41] J. Spino, H.S. Cruz, R. Jovani-Abril, R. Birtcher, C. Ferrero, “Bulk-nanocrystalline oxide nuclear fuels - An innovative material option for increasing fission gas retention, plasticity and radiation-tolerance”, *J. Nucl. Mater.* 422 (1-3) (2012) 27-44.
- [42] H. György, S. Czifrus, “The utilization of thorium in generation IV reactors”, *Prog. Nucl. Energy* 93 (2016) 306-317.
- [43] D. Heuer, E. Merle-Lucotte, M. Allibert, M. Brovchenko, V. Ghetta, P. Rubiolo, “Towards the thorium fuel cycle with molten salt fast reactors”, *Ann. Nucl. Energy* 64 (2014) 421-429.
- [44] G.L. Hofman, L.C. Walters, T.H. Bauer, “Metallic fast reactor fuels”, *Prog. Nucl. Energy* 31(1-2) (1997) 83-110.
- [45] W.J. Carmack, D.L. Porter, Y.I. Chang, S.L. Hayes, M.K. Meyer, D.E. Burkes, C.B. Lee, T. Mizuno, F. Delage, J. Somers, “Metallic fuels for advanced reactors”, *J. Nucl. Mater.* 392 (2) (2009) 139-150.
- [46] Idaho National Laboratory, “Experimental breeder reactor-I (EBR-I) (Web-link: <https://inl.gov/experimental-breeder-reactor-i/>).
- [47] L.C. Walters, “Thirty years of fuels and materials information from EBR-II”, *J. Nucl. Mater.* 270(1) (1999) 39-48.

## References

- [48] K. D. Weaver, J. Gilleland, C. Whitmer, G. Zimmerman, “High burn-up fuels for fast reactors: past experience and novel applications”, International Congress on Advances in Nuclear Power Plants (ICAPP 2009) (2009) 795.
- [49] G. Locatelli, M. Mancini, N. Todeschini, “Generation IV nuclear reactors: Current status and future prospects”, *Energ. Policy* 61 (2013) 1503-1520.
- [50] Z.S. Takibaev, “Fast homogeneous nuclear reactor”, *Atom. Energy* 100 (2006) 154-156.
- [51] T. Jayakumar, M.D. Mathew, K. Laha, R. Sandhya, “Materials development for fast reactor applications”, *Nucl. Eng. Des.* 265 (2013) 1175-1180.
- [52] A. Riyas, P. Mohanakrishnan, “Studies on physics parameters of metal (U-Pu-Zr) fuelled FBR cores”, *Ann. Nucl. Energy* 35(1) (2008) 87-92.
- [53] P. Chellapandi, V. Balasubramaniyan, P. Puthiyavinayagam, R. Sundararajan, M. Kanakkil, P. Selvaraj, P.R. Vasudeva Rao, “Design of 500 MWe metal fuel demonstration fast reactor”, *Proc. Int. Conf. Nucl. Eng.* (2014) (DOI: <https://doi.org/10.1115/ICONE22-30727>).
- [54] Indira Gandhi Centre for Atomic Research, “Fast Breeder Test Reactor”, (Web-link: <http://www.igcar.gov.in/rfg/fbtrhist.html>).
- [55] B. Blumenthal, J.E. Sanecki, D.E. Busch, D.R. O’Boyle, “Thorium-uranium-plutonium alloys as potential fast power reactor fuels; part-II: Properties and irradiation behavior of thorium-uranium-plutonium alloys”, ANL-7259, Argonne National laboratory, Illinois (October 1969).
- [56] S.Z. Ghayeb, “Investigations of thorium-based fuels to improve actinide burning rate in S-PRISM reactor”, M.Sc. Thesis, The Pennsylvania State University (2008) (Web-link: <https://etda.libraries.psu.edu/catalog/9160>).

## References

- [57] R.G. Wymer, D.A. Douglas Jr., “Status and progress report for thorium fuel cycle development for period ending December 31, 1964”, Report no.: ORNL-3831, Oak Ridge National laboratory, Tennessee (May 1966).
- [58] “Fast spectrum reactors”, (Eds.: A.E. Waltar, D. Todd, P.V. Tsvetkov) Springer (2011) (ISBN 978-1-4419-9572-8).
- [59] D.E. Peterson, “The (Th-U) Thorium-uranium system”, Bull. Alloy Phase Diagr. 6 (5) (1985) 443-445.
- [60] S. Peterson, R.E. Adams, D.A. Douglas Jr., “Properties of thorium, its alloys and its compounds”, Report no.: ORNL-TM-1144, Oak Ridge National laboratory, Tennessee (June 1965).
- [61] D.R. Marr, D.A. Cantley, J.C. Chandler, D.C. McCurry, R.P. Omberg, “Performance of thorium fuelled fast breeders”, Report no.: HEDL-SA-1327-FP, Hanford Engineering Development Laboratory, Richland, USA (October 1977).
- [62] G.L. Copeland, “Evaluation of thorium-uranium alloys for the unclad metal breeder reactor”, Report no.: ORNL-4557, Oak Ridge National Laboratory, Tennessee (June 1970).
- [63] B. Blumenthal, J.E. Sanecki, D.E. Busch, “Thorium-uranium-plutonium alloys as potential fast power reactor fuels; part-I: Thorium-uranium-plutonium phase diagram”, Report no.: ANL-7258, Argonne National Laboratory, Illinois (September 1968).
- [64] C.S. Holden, “Rapid computational path for sustainable and renewable nuclear energy using metallic thorium fuels”, Proceedings of 2<sup>nd</sup> Thorium energy conference (ThEC-2010), Mountain View CA (2010).
- [65] R.M. Carroll, “The effects of reactor irradiation on thorium-uranium alloy fuel plates”, Report no.: ORNL-1938, Oak Ridge National Laboratory, Tennessee (August 1955).

## References

- [66] B.R. Hayward, P. Corzine, "Thorium uranium fuel elements for SRE", Proc. 2<sup>nd</sup> UN Int. Conf. Peaceful uses of Atom. Energy, Geneva (October 1958).
- [67] J.L. Ballif, B.R. Hayward, J.W. Walter, "Engineering evaluation of a mixed alloy fuel element irradiated at elevated temperatures in SRE", Technical report no.: NAA-SR-3888, Atomics International Division, North American Aviation Incorporation, California, USA (June 1960).
- [68] A.R. Olsen, "Thorium and thorium alloys: Preliminary corrosion tests", Report no.: ORNL-1066, Oak Ridge National Laboratory, Tennessee (November 1951).
- [69] M.S. Farkas, A.A. Bauer, R.F. Dickerson, "Development of thorium-uranium-base fuel alloys," Report no.: BMI-1428, Battelle Memorial Institute, Columbus, Ohio (March 1960).
- [70] R.H. Cole, L.E. Wilkinson, "Development of high strength ternary and quaternary thorium-uranium base alloys", Technical report no.: ATL-A-128, Advanced Technology Laboratory, California (1961).
- [71] J.H. Kittel, J.A. Horak, W.F. Murphy, S.H. Paine, "Effect of irradiation on thorium and thorium-uranium alloys", Technical report no.: ANL-5674, Argonne National laboratory, Illinois, USA (April 1963).
- [72] A.L. Bement, "Burn-up and specific power calculations for the thermal neutron irradiation on thorium-uranium alloys", Technical report no: HW-56631, General Electric Co. Hanford Atomic Products Operation, Richland, Washington (1958).
- [73] F.W. Dodge, E.W. Murbach, L.A. Hanson, "Low decontamination reprocessing of thorium-uranium alloys by induction drip melting", Nucl. Sci. Eng. 6 (6) (1959) 533-536.
- [74] P. Chiotti, A.F. Voigt, "Pyrometallurgical processing", Technical report: A/CONF.15/P/517; ISC-1018, Ames Laboratory, Iowa (October 1958).

- [75] W.N. Hensen, "Electrolysis of thorium and uranium", US-Patent no.: US 2951793 (1960).
- [76] S. Jiang, K. Liu, Y. Liu, T. Yin, Z. Chai, W. Shi, "Electrochemical behavior of Th(IV) on the bismuth electrode in LiCl–KCl eutectic", *J. Nucl. Mater.* 523 (2019) 268-275.
- [77] G.B. Zorzoli, "Use of metallic thorium for LWBRs and LWRs", *Nucl. Tech.* 20 (1973) 109-113.
- [78] F. Correa, D.J. Driscoll, D.D. Lanning, "An evaluation of tight pitch PWR cores", technical report no.: MIT-EL-79-022, Massachusetts Institute of Technology, Cambridge, Massachusetts (1979).
- [79] Z.S. Li, X.J. Liu, C.P. Wang, "Thermodynamic modelling of the Th-U, Th-Zr and Th-U-Zr systems", *J. Alloy Compd.* 473 (2009) 193-198.
- [80] S.Z. Ghrayeb, K.N. Ivanov, S.H. Levine, E.P. Loewen, "Burn-up performance of sodium-cooled fast reactors utilizing thorium-based fuels", *Nucl. Tech.* 176 (2011) 188-194.
- [81] T. Okawa, H. Sekimoto, S. Nakayama, "Design study on power flattening to sodium cooled large scale CANDLE burning reactor with using thorium fuel", *Proc. 18<sup>th</sup> Int. Conf. Nucl. Eng., ICON18, China, (2010).*
- [82] M.T. Simnad, "The U-ZrH<sub>x</sub> alloy: Its properties and use in TRIGA fuel", *Nucl. Engg. Des.* 64 (1981) 403-422.
- [83] K. Konashi, B.A. Pudjanto, T. Terai, M. Yamawaki, "Thermodynamic stability of ThZr<sub>2</sub>H<sub>x</sub> at high temperature", *J. Phys. Chem. Solids* 66 (2–4) (2005) 625-628.
- [84] T. Yamamoto, H. Suwarno, F. Ono, H. Kayano, M. Yamawaki, "Preparation, analysis and irradiation of hydride Th-U-Zr alloy samples for a new fuel", *J. Alloy Compd.* 271-273 (1998) 702-706.

- [85] S. Das, R. Kumar, S.B. Roy, A.K. Suri, "Development study on metallic thorium and uranium-thorium alloy", BARC Newsletter-Founder's Day Special issue (2011) 72-76.
- [86] S. Das, R. Kumar, S. Kaity, S. Neogy, K.N. Hareendran, S.B. Roy, G.K. Dey, B.S.S. Daniel, G.P. Chaudhari, "Characterization of microstructural, mechanical and thermal properties and ageing study of Th-3 wt.% U alloy" Nucl. Eng. Des. 282 (2015) 116-125.
- [87] S. Das, S. Kaity, R. Kumar, J. Banerjee, S.B. Roy, G.P. Chaudhari, B.S.S. Daniel, "Characterization of microstructural, mechanical and thermophysical properties of Th-52 U alloy", J. Nucl. Mater. 480 (2016) 223-234.
- [88] S. Das, S.B. Roy, G.P. Chaudhari, B.S.S. Daniel, "Microstructural evolution of as-cast Th-U alloys", Prog. Nucl. Energy 88 (2016) 285-296.
- [89] R. Kumar, S. Das, S.B. Roy, R. Agarwal, J. Banerjee, S.K. Satpati, "Effect of Mo addition on the microstructural evolution and  $\gamma$ -U stability in Th-U alloys", J. Nucl. Mater. 539 (2020) 152317.
- [90] S. Vaidyanathan, "Thorium utilization in pressurized water reactors using bimetallic thorium-zirconium alloy cladding", Nucl. Tech. (2020) (DOI: <https://doi.org/10.1080/00295450.2019.1706377>).
- [91] D. Escorcia-Ortiz, J. François, C. Martín-del-Campo, "Comparative study of the neutronic performance of thorium-based metallic fuel and MOX fuel in an ASTRID-like fast reactor core", Nucl. Eng. Des. 347 (2019) 122-131.
- [92] J.K. Startt, C.S. Deo, "First principles study of the structure and elastic properties of thorium metal", MRS Adv. 1 (35) (2016) 2447-2452.
- [93] A. Karahan, J. Buongiorno, "A new code for predicting the thermo-mechanical and irradiation behavior of metallic fuels in sodium fast reactors", J. Nucl. Mater. 396 (2010) 283-293.

## References

- [94] K. Lassmann, "TRANSURANUS: a fuel rod analysis code ready for use", *J. Nucl. Mater.* 188 (1992) 295-302.
- [95] J.P. Hamond, "Physical, mechanical and irradiation properties of thorium and thorium alloys", ORNL-4218, Oak Ridge National Laboratory, USA (1968) 29-30.
- [96] J.K. Fink, M.G. Chasanov, L. Leibowitz, "Thermophysical properties of thorium and uranium systems for use in reactor safety analysis", Report no.: ANL-CEN-RSD-77-1, Argonne National Laboratory (1977) 11-12.
- [97] M. Lung, "A present review of the thorium nuclear fuel cycles", European commission report no.: EUR-17771-EN, (1997).
- [98] S. Kolay, S. Phapale, R. Dawar, M. Jafar, S. N. Achary, A. K. Tyagi, R. Mishra, M. Basu, "Phase characterization and thermal study of SrF<sub>2</sub> and NdF<sub>3</sub> doped fluoride salt containing 78 mol % LiF - 20 mol % ThF<sub>4</sub> - 2 mol % UF<sub>4</sub>", *J. Radioanal. Nucl. Chem.* 314 (2) (2017) 1267-1271.
- [99] M. Verwerft, B. Boer, "Thorium oxide nuclear fuels", *Comprehensive nuclear materials* (Second edition) 5 (2020) 139-168 (DOI: <https://doi.org/10.1016/B978-0-12-803581-8.11770-9>).
- [100] S. Usha, R.R. Ramanarayanan, P. Mohanakrishnan, R.P. Kapoor, "Research reactor KAMINI", *Nucl. Eng. Des.* 236 (7-8) (2006) 872-880.
- [101] T.K. Mukherjee, "Processing of Indian monazite for the recovery of thorium and uranium values", *Proceedings of International Conference on Characterisation and Quality Control of Nuclear Fuels* (Eds.: C. Ganguly, R.N. Jayaraj) Allied Publishers Pvt. Ltd. (2002) 187-195.
- [102] J.R. Johnson, C.E. Curtis, "Note on sintering of ThO<sub>2</sub>", *J. Am. Ceram. Soc.* 37(12) (1954) 611.

## References

- [103] T.R.G. Kutty, K.B. Khan, P.V. Hegde, J. Banerjee, A.K. Sengupta, S. Majumdar, H.S. Kamath, "Development of a master sintering curve for ThO<sub>2</sub>", *J. Nucl. Mater.* 327(2-3) (2004) 211-219.
- [104] P. Balakrishna, B.P. Varma, T.S. Krishnan, T.R.R. Mohan, P. Ramakrishnan, "Thorium oxide: Calcination, compaction and sintering", *J. Nucl. Mater.* 160(1) (1988) 88-94.
- [105] N. Clavier, R. Podor, L. Deliere, J. Ravoux, N. Dacheux, "Combining in situ HT-ESEM observations and dilatometry: An original and fast way to the sintering map of ThO<sub>2</sub>", *Mater. Chem. Phys.* 137(3) (2013) 742-749.
- [106] K. Ananthasivan, S. Balakrishnan, S. Anthonysamy, R. Divakar, E. Mohandas, V. Ganesan, "Synthesis and sintering of nanocrystalline thoria doped with CaO and MgO derived through oxalate-deagglomeration", *J. Nucl. Mater.* 434 (1-3) (2013) 223-229.
- [107] G.P. Halbfinger, M. Kolodney, "Activated Sintering of ThO<sub>2</sub> and ThO<sub>2</sub>-Y<sub>2</sub>O<sub>3</sub> with NiO", *J. Am. Ceram. Soc.* 55(10) (1972) 519-524.
- [108] A. Baena, T. Cardinaels, J. Vleugels, K. Binnemans, M. Verwerft, "Activated sintering of ThO<sub>2</sub> with Al<sub>2</sub>O<sub>3</sub> under reducing and oxidizing conditions", *J. Nucl. Mater.* 470 (2016) 34-43.
- [109] K. Ananthasivan, S. Anthonysamy, C. Sudha, A.L.E. Terrance, P.R. Vasudeva Rao, "Thoria doped with cations of group VB-synthesis and sintering", *J. Nucl. Mater.* 300(2-3) (2002) 217-229.
- [110] T.R.G. Kutty, P.V. Hegde, K.B. Khan, T. Jarvis, A.K. Sengupta, S. Majumdar, H.S. Kamath, "Characterization and densification studies on ThO<sub>2</sub>-UO<sub>2</sub> pellets derived from ThO<sub>2</sub> and U<sub>3</sub>O<sub>8</sub> powders", *J. Nucl. Mater.* 335 (3) (2004) 462-470.
- [111] V. Tyrpekl, M. Cologna, D. Robba, J. Somers, "Sintering behaviour of nanocrystalline ThO<sub>2</sub> powder using spark plasma sintering", *J. Eur. Ceram. Soc.* 36(3) (2016) 767-772.

- [112] W. Straka, S. Amoah, J. Schwartz, “Densification of thoria through flash sintering”, *MRS Commun.* 7(3) (2017) 677-682.
- [113] D. Sanjay Kumar, K. Ananthasivan, R.V. Krishnan, S. Amirthapandian, A. Dasgupta, “Studies on the synthesis of nanocrystalline  $Y_2O_3$  and  $ThO_2$  through volume combustion and their sintering”, *J. Nucl. Mater.* 479 (2016) 585-592.
- [114] R.D. Purohit, S. Saha, A.K. Tyagi, “Nanocrystalline thoria powders via glycine-nitrate combustion” *J. Nucl. Mater.* 288 (1) (2001) 7-10. [114a] F. Cappia, D. Hudry, E. Courtois, A. Janßen, L. Luzzi, R.J.M. Konings, D. Manara, High-temperature and melting behavior of nanocrystalline refractory compounds: an experimental approach applied to thorium dioxide, *Mater. Res. Express* 1 (2014) 0250341-12.
- [115] J. Spino, K. Vennix, M. Coquerelle, “Detailed characterisation of the rim microstructure in PWR fuels in the burn-up range 40–67 GWd/tM”, *J. Nucl. Mater.* 231 (3) (1996) 179-190.
- [116] L. Bonato, M. Viot, X. Le Goff, P. Moisy, S.I. Nikitenko, “Sonochemical dissolution of nanoscale  $ThO_2$  and partial conversion into a thorium peroxo sulphate”, *Ultrason. Sonochem.* 69 (2020) 105235.
- [117] S. Dash, A. Singh, P.K. Ajikumar, H. Subramanian, M. Rajalakshmi, A.K. Tyagi, A.K. Arora, S.V. Narasimhan, B. Raj, “Synthesis and characterization of nanocrystalline thoria obtained from thermally decomposed thorium carbonate”, *J. Nucl. Mater.* 303 (2–3) (2002) 156-168.
- [118] S. Dash, R. Krishnan, M. Kamruddin, A.K. Tyagi, B. Raj, “Temperature programmed decomposition of thorium oxalate hexahydrate”, *J. Nucl. Mater.* 295(2-3) (2001) 281-289.

## References

- [119] S. Dash, M. Kamruddin, P.K. Ajikumar, A.K. Tyagi, B. Raj, S. Bera, S.V. Narasimhan, “Temperature programmed decomposition of thorium nitrate pentahydrate”, *J. Nucl. Mater.* 278 (2–3) (2000) 173-185.
- [120] T.V. Plakhova, A.Y. Romanchuk, D.V. Likhosherstova, A.E. Baranchikov, P.V. Dorovatovskii, R.D. Svetogorov, T.B. Shatalova, T.B. Egorova, A.L. Trigub, K.O. Kvashnina, V.K. Ivanov, S.N. Kalmykov, “Size effects in nanocrystalline thoria”, *J. Phys. Chem. C* 123 (37) (2019) 23167-23176. [120a] D. Hudry, C. Apostolidis, O. Walter, T. Gouder, E. Courtois, C. Kübel, D. Meyer, Controlled Synthesis of Thorium and Uranium Oxide Nanocrystals, *Chem. Eur. J.*, 19 (2013) 5297-5305.
- [121] F. Deganello, A.K. Tyagi, “Solution combustion synthesis, energy and environment: Best parameters for better materials”, *Prog. Cryst. Growth Char.* 64 (2018) 23-61.
- [122] A. Varma, A.S. Mukasyan, A.S. Rogachev, K.V. Manukyan, “Solution combustion synthesis of nanoscale materials”, *Chem. Rev.* 116 (2016) 14493-14586.
- [123] V. Chandramouli, S. Anthonysamy, P.R. Vasudeva Rao, “Combustion synthesis of thoria - A feasibility study”, *J. Nucl. Mater.* 265(3) (1999) 255-261.
- [124] S. Anthonysamy, K. Ananthasivan, V. Chandramouli, I. Kaliappan, P.R. Vasudeva Rao, “Combustion synthesis of urania-thoria solid solutions”, *J. Nucl. Mater.* 278(2) (2000) 346-357.
- [125] D. Sanjay Kumar, K. Ananthasivan, S. Amirthapandian, A. Dasgupta, G. Jogeswara Rao, “Citrate gel-combustion synthesis and sintering of nanocrystalline ThO<sub>2</sub> powders”, *J. Nucl. Mater.* 497 (2017) 16-29.
- [126] R.D. Purohit, S. Saha, A.K. Tyagi, “Combustion synthesis of 5 and 10 mol% YO<sub>1.5</sub> doped ThO<sub>2</sub> powders”, *J. Nucl. Mater.* 323 (1) (2003) 36-40.

- [127] K.C. Patil, M.S. Hegde, T. Rattan, S.T. Aruna, "Chemistry of nanocrystalline oxide materials combustion synthesis, properties and applications", World Scientific Publications (2008) (DOI: <https://doi.org/10.1142/6754>).
- [128] F.-T Li, J. Ran, M. Jaroniec, S.Z. Qiao, "Solution combustion synthesis of metal oxide nanomaterials for energy storage and conversion", *Nanoscale* 7(42) (2015) 17590-17610.
- [129] A. Kumar, E.E. Wolf, A.S. Mukasyan, "Solution combustion synthesis of metal nanopowders: nickel-reaction pathways", *AIChE J.* 57(8) (2011) 2207-2214.
- [130] A. Kumar, E.E. Wolf, A.S. Mukasyan, "Solution combustion synthesis of metal nanopowders: Copper and copper / nickel alloys", *AIChE J.* 57(12) (2011) 3473-3479.
- [131] S. Zhang, Z.A. Munir, "The combustion synthesis of refractory nitrides: Part II the synthesis of niobium nitride", *J. Mater. Sci.* 26 (1991) 3380–3385.
- [132] "Nitride ceramics: Combustion synthesis, properties, and applications", (Eds.: A.A. Gromov, L.N. Chukhlomina) Wiley-VCH Verlag GmbH (2015) (DOI:10.1002/9783527684533).
- [133] H.V. Kirakosyan, K.T. Nazaretyan, R.A. Mnatsakanyan, S.V. Aydinyan, S.L. Kharatyan, "Solution combustion synthesis of nanostructured molybdenum carbide", *J. Nanopart. Res.* 20 (2018) 214.
- [134] N.A. Marand, S.M. Masoudpanah, M. Sh. Bafghi, "Solution combustion synthesis of nickel sulfide composite powders", *Ceram. Int.* 44 (14) (2018) 17277-17282.
- [135] K. Rajeshwar, N.R. De Tacconi, "Solution combustion synthesis of oxide semiconductors for solar energy conversion and environmental remediation", *Chem. Soc. Rev.* 38 (7) (2009) 1984-1998.

- [136] K.C. Thomas, J.R. Kale, R.G. Dalavi, K. Venkatesh, R. Kameswaran, A.V.R. Reddy  
"Development of an IR-based carbon analyser for uranium metal", BARC Newsletter  
311 (2009) 2-6 (Web-link: <http://barc.gov.in/publications/nl/2009/200912.pdf/>)
- [137] B.D. Cullity, "Elements of X-ray diffraction", Addison-Wesley Publishing Company  
Inc. (1956).
- [138] R. Tilley, "Crystals and crystal structures", John Wiley & Sons, Ltd. (2006) (ISBN-13  
978-0-470-01820-0).
- [139] E. Smith, G. Dent, "Modern Raman spectroscopy - A practical approach", John Wiley  
& Sons, Ltd. (2006) (ISBN 0-471-49794-0).
- [140] M. Roessle, D.I. Svergun, "Small angle X-ray scattering", In "Encyclopaedia of  
biophysics" (Eds.: G.C.K. Roberts) Springer, Berlin, Heidelberg (2013) (DOI:  
[https://doi.org/10.1007/978-3-642-16712-6\\_284](https://doi.org/10.1007/978-3-642-16712-6_284)).
- [141] P.W. Schmidt, R. Height, "Slit height corrections in small angle X-ray scattering", Acta  
Crystallogr. 13 (1960) 480-483.
- [142] G. Höhne, W.F. Hemminger, H.J. Flammersheim, "Differential scanning calorimetry",  
Springer-Verlag. (2003) (ISBN 978-3-540-00467-7).
- [143] M. Reading, A. Luget, R. Wilson, "Modulated differential scanning calorimetry",  
Thermochim. Acta 238(C) (1994) 295-307.
- [144] J.E.K. Schawe, T. Hutter, C. Heitz, I. Alig, D. Lellinger, "Stochastic temperature  
modulation: A new technique in temperature-modulated DSC", Thermochim. Acta 446  
(2006) 147-155.
- [145] N. Manoj, D. Jain, J.K. Gautam, K.C. Thomas, V. Sudarsan, C.G.S. Pillai, R.K. Vatsa,  
A.K. Tyagi, "A simple, reliable and cost-effective, high temperature dilatometer for  
bulk thermal expansion studies on solids", Measurement 92 (2016) 318-325.

- [146] W.J. Parker, R.J. Jenkins, C.P. Butler, G.L. Abbott, “Flash method of determining thermal diffusivity, heat capacity, and thermal conductivity”, *J. Appl. Phys.* 32 (1961) 1679-1684.
- [147] H.S. Carslaw, J.C. Jaeger, “Conduction of heat in solids”, 2nd edition, Oxford University Press, New York, (1959).
- [148] D. Jain, D. Das, B.N. Jagatap, “Thorium-based fuels for advanced nuclear reactors: Thermophysical, thermochemical and thermodynamic properties”, in A.K. Nayak, B.R. Sehgal (Eds.), *Thorium—Energy for the Future*, Springer (2019) (ISBN 978-981-13-2658-5) 257-275.
- [149] Y.S. Touloukian, R.W. Powell, C.Y. Ho, P.G. Klemens, “Thermophysical properties of matter - The TPRC data series. Volume 1. Thermal conductivity - metallic elements and alloys”, (1970) 429-440; 381-384.
- [150] Y.S. Touloukian, R.W. Powell, C.Y. Ho, M.C. Nicolaou, “Thermophysical properties of matter - The TPRC data series. Volume 10. Thermal diffusivity”, (1974) 205-208.
- [151] Y.S. Touloukian, E.H. Buyco, “Thermophysical properties of matter - The TPRC data series. Volume 4. Specific heat - metallic elements and alloys”, (1971) 268-270.
- [152] Y.S. Touloukian, R.K. Kirby, R.E. Taylor, P.D. Desai, “Thermophysical properties of matter - The TPRC data series. Volume 12. Thermal expansion metallic elements and alloys”, (1975) 365-372.
- [153] H.G. Schettler, J.J. Martin, F.A. Schmidt, G.C. Danielson, “Thermal conductivity of high purity thorium”, *Phys. Rev.* 187 (3) (1969) 801-804.
- [154] T.A. Sandenaw, “Thermal conductivity of uranium: Effects of purity and microstructure”, Report no.: LA-6092-MS, United States (1975) 1-8.
- [155] Y. Takahashi, M. Yamawaki, K. Yamamoto, “Thermophysical properties of uranium-zirconium alloys”, *J. Nucl. Mater.* 154 (1988) 141-144.

## References

- [156] R.W. Logan, D.H. Wood, "Thermal expansion of rolled and extruded uranium", *J. Less-Common Met.* 90 (1983) 233-241.
- [157] J. Nakamura, Y. Takahashi, S. Izumi, M. Kanno, "Heat capacity of metallic uranium and thorium from 80 to 1000 K", *J. Nucl. Mater.* 88 (1980) 64-72.
- [158] M. Boivineau, H. Colin, J.M. Vermeulen, Th. Thévenin, "Thermophysical properties of solid and liquid thorium", *Int. J. Thermophys.* 17(5) (1996) 1001-1010.
- [159] S. Zhou, R. Jacobs, W. Xie, E. Tea, C. Hin, D. Morgan, "Combined ab-initio and empirical model of the thermal conductivity of uranium, uranium-zirconium, and uranium-molybdenum", *Phys. Rev. Mater.* 2 (2018) 083401-1-21.
- [160] Y. Li, A. Chernatynskiy, J.R. Kennedy, S.B. Sinnott, S.R. Phillpot, Lattice expansion by intrinsic defects in uranium by molecular dynamics simulation, *J. Nucl. Mater.* 475 (2016) 6-18.
- [161] K.D. Joshi, S.C. Gupta, S. Banerjee, "Ab-initio theoretical analysis of thermal expansivity, thermal vibrations and melting of thorium", *Phil. Mag.* 88 (27) (2008) 3145-3152.
- [162] S. Jaroszewicz, H.O. Mosca, J.E. Garcés, "The temperature behaviour of the elastic and thermodynamic properties of fcc thorium", *J. Nucl. Mater.* 429(1-3) (2012) 136-142.
- [163] L. Kývala, D. Legut, "Lattice dynamics and thermal properties of thorium metal and thorium monocarbide" *Phys. Rev. B* 101 (2020) 075117.
- [164] P.L. Vijay, J.C. Sehra, C.V. Sundaram, K.R. Gurumurthy, R.V. Raghavan, "Studies on the preparation of thorium metal sponge from thorium oxalate", *BARC Report no.:* 969 (1978) 1-11.
- [165] M.D. Smith, R.W.K. Honeycombe, "The effect of oxygen, carbon and nitrogen on the properties of sintered thorium", *J. Nucl. Mater.* 4 (1959) 345-355.

- [166] Inorganic Crystal Structure Database (ICSD FIZ Karlsruhe GmbH, Version 4.4.0 (2020); collection code: 653236); from: J. Bohet, W. Müller, “Preparation and structure studies of “Van Arkel” protactinium”, *J. Less-Common Met.* 57 (2) (1978) 185-1995.
- [167] International Centre for Diffraction Data (ICDD Database; JCPDF card no.: 720659).
- [168] Inorganic Crystal Structure Database (ICSD FIZ Karlsruhe GmbH, Version 4.4.0 (2020) collection code: 253564) from: V.K. Tripathi, R. Nagarajan, “Sol–gel synthesis of high-purity actinide oxide ThO<sub>2</sub> and its solid solutions with technologically important tin and zinc ions” *Inorg. Chem.* 55 (24) (2016) 12798-12806.
- [169] Inorganic Crystal Structure Database (ICSD FIZ Karlsruhe GmbH, Version 4.4.0 (2020) collection code: 35204); from: S.A. Barrett, A.J. Jacobson, B.C. Tofield, B.E.F. Fender, “The preparation and structure of barium uranium oxide BaUO<sub>3+x</sub>”, *Acta Crystallogr. B* 38 (1982) 2775-2781. [169a] S. Ellison, A. Williams, Eurachem / CITAC guide: Quantifying Uncertainty in Analytical Measurement (2012) ISBN 978-0-948926-30-3 (Web-link: [www.eurachem.org](http://www.eurachem.org)).
- [170] Inorganic Crystal Structure Database (ICSD FIZ Karlsruhe GmbH, Version 4.4.0 (2020) collection code: 24223); from: R.E. Rundle, N.C. Baenziger, A.S. Wilson, R.A. McDonald, “The structures of the carbides, nitrides and oxides of uranium”, *J. Am. Chem. Soc.* 70 (1948) 99-105.
- [171] Inorganic Crystal Structure Database (ICSD FIZ Karlsruhe GmbH, Version 4.4.0 (2020) collection code: 26476); from: A.E. Austin, “Carbon positions in uranium carbides”, *Acta Crystallogr.* 12 (1959) 159-161.
- [172] “Augmented uranium metal production facility”, BARC Newsletter 200 (2000) 15-18 (Web-link: <http://barc.gov.in/publications/nl/2000/200009.pdf>).
- [173] G.C. Allen, P.M. Tucker, “Surface oxidation of uranium metal as studied by X-ray photoelectron spectroscopy”, *J. Chem. Soc. Dalton* 5 (1973) 470-474.

- [174] R. Rao, R.K. Bhagat, N.P. Salke, A. Kumar, "Raman spectroscopic investigation of thorium dioxide-uranium dioxide ( $\text{ThO}_2\text{-UO}_2$ ) fuel materials", *Appl. Spectrosc.* 68(1) (2014) 44-48.
- [175] "Thermophysical properties of materials for nuclear engineering: A tutorial and collection of data", (IAEA-THPH), International Atomic Energy Agency, Vienna (2008).
- [176] I.F. Barwood, B.R. Butcher, "The  $\alpha \rightarrow \beta$  phase transformation in uranium", *J. Nucl. Mater.* 8 (1963) 232-240.
- [177] C. Yoo, H. Cynn, P. Söderlind, "Phase diagram of uranium at high pressures and temperatures", *Phys. Rev. B* 57 (1998) 10359-10362.
- [178] P. Zhou, X. Wang, H. Yang, X. Fu, "Effect of vacuum heat treatment on oxidation of uranium surfaces", *Rare Metal Mat. Eng.* 37 (2008) 94-97.
- [179] G. Erez, U. Even, "The Wiedemann-Franz ratio of metallic uranium at elevated temperatures", *J. Appl. Phys.* 37 (1966) 4633-4644.
- [180] S. Nasu, S. Fukushima, T. Ohmichi, T. Kikuchi, "Thermal diffusivity of uranium by laser pulse method from 20° to 850°C", *Jap. J. Appl. Phys.* 7 (1968) 682.
- [181] D. Jain, C.G.S. Pillai, B.S. Rao, R.V. Kulkarni, E. Ramdasan and K.C. Sahoo, "Thermal diffusivity and thermal conductivity studies on thoria-lanthana solid solutions up to 10 mol. %  $\text{LaO}_{1.5}$ ", *J. Nucl. Mater.* 353 (2006) 35-41.
- [182] S.S. Parker, J.T. White, P. Hosemann, A.T. Nelson, "Thermophysical properties of thorium mononitride from 298 to 1700 K", *J. Nucl. Mater.* 526 (2019) 151760.
- [183] H. He, J. Majewski, D.D. Allred, P. Wang, X. Wen, K.D. Rector, "Formation of solid thorium monoxide at near-ambient conditions as observed by neutron reflectometry and interpreted by screened hybrid functional calculations", *J. Nucl. Mater.* 487 (2017) 288-296.

## References

- [184] B.R. Butcher, A.H. Rowe, "Phase transformation in uranium", *Nature* (1953) 817.
- [185] H.H. Klpefer, P. Chiotti, "Characteristics of the solid state transformations in uranium", USAEC Report no.: ISC-893 (1957) 1-113.
- [186] W.S. Blackburn, " $\alpha$ - $\beta$  Thermal cycling of uranium", *J. Nucl. Mater.* 2 (1960) 191.
- [187] J.J. Stobo, "Alpha beta cycling of uranium", *J. Nucl. Mater.* 2 (1960) 97-109.
- [188] L.T. Lloyd, "Thermal expansion of alpha-uranium single crystals", *J. Nucl. Mater.* 3 (1961) 67-71.
- [189] L.T. Lloyd, C.S. Barrett, "Thermal expansion of alpha uranium", *J. Nucl. Mater.* 18 (1966) 55-59.
- [190] E.S. Fisher, "Preparation of alpha uranium single crystals by a grain-coarsening method", *J. Metals* 9 (1957) 882-888.
- [191] D.C. Wallace, "Specific heat of thorium at high temperatures", *Phys. Rev.* 120 (1) (1960) 84-88.
- [192] E.A. Mit'kina, "Experimental determination of the true specific heats of uranium, thorium, and other metals", *Sov. Atom Energy* 7 (2) (1959) 163-165.
- [193] F.L. Oetting, D.T. Peterson, "Heat capacity of well characterized thorium metal from 298 to 700 K", *J. Less-Common Met.* 128 (1987) 231-239.
- [194] D.C. Ginnings, R.J. Corruccini, "Heat capacities at high temperatures of uranium, uranium trichloride, and uranium tetrachloride, *J. Res. Nat. Bur. Stand.* 39 (1947) 309-316.
- [195] F.K. Oetting, M.H. Rand, R.J. Ackermann, "The chemical thermodynamics of actinide elements and compounds, Part 1, The actinide elements", International Atomic Energy Agency (IAEA), Vienna (1976).
- [196] A.L. Loeb, "Thermal conductivity: VIII, A theory of thermal conductivity of porous materials", *J. Am. Ceram. Soc.* 37 (1954) 96-99.

## References

- [197] S. Kaity, J. Banerjee, M.R. Nair, K. Ravi, S. Dash, T.R.G. Kutty, A. Kumar, R.P. Singh, "Microstructural and thermophysical properties of U-6 wt.% Zr alloy for fast reactor application", *J. Nucl. Mater.* 427 (2012) 1-11.
- [198] C. Hin, "Thermal conductivity of metallic uranium", NEUP 14-6767 (2018) (Web-link: <https://www.osti.gov/servlets/purl/1433931>).
- [199] M. Floyd, B. Bromley, J. Pencer, "A Canadian perspective on progress in thorium fuel science and technology", *CNL Nucl. Rev.* 6 (1) (2017) 1-17.
- [200] S. Thakur, P.S.R. Krishna, A.B. Shinde, R. Kumar, S.B. Roy, "Quantitative analysis of thorium phase in Th-U alloys using diffraction studies", *AIP Conf. Proc.* 1832 (2017) 060012.
- [201] P. Chiotti, "High temperature crystal structure of thorium", *J. Electrochem. Soc.* (1955) 567-570.
- [202] G.G. Bente, "A Physical Metallurgical Study of Thorium-Rich Thorium-Uranium Alloys", Report no.: NAA-SR-2069 (1958).
- [203] G.H. Bannister, R.C. Burnett, J.R. Murray, "Ageing and hot hardness characteristics of certain thorium alloys", *J. Nucl. Mater.* 2(1) (1960) 51-61.
- [204] "Chemical technology division annual technical report for 1986," ANL-87-19, Argonne National Laboratory (1987) 122.
- [205] V. Crewe, S. Lawroski, "Reactor development program progress report", Argonne National Laboratory, ANL-7230, Lemont, IL, USA (1966).
- [206] O. Beneš D. Manara R.J.M. Konings, "Thermodynamic assessment of the Th-U-Pu system", *J. Nucl. Mater.* 449 (1-3) (2014) 15-22.
- [207] S. Kneppel, "Aqueous corrosion of thorium alloys and zircaloy-clad thorium alloys", NMI-1226, United States Atomic Energy Commission (1960) 1-49 (Web-link: <https://play.google.com/books/reader?id=OGCWvHY4xRwC&hl=en&pg=GBS.PA1>)

## References

- [208] D.S. Evans, G.V. Raynor, "The solubility of zirconium in  $\alpha$ -thorium", *J. Nucl. Mater.* 4 (1) (1961) 66-69.
- [209] R.I. Sheldon, D.E. Peterson, "The (U-Zr) Uranium-zirconium system", *Bull. Alloy Phase Diagr.* 10 (2) (1989) 165-171.
- [210] O.N. Carlson, "Some studies on the uranium-thorium-zirconium ternary alloy system", AECD-3206, United States Atomic Energy Commission (1950) 1-72.
- [211] J.W. Goffard, R.K. Marshall, "Irradiation behavior of Zircaloy-2 clad thorium-uranium-zirconium alloy fuel elements Interim report 1", BNWL-479, Pacific Northwest Laboratory, United States Atomic Energy Commission (1967).
- [212] T. Okawa, S. Nakayama, H. Sekimoto, "Design study on power flattening to sodium cooled large-scale CANDLE burning reactor with using thorium fuel", *Energ. Convers. Manage.* 53 (1) (2012) 182-188.
- [213] Inorganic crystal Structure Database (ICSD FIZ Karlsruhe GmbH, Version 4.4.0 (2020) collection code: 164572) from: A.I. Kolesnikov, A.M. Balagurov, I.O. Bashkin, A.V. Belushkin, E.G. Ponyatovsky, M. Prager, "Neutron scattering studies of ordered gamma -ZrD", *J. Phys. Condens-Mat.* 6 (43) (1994) 8977-8988.
- [214] Inorganic crystal Structure Database (ICSD FIZ Karlsruhe GmbH, Version 4.4.0 (2020) collection code: 16559) from: B.O. Loopstra, "Neutron diffraction investigation of  $U_3O_8$ ", *Acta Crystallogr.* 17 (1964) 651-654.
- [215] Inorganic crystal Structure Database (ICSD FIZ Karlsruhe GmbH, Version 4.4.0 (2020) collection code: 246035) from: S.K. Sali, N.K. Kulkarni, K. Krishnan, S.N. Achary, A.K. Tyagi, "Oxidation / reduction studies on  $Zr_yU_{1-y}O_{2+x}$  and delineation of a new orthorhombic phase in U-Zr-O system", *J. Solid-State Chem.* 181 (8) (2008) 1859-1866.

## References

- [216] Inorganic crystal Structure Database (ICSD FIZ Karlsruhe GmbH, Version 4.4.0 (2020) collection code: 108756) from: H.L. Luo, J.G. Huber, "Superconductivity in Th-Zr alloys", *J. Less-Common Met.* 65 (1) (1979) 13-17.
- [217] J.M. Elorrieta, L.J. Bonales, M. Najj, D. Manara, V.G. Baonza, J. Cobos, "Laser-induced oxidation of  $\text{UO}_2$ : A Raman study", *J. Raman Spectrosc.* 49 (5) (2018) 878-884.
- [218] H. He, D. Shoesmith, "Raman spectroscopic studies of defect structures and phase transition in hyper-stoichiometric  $\text{UO}_{2+x}$ ", *Phys. Chem. Chem. Phys.* 12 (2010) 8109-8118.
- [219] X. Zhao, D. Vanderbilt, "Phonons and lattice dielectric properties of zirconia", *Phys. Rev. B* 65 (2002) 075105.
- [220] E. Hashem, A. Seibert, J-F. Vigier, M. Najj, S. Mastromarino, A. Ciccioli, D. Manara, "Solid-liquid equilibria in the  $\text{ThO}_2$ - $\text{ZrO}_2$  system: An experimental study" *J. Nucl. Mater.* 521 (2019) 99-108.
- [221] O.N. Carlson, E.R. Stevens, "A compilation of thorium binary phase diagrams", USAEC Report (1968) (Web-link: <https://www.osti.gov/servlets/purl/4529064>).
- [222] G.B. Skinner, H.L. Johnston, "Thermal Expansion of zirconium between 298°K and 1600°K", *J. Chem Phys.* 21 (1953) 1383.
- [223] P.L. Brown, E. Curti, B. Grambow, C. Ekberg, "Chemical thermodynamics of zirconium", OECD Nuclear energy agency, data bank (Eds.: F.J. Mompean, J. Perrone, M. Illemassene) (2005) (Web-link: <https://www.oecd-nea.org/dbtdb/pubs/vol8-zirconium.pdf>).
- [224] C.G.S. Pillai, P. Raj, "Thermal Conductivity of  $\text{ThO}_2$  and  $\text{Th}_{0.98}\text{U}_{0.02}\text{O}_2$ ", *J. Nucl. Mater.* 277 (2000) 116-119.

- [225] S.S. Manoharan, K.C. Patil, "Combustion synthesis of metal chromite powders", *J. Am. Ceram. Soc.* 75 (1992) 1012-1015.
- [226] S.R. Jain, K.C. Adiga, V.R. Pai Verneker, "A new approach to thermochemical calculations of condensed fuel-oxidizer mixtures," *Combust. Flame* 40 (6) (1981) 71-79.
- [227] S. Roy, A. Das Sharma, S.N. Roy, H.S. Maiti, "Synthesis of  $\text{YBa}_2\text{Cu}_3\text{O}_{7-x}$  Powder by Autoignition of Citrate-Nitrate Gel", *J. Mater. Res.* 8(11) (1993) 2761-2766.
- [228] M. Gizowska, I. Kobus, K. Perkowski, M. Piatek, G. Konopka, I. Witosławska, M. Osuchowski, "Size and morphology of yttria nanopowders obtained by solution combustion synthesis" *Arch. Metall. Mater.* 63(2) (2018) 743-748.
- [229] G.A.M. Hussein, H.M. Ismail, "Texture assessment of thoria as a final decomposition product of hydrated thorium nitrate and oxycarbonate", *Colloids Surf. A*: 99 (1995) 129-139.
- [230] I.M. Weiss, C. Muth, R. Drumm, H.O.K. Kirchner, "Thermal decomposition of the amino acids glycine, cysteine, aspartic acid, asparagine, glutamic acid, glutamine, arginine and histidine", *BMC Biophys.* 11 (2018) 1-15.
- [231] N. Raje, A.V.R. Reddy, "Mechanistic aspects of thermal decomposition of thorium oxalate hexahydrate: A review", *Thermochim. Acta* 505 (2010) 53-58.
- [232] H. Hayashi, T. Watanabe, "Properties of thoria obtained by thermal decomposition of thorium salts", *Nippon Kagaku Kaishi* 4 (1973) 858-860.
- [233] Y. Saito, "Thermal decomposition of thorium oxalate", *J. Jpn. Soc. Powder Metall.* 17(1971) 235-242.
- [234] M.T. Aybers, "Kinetic study of the thermal decomposition of thorium oxalate dehydrate", *J. Nucl. Mater.* 252 (1998) 28-33.
- [235] D.Y. Chung, E. H. Lee, "Microwave-induced combustion synthesis of  $\text{Ce}_{1-x}\text{Sm}_x\text{O}_{2-x/2}$  powder and its characterization", *J. Alloys Compd.* 374 (2004) 69-73.

## References

- [236] "The Aldrich Library of FT-IR Spectra, Edition-II, Volume-1", 1 898 A 897-898.
- [237] S. Kumar, A.K. Rai, V.B. Singh, S.B. Rai, "Vibrational spectrum of glycine molecule", *Spectrochim. Acta A* 61 (2005) 2741-2746.
- [238] J. R. Ferraro, A. Walker, "Comparison of the infrared spectra of the hydrates and anhydrous salts in the systems  $\text{UO}_2(\text{NO}_3)_2$  and  $\text{Th}(\text{NO}_3)_4$ ", *J. Chem. Phys.* 45 (1966) 550-552.
- [239] J.H-Paredes, D.G-Mitnik, H.E. E-Ponce, M.E. A-Ramos, A.D-Moller, "Band structure, optical properties and infrared spectrum of glycine–sodium nitrate crystal", *J. Mole. Str.* 875 (2008) 295-301.
- [240] S.L. Estes, M.R. Antonio, L. Soderholm, "Tetravalent Ce in the nitrate-decorated hexanuclear cluster  $[\text{Ce}_6(\mu_3\text{-O})_4(\mu_3\text{-OH})_4]^{12+}$ : A structural end point for ceria nanoparticles, *J. Phys. Chem. C* 120 (2016) 5810-5818.
- [241] M. Rand, L. Fuger, I. Grenthe, V. Neck, D. Rai, "Chemical thermodynamics: Chemical thermodynamics of thorium", (OECD, NEA-TDB) Vol. 11, Elsevier, Amsterdam (2007).
- [242] C. Hennig, K. Schmeide, V. Brendler, H. Moll, S. Tsushima, A.C. Scheinost, "EXAFS Investigation of U(VI), U(IV), and Th(IV) sulfato complexes in aqueous solution", *Inorg. Chem.* 46 (2007) 5882-5892.
- [243] J. Rothe, M.A. Denecke, V. Neck, R. Muller, J.I. Kim, XAFS "Investigation of the structure of aqueous thorium(IV) species, colloids, and solid thorium(IV) oxide / hydroxide", *Inorg. Chem.* 41 (2002) 249-258.
- [244] C. Hennig, S. Takao, K. Takao, S. Weiss, W. Kraus, F. Emmerling, A.C. Scheinosta, "Structure and stability range of a hexanuclear Th(IV)-glycine complex", *Dalton Trans.* 41 (2012) 12818-12823.

## References

- [245] Y. Hu, K.E. Knope, S. Skanthakumar, L. Soderholm, "Understanding the ligand-directed assembly of a hexanuclear Th<sup>IV</sup> molecular cluster in aqueous solution", *Eur. J. Inorg. Chem.* 24 (2013) 4159-4163.
- [246] M. Nourmand, N. Meissami, "Complex formation between uranium(VI) and thorium (IV) ions with some  $\alpha$ -amino-acids", *J. Chem. Soc. Dalton* 8 (1983) 1529-1533.
- [247] Bismondo, L. Rizzo, G. Tomat, "Thermodynamic properties of actinide complexes. uranyl (VI)- and thorium (IV)-glycine systems", *Inorg. Chim. Acta* 74 (1983) 21-24.
- [248] B.G. Oliver, A.R. Davis, "The structure of aqueous thorium nitrate solution by laser Raman spectroscopy", *J. Inorg. Nucl. Chem.* 34 (1972) 2851-2860.
- [249] Z. Huang, X. Chen, Y. Li, J. Chen, J. Lin, J. Wang, J. Lei, R. Chen, "Quantitative determination of citric acid in seminal plasma by using Raman spectroscopy", *Appl. Spectrosc.* 67 (7) (2013) 757-760.
- [250] A.K. Arora, M. Rajalakshmi, T.R. Ravindran, V. Sivasubramanian, "Raman spectroscopy of optical phonon confinement in nanostructured materials", *J. Raman Spectrosc.* 38 (2007) 604-617.
- [251] D. Langmuir, J.S. Herman, "The mobility of thorium in natural waters at low temperatures", *Geochim. Cosmochim. Ac.* 44 (1980) 1753-1766.
- [252] M. Bobtelsky, B. Graus, "Thorium citrate complexes, their composition, structure and behavior", *J. Am. Chem. Soc.* 76 (6) (1954,) 1536-1539.
- [253] G.R. Choppin, H.N. Erten, Y. Xia, "Variation of stability constants of thorium citrate complexes with ionic strength", *Radiochim. Acta* 74 (1996) 123-127.
- [254] D.P. Raymond, J.R. Duffield, D.R. Williams, "Complexation of plutonium and thorium in aqueous environments", *Inorg. Chim. Acta* 140 (1987) 309-313.
- [255] M.M. Barbooti, D.A. Al-Sammerrai, "Thermal decomposition of citric acid", *Thermochim. Acta* 98 (1986) 119-126.

- [256] D. Hennings, W. Mayr, "Thermal decomposition of (BaTi) citrates into barium titanate", *J. Solid State Chem.* 26 (1978) 329-338.
- [257] N.S. Gajbhiye, S. Prasad, "Thermal decomposition of hexahydrated nickel iron citrate", *Thermochim. Acta* 285 (1996) 325-336.
- [258] J. Tsay, T. Fang, "Effects of molar ratio of citric acid to cations and of pH value on the formation and thermal-decomposition behavior of barium titanium citrate", *J. Am. Ceram. Soc.* 82(6) (1999) 1409-1415.
- [259] A. Marcilla, A. Gómez-Siurana, M. Beltrán, I. Martínez-Castellanos, I. Blasco, D. Berenguer, "TGA-FTIR study of the pyrolysis of sodium citrate and its effect on the pyrolysis of tobacco and tobacco/SBA-15 mixtures under N<sub>2</sub> and air atmospheres", *J. Sci. Food Agr.* 98 (15) (2018) 5916-5931.
- [260] O. Glatter, O. Kratky, "Small angle X-ray scattering", Academic, London (1982).
- [261] A. Guinier, G. Fournet, "Small angle scattering of X-rays", Wiley, New York (1955).
- [262] J. Aitchison, J.A.C. Brown, "The log normal distribution", Cambridge University Press, Cambridge (1957).
- [263] R.D. Purohit, B.P. Sharma, K.T. Pillai, A.K. Tyagi, "Ultrafine ceria powders via glycine-nitrate combustion", *Mater. Res. Bull.* 36 (15) (2001) 2711-2721.
- [264] V.R. Choudhary, A.M. Rajput, B. Prabhakar, A.S. Mamman, "Partial oxidation of methane to CO and H<sub>2</sub> over nickel and/or cobalt containing ZrO<sub>2</sub>, ThO<sub>2</sub>, UO<sub>2</sub>, TiO<sub>2</sub> and SiO<sub>2</sub> catalysts", *Fuel* 77 (15) (1998) 1803-1807.
- [265] V. Múčka, J. Podlaha, R. Silber, "NiO-ThO<sub>2</sub> mixed catalysts in hydrogen peroxide decomposition and influence of ionizing radiation", *Radiat. Phys. Chem.* 59 (5-6) (2000) 467-475.

## References

- [266] P. Balakrishna, B.N. Murty, K.P. Chakraborty, R.N. Jayaraj, C. Ganguly, "Special features in powder preparation, pressing, and sintering of uranium dioxide", *Mater. Manuf. Process.* 15(5) (2000) 679-693.
- [267] C.S. Morgan, K.H. McCorkle, G.L. Powell, "Sintering and desintering of thoria", In: Kuczynski G.C. (Eds.) *Sintering and Related Phenomena*. Materials Science Research, Vol. 6, Springer, Boston, MA (1973).
- [268] J.M. Pope, K.C. Radford, "Physical properties of some thoria powders and their influence on sinterability", *J. Nucl. Mater.* 52 (1974) 241-254.
- [269] Z. Chen, J. Mabon, J. Wen, R. Trice, "Degradation of plasma-sprayed yttria-stabilized zirconia coatings via ingress of vanadium oxide", *J. Eur. Ceram. Soc.* 29(9) (2009) 1647-1656.
- [270] M.A. Delfrate, J. Lemaitre, V. Buscaglia, M. Leoni, P. Nanni, "Slip casting of submicron BaTiO<sub>3</sub> produced by low-temperature aqueous synthesis", *J. Eur. Ceram. Soc.* 16(9) (1996) 975-984.
- [271] T.K. Gupta, R.L. Coble, "Sintering of ZnO: II, density decrease and pore growth during the final stage of the process", *J. Am. Ceram. Soc.* 51 (9) (1968) 525-528.
- [272] C.-H. Chang, J.F. Rufner, K.V. Benthem, R.H.R. Castro, "Design of desintering in tin dioxide nanoparticles", *Chem. Mater.* 25(21) (2013) 4262-4268.
- [273] P. Duran, J. Tartaj, C. Moure, "Sintering behaviour and microstructural evolution of agglomerated spherical particles of high-purity barium titanate", *Ceram. Int.* 29(4) (2003) 419-425.
- [274] C.-Y. Tsao, W.-H. Tuan, K.-C. Feng, "De-sintering of Ba<sub>5</sub>Nb<sub>4</sub>O<sub>15</sub> ceramic and its influence on microwave characteristics", *J. Eur. Ceram. Soc.* 37(4) (2017) 1517-1521.
- [275] Cs. Balázsi, F.S. Cinar, O. Addemir, F. Wéber, P. Arató, "Manufacture and examination of C/Si<sub>3</sub>N<sub>4</sub> nanocomposites" *J. Eur. Ceram. Soc.* 24(12) (2004) 3287-3294.

- [276] R. Besler, M.R. da Silva, J.J. do Rosario, M. Dosta, S. Heinrich, R. Janssen, “Sintering simulation of periodic macro porous alumina”, *J. Am. Ceram. Soc.* 98(11) (2015) 3496-3502.
- [277] K. Ananthasivan, S. Anthonysamy, A. Singh, P.R. Vasudeva Rao, “De-agglomeration of thorium oxalate - A method for the synthesis of sinter active thoria”, *J. Nucl. Mater.* 306 (1) (2002) 1-9.
- [278] R.H.R. Castro, “Controlling sintering and grain growth of nanoceramics”, *Cerâmica* 65 (373) (2019) 122-129. **[278a]** Thermodynamics of sintering, R.M. German, *Sintering of advanced materials: Fundamentals and processes* (Ed.: Z.Z. Fang) Woodhead Publishing Ltd. (2010), ISBN 978-1-84569-562-0. **[278b]** G.S. Upadhyaya, *Sintered metallic and ceramic Materials*, John Wiley & Sons Ltd. (1999) ISBN 0-471-98155-9.
- [279] O. Sudre, F.F. Lange, “The effect of inclusions on densification; III, The desintering phenomenon”, *J. Am. Ceram. Soc.* 75 (12) (1992) 3241-3251.
- [280] F. Li, J. Pan, A. Cocks, “Defect healing and cracking in ceramic films during constrained sintering” *J. Am. Ceram. Soc.* 95(12) (2012) 3743-3749.
- [281] S. Knight, R. Korlacki, C. Dugan, J.C. Petrosky, A. Mock, P.A. Dowben, J. Matthew Mann, M.M. Kimani, M. Schubert, “Infrared-active phonon modes in single-crystal thorium dioxide and uranium dioxide”, *J. Appl. Phys.* 127 (2020) 125103.

## CHAPTER 3

### Thermophysical studies on reactor-grade uranium and thorium metals

---

#### 1.1. Introduction

As discussed earlier, it is planned to develop liquid sodium cooled fast breeder reactors (FBRs) fuelled with metallic alloys in the 2<sup>nd</sup> stage of nuclear power program to achieve rapid expansion of nuclear energy capacity in India [18, 19, 52]. Advantages of metallic alloy fuelled reactors such as of higher fissile and fertile material density, superior thermophysical properties, higher breeding ratios, inherent safety characteristics, minor actinide transmutation, facile fuel reprocessing by pyro-processing with minimum waste generation, etc. have already been discussed in chapter-1 (Section 1.3.) [44, 45]. In this regard, uranium and thorium-based binary (U-Zr, Th-U) and ternary (U-Pu-Zr, Th-U-Zr) alloy fuels are being developed [35, 148]. Systematic basic research is needed on these alloys to understand their physico-chemical properties. Reliable database on these properties has to be generated, which is required to predict their performance under normal and off-normal reactor operation conditions using suitable fuel performance codes [93, 94]. Thermophysical properties, which are essential for assessment of fuel's performance potential, include thermal diffusivity, thermal expansion, specific heat and thermal conductivity for solid fuels. In case of liquid fuels such as molten salts, viscosity is another important thermophysical property in addition to above. For uranium and thorium metals, which are invariable constituents of most of the metallic alloy fuels being developed, recommended data for their thermophysical properties are available in Thermophysical Properties Research Centre (TPRC) data series volumes [149-152], a number of research articles and technical reports [60, 153]. Mostly, this

information is based on data reported during early years (1950-1970) of metal fuel development. While there have been few experimental studies thereafter [154-158], recent reports indicate increasing use of computational tools to estimate various thermophysical and thermal properties of these metals [159-163]. In spite of availability of thermophysical properties data of thorium and uranium metals in literature, following gap areas can be noted: (i) there is wide variation in the reported data, mostly due to variation in metal purity, crystallinity and metallurgical history. As an illustration, thermal conductivity of uranium metal as reported in literature is shown in Fig. 3.1, which shows the extent of scatter up to ~50%. Table 3.1 presents the relevant details on uranium sample purity and method used for thermal conductivity determination for data plotted in Fig. 3.1. (ii) Thermal conductivity variation trends for high temperature uranium allotropes are not accessible. (iii) Effect of structural phase transitions on uranium's thermophysical properties is not well reported and (iv) information on thermophysical properties of thorium metal with complete sample characterization details are not available. To address these issues, experimental investigations have been carried out on temperature dependent thermal diffusivity, linear thermal expansion and specific heat of thorium and uranium metals that are being prepared in nuclear fuel manufacturing facilities in India. Results of these studies are detailed in the present chapter.

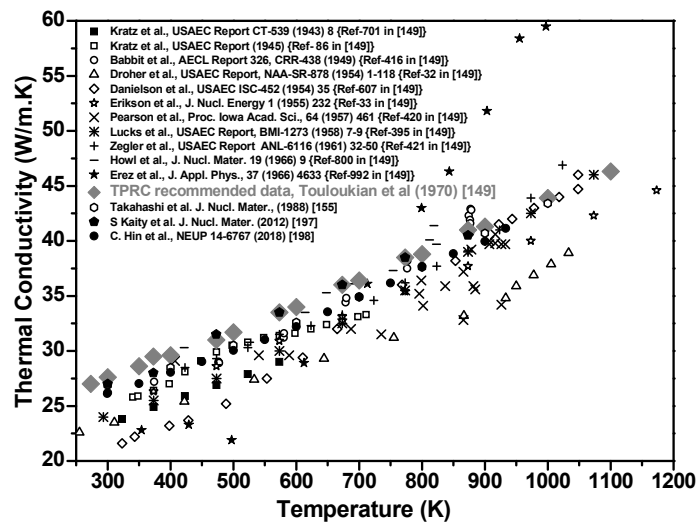


Fig. 3.1. Graphical comparison of reported thermal conductivity data for uranium

**Table 3.1. Details of uranium sample purity and method used for thermal conductivity determination for literature data plotted in Fig. 3.1**

Year	Author & Reference	Sample details	Method	Error
1943	Kartz <i>et al.</i> , USAEC Report, CT-539 (1943) 8.	Extruded natural uranium; > 99.5%	Comparator method	Not available
1945	Kartz <i>et al.</i> , USAEC Report, CP-2315 (1945) 1-14.	Extruded natural uranium; > 99.5% (C = 720, Fe = 150, Ag = 100, N = 28, Ni = 20, Si = 18, Cu = 5, Cr = 3, B = 1 (all in ppm))	Comparator method	Not available
1949	Babbitt <i>et al.</i> , AECL Report-326, CRR-438 (1949) 1-37.	Natural uranium extruded in $\gamma$ -phase; pre-heated at 973 K (Si = 260, Fe = 188, Ni = 36, Mn = 30, Cu = 1, others < 1 (all in ppm))	Longitudinal heat flow	Not available
1954	Droher <i>et al.</i> , USAEC Report, NAA-SR-878 (1954) 1-118.	> 99.5% pure natural uranium rolled in $\alpha$ -phase; pre-heated at 1023 K and water quenched	Radial heat flow	Not available
1954	Danielson <i>et al.</i> , USAEC Report, ISC-452 (1954) 9-35.	Ames uranium produced by metallothermic reduction of uranium oxide	Plate / disc (Diffusivity)	Not available
1955	Erikson <i>et al.</i> , J. Nucl. Energy 1 (1955) 232.	> 99.5% pure uranium; density $\sim 18.6 \text{ g.cm}^{-3}$ ;	Electrical heating	$\pm 5\%$
1957	Pearson <i>et al.</i> , Proc. Iowa Acad. Sci. 64 (1957) 461.	> 99.5% pure uranium; measurements made in vacuum ( $P \sim 10^{-6}$ mm Hg)	Comparator method	$\pm 7\%$
1958	Lucks <i>et al.</i> , USAEC Report, BMI-1273 (1958) 7-9.	> 99.5% pure uranium; measurements made in vacuum, Zircaloy-2 used as comparator	Comparator method	$\pm 5\%$
1961	Zegler <i>et al.</i> , USAEC Report, ANL-6116 (1961) 32-50.	K, P, Ti, Zn (each 5), Si, Ca, Mo (each 2), C = 2, As, Na (each 1), rest impurities < 1 (in ppm)	Comparator method	Not available
1966	Howl <i>et al.</i> , J. Nucl. Mater. 19 (1966) 9.	Springfield uranium, $\beta$ -quenched and $\alpha$ -annealed specimen	Comparator method	$\pm 5\%$
1966	Erez <i>et al.</i> , J. Appl. Phys. 37 (1966) 4633.	Melt-cast uranium, total impurities < 300 ppm	Electrical resistivity	Not available
1970	Touloukian <i>et al.</i> , TPRC recommended data, (1970) [149].	Well annealed high purity uranium, residual electrical resistivity $\sim 2.2 \mu\Omega\text{-cm}$ ,	Compiled database	Up to $\pm 10\%$ -
1988	Takahashi <i>et al.</i> , J. Nucl. Mater. 154 (1988) 141 [155].	$\sim 99.9\%$ pure uranium (C < 400, Si < 100, Al < 100, Cu < 20, total impurities < 1000; in ppm)	Laser flash method	$> \pm 5\%$
2012	Kaity <i>et al.</i> , J. Nucl. Mater. 427 (2012) 1 [197].	$\sim 99.9\%$ pure uranium (Al = 26, Fe = 20, Ni = 9, Ca = 6; all in ppm); C, N, O no reported	Transient plane source	Not available
2018	C. Hin <i>et al.</i> , NEUP 14-6767 (2018) [198]	Computational evaluation on pure uranium	Ab-initio method	N/A

## 1.2. Experimental

Nuclear-grade natural uranium and thorium metals were thoroughly characterized and used for thermophysical properties measurements. Metal handling was carried out under inert atmosphere, as described in chapter-2 (Section-2.3.1.1. to section-2.3.1.2.). Surface cleaned metal samples were characterized for their crystal structure, composition and morphology by

X-ray diffraction (XRD), elemental analysis and scanning electron microscopy (SEM), respectively. For XRD measurements, a thin layer of silicon vacuum grease was applied over the sample surface to minimize surface oxidation during XRD runs. Unit cell parameters of thorium and uranium metals were determined using least-square refinement fitting program.

Thorium metal ingot was prepared by arc-melting the surface cleaned thorium tube. Arc-melted ingot was vacuum annealed at 973 K ( $P < 2 \times 10^{-6}$  Torr; Duration = ~220 h) and slowly cooled (1 K / min.) to ambient temperature. Elemental analysis (C, N and O) was carried out on small samples (~100-150 mg), cut from surface cleaned metals. Ultrasonically cleaned samples were used for elemental analysis as described in chapter-2 (Section-2.3.2.1). Surface morphology of polished metals was analyzed by scanning electron microscopic (SEM) technique while elemental analysis was performed using energy dispersive spectrometer (EDS). Cylindrical pellets for thermophysical characterization were prepared by machining the metal ingots on a mechanical lathe, followed by surface cleaning (polishing → ultrasonication → drying).

Thermal diffusivity was measured on cylindrical samples (~12.5 mm diameter, 3-4 mm thickness) using laser flash apparatus (LFA). Measurements were carried out on graphite coated samples over 298 K to 1273 K under dynamic vacuum ( $P \leq 2 \times 10^{-6}$  mbar). Diffusivity was measured over 298 K to 1273 K at 50 K interval, which was reduced to 25 K near the phase transition regions of uranium metal. Linear thermal expansion of thorium and uranium was measured from 298 K up to 1373 K (1273 K for U) on small cylindrical samples (diameter ~6 mm; thickness ~4-5 mm) using TMA under highly purified argon gas atmosphere ( $P_{O_2 \text{ in argon}} \sim 10^{-18}$  atmosphere). Isobaric specific heat ( $C_p$ ) of both the metals was measured using temperature modulated differential scanning calorimetry (TMDSC) on small

disc-shaped samples (~150 mg to ~200 mg) kept inside aluminum pans (40  $\mu$ l), which were hermitically sealed using aluminum lid. Heat flow data measured under modulated temperature program (underlying heating rate = 2 K/min., modulation amplitude =  $\pm$  0.1 K, pulse duration range = 15 s to 30 s) were treated using the multi-frequency modulation software package (TOPEM<sup>®</sup>) [144]. Specific heat ‘C<sub>p</sub>’ was evaluated from reversible heat flow component. Since, it was not possible to perform DSC experiments over complete temperature range (298 K to 1373 K), literature C<sub>p</sub> data for thorium and uranium were also used for thermal conductivity evaluation. Thermal conductivity ‘ $\lambda(T)$ ’ was evaluated by using the following relation (equation-3.1):

$$\lambda(T) = D(T) \times \rho(T) \times C_p(T) \quad (3.1)$$

Where ‘ $\lambda(T)$ ’, ‘D(T)’, ‘ $\rho(T)$ ’ and ‘C<sub>p</sub>(T)’ are thermal conductivity, thermal diffusivity, density and isobaric specific heat at temperature ‘T’, respectively. Density ‘ $\rho(T)$ ’ was evaluated from experimental thermal expansion data, assuming isotropic expansion of polycrystalline samples in all directions. Specific heat ‘C<sub>p</sub>(T)’ was taken from measured values and / or reported data.

### 1.3. Results and Discussion

#### 1.3.1. Impurity analysis

Table 3.2 shows the average values of C, N and O content in studied thorium and uranium metals. The most prevalent non-metallic impurity in uranium is carbon (~1100 ppm) while that in thorium is oxygen (~2000 ppm). Remaining two impurities (N and O in uranium; C and N in thorium) are present to significantly lower extent. The origin of these impurities in uranium and thorium can be attributed to their metallurgical history. Uranium picks up

carbon from the graphite crucibles during magensiothermic reduction of uranium tetra fluoride ( $UF_4$ ). Higher oxygen impurity in thorium can be attributed to (i) residual un-reacted oxide during calciothermic reduction of thoria (or  $ThCl_4$ ) to obtain thorium metal powder [85, 164] and (ii) oxygen pickup by reactive thorium metal powder during various processing stages (washing, pressing, sintering, melting, shaping, etc.) due to very high chemical affinity of the two elements [165].

**Table 3.2. Carbon, oxygen and nitrogen content of thorium and uranium metals**

Impurity →	Carbon (ppm)		Oxygen (ppm)		Nitrogen (ppm)	
	Average value	Error (2 $\sigma$ ; 95% CL)	Average value	Error (2 $\sigma$ ; 95% CL)	Average value	Error (2 $\sigma$ ; 95% CL)
<b>Thorium</b>	300	300.7 $\pm$ 18.7	2000	2000 $\pm$ 50.1	200	200.2 $\pm$ 7.3
<b>Uranium</b>	1100	1100 $\pm$ 35.8	110	110.4 $\pm$ 7.3	100	100.4 $\pm$ 5.3

Rest of the impurities (N and O in uranium; C and N in thorium) can be attributed to various metallurgical process steps to produce these metals. While all these impurities are on a higher side as compared to high purity metals usually employed for thermophysical characterization, these represent the metal quality that are likely to be produced in nuclear fuel manufacturing facilities for large-scale metallic fuel fabrication. Thermophysical assessment of these metal samples therefore provides a realistic assessment of their behavior in routinely manufactured nuclear fuels.

Figure 3.2 (a) and (b) show representative EDS curves recorded over the polished surface of thorium and uranium metals, respectively using low accelerating voltage ( $\sim 5$  kV). Lower

accelerating voltage was used to suppress the background at lower energy region. Representative SEM micrographs, over which EDS spectra were recorded, are also shown as insets. These results also confirm no major impurity (metallic / non-metallic) other than carbon and oxygen. No effort was made to quantify carbon / oxygen content from EDS results due to poor sensitivity of EDS detector for lighter ( $Z < 11$ ) elements.

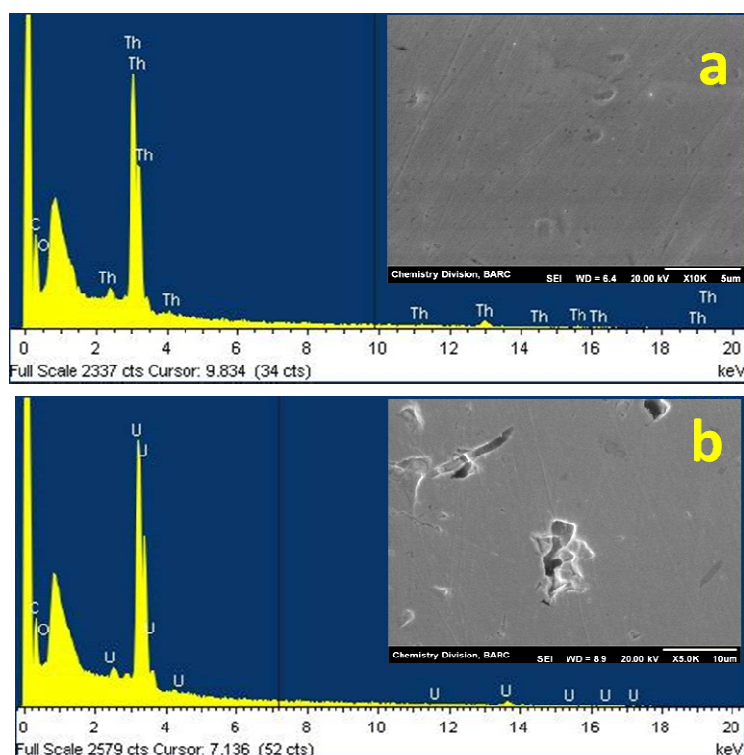


**Fig. 3.2.** EDS spectra recorded on (a) polished thorium and (b) polished uranium metal.

**Insets show the SEM micrographs over which the EDS spectra were recorded**

### 1.3.2. Structural characterization

Figure 3.3 shows the XRD pattern recorded on (a) polished thorium and (b) uranium surface at ambient temperature. Observed reflections were fit into FCC and orthorhombic phase of thorium (space group:  $Fm-3m$  (225)) and uranium (space group:  $Cmcm$  (63)), respectively using least-square refinement program and lattice parameters were obtained for both thorium ( $a = b = c = 5.098(3) \text{ \AA}$ ,  $\alpha = \beta = \gamma = 90^\circ$ , unit cell volume =  $132.50 \pm 0.27 \text{ \AA}^3$ ) and uranium (a

= 2.860(2) Å, b = 5.880(3) Å, c = 4.968(6) Å,  $\alpha = \beta = \gamma = 90^\circ$ , unit cell volume =  $83.58 \pm 0.20$  Å<sup>3</sup>). Comparison with reported values of thorium (a = b = c = 5.0838 (3) Å,  $\alpha = \beta = \gamma = 90^\circ$ , unit cell volume = 131.39 Å<sup>3</sup>) [166] and uranium (a = 2.8535 Å, b = 5.8648 Å, c = 4.9543 Å,  $\alpha = \beta = \gamma = 90^\circ$ , unit cell volume = 83.01 Å<sup>3</sup>) [167] showed slightly enlarged unit cell of both the metal samples as compared to reported data. This could be due to the presence of higher extent of non-metallic impurities such as C, N, and O. Inset in Fig. 3.3(a) shows a weak reflection ( $2\theta \sim 27.49^\circ$ ) that corresponds to (111) plane of fluorite ThO<sub>2</sub> phase ( $2\theta \sim 27.57^\circ$ ) [168] and indicate the presence of thorium oxide as one of the major oxygen-bearing impurity phase. This is quite likely as 2000 ppm of oxygen (by weight) corresponds to  $\sim 2.82$  atom % oxygen, which is primarily present in the form of ThO<sub>2</sub> and is sufficient to give X-ray reflection peak. Surface oxidation of polished thorium metal surface could also contribute to this XRD peak. Slightly lower value of diffraction angle ( $2\theta \sim 27.49^\circ$ ) as compared to reported value ( $2\theta \sim 27.57^\circ$ ) [168] could be due to presence of ultrafine ThO<sub>2</sub> crystallites, which have relatively large inter-planer spacing and therefore result into X-ray reflection peaks at lower angles. Apart from clearly identifiable ThO<sub>2</sub> impurity phase, XRD pattern of thorium metal does not indicate any other phase.

For uranium metal (Fig. 3.2(b)), inset shows two distinct reflections, which do not match with  $\alpha$ -uranium phase. These reflections match well with that of cubic UO<sub>2</sub> ( $2\theta_{100\% \text{ intensity}} = 28.2^\circ$ ) [169], rock-salt type UO ( $2\theta_{100\% \text{ intensity}} = 31.5^\circ$ ) [170] and UC ( $2\theta_{100\% \text{ intensity}} = 31.18^\circ$ ) [171]. Although utmost experimental care was taken, formation of oxide film on polished surface is possible; given the fact that uranium metal is highly electropositive with high surface reactivity towards atmospheric oxygen, even under ambient conditions.

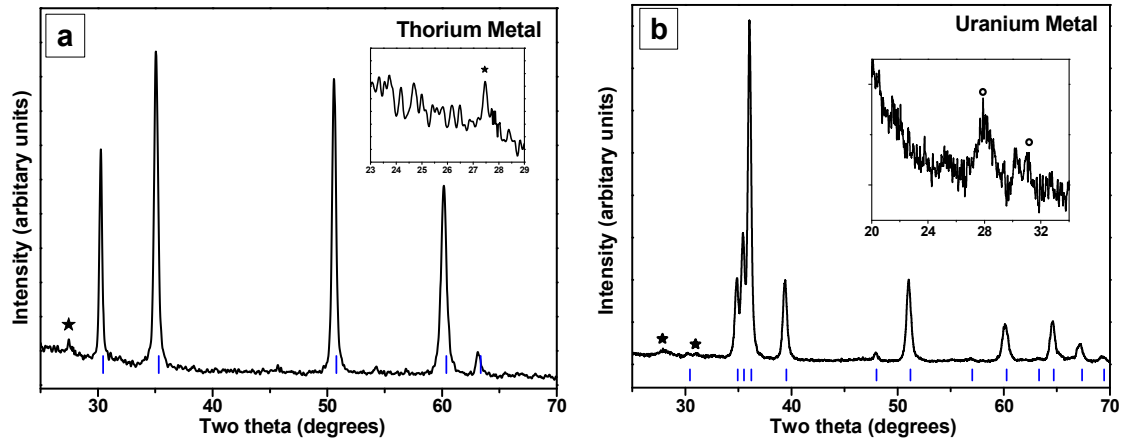


**Fig. 3.3. Room temperature XRD pattern recorded over polished pellet of (a) thorium metal and (b) uranium metal. Black curves show experimental data while blue lines are peak positions corresponding to reported XRD patterns of FCC thorium [166] and orthorhombic uranium [167]. Insets show the presence of weak reflections due to impurity phases. Peaks marked with “\*” and ‘o’ symbols represent  $\text{ThO}_2$  and  $\text{UO}_2 / \text{UO} / \text{UC}$  phases**

Easily visible tarnishing of polished uranium surface was also noted within a span of few minutes. It is also known that oxides of uranium form non-passivating surface layer and may therefore allow further oxidation beyond few atom layers at ambient temperatures. Oxide layers of such high-Z elements are therefore detectable by XRD. Presence of carbide phase (UC) is also likely due to higher carbon content ( $\sim 1100 \pm 36$  ppm) in as-received metal. Carbon is generally picked up by molten uranium during the magensiothermic reduction of  $\text{UF}_4$  in graphite crucibles at higher temperatures [172]. Carbon content is  $\sim 2.14$  at.%, which can be detected by carefully performed XRD measurements. Earlier reports on surface oxidation behavior of uranium metal also suggests that presence of UC impurity phase in metal assists in stabilizing the surface layers consisting of a mixture of  $\text{UO}_2 + \text{UO}$ , even under highly inert conditions [173].

### 1.3.3. Surface morphology and Raman Spectroscopy analysis

Figure 3.4 (a)-(e) shows SEM micrographs of thorium and uranium metals at different process stages. Fig. 3.4 (a) shows the micrograph of thorium powder compact (fractured surface) consisting of uniformly distributed micron-sized bulk thorium metal grains. Detailed elemental mapping results obtained by EDS technique showed oxygen-rich sub-micron sized inclusions, which correspond to  $\text{ThO}_2$  impurity phase in powdered thorium metal. Figure 3.4 (b) and (c) show micrographs of surface cleaned thorium and uranium metal pellets obtained after arc melting and vacuum annealing (973 K; 220 h), respectively. Apart from polishing scratch marks, the micrographs appear featureless except few bright dots seen over the surface of thorium metal surface. These regions were further scanned and Fig. 3.4 (d) shows EDS spectrum recorded on two different regions over the surface of thorium pellet. Under identical measurement conditions, the inclusion regions (spectrum-1) showed significantly higher oxygen concentration as compared to the featureless background region (spectrum-2), which indicated the presence of  $\text{ThO}_2$  inclusions in thorium metal. No such oxide inclusions were observed in uranium metal. Elemental mapping results shown in Fig. 3.5 also confirmed the presence of  $\text{ThO}_2$  inclusions in thorium metal.

Presence of  $\text{ThO}_2$  inclusions in thorium metal was further confirmed by Raman spectroscopy. Fig. 3.4 (e) shows a representative Raman spectrum recorded on thorium metal surface which clearly showed the first order Raman peak ( $465 \text{ cm}^{-1}$ ) [174] corresponding to cubic fluorite  $\text{ThO}_2$ . Inset in Fig. 3.4 (e) shows the optical micrograph of inclusion region in thorium metal over which Raman spectrum was recorded.

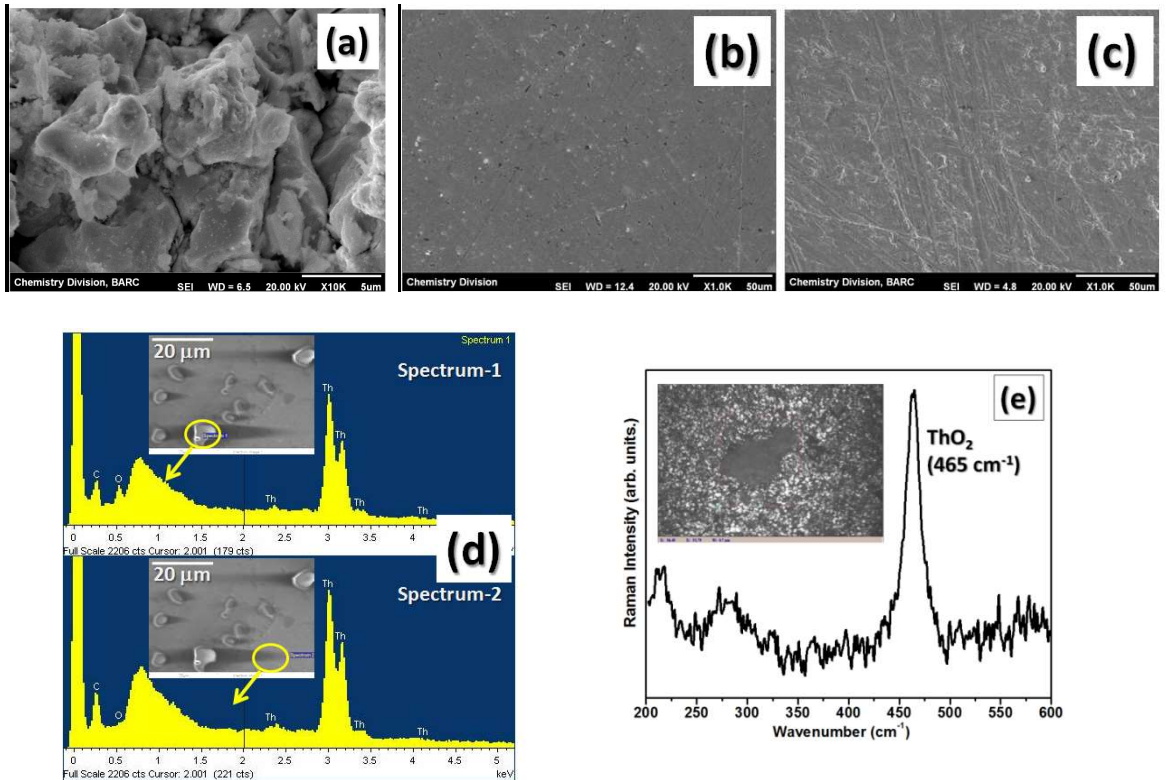


**Fig. 3.4. (a) SEM micrograph of thorium metal power compact (fractured surface), (b) arc-melted and polished thorium metal pellet surface, (c) arc-melted and polished uranium metal pellet, (d) EDS spectra of arc-melted thorium pellet showing distinct oxygen-rich regions (ThO<sub>2</sub> inclusions), (e) Raman spectrum recorded over arc-melted thorium pellet. Optical micrograph of ThO<sub>2</sub> inclusion is shown in inset of Fig. 3.4(e)**

Surface morphology and Raman spectroscopic results showed that while no oxide / carbide inclusions were detected in uranium, thorium metal had oxygen impurity mainly in the form of oxide inclusions apart from surface oxidation layer.

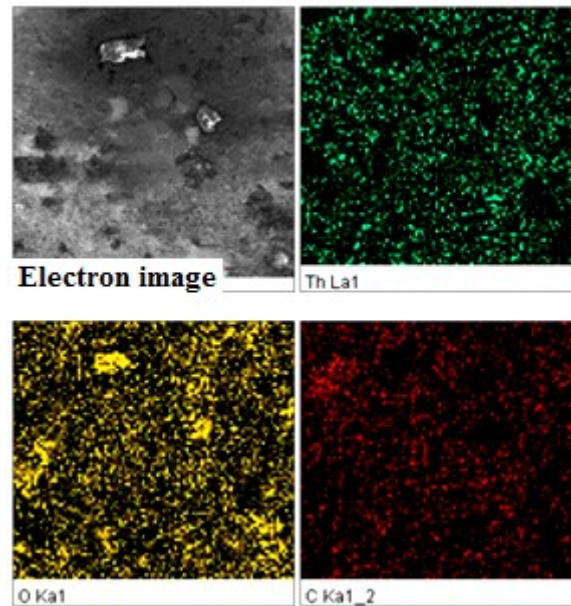


**Fig. 3.5. X-ray elemental mapping results performed over thorium metal surface.**

**Presence of ThO<sub>2</sub> inclusions is clearly seen from elemental mapping results**

#### 1.3.4. Thermal diffusivity of thorium and uranium

Figure 3.6 (a) shows as-measured thermal diffusivity of thorium and uranium as a function of temperature. Quality of data and average error in diffusivity measurements has been shown in Fig. 3.6 (b) in terms of results obtained on Inconel-600 reference measured under identical experimental conditions. Diffusivity results are obtained within  $\pm 2\%$  error. Thermal diffusivity of thorium is nearly three times higher than that of uranium, which shows its superior behavior towards heat transport when used as a nuclear fuel. While thermal diffusivity of thorium gradually decreases with temperature that of uranium shows an increasing trend. Similar trends of thermal diffusivity variation are also reported earlier. The most plausible reason for decreasing trend of thermal diffusivity of thorium with increasing temperature could be due to the contribution of thoria inclusions in thorium metal (as discussed in previous section), which itself is a poor heat conductor. Thoria inclusions may impede heat transport in the metal matrix. As a result of this, thermal diffusivity shows

decreasing trend with increasing temperature. On the other hand, increasing thermal diffusivity of uranium with temperature shows that the metal is devoid of poorly conducting oxide inclusions. It also indicates that the higher extent of carbon (~1100 ppm), which could be present both, as free carbon and/or bound carbide / oxycarbide phase, does not reduce the thermal diffusivity. Since carbides of uranium and thorium have better heat transport properties [175] as compared to oxides, their presence in metals as minor impurity phase is not likely to impede the overall heat transport behavior. Results obtained during present investigations also show notable variation from the literature recommended values for both thorium and uranium [150]. While reported data on thorium indicate a linear drop in thermal diffusivity with higher slope, present results show slower decrease in thermal diffusivity.

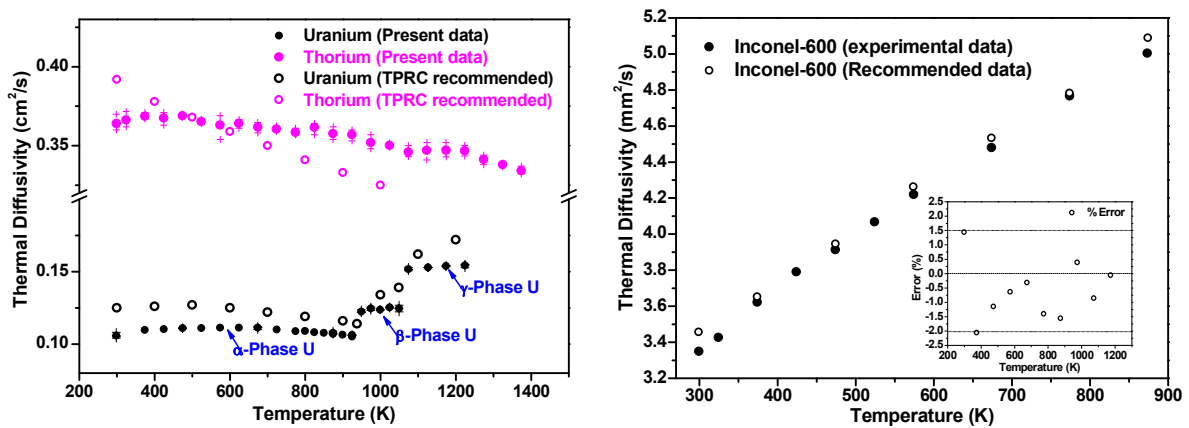


**Fig. 3.6. (a) Thermal diffusivity of thorium and uranium as a function of temperature.**

**Solid dots represent average value of four laser shots on each temperature, while plus symbols show as-measured individual data. Open dots are values recommended by**

**Touloukian et al., [150]; (b) thermal diffusivity results on Inconel-600 reference**

**material obtained under identical experimental conditions. Inset shows percentage**

**error in diffusivity measurements**

Thermal diffusivity of thorium varies continuously with temperature from  $\sim 0.36 \text{ cm}^2/\text{s}$  at ambient temperature to  $\sim 0.33 \text{ cm}^2/\text{s}$  at 1373 K, which is expected from the phase stability of  $\alpha$ -phase (face centred cubic; FCC) of thorium over the temperature range of investigation. On the other hand, results obtained on uranium metal show distinct behavior. In case of uranium, diffusivity values remain nearly constant ( $0.10 \text{ cm}^2/\text{s}$  to  $0.11 \text{ cm}^2/\text{s}$ ) over 298 K to 923 K. It increases systematically in the beginning (298 K – 673 K), followed by a reducing trend afterwards till 923 K. Diffusivity increases sharply (by  $\sim 15\%$  of the value at 923 K) at  $T \geq 949 \text{ K}$ , which marks the first allotropic phase transition from  $\alpha$ -phase (orthorhombic) to  $\beta$ -phase (body centred tetragonal) of uranium ( $\sim 942 \text{ K}$ ) [176]. From 949 K to 1049 K, diffusivity increases steadily. Above 1049 K, it again shows a steep rise (by  $\sim 21\%$  of the value at 1049 K), indicating the second allotropic phase transition from  $\beta$ -phase (body centred tetragonal) to  $\gamma$ -phase (body centred cubic; BCC) of uranium [177]. Diffusivity increases steadily thereafter up to 1273 K.

Weight measurements taken before and after the diffusivity experiments showed marginal gain ( $\leq 0.005 \text{ wt.}\%$ ) for both thorium and uranium, for samples weighing around 9 g to 10 g. This indicated that diffusivity data were only marginally affected by surface oxidation during the measurements. Post-experiments, while graphite coating could easily be removed by ultrasonication in hexane, polishing the uranium metal surface back to silvery-white lustre required mild grinding over silicon carbide (SiC) abrasive (1000 grit). Thorium metal did not require such grinding and was restored to bright metallic lustre with mild rubbing over diamond impregnated polishing cloth. This indicated surface modification of uranium during thermal cycling (298 K to 1273 K) even under dynamic vacuum ( $P \leq 10^{-6} \text{ mbar}$ ) and also showed relative higher stability of thorium towards surface reaction with graphite under similar experimental conditions. Based on earlier reports [178], such surface modification

may occur due to formation of thin layer of uranium oxycarbide phase(s) ( $UC_xO_{1-x}$ ) by high temperature interfacial reactions in U-C-O system (uranium metal + free carbon/UC + surface-oxide + residual atmospheric  $O_2$ ). These oxycarbides with cubic close packed crystal structure are known to adhere well to uranium surface, thereby preventing further corrosion during heat treatment. Formation of such interfacial layer can also explain the marginal decreasing trend of measured thermal diffusivity from 673 K to 923 K, as shown in Fig. 3.6. Erez et al., [179] have studied thermal and electrical properties of high purity uranium (total impurities < 300 ppm) under dynamic vacuum, without providing any surface coating. They observed continuously increasing trend in thermal diffusivity from 523 K up to the first phase transformation ( $\alpha \rightarrow \beta$ ) temperature ( $\sim 943$  K). Apparent difference between samples studied by us and those used by Erez et al. [179] is higher carbon content ( $\sim 1100 \pm 36$  ppm, Table 3.2) in our samples. Apart from that, there could be microstructural variations in different samples of uranium due to anisotropic crystal structure and metal processing history. Both, microstructure and impurities influence thermal transport properties. In order to attain an average equilibrium microstructure, the data reported here was taken after multiple thermal cycles (298 K to 1273 K). Therefore, the observed decrease in thermal diffusivity (over 673 K to 923 K) was attributed predominantly to the formation of oxycarbide layer and only marginally due to microstructural variations. Similar decreasing trend in thermal diffusivity of uranium has been reported earlier [155, 175, 180], but no plausible explanation was given. Our explanation may therefore be useful for data interpretation in future studies.

Figure 3.6 also shows that measured thermal diffusivity data for both thorium and uranium is on a lower side (especially near ambient temperature) than that recommended by Touloukian et al., [150]. One reason for this could be presence of relatively higher amount of impurities (C, N, O), which would impede heat transfer in bulk metal. To estimate the extent to which

higher impurity contents may affect thermal diffusivity (or thermal conductivity), a model calculation was performed with the help of non-metallic impurity content data in studied samples (Table 3.2). Considering that other than C, O and N, the major matrix is metal (thorium / uranium), the weight fraction formula of studied thorium and uranium samples can be given as {Th(0.9975) + C(0.0003) + N(0.0002) + O(0.002)} and {U(0.99869) + C(0.0011) + O(0.0001) + N(0.00011)}, respectively. Corresponding atom fraction formula may be shown as  $\text{Th}_{0.9631}\text{O}_{0.02808}\text{C}_{0.005601}\text{N}_{0.003198}$  and  $\text{U}_{0.9757449}\text{C}_{0.02183}\text{O}_{0.001871}\text{N}_{0.0014896}$  for thorium and uranium, respectively. It was assumed that (i) non-metallic impurities are present in structurally bound form such as (ThO<sub>2</sub>, ThN and ThC) and (UO<sub>2</sub>, UC and UN), and (ii) heat transport in such composite samples Th-ThO<sub>2</sub>-ThC-ThN and U-UO<sub>2</sub>-UC-UN is an algebraic sum of the fractional contributions of constituent phases as given by equation-3.2 and equation-3.3 for thorium and uranium, respectively. Based on these two assumptions, and using equation-3.2 and equation-3.3, the extent of decrease in thermal diffusivity due to the presence of ThO<sub>2</sub> / UO<sub>2</sub>, ThC / UC and ThN / UN phases was calculated. For uranium, these calculations were performed at three different temperatures (298 K, 573 K and 1073 K) while for thorium these were performed only at 298 K. High temperature values for thorium could not be calculated due to unavailability of reliable high temperature thermal diffusivity data for ThC and ThN. For these calculations, thermal diffusivities of pure phases (ThO<sub>2</sub>, UO<sub>2</sub>, UC and UN) were taken from reported IAEA data [175], while that of thorium and uranium metal was taken from TPRC recommended data [150]. Values for ThO<sub>2</sub>, ThC and ThN were taken from earlier reports [96, 181, 182]. Table 3.3 shows the results of this analysis. Uncertainty in thermal diffusivity values calculated using equation-3.2 and equation-3.3 were estimated based on the uncertainty of measurements reported for thorium ( $\pm 30\%$  between 298 K to 500 K;  $\pm 30\% > 500$  K) [150], uranium metal ( $\pm 13\%$  between 298 K to 900 K;  $\pm 15$  to  $\pm 20\% > 900$  K) [150], uranium compounds ( $< \pm 4\%$  for UO<sub>2</sub>;  $< \pm 15\%$  for UC and  $< \pm$

5% for UN) [174], ThO<sub>2</sub> (< ± 5%) [181], ThC (< ± 5%) [96] and ThN (< ± 4%) [182]. Higher values of uncertainty in reported thermal diffusivity is due to large scatter in individual data. This is why generation of indigenous thermophysical properties database is essential.

$$\alpha_{\text{Total-Th}} = 0.963 \times \alpha_{\text{Thorium}} + 0.0281 \times \alpha_{\text{ThO}_2} + 0.0056 \times \alpha_{\text{ThC}} + 0.0032 \times \alpha_{\text{ThN}} \quad (3.2)$$

$$\alpha_{\text{Total-U}} = 0.976 \times \alpha_{\text{Uranium}} + 0.0218 \times \alpha_{\text{UC}} + 0.00094 \times \alpha_{\text{UO}_2} + 0.0015 \times \alpha_{\text{UN}} \quad (3.3)$$

**Table 3.3. Effects of impurities (C, N, O) on thermal diffusivity of thorium and uranium**

<b>Formula used for total thermal diffusivity of thorium and uranium</b>			
$\alpha_{\text{Total-U}} = 0.976 \times \alpha_{\text{Uranium}} + 0.0218 \times \alpha_{\text{UC}} + 0.00094 \times \alpha_{\text{UO}_2} + 0.0015 \times \alpha_{\text{UN}}$			
$\alpha_{\text{Total-Th}} = 0.963 \times \alpha_{\text{Thorium}} + 0.0281 \times \alpha_{\text{ThO}_2} + 0.0056 \times \alpha_{\text{ThC}} + 0.0032 \times \alpha_{\text{ThN}}$			
<b>Temperature (K)</b>	<b>Recommended thermal diffusivity (mm<sup>2</sup>/s) [150]</b>	<b>Calculated thermal diffusivity of composite (mm<sup>2</sup>/s) [Equation-2 &amp; 3]</b>	<b>Present experimental data (mm<sup>2</sup>/s)</b>
298 (U)	12.5 ± 1.62	12.4 ± 1.60	10.6 ± 0.21
298 (Th)	39.1 ± 11.7	38.02 ± 9.51	36.6 ± 0.62
573 (U)	12.6 ± 1.64	12.5 ± 1.62	11.1 ± 0.15
1073 (U)	14.9 ± 2.98	14.7 ± 2.94	15.1 ± 0.10

From these results, it is clear that non-metallic impurities; to the extent present in studied samples (total < 0.25 wt. % for thorium and < 0.15 wt. % for uranium), do not significantly influence the thermal diffusivity. For thorium, large uncertainty associated with literature reported values (Table 3.3) show the poor reliability of literature data. Also, there might be deviations in actual chemical state of impurities from that assumed while calculating the

thermal diffusivity of composites. For example, carbon, which is the major impurity phase in uranium, may not be present as bound carbon alone (UC) but remain as a mix of bound and free carbon (UC + C). Similarly, carbon may be dissolved in thorium [165] or present as ThC along with ThC<sub>2</sub>. Presence of reduced oxide of thorium (ThO) also cannot be ruled out [183]. The observed difference between TPRC recommended values and present results therefore can be attributed to combined effect of (i) impurities (ii) chemical state of impurities and (iii) microstructure. Extent of deviation in thermal diffusivity data for anisotropic-phase of uranium is large (up to 16%), which reduces to ~1.5% for the isotropic cubic uranium (1073 K data; Table 3.3). on the other hand, for thorium, which remains in FCC phase throughout the temperature range of present investigations, the average experimental thermal diffusivity (at 298 K) differs from recommended value by ~6% only. These results further suggest that thermal diffusivity (or thermal conductivity) is notably affected by the microstructure of anisotropic solids such as uranium. At high temperatures, when uranium stabilizes in isotropic cubic structure, the contribution of structural anisotropy in impeding the heat transport is expected to reduce. Results presented in Table 3.3 also indicate the same, where experimental data for uranium at 1073 K exceeds the TPRC recommended value as well as the calculated value for the composite (U-UO<sub>2</sub>-UC-UN). It can be seen that uncertainty associated with the results obtained in present investigations are lower than reported literature values for both, thorium and uranium, which also confirm improved reliability of present data.

It is worth mentioning that as compared to results obtained in present investigations, datasets used in recommended compilation [150] have large scatter. For uranium, either these datasets are limited to orthorhombic phase or, are inconsistent in terms of diffusivity variation for its high temperature structural allotropes. Similarly, high temperature thermal diffusivity values

for thorium are not available. Results reported in a recent IAEA publication [175] provide diffusivity values that are back-calculated from experimental data on thermal conductivity, specific heat and density. In comparison to existing literature, present data shows a clear trend of sharp and notable increase in thermal diffusivity of uranium while transforming from orthorhombic to tetragonal to cubic phase. This confirms that the crystal structure has a notable influence on heat transport, and in particular heat transport is facilitated with increasing structural symmetry. Thorium's diffusivity data is generated over a wider temperature range and with significantly improved precision. In light of above discussion, present thermal diffusivity results are more reliable for evaluating thermal conductivity of thorium and uranium.

### 1.3.5. Linear thermal expansion of thorium and uranium

Figure 3.7 (a) shows fractional linear dilation ( $dL/L_0$ ) of thorium and uranium and as a function of temperature; plotted for heating as well as cooling cycle. Figure 3.7 (b) shows linear thermal expansion of sapphire reference; measured under identical experimental conditions. Inset shows percentage deviation in measured expansion of sapphire from NIST recommended values. Based on the results obtained for sapphire, average error in thermal expansion measurements was found to be less than  $\pm 2\%$ . Expansion of thorium is significantly lower than that of uranium, which is an important advantage of its usage as nuclear fuel since it contributes towards lower fuel swelling behavior and therefore better resistance towards fuel-clad interaction (FCMI and FCCI). Cyclic nature of thorium's expansion curve in heating and cooling cycle without any expansion anomaly confirmed the isotropic expansion behavior of FCC thorium over the studied temperature range. Reproducibility of expansion curves obtained during repeated thermal cycling of thorium also indicated its microstructural stability during thermal cycling, which did not affect its

expansion behavior. Thermal expansion results of uranium on the other hand are quite interesting. Two expansion anomalies can be seen at ~948 K and ~1051 K during the heating cycle, which correspond to  $\alpha \rightarrow \beta$  and  $\beta \rightarrow \gamma$  structural phase transformation of uranium, respectively [184]. Transition temperatures also match well with those observed during thermal diffusivity measurements as well as with most reported values for nuclear-grade uranium [177, 185]. Cooling cycle curve also exhibit both the transitions with transition temperatures shifted downwards mainly due to thermal hysteresis observed under relatively fast cooling (30 K/min.). Fig. 3.7 also shows that sample length apparently increases marginally by 0.41% (~18  $\mu\text{m}$ ; for initial sample length ( $L_0$ ) ~4280  $\mu\text{m}$ ) at the end of cooling cycle. This is mainly due to variation in the extent of measured dilation during  $\alpha \leftrightarrow \beta$  transition in heating and cooling cycles.

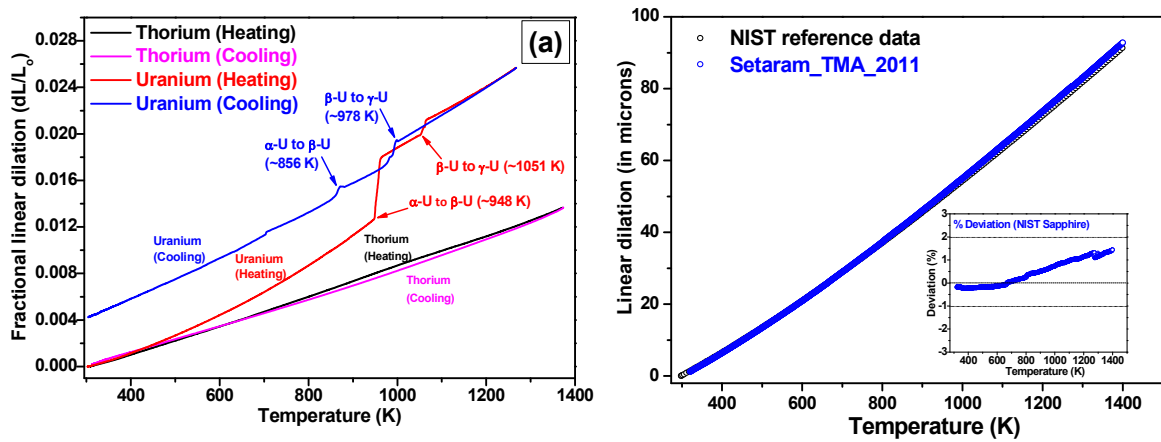


**Fig. 3.7. (a) Linear thermal expansion of polycrystalline thorium and uranium metal as a function of temperature. For uranium, both phase transitions, namely  $\alpha \rightarrow \beta$  and  $\beta \rightarrow \gamma$  are observed during heating as well as cooling cycles; (b) Linear thermal expansion of sapphire reference measured under identical experimental conditions. Inset shows percentage deviation in measured expansion of sapphire from NIST recommended values**

During heating, uranium sample length increases by  $\sim 22 \mu\text{m}$  in the transition ( $\alpha \rightarrow \beta$ ) region, which during cooling cycle transition ( $\beta \rightarrow \alpha$ ), contracts only by  $\sim 5 \mu\text{m}$ , thereby indicating net sample deformation during thermal cycling. No such apparent length change was observed for thorium. Similar changes in dimensions of uranium metal have been reported earlier and attributed to expansion anisotropy in polycrystalline samples, mainly originating from dynamic variation in preferred orientation of grains during solid-solid transitions [156, 186, 187]. To confirm that increase in sample length ( $\sim 18 \mu\text{m}$ ) was not due to surface oxidation, post-experiment sample analysis was performed.

It was observed that uranium sample weight increased by  $\sim 0.0085 \text{ wt.}\%$ . Also, both circular surfaces of sample; perpendicular to which dilation was measured, retained their metallic lustre. It was assumed that sample surface is uniformly oxidized thereby giving rise of oxide layer thickness  $\sim 9 \mu\text{m}$  in presence of oxygen impurity in argon carrier gas as well as degassed oxygen from ceramic components of TMA equipment at high temperatures. It was also assumed that only  $\text{UO}_2$  is formed under inert atmosphere during thermal expansion experiments. Based on above assumptions, the expected weight gain was estimated to be  $\sim 0.06 \text{ wt.}\%$ , which is almost an order of magnitude higher than the observed weight gain ( $\sim 0.0085 \text{ wt.}\%$ ). These results indicated that the observed sample deformation ( $\sim 18 \mu\text{m}$ ) has a minor contribution ( $\sim 10 \%$ ) due to oxide layer growth while the majority of it originates from the expansion anisotropy of metallic uranium. In case of thorium, the extent of weight gain during one thermal cycle (298 K – 1373 K) was  $\sim 0.0034 \text{ wt.}\%$ . However, the nature of thermal expansion curve is completely cycling as seen in Fig. 3.7. Excellent repeatability of expansion curves was observed up to four consecutive thermal cycles. Above results for thorium and uranium confirmed highly reliable quality of measurements. Expansion data was further used for evaluation of volume expansion and temperature dependence of density.

A number of reports are available on thermal expansion behavior of uranium [156, 160, 188, 189]; while very few reports exist on thorium [60, 152]. Reports on uranium invariably indicate the influence of structural anisotropy of both,  $\alpha$ - and  $\beta$ -phase on its expansivity. It is known that at atmospheric pressure, uranium attains three crystallographic forms between ambient temperature and its melting point, through first-order solid-state phase transitions. A conceptual visualization of these transitions inside a defect-free, chemically pure single crystal of  $\alpha$ -uranium (orthorhombic) suggests the following: Upon heating  $\alpha$ -uranium, it transforms to  $\beta$ -phase (tetragonal) as a result of reorganization of U-atoms from their mean positions in the vicinity of transition ( $\sim 942$  K). The  $\beta$ -phase further transforms to isotropic  $\gamma$ -phase (cubic) by yet another event of atomic reorganization around 1050 K. If cooling is started well before the melting ( $\sim 1403$  K), the  $\gamma$ -phase reverts back to  $\alpha$ -phase through the intermediate  $\beta$ -phase. During such thermal cycles, these transitions are likely to result into additional random redistribution of existing defects in the crystal. As a result, thermally cycled crystal would always contain distinct distribution of lattice defects and therefore a residual lattice distortion. Extending this explanation to a polycrystalline uranium sample would require additional involvement of inter-grain effects, especially near their interfaces. Grain to grain orientation (texture) and their fractional content would therefore influence the microstructural changes inside a polycrystalline sample during thermal cycling. As a result of this, a polycrystalline sample of uranium would evolve in terms of its microstructure during thermal cycling over the temperature range encompassing all three phases. A net effect would therefore be seen in terms of expansion anisotropy, as observed in present investigation. As evidence to above explanation, variation in the extent of dilation, especially during the phase transition regions over two different dilation experiments is shown in Fig. 3.8. Inset in Fig. 3.8 shows overlapping dilation curves of thorium recorded over repeated thermal cycles, which confirm its microstructural stability over the investigated temperature range.

Much of the existing literature on thermal expansion of uranium confine to lattice expansion [185]. Few reports are available on bulk thermal expansion using dilatometry [156, 188]. Recently, use of theoretical simulations has also been reported to estimate uranium's lattice thermal expansion behavior [160]. Literature information on thermal expansion behavior of single crystal thorium could not be traced. To compare our results on uranium with those reported earlier, the work of Llyod [188] on high purity single crystals of uranium using dilatometry technique has been referred. Logan et al., [156] also used dilatometry for thermal expansion studies on polycrystalline uranium samples processed by different metallurgical routes.

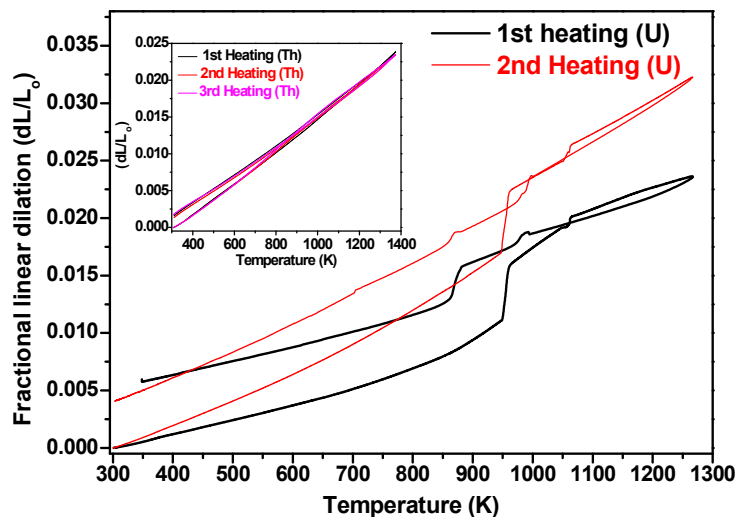


**Fig. 3.8. Effect of thermal cycling on linear thermal expansion of polycrystalline uranium; Inset shows the linear dilation curves for thorium metal over three consecutive thermal cycles**

However, due to unavailability of experimental data or suitable analytical functions, present data could not be compared with their results. In order to estimate average linear expansion of polycrystalline sample using the results obtained on single crystals, following method was

used. Llyod [188] gave the following equations (equation-3.2 to equation-3.4) for linear expansion along three crystallographic directions [100], [010] and [001].

$$\left(\frac{L_T - L_{298K}}{L_{298K}}\right)_{[100]} = 23.53 \times 10^{-6} \times T^1 + 13.74 \times 10^{-9} \times T^2 + 9.94 \times 10^{-12} \times T^3 \quad (3.2)$$

$$\left(\frac{L_T - L_{298K}}{L_{298K}}\right)_{[010]} = 1.16 \times 10^{-6} \times T^1 - 9.43 \times 10^{-9} \times T^2 - 11.79 \times 10^{-12} \times T^3 \quad (3.3)$$

$$\left(\frac{L_T - L_{298K}}{L_{298K}}\right)_{[001]} = 19.38 \times 10^{-6} \times T^1 + 21.58 \times 10^{-9} \times T^2 + 3.32 \times 10^{-12} \times T^3 \quad (3.4)$$

Assuming that the same single crystal is converted into a highly dense polycrystalline sample that is composed of randomly orientated and uniformly distributed small crystallites; the average linear thermal expansion of latter can be estimated as follows.

$$\left(\frac{L_T - L_{298K}}{L_{298K}}\right)_{Polycrystal} = \frac{1}{3} \left(\frac{L_T - L_{298K}}{L_{298K}}\right)_{[100]} + \frac{1}{3} \left(\frac{L_T - L_{298K}}{L_{298K}}\right)_{[010]} + \frac{1}{3} \left(\frac{L_T - L_{298K}}{L_{298K}}\right)_{[001]} \quad (3.5)$$

Using equation-3.5, fractional linear dilation was estimated for a hypothetical polycrystalline sample of uranium having same purity as that of single crystal used by Llyod et al. [189]. Results are plotted along with the dilation curve measured in present investigation and shown in Fig. 3.9. For thorium, results obtained during present studies and those recommended for polycrystalline thorium in TPRC database [152] are also plotted in the same figure.

Reasonable agreement is obtained between the estimated and measured dilation for both the metals with experimental data showing slightly lower fractional dilation as compared to literature. For uranium, the maximum deviation is 0.0009 (~6.6 %) around 943 K (the highest temperature of  $\alpha$ -phase stability region). At this temperature, thorium's experimental data

show much lower deviation (0.0004; ~4 %) from literature data [152]. For uranium, this deviation can be attributed to (i) effect of poor crystallinity at grain boundaries, which may reduce the measured thermal dilation, (ii) variation in purity (Table 3.2) as compared to sample used by Llyod (carbon ~35 ppm, nitrogen ~20 ppm, oxygen: not reported) [190] and (iii) differences in crystallographic anisotropy as well as texture of actual polycrystalline samples against completely randomized and uniformly oriented ideal polycrystalline sample.

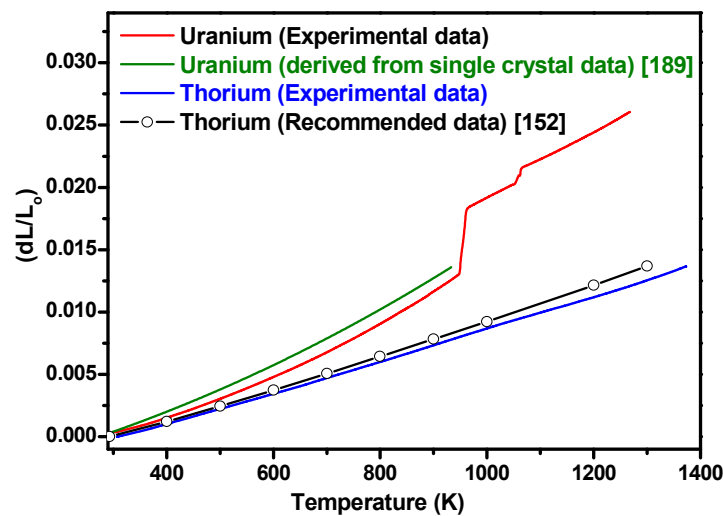


**Fig. 3.9. Comparison of linear thermal dilation behavior of polycrystalline samples of uranium and thorium with literature data on single crystal uranium [189] and polycrystalline thorium [152]**

In case of thorium, the deviation can be attributed mainly to the inclusion of  $\text{ThO}_2$  phase (~2000 ppm oxygen) as well as other impurities. Close agreement between our results and those calculated from equation-(3.5) shows reliability of present measurements. Experimental bulk thermal expansion data on polycrystalline uranium spanning over all three of its solid-state allotropes is not reported. Similarly, presented data on thorium metal is perhaps the first direct experimental linear thermal expansion data over a wide temperature range. Since both thorium and uranium-based alloy nuclear fuels are fabricated in polycrystalline form, present

results would be of significant relevance for understanding their thermo-mechanical properties.

Based on above results, it appeared reasonable to approximate the measured linear expansion data with that of a completely randomized, uniformly oriented polycrystalline sample. Using the measured dilation data, temperature dependent densities ' $\rho(T)$ ' of thorium and uranium were calculated from the following equation.

$$\rho(T) = M_T / V_T \quad (3.6)$$

Here, ' $M_T$ ' is sample mass and ' $V_T$ ' is sample volume at temperature ' $T$ '. ' $V_T$ ' is given as

$$\begin{aligned} V_T &= V_{298\text{ K}} + \Delta V \\ &= V_{298\text{ K}} + V_{298\text{ K}} \times \alpha_V \times (T - 298\text{ K}) \end{aligned} \quad (3.7)$$

Where  $\alpha_V = (dV / dT) / V_{298\text{ K}}$

Assuming that sample has random mixing of fine crystallites, volume expansion coefficient ( $\alpha_V$ ) can be derived from linear expansion coefficient ( $\alpha_L$ ) by using the following relation.

$$\alpha_V = 3\alpha_L \quad (3.8)$$

Where  $\alpha_L = (dL / dT) / L_{298\text{ K}}$  or  $\{(L_T - L_{298\text{ K}}) / (T - 298\text{ K})\} / L_{298\text{ K}}$

Using equation-3.8 in equation-3.7, we get

$$\begin{aligned} V_T &= V_{298\text{ K}} [1 + \alpha_V \times (T - 298\text{ K})] \\ &= V_{298\text{ K}} [1 + 3\alpha_L \times (T - 298\text{ K})] \end{aligned}$$

$$V_T = V_{298\text{ K}} \left[ 1 + 3 \left\{ \frac{L_T - L_{298\text{ K}}}{T - 298\text{ K}} \right\} / L_{298\text{ K}} \times (T - 298\text{ K}) \right]$$

$$V_T = V_{298\text{ K}} \left[ 1 + 3 \left\{ \frac{L_T - L_{298\text{ K}}}{L_{298\text{ K}}} \right\} \right] \quad (3.9)$$

Figure 3.10 shows temperature dependence of density for thorium and uranium, as evaluated by measured linear dilation data. For comparison, densities of nuclear-grade uranium and thorium; as recommended by International Atomic Energy Agency (IAEA) are also plotted [175].

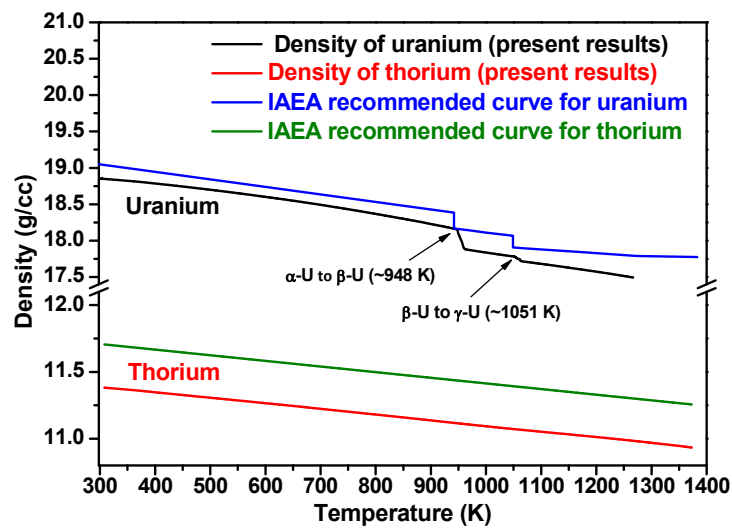


**Fig. 3.10. Bulk density of thorium and uranium metal obtained from measured linear thermal expansion data during heating cycle. IAEA recommended values are also plotted along [175]**

Temperature dependent density of samples investigated in present study was on a lower side (18.86 g/cc for U; 11.39 g/cc for Th; at 300 K) than the IAEA recommended values (19.04 g/cc for U; 11.7 g/cc for Th; at 300 K). This variation can be attributed to (i) lower density at ambient temperature due to relatively higher impurity contents (~1100 ppm carbon in uranium; ~2000 ppm oxygen in thorium), (ii) metallurgical process history and (iii) polycrystallinity. This is further supported by ambient temperature density value obtained from the unit cell parameters (18.91 g/cc for U; 11.62 g/cc for Th; at 298 K). Density

obtained from dilatometry is lower than X-ray density, which may be attributed to the presence of polycrystallinity induced crystal defects and porosity, both of which influence the bulk thermal expansion behavior. However, despite being on the lower side, density values obtained in the present investigation are representative of routinely used metal samples for nuclear fuel fabrication. These density values were used for calculation of thermal conductivity of uranium and thorium. Average coefficients of linear thermal expansion for uranium and thorium metals are presented in Table 3.4. For high temperature tetragonal ( $\beta$ ) and cubic ( $\gamma$ ) phase of uranium, these coefficients were evaluated based on the slope of linear dilation curves in the stability region of these phases.

**Table 3.4. Average coefficient of linear thermal expansion for uranium and thorium**

Sample and temperature range	Coefficient of linear thermal expansion (CTE) ( $\times 10^{-6} \text{ K}^{-1}$ )	Literature reported CTE ( $\times 10^{-6} \text{ K}^{-1}$ )
$\alpha$ -Uranium (Orthorhombic); (298 K – 940 K)	19.74	20.0 [96]
$\beta$ -Uranium (Tetragonal); (960 K – 1050 K)	22.21	17.3 [96]
$\gamma$ -Uranium (BCC) (1060 K – 1270 K)	22.14	23.3 [96] 22.5 $\pm$ 1.3 [185]
$\alpha$ -Thorium (FCC) (298 K – 1373 K)	12.76	12.5 [60]

Thermal expansion of high temperature BCC phase of uranium metal ( $\gamma$ -phase), which is stable between 1048 K up to melting temperature ( $\sim$ 1405 K) is also important. Unit cell of BCC phase has two atoms and shows typical behavior of metallic materials. It is worthwhile to mention here that since the  $\gamma$ -phase is formed at high temperatures (average  $\beta \rightarrow \gamma$  transition temperature  $\sim$ 1045 K), there will always be errors in the estimated values of

coefficient of thermal expansion (CTE), resistivity and density, due to surface oxide layer formation (oxygen contamination), excessive grain growth, etc. In earlier studies reported by Klepfer et al., [185] on purer samples of uranium metal, lattice parameter has been found to increase linearly with increase in temperature for the  $\gamma$ -phase. Based on this, the average coefficient of thermal expansion (CTE) was found to be  $22.5 \pm 1.3 \times 10^{-6}/\text{K}$ . The value agrees reasonably well with that obtained from dilatometry studies reported by the same authors as well as in the present study. Further, Large difference in the values of density between present data and IAEA recommended values for gamma phase of uranium; as shown in Fig. 3.10, must be arising due to the difference in the metallurgical conditions involved in the preparation of the metal as well as the impurities present in it. Thermal expansion coefficient of thorium evaluated from measured dilation data agrees within 2% of literature reported value [60].

### 1.3.6. Specific heat capacity of thorium and uranium

Temperature dependent specific heat ( $C_p$ ) of thorium and uranium, which is required for thermal conductivity evaluation, was taken from existing literature and / or experimental results. A typical heat flow curve obtained by temperature modulated DSC experiment on thorium metal is shown in Fig. 3.11 (a). Specific heat was evaluated from reversing heat flow curve after resolving the heat flow curve into reversing and non-reversing components. Although DSC measurements could only be performed over a limited temperature range (298 K to 773 K), these results served as a guide to compare measured  $C_p$  with the reported values. Figure 3.11 (b) shows specific heat of sapphire reference measured under identical experimental conditions along with the NIST recommended  $C_p$  data. Inset in Fig. 3.11 (b) shows percentage deviation in measured  $C_p$  from recommended values, which is within  $\pm 3\%$  over the studied temperature range (240 K – 723 K).

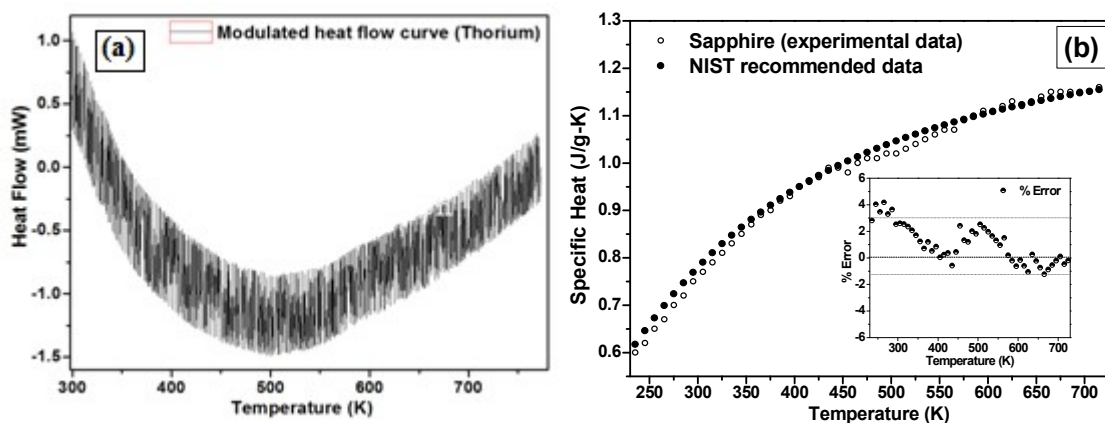


**Fig. 3.11. (a) Representative heat flow curve obtained on thorium metal after a temperature modulated DSC experiment, (b) Specific heat of sapphire measured under identical experimental conditions along with the NIST recommended  $C_p$  data. Inset shows percentage deviation in measured  $C_p$  from recommended values**

Details of samples, for which  $C_p$  data is selected from literature, are presented in Table 3.5 and Table 3.6. Criterion used for selecting the literature data included (i) metal purity and (ii) consistency of reported data. Figure 3.12 (a) and (b) show literature  $C_p$  data for high purity thorium [157, 191-193] and uranium [157, 175, 194, 195], respectively along with results obtained in present investigations using modulated DSC technique.

In case of thorium (Fig. 3.12 (a)), there is more variation in reported  $C_p$  data. Experimental results obtained during present investigations (273 K – 773 K) fall in the middle of these results and match closely with those latest reported by Oetting et al., over the temperature range from 298 K to 700 K [193]. Results reported by Nakamura et al., [157] also have minimum variation from our experimental results and those reported by Oetting et al., [193].

**Table 3.5. Non-metallic impurities in thorium used for  $C_p$  measurements**

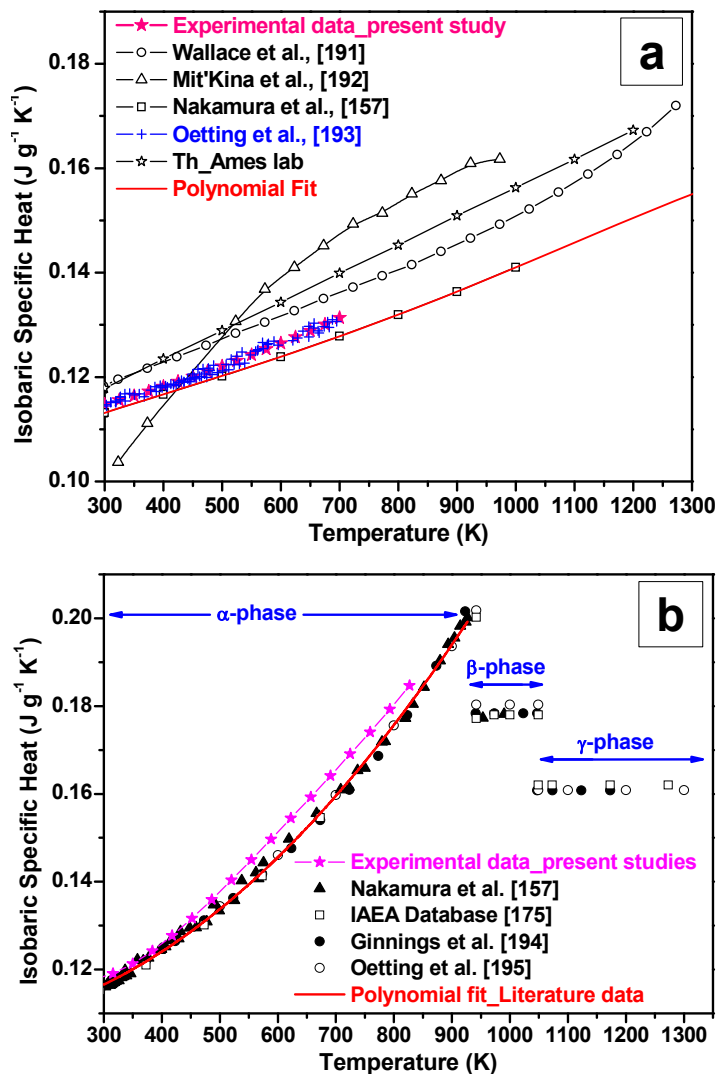
Literature reference	Purity of Th (%)	C Content (ppm)	N Content (ppm)	O Content (ppm)
Present studies	99.75	300	200	2000
Wallace et al., [191]	99.95	75	3.3	58.3
Mit'Kina et al., [192]	~99.81	Not specified	Not specified	Not specified
Nakamura et al., [157]	~99.95	155	29	190
Oetting et al., [193]	99.74	up to 1605	400	600

Table 3.6. Non-metallic impurities in uranium used for  $C_p$  measurements

Literature reference	Purity of U (%)	C Content (ppm)	N Content (ppm)	O Content (ppm)
Present studies	99.8	1100	100	110
Ginnings et al. [196]	$\geq 99.95$	150	30	20
Kaity et al. [197]	High Purity	Not specified	Not specified	Not specified
Nakamura et al. [157]	$\geq 99.9$	$< 720$	$< 20$	190
IAEA report [175]	Nuclear-grade	Not specified	Not specified	Not specified

Weight measurement on thorium sample heated in DSC up to 773 K showed ~1% weight gain. Based on close agreement with present results as well as availability of high temperature  $C_p$  values (up to 1000 K), results of Nakamura et al., [157] were extrapolated up to 1373 K and used for thermal conductivity evaluation. Higher  $C_p$  values obtained during the present investigations could also be attributed to higher extent to  $\text{ThO}_2$  impurity phase, which has higher specific heat than metal.

For uranium on the other hand, measured  $C_p$  values are on a higher side than those reported in literature as shown in Fig. 3.12 (b). Analysis of DSC residue after a single DSC run showed up to 3% weight gain, indicating notable surface oxidation during the DSC experiment. Higher weight gain in the case of uranium could be due to higher surface reactivity of uranium with air as compared to thorium.



**Fig. 3.12. Isobaric specific heat of (a) thorium and (b) uranium as a function of temperature; Black data points show literature reported values. Pink colour data show experimental  $C_p$  obtained from TMDSC measurements (298 K - 773 K)**

It appeared that perfect inert conditions could not be maintained during the experiments, in spite of flowing high purity argon gas over the DSC cell. Surface oxidation could have occurred either from oxygen impurity in argon gas, or from ambient air leak in the lid-type DSC cell. Use of such data would have caused additional uncertainty and hence to prevent that, reported  $C_p$  data [157, 175, 194, 195] was used for thermal conductivity evaluation for uranium.

### 1.3.7. Thermal conductivity of thorium and uranium

Temperature dependent thermal conductivity ' $\lambda(T)$ ' of thorium and uranium was calculated using equation-3.1 from the experimental thermal diffusivity ' $a(T)$ ', density derived from thermal expansion data ' $\rho(T)$ ' and specific heat ' $C_p(T)$ ' values.  $C_p$  data corresponding to temperatures where thermal diffusivity was measured were obtained by 3<sup>rd</sup> order polynomial fitting of literature  $C_p$  data. Figure 3.13 shows the temperature dependence of thermal conductivity of thorium and uranium. Ambient temperature thermal conductivity of thorium ( $\sim 47$  W / m. K) is more than double than that of uranium ( $\sim 23$  W / m. K). Such high thermal conductivity is one of the most important material advantages of thorium-based metallic alloy nuclear fuels. While thermal conductivity of both metals increases with temperature, the extent of increase in thermal conductivity of uranium is higher as it transforms from lower symmetry allotrope (orthorhombic) to isotropic cubic (BCC) allotrope at higher temperatures. Thorium remains in isotropic FCC phase throughout the studied temperature range.

Porosity correction to thermal conductivity of studied samples ( $\rho_{\text{measured-U}} \sim 18.85$  g/cm<sup>3</sup>;  $\rho_{\text{measured-Th}} \sim 11.39$  g/cm<sup>3</sup> at 298 K) was applied using Loeb's equation [196] (equation-3.10) to obtain thermal conductivity of fully dense ( $\rho_{\text{theoretical-U}} \sim 19.16$  g/cm<sup>3</sup>;  $\rho_{\text{theoretical-Th}} \sim 11.70$

g/cm<sup>3</sup> at 298 K) metals. The correction was based on assumption that small isolated pores, which are spherical in shape, are uniformly distributed throughout the sample.

$$\lambda_{\text{Porous}} = \lambda_{100\% \text{ dense}} (1-P) \quad (3.10)$$

$$\text{Where } P \text{ (fractional porosity)} = \{(\rho_{\text{theoretical}} - \rho_{\text{measured}}) / \rho_{\text{theoretical}}\} \quad (3.11)$$

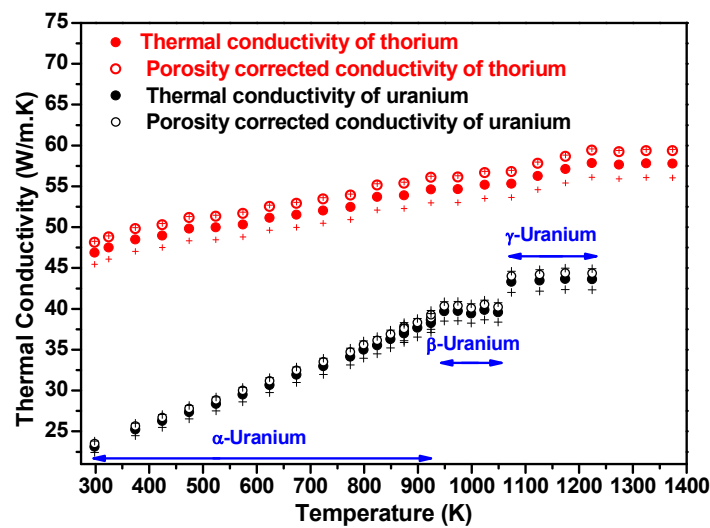


**Fig. 3.13. Thermal Conductivity of nuclear-grade thorium and uranium as a function of temperature. Plus symbols indicate the estimated average error in thermal conductivity measurements**

Porosity corrected thermal conductivity data are also plotted along with as-evaluated data in Fig. 3.13. It can be seen that while small porosity (~ 1%) of has limited effect on thermal conductivity of uranium, the effect is more pronounced for thorium metal where the larger fraction of oxide ceramic phase impurity (ThO<sub>2</sub>) also acts as impedance to efficient heat transfer. Availability of high purity thorium and uranium metals may further improve the quality of such measurements.

Thermal conductivity of uranium increases with increasing temperature. During its transformation to high temperature allotropes ( $\alpha \rightarrow \beta$ ;  $\sim 948$  K,  $\beta \rightarrow \gamma$ ;  $\sim 1051$  K), thermal conductivity increases sharply and the extent of increase is higher for second (tetragonal to cubic) transformation. This can be attributed to higher symmetry of cubic phase, which facilitates heat transport mainly through conduction electrons in a relatively low density, isotropic cubic lattice. Recent theoretical studies on uranium metal [159] have indicated that with increasing temperature, phonon contribution to thermal conductivity decreases while electronic contribution increases. A net effect of the two processes gives true variation in conductivity. Fig. 3.13 also shows that thermal conductivity remains nearly constant with temperature in the stability region of both the high temperature allotropes ( $\beta$  and  $\gamma$  phase). On the contrary, thermal diffusivity steadily increases, while density decreases with temperature as shown in Fig. 3.6 and Fig. 3.10, respectively. Near invariance of thermal conductivity can therefore be attributed to (i) mutually opposing trends in diffusivity and density variation and (ii) near constant values of specific heat in the stability region of both the high temperature allotropes (Fig. 3.12(b)). These results indicate that further careful measurements of specific heat ( $C_p$ ) for uranium are necessary, especially for the high temperature allotropes, in order to obtain more reliable trends in thermal conductivity. It must be noted here that high accuracy  $C_p$  measurements on uranium at elevated temperatures are challenging due to its reactivity with trace amount of  $O_2$ ,  $N_2$ ,  $H_2O_{(vapour)}$ ,  $CO_2$ , etc. Nonetheless, presented results can reliably be taken as the lower bound of thermal conductivity for both the high temperature allotropes ( $\beta$ - and  $\gamma$ -phase). In case of thorium, high temperature specific heat ( $C_p$ ) values (above 1000 K) were extrapolated from the data reported by Nakamura et al., [157]. Since  $C_p$  values reported by them are lower than our experiment values (Fig. 3.12(a)), the present thermal conductivity results can be taken as reliable lower bound values with no over estimation. Stability of  $\alpha$ -phase (FCC) of thorium extends up to  $\sim 1723$  K and thus the extrapolation is

likely to give good approximation of the true  $C_P$  values at higher temperatures. Still, experimental  $C_P$  data in high temperature region (above 1000 K) would be very useful for better accuracy thermal conductivity results.

Figure 3.14 shows a comparison of our thermal conductivity results with those reported earlier [60, 157, 160, 185, 186]. Following inference can be made from these results TPRC recommended thermal conductivity values for thorium [149] are close to values obtained in present investigations. Results reported by Peterson et al., on thorium [60] are more than 20% lower as compared to present results and indicate some systematic deviation in those measurements. Higher accuracy ( $\pm 5\%$ ) and precision ( $\pm 3\%$ ) of present data, based on the results obtained on metallic reference materials (Inconel-600 and high purity iron) measured under similar conditions confirm the reliability of present results.

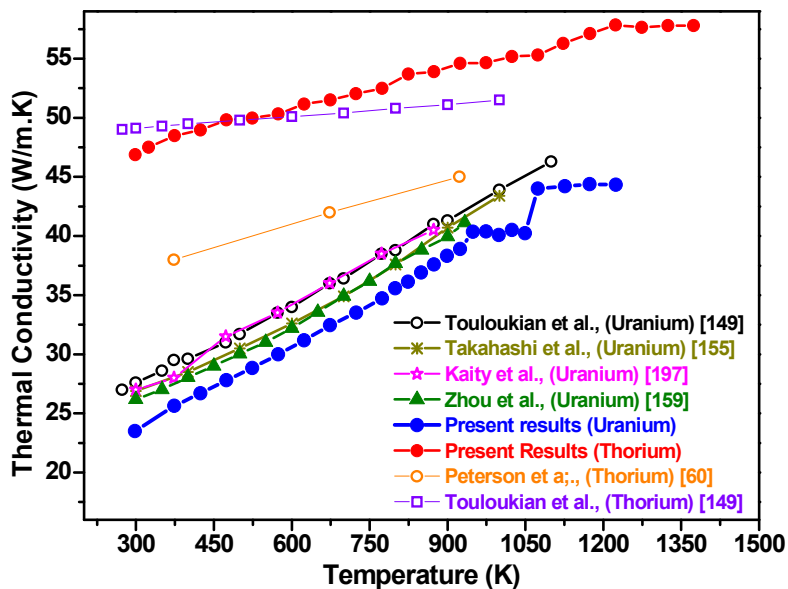


**Fig. 3.14. Comparison of temperature dependence of thermal conductivity of thorium and uranium studied in present investigation with available literature data**

Thermal conductivity of uranium samples studied in present investigation is lower than reported values. This could be due to relatively higher impurity contents in our sample (Table 3.2) as compared to literature. Touloukian et al., [149] recommended their data for well-annealed, high purity uranium. Similarly, both Takahashi et al., [155] and Kaity et al., [197] also reported use of purer uranium metal (total impurities < 1000 ppm).

Theoretical results presented by Zhou et al., [159, 198] were also based on a defect-free, pure uranium crystal. Another reason for lower values of thermal conductivity could be varying degree of structural anisotropy and preferred orientation of crystallites in studied polycrystalline samples, both of which would impede heat transport by acting as additional scattering centres for electrons and phonons. XRD results shown in Fig. 3.3(b) indeed confirm preferred orientation of (002) planes ( $2\theta \sim 36.31^\circ$ ) in studied uranium samples [169]. Further, during thermal cycling (298 K to 1273 K), when uranium metal passes through three structural modifications, its microstructure (grain size, size distribution and orientation) would dynamically evolve (as discussed earlier in this paper). Also, there would be variations in distribution of crystal defects within individual crystallites and also in orientation of grains. This would also affect both, thermal diffusivity and thermal conductivity. As a proof to this, effect of thermal cycling on measured thermal diffusivity of a representative uranium sample is shown in Fig. 3.15. Thermal diffusivity values were reproducible only after four successive thermal cycles in case of uranium samples. Experimental care while obtaining such results is important for reliable use of thermophysical property data for fuel development and safety code evaluation.

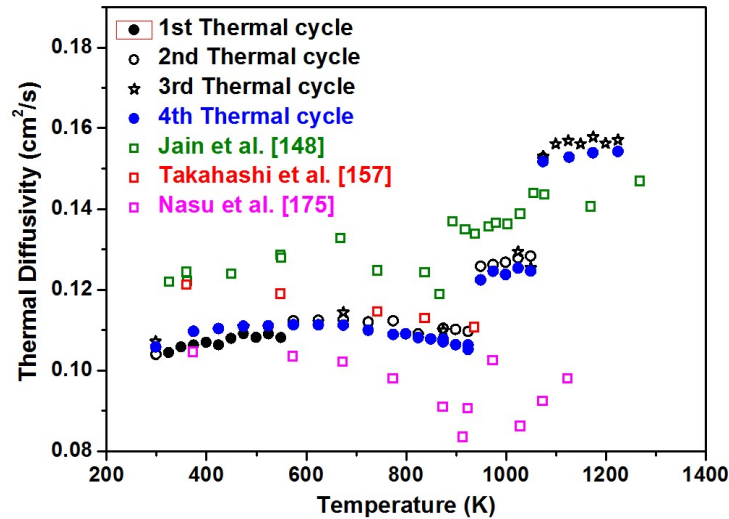


**Fig. 3.15. Effect of thermal cycling on thermal diffusivity of uranium; a comparison with literature reported values is also shown along**

Present results on uranium have also shown trend of thermal conductivity variation in stability region of its high temperature allotropes ( $\beta$ - and  $\gamma$ -phase). So far, literature reports have either focused on thermal conductivity of  $\alpha$ -phase, or have mostly provided the high temperature data based on extrapolation of results obtained on  $\alpha$ -phase, which can be seen from Fig. 3.14. The fact that similar to structural properties that vary during first-order phase transitions, a clear distinction in transport properties should also be reflected at phase transition boundaries; has perhaps been undermined while reporting thermal conductivity of uranium. On the other hand, data obtained in present study clearly shows the effect of phase transition on thermal diffusivity as well as thermal expansion. These two, when combined with specific heat anomalies at phase transitions, clearly show up the effect in thermal conductivity variation. Present results show highest thermal conductivity for cubic ( $\gamma$ -phase) structure of uranium ( $\sim 44 \text{ W.m}^{-1}.\text{K}^{-1}$  at 1075 K), which affirms that isotropic cubic phase of uranium-based metallic alloy fuels would be advantageous in terms of heat transport, along with other advantages such as isotropic swelling, higher fission product retention, high temperature operation, etc.

### 1.3.8. Uncertainty analysis for thermal conductivity of uranium and thorium

Estimation of uncertainty is essential while reporting experimental data on thermophysical properties. For results obtained during the course of this work, uncertainty analysis was performed by following the method reported by Ellison et al. [169a]. As an example, estimation of uncertainty in thermal conductivity of uranium and thorium is summarized. Thermal conductivity ( $\lambda$ ) is evaluated from thermal diffusivity ( $D$ ), specific heat ( $C_p$ ) and density ( $\rho$ ) using equation-3.1.

$$\lambda(T) = D(T) \times C_p(T) \times \rho(T)$$

Uncertainty in  $\lambda(T)$  therefore depends on contributions from uncertainty in  $D(T)$ ,  $C_p(T)$  and  $\rho(T)$  and is given in terms of relative standard deviation) as

$$\text{RSD } (\lambda) = \sqrt{(\text{uncertainty in } D)^2 + (\text{uncertainty in } C_p)^2 + (\text{uncertainty in } \rho)^2} \quad (3.12)$$

Prior to measurements on uranium and thorium metals, experiments were carried out on various reference materials under identical experimental conditions. These included thermal diffusivity measurements on metallic (Inconel-600) and ceramic (Pyroceram-9606) references, bulk thermal expansion on NIST sapphire and specific heat measurements on NIST sapphire as well as 4N purity nickel. Comparison of results obtained on reference materials with recommended values indicated average deviation of  $\pm 2\%$ ,  $\pm 2\%$  and  $\pm 3\%$  in thermal diffusivity ( $D$ ), linear thermal expansion and specific heat ( $C_p$ ), respectively. These results are graphically shown in Fig. 3.6 (b), Fig. 3.7 (b) and Fig. 3.11 (b), respectively.

Uncertainty in density ( $\rho(T)$ ) depends on uncertainty in measurement of ambient temperature density ( $\rho_{298K}$ ) as well as that of thermal expansion data. For cylindrical pellet shaped samples used in present investigations, geometric density was calculated from sample weight and pellet volume.

$$\rho = \frac{M}{V} = \frac{4M}{\pi D^2 h} \quad (3.13)$$

Where M = sample weight, V = volume, D = pellet diameter and h = pellet height (or thickness). Uncertainty in ambient temperature density can be evaluated using the following equation:

$$\frac{\Delta\rho}{\rho} = \sqrt{\left(\left(\frac{\Delta M}{M}\right)^2 + \left(\frac{\Delta h}{h}\right)^2 + \left(\frac{\Delta D}{D}\right)^2 + \left(\frac{\Delta D^2}{D^2}\right)\right)} \quad (3.14)$$

Using equation 3.14, uncertainties in ambient temperature density of uranium (7.868 g sample; 12.5 mm diameter; 3.4 mm height) and thorium (1.612 g sample; 6.1 mm diameter; 5.2 mm height) were found to be ~0.0038 (0.38 %) and ~0.0046 (0.46 %), respectively. Ambient temperature density (in g/cm<sup>3</sup>) of uranium and thorium samples therefore could be given as 18.85 ( $\pm 0.072$ ) and 11.39 ( $\pm 0.052$ ), respectively.

Temperature dependent density ( $\rho(T)$ ) is given as  $M/V(T)$ , where  $V(T)$  is temperature dependent volume obtained from bulk thermal expansion data using equation 3.9.

$$V_T = V_{298 K} + 3\alpha TV_{298 K} \quad (3.15)$$

Uncertainty in  $V_T$  therefore has two components namely, uncertainty ( $e_1$ ) in ambient temperature volume ( $V_{298 K}$ ) and uncertainty ( $e_2$ ) in  $3\alpha TV_{298 K}$ . These can be evaluated as follows:

$$e_1 = V_{298K} * \sqrt{\left(\left(\frac{\Delta h}{h}\right)^2 + \left(\frac{\Delta D}{D}\right)^2 + \left(\frac{\Delta D^2}{D}\right)^2\right)} \quad (3.16)$$

$$e_2 = 3\alpha TV_{298K} * \sqrt{\left(\left(\frac{\Delta \alpha}{\alpha}\right)^2 + (e_1)^2\right)} \quad (3.17)$$

$$= 3\alpha TV_{298K} * \sqrt{(0.02)^2 + (e_1)^2} \quad (\text{Uncertainty in linear thermal expansion} = \pm 2\%)$$

For uranium and thorium samples used in present studies, value of  $e_1$  comes out to be 0.0038 (0.38 %) and 0.0046 (0.46 %), giving rise to their ambient temperature volume (in  $\text{cm}^3$ ) given as 0.4174 ( $\pm 0.0016$ ) and 0.1520 ( $\pm 0.0007$ ), respectively.

Similarly, uncertainty ( $e_2$ ) in uranium and thorium is given as

$$\begin{aligned} e_2(\text{alpha uranium}) &= 3 * 20.0 * 10^{-6} * T * 0.4174 * \sqrt{(0.02)^2 + (0.0038)^2} \\ &= 5.098 * 10^{-7} * T \end{aligned}$$

and

$$\begin{aligned} e_2(\text{alpha thorium}) &= 3 * 12.5 * 10^{-6} * T * 0.1520 * \sqrt{(0.02)^2 + (0.0046)^2} \\ &= 1.169 * 10^{-7} * T \end{aligned}$$

For  $T = 298 \text{ K}$ , values of  $e_2(\text{alpha-U})$  and  $e_2(\text{alpha-Th})$  respectively are 0.00015 and 0.00035, which for  $T = 1273 \text{ K}$  are 0.00065 and 0.00149. These uncertainties are nearly an order of magnitude smaller than the uncertainty ( $e_1$ ) in ambient temperature volume ( $V_{298 \text{ K}}$ ). It is therefore appropriate to say that uncertainty in the thermal expansion coefficient does not significantly influence the uncertainty in volume. For all practical purposes, uncertainty in temperature dependent volume can therefore be taken as 0.38% and 0.46% for uranium and thorium, respectively.

Uncertainty in measurement of sample weight ( $\Delta m/m$ ) is 0.00012 (0.012%) and 0.00062 (0.062 %) for uranium and thorium. Hence, uncertainty in temperature dependent density can be given as

$$\Delta\rho(T) / \rho = \sqrt{\left(\frac{\Delta M}{M}\right)^2 + \left(\frac{\Delta v}{v}\right)^2} \quad (3.18)$$

Using equation-3.18, values of uncertainty comes out to be 0.0038 (0.38%) and 0.0046 (0.46%) for uranium and thorium, respectively. It can be seen that, uncertainty in temperature-dependent densities ( $\rho_{(T)}$ ) is same as that of room temperature density values for both the metals. For uniform analysis, this value is taken as 0.005 (0.5%) for both the metals.

Since thermal conductivity is calculated as product of temperature dependent values of thermal diffusivity, specific heat and density (equation-3.1), uncertainty in thermal conductivity can be evaluated if that of the contributing properties are known. From results obtained on standard reference materials; as shown previously, uncertainty in thermal diffusivity and specific heat is  $\pm 2\%$  and  $\pm 3\%$ , respectively. Combining these values with uncertainty in temperature dependent density ( $\pm 0.5\%$ ), uncertainty in thermal conductivity is calculated as follows:

$$\lambda(T) = \sqrt{0.02^2 + 0.03^2 + 0.005^2}$$

$$\sim 0.037 \text{ (or } 3.7 \%)$$

Hence, it can be said that temperature dependent thermal conductivity results on thorium and uranium metals as well as their alloys have average uncertainty less than  $\pm 4\%$ .

## 1.4. Conclusions

Thermophysical properties of well characterized nuclear-grade thorium and uranium metal over wide temperature range from 298 K up to 1373 K have been investigated. Results obtained on high temperature thermophysical characterization indicate superior heat transport properties of thorium as compared to uranium. Thorium metal shows significantly lower and isotropic thermal expansion behavior, which is desired for nuclear fuel application. Thermal diffusivity and thermal conductivity over 298 K to 1373 K has been reported for the first time. Thermal conductivity of both the metals increases with increasing temperature. Both thermal diffusivity as well as thermal conductivity of uranium shows abrupt rise during metal's allotropic phase transformation from ambient orthorhombic phase to high temperature BCC phase via an intermediate tetragonal phase. Effect of structural symmetry over the heat transport properties of metallic uranium has been brought out with accurate experimental dataset on thermal diffusivity, linear thermal expansion and thermal conductivity of well characterized uranium samples. Cubic ( $\gamma$ -phase) structure of uranium shows very high thermal conductivity ( $\sim 44 \text{ W}\cdot\text{m}^{-1}\cdot\text{K}^{-1}$  at 1075 K), which is still lower than that of FCC thorium ( $\sim 56 \text{ W}\cdot\text{m}^{-1}\cdot\text{K}^{-1}$  at 1075 K). It is expected that high temperature allotrope (BCC phase) of thorium ( $T > 1723 \text{ K}$ ) would have further higher thermal conductivity. Presented data on thermal conductivity would serve as a reference dataset for thorium and uranium-based metallic fuels that will be produced on large-scale for metal fuelled nuclear reactors. Detailed analysis of presented results in comparison to the information already existing in literature would be useful for assessment of various fuel performance and safety analysis codes for development of metallic nuclear fuels. Presented results have brought out clearer representation of thermal conductivity variation over two high temperature allotropic phases of uranium namely, tetragonal and cubic phase and also extended the temperature range over which reliable thermophysical properties information is

known. High temperature isotropic cubic phase of uranium showed the best heat transport properties, which affirmed the need to develop uranium-rich alloy fuels in cubic phase. Presented results assert the need to generate indigenous and reliable in-house database on thermophysical properties of metallic alloy nuclear fuels and constituent elements for development of all-metal fuelled fast reactors in India.

Thorium-based metallic fuels will be used in the form of alloys of thorium with fissile uranium and / or plutonium. Reported studies have indicated that Th-U binary alloys up to 20 wt. % uranium are candidate fuels for fast reactors. Thermophysical characterization of these binary alloys is needed to assess the effect of uranium incorporation on their performance. Preparation, characterization and high temperature thermophysical properties evaluation of thorium-uranium binary metallic alloys was therefore investigated and results are discussed in next chapter (chapter-4).

## References:

- [1] C. Degueudre, M.J. Joyce, “Evidence and uncertainty for uranium and thorium abundance: a review”, *Prog. Nucl. Energy* 124 (2020) 103299.
- [2] L.S. Keith, O.M. Faroon, B.A. Fowler, “Uranium (book chapter); handbook on the toxicology of metals: fourth edition (Eds: G.F. Nordberg, B.A. Fowler, M. Nordberg)”, Elsevier (2015) 1307-1345 (DOI: <https://doi.org/10.1016/C2011-0-07884-5>).
- [3] G. Sadagopan, K.S.V. Nambi, G. Venkataraman, V.K. Shukla, S. Kayasth, “Estimation of thorium in gas mantles to ascertain regulatory compliance”, *Radiat. Prot. Dosim.* 71(1) (1997) 53-56.
- [4] T.E. Leontis, “Properties of magnesium-thorium and magnesium-thorium-cerium alloys”, *J. Min. Metals Mater. Soc.* 4 (3) (1952) 287-294.
- [5] R.A. Glenner, P. Willey, P.S. Sledzik, E.P. Junger, “Dental fillings in civil war skulls: What do they tell us?”, *J. Am. Dent. Assoc.* 127(11) (1996) 1671-1677.
- [6] O. Hahn, F. Strassmann, “Über den nachweis und das verhalten der bei der bestrahlung des urans mittels neutronen entstehenden erdalkalimetalle (English translation: Concerning the existence of alkaline earth metals resulting from neutron irradiation of uranium)”, *Die Naturwissenschaften* 27 (1939) 11-15.
- [7] “The first reactor” The US department of energy report: DOE/NE-0046 (1982) 1-40 (Web-link: <https://www.energy.gov/ne/downloads/first-reactor>).
- [8] R.L. Crowther, “Use of thorium in boiling water reactors”, *J. Nucl. Energy AB* 16(4) (1962) 181-194.
- [9] J.R. Dietrich, “The physics of advanced reactors”, *Brit. J. Appl. Phys.* 7(S5) 302 (1956) S9-S23.
- [10] H.N. Sethna, “India’s atomic energy program: past and future”, *International Atomic Energy Agency (IAEA) Bulletin* 21 (5) (1979) 2-11.

## References

- [11] S. Banerjee, H.P. Gupta, “The evolution of the Indian nuclear power programme”, Prog. Nucl. Energy 101 (2017) 4-18.
- [12] International Atomic Energy Agency “Thorium fuel cycles - potential benefits and challenges”, IAEA-TECDOC-1450, IAEA, Vienna (2005) 1-105.
- [13] P.K. Wattal, “Back end of Indian nuclear fuel cycle - A road to sustainability”, Prog. Nucl. Energy 101 (2017) 133-145.
- [14] R. Natarajan, “Reprocessing of spent nuclear fuel in India: Present challenges and future programme”, Prog. Nucl. Energy 101 (2017) 118-132.
- [15] S.A. Ansari, P. Pathak, P.K. Mohapatra, V.K. Manchanda, “Aqueous partitioning of minor actinides by different processes” Sep. Purif. Rev. 40(1) (2011) 43-76.
- [16] M. Salvatores, “Nuclear fuel cycle strategies including partitioning and transmutation”, Nucl. Eng. Des. 235(7) (2005) 805-816.
- [17] Press Information Bureau, Government of India, “Setting up of ten indigenous nuclear power reactors” (Web-link: <http://pib.nic.in>)
- [18] S.C. Chetal, P. Chellapandi, P. Puthiyavinayagam, S. Raghupathy, V. Balasubramanian, P. Selvaraj, P. Mohanakrishnan, B. Raj, “Current status of fast reactors and future plans in India” Energy. Proced. 7 (2011) 64-73.
- [19] P. Puthiyavinayagam, P. Selvaraj, V. Balasubramanian, S. Raghupathy, K. Velusamy, K. Devan, B.K. Nashine, G.P. Kumar, K.V.S. Kumar, S. Varatharajan, P. Mohanakrishnan, G. Srinivasan, A.K. Bhaduri, “Development of fast breeder reactor technology in India”, Prog. Nucl. Energy 101 (Part A) (2017) 19-42.
- [20] Bharatiya Nabhikiya Vidyut Nigam Limited, Department of Atomic Energy “Present status of 500 MWe Prototype Fast Breeder Reactor (PFBR)”, (Web-link: <http://www.bhavini.nic.in>).

## References

- [21] P. Rodriguez, C.V. Sundaram, “Nuclear and materials aspects of the thorium fuel cycle”, *J. Nucl. Mater.* 100 (1981) 227-249.
- [22] R. Ramanna, S.M. Lee, “The thorium cycle for fast breeder reactors”, *Pramana* 27(1-2) (1986) 129-137.
- [23] R. Chidambaram, C. Ganguly, “Plutonium and thorium in the Indian nuclear programme”, *Curr. Sci. India* 70(1) (1996) 21-35.
- [24] P.K. Vijayan, V. Shivakumar, S. Basu, R.K. Sinha, “Role of thorium in the Indian nuclear power programme”, *Prog. Nucl. Energy* 101 (2017) 43-52.
- [25] “Thoria-based nuclear fuels: thermophysical and thermodynamic properties, fabrication, reprocessing, and waste management”, (Eds.: D. Das, S.R. Bharadwaj) Springer (2013) (DOI: 10.1007/978-1-4471-5589-8).
- [26] “Thorium-energy for the future”, (Eds.: A.K. Nayak, B.R. Sehgal), Springer (2019) (DOI: 10.1007/978-981-13-2658-5).
- [27] S. Mukherji, B.K. Mohan, P.D. Krishnani, V. Jagannathan, S. Ganesan, “Thorium irradiation in Indian PHWRs - applications and limitations of origin code”, *Proceedings of First National Conference in Nuclear Reactor Technology* (2002) (Web-link: [https://inis.iaea.org/search/search.aspx?orig\\_q=RN:34011468](https://inis.iaea.org/search/search.aspx?orig_q=RN:34011468)).
- [28] M. Das, “Design and irradiated experience with thorium based fuels in PHWRs” *Annual International Conference - Canadian Nuclear Association* (1992) 10.1-10.
- [29] P.S. Dhama, J.S. Yadav, K. Agarwal, “Power reactor thoria reprocessing facility (PRTRF), Trombay”, *Proceedings of the Theme Meeting on the Journey of BARC Safety Council for Strengthening Safety Culture in BARC Facilities* (Eds: V.M. Jolly) (2017) (Web-link: [https://inis.iaea.org/search/search.aspx?orig\\_q=RN:48089837](https://inis.iaea.org/search/search.aspx?orig_q=RN:48089837)).
- [30] R.K. Sinha, A. Kakodkar, “Design and development of the AHWR - the Indian thorium fuelled innovative nuclear reactor” *Nucl. Eng. Des.* 236 (7-8) (2006) 683-700.

- [31] R. Sinha, A. Kakodkar, "India's passive breeder", Nucl. Eng. Int. 55(668) (2010) 30-31.
- [32] A. Kakodkar, "Evolution of nuclear reactor containments in India: Addressing the present day challenges", Nucl. Eng. Des. 269 (2014) 3-22.
- [33] S. Sengupta, S.B. Chafle, S. Mammen, K. Sasidharan, V.K. Raina, "Critical facility for AHWR and PHWRs", Proceedings of International Conference on Peaceful uses of Atomic Energy (2009). V. 1. [33a] C. Ronchi, J.-P. Hiernaut, Experimental measurement of pre-melting and melting of thorium dioxide, J. Alloys Comp. 240 (1-2) (1996) 179-185. [33b] R. Böhler, A. Quaini, L. Capriotti, P. Cakir, O. Beneš, K. Boboridis, A. Guiot, L. Luzzi, R.J.M. Konings, D. Manara, "The solidification behavior of the UO<sub>2</sub>-ThO<sub>2</sub> system in a laser heating study" J. Alloys. Comp. 616 (2014) 5-13.
- [34] D. Greneche, W.J. Szymczak, J.M. Buchheit, M. Delpech, A. Vasile, H. Golfier, "Rethinking the thorium fuel cycle: An industrial point of view", Proceedings of ICAPP (Nice, France), (2007) Paper-7367. [34a] S.F. Ashley, G.T. Park, W.J. Nuttall, C. Boxall, R.W. Grimes, "Thorium fuel has risks", Nature 492 (2012) 31-33.
- [35] D. Jain, V. Sudarsan, A.K. Tyagi, "Thorium-based metallic alloys as nuclear fuels: Present status, potential advantages and challenges", SMC Bulletin (Society for Materials Chemistry, India) 4 (1) (2013) pp. 27-40 (Web-link: <https://www.smcindia.org/smc-bulletin.php>).
- [36] P.K. Vijayan, A. Basak, I.V. Dulera, K.K. Vaze, S. Basu, "Conceptual design of Indian molten salt breeder reactor", Pramana - J. Phys. 85 (2015) 539-554.
- [37] T. Yamamoto, H. Suwarno, H. Kayano, M. Yamawaki, "Development of new reactor fuel materials: Hydrogen absorption properties of U-Th, U-Th-Zr and U-Th-Ti-Zr alloys", J. Nucl. Sci. Tech. 32(3) (1995) 260-262.

## References

- [38] K.A. Terrani, G.W.C. Silva, C.B. Yeamans, “Fabrication and characterization of uranium thorium zirconium hydride fuels”, *Trans. Am. Nucl. Soc.* 98 (2008) 1060-1061.
- [39] S.M. McDeavitt, T.J. Downar, A.A. Solomon, S.T. Revankar, M.C. Hash, A.S. Hebden, “Thoria-based cermet nuclear fuel: Cermet fabrication and behavior estimates”, *Proc. Int. Conf. Nucl. Eng. (ICONE 4)* (2002) 59-67.
- [40] C. Lombardi, L. Luzzi, E. Padovani, F. Vettrano, “Thoria and inert matrix fuels for a sustainable nuclear power”, *Prog. Nucl. Energy* 50(8) (2008) 944-953.
- [41] J. Spino, H.S. Cruz, R. Jovani-Abril, R. Birtcher, C. Ferrero, “Bulk-nanocrystalline oxide nuclear fuels - An innovative material option for increasing fission gas retention, plasticity and radiation-tolerance”, *J. Nucl. Mater.* 422 (1-3) (2012) 27-44.
- [42] H. György, S. Czifrus, “The utilization of thorium in generation IV reactors”, *Prog. Nucl. Energy* 93 (2016) 306-317.
- [43] D. Heuer, E. Merle-Lucotte, M. Allibert, M. Brovchenko, V. Ghetta, P. Rubiolo, “Towards the thorium fuel cycle with molten salt fast reactors”, *Ann. Nucl. Energy* 64 (2014) 421-429.
- [44] G.L. Hofman, L.C. Walters, T.H. Bauer, “Metallic fast reactor fuels”, *Prog. Nucl. Energy* 31(1-2) (1997) 83-110.
- [45] W.J. Carmack, D.L. Porter, Y.I. Chang, S.L. Hayes, M.K. Meyer, D.E. Burkes, C.B. Lee, T. Mizuno, F. Delage, J. Somers, “Metallic fuels for advanced reactors”, *J. Nucl. Mater.* 392 (2) (2009) 139-150.
- [46] Idaho National Laboratory, “Experimental breeder reactor-I (EBR-I) (Web-link: <https://inl.gov/experimental-breeder-reactor-i/>).
- [47] L.C. Walters, “Thirty years of fuels and materials information from EBR-II”, *J. Nucl. Mater.* 270(1) (1999) 39-48.

- [48] K. D. Weaver, J. Gilleland, C. Whitmer, G. Zimmerman, “High burn-up fuels for fast reactors: past experience and novel applications”, International Congress on Advances in Nuclear Power Plants (ICAPP 2009) (2009) 795.
- [49] G. Locatelli, M. Mancini, N. Todeschini, “Generation IV nuclear reactors: Current status and future prospects”, *Energ. Policy* 61 (2013) 1503-1520.
- [50] Z.S. Takibaev, “Fast homogeneous nuclear reactor”, *Atom. Energy* 100 (2006) 154-156.
- [51] T. Jayakumar, M.D. Mathew, K. Laha, R. Sandhya, “Materials development for fast reactor applications”, *Nucl. Eng. Des.* 265 (2013) 1175-1180.
- [52] A. Riyas, P. Mohanakrishnan, “Studies on physics parameters of metal (U-Pu-Zr) fuelled FBR cores”, *Ann. Nucl. Energy* 35(1) (2008) 87-92.
- [53] P. Chellapandi, V. Balasubramaniyan, P. Puthiyavinayagam, R. Sundararajan, M. Kanakkil, P. Selvaraj, P.R. Vasudeva Rao, “Design of 500 MWe metal fuel demonstration fast reactor”, *Proc. Int. Conf. Nucl. Eng.* (2014) (DOI: <https://doi.org/10.1115/ICONE22-30727>).
- [54] Indira Gandhi Centre for Atomic Research, “Fast Breeder Test Reactor”, (Web-link: <http://www.igcar.gov.in/rfg/fbtrhist.html>).
- [55] B. Blumenthal, J.E. Sanecki, D.E. Busch, D.R. O’Boyle, “Thorium-uranium-plutonium alloys as potential fast power reactor fuels; part-II: Properties and irradiation behavior of thorium-uranium-plutonium alloys”, ANL-7259, Argonne National laboratory, Illinois (October 1969).
- [56] S.Z. Ghayeb, “Investigations of thorium-based fuels to improve actinide burning rate in S-PRISM reactor”, M.Sc. Thesis, The Pennsylvania State University (2008) (Web-link: <https://etda.libraries.psu.edu/catalog/9160>).

## References

- [57] R.G. Wymer, D.A. Douglas Jr., "Status and progress report for thorium fuel cycle development for period ending December 31, 1964", Report no.: ORNL-3831, Oak Ridge National laboratory, Tennessee (May 1966).
- [58] "Fast spectrum reactors", (Eds.: A.E. Waltar, D. Todd, P.V. Tsvetkov) Springer (2011) (ISBN 978-1-4419-9572-8).
- [59] D.E. Peterson, "The (Th-U) Thorium-uranium system", Bull. Alloy Phase Diagr. 6 (5) (1985) 443-445.
- [60] S. Peterson, R.E. Adams, D.A. Douglas Jr., "Properties of thorium, its alloys and its compounds", Report no.: ORNL-TM-1144, Oak Ridge National laboratory, Tennessee (June 1965).
- [61] D.R. Marr, D.A. Cantley, J.C. Chandler, D.C. McCurry, R.P. Omberg, "Performance of thorium fuelled fast breeders", Report no.: HEDL-SA-1327-FP, Hanford Engineering Development Laboratory, Richland, USA (October 1977).
- [62] G.L. Copeland, "Evaluation of thorium-uranium alloys for the unclad metal breeder reactor", Report no.: ORNL-4557, Oak Ridge National Laboratory, Tennessee (June 1970).
- [63] B. Blumenthal, J.E. Sanecki, D.E. Busch, "Thorium-uranium-plutonium alloys as potential fast power reactor fuels; part-I: Thorium-uranium-plutonium phase diagram", Report no.: ANL-7258, Argonne National Laboratory, Illinois (September 1968).
- [64] C.S. Holden, "Rapid computational path for sustainable and renewable nuclear energy using metallic thorium fuels", Proceedings of 2<sup>nd</sup> Thorium energy conference (ThEC-2010), Mountain View CA (2010).
- [65] R.M. Carroll, "The effects of reactor irradiation on thorium-uranium alloy fuel plates", Report no.: ORNL-1938, Oak Ridge National Laboratory, Tennessee (August 1955).

## References

- [66] B.R. Hayward, P. Corzine, "Thorium uranium fuel elements for SRE", Proc. 2<sup>nd</sup> UN Int. Conf. Peaceful uses of Atom. Energy, Geneva (October 1958).
- [67] J.L. Ballif, B.R. Hayward, J.W. Walter, "Engineering evaluation of a mixed alloy fuel element irradiated at elevated temperatures in SRE", Technical report no.: NAA-SR-3888, Atomics International Division, North American Aviation Incorporation, California, USA (June 1960).
- [68] A.R. Olsen, "Thorium and thorium alloys: Preliminary corrosion tests", Report no.: ORNL-1066, Oak Ridge National Laboratory, Tennessee (November 1951).
- [69] M.S. Farkas, A.A. Bauer, R.F. Dickerson, "Development of thorium-uranium-base fuel alloys," Report no.: BMI-1428, Battelle Memorial Institute, Columbus, Ohio (March 1960).
- [70] R.H. Cole, L.E. Wilkinson, "Development of high strength ternary and quaternary thorium-uranium base alloys", Technical report no.: ATL-A-128, Advanced Technology Laboratory, California (1961).
- [71] J.H. Kittel, J.A. Horak, W.F. Murphy, S.H. Paine, "Effect of irradiation on thorium and thorium-uranium alloys", Technical report no.: ANL-5674, Argonne National laboratory, Illinois, USA (April 1963).
- [72] A.L. Bement, "Burn-up and specific power calculations for the thermal neutron irradiation on thorium-uranium alloys", Technical report no: HW-56631, General Electric Co. Hanford Atomic Products Operation, Richland, Washington (1958).
- [73] F.W. Dodge, E.W. Murbach, L.A. Hanson, "Low decontamination reprocessing of thorium-uranium alloys by induction drip melting", Nucl. Sci. Eng. 6 (6) (1959) 533-536.
- [74] P. Chiotti, A.F. Voigt, "Pyrometallurgical processing", Technical report: A/CONF.15/P/517; ISC-1018, Ames Laboratory, Iowa (October 1958).

- [75] W.N. Hensen, "Electrolysis of thorium and uranium", US-Patent no.: US 2951793 (1960).
- [76] S. Jiang, K. Liu, Y. Liu, T. Yin, Z. Chai, W. Shi, "Electrochemical behavior of Th(IV) on the bismuth electrode in LiCl–KCl eutectic", *J. Nucl. Mater.* 523 (2019) 268-275.
- [77] G.B. Zorzoli, "Use of metallic thorium for LWBRs and LWRs", *Nucl. Tech.* 20 (1973) 109-113.
- [78] F. Correa, D.J. Driscoll, D.D. Lanning, "An evaluation of tight pitch PWR cores", technical report no.: MIT-EL-79-022, Massachusetts Institute of Technology, Cambridge, Massachusetts (1979).
- [79] Z.S. Li, X.J. Liu, C.P. Wang, "Thermodynamic modelling of the Th-U, Th-Zr and Th-U-Zr systems", *J. Alloy Compd.* 473 (2009) 193-198.
- [80] S.Z. Ghrayeb, K.N. Ivanov, S.H. Levine, E.P. Loewen, "Burn-up performance of sodium-cooled fast reactors utilizing thorium-based fuels", *Nucl. Tech.* 176 (2011) 188-194.
- [81] T. Okawa, H. Sekimoto, S. Nakayama, "Design study on power flattening to sodium cooled large scale CANDLE burning reactor with using thorium fuel", *Proc. 18<sup>th</sup> Int. Conf. Nucl. Eng., ICON18, China, (2010).*
- [82] M.T. Simnad, "The U-ZrH<sub>x</sub> alloy: Its properties and use in TRIGA fuel", *Nucl. Engg. Des.* 64 (1981) 403-422.
- [83] K. Konashi, B.A. Pudjanto, T. Terai, M. Yamawaki, "Thermodynamic stability of ThZr<sub>2</sub>H<sub>x</sub> at high temperature", *J. Phys. Chem. Solids* 66 (2–4) (2005) 625-628.
- [84] T. Yamamoto, H. Suwarno, F. Ono, H. Kayano, M. Yamawaki, "Preparation, analysis and irradiation of hydride Th-U-Zr alloy samples for a new fuel", *J. Alloy Compd.* 271-273 (1998) 702-706.

- [85] S. Das, R. Kumar, S.B. Roy, A.K. Suri, "Development study on metallic thorium and uranium-thorium alloy", BARC Newsletter-Founder's Day Special issue (2011) 72-76.
- [86] S. Das, R. Kumar, S. Kaity, S. Neogy, K.N. Hareendran, S.B. Roy, G.K. Dey, B.S.S. Daniel, G.P. Chaudhari, "Characterization of microstructural, mechanical and thermal properties and ageing study of Th-3 wt.% U alloy" Nucl. Eng. Des. 282 (2015) 116-125.
- [87] S. Das, S. Kaity, R. Kumar, J. Banerjee, S.B. Roy, G.P. Chaudhari, B.S.S. Daniel, "Characterization of microstructural, mechanical and thermophysical properties of Th-52 U alloy", J. Nucl. Mater. 480 (2016) 223-234.
- [88] S. Das, S.B. Roy, G.P. Chaudhari, B.S.S. Daniel, "Microstructural evolution of as-cast Th-U alloys", Prog. Nucl. Energy 88 (2016) 285-296.
- [89] R. Kumar, S. Das, S.B. Roy, R. Agarwal, J. Banerjee, S.K. Satpati, "Effect of Mo addition on the microstructural evolution and  $\gamma$ -U stability in Th-U alloys", J. Nucl. Mater. 539 (2020) 152317.
- [90] S. Vaidyanathan, "Thorium utilization in pressurized water reactors using bimetallic thorium-zirconium alloy cladding", Nucl. Tech. (2020) (DOI: <https://doi.org/10.1080/00295450.2019.1706377>).
- [91] D. Escorcia-Ortiz, J. François, C. Martín-del-Campo, "Comparative study of the neutronic performance of thorium-based metallic fuel and MOX fuel in an ASTRID-like fast reactor core", Nucl. Eng. Des. 347 (2019) 122-131.
- [92] J.K. Startt, C.S. Deo, "First principles study of the structure and elastic properties of thorium metal", MRS Adv. 1 (35) (2016) 2447-2452.
- [93] A. Karahan, J. Buongiorno, "A new code for predicting the thermo-mechanical and irradiation behavior of metallic fuels in sodium fast reactors", J. Nucl. Mater. 396 (2010) 283-293.

## References

- [94] K. Lassmann, "TRANSURANUS: a fuel rod analysis code ready for use", *J. Nucl. Mater.* 188 (1992) 295-302.
- [95] J.P. Hamond, "Physical, mechanical and irradiation properties of thorium and thorium alloys", ORNL-4218, Oak Ridge National Laboratory, USA (1968) 29-30.
- [96] J.K. Fink, M.G. Chasanov, L. Leibowitz, "Thermophysical properties of thorium and uranium systems for use in reactor safety analysis", Report no.: ANL-CEN-RSD-77-1, Argonne National Laboratory (1977) 11-12.
- [97] M. Lung, "A present review of the thorium nuclear fuel cycles", European commission report no.: EUR-17771-EN, (1997).
- [98] S. Kolay, S. Phapale, R. Dawar, M. Jafar, S. N. Achary, A. K. Tyagi, R. Mishra, M. Basu, "Phase characterization and thermal study of SrF<sub>2</sub> and NdF<sub>3</sub> doped fluoride salt containing 78 mol % LiF - 20 mol % ThF<sub>4</sub> - 2 mol % UF<sub>4</sub>", *J. Radioanal. Nucl. Chem.* 314 (2) (2017) 1267-1271.
- [99] M. Verwerft, B. Boer, "Thorium oxide nuclear fuels", *Comprehensive nuclear materials* (Second edition) 5 (2020) 139-168 (DOI: <https://doi.org/10.1016/B978-0-12-803581-8.11770-9>).
- [100] S. Usha, R.R. Ramanarayanan, P. Mohanakrishnan, R.P. Kapoor, "Research reactor KAMINI", *Nucl. Eng. Des.* 236 (7-8) (2006) 872-880.
- [101] T.K. Mukherjee, "Processing of Indian monazite for the recovery of thorium and uranium values", *Proceedings of International Conference on Characterisation and Quality Control of Nuclear Fuels* (Eds.: C. Ganguly, R.N. Jayaraj) Allied Publishers Pvt. Ltd. (2002) 187-195.
- [102] J.R. Johnson, C.E. Curtis, "Note on sintering of ThO<sub>2</sub>", *J. Am. Ceram. Soc.* 37(12) (1954) 611.

## References

- [103] T.R.G. Kutty, K.B. Khan, P.V. Hegde, J. Banerjee, A.K. Sengupta, S. Majumdar, H.S. Kamath, "Development of a master sintering curve for ThO<sub>2</sub>", *J. Nucl. Mater.* 327(2-3) (2004) 211-219.
- [104] P. Balakrishna, B.P. Varma, T.S. Krishnan, T.R.R. Mohan, P. Ramakrishnan, "Thorium oxide: Calcination, compaction and sintering", *J. Nucl. Mater.* 160(1) (1988) 88-94.
- [105] N. Clavier, R. Podor, L. Deliere, J. Ravoux, N. Dacheux, "Combining in situ HT-ESEM observations and dilatometry: An original and fast way to the sintering map of ThO<sub>2</sub>", *Mater. Chem. Phys.* 137(3) (2013) 742-749.
- [106] K. Ananthasivan, S. Balakrishnan, S. Anthonysamy, R. Divakar, E. Mohandas, V. Ganesan, "Synthesis and sintering of nanocrystalline thoria doped with CaO and MgO derived through oxalate-deagglomeration", *J. Nucl. Mater.* 434 (1-3) (2013) 223-229.
- [107] G.P. Halbfinger, M. Kolodney, "Activated Sintering of ThO<sub>2</sub> and ThO<sub>2</sub>-Y<sub>2</sub>O<sub>3</sub> with NiO", *J. Am. Ceram. Soc.* 55(10) (1972) 519-524.
- [108] A. Baena, T. Cardinaels, J. Vleugels, K. Binnemans, M. Verwerft, "Activated sintering of ThO<sub>2</sub> with Al<sub>2</sub>O<sub>3</sub> under reducing and oxidizing conditions", *J. Nucl. Mater.* 470 (2016) 34-43.
- [109] K. Ananthasivan, S. Anthonysamy, C. Sudha, A.L.E. Terrance, P.R. Vasudeva Rao, "Thoria doped with cations of group VB-synthesis and sintering", *J. Nucl. Mater.* 300(2-3) (2002) 217-229.
- [110] T.R.G. Kutty, P.V. Hegde, K.B. Khan, T. Jarvis, A.K. Sengupta, S. Majumdar, H.S. Kamath, "Characterization and densification studies on ThO<sub>2</sub>-UO<sub>2</sub> pellets derived from ThO<sub>2</sub> and U<sub>3</sub>O<sub>8</sub> powders", *J. Nucl. Mater.* 335 (3) (2004) 462-470.
- [111] V. Tyrpekl, M. Cologna, D. Robba, J. Somers, "Sintering behaviour of nanocrystalline ThO<sub>2</sub> powder using spark plasma sintering", *J. Eur. Ceram. Soc.* 36(3) (2016) 767-772.

- [112] W. Straka, S. Amoah, J. Schwartz, “Densification of thoria through flash sintering”, *MRS Commun.* 7(3) (2017) 677-682.
- [113] D. Sanjay Kumar, K. Ananthasivan, R.V. Krishnan, S. Amirthapandian, A. Dasgupta, “Studies on the synthesis of nanocrystalline  $Y_2O_3$  and  $ThO_2$  through volume combustion and their sintering”, *J. Nucl. Mater.* 479 (2016) 585-592.
- [114] R.D. Purohit, S. Saha, A.K. Tyagi, “Nanocrystalline thoria powders via glycine-nitrate combustion” *J. Nucl. Mater.* 288 (1) (2001) 7-10. [114a] F. Cappia, D. Hudry, E. Courtois, A. Janßen, L. Luzzi, R.J.M. Konings, D. Manara, High-temperature and melting behavior of nanocrystalline refractory compounds: an experimental approach applied to thorium dioxide, *Mater. Res. Express* 1 (2014) 0250341-12.
- [115] J. Spino, K. Vennix, M. Coquerelle, “Detailed characterisation of the rim microstructure in PWR fuels in the burn-up range 40–67 GWd/tM”, *J. Nucl. Mater.* 231 (3) (1996) 179-190.
- [116] L. Bonato, M. Viot, X. Le Goff, P. Moisy, S.I. Nikitenko, “Sonochemical dissolution of nanoscale  $ThO_2$  and partial conversion into a thorium peroxo sulphate”, *Ultrason. Sonochem.* 69 (2020) 105235.
- [117] S. Dash, A. Singh, P.K. Ajikumar, H. Subramanian, M. Rajalakshmi, A.K. Tyagi, A.K. Arora, S.V. Narasimhan, B. Raj, “Synthesis and characterization of nanocrystalline thoria obtained from thermally decomposed thorium carbonate”, *J. Nucl. Mater.* 303 (2–3) (2002) 156-168.
- [118] S. Dash, R. Krishnan, M. Kamruddin, A.K. Tyagi, B. Raj, “Temperature programmed decomposition of thorium oxalate hexahydrate”, *J. Nucl. Mater.* 295(2-3) (2001) 281-289.

## References

- [119] S. Dash, M. Kamruddin, P.K. Ajikumar, A.K. Tyagi, B. Raj, S. Bera, S.V. Narasimhan, “Temperature programmed decomposition of thorium nitrate pentahydrate”, *J. Nucl. Mater.* 278 (2–3) (2000) 173-185.
- [120] T.V. Plakhova, A.Y. Romanchuk, D.V. Likhosherstova, A.E. Baranchikov, P.V. Dorovatovskii, R.D. Svetogorov, T.B. Shatalova, T.B. Egorova, A.L. Trigub, K.O. Kvashnina, V.K. Ivanov, S.N. Kalmykov, “Size effects in nanocrystalline thoria”, *J. Phys. Chem. C* 123 (37) (2019) 23167-23176. [120a] D. Hudry, C. Apostolidis, O. Walter, T. Gouder, E. Courtois, C. Kübel, D. Meyer, Controlled Synthesis of Thorium and Uranium Oxide Nanocrystals, *Chem. Eur. J.*, 19 (2013) 5297-5305.
- [121] F. Deganello, A.K. Tyagi, “Solution combustion synthesis, energy and environment: Best parameters for better materials”, *Prog. Cryst. Growth Char.* 64 (2018) 23-61.
- [122] A. Varma, A.S. Mukasyan, A.S. Rogachev, K.V. Manukyan, “Solution combustion synthesis of nanoscale materials”, *Chem. Rev.* 116 (2016) 14493-14586.
- [123] V. Chandramouli, S. Anthonysamy, P.R. Vasudeva Rao, “Combustion synthesis of thoria - A feasibility study”, *J. Nucl. Mater.* 265(3) (1999) 255-261.
- [124] S. Anthonysamy, K. Ananthasivan, V. Chandramouli, I. Kaliappan, P.R. Vasudeva Rao, “Combustion synthesis of urania-thoria solid solutions”, *J. Nucl. Mater.* 278(2) (2000) 346-357.
- [125] D. Sanjay Kumar, K. Ananthasivan, S. Amirthapandian, A. Dasgupta, G. Jogeswara Rao, “Citrate gel-combustion synthesis and sintering of nanocrystalline ThO<sub>2</sub> powders”, *J. Nucl. Mater.* 497 (2017) 16-29.
- [126] R.D. Purohit, S. Saha, A.K. Tyagi, “Combustion synthesis of 5 and 10 mol% YO<sub>1.5</sub> doped ThO<sub>2</sub> powders”, *J. Nucl. Mater.* 323 (1) (2003) 36-40.

- [127] K.C. Patil, M.S. Hegde, T. Rattan, S.T. Aruna, "Chemistry of nanocrystalline oxide materials combustion synthesis, properties and applications", World Scientific Publications (2008) (DOI: <https://doi.org/10.1142/6754>).
- [128] F.-T Li, J. Ran, M. Jaroniec, S.Z. Qiao, "Solution combustion synthesis of metal oxide nanomaterials for energy storage and conversion", *Nanoscale* 7(42) (2015) 17590-17610.
- [129] A. Kumar, E.E. Wolf, A.S. Mukasyan, "Solution combustion synthesis of metal nanopowders: nickel-reaction pathways", *AIChE J.* 57(8) (2011) 2207-2214.
- [130] A. Kumar, E.E. Wolf, A.S. Mukasyan, "Solution combustion synthesis of metal nanopowders: Copper and copper / nickel alloys", *AIChE J.* 57(12) (2011) 3473-3479.
- [131] S. Zhang, Z.A. Munir, "The combustion synthesis of refractory nitrides: Part II the synthesis of niobium nitride", *J. Mater. Sci.* 26 (1991) 3380–3385.
- [132] "Nitride ceramics: Combustion synthesis, properties, and applications", (Eds.: A.A. Gromov, L.N. Chukhlomina) Wiley-VCH Verlag GmbH (2015) (DOI:10.1002/9783527684533).
- [133] H.V. Kirakosyan, K.T. Nazaretyan, R.A. Mnatsakanyan, S.V. Aydinyan, S.L. Kharatyan, "Solution combustion synthesis of nanostructured molybdenum carbide", *J. Nanopart. Res.* 20 (2018) 214.
- [134] N.A. Marand, S.M. Masoudpanah, M. Sh. Bafghi, "Solution combustion synthesis of nickel sulfide composite powders", *Ceram. Int.* 44 (14) (2018) 17277-17282.
- [135] K. Rajeshwar, N.R. De Tacconi, "Solution combustion synthesis of oxide semiconductors for solar energy conversion and environmental remediation", *Chem. Soc. Rev.* 38 (7) (2009) 1984-1998.

- [136] K.C. Thomas, J.R. Kale, R.G. Dalavi, K. Venkatesh, R. Kameswaran, A.V.R. Reddy  
"Development of an IR-based carbon analyser for uranium metal", BARC Newsletter  
311 (2009) 2-6 (Web-link: <http://barc.gov.in/publications/nl/2009/200912.pdf/>)
- [137] B.D. Cullity, "Elements of X-ray diffraction", Addison-Wesley Publishing Company  
Inc. (1956).
- [138] R. Tilley, "Crystals and crystal structures", John Wiley & Sons, Ltd. (2006) (ISBN-13  
978-0-470-01820-0).
- [139] E. Smith, G. Dent, "Modern Raman spectroscopy - A practical approach", John Wiley  
& Sons, Ltd. (2006) (ISBN 0-471-49794-0).
- [140] M. Roessle, D.I. Svergun, "Small angle X-ray scattering", In "Encyclopaedia of  
biophysics" (Eds.: G.C.K. Roberts) Springer, Berlin, Heidelberg (2013) (DOI:  
[https://doi.org/10.1007/978-3-642-16712-6\\_284](https://doi.org/10.1007/978-3-642-16712-6_284)).
- [141] P.W. Schmidt, R. Height, "Slit height corrections in small angle X-ray scattering", Acta  
Crystallogr. 13 (1960) 480-483.
- [142] G. Höhne, W.F. Hemminger, H.J. Flammersheim, "Differential scanning calorimetry",  
Springer-Verlag. (2003) (ISBN 978-3-540-00467-7).
- [143] M. Reading, A. Luget, R. Wilson, "Modulated differential scanning calorimetry",  
Thermochim. Acta 238(C) (1994) 295-307.
- [144] J.E.K. Schawe, T. Hutter, C. Heitz, I. Alig, D. Lellinger, "Stochastic temperature  
modulation: A new technique in temperature-modulated DSC", Thermochim. Acta 446  
(2006) 147-155.
- [145] N. Manoj, D. Jain, J.K. Gautam, K.C. Thomas, V. Sudarsan, C.G.S. Pillai, R.K. Vatsa,  
A.K. Tyagi, "A simple, reliable and cost-effective, high temperature dilatometer for  
bulk thermal expansion studies on solids", Measurement 92 (2016) 318-325.

- [146] W.J. Parker, R.J. Jenkins, C.P. Butler, G.L. Abbott, “Flash method of determining thermal diffusivity, heat capacity, and thermal conductivity”, *J. Appl. Phys.* 32 (1961) 1679-1684.
- [147] H.S. Carslaw, J.C. Jaeger, “Conduction of heat in solids”, 2nd edition, Oxford University Press, New York, (1959).
- [148] D. Jain, D. Das, B.N. Jagatap, “Thorium-based fuels for advanced nuclear reactors: Thermophysical, thermochemical and thermodynamic properties”, in A.K. Nayak, B.R. Sehgal (Eds.), *Thorium—Energy for the Future*, Springer (2019) (ISBN 978-981-13-2658-5) 257-275.
- [149] Y.S. Touloukian, R.W. Powell, C.Y. Ho, P.G. Klemens, “Thermophysical properties of matter - The TPRC data series. Volume 1. Thermal conductivity - metallic elements and alloys”, (1970) 429-440; 381-384.
- [150] Y.S. Touloukian, R.W. Powell, C.Y. Ho, M.C. Nicolaou, “Thermophysical properties of matter - The TPRC data series. Volume 10. Thermal diffusivity”, (1974) 205-208.
- [151] Y.S. Touloukian, E.H. Buyco, “Thermophysical properties of matter - The TPRC data series. Volume 4. Specific heat - metallic elements and alloys”, (1971) 268-270.
- [152] Y.S. Touloukian, R.K. Kirby, R.E. Taylor, P.D. Desai, “Thermophysical properties of matter - The TPRC data series. Volume 12. Thermal expansion metallic elements and alloys”, (1975) 365-372.
- [153] H.G. Schettler, J.J. Martin, F.A. Schmidt, G.C. Danielson, “Thermal conductivity of high purity thorium”, *Phys. Rev.* 187 (3) (1969) 801-804.
- [154] T.A. Sandenaw, “Thermal conductivity of uranium: Effects of purity and microstructure”, Report no.: LA-6092-MS, United States (1975) 1-8.
- [155] Y. Takahashi, M. Yamawaki, K. Yamamoto, “Thermophysical properties of uranium-zirconium alloys”, *J. Nucl. Mater.* 154 (1988) 141-144.

- [156] R.W. Logan, D.H. Wood, "Thermal expansion of rolled and extruded uranium", *J. Less-Common Met.* 90 (1983) 233-241.
- [157] J. Nakamura, Y. Takahashi, S. Izumi, M. Kanno, "Heat capacity of metallic uranium and thorium from 80 to 1000 K", *J. Nucl. Mater.* 88 (1980) 64-72.
- [158] M. Boivineau, H. Colin, J.M. Vermeulen, Th. Thévenin, "Thermophysical properties of solid and liquid thorium", *Int. J. Thermophys.* 17(5) (1996) 1001-1010.
- [159] S. Zhou, R. Jacobs, W. Xie, E. Tea, C. Hin, D. Morgan, "Combined ab-initio and empirical model of the thermal conductivity of uranium, uranium-zirconium, and uranium-molybdenum", *Phys. Rev. Mater.* 2 (2018) 083401-1-21.
- [160] Y. Li, A. Chernatynskiy, J.R. Kennedy, S.B. Sinnott, S.R. Phillpot, Lattice expansion by intrinsic defects in uranium by molecular dynamics simulation, *J. Nucl. Mater.* 475 (2016) 6-18.
- [161] K.D. Joshi, S.C. Gupta, S. Banerjee, "Ab-initio theoretical analysis of thermal expansivity, thermal vibrations and melting of thorium", *Phil. Mag.* 88 (27) (2008) 3145-3152.
- [162] S. Jaroszewicz, H.O. Mosca, J.E. Garcés, "The temperature behaviour of the elastic and thermodynamic properties of fcc thorium", *J. Nucl. Mater.* 429(1-3) (2012) 136-142.
- [163] L. Kývala, D. Legut, "Lattice dynamics and thermal properties of thorium metal and thorium monocarbide" *Phys. Rev. B* 101 (2020) 075117.
- [164] P.L. Vijay, J.C. Sehra, C.V. Sundaram, K.R. Gurumurthy, R.V. Raghavan, "Studies on the preparation of thorium metal sponge from thorium oxalate", *BARC Report no.:* 969 (1978) 1-11.
- [165] M.D. Smith, R.W.K. Honeycombe, "The effect of oxygen, carbon and nitrogen on the properties of sintered thorium", *J. Nucl. Mater.* 4 (1959) 345-355.

- [166] Inorganic Crystal Structure Database (ICSD FIZ Karlsruhe GmbH, Version 4.4.0 (2020); collection code: 653236); from: J. Bohet, W. Müller, “Preparation and structure studies of “Van Arkel” protactinium”, *J. Less-Common Met.* 57 (2) (1978) 185-1995.
- [167] International Centre for Diffraction Data (ICDD Database; JCPDF card no.: 720659).
- [168] Inorganic Crystal Structure Database (ICSD FIZ Karlsruhe GmbH, Version 4.4.0 (2020) collection code: 253564) from: V.K. Tripathi, R. Nagarajan, “Sol–gel synthesis of high-purity actinide oxide ThO<sub>2</sub> and its solid solutions with technologically important tin and zinc ions” *Inorg. Chem.* 55 (24) (2016) 12798-12806.
- [169] Inorganic Crystal Structure Database (ICSD FIZ Karlsruhe GmbH, Version 4.4.0 (2020) collection code: 35204); from: S.A. Barrett, A.J. Jacobson, B.C. Tofield, B.E.F. Fender, “The preparation and structure of barium uranium oxide BaUO<sub>3+x</sub>”, *Acta Crystallogr. B* 38 (1982) 2775-2781. [169a] S. Ellison, A. Williams, *Eurachem / CITAC guide: Quantifying Uncertainty in Analytical Measurement* (2012) ISBN 978-0-948926-30-3 (Web-link: [www.eurachem.org](http://www.eurachem.org)).
- [170] Inorganic Crystal Structure Database (ICSD FIZ Karlsruhe GmbH, Version 4.4.0 (2020) collection code: 24223); from: R.E. Rundle, N.C. Baenziger, A.S. Wilson, R.A. McDonald, “The structures of the carbides, nitrides and oxides of uranium”, *J. Am. Chem. Soc.* 70 (1948) 99-105.
- [171] Inorganic Crystal Structure Database (ICSD FIZ Karlsruhe GmbH, Version 4.4.0 (2020) collection code: 26476); from: A.E. Austin, “Carbon positions in uranium carbides”, *Acta Crystallogr.* 12 (1959) 159-161.
- [172] “Augmented uranium metal production facility”, *BARC Newsletter* 200 (2000) 15-18 (Web-link: <http://barc.gov.in/publications/nl/2000/200009.pdf>).
- [173] G.C. Allen, P.M. Tucker, “Surface oxidation of uranium metal as studied by X-ray photoelectron spectroscopy”, *J. Chem. Soc. Dalton* 5 (1973) 470-474.

- [174] R. Rao, R.K. Bhagat, N.P. Salke, A. Kumar, "Raman spectroscopic investigation of thorium dioxide-uranium dioxide ( $\text{ThO}_2\text{-UO}_2$ ) fuel materials", *Appl. Spectrosc.* 68(1) (2014) 44-48.
- [175] "Thermophysical properties of materials for nuclear engineering: A tutorial and collection of data", (IAEA-THPH), International Atomic Energy Agency, Vienna (2008).
- [176] I.F. Barwood, B.R. Butcher, "The  $\alpha \rightarrow \beta$  phase transformation in uranium", *J. Nucl. Mater.* 8 (1963) 232-240.
- [177] C. Yoo, H. Cynn, P. Söderlind, "Phase diagram of uranium at high pressures and temperatures", *Phys. Rev. B* 57 (1998) 10359-10362.
- [178] P. Zhou, X. Wang, H. Yang, X. Fu, "Effect of vacuum heat treatment on oxidation of uranium surfaces", *Rare Metal Mat. Eng.* 37 (2008) 94-97.
- [179] G. Erez, U. Even, "The Wiedemann-Franz ratio of metallic uranium at elevated temperatures", *J. Appl. Phys.* 37 (1966) 4633-4644.
- [180] S. Nasu, S. Fukushima, T. Ohmichi, T. Kikuchi, "Thermal diffusivity of uranium by laser pulse method from 20° to 850°C", *Jap. J. Appl. Phys.* 7 (1968) 682.
- [181] D. Jain, C.G.S. Pillai, B.S. Rao, R.V. Kulkarni, E. Ramdasan and K.C. Sahoo, "Thermal diffusivity and thermal conductivity studies on thoria-lanthana solid solutions up to 10 mol. %  $\text{LaO}_{1.5}$ ", *J. Nucl. Mater.* 353 (2006) 35-41.
- [182] S.S. Parker, J.T. White, P. Hosemann, A.T. Nelson, "Thermophysical properties of thorium mononitride from 298 to 1700 K", *J. Nucl. Mater.* 526 (2019) 151760.
- [183] H. He, J. Majewski, D.D. Allred, P. Wang, X. Wen, K.D. Rector, "Formation of solid thorium monoxide at near-ambient conditions as observed by neutron reflectometry and interpreted by screened hybrid functional calculations", *J. Nucl. Mater.* 487 (2017) 288-296.

## References

- [184] B.R. Butcher, A.H. Rowe, "Phase transformation in uranium", *Nature* (1953) 817.
- [185] H.H. Klpefer, P. Chiotti, "Characteristics of the solid state transformations in uranium", USAEC Report no.: ISC-893 (1957) 1-113.
- [186] W.S. Blackburn, " $\alpha$ - $\beta$  Thermal cycling of uranium", *J. Nucl. Mater.* 2 (1960) 191.
- [187] J.J. Stobo, "Alpha beta cycling of uranium", *J. Nucl. Mater.* 2 (1960) 97-109.
- [188] L.T. Lloyd, "Thermal expansion of alpha-uranium single crystals", *J. Nucl. Mater.* 3 (1961) 67-71.
- [189] L.T. Lloyd, C.S. Barrett, "Thermal expansion of alpha uranium", *J. Nucl. Mater.* 18 (1966) 55-59.
- [190] E.S. Fisher, "Preparation of alpha uranium single crystals by a grain-coarsening method", *J. Metals* 9 (1957) 882-888.
- [191] D.C. Wallace, "Specific heat of thorium at high temperatures", *Phys. Rev.* 120 (1) (1960) 84-88.
- [192] E.A. Mit'kina, "Experimental determination of the true specific heats of uranium, thorium, and other metals", *Sov. Atom Energy* 7 (2) (1959) 163-165.
- [193] F.L. Oetting, D.T. Peterson, "Heat capacity of well characterized thorium metal from 298 to 700 K", *J. Less-Common Met.* 128 (1987) 231-239.
- [194] D.C. Ginnings, R.J. Corruccini, "Heat capacities at high temperatures of uranium, uranium trichloride, and uranium tetrachloride, *J. Res. Nat. Bur. Stand.* 39 (1947) 309-316.
- [195] F.K. Oetting, M.H. Rand, R.J. Ackermann, "The chemical thermodynamics of actinide elements and compounds, Part 1, The actinide elements", International Atomic Energy Agency (IAEA), Vienna (1976).
- [196] A.L. Loeb, "Thermal conductivity: VIII, A theory of thermal conductivity of porous materials", *J. Am. Ceram. Soc.* 37 (1954) 96-99.

## References

- [197] S. Kaity, J. Banerjee, M.R. Nair, K. Ravi, S. Dash, T.R.G. Kutty, A. Kumar, R.P. Singh, "Microstructural and thermophysical properties of U-6 wt.% Zr alloy for fast reactor application", *J. Nucl. Mater.* 427 (2012) 1-11.
- [198] C. Hin, "Thermal conductivity of metallic uranium", NEUP 14-6767 (2018) (Web-link: <https://www.osti.gov/servlets/purl/1433931>).
- [199] M. Floyd, B. Bromley, J. Pencer, "A Canadian perspective on progress in thorium fuel science and technology", *CNL Nucl. Rev.* 6 (1) (2017) 1-17.
- [200] S. Thakur, P.S.R. Krishna, A.B. Shinde, R. Kumar, S.B. Roy, "Quantitative analysis of thorium phase in Th-U alloys using diffraction studies", *AIP Conf. Proc.* 1832 (2017) 060012.
- [201] P. Chiotti, "High temperature crystal structure of thorium", *J. Electrochem. Soc.* (1955) 567-570.
- [202] G.G. Bente, "A Physical Metallurgical Study of Thorium-Rich Thorium-Uranium Alloys", Report no.: NAA-SR-2069 (1958).
- [203] G.H. Bannister, R.C. Burnett, J.R. Murray, "Ageing and hot hardness characteristics of certain thorium alloys", *J. Nucl. Mater.* 2(1) (1960) 51-61.
- [204] "Chemical technology division annual technical report for 1986," ANL-87-19, Argonne National Laboratory (1987) 122.
- [205] V. Crewe, S. Lawroski, "Reactor development program progress report", Argonne National Laboratory, ANL-7230, Lemont, IL, USA (1966).
- [206] O. Beneš D. Manara R.J.M. Konings, "Thermodynamic assessment of the Th-U-Pu system", *J. Nucl. Mater.* 449 (1-3) (2014) 15-22.
- [207] S. Kneppel, "Aqueous corrosion of thorium alloys and zircaloy-clad thorium alloys", NMI-1226, United States Atomic Energy Commission (1960) 1-49 (Web-link: <https://play.google.com/books/reader?id=OGCWvHY4xRwC&hl=en&pg=GBS.PA1>)

- [208] D.S. Evans, G.V. Raynor, "The solubility of zirconium in  $\alpha$ -thorium", *J. Nucl. Mater.* 4 (1) (1961) 66-69.
- [209] R.I. Sheldon, D.E. Peterson, "The (U-Zr) Uranium-zirconium system", *Bull. Alloy Phase Diagr.* 10 (2) (1989) 165-171.
- [210] O.N. Carlson, "Some studies on the uranium-thorium-zirconium ternary alloy system", AECD-3206, United States Atomic Energy Commission (1950) 1-72.
- [211] J.W. Goffard, R.K. Marshall, "Irradiation behavior of Zircaloy-2 clad thorium-uranium-zirconium alloy fuel elements Interim report 1", BNWL-479, Pacific Northwest Laboratory, United States Atomic Energy Commission (1967).
- [212] T. Okawa, S. Nakayama, H. Sekimoto, "Design study on power flattening to sodium cooled large-scale CANDLE burning reactor with using thorium fuel", *Energ. Convers. Manage.* 53 (1) (2012) 182-188.
- [213] Inorganic crystal Structure Database (ICSD FIZ Karlsruhe GmbH, Version 4.4.0 (2020) collection code: 164572) from: A.I. Kolesnikov, A.M. Balagurov, I.O. Bashkin, A.V. Belushkin, E.G. Ponyatovsky, M. Prager, "Neutron scattering studies of ordered gamma -ZrD", *J. Phys. Condens-Mat.* 6 (43) (1994) 8977-8988.
- [214] Inorganic crystal Structure Database (ICSD FIZ Karlsruhe GmbH, Version 4.4.0 (2020) collection code: 16559) from: B.O. Loopstra, "Neutron diffraction investigation of  $U_3O_8$ ", *Acta Crystallogr.* 17 (1964) 651-654.
- [215] Inorganic crystal Structure Database (ICSD FIZ Karlsruhe GmbH, Version 4.4.0 (2020) collection code: 246035) from: S.K. Sali, N.K. Kulkarni, K. Krishnan, S.N. Achary, A.K. Tyagi, "Oxidation / reduction studies on  $Zr_yU_{1-y}O_{2+x}$  and delineation of a new orthorhombic phase in U-Zr-O system", *J. Solid-State Chem.* 181 (8) (2008) 1859-1866.

## References

- [216] Inorganic crystal Structure Database (ICSD FIZ Karlsruhe GmbH, Version 4.4.0 (2020) collection code: 108756) from: H.L. Luo, J.G. Huber, “Superconductivity in Th-Zr alloys”, *J. Less-Common Met.* 65 (1) (1979) 13-17.
- [217] J.M. Elorrieta, L.J. Bonales, M. Naji, D. Manara, V.G. Baonza, J. Cobos, “Laser-induced oxidation of  $\text{UO}_2$ : A Raman study”, *J. Raman Spectrosc.* 49 (5) (2018) 878-884.
- [218] H. He, D. Shoesmith, “Raman spectroscopic studies of defect structures and phase transition in hyper-stoichiometric  $\text{UO}_{2+x}$ ”, *Phys. Chem. Chem. Phys.* 12 (2010) 8109-8118.
- [219] X. Zhao, D. Vanderbilt, “Phonons and lattice dielectric properties of zirconia”, *Phys. Rev. B* 65 (2002) 075105.
- [220] E. Hashem, A. Seibert, J-F. Vigier, M. Naji, S. Mastromarino, A. Ciccioli, D. Manara, “Solid-liquid equilibria in the  $\text{ThO}_2$ - $\text{ZrO}_2$  system: An experimental study” *J. Nucl. Mater.* 521 (2019) 99-108.
- [221] O.N. Carlson, E.R. Stevens, “A compilation of thorium binary phase diagrams”, USAEC Report (1968) (Web-link: <https://www.osti.gov/servlets/purl/4529064>).
- [222] G.B. Skinner, H.L. Johnston, “Thermal Expansion of zirconium between 298°K and 1600°K”, *J. Chem Phys.* 21 (1953) 1383.
- [223] P.L. Brown, E. Curti, B. Grambow, C. Ekberg, “Chemical thermodynamics of zirconium”, OECD Nuclear energy agency, data bank (Eds.: F.J. Mompean, J. Perrone, M. Illemassene) (2005) (Web-link: <https://www.oecd-nea.org/dbtdb/pubs/vol8-zirconium.pdf>).
- [224] C.G.S. Pillai, P. Raj, “Thermal Conductivity of  $\text{ThO}_2$  and  $\text{Th}_{0.98}\text{U}_{0.02}\text{O}_2$ ”, *J. Nucl. Mater.* 277 (2000) 116-119.

- [225] S.S. Manoharan, K.C. Patil, "Combustion synthesis of metal chromite powders", *J. Am. Ceram. Soc.* 75 (1992) 1012-1015.
- [226] S.R. Jain, K.C. Adiga, V.R. Pai Verneker, "A new approach to thermochemical calculations of condensed fuel-oxidizer mixtures," *Combust. Flame* 40 (6) (1981) 71-79.
- [227] S. Roy, A. Das Sharma, S.N. Roy, H.S. Maiti, "Synthesis of  $\text{YBa}_2\text{Cu}_3\text{O}_{7-x}$  Powder by Autoignition of Citrate-Nitrate Gel", *J. Mater. Res.* 8(11) (1993) 2761-2766.
- [228] M. Gizowska, I. Kobus, K. Perkowski, M. Piatek, G. Konopka, I. Witosławska, M. Osuchowski, "Size and morphology of yttria nanopowders obtained by solution combustion synthesis" *Arch. Metall. Mater.* 63(2) (2018) 743-748.
- [229] G.A.M. Hussein, H.M. Ismail, "Texture assessment of thoria as a final decomposition product of hydrated thorium nitrate and oxycarbonate", *Colloids Surf. A*: 99 (1995) 129-139.
- [230] I.M. Weiss, C. Muth, R. Drumm, H.O.K. Kirchner, "Thermal decomposition of the amino acids glycine, cysteine, aspartic acid, asparagine, glutamic acid, glutamine, arginine and histidine", *BMC Biophys.* 11 (2018) 1-15.
- [231] N. Raje, A.V.R. Reddy, "Mechanistic aspects of thermal decomposition of thorium oxalate hexahydrate: A review", *Thermochim. Acta* 505 (2010) 53-58.
- [232] H. Hayashi, T. Watanabe, "Properties of thoria obtained by thermal decomposition of thorium salts", *Nippon Kagaku Kaishi* 4 (1973) 858-860.
- [233] Y. Saito, "Thermal decomposition of thorium oxalate", *J. Jpn. Soc. Powder Metall.* 17(1971) 235-242.
- [234] M.T. Aybers, "Kinetic study of the thermal decomposition of thorium oxalate dehydrate", *J. Nucl. Mater.* 252 (1998) 28-33.
- [235] D.Y. Chung, E. H. Lee, "Microwave-induced combustion synthesis of  $\text{Ce}_{1-x}\text{Sm}_x\text{O}_{2-x/2}$  powder and its characterization", *J. Alloys Compd.* 374 (2004) 69-73.

- [236] “The Aldrich Library of FT-IR Spectra, Edition-II, Volume-1”, 1 898 A 897-898.
- [237] S. Kumar, A.K. Rai, V.B. Singh, S.B. Rai, “Vibrational spectrum of glycine molecule”, *Spectrochim. Acta A* 61 (2005) 2741-2746.
- [238] J. R. Ferraro, A. Walker, “Comparison of the infrared spectra of the hydrates and anhydrous salts in the systems  $\text{UO}_2(\text{NO}_3)_2$  and  $\text{Th}(\text{NO}_3)_4$ ”, *J. Chem. Phys.* 45 (1966) 550-552.
- [239] J.H-Paredes, D.G-Mitnik, H.E. E-Ponce, M.E. A-Ramos, A.D-Moller, “Band structure, optical properties and infrared spectrum of glycine–sodium nitrate crystal”, *J. Mole. Str.* 875 (2008) 295-301.
- [240] S.L. Estes, M.R. Antonio, L. Soderholm, “Tetravalent Ce in the nitrate-decorated hexanuclear cluster  $[\text{Ce}_6(\mu_3\text{-O})_4(\mu_3\text{-OH})_4]^{12+}$ : A structural end point for ceria nanoparticles, *J. Phys. Chem. C* 120 (2016) 5810-5818.
- [241] M. Rand, L. Fuger, I. Grenthe, V. Neck, D. Rai, “Chemical thermodynamics: Chemical thermodynamics of thorium”, (OECD, NEA-TDB) Vol. 11, Elsevier, Amsterdam (2007).
- [242] C. Hennig, K. Schmeide, V. Brendler, H. Moll, S. Tsushima, A.C. Scheinost, “EXAFS Investigation of U(VI), U(IV), and Th(IV) sulfato complexes in aqueous solution”, *Inorg. Chem.* 46 (2007) 5882-5892.
- [243] J. Rothe, M.A. Denecke, V. Neck, R. Muller, J.I. Kim, XAFS “Investigation of the structure of aqueous thorium(IV) species, colloids, and solid thorium(IV) oxide / hydroxide”, *Inorg. Chem.* 41 (2002) 249-258.
- [244] C. Hennig, S. Takao, K. Takao, S. Weiss, W. Kraus, F. Emmerling, A.C. Scheinosta, “Structure and stability range of a hexanuclear Th(IV)-glycine complex”, *Dalton Trans.* 41 (2012) 12818-12823.

## References

- [245] Y. Hu, K.E. Knope, S. Skanthakumar, L. Soderholm, "Understanding the ligand-directed assembly of a hexanuclear Th<sup>IV</sup> molecular cluster in aqueous solution", *Eur. J. Inorg. Chem.* 24 (2013) 4159-4163.
- [246] M. Nourmand, N. Meissami, "Complex formation between uranium(VI) and thorium (IV) ions with some  $\alpha$ -amino-acids", *J. Chem. Soc. Dalton* 8 (1983) 1529-1533.
- [247] Bismondo, L. Rizzo, G. Tomat, "Thermodynamic properties of actinide complexes. uranyl (VI)- and thorium (IV)-glycine systems", *Inorg. Chim. Acta* 74 (1983) 21-24.
- [248] B.G. Oliver, A.R. Davis, "The structure of aqueous thorium nitrate solution by laser Raman spectroscopy", *J. Inorg. Nucl. Chem.* 34 (1972) 2851-2860.
- [249] Z. Huang, X. Chen, Y. Li, J. Chen, J. Lin, J. Wang, J. Lei, R. Chen, "Quantitative determination of citric acid in seminal plasma by using Raman spectroscopy", *Appl. Spectrosc.* 67 (7) (2013) 757-760.
- [250] A.K. Arora, M. Rajalakshmi, T.R. Ravindran, V. Sivasubramanian, "Raman spectroscopy of optical phonon confinement in nanostructured materials", *J. Raman Spectrosc.* 38 (2007) 604-617.
- [251] D. Langmuir, J.S. Herman, "The mobility of thorium in natural waters at low temperatures", *Geochim. Cosmochim. Ac.* 44 (1980) 1753-1766.
- [252] M. Bobtelsky, B. Graus, "Thorium citrate complexes, their composition, structure and behavior", *J. Am. Chem. Soc.* 76 (6) (1954,) 1536-1539.
- [253] G.R. Choppin, H.N. Erten, Y. Xia, "Variation of stability constants of thorium citrate complexes with ionic strength", *Radiochim. Acta* 74 (1996) 123-127.
- [254] D.P. Raymond, J.R. Duffield, D.R. Williams, "Complexation of plutonium and thorium in aqueous environments", *Inorg. Chim. Acta* 140 (1987) 309-313.
- [255] M.M. Barbooti, D.A. Al-Sammerrai, "Thermal decomposition of citric acid", *Thermochim. Acta* 98 (1986) 119-126.

## References

- [256] D. Hennings, W. Mayr, "Thermal decomposition of (BaTi) citrates into barium titanate", *J. Solid State Chem.* 26 (1978) 329-338.
- [257] N.S. Gajbhiye, S. Prasad, "Thermal decomposition of hexahydrated nickel iron citrate", *Thermochim. Acta* 285 (1996) 325-336.
- [258] J. Tsay, T. Fang, "Effects of molar ratio of citric acid to cations and of pH value on the formation and thermal-decomposition behavior of barium titanium citrate", *J. Am. Ceram. Soc.* 82(6) (1999) 1409-1415.
- [259] A. Marcilla, A. Gómez-Siurana, M. Beltrán, I. Martínez-Castellanos, I. Blasco, D. Berenguer, "TGA-FTIR study of the pyrolysis of sodium citrate and its effect on the pyrolysis of tobacco and tobacco/SBA-15 mixtures under N<sub>2</sub> and air atmospheres", *J. Sci. Food Agr.* 98 (15) (2018) 5916-5931.
- [260] O. Glatter, O. Kratky, "Small angle X-ray scattering", Academic, London (1982).
- [261] A. Guinier, G. Fournet, "Small angle scattering of X-rays", Wiley, New York (1955).
- [262] J. Aitchison, J.A.C. Brown, "The log normal distribution", Cambridge University Press, Cambridge (1957).
- [263] R.D. Purohit, B.P. Sharma, K.T. Pillai, A.K. Tyagi, "Ultrafine ceria powders via glycine-nitrate combustion", *Mater. Res. Bull.* 36 (15) (2001) 2711-2721.
- [264] V.R. Choudhary, A.M. Rajput, B. Prabhakar, A.S. Mamman, "Partial oxidation of methane to CO and H<sub>2</sub> over nickel and/or cobalt containing ZrO<sub>2</sub>, ThO<sub>2</sub>, UO<sub>2</sub>, TiO<sub>2</sub> and SiO<sub>2</sub> catalysts", *Fuel* 77 (15) (1998) 1803-1807.
- [265] V. Múčka, J. Podlaha, R. Silber, "NiO-ThO<sub>2</sub> mixed catalysts in hydrogen peroxide decomposition and influence of ionizing radiation", *Radiat. Phys. Chem.* 59 (5-6) (2000) 467-475.

## References

- [266] P. Balakrishna, B.N. Murty, K.P. Chakraborty, R.N. Jayaraj, C. Ganguly, "Special features in powder preparation, pressing, and sintering of uranium dioxide", *Mater. Manuf. Process.* 15(5) (2000) 679-693.
- [267] C.S. Morgan, K.H. McCorkle, G.L. Powell, "Sintering and desintering of thoria", In: Kuczynski G.C. (Eds.) *Sintering and Related Phenomena*. Materials Science Research, Vol. 6, Springer, Boston, MA (1973).
- [268] J.M. Pope, K.C. Radford, "Physical properties of some thoria powders and their influence on sinterability", *J. Nucl. Mater.* 52 (1974) 241-254.
- [269] Z. Chen, J. Mabon, J. Wen, R. Trice, "Degradation of plasma-sprayed yttria-stabilized zirconia coatings via ingress of vanadium oxide", *J. Eur. Ceram. Soc.* 29(9) (2009) 1647-1656.
- [270] M.A. Delfrate, J. Lemaitre, V. Buscaglia, M. Leoni, P. Nanni, "Slip casting of submicron BaTiO<sub>3</sub> produced by low-temperature aqueous synthesis", *J. Eur. Ceram. Soc.* 16(9) (1996) 975-984.
- [271] T.K. Gupta, R.L. Coble, "Sintering of ZnO: II, density decrease and pore growth during the final stage of the process", *J. Am. Ceram. Soc.* 51 (9) (1968) 525-528.
- [272] C.-H. Chang, J.F. Rufner, K.V. Benthem, R.H.R. Castro, "Design of desintering in tin dioxide nanoparticles", *Chem. Mater.* 25(21) (2013) 4262-4268.
- [273] P. Duran, J. Tartaj, C. Moure, "Sintering behaviour and microstructural evolution of agglomerated spherical particles of high-purity barium titanate", *Ceram. Int.* 29(4) (2003) 419-425.
- [274] C.-Y. Tsao, W.-H. Tuan, K.-C. Feng, "De-sintering of Ba<sub>5</sub>Nb<sub>4</sub>O<sub>15</sub> ceramic and its influence on microwave characteristics", *J. Eur. Ceram. Soc.* 37(4) (2017) 1517-1521.
- [275] Cs. Balázs, F.S. Cinar, O. Addemir, F. Wéber, P. Arató, "Manufacture and examination of C/Si<sub>3</sub>N<sub>4</sub> nanocomposites" *J. Eur. Ceram. Soc.* 24(12) (2004) 3287-3294.

- [276] R. Besler, M.R. da Silva, J.J. do Rosario, M. Dosta, S. Heinrich, R. Janssen, “Sintering simulation of periodic macro porous alumina”, *J. Am. Ceram. Soc.* 98(11) (2015) 3496-3502.
- [277] K. Ananthasivan, S. Anthonysamy, A. Singh, P.R. Vasudeva Rao, “De-agglomeration of thorium oxalate - A method for the synthesis of sinter active thoria”, *J. Nucl. Mater.* 306 (1) (2002) 1-9.
- [278] R.H.R. Castro, “Controlling sintering and grain growth of nanoceramics”, *Cerâmica* 65 (373) (2019) 122-129. **[278a]** Thermodynamics of sintering, R.M. German, *Sintering of advanced materials: Fundamentals and processes* (Ed.: Z.Z. Fang) Woodhead Publishing Ltd. (2010), ISBN 978-1-84569-562-0. **[278b]** G.S. Upadhyaya, *Sintered metallic and ceramic Materials*, John Wiley & Sons Ltd. (1999) ISBN 0-471-98155-9.
- [279] O. Sudre, F.F. Lange, “The effect of inclusions on densification; III, The desintering phenomenon”, *J. Am. Ceram. Soc.* 75 (12) (1992) 3241-3251.
- [280] F. Li, J. Pan, A. Cocks, “Defect healing and cracking in ceramic films during constrained sintering” *J. Am. Ceram. Soc.* 95(12) (2012) 3743-3749.
- [281] S. Knight, R. Korlacki, C. Dugan, J.C. Petrosky, A. Mock, P.A. Dowben, J. Matthew Mann, M.M. Kimani, M. Schubert, “Infrared-active phonon modes in single-crystal thorium dioxide and uranium dioxide”, *J. Appl. Phys.* 127 (2020) 125103.

## CHAPTER 4

### Thermophysical studies on thorium-uranium (Th-U)

#### binary metallic alloys

---

##### 4.1. Introduction

In chapter-3, thermophysical properties of well characterized, nuclear-grade thorium and uranium metals have been studied over a wide temperature range (298 K – 1373 K). Detailed comparative assessment of experimentally measured thermophysical properties data on these two metals with the reported values has highlighted the importance of indigenous database for the development of thorium-based metallic nuclear fuels. Being a fertile radionuclide, thorium alone cannot be used as a nuclear fuel and must be combined with a fissile element such as  $^{235}\text{U}$ ,  $^{233}\text{U}$ , plutonium or minor actinides (MAs: Np, Am, Cm, etc.). Only then a controlled fission chain reaction can be sustained to produce electricity; predominantly from the fissile radionuclide while  $^{232}\text{Th}$  undergoes neutron induced transmutation to produce new fissile inventory (breeding) in the form of  $^{233}\text{U}$ . A fraction of as-bred  $^{233}\text{U}$  would also undergo neutron induced fission for energy production during the fuel irradiation while the rest of it remains in the spent fuel.  $^{233}\text{U}$  present in the spent fuel can be separated from remaining thorium and fission products by chemical reprocessing (aqueous or pyrometallurgical). The extracted  $^{233}\text{U}$  can then be used for fuel re-fabrication for fresh cores of new reactors or refuelling of existing reactors.

Similar to binary mixed oxides (MOX) of thorium with fissile actinides  $\{(\text{Th}_{1-x}\text{U}_x)\text{O}_2, (\text{Th}_{1-x}\text{Pu}_x)\text{O}_2, (\text{Th}_{1-x}\text{MA}_x)\text{O}_2\}$ , binary metallic alloys of thorium with uranium (Th-U alloys), plutonium (Th-Pu alloys) and / or MAs (Th-MA alloys) are potential metallic

nuclear fuel candidates. Research carried out mainly during the first three decades of nuclear technology development has clearly indicated the inherent advantages of these binary metallic alloy fuels over uranium-based metallic fuels for use in both fast and thermal reactors [35, 65, 71]. A brief review of literature on thorium-based binary metallic alloy fuels has been presented in Chapter-1 (Section 1.3). Potential of Th-U binary alloys as promising nuclear fuels for fast as well as thermal reactors had been identified during the early developments of nuclear technology. While adequate information on physico-chemical properties, irradiation behavior, reprocessing and waste management aspects of thorium-based binary mixed oxides (MOX) have been accumulated [25, 26, 199], very limited literature exists on thorium-based binary metallic alloy fuels. Further, studies on thorium-based metallic alloys; mainly reported in the form of internal reports also show wide scatter in their physico-chemical properties data. Preparation, microstructure evaluation, mechanical properties and irradiation performance of thorium-uranium binary alloys have been reported for few alloy compositions [85-87, 95, 200]. However, information on their thermophysical properties as a function of temperature is very limited [86, 96]. For development of these alloys as potential fast reactor fuels in India, it is therefore essential to study them in terms of their preparation, characterization and thermophysical properties evaluation. Keeping this in mind, two representative binary alloys, namely Th-10U and Th-20U (in wt. %) have been investigated during the present studies. Earlier irradiation studies reported on these alloy compositions have indicated their potential as power reactor fuels [62, 71]. Excellent stability of Th-U binary alloy fuels up to 10 wt. % uranium has also been reported [66]. For this reason, Th-10U and Th-20U (wt. %) compositions are chosen for the present investigations. With the aim of utilization as metallic nuclear fuels, few other Th-U binary alloys with varied compositions such as Th-65U [85], Th-3U [86], Th-52U [87], (wt. %) have recently been investigated for their phase behavior, microstructural, thermal and mechanical properties.

Experimental results on preparation, characterization and thermophysical properties of Th-10U and Th-20U (wt. %) binary alloys are presented in this chapter.

## 4.2. Experimental

Th-10U and Th-20U alloys (wt. %) were prepared by DC-arc melting of stoichiometric amounts of reactor grade uranium and thorium metals under high purity argon atmosphere (~200 ml/min.). Uranium and thorium metal pieces were cut from metal ingots using slow speed diamond impregnated metal cutting machine as detailed in Chapter 2 (section 2.3.1.3.). Argon gas was purified by passing through heated ( $673 \text{ K} \pm 2 \text{ K}$ ) uranium metal scrap before flowing through the arc melting furnace. Both uranium and thorium metal pieces were thoroughly surface cleaned under dry hexane immersion inside an inert atmosphere (Argon) glove box, ultrasonicated and vacuum dried ( $P < 10^{-2}$  Torr) before melting. Melting was repeated four times by inverting the alloy button each time to obtain better homogeneity and uniformity of constituents' distribution in as-melted alloys. As-melted alloys were surface cleaned; wrapped in tantalum foils and sealed in quartz tube under reduced argon pressure ( $P < 10^{-3}$  Torr) for phase homogenization at 973 K for 220 h. Annealed alloys were slowly cooled to ambient temperature (cooling rate = 1 K /min.) and sealed quartz tubes were break open inside the glove box. Annealed alloyed were used for characterization and thermophysical properties evaluation. Both the alloys were analyzed for non-metallic impurities (C, N, O) using small samples (100-150 mg; in triplicate) cut from the annealed alloy buttons. Phase characterization of alloys was carried out using XRD. A thin layer of silicon vacuum grease was applied over the flat polished surface of alloys to minimize surface oxidation during XRD data collection. Surface morphology and alloy composition of polished alloy samples was studied using scanning electron microscope (SEM) and energy dispersive X-ray spectroscopy (EDS), respectively. Samples for thermophysical properties

measurements were machined from annealed alloy buttons in suitable shapes using a mechanical lathe machine under continuous flow of machine oil over the alloy surface. Cylindrical pellets (~12.5 mm diameter; ~ 3 mm thickness) were prepared for thermal diffusivity measurements. Small pellets (~6 mm diameter; 4-5 mm heights) were machined for thermal expansion studies while thin disc shaped samples (~0.5 mm thickness) were prepared for specific heat measurements. Sample densities were evaluated using measured weight and sample dimensions. Sample weights were recorded after each experiment to assess the extent of oxidation during thermophysical properties measurements.

Bulk linear thermal expansion measurements were performed on a thermo mechanical analyzer (TMA) over 308 K to 1373 K (Heating rate = 10 K / min.; cooling rate = 20 K / min.) under high purity argon flow. Each alloy sample was sandwiched between two high density (~96 % TD) sintered ThO<sub>2</sub> discs to avoid alloy's chemical interaction with TMA push-rod or sample holder. Linear dilation of alloys was evaluated by subtracting the blank corrected dilation of ThO<sub>2</sub>-ThO<sub>2</sub> couple from that of ThO<sub>2</sub>-alloy-ThO<sub>2</sub> stack. Heat flow through the alloy samples was measured over 273 K to 773 K using temperature modulated differential scanning calorimeter (TMDSC) under multi-frequency temperature modulation program (TOPEM<sup>®</sup>). Specific heats of alloys were evaluated from the reversing component of the heat flow obtained by the analysis of modulated heat flow curve. Thermal diffusivities of alloys were measured using laser flash apparatus (LFA) over a temperature range from 298 K to 1373 K under dynamic vacuum ( $P < 3 \times 10^{-6}$  Torr). Four laser shots were fired on each temperature and average of diffusivity values obtained from acceptable shots were taken as final diffusivity values. Thermal conductivity of alloys was evaluated by multiplying measured thermal diffusivity with density (evaluated from measured linear thermal expansion data) and specific heat (experimentally measured from TMDSC as well as literature reported

specific heats of thorium and uranium metals). Sample densities were evaluated from measured weight and sample dimensions.

### 4.3. Results and discussion

#### 4.3.1. Impurity analysis

Information of impurities present in the starting metals (Th and U) as well as Th-U binary alloys is important while reporting their thermophysical properties. Particularly, assessment of extent of non-metallic impurities like carbon, nitrogen, oxygen, hydrogen, etc. is essential since they have notable influence on thermophysical properties. Table 4.1 shows the average concentration of C, N, and O present in Th-10U and Th-20U alloys as measured from elemental analysis.

**Table 4.1. Carbon, oxygen and nitrogen contents in binary alloys (Th-10U, Th-20U) and constituent metals (Th and U)**

<b>Impurity</b> →	<b>Carbon (ppm)</b>	<b>Oxygen (ppm)</b>	<b>Nitrogen (ppm)</b>
<b>Sample</b> ↓	<b>Average value of triplicate analysis ± Error (2 <math>\sigma</math>; 95% CL)</b>	<b>Average value of triplicate analysis ± Error (2 <math>\sigma</math>; 95% CL)</b>	<b>Average value of triplicate analysis ± Error (2 <math>\sigma</math>; 95% CL)</b>
<b>Thorium</b>	300.7 ± 18.7	2000 ± 50.1	200.2 ± 7.3
<b>Th-10U</b>	100.6 ± 12.2	2100 ± 42.7	300.6 ± 6.2
<b>Th-20U</b>	120.4 ± 13.8	2300 ± 39.4	300.1 ± 8.2
<b>Uranium</b>	1100 ± 35.8	110.4 ± 7.3	100.4 ± 5.3

Results obtained on thorium and uranium metals have also been shown for comparison. Based on weighted average rule **{impurity content in (1-x)Th-(x)U alloy = (impurity in Th) × (1-x) + (impurity in U) × (x); ‘x’ is given in wt.%}** and assuming no additional impurity uptake during alloy preparation and processing steps, expected C, O and N contents in Th-10U alloy are ~380 ppm, ~1810 ppm and ~190 ppm, respectively. Similarly, expected impurity contents in Th-20U alloy should be ~460 ppm, ~1620 ppm and ~180 ppm for C, O and N, respectively. As compared to these estimated values, experimental results (Table 4.1) show reduction in carbon content and increase in both, oxygen and nitrogen contents. Increment in oxygen content also increases with fraction of uranium in these alloys. Higher O and N contents in Th-10U and Th-20U alloys can be attributed to oxygen and nitrogen pickup during various metal handling, alloy melting and alloy processing stages, which is dominated by highly reactive uranium metal. It must be noted that in spite of extreme care taken while handling, cutting, surface cleaning of uranium metal, it shows surface tarnishing within short time span, which is indicative of its high reactivity with even traces of air / moisture. While relative increase in oxygen content of Th-10U and Th-20U alloys as compared to thorium metal is ~5% and ~15%, respectively, the absolute values are well within the tolerable limits of metals and alloys used for routine nuclear fuel fabrication. Increase in nitrogen content can also be attributed to strong affinity of both thorium and uranium towards nitrogen. Nitrogen can be picked up from (i) residual air left inside the glove box and argon gas (inside arc melting furnace) and / or (ii) degassing through sealed quartz tube during prolonged annealing (973 K; 220 h). It must be noted that overall weight change observed after arc-melting (alloys were weighed as such just after arc melting) was 0.007%, 0.002%, 0.008% and -0.009% for thorium, Th-10U, Th-20U and uranium metal, respectively. Weight reduction in case of uranium metal indicates net material loss in the form of carbon-species as well as uranium vapours.

In case of carbon, a notable reduction is observed in alloys as compared to values estimated from carbon content of constituent elements. It is known that higher carbon content in uranium metal produced by magnesiothermic reduction of  $UF_4$  originates from carbon pickup by molten uranium from graphite crucibles used for the reduction process [172]. Carbon in uranium / thorium may be present as free carbon (in non ionised elemental form) in the interstitial sites of metal crystals or in chemically bound state in the form of metal carbides (or oxy-carbides) [178], During arc melting, free carbon / carbide phases, which are usually lighter than molten metal/alloys (density values in  $kg.m^{-3}$ : carbon =  $\sim 2336$ ; UC =  $\sim 13630$ ; ThC =  $\sim 10600$ ; U =  $\sim 18950$ ; Th =  $\sim 11720$ ) may preferentially accumulate come over the surface of molten metal / alloy ingots. When these alloy ingots are surface cleaned, carbon / carbide layer over the surface may be removed, which lead to overall decrease in carbon content of alloys. In order to confirm this, one of the as-received uranium metal ingots was melted under identical conditions and its carbon contents were analyzed after two successive melting experiments. Carbon content was found to reduce from  $\sim 1100$  ppm in as received metal to  $\sim 940$  ppm and  $\sim 830$  ppm, which confirmed the observed trend of carbon content results for Th-U alloys and supported the explanation suggested for this reduction.

Fig. 4.1 shows a representative EDS curve recorded on surface cleaned Th-20U alloy surface. Electron micrograph over which the spectrum was recorded (back scattered electron image) is shown in the inset. It can be seen that no other major metallic impurity is detected in EDS analysis, which confirms adequate purity of alloys for further studies. Alloy composition obtained from EDS analysis (after eliminating oxygen and carbon elements from quantification) is (78 wt. % Th – 22 wt. % U), which is quite close to the nominal composition (80 wt. % Th – 20 wt. % U) taken for alloy preparation. Deviation in EDS evaluated composition could be attributed to error associated with EDS analysis (by

eliminating C and O) as well as calibration error in quantification using cobalt standard. EDS curve also confirms the presence of carbon and oxygen, although no attempt was made to quantify them from EDS results due to poor sensitivity of EDS detector for lighter elements ( $Z < 11$ ). Micrograph in inset of Fig. 4.1 shows distribution of dendritic precipitates of  $\text{ThO}_2$  phase in thorium matrix, which will be discussed later in this chapter.

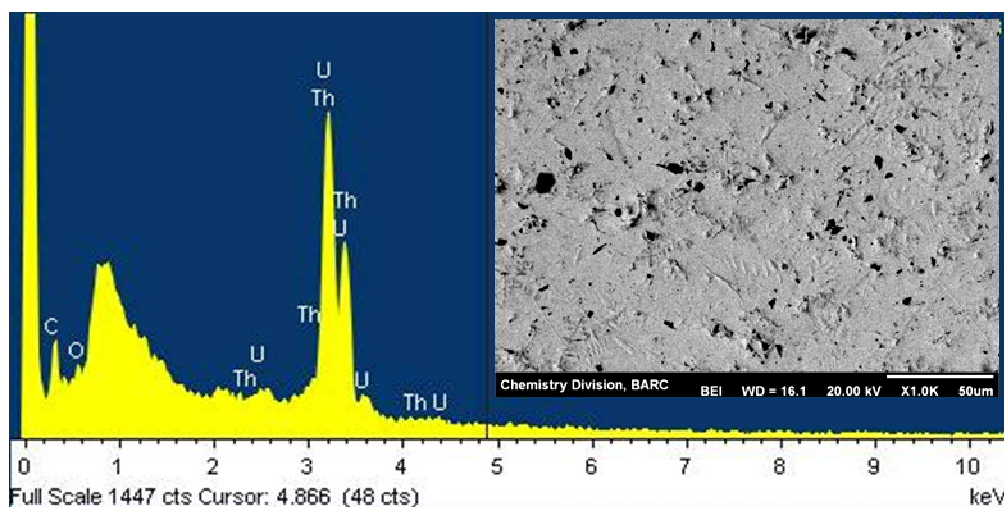


**Fig. 4.1. EDS curve recorded on surface cleaned Th-20U alloy. Inset shows the electron micrograph, over which EDS curve was recorded**

Above results indicate that while there are marginal variations in non-metallic impurity contents of alloys and their constituent metals, the overall quality of alloys is retained well for their utilization as nuclear fuel. Absence of any major metallic impurity, as indicated by EDS results also confirm good quality of studied alloy samples.

#### 4.3.2. Phase analysis of Th-10U and Th-20U alloys (XRD results)

Fig. 4.2 shows XRD patterns recorded on flat surface of polished metals (as-received U and Th) and alloy (vacuum annealed Th-10U, Th-20U) samples. Reported XRD peak positions for orthorhombic uranium [167] and FCC thorium [201] are also shown for comparison. It

can be seen from Fig. 4.2 that both alloys show diffraction peaks corresponding to constituent elements, which indicate the composite nature of these alloys. Equilibrium thorium-uranium binary phase diagram as-reported by Peterson [59] is shown in Fig. 4.3. Phase diagram indicates a binary system with no inter-metallic compound. Also, while thorium has marginal solubility in uranium (0.048 and  $\sim 0.29$  wt. % at 973 K and 1173 K, respectively), uranium is relatively more soluble in thorium (solubility:  $\sim 0.7$ ,  $\sim 1.1$ ,  $\sim 1.1$ ,  $\sim 1.8$  and  $\sim 2.7$  wt. % at 298 K, 873 K, 1073 K, 1273 K, and 1373 K, respectively) [59, 202]. Along with lower solubility of constituent elements in each other, phase diagram indicates a large miscibility gap, which contains two metals intimately mixed only at very high temperatures. Crystallization temperature of thorium-uranium binary alloys has also been reported in 973 K -1073 K range [69], based on which alloy samples were annealed at  $\sim 973$  K (220 h) in present studies.

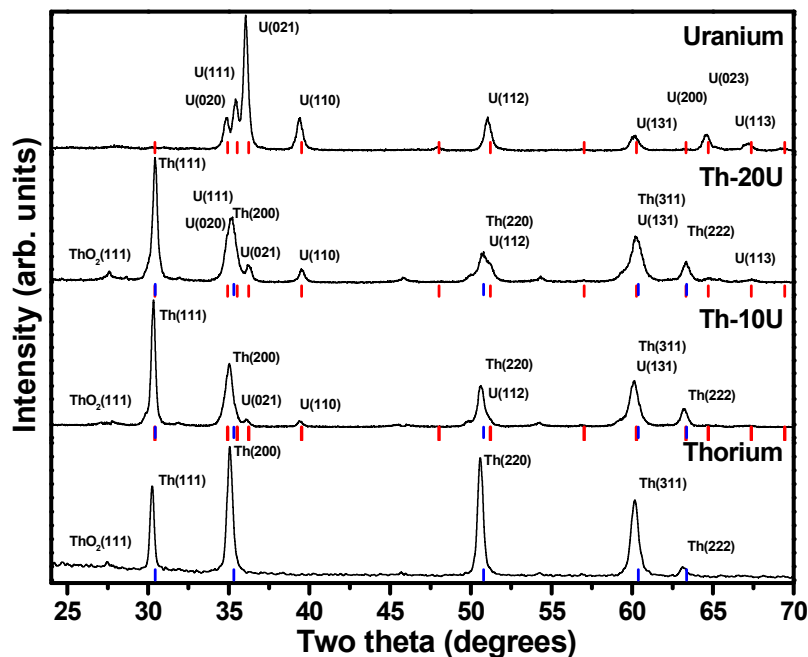
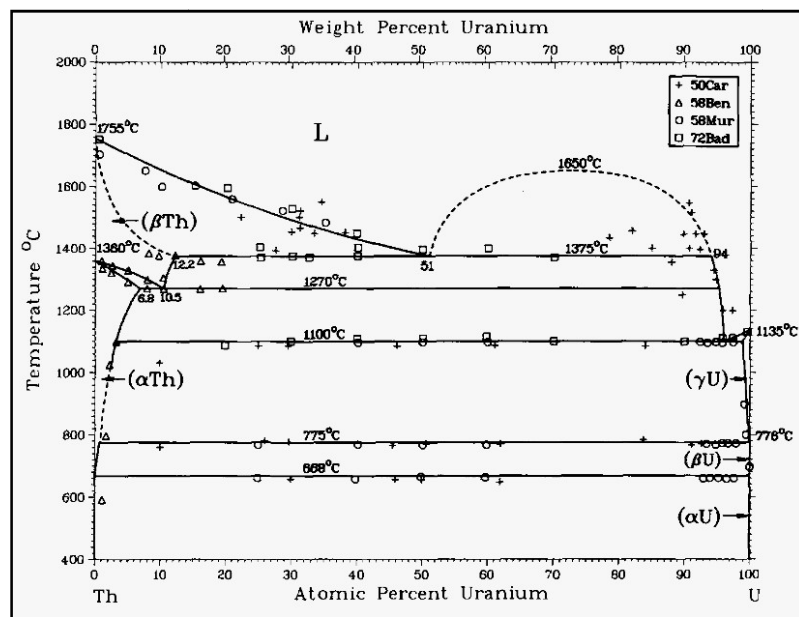


Fig. 4.2. XRD patterns recorded on thorium, uranium, Th-10U and Th-20 U alloy.

Black curves show the measured diffraction data. Red and blue lines show reported peak positions for orthorhombic uranium [167] and FCC thorium [201]

Both the alloys studied here (Th-10U, Th-20U) are in thorium-rich region of phase diagram. Based on the Th-U binary phase diagram [59] and thermal annealing history (~973 K, 220 h; cooled to 298 K at 1 K / min.), bi-phasic alloys consisting of thorium and uranium-rich phases with minimum solubility of the constituents are expected. XRD patterns of these alloys are likely to give reflections from the constituent metals without significant variation in peak positions. XRD patterns shown in Fig. 4.2 confirm the same.



**Fig. 4.3. Thorium-Uranium phase diagram [Bull. Alloy Phase Diagr. 6 (5) (1985) 443-445, © Springer; Reproduced with kind permission of Springer Science & Business Media; Licence number: 4897030537802]**

Peak position of principal reflection corresponding to (111) plane from FCC thorium lattice is observed at  $30.26^\circ$ ,  $30.32^\circ$  and  $30.42^\circ$  for thorium, Th-10U and Th-20U samples, respectively. Lattice parameters were evaluated from peak positions for cubic thorium ( $d_{(hkl)} = \lambda / (2 \sin\theta_{(hkl)})$ );  $a = \{(h^2 + k^2 + l^2) d^2\}^{1/2}$ , which were obtained as 5.1158(5) Å, 5.1043(2) Å and 5.0895(7) Å for thorium, Th-10U and Th-20U, respectively. Since uranium is relatively

more soluble in FCC thorium phase, its incorporation is likely to reduce the lattice parameter as atomic radius of uranium (~230 pm) is smaller than that of thorium (~240 pm). Similarly, peak position corresponding to the (110) plane for orthorhombic uranium lattice is observed at  $39.38^\circ$ ,  $39.40^\circ$  and  $39.44^\circ$  for uranium, Th-10U and Th-20U samples, respectively. Reflection from (110) plane was chosen for analysis of peak position of uranium lattice since it does not overlap with any of the thorium's XRD peaks. These results indicate marginal solid solubility of constituent elements into each other.. This is indeed observed in terms of shift of diffraction peak(s) towards higher angles for both Th-10U and Th-20U alloys. On the other hand, (110) reflection from uranium lattice remains nearly invariant for uranium and Th-U alloys. Broadening of XRD peaks is observed in both the alloys, which can be attributed to (i) overlapping of peaks due to thorium and uranium and (ii) relatively higher structural disorder in the alloy samples especially across the interface of uranium and thorium-rich phases. Peak intensities of thorium and uranium phase also show variation. In as-received thorium and uranium metals, reflections due to (200) and (021) planes show maximum intensities, respectively, which can be attributed to preferred orientation of grains in as-received metals based on their metallurgical history. Upon arc-melting, Th-U alloys solidify with random crystallization from molten phase and attain equilibrium crystallization during thermal annealing. As a result, both alloys show maximum intensities for Th (111) and U (111) reflections, which is expected for their crystalline phase with random orientation of grains. Fig. 4.2 also shows weak reflection due to  $\text{ThO}_2$  phase ( $2\theta \sim 27.56^\circ$ ), which can be attributed to higher oxygen impurity in thorium metal (~2000 ppm), Th-10U (~2100 ppm) and Th-20U (~2300 ppm) alloys. As explained earlier in chapter-3 (Sections 3.3.1. and 3.3.2.), oxygen reacts with thorium to give stable  $\text{ThO}_2$  phase. Quantitative estimation of  $\text{ThO}_2$  impurity phase in Th-U binary alloys has been reported by X-ray and neutron diffraction techniques [200]. XRD results confirm crystalline biphasic alloys (Th-10U, Th-

20U) consisting of thorium- and uranium-rich phases with random distribution of grains. Microstructures of these alloys were studied to obtain further information on phase distribution. These results are discussed now.

#### 4.3.3. Microstructural characterization (SEM studies)

Figure 4.4. shows back scattered electron (BSE) micrographs recorded on polished samples of (a) Th-10U alloy, (b) Th-20U alloy, (c) thorium metal and (d) uranium metal. Both constituent metals appear featureless except polishing marks seen in the micrographs (Fig. 4.4 (c), 4.4 (d)). A few dark spots seen over the surface of both thorium and uranium metal are either due to pits created during grinding / polishing over with coarse SiC abrasive paper (400 grit size) or due to impurity phases (predominantly  $\text{ThO}_2$  in thorium metal and carbon in uranium metal). EDS analysis over the metal surfaces indeed confirmed the presence of carbon and oxygen impurities (chapter-3; Fig. 3.2). Grain structure is not revealed since polished surfaces of as-received metals were not subjected to any surface etching treatment.

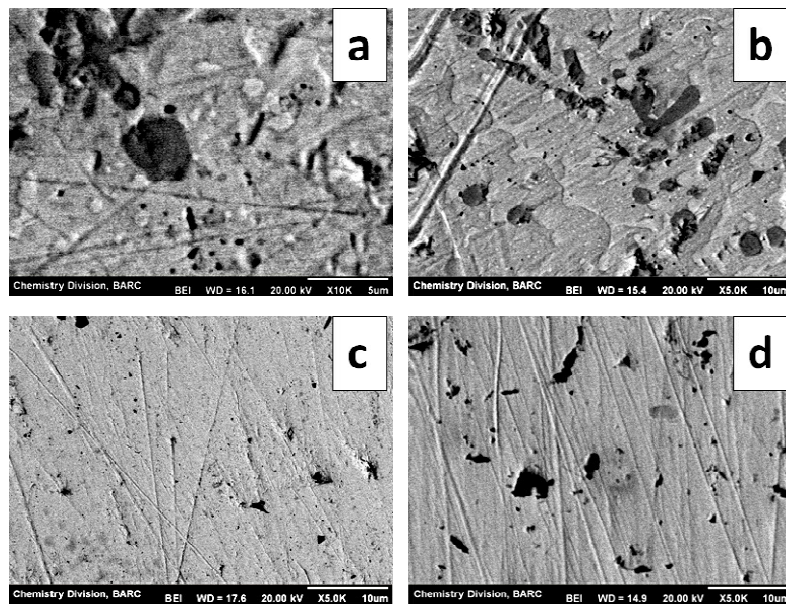


**Fig. 4.4. Back scattered electron (BSE) micrographs of (a) Th-10U alloy, (b) Th-20U alloy (c) thorium metal and (d) uranium metal**

BSE micrograph of Th-10U (Fig. 4a) alloy shows uniformly distributed bright inclusions in the base alloy matrix apart from few dark spots. The bright spots (sub-micron to micron sized) were identified to be uranium particles by EDS analysis. Th-10U alloy therefore behaves as dispersion alloy with uranium precipitates uniformly distributed in the base thorium matrix. Such an alloy microstructure is ideal for optimum utilization of (i) superior mechanical and thermal properties of fertile thorium matrix and (ii) fissile properties of uranium fuel phase in such a way that excessive anisotropic swelling of uranium does not affect the structural integrity of dispersion fuel. Few dark spots seen in micrograph of Th-10U alloy (Fig. 4.4 (a)) are due to  $\text{ThO}_2$  impurity phase from thorium metal, which was confirmed by EDS analysis. In case of Th-20U alloy, the uranium-rich (brighter phase) phase can be seen spread across the grain boundary regions in the bulk thorium matrix (although not well resolved in image recorded on non-etched samples). Similar microstructures with uranium in grain boundary regions of Th-U binary alloys with uranium content exceeding 15 wt. % have been reported by Hammond [95].  $\text{ThO}_2$  phase is also seen in Th-20U alloys in the form of dendrite-like inclusions (see also inset of Fig. 4.1). Similar dendritic  $\text{ThO}_2$  inclusions have been reported by Bannister et al., [203] in arc-melted thorium metal. Uranium concentration at the grain boundaries region is less preferred from the perspective of irradiation performance of dispersion fuels wherein it is desired to have fuel microstructure consisting of uniformly dispersed uranium precipitates in thorium matrix. Microstructure observed in Th-20U alloy may affect the structural integrity of fuel due to uranium's swelling behavior. An upper bound of 20 wt. % U in Th-U binary alloy fuels for fast reactors has also been reported [69]. As indicated by XRD results, microstructures of Th-10U and Th-20U alloys further confirm their biphasic nature with uranium phase distributed in the thorium matrix. Information on thermophysical properties of these alloys will be needed for

assessment of their performance as nuclear fuel. Results of their thermophysical characterization are detailed now.

#### 4.3.4. Thermal diffusivity of Th-U binary alloys

Temperature dependence of thermal diffusivity of phase equilibrated Th-10U and Th-20U alloys (wt. %) is shown in Fig. 4.5. For comparison, thermal diffusivity of thorium and uranium metals is also plotted along. It can be seen that thermal diffusivity of both alloys is significantly lower than that of thorium metal. For example, ambient temperature thermal diffusivity of Th-10U ( $\sim 0.23 \text{ cm}^2 \cdot \text{s}^{-1}$ ) and Th-20U alloy ( $\sim 0.218 \text{ cm}^2 \cdot \text{s}^{-1}$ ) drops by  $\sim 37\%$  and  $\sim 40\%$ , respectively as compared to that of thorium ( $\sim 0.364 \text{ cm}^2 \cdot \text{s}^{-1}$ ). At the same time, it is notably higher (by  $\sim 110\%$  for Th-10U and  $\sim 98\%$  for Th-20U) as compared to ambient temperature thermal diffusivity of uranium ( $\sim 0.11 \text{ cm}^2 \cdot \text{s}^{-1}$ ).

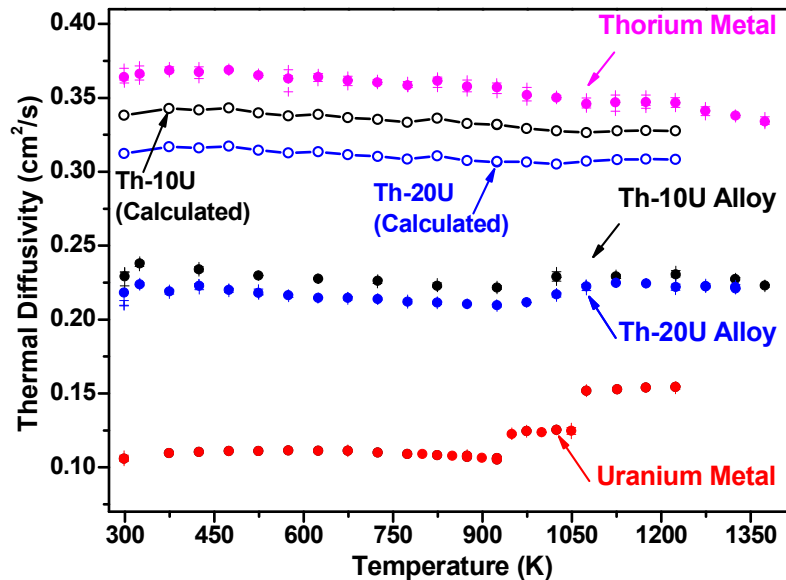


Fig. 4.5. Thermal diffusivities of Th-10U, Th-20U alloys and constituent metals as a function of temperature. Filled circles represent the average value of multiple laser shots while plus symbols show individual data points. Thermal diffusivities of both alloys calculated from weighted average rule are also plotted (open circle symbols)

These results indicate the superior heat transport behavior of thorium-based alloys over uranium-based metallic alloy nuclear fuels such as U-Zr binary alloys or U-Pu-Zr ternary alloys. Thermal diffusivity (**D**) of Th-U binary composite alloys, which consist of randomly distributed uranium and thorium phases, was also estimated from the weighted average rule using the experimentally measured diffusivities of constituent metals as follows:

$$\mathbf{D-calc}_{(Th-10U)} = \mathbf{0.9 \times D-experimental}_{(Th)} + \mathbf{0.1 \times D-experimental}_{(U)} \quad (4.1)$$

$$\mathbf{D-calc}_{(Th-20U)} = \mathbf{0.8 \times D-experimental}_{(Th)} + \mathbf{0.2 \times D-experimental}_{(U)} \quad (4.2)$$

Thermal diffusivities of Th-10U and Th-20U alloys, as estimated from equation-4.1 and equation-4.2 are also plotted in Fig. 4.5. These values are significantly overestimated as compared to the experimental thermal diffusivities data for Th-10U and Th-20U alloys. Experimental thermal diffusivities are notably lower than those calculated using weighted average rule (equation-4.1 and equation-4.2). This difference can be attributed to combined effect of (i) partial solubility of uranium in thorium matrix, (ii) alloy microstructure consisting of randomly distributed uranium and thorium-rich phases, (iii) structural disorder at the interface regions between thorium- and uranium-rich phases and, (iv) additional non-metallic impurities included in these alloys during alloy preparation and processing, as compared to constituent elements. All these factors contribute to scattering of heat carriers (predominantly electrons in case of metals and alloys) and result into lower thermal diffusivities. Extended phase equilibration at higher temperatures (up to 1273 K) may improve the crystallization and minimize the structural disorder at the phase boundaries in these alloys, which would result into higher thermal diffusivity values as compared to those obtained in studied samples. It would therefore be interesting to study the effect of different heat treatment conditions on thermal diffusivity of Th-U binary alloys.

Fig. 4.5 also indicates that Th-10U alloy has higher thermal diffusivity as compared to Th-20U alloys at lower temperatures ( $T < 1000$  K). However, at higher temperatures ( $T > 1000$  K), both alloys have similar diffusivities, which can be attributed to higher diffusivity of high temperature cubic (BCC) allotrope of uranium in Th-20U alloy. Effect of the allotropic phase transformation of uranium is apparent in thermal diffusivity curve of Th-20U alloy in terms of increasing thermal diffusivity values above 1000 K. These results suggest that for metallic nuclear fuels, which are preferred to operate in the stability region of gamma phase (BCC) of uranium ( $T \geq 1050$  K), both Th-10U and Th-20U alloys have comparable heat transport behavior. Analysis of sample weight after each thermal diffusivity experiment indicated marginal weight gain ( $< 0.003$  wt. %), which occurred primarily due to surface oxidation during high temperature measurements. Repeated measurements on same samples after re-polishing the alloy surface confirmed the reproducibility of results. Close match of diffusivity values measured during individual laser shots (shown by plus symbols in Fig. 4.5) also confirm the reliability of results presented here. These results have been used for evaluation of thermal conductivity.

#### 4.3.5. Bulk thermal expansion of Th-U binary alloys

Fig. 4.6 shows the linear thermal expansion behavior of Th-10U and Th-20U alloys (wt. %) as a function of temperature; measured by dilatometry. Experimental thermal expansion behavior of thorium and uranium metal is also plotted for comparison. Thermal expansion of these composite alloys was estimated using the weighted average rule (equation-4.3 and equation-4.4). These results are also shown in Fig. 4.6. Average coefficients of linear thermal expansion (CTE) were evaluated from experimental dilation data using equation-4.5 and their values are given in Table 4.2.

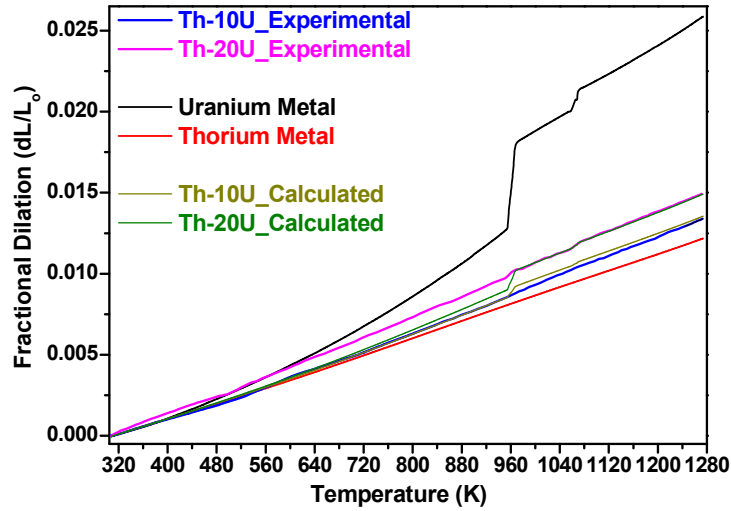


**Fig. 4.6. Linear dilatation of Th-10U alloy, Th-20U alloy, thorium and uranium as a function of temperature. Dilatation estimated from weighted average rule is also shown**

$$dL/L_0(\text{Th-10U}) = 0.9 \times dL/L_0(\text{Th}) + 0.1 \times dL/L_0(\text{U}) \quad (4.3)$$

$$dL/L_0(\text{Th-20U}) = 0.8 \times dL/L_0(\text{Th}) + 0.2 \times dL/L_0(\text{U}) \quad (4.4)$$

$$\text{CTE (between } T_1 \text{ and } T_2) = (1/L_0) \times (\Delta L/\Delta T) \quad (4.5)$$

Here  $\Delta L = (L_{T_2} - L_{T_1})$ ;  $\Delta T = (T_2 - T_1)$ ;  $T_2 > T_1$

**Table 4.2. Average coefficient of linear thermal expansion (CTE) for Th-10U, Th-20U binary alloys and constituent metals (Th and U) in different temperature intervals**

Sample	CTE	CTE	CTE	CTE
	(310 – 950 K) ( $\times 10^6 \text{ K}^{-1}$ )	(975 – 1050 K) ( $\times 10^6 \text{ K}^{-1}$ )	(1075 – 1273 K) ( $\times 10^6 \text{ K}^{-1}$ )	(310 – 1273 K) ( $\times 10^6 \text{ K}^{-1}$ )
<b>Thorium</b>	12.54	12.89	12.87	12.65
<b>Th-10U</b>	13.26	15.81	14.64	13.91
<b>Th-20U</b>	15.08	14.96	14.99	15.49
<b>Uranium</b>	19.71	22.23	22.30	26.84

Results shown in Fig. 4.6 indicate that both, Th-10U and Th-20U alloys show thermal expansion behavior similar to thorium metal. While extent of thermal expansion increases with increasing uranium content, it remains close to the expansion behavior of thorium. Unlike uranium metal, which show sharp expansion anomalies at  $\sim 948$  K and  $\sim 1051$  K, respectively corresponding to  $\alpha$  to  $\beta$  (orthorhombic  $\rightarrow$  tetragonal) and  $\beta$  to  $\gamma$  (tetragonal  $\rightarrow$  BCC) allotropic phase transitions, Th-10U alloy does not show any expansion anomaly. For Th-20U alloy, a marginal upward shift in expansion curve is observed ( $\sim 950$  K) (upon close inspection) corresponding to orthorhombic to tetragonal ( $\alpha \rightarrow \beta$ ) phase transformation of uranium. Uniform expansion behavior of studied alloys without sharp expansion anomalies can be attributed to their microstructures consisting of uranium phase dispersed in thorium matrix. Due to lower density of thorium ( $\sim 11.4 \text{ g.cm}^{-3}$  at  $\sim 298$  K) as compared to uranium ( $\sim 18.9 \text{ g.cm}^{-3}$  at  $\sim 298$  K), and also lower thermal expansivity of thorium ( $\text{CTE} = 12.5 \times 10^{-6} / \text{K}$ ;  $298 \text{ K} - 950 \text{ K}$ ) than that of uranium ( $\text{CTE} = 19.7 \times 10^{-6} / \text{K}$ ;  $298 \text{ K} - 950 \text{ K}$ ), the anisotropic expansion occurring in dispersed uranium phase is masked by thorium matrix in measured dilation curves. This is yet another very significant advantage of thorium-based dispersion-type metallic alloy fuels, in which anisotropic expansion as well as higher expansion-driven swelling of fissile uranium phase does not affect fuel's overall structural integrity. Similar behavior is also expected for dispersion-type Th-Pu binary alloy fuels.

While thermal diffusivities of Th-10U and Th-20U alloys estimated using weighted average rule were largely overestimated from the experimental results (Fig. 4.5), a good correlation with experimental thermal expansion behavior is observed for expansivity values estimated from weighted average rule, as shown in Fig. 4.6. Estimated expansion behavior of Th-10U alloy calculated using equation-4.3 matches fairly well with experimental results over the studied temperature range. Results for Th-20U alloy (obtained from equation-4.4) show

slightly underestimated values over the temperature range of stability for alpha uranium (298 K – 950 K). Estimated and experimental expansion curves for Th-20U match well in high temperature region (950 K – 1373 K). Relatively higher expansion observed in experimental curve of Th-20U alloy could be due to the presence of uranium phase near the grain boundary regions of thorium matrix (Fig. 4.4 (b)), which cause incomplete masking of higher expansion of uranium metal so that it is reflected in measured dilation curve. Close match between estimated and experiment dilation curve of Th-10U alloy can be attributed to dispersion of uranium phase in the forms of small isolated particles in thorium matrix, which results into better masking of uranium's expansion behavior. Expansion anomalies shown in estimated dilation curves do not appear in experimental data for both the alloys.

The reason, for which thermal diffusivity values estimated from weighted average rule for composite binary alloys (Th-10U, Th-20U) do not match with experimental results while a close match is observed for estimated and experimental thermal expansion values, lies in the nature of these two properties and their measurement techniques. Thermal expansion is an equilibrium thermophysical property, which results from an average thermo-mechanical response of a given material subjected to programmed temperature variation. For composite alloys in which the constituent elements have marginal solubility into each other, thermal expansion is affected only to a small extent by the structural disorder at the phase boundaries. It is also not likely to be influenced significantly by marginal increase in non-metallic impurity contents, which get randomly distributed over the alloy phase. Therefore, total expansion of composite alloy with random distribution of constituent phases is likely to be close to the weighted sum of the expansion of individual components consisting of randomly oriented grains. On the other hand, thermal diffusivity is a transient thermophysical property related to flow of heat energy through the material via different heat carriers (electrons,

phonons, excitons, etc.). Factors such as impurities, structural disorder at phase boundaries, solid solubility of constituents even at marginal concentrations, and microstructural variations effectively scatter these heat carriers and therefore significantly decrease the thermal diffusivity of composite alloys. As stated earlier, extended heat treatment at the highest permissible temperatures (under inert atmosphere) followed by slow cooling can minimize the structural disorder in a material, both inside the grains as well as grain (phase) boundary interface regions, which in turn can improve the thermal diffusivity of such alloys.

Assuming that the thermal expansion results shown in Fig. 4.6 are representative of completely randomized, polycrystalline Th-10U and Th-20U alloys, their temperature dependent bulk densities were calculated in a similar manner as detailed in chapter-3 (Section 3.3.5) using equation-4.6.

$$\rho(T) = M_T/V_T \quad (4.6)$$

Here, 'M<sub>T</sub>' is sample mass and 'V<sub>T</sub>' is sample volume at temperature 'T'. 'V<sub>T</sub>' is given as

$$V_T = V_{298\text{ K}} [1 + 3\{(L_T - L_{298\text{ K}})/L_{298\text{ K}}\}] \quad (4.7)$$

Where, V<sub>298 K</sub>, L<sub>T</sub>, L<sub>298 K</sub> are sample volume at 298 K, Sample length at temperature 'T' and sample length at 298 K, respectively. Fig. 4.7 shows temperature dependence of density for both alloys (Th-10U, Th-20U) along with that of thorium and uranium for comparison.

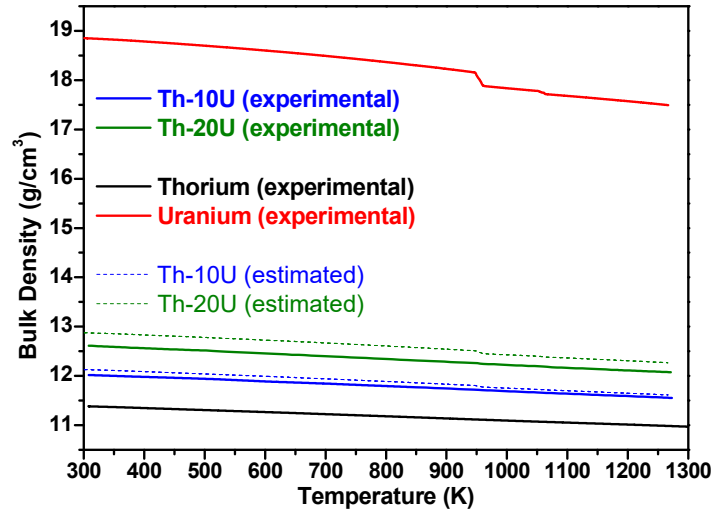


**Fig. 4.7. Temperature dependent bulk density of Th-10U and Th-20U alloys (wt. %) in comparison to that of thorium and uranium metals. Alloy densities estimated from weighted average rule are also shown**

Density ( $\rho$ ) results show that density of alloys increases with increasing uranium fraction. Also, densities are continuously varying function of temperature without any anomaly. Lower densities of Th-U binary alloys as compared to uranium-based alloy fuels (U-Zr, U-Pu-Zr) are advantage in terms of higher space available for fission product accommodation, which helps in lower fuel swelling behavior during neutron irradiation. Low density thorium matrix also serves as buffer space for anisotropic expansion of uranium phase dispersed in the thorium matrix. Densities estimated from weighted average rule  $\{\rho_{(1-x)\text{Th-(x)U alloy}} = (1-x)\cdot\rho_{\text{Th}} + (x)\cdot\rho_{\text{U}}$ ; 'x' is given in wt.%} for these composite alloys show a very good match with density obtained from dilation data (within  $\sim 0.6\%$ ) for Th-10U alloy. For Th-20U alloy, estimated density values are higher (by  $\sim 2\%$ ) than those obtained from dilation data. Lower actual densities of alloys can be attributed to additional non-metallic impurities, structural disorder; particularly at grain / phase boundary regions and, deviation from equilibrium microstructure. These density values were used for thermal conductivity evaluation.

#### 4.3.6. Specific heat of Th-U binary alloys

Figure 4.8 shows temperature dependent isobaric heat capacities ( $C_p$ ) of Th-10U and Th-20U (wt. %) alloys, thorium and uranium metals measured by temperature modulated DSC (298 K to 773 K). Reported  $C_p$  values for thorium and uranium metals are also shown [157, 175, 194]. Effect of allotropic phase transitions of uranium on its  $C_p$  data can also be noted. Literature data on thorium and uranium metals were selected based on close match between impurity contents of samples used for reported data with that of the samples used in present investigation, as detailed in chapter-3 (Section 3.3.6.). It can be seen that our results on uranium and thorium are slightly overestimated as compared to reported values, which is mainly due to higher non-metallic impurity contents and relatively poor control of atmosphere during DSC experiments, which was revealed by  $\sim 3\%$  increase in sample weight after each DSC runs. Similar weight gain was also observed for Th-10U and Th-20U alloys during DSC experiments. Direct comparison of specific heat of alloys could not be done due to non-availability of reported  $C_p$  data except that of Th-10U alloy at 298 K ( $0.1176 \text{ J.g}^{-1}\text{K}^{-1}$ ) reported by Fink et al. [96], which matched well with present results. However, based on the results obtained on thorium and uranium metals, and additional non-metallic impurities present in studied alloys (see Table 4.1), it was reasonable to assume that measured  $C_p$  data of Th-10U and Th-20U alloys are also on higher side. Since calculation of thermal conductivity involves multiplication of specific heat ( $C_p$ ) with thermal diffusivity and density, any overestimation of  $C_p$  data could lead to undesirable overestimation of thermal conductivity. Also measured  $C_p$  data is limited to 773 K due to high temperature limitation of TMDSC technique. Therefore, in order to obtain a reliable lower bound of thermal conductivity values for Th-U binary alloys, it is more appropriate to use reported  $C_p$  values, which are also available over a wide temperature range (298 K to 1373 K). Further, since specific heat is an equilibrium thermodynamic property, for composite-type Th-U binary

alloys, it can be reasonably estimated from the  $C_p$  values of constituent metals (Th and U) using the weighted average rule  $\{C_p (1-x)\text{Th}-x\text{U alloy} = (1-x).C_p(\text{Th}) + x.C_p(\text{U})\}$ . Fig. 4.8 shows the  $C_p$  values obtained from the weighted average rule. As these values are lower than experimental  $C_p$  values obtained from TMDSC data, they can be used for evaluation of the lower bound of thermal conductivity of Th-U binary alloys.

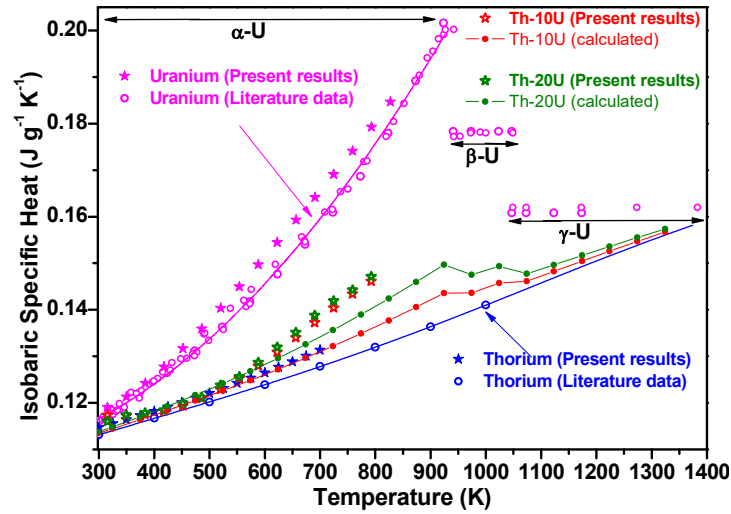


Fig. 4.8. Specific heat ( $C_p$ ) of Th-10U, Th-20U alloys, thorium and uranium metals.

Reported  $C_p$  data on thorium and uranium are also plotted.  $C_p$  of alloys estimated from weighted average rule using reported  $C_p$  of constituent metals is also shown

#### 4.3.7. Thermal conductivity of Th-U binary alloys

Thermal conductivity ' $\lambda(T)$ ' of Th-10U and Th-20U alloys was calculated using equation-4.8.

$$\lambda(T) = D(T) \times \rho(T) \times C_p(T) \quad (4.8)$$

Here ' $D(T)$ ', ' $\rho(T)$ ' and ' $C_p(T)$ ' are experimental thermal diffusivity, density derived from linear thermal expansion data and specific heat evaluated from weighted average values of

reported  $C_p$  of constituent metals, respectively. Fig. 4.9 shows the variation of thermal conductivity of studied alloys as a function of temperature. For comparison, thermal conductivity of thorium and uranium metals, which were used for preparation of these alloys, and reported thermal conductivities of two binary alloys in U-Zr system namely U-14Zr [155] and U-11.4Zr [204], are also plotted in Fig. 4.9.

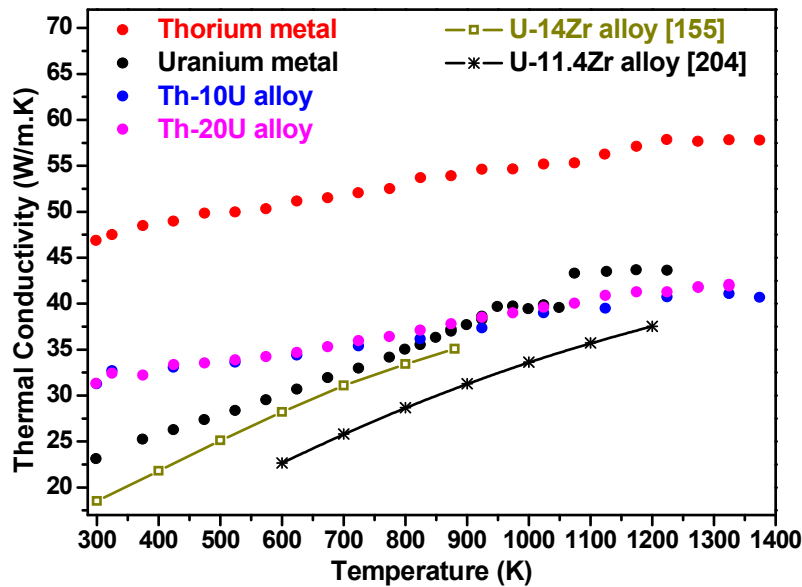


**Fig. 4.9. Thermal conductivity of Th-10U, Th-20U (wt. %) alloys as a function of temperature. Thermal conductivities of thorium and uranium metals (from chapter-3) and reported data on U-14 wt. % Zr alloy [155] and U-11.4 wt. % Zr alloy [204] are also shown for comparison**

At ambient temperature, thermal conductivity of both Th-10U ( $\sim 31.2 \text{ W.m}^{-1}.\text{K}^{-1}$ ) and Th-20U ( $\sim 31.3 \text{ W.m}^{-1}.\text{K}^{-1}$ ) alloys is higher than that of uranium ( $\sim 23.1 \text{ W.m}^{-1}.\text{K}^{-1}$ ). Thermal conductivity of studied alloys is significantly lower than thorium metal ( $\sim 48.2 \text{ W.m}^{-1}.\text{K}^{-1}$ ). Alloys' thermal conductivity variation with temperature do not show any noticeable anomaly at temperatures corresponding to uranium's allotropic phase transitions, which can be attributed to the dispersion-type alloy microstructure. Thermal conductivity of both, Th-10U

and Th-20U alloys is notably higher than that of (i) U-14Zr (Wt.%) binary alloy (by  $\sim 71\%$  at 298 K and,  $\sim 10\%$  at 900 K) [155], (ii) U-11.4wt.% Zr alloy (by  $\sim 53\%$  at 600 K and,  $\sim 11\%$  at 1200 K) [204] and (iii) U-18.4Pu-11.5Zr alloy (wt. %) (by  $\sim 240\%$  at 373 K and,  $\sim 60\%$  at 1200 K) [205], which are uranium-based fast breeder reactors fuel options. The difference in thermal conductivity values becomes smaller at higher temperatures mainly because, uranium-based alloys (U-Zr, U-Pu-Zr) attain isotropic cubic phase at higher temperatures ( $> 900$  K), which has higher thermal conductivity than ambient temperature anisotropic composite phase. On the other hand, Th-U binary alloys remain in composites form up to very high temperatures ( $> 1373$  K) so that scattering of heat carriers by phase boundaries scattering is still dominant. Similar to thorium and uranium, thermal conductivity of Th-U binary alloys continuously increases with temperature. While there is notable difference in thermal diffusivity, density and specific heat of Th-10U and Th-20U alloys, their thermal conductivities are only marginally different, as seen in Fig. 4.9. This is due to the mutually opposite effect of increase in specific heat and density, and decrease in thermal diffusivity of Th-U alloys with increasing uranium concentration. Interestingly, at higher temperatures ( $T > 1050$  K), thermal conductivity of uranium metal exceeds than that of both, Th-10U and Th-20U alloys. At higher temperatures, structural disorder in these alloys across the phase boundary regions reduces (thermal annealing effect), which is likely to improve the heat transport. At the same time, solubility of uranium in thorium increases with increasing temperatures, although both the alloys still remain grossly biphasic in nature [178]. Solubility of uranium in thorium (as well as thorium in uranium) is also likely to impede the heat transfer in resulting FCC thorium solid solution (and BCC uranium solid solution) as compared to pure metals. High temperature also brings about additional scattering of heat carriers (predominantly electrons) by lattice vibrations. The thermal conductivity of alloys is therefore a net outcome of these competing processes. For uranium on the other hand, the

metal transforms from anisotropic tetragonal phase to low density isotropic BCC phase ( $\sim 1048$  K), which greatly facilitates the transport of heat. Apart from transition of a high symmetry phase, low melting uranium metal (melting temperature  $\sim 1404$  K) also undergoes extensive grain growth and rapid minimization of inter-grain structural disorder at these temperatures ( $T > 1050$  K). On the other hand, due to higher melting temperature of thorium ( $\sim 2023$  K), grain growth is relatively slower in alloy matrices at similar temperatures ( $\sim 1050$  K). It is also reported that re-crystallization temperature of thorium increases by  $\sim 100$  K in presence of uranium [201]. As a result, thermal conductivity of uranium metal is higher than Th-10U and Th-20U alloys in high temperature regions. For further understanding of heat transport properties of Th-U binary alloy fuels, it will be useful to anneal these alloys at further higher temperatures (up to  $\sim 1350$  K) for long durations and study the improvement in their thermal conductivity, if any.

#### 4.4. Conclusions

In the present studies, thermophysical properties of Th-U binary alloys as a function of temperature are studied in detail. Results presented in this chapter are useful in terms of detailed experimental thermophysical characterization of Th-10U and Th-20U (wt. %) binary metallic alloys over a wide range of temperature (298 K – 1373 K). Superior thermophysical behavior of Th-U binary alloys in terms of lower specific heat (low stored energy), lower density (high fission product retention capacity) and higher thermal conductivity (safe and efficient fuel performance) over uranium-based alloys (U-Zr, U-Pu-Zr) has been established. These studies would serve as reference for optimization of alloy composition for metallic nuclear fuel fabrication. Thermophysical properties of these alloys can be further improved by varying the preparation methods, using high purity starting materials (thorium and uranium), and microstructural variations brought about by thermal treatment conditions.

Thermal conductivity results, which have been evaluated using experimental thermal diffusivities and densities along with reported specific heat data, can be reliably taken as a lower bound for these alloys within  $\pm 5\%$ . An important requirement for the future development of these alloy fuels, in terms of thermophysical assessment, is the evaluation of accurate values of specific heats of these binary alloys over a wide temperature range, preferably by high temperature Calvet calorimetry (drop calorimetry), so that upper bound of thermal conductivities of these binary alloys can be obtained.

Uranium-based metallic alloy fuels for fast reactors are taken in the form of U-Zr binary or U-Pu-Zr ternary alloys. Zirconium is added to increase in the solidus temperature of these alloys as well as improve the resistance towards fuel-clad interaction. Addition of zirconium in thorium-based alloys is also envisaged to improve fuel-clad interaction resistance. Th-U-Zr ternary alloys are also considered as potential fuels for thermal neutron spectrum reactors. Addition of zirconium is known to enhance the resistance towards high temperature corrosion with water / steam. Th-U-Zr or Th-Pu-Zr ternary alloys in the form of dispersion fuel can also be used in research reactors. Development of these fuels would also require information on their thermophysical behavior. With this objective, two ternary alloy compositions have been investigated and results obtained are discussed in next chapter (chapter-5).

## References:

- [1] C. Degueudre, M.J. Joyce, “Evidence and uncertainty for uranium and thorium abundance: a review”, *Prog. Nucl. Energy* 124 (2020) 103299.
- [2] L.S. Keith, O.M. Faroon, B.A. Fowler, “Uranium (book chapter); handbook on the toxicology of metals: fourth edition (Eds: G.F. Nordberg, B.A. Fowler, M. Nordberg)”, Elsevier (2015) 1307-1345 (DOI: <https://doi.org/10.1016/C2011-0-07884-5>).
- [3] G. Sadagopan, K.S.V. Nambi, G. Venkataraman, V.K. Shukla, S. Kayasth, “Estimation of thorium in gas mantles to ascertain regulatory compliance”, *Radiat. Prot. Dosim.* 71(1) (1997) 53-56.
- [4] T.E. Leontis, “Properties of magnesium-thorium and magnesium-thorium-cerium alloys”, *J. Min. Metals Mater. Soc.* 4 (3) (1952) 287-294.
- [5] R.A. Glenner, P. Willey, P.S. Sledzik, E.P. Junger, “Dental fillings in civil war skulls: What do they tell us?”, *J. Am. Dent. Assoc.* 127(11) (1996) 1671-1677.
- [6] O. Hahn, F. Strassmann, “Über den nachweis und das verhalten der bei der bestrahlung des urans mittels neutronen entstehenden erdalkalimetalle (English translation: Concerning the existence of alkaline earth metals resulting from neutron irradiation of uranium)”, *Die Naturwissenschaften* 27 (1939) 11-15.
- [7] “The first reactor” The US department of energy report: DOE/NE-0046 (1982) 1-40 (Web-link: <https://www.energy.gov/ne/downloads/first-reactor>).
- [8] R.L. Crowther, “Use of thorium in boiling water reactors”, *J. Nucl. Energy AB* 16(4) (1962) 181-194.
- [9] J.R. Dietrich, “The physics of advanced reactors”, *Brit. J. Appl. Phys.* 7(S5) 302 (1956) S9-S23.
- [10] H.N. Sethna, “India’s atomic energy program: past and future”, *International Atomic Energy Agency (IAEA) Bulletin* 21 (5) (1979) 2-11.

## References

- [11] S. Banerjee, H.P. Gupta, “The evolution of the Indian nuclear power programme”, Prog. Nucl. Energy 101 (2017) 4-18.
- [12] International Atomic Energy Agency “Thorium fuel cycles - potential benefits and challenges”, IAEA-TECDOC-1450, IAEA, Vienna (2005) 1-105.
- [13] P.K. Wattal, “Back end of Indian nuclear fuel cycle - A road to sustainability”, Prog. Nucl. Energy 101 (2017) 133-145.
- [14] R. Natarajan, “Reprocessing of spent nuclear fuel in India: Present challenges and future programme”, Prog. Nucl. Energy 101 (2017) 118-132.
- [15] S.A. Ansari, P. Pathak, P.K. Mohapatra, V.K. Manchanda, “Aqueous partitioning of minor actinides by different processes” Sep. Purif. Rev. 40(1) (2011) 43-76.
- [16] M. Salvatores, “Nuclear fuel cycle strategies including partitioning and transmutation”, Nucl. Eng. Des. 235(7) (2005) 805-816.
- [17] Press Information Bureau, Government of India, “Setting up of ten indigenous nuclear power reactors” (Web-link: <http://pib.nic.in>)
- [18] S.C. Chetal, P. Chellapandi, P. Puthiyavinayagam, S. Raghupathy, V. Balasubramanian, P. Selvaraj, P. Mohanakrishnan, B. Raj, “Current status of fast reactors and future plans in India” Energy. Proced. 7 (2011) 64-73.
- [19] P. Puthiyavinayagam, P. Selvaraj, V. Balasubramanian, S. Raghupathy, K. Velusamy, K. Devan, B.K. Nashine, G.P. Kumar, K.V.S. Kumar, S. Varatharajan, P. Mohanakrishnan, G. Srinivasan, A.K. Bhaduri, “Development of fast breeder reactor technology in India”, Prog. Nucl. Energy 101 (Part A) (2017) 19-42.
- [20] Bharatiya Nabhikiya Vidyut Nigam Limited, Department of Atomic Energy “Present status of 500 MWe Prototype Fast Breeder Reactor (PFBR)”, (Web-link: <http://www.bhavini.nic.in>).

## References

- [21] P. Rodriguez, C.V. Sundaram, "Nuclear and materials aspects of the thorium fuel cycle", *J. Nucl. Mater.* 100 (1981) 227-249.
- [22] R. Ramanna, S.M. Lee, "The thorium cycle for fast breeder reactors", *Pramana* 27(1-2) (1986) 129-137.
- [23] R. Chidambaram, C. Ganguly, "Plutonium and thorium in the Indian nuclear programme", *Curr. Sci. India* 70(1) (1996) 21-35.
- [24] P.K. Vijayan, V. Shivakumar, S. Basu, R.K. Sinha, "Role of thorium in the Indian nuclear power programme", *Prog. Nucl. Energy* 101 (2017) 43-52.
- [25] "Thoria-based nuclear fuels: thermophysical and thermodynamic properties, fabrication, reprocessing, and waste management", (Eds.: D. Das, S.R. Bharadwaj) Springer (2013) (DOI: 10.1007/978-1-4471-5589-8).
- [26] "Thorium-energy for the future", (Eds.: A.K. Nayak, B.R. Sehgal), Springer (2019) (DOI: 10.1007/978-981-13-2658-5).
- [27] S. Mukherji, B.K. Mohan, P.D. Krishnani, V. Jagannathan, S. Ganesan, "Thorium irradiation in Indian PHWRs - applications and limitations of origin code", *Proceedings of First National Conference in Nuclear Reactor Technology* (2002) (Web-link: [https://inis.iaea.org/search/search.aspx?orig\\_q=RN:34011468](https://inis.iaea.org/search/search.aspx?orig_q=RN:34011468)).
- [28] M. Das, "Design and irradiated experience with thorium based fuels in PHWRs" *Annual International Conference - Canadian Nuclear Association* (1992) 10.1-10.
- [29] P.S. Dharmi, J.S. Yadav, K. Agarwal, "Power reactor thoria reprocessing facility (PRTRF), Trombay", *Proceedings of the Theme Meeting on the Journey of BARC Safety Council for Strengthening Safety Culture in BARC Facilities* (Eds: V.M. Jolly) (2017) (Web-link: [https://inis.iaea.org/search/search.aspx?orig\\_q=RN:48089837](https://inis.iaea.org/search/search.aspx?orig_q=RN:48089837)).
- [30] R.K. Sinha, A. Kakodkar, "Design and development of the AHWR - the Indian thorium fuelled innovative nuclear reactor" *Nucl. Eng. Des.* 236 (7-8) (2006) 683-700.

- [31] R. Sinha, A. Kakodkar, "India's passive breeder", Nucl. Eng. Int. 55(668) (2010) 30-31.
- [32] A. Kakodkar, "Evolution of nuclear reactor containments in India: Addressing the present day challenges", Nucl. Eng. Des. 269 (2014) 3-22.
- [33] S. Sengupta, S.B. Chafle, S. Mammen, K. Sasidharan, V.K. Raina, "Critical facility for AHWR and PHWRs", Proceedings of International Conference on Peaceful uses of Atomic Energy (2009). V. 1. **[33a]** C. Ronchi, J.-P. Hiernaut, Experimental measurement of pre-melting and melting of thorium dioxide, J. Alloys Comp. 240 (1-2) (1996) 179-185. **[33b]** R. Böhler, A. Quaini, L. Capriotti, P. Cakir, O. Beneš, K. Boboridis, A. Guiot, L. Luzzi, R.J.M. Konings, D. Manara, "The solidification behavior of the UO<sub>2</sub>-ThO<sub>2</sub> system in a laser heating study" J. Alloys. Comp. 616 (2014) 5-13.
- [34] D. Greneche, W.J. Szymczak, J.M. Buchheit, M. Delpech, A. Vasile, H. Golfier, "Rethinking the thorium fuel cycle: An industrial point of view", Proceedings of ICAPP (Nice, France), (2007) Paper-7367. **[34a]** S.F. Ashley, G.T. Park, W.J. Nuttall, C. Boxall, R.W. Grimes, "Thorium fuel has risks", Nature 492 (2012) 31-33.
- [35] D. Jain, V. Sudarsan, A.K. Tyagi, "Thorium-based metallic alloys as nuclear fuels: Present status, potential advantages and challenges", SMC Bulletin (Society for Materials Chemistry, India) 4 (1) (2013) pp. 27-40 (Web-link: <https://www.smcindia.org/smc-bulletin.php>).
- [36] P.K. Vijayan, A. Basak, I.V. Dulera, K.K. Vaze, S. Basu, "Conceptual design of Indian molten salt breeder reactor", Pramana - J. Phys. 85 (2015) 539–554.
- [37] T. Yamamoto, H. Suwarno, H. Kayano, M. Yamawaki, "Development of new reactor fuel materials: Hydrogen absorption properties of U-Th, U-Th-Zr and U-Th-Ti-Zr alloys", J. Nucl. Sci. Tech. 32(3) (1995) 260-262.

## References

- [38] K.A. Terrani, G.W.C. Silva, C.B. Yeamans, "Fabrication and characterization of uranium thorium zirconium hydride fuels", *Trans. Am. Nucl. Soc.* 98 (2008) 1060-1061.
- [39] S.M. McDeavitt, T.J. Downar, A.A. Solomon, S.T. Revankar, M.C. Hash, A.S. Hebden, "Thoria-based cermet nuclear fuel: Cermet fabrication and behavior estimates", *Proc. Int. Conf. Nucl. Eng. (ICONE 4)* (2002) 59-67.
- [40] C. Lombardi, L. Luzzi, E. Padovani, F. Vettrano, "Thoria and inert matrix fuels for a sustainable nuclear power", *Prog. Nucl. Energy* 50(8) (2008) 944-953.
- [41] J. Spino, H.S. Cruz, R. Jovani-Abril, R. Birtcher, C. Ferrero, "Bulk-nanocrystalline oxide nuclear fuels - An innovative material option for increasing fission gas retention, plasticity and radiation-tolerance", *J. Nucl. Mater.* 422 (1-3) (2012) 27-44.
- [42] H. György, S. Czifrus, "The utilization of thorium in generation IV reactors", *Prog. Nucl. Energy* 93 (2016) 306-317.
- [43] D. Heuer, E. Merle-Lucotte, M. Allibert, M. Brovchenko, V. Ghetta, P. Rubiolo, "Towards the thorium fuel cycle with molten salt fast reactors", *Ann. Nucl. Energy* 64 (2014) 421-429.
- [44] G.L. Hofman, L.C. Walters, T.H. Bauer, "Metallic fast reactor fuels", *Prog. Nucl. Energy* 31(1-2) (1997) 83-110.
- [45] W.J. Carmack, D.L. Porter, Y.I. Chang, S.L. Hayes, M.K. Meyer, D.E. Burkes, C.B. Lee, T. Mizuno, F. Delage, J. Somers, "Metallic fuels for advanced reactors", *J. Nucl. Mater.* 392 (2) (2009) 139-150.
- [46] Idaho National Laboratory, "Experimental breeder reactor-I (EBR-I) (Web-link: <https://inl.gov/experimental-breeder-reactor-i/>).
- [47] L.C. Walters, "Thirty years of fuels and materials information from EBR-II", *J. Nucl. Mater.* 270(1) (1999) 39-48.

- [48] K. D. Weaver, J. Gilleland, C. Whitmer, G. Zimmerman, “High burn-up fuels for fast reactors: past experience and novel applications”, International Congress on Advances in Nuclear Power Plants (ICAPP 2009) (2009) 795.
- [49] G. Locatelli, M. Mancini, N. Todeschini, “Generation IV nuclear reactors: Current status and future prospects”, *Energ. Policy* 61 (2013) 1503-1520.
- [50] Z.S. Takibaev, “Fast homogeneous nuclear reactor”, *Atom. Energy* 100 (2006) 154-156.
- [51] T. Jayakumar, M.D. Mathew, K. Laha, R. Sandhya, “Materials development for fast reactor applications”, *Nucl. Eng. Des.* 265 (2013) 1175-1180.
- [52] A. Riyas, P. Mohanakrishnan, “Studies on physics parameters of metal (U-Pu-Zr) fuelled FBR cores”, *Ann. Nucl. Energy* 35(1) (2008) 87-92.
- [53] P. Chellapandi, V. Balasubramaniyan, P. Puthiyavinayagam, R. Sundararajan, M. Kanakkil, P. Selvaraj, P.R. Vasudeva Rao, “Design of 500 MWe metal fuel demonstration fast reactor”, *Proc. Int. Conf. Nucl. Eng.* (2014) (DOI: <https://doi.org/10.1115/ICONE22-30727>).
- [54] Indira Gandhi Centre for Atomic Research, “Fast Breeder Test Reactor”, (Web-link: <http://www.igcar.gov.in/rfg/fbtrhist.html>).
- [55] B. Blumenthal, J.E. Sanecki, D.E. Busch, D.R. O’Boyle, “Thorium-uranium-plutonium alloys as potential fast power reactor fuels; part-II: Properties and irradiation behavior of thorium-uranium-plutonium alloys”, ANL-7259, Argonne National laboratory, Illinois (October 1969).
- [56] S.Z. Ghayeb, “Investigations of thorium-based fuels to improve actinide burning rate in S-PRISM reactor”, M.Sc. Thesis, The Pennsylvania State University (2008) (Web-link: <https://etda.libraries.psu.edu/catalog/9160>).

## References

- [57] R.G. Wymer, D.A. Douglas Jr., “Status and progress report for thorium fuel cycle development for period ending December 31, 1964”, Report no.: ORNL-3831, Oak Ridge National laboratory, Tennessee (May 1966).
- [58] “Fast spectrum reactors”, (Eds.: A.E. Waltar, D. Todd, P.V. Tsvetkov) Springer (2011) (ISBN 978-1-4419-9572-8).
- [59] D.E. Peterson, “The (Th-U) Thorium-uranium system”, Bull. Alloy Phase Diagr. 6 (5) (1985) 443-445.
- [60] S. Peterson, R.E. Adams, D.A. Douglas Jr., “Properties of thorium, its alloys and its compounds”, Report no.: ORNL-TM-1144, Oak Ridge National laboratory, Tennessee (June 1965).
- [61] D.R. Marr, D.A. Cantley, J.C. Chandler, D.C. McCurry, R.P. Omberg, “Performance of thorium fuelled fast breeders”, Report no.: HEDL-SA-1327-FP, Hanford Engineering Development Laboratory, Richland, USA (October 1977).
- [62] G.L. Copeland, “Evaluation of thorium-uranium alloys for the unclad metal breeder reactor”, Report no.: ORNL-4557, Oak Ridge National Laboratory, Tennessee (June 1970).
- [63] B. Blumenthal, J.E. Sanecki, D.E. Busch, “Thorium-uranium-plutonium alloys as potential fast power reactor fuels; part-I: Thorium-uranium-plutonium phase diagram”, Report no.: ANL-7258, Argonne National Laboratory, Illinois (September 1968).
- [64] C.S. Holden, “Rapid computational path for sustainable and renewable nuclear energy using metallic thorium fuels”, Proceedings of 2<sup>nd</sup> Thorium energy conference (ThEC-2010), Mountain View CA (2010).
- [65] R.M. Carroll, “The effects of reactor irradiation on thorium-uranium alloy fuel plates”, Report no.: ORNL-1938, Oak Ridge National Laboratory, Tennessee (August 1955).

## References

- [66] B.R. Hayward, P. Corzine, "Thorium uranium fuel elements for SRE", Proc. 2<sup>nd</sup> UN Int. Conf. Peaceful uses of Atom. Energy, Geneva (October 1958).
- [67] J.L. Ballif, B.R. Hayward, J.W. Walter, "Engineering evaluation of a mixed alloy fuel element irradiated at elevated temperatures in SRE", Technical report no.: NAA-SR-3888, Atomics International Division, North American Aviation Incorporation, California, USA (June 1960).
- [68] A.R. Olsen, "Thorium and thorium alloys: Preliminary corrosion tests", Report no.: ORNL-1066, Oak Ridge National Laboratory, Tennessee (November 1951).
- [69] M.S. Farkas, A.A. Bauer, R.F. Dickerson, "Development of thorium-uranium-base fuel alloys," Report no.: BMI-1428, Battelle Memorial Institute, Columbus, Ohio (March 1960).
- [70] R.H. Cole, L.E. Wilkinson, "Development of high strength ternary and quaternary thorium-uranium base alloys", Technical report no.: ATL-A-128, Advanced Technology Laboratory, California (1961).
- [71] J.H. Kittel, J.A. Horak, W.F. Murphy, S.H. Paine, "Effect of irradiation on thorium and thorium-uranium alloys", Technical report no.: ANL-5674, Argonne National laboratory, Illinois, USA (April 1963).
- [72] A.L. Bement, "Burn-up and specific power calculations for the thermal neutron irradiation on thorium-uranium alloys", Technical report no: HW-56631, General Electric Co. Hanford Atomic Products Operation, Richland, Washington (1958).
- [73] F.W. Dodge, E.W. Murbach, L.A. Hanson, "Low decontamination reprocessing of thorium-uranium alloys by induction drip melting", Nucl. Sci. Eng. 6 (6) (1959) 533-536.
- [74] P. Chiotti, A.F. Voigt, "Pyrometallurgical processing", Technical report: A/CONF.15/P/517; ISC-1018, Ames Laboratory, Iowa (October 1958).

- [75] W.N. Hensen, "Electrolysis of thorium and uranium", US-Patent no.: US 2951793 (1960).
- [76] S. Jiang, K. Liu, Y. Liu, T. Yin, Z. Chai, W. Shi, "Electrochemical behavior of Th(IV) on the bismuth electrode in LiCl–KCl eutectic", *J. Nucl. Mater.* 523 (2019) 268-275.
- [77] G.B. Zorzoli, "Use of metallic thorium for LWBRs and LWRs", *Nucl. Tech.* 20 (1973) 109-113.
- [78] F. Correa, D.J. Driscoll, D.D. Lanning, "An evaluation of tight pitch PWR cores", technical report no.: MIT-EL-79-022, Massachusetts Institute of Technology, Cambridge, Massachusetts (1979).
- [79] Z.S. Li, X.J. Liu, C.P. Wang, "Thermodynamic modelling of the Th-U, Th-Zr and Th-U-Zr systems", *J. Alloy Compd.* 473 (2009) 193-198.
- [80] S.Z. Ghrayeb, K.N. Ivanov, S.H. Levine, E.P. Loewen, "Burn-up performance of sodium-cooled fast reactors utilizing thorium-based fuels", *Nucl. Tech.* 176 (2011) 188-194.
- [81] T. Okawa, H. Sekimoto, S. Nakayama, "Design study on power flattening to sodium cooled large scale CANDLE burning reactor with using thorium fuel", *Proc. 18<sup>th</sup> Int. Conf. Nucl. Eng., ICON18, China, (2010).*
- [82] M.T. Simnad, "The U-ZrH<sub>x</sub> alloy: Its properties and use in TRIGA fuel", *Nucl. Engg. Des.* 64 (1981) 403-422.
- [83] K. Konashi, B.A. Pudjanto, T. Terai, M. Yamawaki, "Thermodynamic stability of ThZr<sub>2</sub>H<sub>x</sub> at high temperature", *J. Phys. Chem. Solids* 66 (2–4) (2005) 625-628.
- [84] T. Yamamoto, H. Suwarno, F. Ono, H. Kayano, M. Yamawaki, "Preparation, analysis and irradiation of hydride Th-U-Zr alloy samples for a new fuel", *J. Alloy Compd.* 271-273 (1998) 702-706.

- [85] S. Das, R. Kumar, S.B. Roy, A.K. Suri, "Development study on metallic thorium and uranium-thorium alloy", BARC Newsletter-Founder's Day Special issue (2011) 72-76.
- [86] S. Das, R. Kumar, S. Kaity, S. Neogy, K.N. Hareendran, S.B. Roy, G.K. Dey, B.S.S. Daniel, G.P. Chaudhari, "Characterization of microstructural, mechanical and thermal properties and ageing study of Th-3 wt.% U alloy" Nucl. Eng. Des. 282 (2015) 116-125.
- [87] S. Das, S. Kaity, R. Kumar, J. Banerjee, S.B. Roy, G.P. Chaudhari, B.S.S. Daniel, "Characterization of microstructural, mechanical and thermophysical properties of Th-52 U alloy", J. Nucl. Mater. 480 (2016) 223-234.
- [88] S. Das, S.B. Roy, G.P. Chaudhari, B.S.S. Daniel, "Microstructural evolution of as-cast Th-U alloys", Prog. Nucl. Energy 88 (2016) 285-296.
- [89] R. Kumar, S. Das, S.B. Roy, R. Agarwal, J. Banerjee, S.K. Satpati, "Effect of Mo addition on the microstructural evolution and  $\gamma$ -U stability in Th-U alloys", J. Nucl. Mater. 539 (2020) 152317.
- [90] S. Vaidyanathan, "Thorium utilization in pressurized water reactors using bimetallic thorium-zirconium alloy cladding", Nucl. Tech. (2020) (DOI: <https://doi.org/10.1080/00295450.2019.1706377>).
- [91] D. Escorcia-Ortiz, J. François, C. Martín-del-Campo, "Comparative study of the neutronic performance of thorium-based metallic fuel and MOX fuel in an ASTRID-like fast reactor core", Nucl. Eng. Des. 347 (2019) 122-131.
- [92] J.K. Startt, C.S. Deo, "First principles study of the structure and elastic properties of thorium metal", MRS Adv. 1 (35) (2016) 2447-2452.
- [93] A. Karahan, J. Buongiorno, "A new code for predicting the thermo-mechanical and irradiation behavior of metallic fuels in sodium fast reactors", J. Nucl. Mater. 396 (2010) 283-293.

## References

- [94] K. Lassmann, "TRANSURANUS: a fuel rod analysis code ready for use", *J. Nucl. Mater.* 188 (1992) 295-302.
- [95] J.P. Hamond, "Physical, mechanical and irradiation properties of thorium and thorium alloys", ORNL-4218, Oak Ridge National Laboratory, USA (1968) 29-30.
- [96] J.K. Fink, M.G. Chasanov, L. Leibowitz, "Thermophysical properties of thorium and uranium systems for use in reactor safety analysis", Report no.: ANL-CEN-RSD-77-1, Argonne National Laboratory (1977) 11-12.
- [97] M. Lung, "A present review of the thorium nuclear fuel cycles", European commission report no.: EUR-17771-EN, (1997).
- [98] S. Kolay, S. Phapale, R. Dawar, M. Jafar, S. N. Achary, A. K. Tyagi, R. Mishra, M. Basu, "Phase characterization and thermal study of SrF<sub>2</sub> and NdF<sub>3</sub> doped fluoride salt containing 78 mol % LiF - 20 mol % ThF<sub>4</sub> - 2 mol % UF<sub>4</sub>", *J. Radioanal. Nucl. Chem.* 314 (2) (2017) 1267-1271.
- [99] M. Verwerft, B. Boer, "Thorium oxide nuclear fuels", *Comprehensive nuclear materials* (Second edition) 5 (2020) 139-168 (DOI: <https://doi.org/10.1016/B978-0-12-803581-8.11770-9>).
- [100] S. Usha, R.R. Ramanarayanan, P. Mohanakrishnan, R.P. Kapoor, "Research reactor KAMINI", *Nucl. Eng. Des.* 236 (7-8) (2006) 872-880.
- [101] T.K. Mukherjee, "Processing of Indian monazite for the recovery of thorium and uranium values", *Proceedings of International Conference on Characterisation and Quality Control of Nuclear Fuels* (Eds.: C. Ganguly, R.N. Jayaraj) Allied Publishers Pvt. Ltd. (2002) 187-195.
- [102] J.R. Johnson, C.E. Curtis, "Note on sintering of ThO<sub>2</sub>", *J. Am. Ceram. Soc.* 37(12) (1954) 611.

## References

- [103] T.R.G. Kutty, K.B. Khan, P.V. Hegde, J. Banerjee, A.K. Sengupta, S. Majumdar, H.S. Kamath, "Development of a master sintering curve for ThO<sub>2</sub>", *J. Nucl. Mater.* 327(2-3) (2004) 211-219.
- [104] P. Balakrishna, B.P. Varma, T.S. Krishnan, T.R.R. Mohan, P. Ramakrishnan, "Thorium oxide: Calcination, compaction and sintering", *J. Nucl. Mater.* 160(1) (1988) 88-94.
- [105] N. Clavier, R. Podor, L. Deliere, J. Ravoux, N. Dacheux, "Combining in situ HT-ESEM observations and dilatometry: An original and fast way to the sintering map of ThO<sub>2</sub>", *Mater. Chem. Phys.* 137(3) (2013) 742-749.
- [106] K. Ananthasivan, S. Balakrishnan, S. Anthonysamy, R. Divakar, E. Mohandas, V. Ganesan, "Synthesis and sintering of nanocrystalline thoria doped with CaO and MgO derived through oxalate-deagglomeration", *J. Nucl. Mater.* 434 (1-3) (2013) 223-229.
- [107] G.P. Halbfinger, M. Kolodney, "Activated Sintering of ThO<sub>2</sub> and ThO<sub>2</sub>-Y<sub>2</sub>O<sub>3</sub> with NiO", *J. Am. Ceram. Soc.* 55(10) (1972) 519-524.
- [108] A. Baena, T. Cardinaels, J. Vleugels, K. Binnemans, M. Verwerft, "Activated sintering of ThO<sub>2</sub> with Al<sub>2</sub>O<sub>3</sub> under reducing and oxidizing conditions", *J. Nucl. Mater.* 470 (2016) 34-43.
- [109] K. Ananthasivan, S. Anthonysamy, C. Sudha, A.L.E. Terrance, P.R. Vasudeva Rao, "Thoria doped with cations of group VB-synthesis and sintering", *J. Nucl. Mater.* 300(2-3) (2002) 217-229.
- [110] T.R.G. Kutty, P.V. Hegde, K.B. Khan, T. Jarvis, A.K. Sengupta, S. Majumdar, H.S. Kamath, "Characterization and densification studies on ThO<sub>2</sub>-UO<sub>2</sub> pellets derived from ThO<sub>2</sub> and U<sub>3</sub>O<sub>8</sub> powders", *J. Nucl. Mater.* 335 (3) (2004) 462-470.
- [111] V. Tyrpekl, M. Cologna, D. Robba, J. Somers, "Sintering behaviour of nanocrystalline ThO<sub>2</sub> powder using spark plasma sintering", *J. Eur. Ceram. Soc.* 36(3) (2016) 767-772.

## References

- [112] W. Straka, S. Amoah, J. Schwartz, “Densification of thoria through flash sintering”, *MRS Commun.* 7(3) (2017) 677-682.
- [113] D. Sanjay Kumar, K. Ananthasivan, R.V. Krishnan, S. Amirthapandian, A. Dasgupta, “Studies on the synthesis of nanocrystalline  $Y_2O_3$  and  $ThO_2$  through volume combustion and their sintering”, *J. Nucl. Mater.* 479 (2016) 585-592.
- [114] R.D. Purohit, S. Saha, A.K. Tyagi, “Nanocrystalline thoria powders via glycine-nitrate combustion” *J. Nucl. Mater.* 288 (1) (2001) 7-10. [114a] F. Cappia, D. Hudry, E. Courtois, A. Janßen, L. Luzzi, R.J.M. Konings, D. Manara, High-temperature and melting behavior of nanocrystalline refractory compounds: an experimental approach applied to thorium dioxide, *Mater. Res. Express* 1 (2014) 0250341-12.
- [115] J. Spino, K. Vennix, M. Coquerelle, “Detailed characterisation of the rim microstructure in PWR fuels in the burn-up range 40–67 GWd/tM”, *J. Nucl. Mater.* 231 (3) (1996) 179-190.
- [116] L. Bonato, M. Viot, X. Le Goff, P. Moisy, S.I. Nikitenko, “Sonochemical dissolution of nanoscale  $ThO_2$  and partial conversion into a thorium peroxo sulphate”, *Ultrason. Sonochem.* 69 (2020) 105235.
- [117] S. Dash, A. Singh, P.K. Ajikumar, H. Subramanian, M. Rajalakshmi, A.K. Tyagi, A.K. Arora, S.V. Narasimhan, B. Raj, “Synthesis and characterization of nanocrystalline thoria obtained from thermally decomposed thorium carbonate”, *J. Nucl. Mater.* 303 (2–3) (2002) 156-168.
- [118] S. Dash, R. Krishnan, M. Kamruddin, A.K. Tyagi, B. Raj, “Temperature programmed decomposition of thorium oxalate hexahydrate”, *J. Nucl. Mater.* 295(2-3) (2001) 281-289.

## References

- [119] S. Dash, M. Kamruddin, P.K. Ajikumar, A.K. Tyagi, B. Raj, S. Bera, S.V. Narasimhan, “Temperature programmed decomposition of thorium nitrate pentahydrate”, *J. Nucl. Mater.* 278 (2–3) (2000) 173-185.
- [120] T.V. Plakhova, A.Y. Romanchuk, D.V. Likhosherstova, A.E. Baranchikov, P.V. Dorovatovskii, R.D. Svetogorov, T.B. Shatalova, T.B. Egorova, A.L. Trigub, K.O. Kvashnina, V.K. Ivanov, S.N. Kalmykov, “Size effects in nanocrystalline thoria”, *J. Phys. Chem. C* 123 (37) (2019) 23167-23176. [120a] D. Hudry, C. Apostolidis, O. Walter, T. Gouder, E. Courtois, C. Kübel, D. Meyer, Controlled Synthesis of Thorium and Uranium Oxide Nanocrystals, *Chem. Eur. J.*, 19 (2013) 5297-5305.
- [121] F. Deganello, A.K. Tyagi, “Solution combustion synthesis, energy and environment: Best parameters for better materials”, *Prog. Cryst. Growth Char.* 64 (2018) 23-61.
- [122] A. Varma, A.S. Mukasyan, A.S. Rogachev, K.V. Manukyan, “Solution combustion synthesis of nanoscale materials”, *Chem. Rev.* 116 (2016) 14493-14586.
- [123] V. Chandramouli, S. Anthonysamy, P.R. Vasudeva Rao, “Combustion synthesis of thoria - A feasibility study”, *J. Nucl. Mater.* 265(3) (1999) 255-261.
- [124] S. Anthonysamy, K. Ananthasivan, V. Chandramouli, I. Kaliappan, P.R. Vasudeva Rao, “Combustion synthesis of urania-thoria solid solutions”, *J. Nucl. Mater.* 278(2) (2000) 346-357.
- [125] D. Sanjay Kumar, K. Ananthasivan, S. Amirthapandian, A. Dasgupta, G. Jogeswara Rao, “Citrate gel-combustion synthesis and sintering of nanocrystalline ThO<sub>2</sub> powders”, *J. Nucl. Mater.* 497 (2017) 16-29.
- [126] R.D. Purohit, S. Saha, A.K. Tyagi, “Combustion synthesis of 5 and 10 mol% YO<sub>1.5</sub> doped ThO<sub>2</sub> powders”, *J. Nucl. Mater.* 323 (1) (2003) 36-40.

- [127] K.C. Patil, M.S. Hegde, T. Rattan, S.T. Aruna, "Chemistry of nanocrystalline oxide materials combustion synthesis, properties and applications", World Scientific Publications (2008) (DOI: <https://doi.org/10.1142/6754>).
- [128] F.-T Li, J. Ran, M. Jaroniec, S.Z. Qiao, "Solution combustion synthesis of metal oxide nanomaterials for energy storage and conversion", *Nanoscale* 7(42) (2015) 17590-17610.
- [129] A. Kumar, E.E. Wolf, A.S. Mukasyan, "Solution combustion synthesis of metal nanopowders: nickel-reaction pathways", *AIChE J.* 57(8) (2011) 2207-2214.
- [130] A. Kumar, E.E. Wolf, A.S. Mukasyan, "Solution combustion synthesis of metal nanopowders: Copper and copper / nickel alloys", *AIChE J.* 57(12) (2011) 3473-3479.
- [131] S. Zhang, Z.A. Munir, "The combustion synthesis of refractory nitrides: Part II the synthesis of niobium nitride", *J. Mater. Sci.* 26 (1991) 3380–3385.
- [132] "Nitride ceramics: Combustion synthesis, properties, and applications", (Eds.: A.A. Gromov, L.N. Chukhlomina) Wiley-VCH Verlag GmbH (2015) (DOI:10.1002/9783527684533).
- [133] H.V. Kirakosyan, K.T. Nazaretyan, R.A. Mnatsakanyan, S.V. Aydinyan, S.L. Kharatyan, "Solution combustion synthesis of nanostructured molybdenum carbide", *J. Nanopart. Res.* 20 (2018) 214.
- [134] N.A. Marand, S.M. Masoudpanah, M. Sh. Bafghi, "Solution combustion synthesis of nickel sulfide composite powders", *Ceram. Int.* 44 (14) (2018) 17277-17282.
- [135] K. Rajeshwar, N.R. De Tacconi, "Solution combustion synthesis of oxide semiconductors for solar energy conversion and environmental remediation", *Chem. Soc. Rev.* 38 (7) (2009) 1984-1998.

- [136] K.C. Thomas, J.R. Kale, R.G. Dalavi, K. Venkatesh, R. Kameswaran, A.V.R. Reddy  
"Development of an IR-based carbon analyser for uranium metal", BARC Newsletter  
311 (2009) 2-6 (Web-link: <http://barc.gov.in/publications/nl/2009/200912.pdf/>)
- [137] B.D. Cullity, "Elements of X-ray diffraction", Addison-Wesley Publishing Company  
Inc. (1956).
- [138] R. Tilley, "Crystals and crystal structures", John Wiley & Sons, Ltd. (2006) (ISBN-13  
978-0-470-01820-0).
- [139] E. Smith, G. Dent, "Modern Raman spectroscopy - A practical approach", John Wiley  
& Sons, Ltd. (2006) (ISBN 0-471-49794-0).
- [140] M. Roessle, D.I. Svergun, "Small angle X-ray scattering", In "Encyclopaedia of  
biophysics" (Eds.: G.C.K. Roberts) Springer, Berlin, Heidelberg (2013) (DOI:  
[https://doi.org/10.1007/978-3-642-16712-6\\_284](https://doi.org/10.1007/978-3-642-16712-6_284)).
- [141] P.W. Schmidt, R. Height, "Slit height corrections in small angle X-ray scattering", Acta  
Crystallogr. 13 (1960) 480-483.
- [142] G. Höhne, W.F. Hemminger, H.J. Flammersheim, "Differential scanning calorimetry",  
Springer-Verlag. (2003) (ISBN 978-3-540-00467-7).
- [143] M. Reading, A. Luget, R. Wilson, "Modulated differential scanning calorimetry",  
Thermochim. Acta 238(C) (1994) 295-307.
- [144] J.E.K. Schawe, T. Hutter, C. Heitz, I. Alig, D. Lellinger, "Stochastic temperature  
modulation: A new technique in temperature-modulated DSC", Thermochim. Acta 446  
(2006) 147-155.
- [145] N. Manoj, D. Jain, J.K. Gautam, K.C. Thomas, V. Sudarsan, C.G.S. Pillai, R.K. Vatsa,  
A.K. Tyagi, "A simple, reliable and cost-effective, high temperature dilatometer for  
bulk thermal expansion studies on solids", Measurement 92 (2016) 318-325.

- [146] W.J. Parker, R.J. Jenkins, C.P. Butler, G.L. Abbott, “Flash method of determining thermal diffusivity, heat capacity, and thermal conductivity”, *J. Appl. Phys.* 32 (1961) 1679-1684.
- [147] H.S. Carslaw, J.C. Jaeger, “Conduction of heat in solids”, 2nd edition, Oxford University Press, New York, (1959).
- [148] D. Jain, D. Das, B.N. Jagatap, “Thorium-based fuels for advanced nuclear reactors: Thermophysical, thermochemical and thermodynamic properties”, in A.K. Nayak, B.R. Sehgal (Eds.), *Thorium—Energy for the Future*, Springer (2019) (ISBN 978-981-13-2658-5) 257-275.
- [149] Y.S. Touloukian, R.W. Powell, C.Y. Ho, P.G. Klemens, “Thermophysical properties of matter - The TPRC data series. Volume 1. Thermal conductivity - metallic elements and alloys”, (1970) 429-440; 381-384.
- [150] Y.S. Touloukian, R.W. Powell, C.Y. Ho, M.C. Nicolaou, “Thermophysical properties of matter - The TPRC data series. Volume 10. Thermal diffusivity”, (1974) 205-208.
- [151] Y.S. Touloukian, E.H. Buyco, “Thermophysical properties of matter - The TPRC data series. Volume 4. Specific heat - metallic elements and alloys”, (1971) 268-270.
- [152] Y.S. Touloukian, R.K. Kirby, R.E. Taylor, P.D. Desai, “Thermophysical properties of matter - The TPRC data series. Volume 12. Thermal expansion metallic elements and alloys”, (1975) 365-372.
- [153] H.G. Schettler, J.J. Martin, F.A. Schmidt, G.C. Danielson, “Thermal conductivity of high purity thorium”, *Phys. Rev.* 187 (3) (1969) 801-804.
- [154] T.A. Sandenaw, “Thermal conductivity of uranium: Effects of purity and microstructure”, Report no.: LA-6092-MS, United States (1975) 1-8.
- [155] Y. Takahashi, M. Yamawaki, K. Yamamoto, “Thermophysical properties of uranium-zirconium alloys”, *J. Nucl. Mater.* 154 (1988) 141-144.

## References

- [156] R.W. Logan, D.H. Wood, "Thermal expansion of rolled and extruded uranium", *J. Less-Common Met.* 90 (1983) 233-241.
- [157] J. Nakamura, Y. Takahashi, S. Izumi, M. Kanno, "Heat capacity of metallic uranium and thorium from 80 to 1000 K", *J. Nucl. Mater.* 88 (1980) 64-72.
- [158] M. Boivineau, H. Colin, J.M. Vermeulen, Th. Thévenin, "Thermophysical properties of solid and liquid thorium", *Int. J. Thermophys.* 17(5) (1996) 1001-1010.
- [159] S. Zhou, R. Jacobs, W. Xie, E. Tea, C. Hin, D. Morgan, "Combined ab-initio and empirical model of the thermal conductivity of uranium, uranium-zirconium, and uranium-molybdenum", *Phys. Rev. Mater.* 2 (2018) 083401-1-21.
- [160] Y. Li, A. Chernatynskiy, J.R. Kennedy, S.B. Sinnott, S.R. Phillpot, Lattice expansion by intrinsic defects in uranium by molecular dynamics simulation, *J. Nucl. Mater.* 475 (2016) 6-18.
- [161] K.D. Joshi, S.C. Gupta, S. Banerjee, "Ab-initio theoretical analysis of thermal expansivity, thermal vibrations and melting of thorium", *Phil. Mag.* 88 (27) (2008) 3145-3152.
- [162] S. Jaroszewicz, H.O. Mosca, J.E. Garcés, "The temperature behaviour of the elastic and thermodynamic properties of fcc thorium", *J. Nucl. Mater.* 429(1-3) (2012) 136-142.
- [163] L. Kývala, D. Legut, "Lattice dynamics and thermal properties of thorium metal and thorium monocarbide" *Phys. Rev. B* 101 (2020) 075117.
- [164] P.L. Vijay, J.C. Sehra, C.V. Sundaram, K.R. Gurumurthy, R.V. Raghavan, "Studies on the preparation of thorium metal sponge from thorium oxalate", *BARC Report no.:* 969 (1978) 1-11.
- [165] M.D. Smith, R.W.K. Honeycombe, "The effect of oxygen, carbon and nitrogen on the properties of sintered thorium", *J. Nucl. Mater.* 4 (1959) 345-355.

- [166] Inorganic Crystal Structure Database (ICSD FIZ Karlsruhe GmbH, Version 4.4.0 (2020); collection code: 653236); from: J. Bohet, W. Müller, “Preparation and structure studies of “Van Arkel” protactinium”, *J. Less-Common Met.* 57 (2) (1978) 185-1995.
- [167] International Centre for Diffraction Data (ICDD Database; JCPDF card no.: 720659).
- [168] Inorganic Crystal Structure Database (ICSD FIZ Karlsruhe GmbH, Version 4.4.0 (2020) collection code: 253564) from: V.K. Tripathi, R. Nagarajan, “Sol–gel synthesis of high-purity actinide oxide ThO<sub>2</sub> and its solid solutions with technologically important tin and zinc ions” *Inorg. Chem.* 55 (24) (2016) 12798-12806.
- [169] Inorganic Crystal Structure Database (ICSD FIZ Karlsruhe GmbH, Version 4.4.0 (2020) collection code: 35204); from: S.A. Barrett, A.J. Jacobson, B.C. Tofield, B.E.F. Fender, “The preparation and structure of barium uranium oxide BaUO<sub>3+x</sub>”, *Acta Crystallogr. B* 38 (1982) 2775-2781. [169a] S. Ellison, A. Williams, Eurachem / CITAC guide: Quantifying Uncertainty in Analytical Measurement (2012) ISBN 978-0-948926-30-3 (Web-link: [www.eurachem.org](http://www.eurachem.org)).
- [170] Inorganic Crystal Structure Database (ICSD FIZ Karlsruhe GmbH, Version 4.4.0 (2020) collection code: 24223); from: R.E. Rundle, N.C. Baenziger, A.S. Wilson, R.A. McDonald, “The structures of the carbides, nitrides and oxides of uranium”, *J. Am. Chem. Soc.* 70 (1948) 99-105.
- [171] Inorganic Crystal Structure Database (ICSD FIZ Karlsruhe GmbH, Version 4.4.0 (2020) collection code: 26476); from: A.E. Austin, “Carbon positions in uranium carbides”, *Acta Crystallogr.* 12 (1959) 159-161.
- [172] “Augmented uranium metal production facility”, BARC Newsletter 200 (2000) 15-18 (Web-link: <http://barc.gov.in/publications/nl/2000/200009.pdf>).
- [173] G.C. Allen, P.M. Tucker, “Surface oxidation of uranium metal as studied by X-ray photoelectron spectroscopy”, *J. Chem. Soc. Dalton* 5 (1973) 470-474.

- [174] R. Rao, R.K. Bhagat, N.P. Salke, A. Kumar, "Raman spectroscopic investigation of thorium dioxide-uranium dioxide ( $\text{ThO}_2\text{-UO}_2$ ) fuel materials", *Appl. Spectrosc.* 68(1) (2014) 44-48.
- [175] "Thermophysical properties of materials for nuclear engineering: A tutorial and collection of data", (IAEA-THPH), International Atomic Energy Agency, Vienna (2008).
- [176] I.F. Barwood, B.R. Butcher, "The  $\alpha \rightarrow \beta$  phase transformation in uranium", *J. Nucl. Mater.* 8 (1963) 232-240.
- [177] C. Yoo, H. Cynn, P. Söderlind, "Phase diagram of uranium at high pressures and temperatures", *Phys. Rev. B* 57 (1998) 10359-10362.
- [178] P. Zhou, X. Wang, H. Yang, X. Fu, "Effect of vacuum heat treatment on oxidation of uranium surfaces", *Rare Metal Mat. Eng.* 37 (2008) 94-97.
- [179] G. Erez, U. Even, "The Wiedemann-Franz ratio of metallic uranium at elevated temperatures", *J. Appl. Phys.* 37 (1966) 4633-4644.
- [180] S. Nasu, S. Fukushima, T. Ohmichi, T. Kikuchi, "Thermal diffusivity of uranium by laser pulse method from 20° to 850°C", *Jap. J. Appl. Phys.* 7 (1968) 682.
- [181] D. Jain, C.G.S. Pillai, B.S. Rao, R.V. Kulkarni, E. Ramdasan and K.C. Sahoo, "Thermal diffusivity and thermal conductivity studies on thoria-lanthana solid solutions up to 10 mol. %  $\text{LaO}_{1.5}$ ", *J. Nucl. Mater.* 353 (2006) 35-41.
- [182] S.S. Parker, J.T. White, P. Hosemann, A.T. Nelson, "Thermophysical properties of thorium mononitride from 298 to 1700 K", *J. Nucl. Mater.* 526 (2019) 151760.
- [183] H. He, J. Majewski, D.D. Allred, P. Wang, X. Wen, K.D. Rector, "Formation of solid thorium monoxide at near-ambient conditions as observed by neutron reflectometry and interpreted by screened hybrid functional calculations", *J. Nucl. Mater.* 487 (2017) 288-296.

## References

- [184] B.R. Butcher, A.H. Rowe, "Phase transformation in uranium", *Nature* (1953) 817.
- [185] H.H. Klpefer, P. Chiotti, "Characteristics of the solid state transformations in uranium", USAEC Report no.: ISC-893 (1957) 1-113.
- [186] W.S. Blackburn, " $\alpha$ - $\beta$  Thermal cycling of uranium", *J. Nucl. Mater.* 2 (1960) 191.
- [187] J.J. Stobo, "Alpha beta cycling of uranium", *J. Nucl. Mater.* 2 (1960) 97-109.
- [188] L.T. Lloyd, "Thermal expansion of alpha-uranium single crystals", *J. Nucl. Mater.* 3 (1961) 67-71.
- [189] L.T. Lloyd, C.S. Barrett, "Thermal expansion of alpha uranium", *J. Nucl. Mater.* 18 (1966) 55-59.
- [190] E.S. Fisher, "Preparation of alpha uranium single crystals by a grain-coarsening method", *J. Metals* 9 (1957) 882-888.
- [191] D.C. Wallace, "Specific heat of thorium at high temperatures", *Phys. Rev.* 120 (1) (1960) 84-88.
- [192] E.A. Mit'kina, "Experimental determination of the true specific heats of uranium, thorium, and other metals", *Sov. Atom Energy* 7 (2) (1959) 163-165.
- [193] F.L. Oetting, D.T. Peterson, "Heat capacity of well characterized thorium metal from 298 to 700 K", *J. Less-Common Met.* 128 (1987) 231-239.
- [194] D.C. Ginnings, R.J. Corruccini, "Heat capacities at high temperatures of uranium, uranium trichloride, and uranium tetrachloride, *J. Res. Nat. Bur. Stand.* 39 (1947) 309-316.
- [195] F.K. Oetting, M.H. Rand, R.J. Ackermann, "The chemical thermodynamics of actinide elements and compounds, Part 1, The actinide elements", International Atomic Energy Agency (IAEA), Vienna (1976).
- [196] A.L. Loeb, "Thermal conductivity: VIII, A theory of thermal conductivity of porous materials", *J. Am. Ceram. Soc.* 37 (1954) 96-99.

## References

- [197] S. Kaity, J. Banerjee, M.R. Nair, K. Ravi, S. Dash, T.R.G. Kutty, A. Kumar, R.P. Singh, "Microstructural and thermophysical properties of U-6 wt.% Zr alloy for fast reactor application", *J. Nucl. Mater.* 427 (2012) 1-11.
- [198] C. Hin, "Thermal conductivity of metallic uranium", NEUP 14-6767 (2018) (Web-link: <https://www.osti.gov/servlets/purl/1433931>).
- [199] M. Floyd, B. Bromley, J. Pencer, "A Canadian perspective on progress in thorium fuel science and technology", *CNL Nucl. Rev.* 6 (1) (2017) 1-17.
- [200] S. Thakur, P.S.R. Krishna, A.B. Shinde, R. Kumar, S.B. Roy, "Quantitative analysis of thorium phase in Th-U alloys using diffraction studies", *AIP Conf. Proc.* 1832 (2017) 060012.
- [201] P. Chiotti, "High temperature crystal structure of thorium", *J. Electrochem. Soc.* (1955) 567-570.
- [202] G.G. Bente, "A Physical Metallurgical Study of Thorium-Rich Thorium-Uranium Alloys", Report no.: NAA-SR-2069 (1958).
- [203] G.H. Bannister, R.C. Burnett, J.R. Murray, "Ageing and hot hardness characteristics of certain thorium alloys", *J. Nucl. Mater.* 2(1) (1960) 51-61.
- [204] "Chemical technology division annual technical report for 1986," ANL-87-19, Argonne National Laboratory (1987) 122.
- [205] V. Crewe, S. Lawroski, "Reactor development program progress report", Argonne National Laboratory, ANL-7230, Lemont, IL, USA (1966).
- [206] O. Beneš D. Manara R.J.M. Konings, "Thermodynamic assessment of the Th-U-Pu system", *J. Nucl. Mater.* 449 (1-3) (2014) 15-22.
- [207] S. Kneppel, "Aqueous corrosion of thorium alloys and zircaloy-clad thorium alloys", NMI-1226, United States Atomic Energy Commission (1960) 1-49 (Web-link: <https://play.google.com/books/reader?id=OGCWvHY4xRwC&hl=en&pg=GBS.PA1>)

- [208] D.S. Evans, G.V. Raynor, "The solubility of zirconium in  $\alpha$ -thorium", *J. Nucl. Mater.* 4 (1) (1961) 66-69.
- [209] R.I. Sheldon, D.E. Peterson, "The (U-Zr) Uranium-zirconium system", *Bull. Alloy Phase Diagr.* 10 (2) (1989) 165-171.
- [210] O.N. Carlson, "Some studies on the uranium-thorium-zirconium ternary alloy system", AECD-3206, United States Atomic Energy Commission (1950) 1-72.
- [211] J.W. Goffard, R.K. Marshall, "Irradiation behavior of Zircaloy-2 clad thorium-uranium-zirconium alloy fuel elements Interim report 1", BNWL-479, Pacific Northwest Laboratory, United States Atomic Energy Commission (1967).
- [212] T. Okawa, S. Nakayama, H. Sekimoto, "Design study on power flattening to sodium cooled large-scale CANDLE burning reactor with using thorium fuel", *Energ. Convers. Manage.* 53 (1) (2012) 182-188.
- [213] Inorganic crystal Structure Database (ICSD FIZ Karlsruhe GmbH, Version 4.4.0 (2020) collection code: 164572) from: A.I. Kolesnikov, A.M. Balagurov, I.O. Bashkin, A.V. Belushkin, E.G. Ponyatovsky, M. Prager, "Neutron scattering studies of ordered gamma -ZrD", *J. Phys. Condens-Mat.* 6 (43) (1994) 8977-8988.
- [214] Inorganic crystal Structure Database (ICSD FIZ Karlsruhe GmbH, Version 4.4.0 (2020) collection code: 16559) from: B.O. Loopstra, "Neutron diffraction investigation of  $U_3O_8$ ", *Acta Crystallogr.* 17 (1964) 651-654.
- [215] Inorganic crystal Structure Database (ICSD FIZ Karlsruhe GmbH, Version 4.4.0 (2020) collection code: 246035) from: S.K. Sali, N.K. Kulkarni, K. Krishnan, S.N. Achary, A.K. Tyagi, "Oxidation / reduction studies on  $Zr_yU_{1-y}O_{2+x}$  and delineation of a new orthorhombic phase in U-Zr-O system", *J. Solid-State Chem.* 181 (8) (2008) 1859-1866.

## References

- [216] Inorganic crystal Structure Database (ICSD FIZ Karlsruhe GmbH, Version 4.4.0 (2020) collection code: 108756) from: H.L. Luo, J.G. Huber, “Superconductivity in Th-Zr alloys”, *J. Less-Common Met.* 65 (1) (1979) 13-17.
- [217] J.M. Elorrieta, L.J. Bonales, M. Naji, D. Manara, V.G. Baonza, J. Cobos, “Laser-induced oxidation of  $\text{UO}_2$ : A Raman study”, *J. Raman Spectrosc.* 49 (5) (2018) 878-884.
- [218] H. He, D. Shoesmith, “Raman spectroscopic studies of defect structures and phase transition in hyper-stoichiometric  $\text{UO}_{2+x}$ ”, *Phys. Chem. Chem. Phys.* 12 (2010) 8109-8118.
- [219] X. Zhao, D. Vanderbilt, “Phonons and lattice dielectric properties of zirconia”, *Phys. Rev. B* 65 (2002) 075105.
- [220] E. Hashem, A. Seibert, J-F. Vigier, M. Naji, S. Mastromarino, A. Ciccioli, D. Manara, “Solid-liquid equilibria in the  $\text{ThO}_2$ - $\text{ZrO}_2$  system: An experimental study” *J. Nucl. Mater.* 521 (2019) 99-108.
- [221] O.N. Carlson, E.R. Stevens, “A compilation of thorium binary phase diagrams”, USAEC Report (1968) (Web-link: <https://www.osti.gov/servlets/purl/4529064>).
- [222] G.B. Skinner, H.L. Johnston, “Thermal Expansion of zirconium between 298°K and 1600°K”, *J. Chem Phys.* 21 (1953) 1383.
- [223] P.L. Brown, E. Curti, B. Grambow, C. Ekberg, “Chemical thermodynamics of zirconium”, OECD Nuclear energy agency, data bank (Eds.: F.J. Mompean, J. Perrone, M. Illemassene) (2005) (Web-link: <https://www.oecd-nea.org/dbtdb/pubs/vol8-zirconium.pdf>).
- [224] C.G.S. Pillai, P. Raj, “Thermal Conductivity of  $\text{ThO}_2$  and  $\text{Th}_{0.98}\text{U}_{0.02}\text{O}_2$ ”, *J. Nucl. Mater.* 277 (2000) 116-119.

- [225] S.S. Manoharan, K.C. Patil, "Combustion synthesis of metal chromite powders", *J. Am. Ceram. Soc.* 75 (1992) 1012-1015.
- [226] S.R. Jain, K.C. Adiga, V.R. Pai Verneker, "A new approach to thermochemical calculations of condensed fuel-oxidizer mixtures," *Combust. Flame* 40 (6) (1981) 71-79.
- [227] S. Roy, A. Das Sharma, S.N. Roy, H.S. Maiti, "Synthesis of  $\text{YBa}_2\text{Cu}_3\text{O}_{7-x}$  Powder by Autoignition of Citrate-Nitrate Gel", *J. Mater. Res.* 8(11) (1993) 2761-2766.
- [228] M. Gizowska, I. Kobus, K. Perkowski, M. Piatek, G. Konopka, I. Witosławska, M. Osuchowski, "Size and morphology of yttria nanopowders obtained by solution combustion synthesis" *Arch. Metall. Mater.* 63(2) (2018) 743-748.
- [229] G.A.M. Hussein, H.M. Ismail, "Texture assessment of thoria as a final decomposition product of hydrated thorium nitrate and oxycarbonate", *Colloids Surf. A*: 99 (1995) 129-139.
- [230] I.M. Weiss, C. Muth, R. Drumm, H.O.K. Kirchner, "Thermal decomposition of the amino acids glycine, cysteine, aspartic acid, asparagine, glutamic acid, glutamine, arginine and histidine", *BMC Biophys.* 11 (2018) 1-15.
- [231] N. Raje, A.V.R. Reddy, "Mechanistic aspects of thermal decomposition of thorium oxalate hexahydrate: A review", *Thermochim. Acta* 505 (2010) 53-58.
- [232] H. Hayashi, T. Watanabe, "Properties of thoria obtained by thermal decomposition of thorium salts", *Nippon Kagaku Kaishi* 4 (1973) 858-860.
- [233] Y. Saito, "Thermal decomposition of thorium oxalate", *J. Jpn. Soc. Powder Metall.* 17(1971) 235-242.
- [234] M.T. Aybers, "Kinetic study of the thermal decomposition of thorium oxalate dehydrate", *J. Nucl. Mater.* 252 (1998) 28-33.
- [235] D.Y. Chung, E. H. Lee, "Microwave-induced combustion synthesis of  $\text{Ce}_{1-x}\text{Sm}_x\text{O}_{2-x/2}$  powder and its characterization", *J. Alloys Compd.* 374 (2004) 69-73.

- [236] “The Aldrich Library of FT-IR Spectra, Edition-II, Volume-1”, 1 898 A 897-898.
- [237] S. Kumar, A.K. Rai, V.B. Singh, S.B. Rai, “Vibrational spectrum of glycine molecule”, *Spectrochim. Acta A* 61 (2005) 2741-2746.
- [238] J. R. Ferraro, A. Walker, “Comparison of the infrared spectra of the hydrates and anhydrous salts in the systems  $\text{UO}_2(\text{NO}_3)_2$  and  $\text{Th}(\text{NO}_3)_4$ ”, *J. Chem. Phys.* 45 (1966) 550-552.
- [239] J.H-Paredes, D.G-Mitnik, H.E. E-Ponce, M.E. A-Ramos, A.D-Moller, “Band structure, optical properties and infrared spectrum of glycine–sodium nitrate crystal”, *J. Mole. Str.* 875 (2008) 295-301.
- [240] S.L. Estes, M.R. Antonio, L. Soderholm, “Tetravalent Ce in the nitrate-decorated hexanuclear cluster  $[\text{Ce}_6(\mu_3\text{-O})_4(\mu_3\text{-OH})_4]^{12+}$ : A structural end point for ceria nanoparticles, *J. Phys. Chem. C* 120 (2016) 5810-5818.
- [241] M. Rand, L. Fuger, I. Grenthe, V. Neck, D. Rai, “Chemical thermodynamics: Chemical thermodynamics of thorium”, (OECD, NEA-TDB) Vol. 11, Elsevier, Amsterdam (2007).
- [242] C. Hennig, K. Schmeide, V. Brendler, H. Moll, S. Tsushima, A.C. Scheinost, “EXAFS Investigation of U(VI), U(IV), and Th(IV) sulfato complexes in aqueous solution”, *Inorg. Chem.* 46 (2007) 5882-5892.
- [243] J. Rothe, M.A. Denecke, V. Neck, R. Muller, J.I. Kim, XAFS “Investigation of the structure of aqueous thorium(IV) species, colloids, and solid thorium(IV) oxide / hydroxide”, *Inorg. Chem.* 41 (2002) 249-258.
- [244] C. Hennig, S. Takao, K. Takao, S. Weiss, W. Kraus, F. Emmerling, A.C. Scheinosta, “Structure and stability range of a hexanuclear Th(IV)-glycine complex”, *Dalton Trans.* 41 (2012) 12818-12823.

## References

- [245] Y. Hu, K.E. Knope, S. Skanthakumar, L. Soderholm, "Understanding the ligand-directed assembly of a hexanuclear Th<sup>IV</sup> molecular cluster in aqueous solution", *Eur. J. Inorg. Chem.* 24 (2013) 4159-4163.
- [246] M. Nourmand, N. Meissami, "Complex formation between uranium(VI) and thorium (IV) ions with some  $\alpha$ -amino-acids", *J. Chem. Soc. Dalton* 8 (1983) 1529-1533.
- [247] Bismondo, L. Rizzo, G. Tomat, "Thermodynamic properties of actinide complexes. uranyl (VI)- and thorium (IV)-glycine systems", *Inorg. Chim. Acta* 74 (1983) 21-24.
- [248] B.G. Oliver, A.R. Davis, "The structure of aqueous thorium nitrate solution by laser Raman spectroscopy", *J. Inorg. Nucl. Chem.* 34 (1972) 2851-2860.
- [249] Z. Huang, X. Chen, Y. Li, J. Chen, J. Lin, J. Wang, J. Lei, R. Chen, "Quantitative determination of citric acid in seminal plasma by using Raman spectroscopy", *Appl. Spectrosc.* 67 (7) (2013) 757-760.
- [250] A.K. Arora, M. Rajalakshmi, T.R. Ravindran, V. Sivasubramanian, "Raman spectroscopy of optical phonon confinement in nanostructured materials", *J. Raman Spectrosc.* 38 (2007) 604-617.
- [251] D. Langmuir, J.S. Herman, "The mobility of thorium in natural waters at low temperatures", *Geochim. Cosmochim. Ac.* 44 (1980) 1753-1766.
- [252] M. Bobtelsky, B. Graus, "Thorium citrate complexes, their composition, structure and behavior", *J. Am. Chem. Soc.* 76 (6) (1954,) 1536-1539.
- [253] G.R. Choppin, H.N. Erten, Y. Xia, "Variation of stability constants of thorium citrate complexes with ionic strength", *Radiochim. Acta* 74 (1996) 123-127.
- [254] D.P. Raymond, J.R. Duffield, D.R. Williams, "Complexation of plutonium and thorium in aqueous environments", *Inorg. Chim. Acta* 140 (1987) 309-313.
- [255] M.M. Barbooti, D.A. Al-Sammerrai, "Thermal decomposition of citric acid", *Thermochim. Acta* 98 (1986) 119-126.

## References

- [256] D. Hennings, W. Mayr, "Thermal decomposition of (BaTi) citrates into barium titanate", *J. Solid State Chem.* 26 (1978) 329-338.
- [257] N.S. Gajbhiye, S. Prasad, "Thermal decomposition of hexahydrated nickel iron citrate", *Thermochim. Acta* 285 (1996) 325-336.
- [258] J. Tsay, T. Fang, "Effects of molar ratio of citric acid to cations and of pH value on the formation and thermal-decomposition behavior of barium titanium citrate", *J. Am. Ceram. Soc.* 82(6) (1999) 1409-1415.
- [259] A. Marcilla, A. Gómez-Siurana, M. Beltrán, I. Martínez-Castellanos, I. Blasco, D. Berenguer, "TGA-FTIR study of the pyrolysis of sodium citrate and its effect on the pyrolysis of tobacco and tobacco/SBA-15 mixtures under N<sub>2</sub> and air atmospheres", *J. Sci. Food Agr.* 98 (15) (2018) 5916-5931.
- [260] O. Glatter, O. Kratky, "Small angle X-ray scattering", Academic, London (1982).
- [261] A. Guinier, G. Fournet, "Small angle scattering of X-rays", Wiley, New York (1955).
- [262] J. Aitchison, J.A.C. Brown, "The log normal distribution", Cambridge University Press, Cambridge (1957).
- [263] R.D. Purohit, B.P. Sharma, K.T. Pillai, A.K. Tyagi, "Ultrafine ceria powders via glycine-nitrate combustion", *Mater. Res. Bull.* 36 (15) (2001) 2711-2721.
- [264] V.R. Choudhary, A.M. Rajput, B. Prabhakar, A.S. Mamman, "Partial oxidation of methane to CO and H<sub>2</sub> over nickel and/or cobalt containing ZrO<sub>2</sub>, ThO<sub>2</sub>, UO<sub>2</sub>, TiO<sub>2</sub> and SiO<sub>2</sub> catalysts", *Fuel* 77 (15) (1998) 1803-1807.
- [265] V. Múčka, J. Podlaha, R. Silber, "NiO-ThO<sub>2</sub> mixed catalysts in hydrogen peroxide decomposition and influence of ionizing radiation", *Radiat. Phys. Chem.* 59 (5-6) (2000) 467-475.

## References

- [266] P. Balakrishna, B.N. Murty, K.P. Chakraborty, R.N. Jayaraj, C. Ganguly, "Special features in powder preparation, pressing, and sintering of uranium dioxide", *Mater. Manuf. Process.* 15(5) (2000) 679-693.
- [267] C.S. Morgan, K.H. McCorkle, G.L. Powell, "Sintering and desintering of thoria", In: Kuczynski G.C. (Eds.) *Sintering and Related Phenomena*. Materials Science Research, Vol. 6, Springer, Boston, MA (1973).
- [268] J.M. Pope, K.C. Radford, "Physical properties of some thoria powders and their influence on sinterability", *J. Nucl. Mater.* 52 (1974) 241-254.
- [269] Z. Chen, J. Mabon, J. Wen, R. Trice, "Degradation of plasma-sprayed yttria-stabilized zirconia coatings via ingress of vanadium oxide", *J. Eur. Ceram. Soc.* 29(9) (2009) 1647-1656.
- [270] M.A. Delfrate, J. Lemaitre, V. Buscaglia, M. Leoni, P. Nanni, "Slip casting of submicron BaTiO<sub>3</sub> produced by low-temperature aqueous synthesis", *J. Eur. Ceram. Soc.* 16(9) (1996) 975-984.
- [271] T.K. Gupta, R.L. Coble, "Sintering of ZnO: II, density decrease and pore growth during the final stage of the process", *J. Am. Ceram. Soc.* 51 (9) (1968) 525-528.
- [272] C.-H. Chang, J.F. Rufner, K.V. Benthem, R.H.R. Castro, "Design of desintering in tin dioxide nanoparticles", *Chem. Mater.* 25(21) (2013) 4262-4268.
- [273] P. Duran, J. Tartaj, C. Moure, "Sintering behaviour and microstructural evolution of agglomerated spherical particles of high-purity barium titanate", *Ceram. Int.* 29(4) (2003) 419-425.
- [274] C.-Y. Tsao, W.-H. Tuan, K.-C. Feng, "De-sintering of Ba<sub>5</sub>Nb<sub>4</sub>O<sub>15</sub> ceramic and its influence on microwave characteristics", *J. Eur. Ceram. Soc.* 37(4) (2017) 1517-1521.
- [275] Cs. Balázs, F.S. Cinar, O. Addemir, F. Wéber, P. Arató, "Manufacture and examination of C/Si<sub>3</sub>N<sub>4</sub> nanocomposites" *J. Eur. Ceram. Soc.* 24(12) (2004) 3287-3294.

- [276] R. Besler, M.R. da Silva, J.J. do Rosario, M. Dosta, S. Heinrich, R. Janssen, “Sintering simulation of periodic macro porous alumina”, *J. Am. Ceram. Soc.* 98(11) (2015) 3496-3502.
- [277] K. Ananthasivan, S. Anthonysamy, A. Singh, P.R. Vasudeva Rao, “De-agglomeration of thorium oxalate - A method for the synthesis of sinter active thoria”, *J. Nucl. Mater.* 306 (1) (2002) 1-9.
- [278] R.H.R. Castro, “Controlling sintering and grain growth of nanoceramics”, *Cerâmica* 65 (373) (2019) 122-129. **[278a]** Thermodynamics of sintering, R.M. German, *Sintering of advanced materials: Fundamentals and processes* (Ed.: Z.Z. Fang) Woodhead Publishing Ltd. (2010), ISBN 978-1-84569-562-0. **[278b]** G.S. Upadhyaya, *Sintered metallic and ceramic Materials*, John Wiley & Sons Ltd. (1999) ISBN 0-471-98155-9.
- [279] O. Sudre, F.F. Lange, “The effect of inclusions on densification; III, The desintering phenomenon”, *J. Am. Ceram. Soc.* 75 (12) (1992) 3241-3251.
- [280] F. Li, J. Pan, A. Cocks, “Defect healing and cracking in ceramic films during constrained sintering” *J. Am. Ceram. Soc.* 95(12) (2012) 3743-3749.
- [281] S. Knight, R. Korlacki, C. Dugan, J.C. Petrosky, A. Mock, P.A. Dowben, J. Matthew Mann, M.M. Kimani, M. Schubert, “Infrared-active phonon modes in single-crystal thorium dioxide and uranium dioxide”, *J. Appl. Phys.* 127 (2020) 125103.

## CHAPTER 5

### Thermophysical studies on thorium-uranium-zirconium

#### (Th-U-Zr) ternary metallic alloys

---

##### 5.1. Introduction

In chapter-4, temperature dependent thermophysical properties of two Th-U binary alloys namely, Th-10U and Th-20U (wt. %), which are potential fuels for nuclear reactors, have been discussed in detail. Results shown in chapter-4 have confirmed that as compared to uranium-based metallic alloy fuels (U-10Zr, U-19Pu-10Zr, etc.), studied Th-U binary alloys have superior properties in terms of dispersion type fuel microstructure in isotropic FCC thorium matrix, lower values of thermal expansion coefficients and specific heat capacities, and higher thermal conductivity over the studied temperature range (298 K – 1373 K). In case of uranium-based metallic alloy nuclear fuels, it is known that addition of zirconium (up to 10 wt. %) benefits in terms of increasing fuel's solidus (melting) temperature as well as enhancing the fuel-clad interaction (FCCI and FCMI) resistance [44, 45]. Beyond 10 wt. % zirconium addition, fuel's solidus temperature increases more than the softening temperature of the fused quartz moulds that are used for vacuum injection casting of uranium-based metallic fuels and pose additional fuel fabrication challenges. For Th-U binary alloys, due to higher melting temperature of thorium (~2023 K), solidus temperatures of thorium-rich alloys are sufficiently higher (> 1500 K) [59], which enable safe fuel irradiation at high temperatures. Even Th-20U-10Pu ternary alloy (wt. %), which is a candidate fast reactor fuel possesses sufficiently higher solidus temperatures (> 1160 K) [206]. As long as Th-U alloy microstructure remains truly dispersion type (i.e., uniform distribution of small isolated uranium metal phase in bulk thorium matrix; typically observed up to 10 wt. % U),

fuel's swelling would be lower as compared to U-Zr or U-Pu-Zr alloys. It is to be noted here that swelling occurs due to thermal expansion, accommodation of fission products, accumulation of fission gas bubbles and microstructural changes due to thermal cycling. In view of higher solidus temperature and lower swelling behavior, Th-U alloys are inherently superior to U-Zr and U-Pu-Zr alloys. Also, zirconium addition is not required for increasing the solidus temperature. However, zirconium addition may improve the resistance towards fuel-clad interaction, in case fuel comes in contact with clad surface. On the other hand, for potential applications of thorium-uranium alloy fuels in thermal (or epithermal) spectrum nuclear reactors, where zirconium-based cladding materials are most commonly used with water as the primary coolant, it is necessary to understand Th-U alloy fuel interaction with zirconium-based cladding materials and, fuel's corrosion behavior in high temperature-high pressure water (steam) in case of any event of clad breach. It has been reported that zirconium addition ( $\sim 5-10$  wt. %) in thorium increases the resistance of Th-Zr alloys towards high temperature aqueous corrosion by five to six times as compared to unalloyed thorium [207]. Zirconium has very small neutron absorption cross-section ( $\sim 0.006$  barns) and does not hamper the neutron economy in any way. Th-U-Zr alloys can therefore be used as fuel for thermal breeder reactors [37]. For uranium containing Th-Zr alloys, adequate resistance towards aqueous corrosion has been reported up to 9 wt. % uranium [207]. For fast reactor fuels, addition of zirconium in Th-U alloys is not likely to bring significant advantages in terms of solidus temperature. At the same time, it is not a disadvantage also. For lower concentrations of zirconium ( $< 5-10$  wt. %), the loss in heavy metal (actinide) fraction in Th-U-Zr ternary alloys can be compensated by increasing the uranium enrichment or by using slightly higher fractions of uranium. Zirconium also has higher solubility ( $\sim 3$  wt. % at  $\sim 673$  K) in thorium than in uranium ( $\sim 0.2$  wt. % at  $\sim 663$  K), and it increases with temperature [208, 209]. As a result, thorium-rich Th-U-Zr ternary alloys are likely to have phase

distribution with more zirconium in FCC thorium phase than zirconium in  $\alpha$ -uranium (orthorhombic) as is the case of U-Zr alloys. Microstructures of these ternary alloys would also be different than their binary component systems (Th-U, Th-Zr, U-Zr), which would affect the thermophysical properties. In view of this, Th-U-Zr ternary alloys with low Zr fraction ( $< 10$  wt. %) is worth investigating as these can be potential nuclear fuels. There are very few studies on alloys based on Th-U-Zr ternary system. Carlson has reported experimental phase relations in Th-U-Zr ternary system over wide composition range [210] while Li et al., [79] reported phase equilibrium and thermodynamic parameters using computational thermodynamics. Neutron irradiation behavior of zircaloy clad Th-2.5U-1Zr alloy (wt.%; highly enriched uranium) in thermal reactors has been reported by Goffard et al., [211]. Their results indicated burn-up potential of these alloys up to 3 atom %. Th-U-10Zr alloys (wt. %) have also been proposed as potential fuel for sodium cooled CANDU (Constant Axial shape of Neutron flux, nuclide densities and power shape During Life of Energy production) burning reactors [212]. High temperature thermophysical properties of these alloys are not available in open literature. With this objective, phase characterization and evaluation of high temperature thermophysical properties have been carried out for two representative alloys, namely, Th-3U-7Zr and Th-7U-3Zr (in wt. %) prepared by arc-melting technique. Effect of thermal cycling on thermal diffusivity of as-cast alloys has also been studied and the results are presented in this chapter.

## 5.2. Experimental

Two alloys with nominal composition Th-3U-7Zr and Th-7U-3Zr (in wt. %) were prepared by DC arc melting technique using nuclear-grade thorium, uranium and zirconium metals under inert atmosphere. As-melted alloy ingots were machined in the form of small pellets using mechanical lathe under continuous flow of lubricant (machine oil) over the alloy

surface. These alloys and constituent metals were handled inside argon filled glove box for cutting, surface cleaning, polishing, etc. Both the alloys as well as constituent metals were phase characterized by X-ray diffraction technique. Microstructures of as-melted alloys were studied by optical and scanning electron microscopic (SEM) techniques. Characterization of oxide inclusions ( $\text{ThO}_2$  /  $\text{ZrO}_2$ ) in studied alloys was performed by micro-Raman spectroscopy using He-Ne laser (632.8 nm; ~15 mW maximum energy) as the excitation source. Elemental analysis was performed using energy dispersive spectroscopy (EDS) technique attached with SEM unit. Thermal diffusivity of as-melted alloys were measured by laser flash technique over a temperature range from 298 K to 1273 K under dynamic vacuum conditions ( $P < 3 \times 10^{-5}$  Torr). Effect of thermal cycling on thermal diffusivity of Th-U-Zr alloys was studied by measuring the thermal diffusivity of both alloys over repeated thermal cycles with re-polishing the sample after each cycle. Linear thermal expansion of thermally cycled alloy specimen was measured using thermo mechanical analyzer (TMA) over a temperature range from 308 K to 1273 K. Thermal conductivity was estimated using measured thermal diffusivity, temperature dependent density (evaluated from thermal expansion data) and reported specific heat capacities of constituent metals.

### **5.3. Results and discussion**

#### **5.3.1. Phase characterization of ternary alloys**

Figure 5.1 show the optical micrographs recorded over well polished surface of as-melted Th-7U-3Zr and Th-3U-7Zr alloys. These micrographs were recorded using the optical microscope attached with laser Raman spectrometer and sample surface was illuminated with halogen lamp. Back scattered electron images of thorium and uranium metals that were used for alloy preparation are also shown.

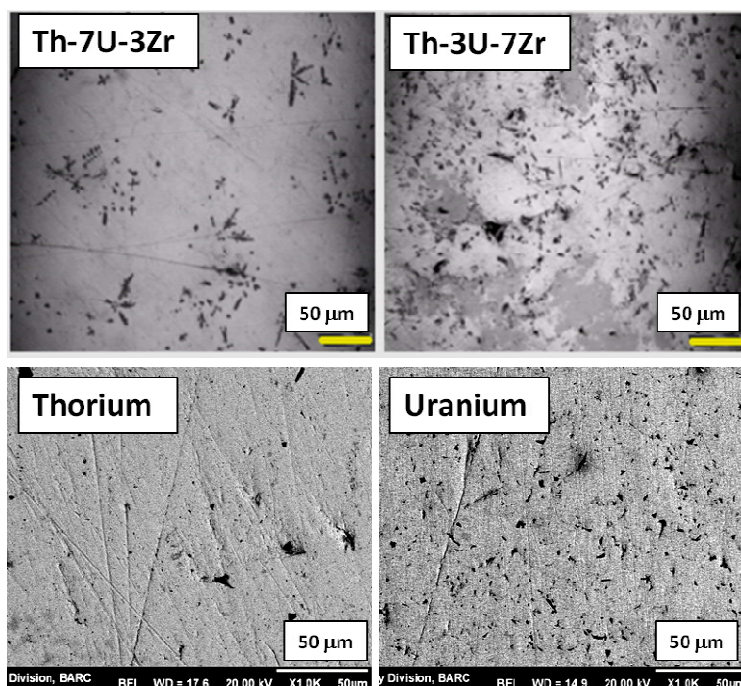


**Fig. 5.1. Optical micrographs of as-melted Th-7U-3Zr and Th-3U-7Zr (wt. %) alloys. Representative back scattered electron (BSE) images of thorium and uranium metals used for preparation of ternary alloys are also shown**

Optical micrographs shown in Fig. 5.1 indicate that both as-melted alloys have randomly distributed dark coloured inclusions, which are distributed in the form of dendritic precipitates. Similar inclusions with dendritic morphology were also seen in Th-U binary alloys studied by us. Back scattered electron images of thorium and uranium metals do not show such inclusions, although, dark regions distributed in electron micrographs of thorium show pores created during surface grinding / polishing and those in uranium shows carbon inclusion, which was confirmed by EDS analysis. No such inclusions were also seen in optical micrographs of high purity zirconium metal (> 99.99 %). Optical micrograph of alloy containing 7 wt. % zirconium shows grey-shaded phase. These results indicate that dendritic inclusions might have formed in during arc-melting of alloys. In order to identify the phases formed in as-melted alloys and to characterize these dendritic inclusions, XRD studies were carried out on polished alloy samples. Results of XRD analysis are discussed now.

X-ray diffraction patterns of as-melted Th-7U-3Zr and Th-3U-7Zr alloys, recorded at ambient temperature are shown in Fig. 5.2. Corresponding patterns for thorium, uranium and zirconium, which were used to prepare these alloys, are also shown for comparison. Diffraction peak positions (in terms of  $2\theta$  values) reported for orthorhombic  $\alpha$ -uranium [167], FCC  $\alpha$ -thorium [201] and HCP  $\alpha$ -zirconium [213] are indicated in the plot.

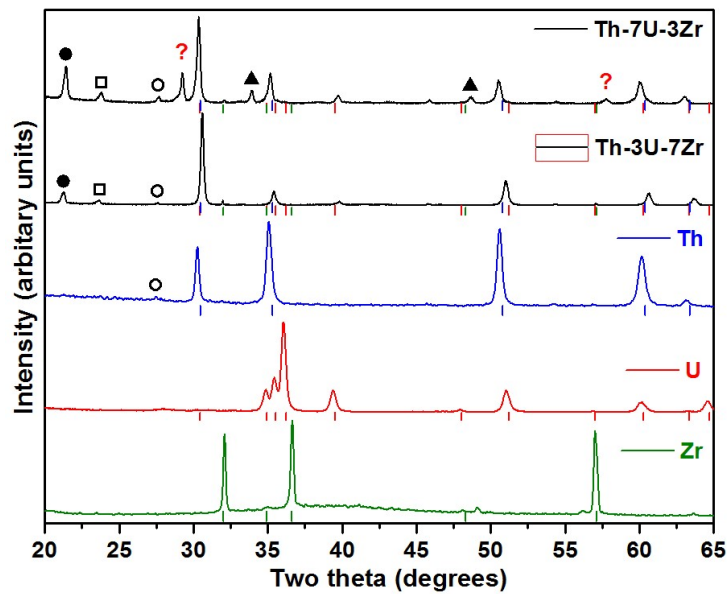


**Fig. 5.2. Ambient temperature XRD patterns of Th-3U-7Zr and Th-7U-3Zr alloys and constituent elements (Th, U and Zr). Reported diffraction peak positions for ambient temperature allotropes of Th [167], U [201] and Zr [213] also indicated. Symbols have following meaning: • ( $U_3O_8$ ); □ ( $U_{0.67}Zr_{0.33}O_{2.33}$ ); ○ ( $ThO_2$ ); ▲ ( $Th_{0.33}Zr_{0.67}$ )**

Diffraction patterns of both ternary alloys show all major peaks corresponding to FCC thorium metal, which is the major matrix (90 wt. %). Apart from that, diffraction peaks due to (111) plane of uranium ( $2\theta \sim 39.54^\circ$ ; which is not overlapping with any of thorium metal diffraction peaks) and (110) plane of hexagonal zirconium ( $2\theta \sim 31.96^\circ$ ) can also be seen. Other peaks due to orthorhombic uranium lattice are mostly overlapping with those of

thorium, as revealed by the relative broadening of thorium peaks in both the alloys. Peak due to (111) plane of FCC thorium phase ( $2\theta \sim 30.26^\circ$ ) is shifted to higher angles for Th-7U-3Zr alloy ( $2\theta \sim 30.42^\circ$ ) and Th-3U-7Zr ( $2\theta \sim 30.58^\circ$ ). This can be attributed to formation of solid solution of zirconium into thorium [208] where incorporation of smaller zirconium atoms (atomic radius  $\sim 160$  pm) into thorium lattice (atomic radius  $\sim 240$  pm) causes net lattice shrinkage, leading to shift in diffraction peak towards higher angles with increasing zirconium concentration. Slight solubility of uranium into thorium ( $\sim 0.2$  wt. % at 673 K) is also expected as per Th-U binary phase diagram [209], which also would lead to thorium XRD peaks shift towards higher angles. Presence of  $\text{ThO}_2$  impurity phase ( $2\theta \sim 27.64^\circ$ ; indicated by symbol 'o') is also seen in both ternary alloys as well as thorium metal.  $\text{ThO}_2$  impurity comes from higher oxygen impurity in thorium metal ( $\sim 2000$  ppm) as discussed earlier in chapter-3.

Apart from diffraction peaks due to constituent metals, some additional peaks are also observed. These are positioned at  $2\theta$  values  $\sim 21.42^\circ$  (symbol '•'),  $\sim 23.76^\circ$  (symbol '□'),  $\sim 29.20^\circ$  and  $\sim 57.76^\circ$  (both shown as '?') and,  $33.92^\circ$  and  $48.64^\circ$  (both shown by symbol '▲') as shown in Fig. 2. These peaks correspond to new phases present in as-melted ternary alloys. Intensities of these peaks are higher for Th-7U-3Zr alloy as compared to Th-3U-7Zr, which indicate a possible role of uranium concentration in the origin of these peaks. Based on phase behavior of binary components as reported in Th-U, Th-Zr and U-Zr phase diagrams, attempt was made to identify the origin of these additional diffraction peaks. During arc-melting process, molten alloys are cooled rapidly upon stopping the arc. Therefore, one may expect quenching of high temperature allotropic phases in as-melted alloys. Observed additional peaks however did not match with those reported for high temperature allotropes of individual metals namely,  $\beta$ -uranium (tetragonal;  $2\theta \sim 34.36^\circ, \sim 37.96^\circ$ ),  $\gamma$ -uranium (BCC;  $2\theta$

~ 35.96°, ~ 51.70°),  $\beta$ -thorium (BCC;  $2\theta \sim 30.76^\circ, \sim 54.70^\circ$ ) and  $\beta$ -zirconium (BCC;  $2\theta \sim 35.58^\circ, \sim 63.90^\circ$ ). Th-U [59] and Th-Zr [208, 79] binary system also do not show any line compound. Th-Zr system shows relatively higher Zr solubility in thorium lattice, which has been seen in terms of shift of diffraction peaks towards higher angles. U-Zr Binary phase diagram indicates formation of U-Zr solid solution (BCC) at high temperatures and  $\text{UZr}_2$  phase [209]. Reported diffraction pattern of  $\text{UZr}_2$  (hexagonal;  $2\theta \sim 28.90^\circ, \sim 35.70^\circ, \sim 20.38^\circ$ ) also did not match with observed additional peaks in Th-U-Zr ternary alloys. These peaks matched well with principal reflections reported for  $\text{U}_3\text{O}_8$  ( $2\theta = 21.42^\circ$  and  $33.96^\circ$ ; [214]),  $\text{U}_{0.67}\text{Zr}_{0.33}\text{O}_2$  ( $2\theta = 23.66^\circ, 28.66^\circ$  [215]), and  $\text{Th}_{0.33}\text{Zr}_{0.67}$  ( $2\theta = 33.86^\circ, 48.66^\circ$ ; [216]) Peaks ~ 29.20° and ~ 57.76° (both marked with symbol ‘?’) could not be exactly matched with any reported phase. Formation of oxides of uranium is possible during arc-melting process, if oxygen is present in the cover gas. High reactivity of both, uranium and zirconium with oxygen at elevated temperatures (molten form during arc-melting) also favours oxidation of these metals. For purification of inert gases, both uranium and zirconium were used as excellent oxygen getters, particularly at high temperatures ( $T > 600$  K). Intensity of diffraction peak at  $2\theta \sim 21.42^\circ$  increases for alloy containing higher uranium concentration, which suggests uranium oxide formation. Dark colours of dendritic inclusions seen in optical micrographs (Fig. 5.1) also suggest presence of uranium oxides, which are typically dark green to black in colour. To further characterize these inclusions, Raman spectroscopic analysis was performed on as-melted alloys. These results are discussed as follows.

Figure 5.3 show Raman spectra recorded on polished surface of Th-3U-7Zr alloy. Optical micrographs showing the regions over which different Raman spectra were recorded are also shown in the inset of this figure. Spectra recorded on white (S-1) and grey regions (S-2) do not show any Raman band / peak, which is typical of metallic alloy phase. White and grey

regions could be different immiscible metallic phases in these multi-phase composite alloy systems, identification of which is not possible by Raman spectroscopy.

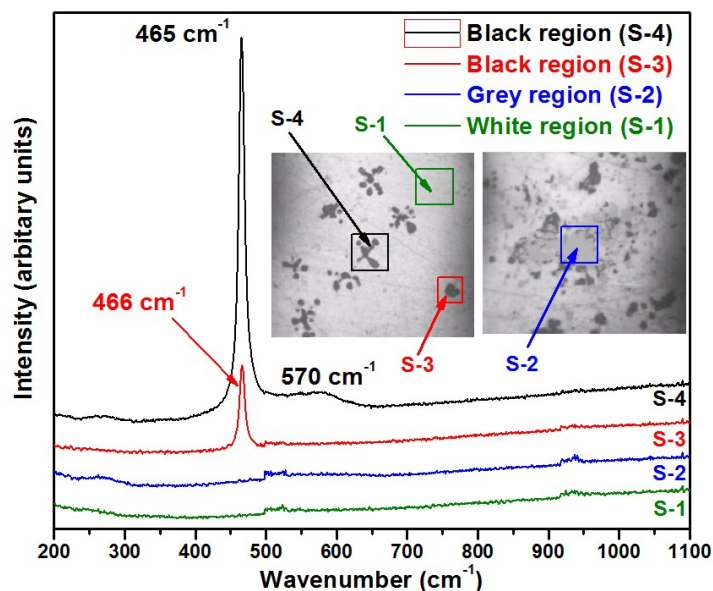


**Fig. 5.3. Raman spectra corresponding to different regions of Th-3U-7Zr ternary alloy (polished surface); recorded at ambient temperature. Different regions in optical micrographs of alloy, over which Raman spectra were acquired, are shown in the inset**

On the other hand, Raman spectra recorded on dark inclusions show sharp peak located at  $\sim 465 \text{ cm}^{-1}$ . Both, isolated inclusions (S-3) as well as dendritic inclusions (S-4) showed sharp Raman peak. Spectrum recorded on dendritic inclusions also show a weak high energy Raman band centred around  $570 \text{ cm}^{-1}$ . Raman peak observed in dendritic regions is relatively broad and asymmetric in nature. A sharp Raman peak  $\sim 465 \text{ cm}^{-1}$  is characteristic of  $F_{2g}$  vibrational modes of fluorite structured bulk  $\text{ThO}_2$  [174]. In case of  $\text{UO}_2$ , this mode is observed at  $\sim 445 \text{ cm}^{-1}$ , however, pure  $\text{UO}_2$  is characterized by a sharp Raman peak (2LO mode)  $\sim 1145 \text{ cm}^{-1}$  [217]. Similar to the broad band ( $\sim 570 \text{ cm}^{-1}$ ) observed in Raman spectrum of dendritic inclusions in studied ternary alloy, a broad Raman band has been reported for  $(\text{Th}_{0.80}\text{U}_{0.20})\text{O}_2$  mixed oxide solid solutions [174]. Similar LO phonon band ( $\sim 570 \text{ cm}^{-1}$ ) has

also been reported for hyper-stoichiometric  $\text{UO}_{2+x}$  and attributed to structural defects in fluorite lattice [218]. Raman spectroscopic studies on  $\text{UO}_2\text{-ZrO}_2$  solid solutions are not reported in literature. Asymmetry at the lower wave number end of  $\text{F}_{2g}$  vibrational peak has also been reported for  $(\text{Th-U})\text{O}_2$  solid solutions [174]. Observed Raman results do not match with those reported for pure oxides of uranium ( $\text{UO}_2$ ,  $\text{UO}_3$ ,  $\text{U}_4\text{O}_9$  and  $\text{U}_3\text{O}_8$ ) [217], zirconium (monoclinic- $\text{ZrO}_2$ , tetragonal- $\text{ZrO}_2$ , cubic/stabilized  $\text{ZrO}_2$ ) [219] and  $\text{ThO}_2\text{-ZrO}_2$  solid solutions [220]. From these results, the observed inclusions in Th-U-Zr ternary alloys were attributed to the presence of thoria-rich oxides having structural defects as well as uranium inclusion. Spectra observed with and without the high wave number broad Raman band ( $\sim 570 \text{ cm}^{-1}$ ), as shown in Fig. 5.3 (spectrum S-3 and S-4), indicate that during arc-melting,  $\text{ThO}_2$  impurity phase present in thorium metal may undergo solid-state reaction with uranium / zirconium in the molten alloy and form such solid solutions. Presence of air in cover gas during arc melting may also contribute towards formation of these inclusions in actinide alloys. Presence of  $\text{U}_3\text{O}_8$  phase, as suggested by XRD analysis (peak at  $2\theta \sim 21.42^\circ$ ; Fig. 5.2) could not be confirmed by Raman measurements. However, its formation by oxidation of uranium-rich phases during arc-melting (due to impure cover gas) or during the processing of alloys cannot be ruled out. Detailed characterization of such inclusions would require systematic EPMA analysis on highly polished and chemically etched alloys.

Figure 5.4 shows the SEM micrographs recorded on polished surface of as-melted Th-7U-3Zr and Th-3U-7Zr alloys at two different magnifications (1000 X and 5000 X). Th-7U-3Zr alloy shows uniform microstructure with well defined grains (Grey coloured background), sub-micron sized precipitates (bright spots) and dark inclusions (mostly due to oxide impurity phases). On the other hand, Th-3U-7Zr alloy shows a distinct morphology with semi-continuous phase (dark grey shaded) distributed around the grain interface regions. Unlike

Th-7U-3Zr alloy, sub-micron sized precipitates (bright spots) are not observed in micrographs of Th-3U-7Zr alloy. Dark inclusions are however seen here also.

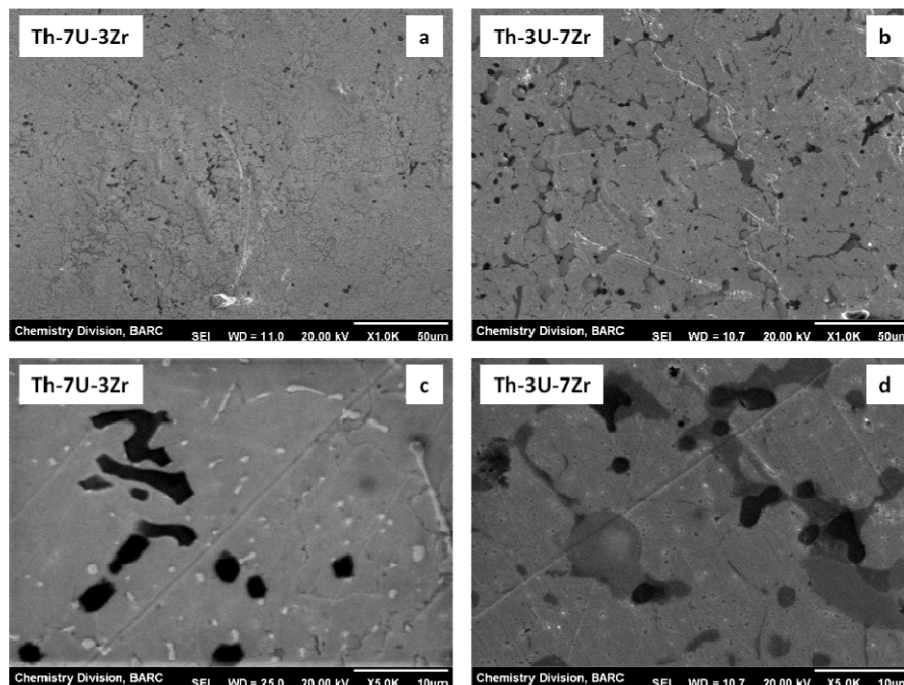
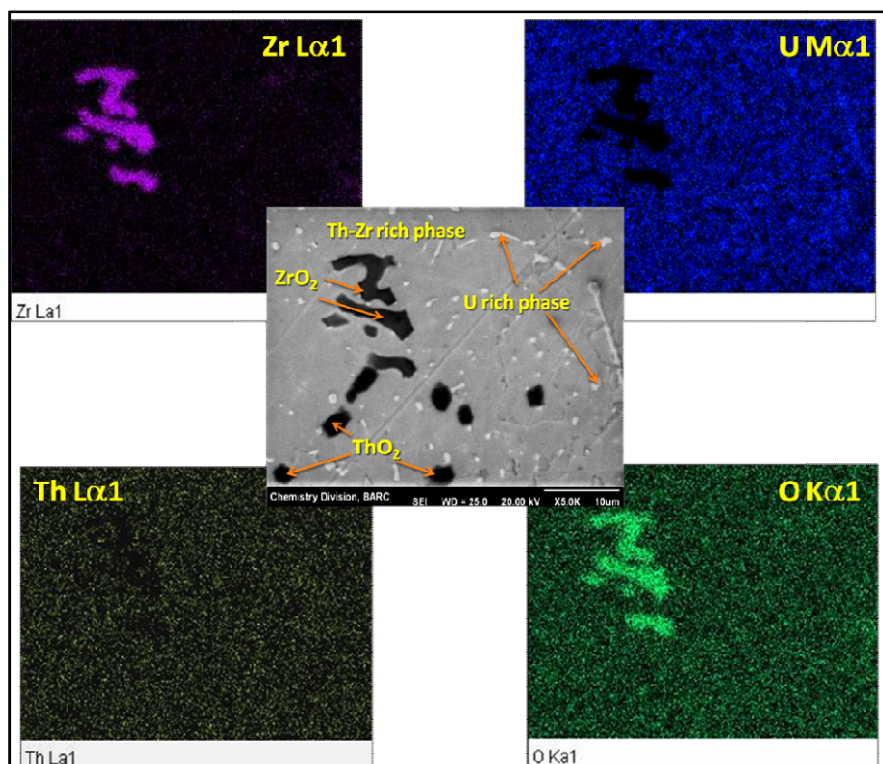


Fig. 5.4. SEM micrographs of (a, c) Th-7U-3Zr and (b, d) Th-3U-7Zr alloys

In case of Th-7U-3Zr alloy, uranium content is relatively higher. Also uranium has marginal solubility in thorium or zirconium at ambient temperature [59, 209]. Therefore, when arc-melted alloy solidifies upon cooling, the excess uranium phase precipitates in the form of finely dispersed phase, which is seen in the form of sub-micron sized bright spots in Fig. 5.4c. For Th-3U-7Zr alloy, since uranium fraction is lower and part of it is dissolved in thorium and zirconium matrix, clearly identifiable uranium phase is not observed in SEM micrographs (Fig. 5.4d). On the other hand, the semi-continuous phase observed in Th-3U-7Zr alloy could be attributed to Th-Zr or U-Zr phase. For elemental information on different phases seen in SEM micrographs, EDS analysis was performed. Fig. 5.5 shows the results of EDS analysis with elemental mapping on an electron micrograph of Th-7U-3Zr alloy (image

shown in Fig 5.4c). Results indicate that  $\text{ThO}_2$  and  $\text{ZrO}_2$ -based inclusions are present in these alloys, which might have come from base metal and formed during arc-melting.



**Fig. 5.5. Results of elemental mapping analysis on Th-7U-3Zr alloy**

Fine particles of uranium-rich metallic phase dispersed in base Th-Zr matrix could also be identified. Presence of zirconium dissolved in thorium matrix is also observed. Fig. 5.6 shows the EDS pattern recorded on different regions of the micrograph. Based on elemental compositions evaluated from EDS; phase identification has been carried out. Carbon and oxygen were not taken for quantification due to poor sensitivity of EDS detectors for light elements ( $Z < 11$ ). Apart from observation of uranium-rich metallic phase dispersed in Th-Zr alloy matrix, results of EDS analysis on Th-3U-7Zr alloy were comparable to those obtained of Th-7U-3Zr alloy.

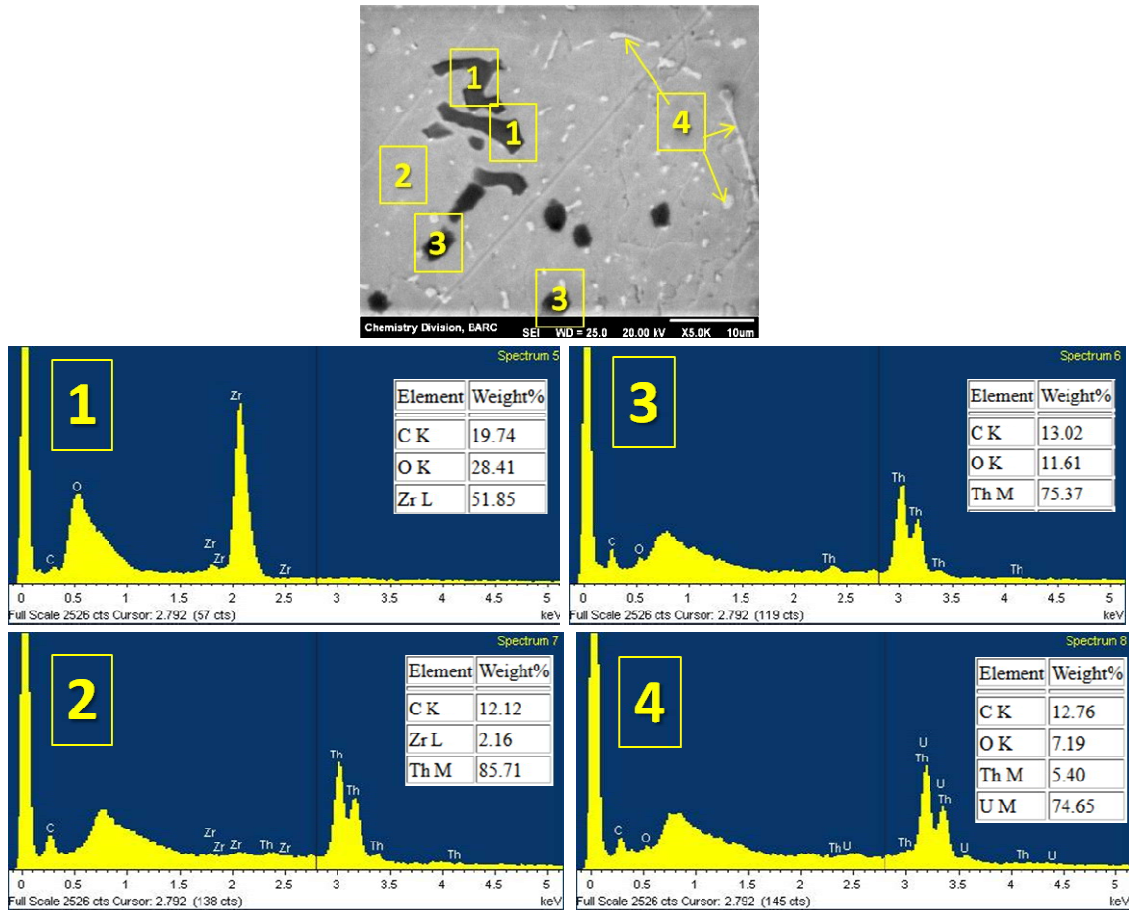


**Fig. 5.6. EDS patterns recorded from different regions of Th-7U-3Zr alloy, as marked in the electron micrograph image**

Results obtained from XRD, Raman, EDS and optical image analysis of both ternary alloys indicate (i) partial dissolution of zirconium into thorium, (2) dispersion of uranium phase into Th-Zr base alloy matrix, (3) presence of thorium-based oxides and  $ZrO_2$  inclusions. Thermophysical properties of these alloys were measured and results obtained are discussed in the following section.

### 5.3.2. Thermal diffusivity of Th-U-Zr ternary alloys

Thermal diffusivity of both, Th-3U-7Zr and Th-7U-3Zr alloys, measured over three successive repeat thermal cycles is shown in Fig. 5.7 (a) and 7(b), respectively. Alloy

samples were removed from the laser flash apparatus (LFA) after each thermal cycle (298 K  $\rightarrow$  1273 K  $\rightarrow$  298 K; dynamic vacuum;  $P < 3 \times 10^{-6}$  Torr), surface cleaned and polished using diamond paste ( $\sim 250$  nm particle size) under inert atmosphere until bright metallic lustre (as shown in the insets of Fig. 5.7(a) and 7(b)) was obtained. The polishing treatment ensured that any oxide layer formed over the alloy surface during high temperature thermal diffusivity measurements is removed. Results indicate notable variation in thermal diffusivity of both the alloys upon thermal cycling. Thermal diffusivity of as-melted alloys (Run-1) was always lower than the subsequent measurements on same sample.

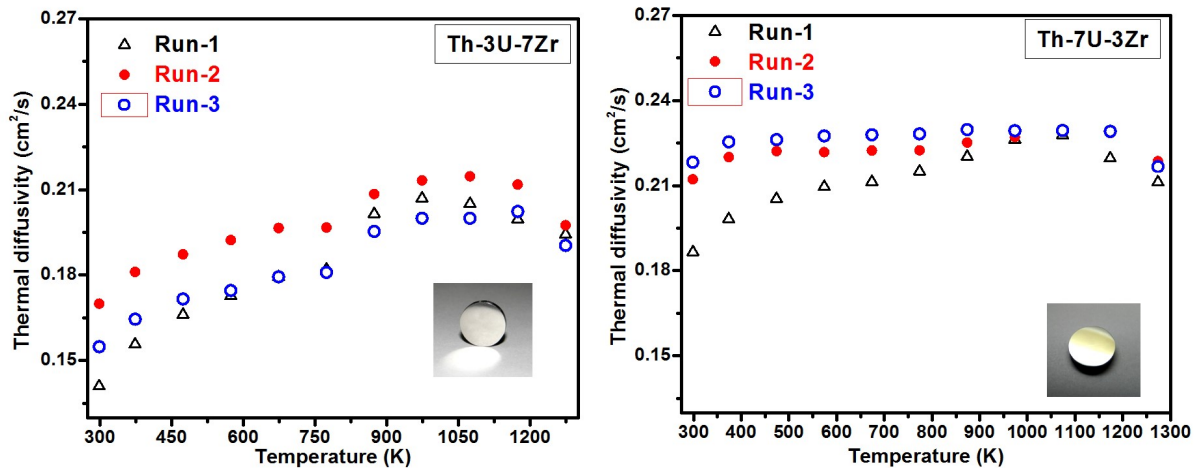


**Fig. 5.7. Thermal diffusivities of Th-3U-7Zr and Th-7U-3Zr alloys measured over three thermal cycles (298 K  $\rightarrow$  1273 K  $\rightarrow$  298 K)**

Variation in thermal diffusivity of Th-3U-7Zr alloy measured over three cycles is  $\sim 20\%$  at 298 K and  $\sim 5\%$  at 1273 K. Extent of diffusivity variation for Th-7U-3Zr alloys is  $\sim 17\%$  at 298 K and  $\sim 3\%$  at 1273 K. Increase in sample mass (due to surface oxidation) after any thermal cycle on both the alloy samples did not exceed  $\sim 0.0006$  wt. % (sample mass  $\sim 3.5$  g), which indicated reliable quality of diffusivity experiments. Variation in thermal diffusivity upon repeated thermal cycling can be attributed to phase homogenization of arc-

melted alloys, in which high temperature phases are mostly quenched during rapid cooling. Thorium-zirconium (Th-Zr) binary phase diagram [221] indicates various phase reactions over  $\sim 923$  K to  $\sim 1228$  K. During cooling of Th-Zr alloys, BCC solid solution of thorium and zirconium ( $\beta$ -Th,  $\beta$ -Zr) decomposes to HCP zirconium ( $\alpha$ -phase) and FCC thorium ( $\alpha$ -phase) phase at  $\sim 923$  K via eutectoid reaction. At  $\sim 1183$  K, BCC solid solution of thorium and zirconium ( $\beta$ -Th,  $\beta$ -Zr) transforms to BCC zirconium ( $\beta$ -phase) and FCC thorium ( $\alpha$ -phase) via monotectoid reaction. Similarly,  $\sim 1228$  K, a solid-solid miscibility gap (loop) is present with co-existing BCC thorium ( $\beta$ -phase) and BCC zirconium ( $\beta$ -phase) for a very narrow composition range. Also, zirconium solubility in FCC thorium ( $\sim 3$  wt. % at 298 K) increases with temperature and goes up to  $\sim 6$  wt. % at  $\sim 1173$  K. Occurrence of such phase reactions lead to microstructural variations in these alloys. Similar phase reactions occur in Th-U alloys also [59]. However, their equilibrium temperatures ( $> 1373$  K) are higher than the maximum temperature ( $\sim 1273$  K) up to which thermal diffusivity was measured in present investigation. U-Zr binary phase diagram also indicate various phase reactions over the temperature range 880 K to 966 K [209]. Upon repeated heating and cooling cycles, Th-U-Zr alloys pass through above mentioned phase reactions, which result into microstructural reorganization. Since heat transfer is dependent on microstructure of materials, thermal diffusivity of as-melted alloys is different from phase-equilibrated alloys obtained after repeated thermal cycling. These results indicate that even though metallic alloy nuclear fuels are usually fabricated from as-cast alloys, their thermophysical properties should always be evaluated on both as-cast as well as phase equilibrated samples so that appropriate margins can be included in fuel analysis codes and for safety assessment purpose of alloy fuels.

Figure 5.8 shows the thermal diffusivities of phase equilibrated ternary alloys obtained after six successive thermal cycles (298 K  $\rightarrow$  1273 K  $\rightarrow$  298 K). Diffusivity data obtained after six

thermal cycles were fully reproducible. Thermal diffusivities of thorium, uranium and Th-10 wt. % Zr binary alloys measured during present studies, and reported diffusivity data on zirconium [150] are also plotted in the same figure for comparison.

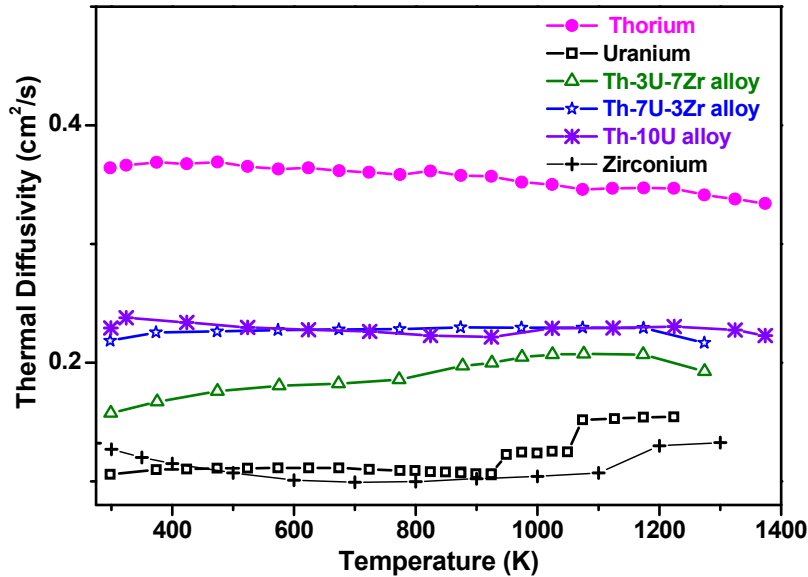


**Fig. 5.8. Thermal diffusivities of Th-3U-7Zr and Th-7U-3Zr alloys (298 K - 1273 K).**

**Thermal diffusivities of thorium, uranium, Th-10U alloy measured during present investigations and reported diffusivity data of zirconium [150] are also plotted**

It can be seen that thermal diffusivities of both ternary alloys (Th-3U-7Zr and Th-7U-3Zr) are higher than that of uranium metal, which is advantageous for their application as nuclear fuels. Both alloys show notable reduction in thermal diffusivity as compared to thorium metal, which can be attributed to multi-phase composite morphology of these alloys. Even though uranium and zirconium have comparable thermal diffusivities (especially at lower temperatures), thermal diffusivity of ternary alloy containing higher uranium concentration (Th-7U-3Zr) is higher than that of Th-3U-7Zr alloy. This can be attributed to presence of zirconium-rich phase in alloy containing higher zirconium concentration, which is present as semi-continuous network along the phase boundaries of thorium-rich matrix. Such

microstructure could cause scattering of heat carriers across the phase boundary regions and result into lower thermal diffusivity of Th-3U-7Zr alloys as compared to Th-7U-3Zr alloys. Relatively higher solubility of zirconium in thorium could also affect thermal diffusivity of ternary alloys. Another important observation from Fig. 5.8 is nearly comparable thermal diffusivities of Th-10 wt. % U binary alloy and Th-7U-3Zr alloys. Apart from different phases present in ternary alloys, oxide inclusions such as  $ZrO_2$  and  $ThO_2$ -based oxides, as observed in studied samples would also lower the net thermal diffusivity by impeding the movement of heat carriers. Thermal diffusivity data on studied ternary alloys are being reported for the first time. It may be noted that these results were used for thermal conductivity evaluation.

### 5.3.3. Linear thermal expansion of Th-U-Zr ternary alloys

Figure 5.9 shows the as-measured linear thermal expansion data for vacuum annealed Th-3U-7Zr and Th-7U-3Zr ternary alloys. Thermal expansion behavior of thorium, uranium and zirconium are also shown for comparison.

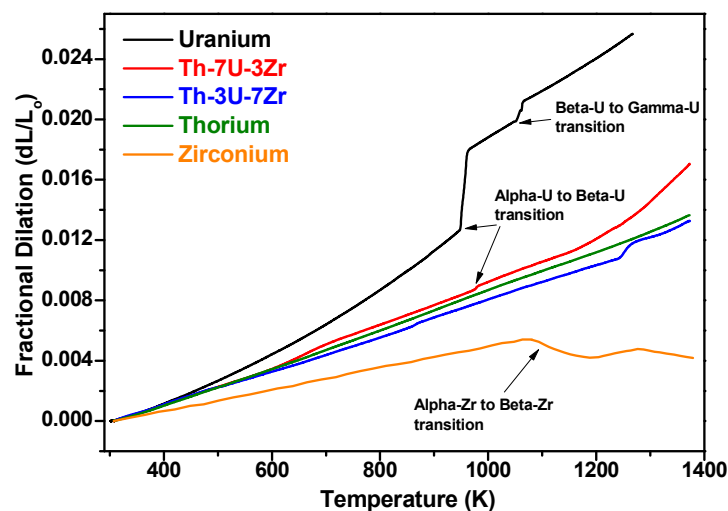


**Fig. 5.9. Linear thermal expansion of Th-3U-7Zr, Th-7U-3Zr ternary alloys and constituent metals (thorium, uranium and zirconium) (308 K – 1373 K)**

Thermal expansion of zirconium metal was measured by sandwiching the metal sample either between two graphite discs or two sintered thoria discs. Results obtained with ThO<sub>2</sub>-Zr-ThO<sub>2</sub> sandwich configurations were highly reproducible. A maximum weight gain of ~ 0.1 % was observed after four successive thermal cycles (298 K – 1373 K) in purified argon atmospheres, which indicated reliable quality of thermal expansion data. An expansion anomaly was observed for zirconium metal ~ 1135 K, which corresponded to its allotropic phase transition from HCP ( $\alpha$ -phase) to BCC ( $\beta$ -phase) [219]. Values of average coefficient of thermal expansion (CTE), as evaluated from linear dilation data are presented in Table 5.1.

**Table 5.1. Average coefficient of linear thermal expansion for Th-3U-7Zr, Th-7U-3Zr ternary alloys and constituent metals (Th, U and Zr) in different temperature intervals**

Sample	CTE	CTE	CTE	CTE
	(310 – 950 K) (( $\times 10^6$ K <sup>-1</sup> ))	(975 – 1050 K) (( $\times 10^6$ K <sup>-1</sup> ))	(1075 – 1273 K) (( $\times 10^6$ K <sup>-1</sup> ))	(310 – 1273 K) (( $\times 10^6$ K <sup>-1</sup> ))
<b>Thorium</b>	12.54	12.89	12.87	12.65
<b>Th-3U-7Zr</b>	11.65	12.07	10.95	11.57
<b>Th-7U-3Zr</b>	13.01	13.98	17.61	14.26
<b>Uranium</b>	19.71	22.23	22.30	26.84
<b>Zirconium</b>	7.18	7.18	---	7.20 (310 – 1100 K)

Thermal expansion of both ternary alloys is similar to that of thorium metal. Th-3U-7Zr alloy show lower expansion than thorium metal, which can be attributed to (i) higher solubility of Zr into thorium to form FCC Th<sub>1-x</sub>Zr<sub>x</sub> solid solution and (ii) lower thermal expansion of Zr (excess Zr remaining after solid solubility limit) as compared to Th and U. An expansion

anomaly was observed  $\sim 1248$  K for Th-3U-7Zr alloy, origin of which could not be identified. In case of Th-7U-3Zr alloy, thermal expansion is higher than that of thorium. Since uranium has limited solubility in thorium and zirconium at ambient temperatures, higher expansion of Th-7U-3Zr alloy could be attributed to presence of uranium-rich phase. Expansion anomaly due to orthorhombic to tetragonal ( $\alpha$  to  $\beta$ ) allotropic phase transition in uranium is also observed in the linear dilation curve (Fig. 5.9). Tetragonal to cubic ( $\beta$  to  $\gamma$ ) transition of uranium could not be seen, possibly due to small dilation anomaly associated with it.

At higher temperatures ( $> 1200$  K), slope of curve increases rapidly for Th-7U-3Zr alloy, which could also be due to higher expansion of uranium. Expansion anomaly related to zirconium's allotropic phase transition is not observed in both the alloys, which can be attributed to higher solubility of zirconium into thorium at higher temperatures. Relatively lower values of average coefficients of linear thermal expansion (Table 5.1) indicate lower swelling behavior of studied Th-U-Zr ternary alloys as compared to uranium. CTE of zirconium metal also matches with the reported data [222]. Thermal expansion results confirm that both ternary alloys have nearly isotropic expansion behavior and thermal expansion coefficients are lower than those observed for uranium-based metallic alloy fuels. Assuming isotropic polycrystalline nature of vacuum annealed ternary alloy samples, temperature dependence of their densities was calculated from ambient temperature density values and linear dilation behavior in a similar manner as detailed in chapter-3 (Section 3.3.5) using the following equation.

$$\rho(T) = M_T/V_T \quad (5.1)$$

Here, ' $M_T$ ' is sample mass and ' $V_T$ ' is sample volume at temperature ' $T$ '. ' $V_T$ ' is given as

$$V_T = V_{298\text{ K}} [1 + 3\{(L_T - L_{298\text{ K}})/L_{298\text{ K}}\}] \quad (5.2)$$

Figure 5.10 shows the densities of Th-U-Zr ternary alloys as a function of temperature along with that of uranium and thorium metals. Temperature dependent density zirconium is shown in the inset.

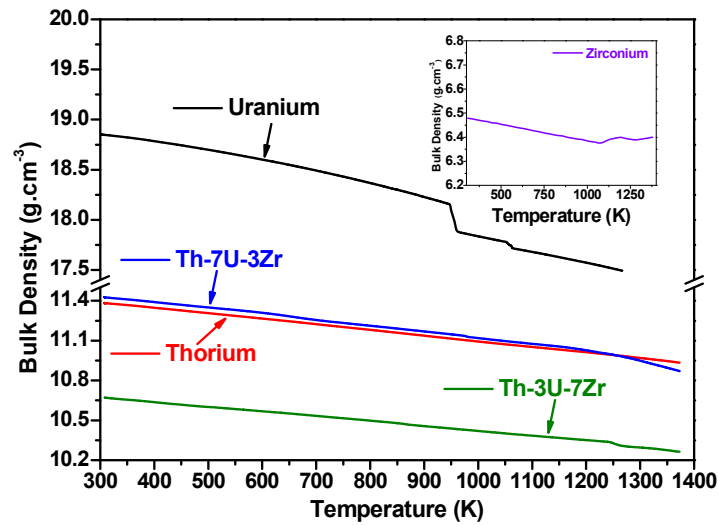


**Fig. 5.10. Variation of density as a function of temperature for Th-3U-7Zr, Th-7U-3Zr alloys along with that of Th and U metals. Inset shows the temperature dependent density for zirconium**

These results show that density of Th-7U-3Zr alloy ( $\sim 11.42 \text{ g.cm}^{-3}$ ; at 298 K) is comparable to that of thorium. Th-3U-7Zr alloy ( $\sim 10.67 \text{ g.cm}^{-3}$ ; at 298 K) has lower density than that of Thorium or Th-7U-3Zr alloy. Low density of both the ternary alloys can be attributed to low density of zirconium ( $\sim 6.48 \text{ g.cm}^{-3}$ ; at 298 K) as compared to thorium ( $\sim 11.4 \text{ g.cm}^{-3}$ ; at 298 K) or uranium ( $\sim 18.8 \text{ g.cm}^{-3}$ ; at 298 K). It is important to note that these densities are comparable to  $\text{ThO}_2$  ( $\sim 10 \text{ g.cm}^{-3}$ ; at 298 K),  $\text{UO}_2$  ( $\sim 10.96 \text{ g.cm}^{-3}$ ; at 298 K) and  $\text{PuO}_2$  ( $\sim 11.46 \text{ g.cm}^{-3}$ ; at 298 K), which are commonly used oxide ceramic fuel materials for thermal

spectrum nuclear reactors [12]. Mixed oxide (MOX) fuels such as (U,Pu)O<sub>2</sub>, (Th,U)O<sub>2</sub> and (Th,Pu)O<sub>2</sub> also have densities in the range from 10 to 11 g.cm<sup>-3</sup> at ambient temperatures. Such fuels usually show significant fission product retention capacity. For this reason as well as higher melting temperature of thorium, fission product induced swelling is likely to be lower in Th-U-Zr ternary alloys. Density values shown in Fig. 5.10 were used for evaluation of thermal conductivity of Th-U-Zr ternary alloys along with as-measured thermal diffusivity and specific heat values calculated from reported specific heat capacities of constituent metals.

#### 5.3.4. Thermal conductivity of Th-U-Zr ternary alloys

Based on results reported on thorium and uranium metals (chapter-3; section 3.3.6) as well as Th-U binary alloys (chapter-4; section 4.3.6), specific heat values measured by DSC technique in the present study are always found to be higher than reported values. Also, significant gain in samples weight was observed (up to 3 wt. %) during DSC measurements on constituent metals (Th and U) as well as Th-U binary alloys. In order to refrain from overestimation of thermal conductivity of Th-U-Zr ternary alloys, which is obtained by multiplying the specific heat with density and thermal diffusivity, specific heat data reported for thorium, uranium and zirconium were used for thermal conductivity calculation. Specific heat of ternary alloys was estimated by weighted average rule using the reported specific heat values of thorium, uranium and zirconium [157, 223]. Using these specific heat values, thermal conductivity was evaluated from equation-5.3.

$$\lambda(T) = D(T) \times \rho(T) \times C_p(T) \quad (5.3)$$

Where ' $\lambda(T)$ ', ' $D(T)$ ', ' $\rho(T)$ ' and ' $C_p(T)$ ' are thermal conductivity, thermal diffusivity, density and isobaric specific heat at temperature ' $T$ ', respectively. Results of thermal conductivity variation as a function of temperature are shown in Fig. 5.11.

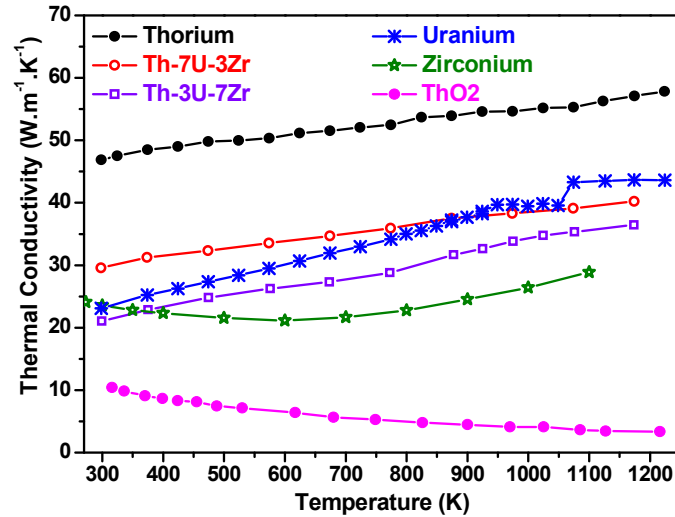


**Fig. 5.11. Temperature dependent thermal conductivity of Th-3U-7Zr and Th-7U-3Zr alloys, constituent metals (Th, U, Zr) and ThO<sub>2</sub> [224]**

These results show that thermal conductivity of both ternary alloys increases with temperature and is two to three times higher than that reported for high density (> 93 %) nuclear-grade thoria ceramics [224]. This is a significant advantage of ternary metallic alloys for their utilization as fuel in nuclear reactors. Thermal conductivity of both ternary alloys is significantly lower than that of thorium. This can be attributed to multi-phase nature of these alloys which consist of Th-rich matrix with zirconium as well as uranium dissolved in it, uranium-rich precipitates, zirconium-rich phase, oxide inclusions, etc. Such composite alloy would have additional scattering of heat carriers within the grains as well as phase boundaries. As a result, thermal conductivity of ternary alloys is significantly lower than that of thorium. Ternary alloy with higher uranium concentration (Th-7U-3Zr) have higher

thermal conductivity than alloy containing higher zirconium (Th-3U-7Zr). Even though both uranium and zirconium have comparable thermal conductivities ( $\sim 23 \text{ W.m}^{-1}\text{K}^{-1}$ ) at ambient temperature, higher extent of uranium incorporation in ternary alloys result into notably higher thermal conductivity. This can be attributed to nature of thermal conductivity variation with temperature for uranium and zirconium. While uranium's thermal conductivity continuously increases with temperature, for zirconium it first decreases up to  $\sim 700 \text{ K}$  and then increases marginally at further higher temperatures. A quantitative correlation of thermophysical properties with respect to microstructures of phase homogenized ternary alloys would help to further understand the observed variation in thermophysical properties and such studies are planned to be carried out in future.

#### 5.4. Conclusions

In present study, thermophysical properties of thorium-based ternary alloys namely, Th-3U-7Zr and Th-7U-3Zr (in wt. %) as a function of temperature (298 K – 1273 K) have been evaluated. Studies confirmed superior heat transport behavior of ternary alloy fuels in comparison to uranium-based metallic alloys as well as conventional thorium-based oxides. Thermal expansion behavior of the alloys indicates their potential to accommodate fission products to a higher extent as compared to uranium-based metallic alloy fuels. It has also been highlighted that preparation of such alloys in phase pure form with minimum contamination during alloy preparation / processing is very important step in development of metallic alloy fuels. These results will be useful for assessment of ternary alloys, which are potential fuel candidates for advanced nuclear reactors.

## References:

- [1] C. Degueudre, M.J. Joyce, “Evidence and uncertainty for uranium and thorium abundance: a review”, *Prog. Nucl. Energy* 124 (2020) 103299.
- [2] L.S. Keith, O.M. Faroon, B.A. Fowler, “Uranium (book chapter); handbook on the toxicology of metals: fourth edition (Eds: G.F. Nordberg, B.A. Fowler, M. Nordberg)”, Elsevier (2015) 1307-1345 (DOI: <https://doi.org/10.1016/C2011-0-07884-5>).
- [3] G. Sadagopan, K.S.V. Nambi, G. Venkataraman, V.K. Shukla, S. Kayasth, “Estimation of thorium in gas mantles to ascertain regulatory compliance”, *Radiat. Prot. Dosim.* 71(1) (1997) 53-56.
- [4] T.E. Leontis, “Properties of magnesium-thorium and magnesium-thorium-cerium alloys”, *J. Min. Metals Mater. Soc.* 4 (3) (1952) 287-294.
- [5] R.A. Glenner, P. Willey, P.S. Sledzik, E.P. Junger, “Dental fillings in civil war skulls: What do they tell us?”, *J. Am. Dent. Assoc.* 127(11) (1996) 1671-1677.
- [6] O. Hahn, F. Strassmann, “Über den nachweis und das verhalten der bei der bestrahlung des urans mittels neutronen entstehenden erdalkalimetalle (English translation: Concerning the existence of alkaline earth metals resulting from neutron irradiation of uranium)”, *Die Naturwissenschaften* 27 (1939) 11-15.
- [7] “The first reactor” The US department of energy report: DOE/NE-0046 (1982) 1-40 (Web-link: <https://www.energy.gov/ne/downloads/first-reactor>).
- [8] R.L. Crowther, “Use of thorium in boiling water reactors”, *J. Nucl. Energy AB* 16(4) (1962) 181-194.
- [9] J.R. Dietrich, “The physics of advanced reactors”, *Brit. J. Appl. Phys.* 7(S5) 302 (1956) S9-S23.
- [10] H.N. Sethna, “India’s atomic energy program: past and future”, *International Atomic Energy Agency (IAEA) Bulletin* 21 (5) (1979) 2-11.

## References

- [11] S. Banerjee, H.P. Gupta, “The evolution of the Indian nuclear power programme”, Prog. Nucl. Energy 101 (2017) 4-18.
- [12] International Atomic Energy Agency “Thorium fuel cycles - potential benefits and challenges”, IAEA-TECDOC-1450, IAEA, Vienna (2005) 1-105.
- [13] P.K. Wattal, “Back end of Indian nuclear fuel cycle - A road to sustainability”, Prog. Nucl. Energy 101 (2017) 133-145.
- [14] R. Natarajan, “Reprocessing of spent nuclear fuel in India: Present challenges and future programme”, Prog. Nucl. Energy 101 (2017) 118-132.
- [15] S.A. Ansari, P. Pathak, P.K. Mohapatra, V.K. Manchanda, “Aqueous partitioning of minor actinides by different processes” Sep. Purif. Rev. 40(1) (2011) 43-76.
- [16] M. Salvatores, “Nuclear fuel cycle strategies including partitioning and transmutation”, Nucl. Eng. Des. 235(7) (2005) 805-816.
- [17] Press Information Bureau, Government of India, “Setting up of ten indigenous nuclear power reactors” (Web-link: <http://pib.nic.in>)
- [18] S.C. Chetal, P. Chellapandi, P. Puthiyavinayagam, S. Raghupathy, V. Balasubramanian, P. Selvaraj, P. Mohanakrishnan, B. Raj, “Current status of fast reactors and future plans in India” Energy. Proced. 7 (2011) 64-73.
- [19] P. Puthiyavinayagam, P. Selvaraj, V. Balasubramanian, S. Raghupathy, K. Velusamy, K. Devan, B.K. Nashine, G.P. Kumar, K.V.S. Kumar, S. Varatharajan, P. Mohanakrishnan, G. Srinivasan, A.K. Bhaduri, “Development of fast breeder reactor technology in India”, Prog. Nucl. Energy 101 (Part A) (2017) 19-42.
- [20] Bharatiya Nabhikiya Vidyut Nigam Limited, Department of Atomic Energy “Present status of 500 MWe Prototype Fast Breeder Reactor (PFBR)”, (Web-link: <http://www.bhavini.nic.in>).

## References

- [21] P. Rodriguez, C.V. Sundaram, “Nuclear and materials aspects of the thorium fuel cycle”, *J. Nucl. Mater.* 100 (1981) 227-249.
- [22] R. Ramanna, S.M. Lee, “The thorium cycle for fast breeder reactors”, *Pramana* 27(1-2) (1986) 129-137.
- [23] R. Chidambaram, C. Ganguly, “Plutonium and thorium in the Indian nuclear programme”, *Curr. Sci. India* 70(1) (1996) 21-35.
- [24] P.K. Vijayan, V. Shivakumar, S. Basu, R.K. Sinha, “Role of thorium in the Indian nuclear power programme”, *Prog. Nucl. Energy* 101 (2017) 43-52.
- [25] “Thoria-based nuclear fuels: thermophysical and thermodynamic properties, fabrication, reprocessing, and waste management”, (Eds.: D. Das, S.R. Bharadwaj) Springer (2013) (DOI: 10.1007/978-1-4471-5589-8).
- [26] “Thorium-energy for the future”, (Eds.: A.K. Nayak, B.R. Sehgal), Springer (2019) (DOI: 10.1007/978-981-13-2658-5).
- [27] S. Mukherji, B.K. Mohan, P.D. Krishnani, V. Jagannathan, S. Ganesan, “Thorium irradiation in Indian PHWRs - applications and limitations of origin code”, *Proceedings of First National Conference in Nuclear Reactor Technology* (2002) (Web-link: [https://inis.iaea.org/search/search.aspx?orig\\_q=RN:34011468](https://inis.iaea.org/search/search.aspx?orig_q=RN:34011468)).
- [28] M. Das, “Design and irradiated experience with thorium based fuels in PHWRs” *Annual International Conference - Canadian Nuclear Association* (1992) 10.1-10.
- [29] P.S. Dhama, J.S. Yadav, K. Agarwal, “Power reactor thoria reprocessing facility (PRTRF), Trombay”, *Proceedings of the Theme Meeting on the Journey of BARC Safety Council for Strengthening Safety Culture in BARC Facilities* (Eds: V.M. Jolly) (2017) (Web-link: [https://inis.iaea.org/search/search.aspx?orig\\_q=RN:48089837](https://inis.iaea.org/search/search.aspx?orig_q=RN:48089837)).
- [30] R.K. Sinha, A. Kakodkar, “Design and development of the AHWR - the Indian thorium fuelled innovative nuclear reactor” *Nucl. Eng. Des.* 236 (7-8) (2006) 683-700.

- [31] R. Sinha, A. Kakodkar, "India's passive breeder", Nucl. Eng. Int. 55(668) (2010) 30-31.
- [32] A. Kakodkar, "Evolution of nuclear reactor containments in India: Addressing the present day challenges", Nucl. Eng. Des. 269 (2014) 3-22.
- [33] S. Sengupta, S.B. Chafle, S. Mammen, K. Sasidharan, V.K. Raina, "Critical facility for AHWR and PHWRs", Proceedings of International Conference on Peaceful uses of Atomic Energy (2009). V. 1. **[33a]** C. Ronchi, J.-P. Hiernaut, Experimental measurement of pre-melting and melting of thorium dioxide, J. Alloys Comp. 240 (1-2) (1996) 179-185. **[33b]** R. Böhler, A. Quaini, L. Capriotti, P. Cakir, O. Beneš, K. Boboridis, A. Guiot, L. Luzzi, R.J.M. Konings, D. Manara, "The solidification behavior of the UO<sub>2</sub>-ThO<sub>2</sub> system in a laser heating study" J. Alloys. Comp. 616 (2014) 5-13.
- [34] D. Greneche, W.J. Szymczak, J.M. Buchheit, M. Delpech, A. Vasile, H. Golfier, "Rethinking the thorium fuel cycle: An industrial point of view", Proceedings of ICAPP (Nice, France), (2007) Paper-7367. **[34a]** S.F. Ashley, G.T. Park, W.J. Nuttall, C. Boxall, R.W. Grimes, "Thorium fuel has risks", Nature 492 (2012) 31-33.
- [35] D. Jain, V. Sudarsan, A.K. Tyagi, "Thorium-based metallic alloys as nuclear fuels: Present status, potential advantages and challenges", SMC Bulletin (Society for Materials Chemistry, India) 4 (1) (2013) pp. 27-40 (Web-link: <https://www.smcindia.org/smc-bulletin.php>).
- [36] P.K. Vijayan, A. Basak, I.V. Dulera, K.K. Vaze, S. Basu, "Conceptual design of Indian molten salt breeder reactor", Pramana - J. Phys. 85 (2015) 539-554.
- [37] T. Yamamoto, H. Suwarno, H. Kayano, M. Yamawaki, "Development of new reactor fuel materials: Hydrogen absorption properties of U-Th, U-Th-Zr and U-Th-Ti-Zr alloys", J. Nucl. Sci. Tech. 32(3) (1995) 260-262.

## References

- [38] K.A. Terrani, G.W.C. Silva, C.B. Yeamans, "Fabrication and characterization of uranium thorium zirconium hydride fuels", *Trans. Am. Nucl. Soc.* 98 (2008) 1060-1061.
- [39] S.M. McDeavitt, T.J. Downar, A.A. Solomon, S.T. Revankar, M.C. Hash, A.S. Hebden, "Thoria-based cermet nuclear fuel: Cermet fabrication and behavior estimates", *Proc. Int. Conf. Nucl. Eng. (ICONE 4)* (2002) 59-67.
- [40] C. Lombardi, L. Luzzi, E. Padovani, F. Vettrano, "Thoria and inert matrix fuels for a sustainable nuclear power", *Prog. Nucl. Energy* 50(8) (2008) 944-953.
- [41] J. Spino, H.S. Cruz, R. Jovani-Abril, R. Birtcher, C. Ferrero, "Bulk-nanocrystalline oxide nuclear fuels - An innovative material option for increasing fission gas retention, plasticity and radiation-tolerance", *J. Nucl. Mater.* 422 (1-3) (2012) 27-44.
- [42] H. György, S. Czifrus, "The utilization of thorium in generation IV reactors", *Prog. Nucl. Energy* 93 (2016) 306-317.
- [43] D. Heuer, E. Merle-Lucotte, M. Allibert, M. Brovchenko, V. Ghetta, P. Rubiolo, "Towards the thorium fuel cycle with molten salt fast reactors", *Ann. Nucl. Energy* 64 (2014) 421-429.
- [44] G.L. Hofman, L.C. Walters, T.H. Bauer, "Metallic fast reactor fuels", *Prog. Nucl. Energy* 31(1-2) (1997) 83-110.
- [45] W.J. Carmack, D.L. Porter, Y.I. Chang, S.L. Hayes, M.K. Meyer, D.E. Burkes, C.B. Lee, T. Mizuno, F. Delage, J. Somers, "Metallic fuels for advanced reactors", *J. Nucl. Mater.* 392 (2) (2009) 139-150.
- [46] Idaho National Laboratory, "Experimental breeder reactor-I (EBR-I) (Web-link: <https://inl.gov/experimental-breeder-reactor-i/>).
- [47] L.C. Walters, "Thirty years of fuels and materials information from EBR-II", *J. Nucl. Mater.* 270(1) (1999) 39-48.

- [48] K. D. Weaver, J. Gilleland, C. Whitmer, G. Zimmerman, “High burn-up fuels for fast reactors: past experience and novel applications”, International Congress on Advances in Nuclear Power Plants (ICAPP 2009) (2009) 795.
- [49] G. Locatelli, M. Mancini, N. Todeschini, “Generation IV nuclear reactors: Current status and future prospects”, *Energ. Policy* 61 (2013) 1503-1520.
- [50] Z.S. Takibaev, “Fast homogeneous nuclear reactor”, *Atom. Energy* 100 (2006) 154-156.
- [51] T. Jayakumar, M.D. Mathew, K. Laha, R. Sandhya, “Materials development for fast reactor applications”, *Nucl. Eng. Des.* 265 (2013) 1175-1180.
- [52] A. Riyas, P. Mohanakrishnan, “Studies on physics parameters of metal (U-Pu-Zr) fuelled FBR cores”, *Ann. Nucl. Energy* 35(1) (2008) 87-92.
- [53] P. Chellapandi, V. Balasubramaniyan, P. Puthiyavinayagam, R. Sundararajan, M. Kanakkil, P. Selvaraj, P.R. Vasudeva Rao, “Design of 500 MWe metal fuel demonstration fast reactor”, *Proc. Int. Conf. Nucl. Eng.* (2014) (DOI: <https://doi.org/10.1115/ICONE22-30727>).
- [54] Indira Gandhi Centre for Atomic Research, “Fast Breeder Test Reactor”, (Web-link: <http://www.igcar.gov.in/rfg/fbtrhist.html>).
- [55] B. Blumenthal, J.E. Sanecki, D.E. Busch, D.R. O’Boyle, “Thorium-uranium-plutonium alloys as potential fast power reactor fuels; part-II: Properties and irradiation behavior of thorium-uranium-plutonium alloys”, ANL-7259, Argonne National laboratory, Illinois (October 1969).
- [56] S.Z. Ghayeb, “Investigations of thorium-based fuels to improve actinide burning rate in S-PRISM reactor”, M.Sc. Thesis, The Pennsylvania State University (2008) (Web-link: <https://etda.libraries.psu.edu/catalog/9160>).

## References

- [57] R.G. Wymer, D.A. Douglas Jr., "Status and progress report for thorium fuel cycle development for period ending December 31, 1964", Report no.: ORNL-3831, Oak Ridge National laboratory, Tennessee (May 1966).
- [58] "Fast spectrum reactors", (Eds.: A.E. Waltar, D. Todd, P.V. Tsvetkov) Springer (2011) (ISBN 978-1-4419-9572-8).
- [59] D.E. Peterson, "The (Th-U) Thorium-uranium system", Bull. Alloy Phase Diagr. 6 (5) (1985) 443-445.
- [60] S. Peterson, R.E. Adams, D.A. Douglas Jr., "Properties of thorium, its alloys and its compounds", Report no.: ORNL-TM-1144, Oak Ridge National laboratory, Tennessee (June 1965).
- [61] D.R. Marr, D.A. Cantley, J.C. Chandler, D.C. McCurry, R.P. Omberg, "Performance of thorium fuelled fast breeders", Report no.: HEDL-SA-1327-FP, Hanford Engineering Development Laboratory, Richland, USA (October 1977).
- [62] G.L. Copeland, "Evaluation of thorium-uranium alloys for the unclad metal breeder reactor", Report no.: ORNL-4557, Oak Ridge National Laboratory, Tennessee (June 1970).
- [63] B. Blumenthal, J.E. Sanecki, D.E. Busch, "Thorium-uranium-plutonium alloys as potential fast power reactor fuels; part-I: Thorium-uranium-plutonium phase diagram", Report no.: ANL-7258, Argonne National Laboratory, Illinois (September 1968).
- [64] C.S. Holden, "Rapid computational path for sustainable and renewable nuclear energy using metallic thorium fuels", Proceedings of 2<sup>nd</sup> Thorium energy conference (ThEC-2010), Mountain View CA (2010).
- [65] R.M. Carroll, "The effects of reactor irradiation on thorium-uranium alloy fuel plates", Report no.: ORNL-1938, Oak Ridge National Laboratory, Tennessee (August 1955).

## References

- [66] B.R. Hayward, P. Corzine, "Thorium uranium fuel elements for SRE", Proc. 2<sup>nd</sup> UN Int. Conf. Peaceful uses of Atom. Energy, Geneva (October 1958).
- [67] J.L. Ballif, B.R. Hayward, J.W. Walter, "Engineering evaluation of a mixed alloy fuel element irradiated at elevated temperatures in SRE", Technical report no.: NAA-SR-3888, Atomics International Division, North American Aviation Incorporation, California, USA (June 1960).
- [68] A.R. Olsen, "Thorium and thorium alloys: Preliminary corrosion tests", Report no.: ORNL-1066, Oak Ridge National Laboratory, Tennessee (November 1951).
- [69] M.S. Farkas, A.A. Bauer, R.F. Dickerson, "Development of thorium-uranium-base fuel alloys," Report no.: BMI-1428, Battelle Memorial Institute, Columbus, Ohio (March 1960).
- [70] R.H. Cole, L.E. Wilkinson, "Development of high strength ternary and quaternary thorium-uranium base alloys", Technical report no.: ATL-A-128, Advanced Technology Laboratory, California (1961).
- [71] J.H. Kittel, J.A. Horak, W.F. Murphy, S.H. Paine, "Effect of irradiation on thorium and thorium-uranium alloys", Technical report no.: ANL-5674, Argonne National laboratory, Illinois, USA (April 1963).
- [72] A.L. Bement, "Burn-up and specific power calculations for the thermal neutron irradiation on thorium-uranium alloys", Technical report no: HW-56631, General Electric Co. Hanford Atomic Products Operation, Richland, Washington (1958).
- [73] F.W. Dodge, E.W. Murbach, L.A. Hanson, "Low decontamination reprocessing of thorium-uranium alloys by induction drip melting", Nucl. Sci. Eng. 6 (6) (1959) 533-536.
- [74] P. Chiotti, A.F. Voigt, "Pyrometallurgical processing", Technical report: A/CONF.15/P/517; ISC-1018, Ames Laboratory, Iowa (October 1958).

- [75] W.N. Hensen, "Electrolysis of thorium and uranium", US-Patent no.: US 2951793 (1960).
- [76] S. Jiang, K. Liu, Y. Liu, T. Yin, Z. Chai, W. Shi, "Electrochemical behavior of Th(IV) on the bismuth electrode in LiCl–KCl eutectic", *J. Nucl. Mater.* 523 (2019) 268-275.
- [77] G.B. Zorzoli, "Use of metallic thorium for LWBRs and LWRs", *Nucl. Tech.* 20 (1973) 109-113.
- [78] F. Correa, D.J. Driscoll, D.D. Lanning, "An evaluation of tight pitch PWR cores", technical report no.: MIT-EL-79-022, Massachusetts Institute of Technology, Cambridge, Massachusetts (1979).
- [79] Z.S. Li, X.J. Liu, C.P. Wang, "Thermodynamic modelling of the Th-U, Th-Zr and Th-U-Zr systems", *J. Alloy Compd.* 473 (2009) 193-198.
- [80] S.Z. Ghrayeb, K.N. Ivanov, S.H. Levine, E.P. Loewen, "Burn-up performance of sodium-cooled fast reactors utilizing thorium-based fuels", *Nucl. Tech.* 176 (2011) 188-194.
- [81] T. Okawa, H. Sekimoto, S. Nakayama, "Design study on power flattening to sodium cooled large scale CANDLE burning reactor with using thorium fuel", *Proc. 18<sup>th</sup> Int. Conf. Nucl. Eng., ICONE18, China, (2010).*
- [82] M.T. Simnad, "The U-ZrH<sub>x</sub> alloy: Its properties and use in TRIGA fuel", *Nucl. Engg. Des.* 64 (1981) 403-422.
- [83] K. Konashi, B.A. Pudjanto, T. Terai, M. Yamawaki, "Thermodynamic stability of ThZr<sub>2</sub>H<sub>x</sub> at high temperature", *J. Phys. Chem. Solids* 66 (2–4) (2005) 625-628.
- [84] T. Yamamoto, H. Suwarno, F. Ono, H. Kayano, M. Yamawaki, "Preparation, analysis and irradiation of hydride Th-U-Zr alloy samples for a new fuel", *J. Alloy Compd.* 271-273 (1998) 702-706.

- [85] S. Das, R. Kumar, S.B. Roy, A.K. Suri, "Development study on metallic thorium and uranium-thorium alloy", BARC Newsletter-Founder's Day Special issue (2011) 72-76.
- [86] S. Das, R. Kumar, S. Kaity, S. Neogy, K.N. Hareendran, S.B. Roy, G.K. Dey, B.S.S. Daniel, G.P. Chaudhari, "Characterization of microstructural, mechanical and thermal properties and ageing study of Th-3 wt.% U alloy" Nucl. Eng. Des. 282 (2015) 116-125.
- [87] S. Das, S. Kaity, R. Kumar, J. Banerjee, S.B. Roy, G.P. Chaudhari, B.S.S. Daniel, "Characterization of microstructural, mechanical and thermophysical properties of Th-52 U alloy", J. Nucl. Mater. 480 (2016) 223-234.
- [88] S. Das, S.B. Roy, G.P. Chaudhari, B.S.S. Daniel, "Microstructural evolution of as-cast Th-U alloys", Prog. Nucl. Energy 88 (2016) 285-296.
- [89] R. Kumar, S. Das, S.B. Roy, R. Agarwal, J. Banerjee, S.K. Satpati, "Effect of Mo addition on the microstructural evolution and  $\gamma$ -U stability in Th-U alloys", J. Nucl. Mater. 539 (2020) 152317.
- [90] S. Vaidyanathan, "Thorium utilization in pressurized water reactors using bimetallic thorium-zirconium alloy cladding", Nucl. Tech. (2020) (DOI: <https://doi.org/10.1080/00295450.2019.1706377>).
- [91] D. Escorcia-Ortiz, J. François, C. Martín-del-Campo, "Comparative study of the neutronic performance of thorium-based metallic fuel and MOX fuel in an ASTRID-like fast reactor core", Nucl. Eng. Des. 347 (2019) 122-131.
- [92] J.K. Startt, C.S. Deo, "First principles study of the structure and elastic properties of thorium metal", MRS Adv. 1 (35) (2016) 2447-2452.
- [93] A. Karahan, J. Buongiorno, "A new code for predicting the thermo-mechanical and irradiation behavior of metallic fuels in sodium fast reactors", J. Nucl. Mater. 396 (2010) 283-293.

## References

- [94] K. Lassmann, "TRANSURANUS: a fuel rod analysis code ready for use", *J. Nucl. Mater.* 188 (1992) 295-302.
- [95] J.P. Hamond, "Physical, mechanical and irradiation properties of thorium and thorium alloys", ORNL-4218, Oak Ridge National Laboratory, USA (1968) 29-30.
- [96] J.K. Fink, M.G. Chasanov, L. Leibowitz, "Thermophysical properties of thorium and uranium systems for use in reactor safety analysis", Report no.: ANL-CEN-RSD-77-1, Argonne National Laboratory (1977) 11-12.
- [97] M. Lung, "A present review of the thorium nuclear fuel cycles", European commission report no.: EUR-17771-EN, (1997).
- [98] S. Kolay, S. Phapale, R. Dawar, M. Jafar, S. N. Achary, A. K. Tyagi, R. Mishra, M. Basu, "Phase characterization and thermal study of SrF<sub>2</sub> and NdF<sub>3</sub> doped fluoride salt containing 78 mol % LiF - 20 mol % ThF<sub>4</sub> - 2 mol % UF<sub>4</sub>", *J. Radioanal. Nucl. Chem.* 314 (2) (2017) 1267-1271.
- [99] M. Verwerft, B. Boer, "Thorium oxide nuclear fuels", *Comprehensive nuclear materials* (Second edition) 5 (2020) 139-168 (DOI: <https://doi.org/10.1016/B978-0-12-803581-8.11770-9>).
- [100] S. Usha, R.R. Ramanarayanan, P. Mohanakrishnan, R.P. Kapoor, "Research reactor KAMINI", *Nucl. Eng. Des.* 236 (7-8) (2006) 872-880.
- [101] T.K. Mukherjee, "Processing of Indian monazite for the recovery of thorium and uranium values", *Proceedings of International Conference on Characterisation and Quality Control of Nuclear Fuels* (Eds.: C. Ganguly, R.N. Jayaraj) Allied Publishers Pvt. Ltd. (2002) 187-195.
- [102] J.R. Johnson, C.E. Curtis, "Note on sintering of ThO<sub>2</sub>", *J. Am. Ceram. Soc.* 37(12) (1954) 611.

## References

- [103] T.R.G. Kutty, K.B. Khan, P.V. Hegde, J. Banerjee, A.K. Sengupta, S. Majumdar, H.S. Kamath, "Development of a master sintering curve for ThO<sub>2</sub>", *J. Nucl. Mater.* 327(2-3) (2004) 211-219.
- [104] P. Balakrishna, B.P. Varma, T.S. Krishnan, T.R.R. Mohan, P. Ramakrishnan, "Thorium oxide: Calcination, compaction and sintering", *J. Nucl. Mater.* 160(1) (1988) 88-94.
- [105] N. Clavier, R. Podor, L. Deliere, J. Ravoux, N. Dacheux, "Combining in situ HT-ESEM observations and dilatometry: An original and fast way to the sintering map of ThO<sub>2</sub>", *Mater. Chem. Phys.* 137(3) (2013) 742-749.
- [106] K. Ananthasivan, S. Balakrishnan, S. Anthonysamy, R. Divakar, E. Mohandas, V. Ganesan, "Synthesis and sintering of nanocrystalline thoria doped with CaO and MgO derived through oxalate-deagglomeration", *J. Nucl. Mater.* 434 (1-3) (2013) 223-229.
- [107] G.P. Halbfinger, M. Kolodney, "Activated Sintering of ThO<sub>2</sub> and ThO<sub>2</sub>-Y<sub>2</sub>O<sub>3</sub> with NiO", *J. Am. Ceram. Soc.* 55(10) (1972) 519-524.
- [108] A. Baena, T. Cardinaels, J. Vleugels, K. Binnemans, M. Verwerft, "Activated sintering of ThO<sub>2</sub> with Al<sub>2</sub>O<sub>3</sub> under reducing and oxidizing conditions", *J. Nucl. Mater.* 470 (2016) 34-43.
- [109] K. Ananthasivan, S. Anthonysamy, C. Sudha, A.L.E. Terrance, P.R. Vasudeva Rao, "Thoria doped with cations of group VB-synthesis and sintering", *J. Nucl. Mater.* 300(2-3) (2002) 217-229.
- [110] T.R.G. Kutty, P.V. Hegde, K.B. Khan, T. Jarvis, A.K. Sengupta, S. Majumdar, H.S. Kamath, "Characterization and densification studies on ThO<sub>2</sub>-UO<sub>2</sub> pellets derived from ThO<sub>2</sub> and U<sub>3</sub>O<sub>8</sub> powders", *J. Nucl. Mater.* 335 (3) (2004) 462-470.
- [111] V. Tyrpekl, M. Cologna, D. Robba, J. Somers, "Sintering behaviour of nanocrystalline ThO<sub>2</sub> powder using spark plasma sintering", *J. Eur. Ceram. Soc.* 36(3) (2016) 767-772.

- [112] W. Straka, S. Amoah, J. Schwartz, “Densification of thoria through flash sintering”, *MRS Commun.* 7(3) (2017) 677-682.
- [113] D. Sanjay Kumar, K. Ananthasivan, R.V. Krishnan, S. Amirthapandian, A. Dasgupta, “Studies on the synthesis of nanocrystalline  $Y_2O_3$  and  $ThO_2$  through volume combustion and their sintering”, *J. Nucl. Mater.* 479 (2016) 585-592.
- [114] R.D. Purohit, S. Saha, A.K. Tyagi, “Nanocrystalline thoria powders via glycine-nitrate combustion” *J. Nucl. Mater.* 288 (1) (2001) 7-10. [114a] F. Cappia, D. Hudry, E. Courtois, A. Janßen, L. Luzzi, R.J.M. Konings, D. Manara, High-temperature and melting behavior of nanocrystalline refractory compounds: an experimental approach applied to thorium dioxide, *Mater. Res. Express* 1 (2014) 0250341-12.
- [115] J. Spino, K. Vennix, M. Coquerelle, “Detailed characterisation of the rim microstructure in PWR fuels in the burn-up range 40–67 GWd/tM”, *J. Nucl. Mater.* 231 (3) (1996) 179-190.
- [116] L. Bonato, M. Viot, X. Le Goff, P. Moisy, S.I. Nikitenko, “Sonochemical dissolution of nanoscale  $ThO_2$  and partial conversion into a thorium peroxo sulphate”, *Ultrason. Sonochem.* 69 (2020) 105235.
- [117] S. Dash, A. Singh, P.K. Ajikumar, H. Subramanian, M. Rajalakshmi, A.K. Tyagi, A.K. Arora, S.V. Narasimhan, B. Raj, “Synthesis and characterization of nanocrystalline thoria obtained from thermally decomposed thorium carbonate”, *J. Nucl. Mater.* 303 (2–3) (2002) 156-168.
- [118] S. Dash, R. Krishnan, M. Kamruddin, A.K. Tyagi, B. Raj, “Temperature programmed decomposition of thorium oxalate hexahydrate”, *J. Nucl. Mater.* 295(2-3) (2001) 281-289.

## References

- [119] S. Dash, M. Kamruddin, P.K. Ajikumar, A.K. Tyagi, B. Raj, S. Bera, S.V. Narasimhan, “Temperature programmed decomposition of thorium nitrate pentahydrate”, *J. Nucl. Mater.* 278 (2–3) (2000) 173-185.
- [120] T.V. Plakhova, A.Y. Romanchuk, D.V. Likhosherstova, A.E. Baranchikov, P.V. Dorovatovskii, R.D. Svetogorov, T.B. Shatalova, T.B. Egorova, A.L. Trigub, K.O. Kvashnina, V.K. Ivanov, S.N. Kalmykov, “Size effects in nanocrystalline thoria”, *J. Phys. Chem. C* 123 (37) (2019) 23167-23176. [120a] D. Hudry, C. Apostolidis, O. Walter, T. Gouder, E. Courtois, C. Kübel, D. Meyer, Controlled Synthesis of Thorium and Uranium Oxide Nanocrystals, *Chem. Eur. J.*, 19 (2013) 5297-5305.
- [121] F. Deganello, A.K. Tyagi, “Solution combustion synthesis, energy and environment: Best parameters for better materials”, *Prog. Cryst. Growth Char.* 64 (2018) 23-61.
- [122] A. Varma, A.S. Mukasyan, A.S. Rogachev, K.V. Manukyan, “Solution combustion synthesis of nanoscale materials”, *Chem. Rev.* 116 (2016) 14493-14586.
- [123] V. Chandramouli, S. Anthonysamy, P.R. Vasudeva Rao, “Combustion synthesis of thoria - A feasibility study”, *J. Nucl. Mater.* 265(3) (1999) 255-261.
- [124] S. Anthonysamy, K. Ananthasivan, V. Chandramouli, I. Kaliappan, P.R. Vasudeva Rao, “Combustion synthesis of urania-thoria solid solutions”, *J. Nucl. Mater.* 278(2) (2000) 346-357.
- [125] D. Sanjay Kumar, K. Ananthasivan, S. Amirthapandian, A. Dasgupta, G. Jogeswara Rao, “Citrate gel-combustion synthesis and sintering of nanocrystalline  $\text{ThO}_2$  powders”, *J. Nucl. Mater.* 497 (2017) 16-29.
- [126] R.D. Purohit, S. Saha, A.K. Tyagi, “Combustion synthesis of 5 and 10 mol%  $\text{YO}_{1.5}$  doped  $\text{ThO}_2$  powders”, *J. Nucl. Mater.* 323 (1) (2003) 36-40.

- [127] K.C. Patil, M.S. Hegde, T. Rattan, S.T. Aruna, "Chemistry of nanocrystalline oxide materials combustion synthesis, properties and applications", World Scientific Publications (2008) (DOI: <https://doi.org/10.1142/6754>).
- [128] F.-T Li, J. Ran, M. Jaroniec, S.Z. Qiao, "Solution combustion synthesis of metal oxide nanomaterials for energy storage and conversion", *Nanoscale* 7(42) (2015) 17590-17610.
- [129] A. Kumar, E.E. Wolf, A.S. Mukasyan, "Solution combustion synthesis of metal nanopowders: nickel-reaction pathways", *AIChE J.* 57(8) (2011) 2207-2214.
- [130] A. Kumar, E.E. Wolf, A.S. Mukasyan, "Solution combustion synthesis of metal nanopowders: Copper and copper / nickel alloys", *AIChE J.* 57(12) (2011) 3473-3479.
- [131] S. Zhang, Z.A. Munir, "The combustion synthesis of refractory nitrides: Part II the synthesis of niobium nitride", *J. Mater. Sci.* 26 (1991) 3380–3385.
- [132] "Nitride ceramics: Combustion synthesis, properties, and applications", (Eds.: A.A. Gromov, L.N. Chukhlomina) Wiley-VCH Verlag GmbH (2015) (DOI:10.1002/9783527684533).
- [133] H.V. Kirakosyan, K.T. Nazaretyan, R.A. Mnatsakanyan, S.V. Aydinyan, S.L. Kharatyan, "Solution combustion synthesis of nanostructured molybdenum carbide", *J. Nanopart. Res.* 20 (2018) 214.
- [134] N.A. Marand, S.M. Masoudpanah, M. Sh. Bafghi, "Solution combustion synthesis of nickel sulfide composite powders", *Ceram. Int.* 44 (14) (2018) 17277-17282.
- [135] K. Rajeshwar, N.R. De Tacconi, "Solution combustion synthesis of oxide semiconductors for solar energy conversion and environmental remediation", *Chem. Soc. Rev.* 38 (7) (2009) 1984-1998.

- [136] K.C. Thomas, J.R. Kale, R.G. Dalavi, K. Venkatesh, R. Kameswaran, A.V.R. Reddy "Development of an IR-based carbon analyser for uranium metal", BARC Newsletter 311 (2009) 2-6 (Web-link: <http://barc.gov.in/publications/nl/2009/200912.pdf/>)
- [137] B.D. Cullity, "Elements of X-ray diffraction", Addison-Wesley Publishing Company Inc. (1956).
- [138] R. Tilley, "Crystals and crystal structures", John Wiley & Sons, Ltd. (2006) (ISBN-13 978-0-470-01820-0).
- [139] E. Smith, G. Dent, "Modern Raman spectroscopy - A practical approach", John Wiley & Sons, Ltd. (2006) (ISBN 0-471-49794-0).
- [140] M. Roessle, D.I. Svergun, "Small angle X-ray scattering", In "Encyclopaedia of biophysics" (Eds.: G.C.K. Roberts) Springer, Berlin, Heidelberg (2013) (DOI: [https://doi.org/10.1007/978-3-642-16712-6\\_284](https://doi.org/10.1007/978-3-642-16712-6_284)).
- [141] P.W. Schmidt, R. Height, "Slit height corrections in small angle X-ray scattering", Acta Crystallogr. 13 (1960) 480-483.
- [142] G. Höhne, W.F. Hemminger, H.J. Flammersheim, "Differential scanning calorimetry", Springer-Verlag. (2003) (ISBN 978-3-540-00467-7).
- [143] M. Reading, A. Luget, R. Wilson, "Modulated differential scanning calorimetry", Thermochim. Acta 238(C) (1994) 295-307.
- [144] J.E.K. Schawe, T. Hutter, C. Heitz, I. Alig, D. Lellinger, "Stochastic temperature modulation: A new technique in temperature-modulated DSC", Thermochim. Acta 446 (2006) 147-155.
- [145] N. Manoj, D. Jain, J.K. Gautam, K.C. Thomas, V. Sudarsan, C.G.S. Pillai, R.K. Vatsa, A.K. Tyagi, "A simple, reliable and cost-effective, high temperature dilatometer for bulk thermal expansion studies on solids", Measurement 92 (2016) 318-325.

- [146] W.J. Parker, R.J. Jenkins, C.P. Butler, G.L. Abbott, “Flash method of determining thermal diffusivity, heat capacity, and thermal conductivity”, *J. Appl. Phys.* 32 (1961) 1679-1684.
- [147] H.S. Carslaw, J.C. Jaeger, “Conduction of heat in solids”, 2nd edition, Oxford University Press, New York, (1959).
- [148] D. Jain, D. Das, B.N. Jagatap, “Thorium-based fuels for advanced nuclear reactors: Thermophysical, thermochemical and thermodynamic properties”, in A.K. Nayak, B.R. Sehgal (Eds.), *Thorium—Energy for the Future*, Springer (2019) (ISBN 978-981-13-2658-5) 257-275.
- [149] Y.S. Touloukian, R.W. Powell, C.Y. Ho, P.G. Klemens, “Thermophysical properties of matter - The TPRC data series. Volume 1. Thermal conductivity - metallic elements and alloys”, (1970) 429-440; 381-384.
- [150] Y.S. Touloukian, R.W. Powell, C.Y. Ho, M.C. Nicolaou, “Thermophysical properties of matter - The TPRC data series. Volume 10. Thermal diffusivity”, (1974) 205-208.
- [151] Y.S. Touloukian, E.H. Buyco, “Thermophysical properties of matter - The TPRC data series. Volume 4. Specific heat - metallic elements and alloys”, (1971) 268-270.
- [152] Y.S. Touloukian, R.K. Kirby, R.E. Taylor, P.D. Desai, “Thermophysical properties of matter - The TPRC data series. Volume 12. Thermal expansion metallic elements and alloys”, (1975) 365-372.
- [153] H.G. Schettler, J.J. Martin, F.A. Schmidt, G.C. Danielson, “Thermal conductivity of high purity thorium”, *Phys. Rev.* 187 (3) (1969) 801-804.
- [154] T.A. Sandenaw, “Thermal conductivity of uranium: Effects of purity and microstructure”, Report no.: LA-6092-MS, United States (1975) 1-8.
- [155] Y. Takahashi, M. Yamawaki, K. Yamamoto, “Thermophysical properties of uranium-zirconium alloys”, *J. Nucl. Mater.* 154 (1988) 141-144.

## References

- [156] R.W. Logan, D.H. Wood, "Thermal expansion of rolled and extruded uranium", *J. Less-Common Met.* 90 (1983) 233-241.
- [157] J. Nakamura, Y. Takahashi, S. Izumi, M. Kanno, "Heat capacity of metallic uranium and thorium from 80 to 1000 K", *J. Nucl. Mater.* 88 (1980) 64-72.
- [158] M. Boivineau, H. Colin, J.M. Vermeulen, Th. Thévenin, "Thermophysical properties of solid and liquid thorium", *Int. J. Thermophys.* 17(5) (1996) 1001-1010.
- [159] S. Zhou, R. Jacobs, W. Xie, E. Tea, C. Hin, D. Morgan, "Combined ab-initio and empirical model of the thermal conductivity of uranium, uranium-zirconium, and uranium-molybdenum", *Phys. Rev. Mater.* 2 (2018) 083401-1-21.
- [160] Y. Li, A. Chernatynskiy, J.R. Kennedy, S.B. Sinnott, S.R. Phillpot, Lattice expansion by intrinsic defects in uranium by molecular dynamics simulation, *J. Nucl. Mater.* 475 (2016) 6-18.
- [161] K.D. Joshi, S.C. Gupta, S. Banerjee, "Ab-initio theoretical analysis of thermal expansivity, thermal vibrations and melting of thorium", *Phil. Mag.* 88 (27) (2008) 3145-3152.
- [162] S. Jaroszewicz, H.O. Mosca, J.E. Garcés, "The temperature behaviour of the elastic and thermodynamic properties of fcc thorium", *J. Nucl. Mater.* 429(1-3) (2012) 136-142.
- [163] L. Kývala, D. Legut, "Lattice dynamics and thermal properties of thorium metal and thorium monocarbide" *Phys. Rev. B* 101 (2020) 075117.
- [164] P.L. Vijay, J.C. Sehra, C.V. Sundaram, K.R. Gurumurthy, R.V. Raghavan, "Studies on the preparation of thorium metal sponge from thorium oxalate", *BARC Report no.:* 969 (1978) 1-11.
- [165] M.D. Smith, R.W.K. Honeycombe, "The effect of oxygen, carbon and nitrogen on the properties of sintered thorium", *J. Nucl. Mater.* 4 (1959) 345-355.

- [166] Inorganic Crystal Structure Database (ICSD FIZ Karlsruhe GmbH, Version 4.4.0 (2020); collection code: 653236); from: J. Bohet, W. Müller, “Preparation and structure studies of “Van Arkel” protactinium”, *J. Less-Common Met.* 57 (2) (1978) 185-1995.
- [167] International Centre for Diffraction Data (ICDD Database; JCPDF card no.: 720659).
- [168] Inorganic Crystal Structure Database (ICSD FIZ Karlsruhe GmbH, Version 4.4.0 (2020) collection code: 253564) from: V.K. Tripathi, R. Nagarajan, “Sol–gel synthesis of high-purity actinide oxide ThO<sub>2</sub> and its solid solutions with technologically important tin and zinc ions” *Inorg. Chem.* 55 (24) (2016) 12798-12806.
- [169] Inorganic Crystal Structure Database (ICSD FIZ Karlsruhe GmbH, Version 4.4.0 (2020) collection code: 35204); from: S.A. Barrett, A.J. Jacobson, B.C. Tofield, B.E.F. Fender, “The preparation and structure of barium uranium oxide BaUO<sub>3+x</sub>”, *Acta Crystallogr. B* 38 (1982) 2775-2781. [169a] S. Ellison, A. Williams, *Eurachem / CITAC guide: Quantifying Uncertainty in Analytical Measurement* (2012) ISBN 978-0-948926-30-3 (Web-link: [www.eurachem.org](http://www.eurachem.org)).
- [170] Inorganic Crystal Structure Database (ICSD FIZ Karlsruhe GmbH, Version 4.4.0 (2020) collection code: 24223); from: R.E. Rundle, N.C. Baenziger, A.S. Wilson, R.A. McDonald, “The structures of the carbides, nitrides and oxides of uranium”, *J. Am. Chem. Soc.* 70 (1948) 99-105.
- [171] Inorganic Crystal Structure Database (ICSD FIZ Karlsruhe GmbH, Version 4.4.0 (2020) collection code: 26476); from: A.E. Austin, “Carbon positions in uranium carbides”, *Acta Crystallogr.* 12 (1959) 159-161.
- [172] “Augmented uranium metal production facility”, *BARC Newsletter* 200 (2000) 15-18 (Web-link: <http://barc.gov.in/publications/nl/2000/200009.pdf>).
- [173] G.C. Allen, P.M. Tucker, “Surface oxidation of uranium metal as studied by X-ray photoelectron spectroscopy”, *J. Chem. Soc. Dalton* 5 (1973) 470-474.

- [174] R. Rao, R.K. Bhagat, N.P. Salke, A. Kumar, "Raman spectroscopic investigation of thorium dioxide-uranium dioxide ( $\text{ThO}_2\text{-UO}_2$ ) fuel materials", *Appl. Spectrosc.* 68(1) (2014) 44-48.
- [175] "Thermophysical properties of materials for nuclear engineering: A tutorial and collection of data", (IAEA-THPH), International Atomic Energy Agency, Vienna (2008).
- [176] I.F. Barwood, B.R. Butcher, "The  $\alpha \rightarrow \beta$  phase transformation in uranium", *J. Nucl. Mater.* 8 (1963) 232-240.
- [177] C. Yoo, H. Cynn, P. Söderlind, "Phase diagram of uranium at high pressures and temperatures", *Phys. Rev. B* 57 (1998) 10359-10362.
- [178] P. Zhou, X. Wang, H. Yang, X. Fu, "Effect of vacuum heat treatment on oxidation of uranium surfaces", *Rare Metal Mat. Eng.* 37 (2008) 94-97.
- [179] G. Erez, U. Even, "The Wiedemann-Franz ratio of metallic uranium at elevated temperatures", *J. Appl. Phys.* 37 (1966) 4633-4644.
- [180] S. Nasu, S. Fukushima, T. Ohmichi, T. Kikuchi, "Thermal diffusivity of uranium by laser pulse method from 20° to 850°C", *Jap. J. Appl. Phys.* 7 (1968) 682.
- [181] D. Jain, C.G.S. Pillai, B.S. Rao, R.V. Kulkarni, E. Ramdasan and K.C. Sahoo, "Thermal diffusivity and thermal conductivity studies on thoria-lanthana solid solutions up to 10 mol. %  $\text{LaO}_{1.5}$ ", *J. Nucl. Mater.* 353 (2006) 35-41.
- [182] S.S. Parker, J.T. White, P. Hosemann, A.T. Nelson, "Thermophysical properties of thorium mononitride from 298 to 1700 K", *J. Nucl. Mater.* 526 (2019) 151760.
- [183] H. He, J. Majewski, D.D. Allred, P. Wang, X. Wen, K.D. Rector, "Formation of solid thorium monoxide at near-ambient conditions as observed by neutron reflectometry and interpreted by screened hybrid functional calculations", *J. Nucl. Mater.* 487 (2017) 288-296.

## References

- [184] B.R. Butcher, A.H. Rowe, "Phase transformation in uranium", *Nature* (1953) 817.
- [185] H.H. Klpefer, P. Chiotti, "Characteristics of the solid state transformations in uranium", USAEC Report no.: ISC-893 (1957) 1-113.
- [186] W.S. Blackburn, " $\alpha$ - $\beta$  Thermal cycling of uranium", *J. Nucl. Mater.* 2 (1960) 191.
- [187] J.J. Stobo, "Alpha beta cycling of uranium", *J. Nucl. Mater.* 2 (1960) 97-109.
- [188] L.T. Lloyd, "Thermal expansion of alpha-uranium single crystals", *J. Nucl. Mater.* 3 (1961) 67-71.
- [189] L.T. Lloyd, C.S. Barrett, "Thermal expansion of alpha uranium", *J. Nucl. Mater.* 18 (1966) 55-59.
- [190] E.S. Fisher, "Preparation of alpha uranium single crystals by a grain-coarsening method", *J. Metals* 9 (1957) 882-888.
- [191] D.C. Wallace, "Specific heat of thorium at high temperatures", *Phys. Rev.* 120 (1) (1960) 84-88.
- [192] E.A. Mit'kina, "Experimental determination of the true specific heats of uranium, thorium, and other metals", *Sov. Atom Energy* 7 (2) (1959) 163-165.
- [193] F.L. Oetting, D.T. Peterson, "Heat capacity of well characterized thorium metal from 298 to 700 K", *J. Less-Common Met.* 128 (1987) 231-239.
- [194] D.C. Ginnings, R.J. Corruccini, "Heat capacities at high temperatures of uranium, uranium trichloride, and uranium tetrachloride, *J. Res. Nat. Bur. Stand.* 39 (1947) 309-316.
- [195] F.K. Oetting, M.H. Rand, R.J. Ackermann, "The chemical thermodynamics of actinide elements and compounds, Part 1, The actinide elements", International Atomic Energy Agency (IAEA), Vienna (1976).
- [196] A.L. Loeb, "Thermal conductivity: VIII, A theory of thermal conductivity of porous materials", *J. Am. Ceram. Soc.* 37 (1954) 96-99.

## References

- [197] S. Kaity, J. Banerjee, M.R. Nair, K. Ravi, S. Dash, T.R.G. Kutty, A. Kumar, R.P. Singh, "Microstructural and thermophysical properties of U-6 wt.% Zr alloy for fast reactor application", *J. Nucl. Mater.* 427 (2012) 1-11.
- [198] C. Hin, "Thermal conductivity of metallic uranium", NEUP 14-6767 (2018) (Web-link: <https://www.osti.gov/servlets/purl/1433931>).
- [199] M. Floyd, B. Bromley, J. Pencer, "A Canadian perspective on progress in thorium fuel science and technology", *CNL Nucl. Rev.* 6 (1) (2017) 1-17.
- [200] S. Thakur, P.S.R. Krishna, A.B. Shinde, R. Kumar, S.B. Roy, "Quantitative analysis of thorium phase in Th-U alloys using diffraction studies", *AIP Conf. Proc.* 1832 (2017) 060012.
- [201] P. Chiotti, "High temperature crystal structure of thorium", *J. Electrochem. Soc.* (1955) 567-570.
- [202] G.G. Bente, "A Physical Metallurgical Study of Thorium-Rich Thorium-Uranium Alloys", Report no.: NAA-SR-2069 (1958).
- [203] G.H. Bannister, R.C. Burnett, J.R. Murray, "Ageing and hot hardness characteristics of certain thorium alloys", *J. Nucl. Mater.* 2(1) (1960) 51-61.
- [204] "Chemical technology division annual technical report for 1986," ANL-87-19, Argonne National Laboratory (1987) 122.
- [205] V. Crewe, S. Lawroski, "Reactor development program progress report", Argonne National Laboratory, ANL-7230, Lemont, IL, USA (1966).
- [206] O. Beneš D. Manara R.J.M. Konings, "Thermodynamic assessment of the Th-U-Pu system", *J. Nucl. Mater.* 449 (1-3) (2014) 15-22.
- [207] S. Kneppel, "Aqueous corrosion of thorium alloys and zircaloy-clad thorium alloys", NMI-1226, United States Atomic Energy Commission (1960) 1-49 (Web-link: <https://play.google.com/books/reader?id=OGCWvHY4xRwC&hl=en&pg=GBS.PA1>)

- [208] D.S. Evans, G.V. Raynor, "The solubility of zirconium in  $\alpha$ -thorium", *J. Nucl. Mater.* 4 (1) (1961) 66-69.
- [209] R.I. Sheldon, D.E. Peterson, "The (U-Zr) Uranium-zirconium system", *Bull. Alloy Phase Diagr.* 10 (2) (1989) 165-171.
- [210] O.N. Carlson, "Some studies on the uranium-thorium-zirconium ternary alloy system", AECD-3206, United States Atomic Energy Commission (1950) 1-72.
- [211] J.W. Goffard, R.K. Marshall, "Irradiation behavior of Zircaloy-2 clad thorium-uranium-zirconium alloy fuel elements Interim report 1", BNWL-479, Pacific Northwest Laboratory, United States Atomic Energy Commission (1967).
- [212] T. Okawa, S. Nakayama, H. Sekimoto, "Design study on power flattening to sodium cooled large-scale CANDU burning reactor with using thorium fuel", *Energ. Convers. Manage.* 53 (1) (2012) 182-188.
- [213] Inorganic crystal Structure Database (ICSD FIZ Karlsruhe GmbH, Version 4.4.0 (2020) collection code: 164572) from: A.I. Kolesnikov, A.M. Balagurov, I.O. Bashkin, A.V. Belushkin, E.G. Ponyatovsky, M. Prager, "Neutron scattering studies of ordered gamma -ZrD", *J. Phys. Condens-Mat.* 6 (43) (1994) 8977-8988.
- [214] Inorganic crystal Structure Database (ICSD FIZ Karlsruhe GmbH, Version 4.4.0 (2020) collection code: 16559) from: B.O. Loopstra, "Neutron diffraction investigation of  $U_3O_8$ ", *Acta Crystallogr.* 17 (1964) 651-654.
- [215] Inorganic crystal Structure Database (ICSD FIZ Karlsruhe GmbH, Version 4.4.0 (2020) collection code: 246035) from: S.K. Sali, N.K. Kulkarni, K. Krishnan, S.N. Achary, A.K. Tyagi, "Oxidation / reduction studies on  $Zr_yU_{1-y}O_{2+x}$  and delineation of a new orthorhombic phase in U-Zr-O system", *J. Solid-State Chem.* 181 (8) (2008) 1859-1866.

## References

- [216] Inorganic crystal Structure Database (ICSD FIZ Karlsruhe GmbH, Version 4.4.0 (2020) collection code: 108756) from: H.L. Luo, J.G. Huber, “Superconductivity in Th-Zr alloys”, *J. Less-Common Met.* 65 (1) (1979) 13-17.
- [217] J.M. Elorrieta, L.J. Bonales, M. Naji, D. Manara, V.G. Baonza, J. Cobos, “Laser-induced oxidation of  $\text{UO}_2$ : A Raman study”, *J. Raman Spectrosc.* 49 (5) (2018) 878-884.
- [218] H. He, D. Shoesmith, “Raman spectroscopic studies of defect structures and phase transition in hyper-stoichiometric  $\text{UO}_{2+x}$ ”, *Phys. Chem. Chem. Phys.* 12 (2010) 8109-8118.
- [219] X. Zhao, D. Vanderbilt, “Phonons and lattice dielectric properties of zirconia”, *Phys. Rev. B* 65 (2002) 075105.
- [220] E. Hashem, A. Seibert, J-F. Vigier, M. Naji, S. Mastromarino, A. Ciccioli, D. Manara, “Solid-liquid equilibria in the  $\text{ThO}_2$ - $\text{ZrO}_2$  system: An experimental study” *J. Nucl. Mater.* 521 (2019) 99-108.
- [221] O.N. Carlson, E.R. Stevens, “A compilation of thorium binary phase diagrams”, USAEC Report (1968) (Web-link: <https://www.osti.gov/servlets/purl/4529064>).
- [222] G.B. Skinner, H.L. Johnston, “Thermal Expansion of zirconium between 298°K and 1600°K”, *J. Chem Phys.* 21 (1953) 1383.
- [223] P.L. Brown, E. Curti, B. Grambow, C. Ekberg, “Chemical thermodynamics of zirconium”, OECD Nuclear energy agency, data bank (Eds.: F.J. Mompean, J. Perrone, M. Illemassene) (2005) (Web-link: <https://www.oecd-nea.org/dbtdb/pubs/vol8-zirconium.pdf>).
- [224] C.G.S. Pillai, P. Raj, “Thermal Conductivity of  $\text{ThO}_2$  and  $\text{Th}_{0.98}\text{U}_{0.02}\text{O}_2$ ”, *J. Nucl. Mater.* 277 (2000) 116-119.

- [225] S.S. Manoharan, K.C. Patil, "Combustion synthesis of metal chromite powders", *J. Am. Ceram. Soc.* 75 (1992) 1012-1015.
- [226] S.R. Jain, K.C. Adiga, V.R. Pai Verneker, "A new approach to thermochemical calculations of condensed fuel-oxidizer mixtures," *Combust. Flame* 40 (6) (1981) 71-79.
- [227] S. Roy, A. Das Sharma, S.N. Roy, H.S. Maiti, "Synthesis of  $\text{YBa}_2\text{Cu}_3\text{O}_{7-x}$  Powder by Autoignition of Citrate-Nitrate Gel", *J. Mater. Res.* 8(11) (1993) 2761-2766.
- [228] M. Gizowska, I. Kobus, K. Perkowski, M. Piatek, G. Konopka, I. Witosławska, M. Osuchowski, "Size and morphology of yttria nanopowders obtained by solution combustion synthesis" *Arch. Metall. Mater.* 63(2) (2018) 743-748.
- [229] G.A.M. Hussein, H.M. Ismail, "Texture assessment of thoria as a final decomposition product of hydrated thorium nitrate and oxycarbonate", *Colloids Surf. A*: 99 (1995) 129-139.
- [230] I.M. Weiss, C. Muth, R. Drumm, H.O.K. Kirchner, "Thermal decomposition of the amino acids glycine, cysteine, aspartic acid, asparagine, glutamic acid, glutamine, arginine and histidine", *BMC Biophys.* 11 (2018) 1-15.
- [231] N. Raje, A.V.R. Reddy, "Mechanistic aspects of thermal decomposition of thorium oxalate hexahydrate: A review", *Thermochim. Acta* 505 (2010) 53-58.
- [232] H. Hayashi, T. Watanabe, "Properties of thoria obtained by thermal decomposition of thorium salts", *Nippon Kagaku Kaishi* 4 (1973) 858-860.
- [233] Y. Saito, "Thermal decomposition of thorium oxalate", *J. Jpn. Soc. Powder Metall.* 17(1971) 235-242.
- [234] M.T. Aybers, "Kinetic study of the thermal decomposition of thorium oxalate dehydrate", *J. Nucl. Mater.* 252 (1998) 28-33.
- [235] D.Y. Chung, E. H. Lee, "Microwave-induced combustion synthesis of  $\text{Ce}_{1-x}\text{Sm}_x\text{O}_{2-x/2}$  powder and its characterization", *J. Alloys Compd.* 374 (2004) 69-73.

- [236] “The Aldrich Library of FT-IR Spectra, Edition-II, Volume-1”, 1 898 A 897-898.
- [237] S. Kumar, A.K. Rai, V.B. Singh, S.B. Rai, “Vibrational spectrum of glycine molecule”, *Spectrochim. Acta A* 61 (2005) 2741-2746.
- [238] J. R. Ferraro, A. Walker, “Comparison of the infrared spectra of the hydrates and anhydrous salts in the systems  $\text{UO}_2(\text{NO}_3)_2$  and  $\text{Th}(\text{NO}_3)_4$ ”, *J. Chem. Phys.* 45 (1966) 550-552.
- [239] J.H-Paredes, D.G-Mitnik, H.E. E-Ponce, M.E. A-Ramos, A.D-Moller, “Band structure, optical properties and infrared spectrum of glycine–sodium nitrate crystal”, *J. Mole. Str.* 875 (2008) 295-301.
- [240] S.L. Estes, M.R. Antonio, L. Soderholm, “Tetravalent Ce in the nitrate-decorated hexanuclear cluster  $[\text{Ce}_6(\mu_3\text{-O})_4(\mu_3\text{-OH})_4]^{12+}$ : A structural end point for ceria nanoparticles, *J. Phys. Chem. C* 120 (2016) 5810-5818.
- [241] M. Rand, L. Fuger, I. Grenthe, V. Neck, D. Rai, “Chemical thermodynamics: Chemical thermodynamics of thorium”, (OECD, NEA-TDB) Vol. 11, Elsevier, Amsterdam (2007).
- [242] C. Hennig, K. Schmeide, V. Brendler, H. Moll, S. Tsushima, A.C. Scheinost, “EXAFS Investigation of U(VI), U(IV), and Th(IV) sulfato complexes in aqueous solution”, *Inorg. Chem.* 46 (2007) 5882-5892.
- [243] J. Rothe, M.A. Denecke, V. Neck, R. Muller, J.I. Kim, XAFS “Investigation of the structure of aqueous thorium(IV) species, colloids, and solid thorium(IV) oxide / hydroxide”, *Inorg. Chem.* 41 (2002) 249-258.
- [244] C. Hennig, S. Takao, K. Takao, S. Weiss, W. Kraus, F. Emmerling, A.C. Scheinosta, “Structure and stability range of a hexanuclear Th(IV)-glycine complex”, *Dalton Trans.* 41 (2012) 12818-12823.

## References

- [245] Y. Hu, K.E. Knope, S. Skanthakumar, L. Soderholm, "Understanding the ligand-directed assembly of a hexanuclear Th<sup>IV</sup> molecular cluster in aqueous solution", *Eur. J. Inorg. Chem.* 24 (2013) 4159-4163.
- [246] M. Nourmand, N. Meissami, "Complex formation between uranium(VI) and thorium (IV) ions with some  $\alpha$ -amino-acids", *J. Chem. Soc. Dalton* 8 (1983) 1529-1533.
- [247] Bismondo, L. Rizzo, G. Tomat, "Thermodynamic properties of actinide complexes. uranyl (VI)- and thorium (IV)-glycine systems", *Inorg. Chim. Acta* 74 (1983) 21-24.
- [248] B.G. Oliver, A.R. Davis, "The structure of aqueous thorium nitrate solution by laser Raman spectroscopy", *J. Inorg. Nucl. Chem.* 34 (1972) 2851-2860.
- [249] Z. Huang, X. Chen, Y. Li, J. Chen, J. Lin, J. Wang, J. Lei, R. Chen, "Quantitative determination of citric acid in seminal plasma by using Raman spectroscopy", *Appl. Spectrosc.* 67 (7) (2013) 757-760.
- [250] A.K. Arora, M. Rajalakshmi, T.R. Ravindran, V. Sivasubramanian, "Raman spectroscopy of optical phonon confinement in nanostructured materials", *J. Raman Spectrosc.* 38 (2007) 604-617.
- [251] D. Langmuir, J.S. Herman, "The mobility of thorium in natural waters at low temperatures", *Geochim. Cosmochim. Ac.* 44 (1980) 1753-1766.
- [252] M. Bobtelsky, B. Graus, "Thorium citrate complexes, their composition, structure and behavior", *J. Am. Chem. Soc.* 76 (6) (1954,) 1536-1539.
- [253] G.R. Choppin, H.N. Erten, Y. Xia, "Variation of stability constants of thorium citrate complexes with ionic strength", *Radiochim. Acta* 74 (1996) 123-127.
- [254] D.P. Raymond, J.R. Duffield, D.R. Williams, "Complexation of plutonium and thorium in aqueous environments", *Inorg. Chim. Acta* 140 (1987) 309-313.
- [255] M.M. Barbooti, D.A. Al-Sammerrai, "Thermal decomposition of citric acid", *Thermochim. Acta* 98 (1986) 119-126.

## References

- [256] D. Hennings, W. Mayr, "Thermal decomposition of (BaTi) citrates into barium titanate", *J. Solid State Chem.* 26 (1978) 329-338.
- [257] N.S. Gajbhiye, S. Prasad, "Thermal decomposition of hexahydrated nickel iron citrate", *Thermochim. Acta* 285 (1996) 325-336.
- [258] J. Tsay, T. Fang, "Effects of molar ratio of citric acid to cations and of pH value on the formation and thermal-decomposition behavior of barium titanium citrate", *J. Am. Ceram. Soc.* 82(6) (1999) 1409-1415.
- [259] A. Marcilla, A. Gómez-Siurana, M. Beltrán, I. Martínez-Castellanos, I. Blasco, D. Berenguer, "TGA-FTIR study of the pyrolysis of sodium citrate and its effect on the pyrolysis of tobacco and tobacco/SBA-15 mixtures under N<sub>2</sub> and air atmospheres", *J. Sci. Food Agr.* 98 (15) (2018) 5916-5931.
- [260] O. Glatter, O. Kratky, "Small angle X-ray scattering", Academic, London (1982).
- [261] A. Guinier, G. Fournet, "Small angle scattering of X-rays", Wiley, New York (1955).
- [262] J. Aitchison, J.A.C. Brown, "The log normal distribution", Cambridge University Press, Cambridge (1957).
- [263] R.D. Purohit, B.P. Sharma, K.T. Pillai, A.K. Tyagi, "Ultrafine ceria powders via glycine-nitrate combustion", *Mater. Res. Bull.* 36 (15) (2001) 2711-2721.
- [264] V.R. Choudhary, A.M. Rajput, B. Prabhakar, A.S. Mamman, "Partial oxidation of methane to CO and H<sub>2</sub> over nickel and/or cobalt containing ZrO<sub>2</sub>, ThO<sub>2</sub>, UO<sub>2</sub>, TiO<sub>2</sub> and SiO<sub>2</sub> catalysts", *Fuel* 77 (15) (1998) 1803-1807.
- [265] V. Múčka, J. Podlaha, R. Silber, "NiO-ThO<sub>2</sub> mixed catalysts in hydrogen peroxide decomposition and influence of ionizing radiation", *Radiat. Phys. Chem.* 59 (5-6) (2000) 467-475.

## References

- [266] P. Balakrishna, B.N. Murty, K.P. Chakraborty, R.N. Jayaraj, C. Ganguly, "Special features in powder preparation, pressing, and sintering of uranium dioxide", *Mater. Manuf. Process.* 15(5) (2000) 679-693.
- [267] C.S. Morgan, K.H. McCorkle, G.L. Powell, "Sintering and desintering of thoria", In: Kuczynski G.C. (Eds.) *Sintering and Related Phenomena*. Materials Science Research, Vol. 6, Springer, Boston, MA (1973).
- [268] J.M. Pope, K.C. Radford, "Physical properties of some thoria powders and their influence on sinterability", *J. Nucl. Mater.* 52 (1974) 241-254.
- [269] Z. Chen, J. Mabon, J. Wen, R. Trice, "Degradation of plasma-sprayed yttria-stabilized zirconia coatings via ingress of vanadium oxide", *J. Eur. Ceram. Soc.* 29(9) (2009) 1647-1656.
- [270] M.A. Delfrate, J. Lemaitre, V. Buscaglia, M. Leoni, P. Nanni, "Slip casting of submicron BaTiO<sub>3</sub> produced by low-temperature aqueous synthesis", *J. Eur. Ceram. Soc.* 16(9) (1996) 975-984.
- [271] T.K. Gupta, R.L. Coble, "Sintering of ZnO: II, density decrease and pore growth during the final stage of the process", *J. Am. Ceram. Soc.* 51 (9) (1968) 525-528.
- [272] C.-H. Chang, J.F. Rufner, K.V. Benthem, R.H.R. Castro, "Design of desintering in tin dioxide nanoparticles", *Chem. Mater.* 25(21) (2013) 4262-4268.
- [273] P. Duran, J. Tartaj, C. Moure, "Sintering behaviour and microstructural evolution of agglomerated spherical particles of high-purity barium titanate", *Ceram. Int.* 29(4) (2003) 419-425.
- [274] C.-Y. Tsao, W.-H. Tuan, K.-C. Feng, "De-sintering of Ba<sub>5</sub>Nb<sub>4</sub>O<sub>15</sub> ceramic and its influence on microwave characteristics", *J. Eur. Ceram. Soc.* 37(4) (2017) 1517-1521.
- [275] Cs. Balázsi, F.S. Cinar, O. Addemir, F. Wéber, P. Arató, "Manufacture and examination of C/Si<sub>3</sub>N<sub>4</sub> nanocomposites" *J. Eur. Ceram. Soc.* 24(12) (2004) 3287-3294.

- [276] R. Besler, M.R. da Silva, J.J. do Rosario, M. Dosta, S. Heinrich, R. Janssen, “Sintering simulation of periodic macro porous alumina”, *J. Am. Ceram. Soc.* 98(11) (2015) 3496-3502.
- [277] K. Ananthasivan, S. Anthonysamy, A. Singh, P.R. Vasudeva Rao, “De-agglomeration of thorium oxalate - A method for the synthesis of sinter active thoria”, *J. Nucl. Mater.* 306 (1) (2002) 1-9.
- [278] R.H.R. Castro, “Controlling sintering and grain growth of nanoceramics”, *Cerâmica* 65 (373) (2019) 122-129. **[278a]** Thermodynamics of sintering, R.M. German, *Sintering of advanced materials: Fundamentals and processes* (Ed.: Z.Z. Fang) Woodhead Publishing Ltd. (2010), ISBN 978-1-84569-562-0. **[278b]** G.S. Upadhyaya, *Sintered metallic and ceramic Materials*, John Wiley & Sons Ltd. (1999) ISBN 0-471-98155-9.
- [279] O. Sudre, F.F. Lange, “The effect of inclusions on densification; III, The desintering phenomenon”, *J. Am. Ceram. Soc.* 75 (12) (1992) 3241-3251.
- [280] F. Li, J. Pan, A. Cocks, “Defect healing and cracking in ceramic films during constrained sintering” *J. Am. Ceram. Soc.* 95(12) (2012) 3743-3749.
- [281] S. Knight, R. Korlacki, C. Dugan, J.C. Petrosky, A. Mock, P.A. Dowben, J. Matthew Mann, M.M. Kimani, M. Schubert, “Infrared-active phonon modes in single-crystal thorium dioxide and uranium dioxide”, *J. Appl. Phys.* 127 (2020) 125103.

## CHAPTER 6

### Combustion synthesis of nanocrystalline ThO<sub>2</sub>:

#### Probing synthesis mechanism by thermal analysis

---

##### 6.1. Introduction

In chapter-1 (Section 1.4), potential of nanocrystalline actinide oxides (ThO<sub>2</sub>, UO<sub>2</sub>, their solid solutions, etc.) and their composites with actinide metal powders (ThO<sub>2</sub>-Th, UO<sub>2</sub>-U, ThO<sub>2</sub>-U, etc.) for fabrication of advanced nuclear fuels (ceramic fuels as well as cermet fuels) has been outlined. In particular, advantages of using nanocrystalline thorium dioxide (ThO<sub>2</sub>) powders for fabrication of (i) thoria-based nuclear fuels, (ii) ultra-high temperature refractory ceramics for reactor core catcher applications, (iii) oxide ion conducting solid electrolytes, (iv) optically transparent ceramics, etc. have been discussed. Nanocrystalline ThO<sub>2</sub> can be used as thermo-chemically stable catalyst support material for various technologically important processes such as noble metal catalyzed uranyl (U<sup>6+</sup>) to uranous (U<sup>4+</sup>) reduction, hydrogen halide (HX) decomposition reactions, etc. Based on the review of various synthesis methods to prepare nanocrystalline ThO<sub>2</sub> powders in large scale with minimum process steps; as presented in chapter-1, it is confirmed that solution combustion method is one of the most advantageous routes. It is a simple, rapid and scalable method, and only requires easily available and cost effective reactants. Solution combustion synthesis of nanocrystalline ThO<sub>2</sub> has been reported earlier by several researchers [109, 113, 114, 123-125]. However, most of these studies have focused on effects of reaction variables (fuel type, oxidant type, nature of combustion, fuel to oxidant ratio, etc.) on powder characteristics and consolidation of powders into bulk ceramics. On the other hand, being a process driven from solution-phase chemical interactions among the reactant species, it is apparent that fine ThO<sub>2</sub> powders with

tailored properties could only be synthesized by combustion route provided the mechanism of combustion process is understood. With this objective, studies on solution combustion synthesis of nanocrystalline ThO<sub>2</sub> have been carried out using glycine-thorium-nitrate and citrate-thorium-nitrate routes over wide range of fuel to oxidant ratios and mechanism of combustion has been investigated using thermal analysis, X-ray diffraction and spectroscopic techniques. Nature of interaction in glycine-Th(IV)-nitrate and citrate-Th(IV)-nitrate aqueous systems and associated thermo chemical-changes prior to the combustion of gels resulting from these solutions for the synthesis of ThO<sub>2</sub> powder have been investigated. Role of such molecular-scale interactions on the combustion process and characteristics of resulting ThO<sub>2</sub> powders has been identified. Results obtained from these investigations are detailed in the present chapter and a roadmap for tailored synthesis of ThO<sub>2</sub> nano powders by solution combustion method has been proposed / suggested.

## 6.2. Experimental

Vacuum dried thorium nitrate pentahydrate (Th(NO<sub>3</sub>)<sub>4</sub>.5H<sub>2</sub>O, > 99% purity), glycine (NH<sub>2</sub>CH<sub>2</sub>COOH, > 99.5% purity), citric acid monohydrate (HOOC-CH<sub>2</sub>)<sub>2</sub>C(OH)COOH.H<sub>2</sub>O, > 99.9% purity) and deionized water were used as starting reagents. Transparent and colorless aqueous solutions consisting of oxidant (thorium nitrate) and fuel (glycine or citric acid) were prepared by dissolving these reactants in deionized water (~2 ml/g Th(NO<sub>3</sub>)<sub>4</sub>.5H<sub>2</sub>O basis). As per the principle of propellant chemistry [225, 226], oxidising valency of thorium nitrate (-20) was equated with reducing valency of glycine (+9) or citric acid (+18) to arrive at fuel to oxidant molar ratios of (20/9) or (20/18) for stoichiometric combustion (F:O = 1) via glycine-nitrate or citrate-nitrate routes, respectively. Oxidation states (valency) of individual species were taken as Th(IV) = + 4, N = 0, O = - 2, H = + 1, and C = + 4 based on the chemical state of their end-products after combustion as ThO<sub>2</sub>, N<sub>2</sub>,

H<sub>2</sub>O and CO<sub>2</sub>, respectively. Fuel-excess (F:O > 1.0) and fuel-deficient (F:O < 1.0) solutions were prepared by mixing fuel and oxidant in above molar ratios multiplied by particular (F:O) value. These solutions were used for thermal analysis and combustion to produce ThO<sub>2</sub> powder. Solution pH was measured using pH paper. A portion of few representative solutions (fuel to oxidant ratio = 0.75, 0.90, 1.00 and 1.25) were stored under ambient conditions (298 K ± 3 K) for slow evaporation of solvent.

Thermal analysis on individual starting reagents and aqueous gels (fuel + oxidant) was performed using a heat-flux DSC. Samples for DSC experiments were prepared by placing a drop of aqueous solution in an aluminum pan (40 µl) followed by drying at ambient temperature inside a desiccator (for 48 h) to remove excess water. Thermograms were recorded on hermetically sealed pans containing aqueous gels under flowing argon (or O<sub>2</sub>) atmosphere (~ 60 ml/min.). Another set of experiments was performed by taking a micro-drop of each solution in DSC pan and recording the thermograms immediately, without allowing for solvent evaporation.

Combustion was performed inside a fume hood. Aqueous solution containing fuel and oxidant was taken in a glass beaker and heated up to ~ 353 K over a hot plate for solvent evaporation. As solution turned into a viscous and transparent gel, beaker mouth was covered with SS sieve (mesh size = 500) to minimize air-borne (aerosol-borne) powder spillage during combustion. No turbidity was observed during gel formation, indicating that no components precipitated out of the gel. Combustion occurred when hot plate temperature was rapidly raised (> 523 K). Apparently, reaction was more vigorous for glycine-nitrate gels as compared to citrate-nitrate gels with excessive frothing and drying observed for the former

gels. Visible flame was noted during combustion process. As-combusted powders were calcined at 973 K for 5 h in air.

Gel-precursors, crystal grown inside aqueous gels and combusted ThO<sub>2</sub> powders were phase characterized by powder XRD. Diffractograms were recorded over 20° to 35° (as-combusted powders) and 10° to 70° (calcined powders) with 0.02° step size. FT-IR measurements (400-4000 cm<sup>-1</sup>) were performed on thin semi-transparent disc-shaped samples prepared from mixture of sample and pre-heated (at 473 K) IR-grade KBr powder (sample to KBr weight ratio = 1:99) using a hydraulic press with the help of tungsten carbide (WC) die-plunger. Temperature dependent structural changes in as-prepared gel were studied by heating the IR discs (KBr + gel) at different temperatures (298 K - 553 K; 25 K interval) followed by soaking for 2 h at a particular temperature. These discs were cooled down to ambient temperature inside a desiccator and FT-IR spectra were recorded on them. Aqueous gels and combusted powders were also characterized by Raman spectroscopy. For glycine-Th(IV)-nitrate system, few representative aqueous gels, solid crystals grown inside fuel-rich gels and as-combusted ThO<sub>2</sub> powders were also characterized by Small-angle X-ray scattering (SAXS) technique.

### 6.3. Results and discussion

Figure 6.1 shows DSC thermograms of stoichiometric glycine-Th(IV)-nitrate and citrate-Th(IV)-nitrate aqueous gels (F:O = 1.0) recorded in flowing argon atmosphere. Thermal behavior of these two gels is quite distinct. Upon heating, glycine-Th(IV)-nitrate gel shows a weak and broad exothermic peak (~ 487 K), which is followed by a sharp and intense exothermic peak (~ 521 K). On the other hand, citrate-Th(IV)-nitrate gel first undergoes a weak endothermic event characterized by a broad endothermic peak (~ 409 K). This is

followed by intense exothermic event characterized by a sharp peak  $\sim 439$  K with peak profile similar to that observed in glycine-Th(IV)-nitrate gel  $\sim 521$  K. Further heating of citrate-Th(IV)-nitrate gel results into two high temperature exothermic peaks ( $\sim 615$  K and  $\sim 660$  K), which are absent in case of glycine-Th(IV)-nitrate gel. Thermograms recorded on DSC residues, which are shown in the inset of Fig. 6.1, are featureless. Absence of any endothermic or exothermic peak in DSC curves of residues confirms the irreversible nature of thermal events observed in glycine-Th(IV)-nitrate and citrate-Th(IV)-nitrate gels during heating cycle.

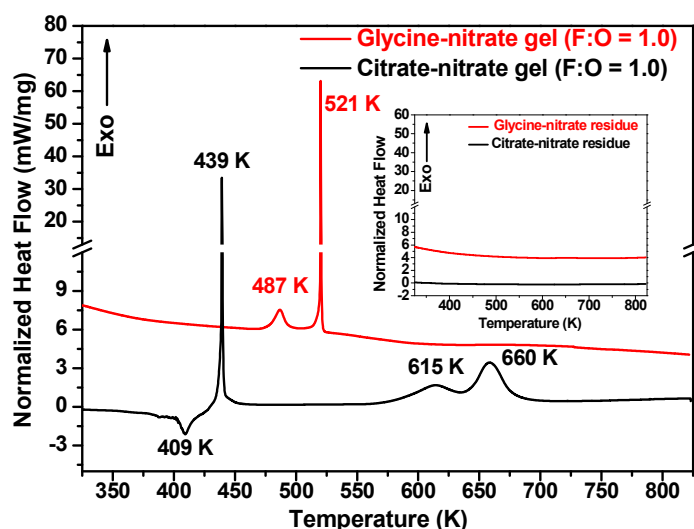


**Fig. 6.1. DSC thermograms of stoichiometric glycine-Th(IV)-nitrate and citric acid-Th(IV)-nitrate aqueous gels. Inset shows thermograms recorded on DSC residues**

Broad endothermic peak in DSC curve of citrate-Th(IV)-nitrate gel with onset temperature  $\sim 390$  K and peak temperature  $\sim 409$  K can be attributed to loss of acidic water vapours from these gels. On the other hand, weak exothermic peak in the case of glycine-Th(IV)-nitrate gels with onset temperature  $\sim 475$  K and peak temperature  $\sim 487$  K is quite interesting and needs to be investigated further for its origin. Sharp and intense exothermic peaks in both gels indicate combustion (auto-ignition) process. High temperature exothermic peaks in citrate-

Th(IV)-nitrate system (~ 615 K and ~ 660 K) are attributed to oxidative decomposition of as-combusted (auto-ignited) mass.

Further elaboration of results on these two routes of solution combustion synthesis of ThO<sub>2</sub> has been sub-divided into three sub-sections namely, (i) mechanism of glycine-nitrate combustion synthesis of nanocrystalline ThO<sub>2</sub>, (ii) mechanism of citrate-nitrate combustion synthesis of nanocrystalline ThO<sub>2</sub> and (iii) Role of fuel to oxidant ratio on the mechanism of glycine-Th(IV)-nitrate combustion synthesis of ThO<sub>2</sub>.

### **6.3.1. Mechanism of glycine-nitrate combustion synthesis of nanocrystalline ThO<sub>2</sub>**

#### **6.3.1.1. Probing glycine-nitrate combustion by thermal analysis (DSC results)**

Figure 6.2 shows DSC thermograms of stoichiometric glycine-Th(IV)-nitrate gel recorded over a limited temperature range during four consecutive heating cycles. Inset shows the thermograms recorded during respective cooling cycles. Experiments were performed with 5 K/min. heating / cooling rate. Thermograms are shifted vertically for clear presentation. During the first heating cycle, an exothermic peak (~ 487 K) is observed. No endotherm is observed in thermogram recorded during the first cooling cycle (inset of Fig. 6.2), which confirms the irreversible nature of process. The same sample upon subjecting to second heating cycle, again show an exothermic peak around same temperature (~ 485 K). However the exothermic peak is broader than that observed in the first heating cycle. In third heating cycle, no exothermic peak is observed in DSC thermogram. Re-occurrence of exothermic peak during second heating cycle and its absence in the third heating cycle indicates that the exothermic process is incomplete in the first heating cycle due to the slow kinetics associated with the process, and it gets completed in the second heating cycle.

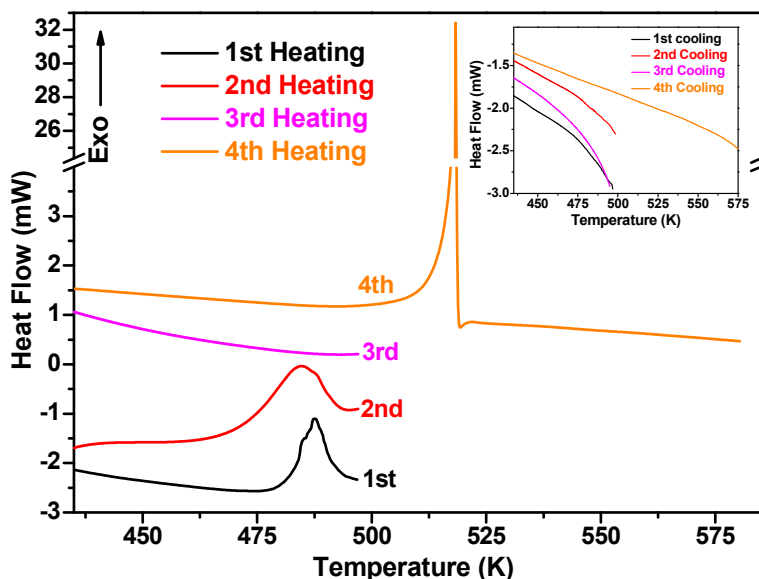


**Fig. 6.2. DSC thermograms recorded on stoichiometric glycine-Th(IV)-nitrate aqueous gel during consecutive heating cycles. Inset shows the cooling cycle thermograms**

The 4<sup>th</sup> heating was carried out up to 580 K, wherein a sharp and intense exothermic peak, ~ 521 K; characteristic of auto-ignition / combustion process is observed. Exothermic peak with identical peak profile is observed for citrate-Th(IV)-nitrate gel (~437 K) as shown in Fig. 6.1. Similar exothermic peaks (~ 430 K), attributed to auto-ignition of citrate-nitrate gel have been reported by Roy et al., [227] for combustion synthesis of oxide superconductors. Kumar et al., [125] reported similar DSC pattern along with TGA-DTA and evolved gas analysis (EGA) results for citrate-Th(IV)-nitrate gel (F:O = 0.45) and attributed the broad exotherm (~ 438 K) to gel pyrolysis. Gizowska et al., [228] also reported similar DSC peak around 514 K for combustion of glycine-Y(III)-nitrate gels. DSC residue obtained after this exothermic peak was in the form of fine powder, which was characterized as nanocrystalline ThO<sub>2</sub> by powder XRD technique. Based on close match of observed peak profile with those reported in literature and, characterization of DSC residue, the high temperature exothermic peak (~ 521 K) observed in glycine-Th(IV)-nitrate gel is attributed to autoignition

(combustion) of dried gel precursor. Thermograms recorded during all the cooling cycle experiments are eventless, which confirm the irreversible nature of exothermic process prior to autoignition.

Figure 6.3 shows DSC thermograms recorded on glycine-Th(IV)-nitrate aqueous gels prepared with varying fuel to oxidant ratios ( $0.65 \leq \text{F:O} \leq 1.20$ ). Similar to results obtained on stoichiometric gel (Fig. 6.1), DSC thermograms recorded on gels with variable F:O ratio show a broad and weak exothermic peak followed by an intense autoignition exotherm. For different F:O values, peak temperatures of these two exotherms vary over 485 K to 500 K and 507 K to 535 K, respectively.

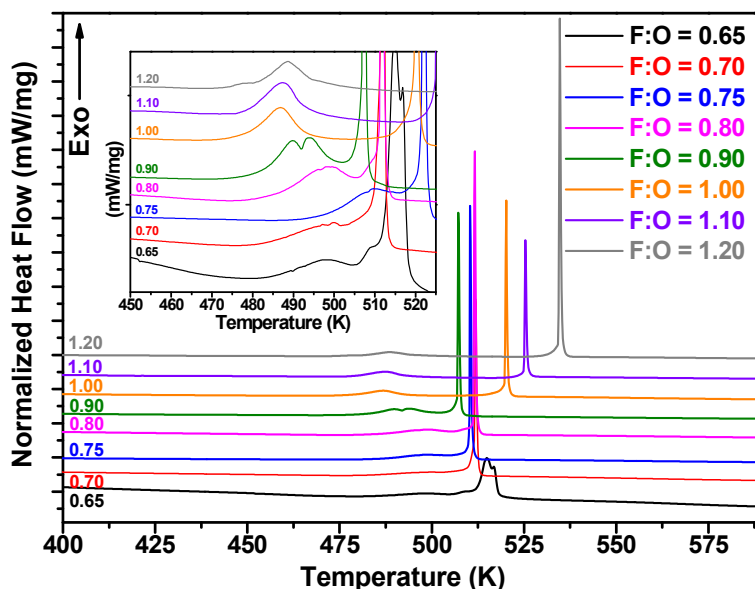


**Fig. 6.3.** DSC thermograms of glycine-Th(IV)-nitrate gels with varying F:O values.

**Insets show expanded view of thermograms in lower temperature region**

Above results show that for all glycine-Th(IV)-nitrate gels studied here ( $0.65 \leq \text{F:O} \leq 1.20$ ), an exothermic event always precedes the combustion, origin of which is not understood.

Detailed experimental studies were carried out to identify the origin of this exothermic peak, which is discussed as follows:

In order to check the contribution of individual starting reagents namely, glycine and Th(NO<sub>3</sub>)<sub>4</sub>·5H<sub>2</sub>O, on the origin of exothermic peak (~ 487 K), DSC thermograms were recorded for aqueous solutions of individual starting reagents Th(NO<sub>3</sub>)<sub>4</sub>·5H<sub>2</sub>O and glycine.

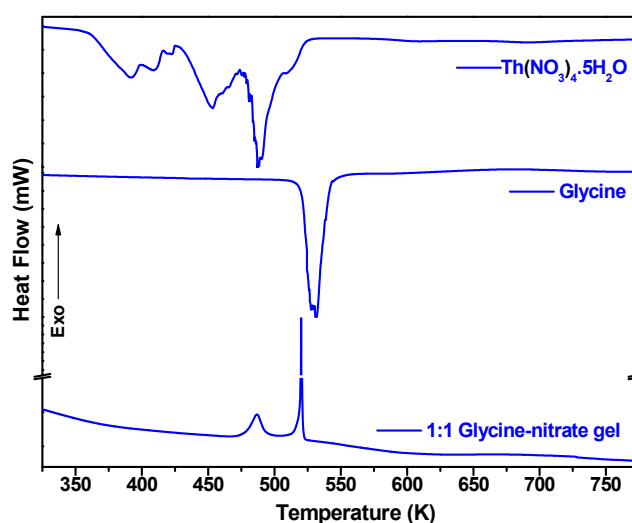


**Fig. 6.4. DSC thermograms of starting materials (Th(NO<sub>3</sub>)<sub>4</sub>·5H<sub>2</sub>O and glycine) in comparison to that of stoichiometric glycine-Th(IV)-nitrate aqueous gel**

These results are shown in Fig. 6.4. DSC patterns match well with that reported earlier for pure glycine and Th(NO<sub>3</sub>)<sub>4</sub>·5H<sub>2</sub>O [229, 230]. It may be noted that under identical experimental conditions, only endothermic peaks are observed in DSC thermograms of glycine as well as Th(NO<sub>3</sub>)<sub>4</sub>·5H<sub>2</sub>O. Absence of exothermic peaks in starting reagents' thermograms suggests that exothermic DSC peak ~ 487 K observed in glycine-Th(IV)-nitrate gel has its genesis in unique structural interaction among the constituent species of gel. Such an interaction among glycine, Th(IV) and nitrate species is expected to have implications on

the powder properties. Understanding the nature of interaction can provide information on molecular level mechanism of combustion.

### 6.3.1.2. Visual evolution of glycine-Th(IV)-nitrate gel during combustion process

As mentioned above, the exothermic DSC peak prior to combustion of glycine-Th(IV)-nitrate gel indicates distinct structural interaction among the constituent species of the gel. Such interaction and associated exothermic process may also result in visual changes and transparency of the gel, which was monitored by recording images during thermal cycling DSC experiments. Fig. 6.5 shows photographs of stoichiometric gel recorded at different temperatures.

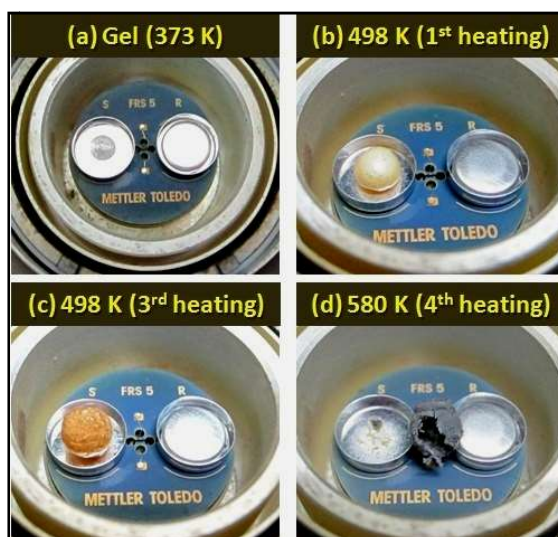


**Fig. 6.5. Photographs of glycine-Th(IV)-nitrate gel and residue obtained during DSC thermal cycling experiments (a) Transparent gel at 373 K, (b) porous yellowish-brown solid obtained after first heating up to 498 K, (c) further swollen porous solid obtained after 3<sup>rd</sup> heating up to 498 K and, (d) as-combusted product popped out of sample pan**

The as-prepared gel, when heated up to ~ 373 K, remains transparent as can be seen from Fig. 6.5(a). Upon increasing the temperature up to 498 K, the transparent gel swells excessively

and converts into a voluminous and opaque porous solid with yellowish brown colour (Fig. 6.5(b)). Swelling indicates that the process is accompanied with evolution of vapours / gases and the yellowish brown colour is arising from the release of gaseous NO<sub>x</sub> species by the gel. This was confirmed by measuring the pH of evolved vapours by maintaining the same experimental conditions in a quartz tube. Presence of NO<sub>x</sub> leads to acidic nature of vapours while presence of ammonia gives basic nature to the evolved vapours. Similar images are observed over repeated heating cycles up to 498 K with darkening of colour of the swollen solid as can be seen from Fig. 6.5(c). Further heating leads to combustion to give ash-like residue (Fig. 6.5(d)), which was later characterized as nanocrystalline ThO<sub>2</sub> (by XRD). These results indicate that the exothermic process (~ 480 K) prior to combustion is also associated with physico-chemical changes like gas evolution and associated colour changes.

### 6.3.1.3. Thermo gravimetric analysis (TGA) of glycine-Th(IV)-nitrate gel

Literature information on thermal analysis of thorium salts (nitrates / carbonates / oxalates) indicates that their decomposition is a multi-step, endothermic phenomenon [229, 231, 232]. In some cases, particularly under oxidizing conditions, exothermic DTA / DSC peaks due to oxidation of gaseous by-products like CO and NO<sub>x</sub> into higher oxides (CO<sub>2</sub> and higher NO<sub>x</sub>) have also been reported [233, 234]. Such peaks are mostly overlapped with endothermic peak(s) at the onset, corresponding to initial material decomposition which requires energy absorption. On the other hand, peak observed ~ 487 K in glycine-Th(IV)-nitrate gel is purely exothermic, consistently seen for varying fuel to oxidant ratios ( $0.65 \leq \text{F:O} \leq 1.20$ ) and under both, inert as well as oxidizing atmosphere. For these reasons, it is unlikely that peak ~ 487 K is due to gel decomposition with release of gaseous by-products and their subsequent oxidation. A DTA pattern similar to present results has been reported by Chung et al., for glycine-nitrate precursor used for the preparation of samarium doped ceria [235]. They also

reported TGA mass loss curve recorded simultaneously with DTA. However, while discussing their results, authors did not provide any explanation for the observed DTA exotherm (~ 473 K). In order to check, whether the exothermic peak observed in the present study is also associated with mass loss, TGA experiments were carried out and are described below.

Off-line TGA was carried out using aqueous gel prepared by heating stoichiometric glycine-Th(IV)-nitrate solution at 363 K. Vial containing this gel was weighed and thereafter heated in a tubular resistive furnace at pre-defined temperatures. It was removed from furnace after 15 minutes soaking at each temperature and cooled inside a desiccator (maintained at < 5% RH), followed by weight measurement. Results of this experiment are shown in Fig. 6.6. Initial heating (360 K -398 K) reveals loss of free solvent (H<sub>2</sub>O). From 398 K to 438 K, sample weight remained nearly constant, which indicated gel's gravimetric stability over this temperature range. Further heating showed two distinct mass loss steps spanning over the temperature range from (i) 438 K to 455 K and (ii) 483 K to 503 K.

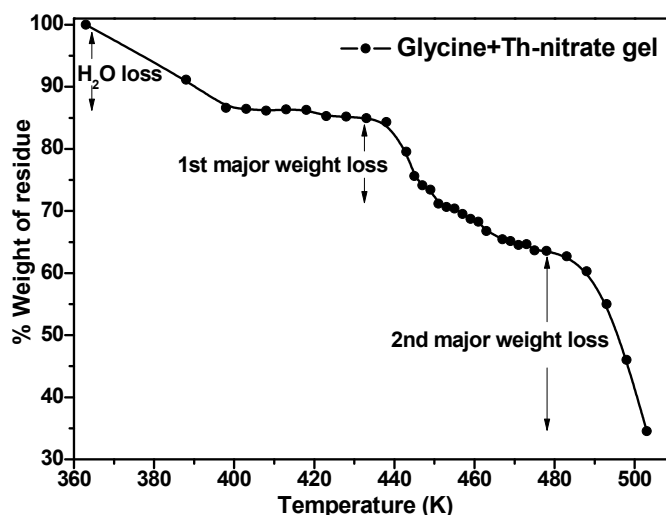


**Fig. 6.6. Variation of weight of residue as a function of temperature obtained for off-line TG experiment on stoichiometric glycine-Th(IV)-nitrate gel**

Compared to DSC results (Fig. 6.1), temperature ranges of these mass loss steps have shifted downward, mainly due to kinetic factors since TGA experiments were performed under steady-state whereas DSC measurements were carried out under dynamic conditions. These results indicate that mass loss over the range 438 K-455 K and 483 K- 503 K are associated with DSC exotherm ( $\sim 487$  K) and combustion ( $\sim 521$  K), respectively. These results are corroborated by weight analysis of DSC residues after each thermal cycling (Fig. 6.2), which showed  $\sim 11\%$ ,  $\sim 24\%$  and  $\sim 61\%$  mass loss after 1<sup>st</sup>, 3<sup>rd</sup> and 4<sup>th</sup> thermal cycle, respectively. Gases / vapours evolved during the first mass-loss step should consist of mainly water vapours and nitrogen oxides as the possibility of decomposition of glycine at this stage is unlikely. This was further confirmed by off-line TG experiments on glycine (298 K to 573 K), which showed onset of mass-loss only above 500 K.

#### 6.3.1.4. X-Ray diffraction studies on glycine-Th(IV)-nitrate gel and ThO<sub>2</sub> powders

For better understanding of the nature of interaction inside the gel precursor at different temperatures, powder XRD studies were carried out. Fig. 6.7 shows XRD patterns of aqueous gel obtained from stoichiometric glycine-Th(IV)-nitrate solution, gel heated up to 373 K and 460 K, along with as-combusted powder. As-prepared gel is amorphous with two broad humps around  $\sim 2\theta = 24^\circ$  and  $42^\circ$ , indicating short range ordering in the gel phase. The pattern remained nearly same for 373 K heated gel except that a low angle, broad diffraction peak appeared  $\sim 12.7^\circ$ , along with two sharp but low intensity peaks  $\sim 22.9^\circ$  and  $\sim 25.7^\circ$ . Low angle peak at  $12.7^\circ$  is due to molecular level ordering resulting from the aggregation of glycine-Th(IV)-nitrate complexes in the gel phase brought about by removal of solvent. Sharp peaks at  $22.9^\circ$  and  $25.7^\circ$  indicate presence of a crystalline phase in gel matrix. However, due to low intensity and poor peak profile, their origin could not be unequivocally identified. XRD pattern of gel heated up to 460 K appeared grossly amorphous with two

broad humps ( $2\theta \sim 28.5^\circ$  and  $\sim 43.5^\circ$ ). Unlike this, XRD pattern of gel dried at ambient temperature, inside a desiccator shows sharp peaks (inset of Fig. 6.7). The pattern does not match with reported XRD patterns of any of the starting materials and their salts namely glycine nitrate, polymorphs of glycine ( $\alpha$ -,  $\beta$ -,  $\gamma$ -glycine) or their oligomers (diglycine and tricine). Powder patterns of Glycine-Th(IV)-nitrate complexes are unavailable in the JCPDF data base and hence exact phase identification could not be done. Upon increasing the temperature to 500 K, combustion occurs leading to the formation of nanocrystalline ThO<sub>2</sub> (average crystallite size  $< 5$  nm) as revealed by the XRD pattern (Fig. 6.7, top pattern).

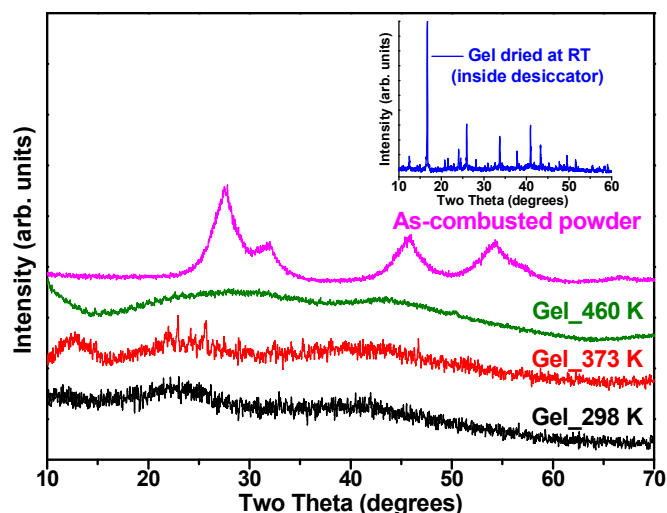


**Fig. 6.7. Powder XRD patterns of as-prepared glycine-Th(IV)-nitrate gel, gel heated to 373 K and 460 K along with as-combusted product. Inset shows XRD pattern of as-prepared gel dried at ambient temperature inside a desiccator**

From the results it is inferred that dry gel mainly comprises of glycine-Th(IV)-nitrate complexes along with residual starting materials (if any) and water. An evidence to this was observed when transparent crystals were harvested from glycine-rich aqueous solutions of

thorium nitrate (F:O = 1.25). Thermal analysis of these crystals showed highly exothermic decomposition to give crystalline ThO<sub>2</sub> as end product.

### 6.3.1.5. FT-IR and Raman spectroscopy studies on aqueous gel and ThO<sub>2</sub> powders

Formation of glycine-Th(IV)-nitrate complexes in the gel phase and their conversion to solid matrix upon heating is further confirmed by FT-IR and Raman spectroscopic techniques.

These results are described as under.

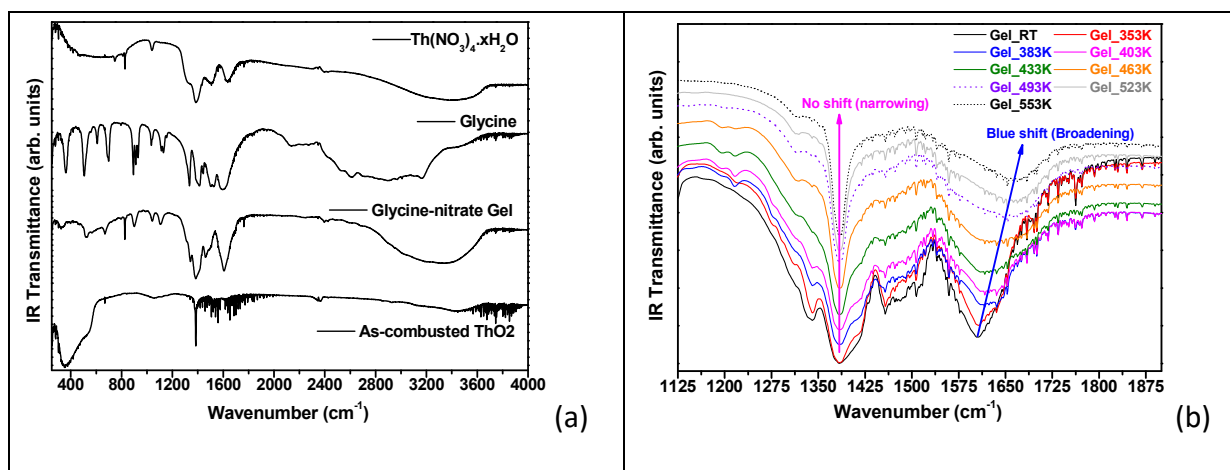


**Fig. 6.8. (a) FT-IR patterns of glycine, Th(NO<sub>3</sub>)<sub>4</sub>.5H<sub>2</sub>O, glycine-Th(IV)-nitrate gel and as-combusted ThO<sub>2</sub>, (b) Corresponding patterns of gel heated at different temperatures**

Figure 6.8 (a) shows FT-IR patterns of starting reactants, as-prepared gel and combustion product. IR patterns of glycine and Th(NO<sub>3</sub>)<sub>4</sub>.5H<sub>2</sub>O match well with that reported earlier [236-238]. For Th(NO<sub>3</sub>)<sub>4</sub>.5H<sub>2</sub>O, peaks were assigned to vibrations of NO<sub>3</sub><sup>-</sup> ions and water of hydration. For glycine, all peaks were indexed to vibrational modes of -OH, -COO, -NH<sub>2</sub> and -CH<sub>2</sub> groups present in the molecule [236, 237]. FT-IR pattern of gel is significantly different from starting reactants as can be seen from Fig. 6.8 (a). The pattern matches fairly well with that of glycine-sodium nitrate crystal reported by Paredes et al., [239]. FT-IR

pattern of as-prepared gel mainly consists of three peaks  $\sim 1383$ ,  $\sim 1606$  and  $\sim 3300$  cm<sup>-1</sup>. Broad peak over 2500 - 3650 cm<sup>-1</sup> with peak maximum  $\sim 3300$  cm<sup>-1</sup> corresponds to overlapping of the stretching vibrations of -OH, -CH and -NH linkages. As the peak is quite broad, no information has been derived from this peak and further discussion of FT-IR results is focused on remaining two peaks. Both peaks  $\sim 1383$  and  $\sim 1606$  cm<sup>-1</sup> are asymmetric, but well resolved shoulder peaks with peak maxima  $\sim 1341$  and  $\sim 1455$  cm<sup>-1</sup> are observed only for 1383 cm<sup>-1</sup> peak. Intense peak at 1383 cm<sup>-1</sup> is due to the asymmetric stretching mode of NO<sub>3</sub><sup>-</sup> ions ( $\nu_4$ -mode), while shoulder peaks (1341 and 1455 cm<sup>-1</sup>) have been attributed to different bending modes ( $\omega$  and  $\delta$ ) of -CH<sub>2</sub> linkages. Peak  $\sim 1610$  cm<sup>-1</sup> is due to asymmetric stretching mode of -COO moiety. There is also a shoulder peak at 1489 cm<sup>-1</sup> at the high energy side of 1455 cm<sup>-1</sup> peak, which arises due to the symmetric bending modes of -NH<sub>3</sub><sup>+</sup> groups. With increase in temperature, the intensity of peaks at 1341, 1455 and 1489 cm<sup>-1</sup> systematically decreases as can be seen from Fig. 6.8(b), suggesting the removal of -CH<sub>2</sub> and -NH<sub>3</sub><sup>+</sup> linkages from the sample. Further peak around 1610 cm<sup>-1</sup>, became broader and blue shifted with respect to that of as-prepared gel. Broadening of this peak is attributed to significant reduction in the extent of free rotation of carboxylate moiety due to aggregation of complex molecules brought about by the decrease in water content of the gel and subsequent formation of a solid matrix (molecular solid). It is interesting to note that asymmetric stretching mode of NO<sub>3</sub><sup>-</sup> ions at 1383 cm<sup>-1</sup> remains nearly unaffected with increase in temperature which suggests that NO<sub>3</sub><sup>-</sup> ions exist as a charge neutralizing species in the outer sphere region of the complex. Hence from the FT-IR results it is inferred that hydrated complex of glycine with Th<sup>4+</sup> ions formed in the gel at room temperature undergoes aggregation upon progressive dehydration brought about by increasing in temperature and finally results in the formation of solid matrix or a molecular solid.

Figure 6.9 shows the Raman spectra of as-prepared gel sample. The pattern matches fairly well with that reported for hexanuclear Ce(IV)-glycine complexes [240], which confirm that similar Th(IV)-glycine complex also exist in the gel phase. Raman spectrum of precursor obtained by heating the gel up to 460 K was also recorded, which showed very high background and therefore did not provide useful information.

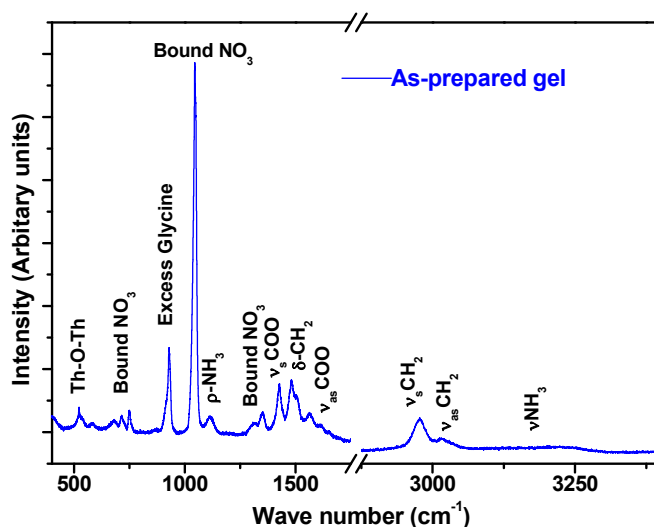


Fig. 6.9. Raman spectrum of as-prepared glycine-Th(IV)-nitrate gel

#### 6.3.1.6. Discussion (Glycine-nitrate solution combustion synthesis of ThO<sub>2</sub>)

Based on the results presented above, a mechanism for glycine-nitrate solution combustion synthesis of ThO<sub>2</sub> is suggested as follows: Starting aqueous solution contains Th(IV)-species, NO<sub>3</sub><sup>-</sup> ions and glycine. Highly acidic nature of this solution was revealed by pH measurement (pH ≤ 1). It is expected since Th(IV) undergoes hydrolysis in aqueous solution to form Th(OH<sub>2</sub>)<sub>n</sub><sup>4+</sup>, Th(OH)<sub>n</sub><sup>(4-n)+</sup> and polynuclear Th<sub>m</sub>(OH)<sub>p</sub><sup>(4m-p)+</sup> species [241, 242]. Presence of strong ligand like glycine in the medium leads to complexation of ligand with Th(IV) species, which act as a competing process for hydrolysis [243]. At ambient temperature, Th(IV)-complexes and hydrolyzed Th(IV) species would co-exist. Their relative concentration would depend on the starting stoichiometry, extent of water content in the medium and temperature.

Heating of such solution leads to evaporation of acidic water vapours. This was confirmed by exposure of evolved vapours to neutral pH paper and monitoring the changes in pH value. A photograph showing colour of pH paper at different sample temperatures (kept inside a quartz tube at the uniform hot zone of the furnace) is shown in Fig. 6.10.



**Fig. 6.10. Estimation of pH of vapours evolved during heating of glycine-Th(IV)-nitrate gel. Gel was heated inside quartz tube and vapours were carried up to pH paper by argon gas flow**

This experiment ruled out the possibility of glycine decomposition up to 423 K, which would have increased the pH due to NH<sub>3</sub> gas evolution as a decomposition product [230]. Upon further heating (490 K - 533 K), pH of evolved vapours increased to a value of 6-7 indicating the occurrence of combustion resulting into NH<sub>3</sub> gas evolution.

With loss of acidic vapours, following changes occur in the aqueous solution: (i) Effective concentrations of constituent species increase until a viscous transparent gel is formed and (ii) pH of gel gradually increases. Concentration increase brings in aggregation of Th(IV)-glycine complexes. Hennig et al., have characterized hexanuclear Th(IV)-glycine complexes in aqueous solutions by EXAFS studies and reported stabilization of these complexes with increasing solution pH [244]. These hexanuclear complexes consist of  $[M_6(\mu_3-O)_4(\mu_3-OH)_4]^{12+}$  polyhedral framework (M = Th(IV), Zr(IV), Ce(IV), etc.) while the formal charge is balanced by glycinate ligand and excess nitrate ions [244, 245]. Since pH is likely to increase with continued heating of glycine-nitrate aqueous solution, such complexes must be getting

stabilized in gel phase. Presence of hexanuclear complexes in gel prepared by us is also evidenced by a very close match of Raman spectrum (Fig. 6.9) with that of solid crystals of hexanuclear Ce(IV)-glycine complex reported by Estes et al. [240]. Apart from hexanuclear complexes, it is possible that other mono / multi-nuclear Th(IV)-glycine complexes can also be present in aqueous solutions under highly acidic conditions [244-247]. Coordination environment of such complexes must be stabilized by water of hydration. Well crystalline powder XRD pattern of gel slowly dried at ambient temperature inside a desiccator (inset in Fig. 6.7), which is different from that of starting reactants / gel provides further evidence that gel mainly consists of different types of Th(IV)-glycine complexes. Along with complexes, gel may also contain residual glycine, hydrolyzed Th(IV)-OH species, nitrate ions and excess water. Actual concentration of these species would primarily depend upon F:O ratio and fractional concentration of various complexes formed inside the gel. When the transparent gel is further heated (400 K - 498 K), it shows onset of weight loss around 438 K (Fig. 6.6), which is quite lower than that of pure glycine decomposition (> 500 K). The observed weight loss is associated with loss of acidic water vapours (confirmed by pH estimation) and subsequent excessive swelling of gel to transform into yellowish-brown porous solid material. Ammonia gas evolution did not occur during the process as revealed by the exposure of the evolved gas to pH paper, which confirmed that decomposition of glycine do not commence ~ 438 K in the gel phase.

In the light of the above observations, exothermic peak observed ~ 487 K in the DSC patterns can be explained in the following way: When the gel containing Th(IV)-glycine complexes and other residual species is heated, acidic vapours get evaporated out. As a result, the gel undergoes a dynamic transformation to a precursor, which mostly consist of mono and multi nuclear, anhydrous Th(IV)-glycine complexes. Such complexes are highly susceptible for

water absorption and this aspect is quite clear from the hygroscopic nature of the precursor. DSC results indicate stability of this precursor up to  $\sim 495$  K. Samples annealed under static conditions also showed precursor's thermal stability up to 463 K (44 h). The molecular complexes existing in the gel phase must be getting aggregated due to lack of water molecules and forming a solid material (molecular solid). Since this process is quite rapid with the complex molecules upon heating, the motifs in the solid matrix might not be getting arranged in a regular fashion leading to a disordered phase. Broad peak observed in the XRD pattern further confirms this conjecture. The facts that an ordered crystalline phase was observed when the gel was dried at ambient temperature inside a desiccator over a period of several days as well as transparent crystals were obtained from glycine-rich solutions; further confirm the aggregation of complexes and formation of solid matrix. Formation of such solid materials from the complexes in solution must be giving rise to exothermic peak in the DSC patterns shown in Fig. 6.1. Also, the heat released in this exothermic process must be sufficiently large as compared to the heat required for endothermic decomposition of nitrate ions and evaporation of water. As a result, a broad exothermic peak ( $\sim 487$  K) is observed in the DSC patterns.

Upon further heating (498 K - 573 K), the dehydrated precursor (poorly crystalline solid) undergoes thermal decomposition, initiated by scission of glycine molecule, which evolves NH<sub>3</sub> gas as by-product. Ammonia so released reacts with nitrate ions and result into rapid and highly exothermic decomposition of the precursor to produce nanocrystalline ThO<sub>2</sub> as end product. This is exhibited in form of intense exothermic DSC peak, characteristic of autoignition (or combustion) process. Since powder properties of combustion synthesized ThO<sub>2</sub> are known to vary significantly with fuel to oxidant ratio, it is likely that this ratio

decides the relative fractions of different type of complexes as well as the composition of the poorly crystalline molecular solid.

To summarize, from the studies reported on glycine-Th(IV)-nitrate aqueous gels, it is concluded that mono and multi-nuclear complexes of Th(IV), glycine and NO<sub>3</sub><sup>-</sup> are formed in the aqueous gel phase. Upon thermal treatment, these complexes undergo rapid aggregation at a temperature ~ 480 K along with loss of acidic water vapours resulting in the formation of poorly crystalline molecular solids. This process is characterized by an exothermic peak in DSC measurements ~ 480 K. Transformation of aqueous gel into a solid molecular precursor consisting of Th(IV)-glycine-nitrate complexes has been supported by results of XRD, FT-IR and Raman Spectroscopy. The molecular solid; above 500 K, undergoes highly exothermic combustion leading to formation of nanocrystalline ThO<sub>2</sub>.

### **6.3.2. Mechanism of citrate-nitrate combustion synthesis of nanocrystalline ThO<sub>2</sub>**

Thermal analysis of stoichiometric citrate-Th(IV)-nitrate aqueous gel (Fig. 6.1) indicates their distinct thermal behavior as compared to glycine-nitrate system (Section 6.3.1.). Detailed studies have been carried out to understand citrate-nitrate combustion synthesis of nanocrystalline ThO<sub>2</sub>. The results are discussed in the following section. Based on the results, a plausible mechanism has been suggested / proposed.

#### **6.3.2.1. Probing citrate-nitrate combustion by thermal analysis (DSC results)**

Figure 6.11 shows DSC thermograms recorded on stoichiometric citrate-Th(IV)-nitrate gel over two consecutive heating cycles. Thermograms are vertically shifted for clear representation. Thermogram recorded during the first heating cycle shows an endothermic peak ~ 409 K, which is neither observed as exotherm during the cooling cycle nor seen again

in the thermogram recorded during second 2<sup>nd</sup> heating cycle. This confirms the irreversible nature of thermal event associated with the endothermic DSC peak. An intense exothermic peak ( $\sim 437$  K), which characterizes autoignition of gel precursor [227, 125] is observed during the second heating cycle.

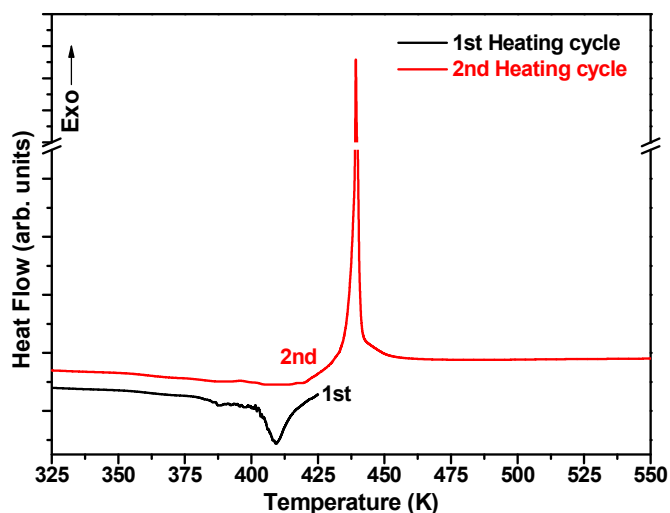


**Fig. 6.11. DSC thermograms recorded on stoichiometric citrate-Th(IV)-nitrate gels during consecutive heating cycles**

Figure 6.12 shows DSC thermograms recorded on citrate-Th(IV)-nitrate aqueous gels prepared with varying fuel to oxidant ratios ( $0.75 \leq \text{F:O} \leq 1.25$ ). Irrespective of F:O value, all citrate-Th(IV)-nitrate gels exhibit weak endothermic peak at same temperature ( $\sim 410$  K) with identical peak profile. It is therefore attributed to loss of acidic water vapours from as-prepared gels. This is followed by autoignition of gel (430 K - 454 K), which appears as a broad peak for fuel-deficient gels ( $\text{F:O} < 1.0$ ) and is quite sharp and intense for fuel-rich gels ( $1.00 \leq \text{F:O} \leq 1.25$ ). With increasing F:O value, autoignition peak temperature systematically decreases from  $\sim 454$  K ( $\text{F:O} = 0.75$ ) to  $\sim 430$  K ( $\text{F:O} = 1.25$ ). To confirm autoignition of citrate-Th(IV)-nitrate gels, separate experiments were performed on few representative

samples (F:O = 0.90 , 1.00, 1.10, 1.20). Gel samples (8-10 mg) kept in open aluminum pans (200  $\mu$ l volume) were heated over a hot plate in air and gel temperature was monitored by IR thermometer. After initial release of vapours in the form of bubbles ( $\sim$  373 K to 400 K), ignition of dried gel with burst release of brown-coloured vapours was observed around 425 K to 430 K. These experiments confirmed that the first exothermic DSC peak (425 K to 440 K) observed in citrate-Th(IV)-nitrate gels, originates from autoignition of gel precursor. Citrate-Th(IV)-nitrate gels undergo autoignition at lower temperatures as compared to corresponding glycine-Th(IV)-nitrate gels ( $>$  505 K; Fig. 6.3).

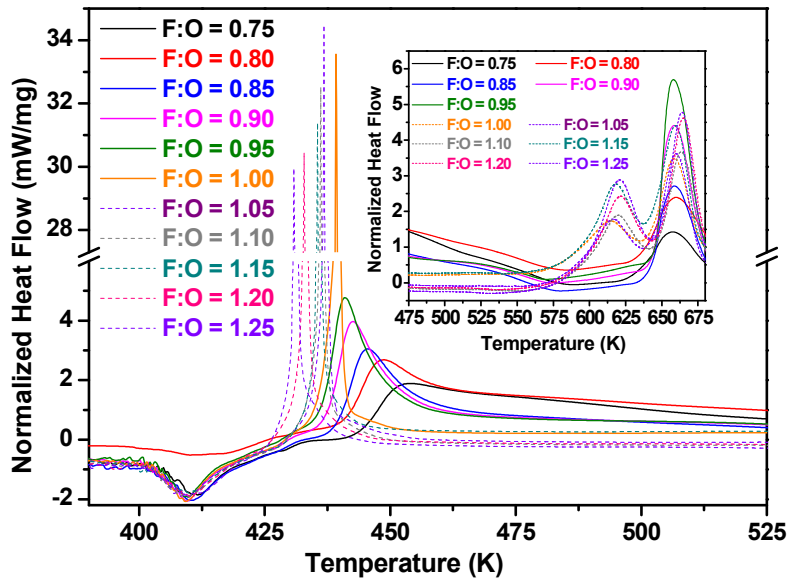


**Fig. 6.12.** DSC thermograms of citrate-nitrate gels ( $0.75 \leq \text{F:O} \leq 1.25$ ). Inset shows expanded view of thermograms over 475 K to 630 K

Inset in Fig. 6.12 shows additional exothermic peaks in high temperature region (600 K to 700 K). For fuel-deficient compositions (F:O  $<$  1.0), a single exothermic peak is observed  $\sim$  660 K. On the other hand, all fuel-rich compositions (F:O  $\geq$  1.0) show two exothermic peaks  $\sim$  620 K and  $\sim$  660 K. These exotherms have been attributed to combustion / oxidation of

residual species after the auto-ignition of gel precursor. These include carbonaceous residue from the fuel and nitrate residue (if any) from the oxidant.

The autoignition peak temperature ( $\sim 435$  K) is lower than the peak temperature for thermal decomposition of starting reactants namely; citric acid ( $\sim 450$  K) and thorium nitrate ( $\sim 453$  K), measured by DSC under identical experimental conditions. These results are shown in Fig. 6.13. Also, none of the studied gel samples showed endothermic peak due to melting of free citric acid ( $\sim 426$  K) prior to decomposition. Endothermic peak observed at  $\sim 410$  K cannot be attributed to melting of free citric acid since its peak profile is quite broad, which is uncharacteristic of melting process. Also, consideration of melting point depression (by  $\sim 15$  K) in the gel phase is unlikely as it would have resulted in variation in temperature (onset / peak) of endothermic peak with different values of F:O. These results indicate absence of free reactants in gel phase. Also, distinct chemical interactions among the constituent species in the gel phase are responsible for its exothermic autoignition, which have been probed further.

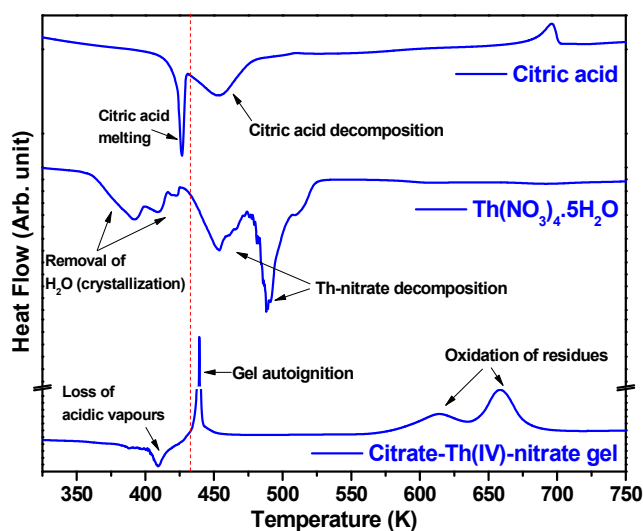


**Fig. 6.13. DSC thermograms of anhydrous citric acid (C<sub>6</sub>H<sub>8</sub>O<sub>7</sub>), (Th(NO<sub>3</sub>)<sub>4</sub>·5H<sub>2</sub>O) and citrate-Th(IV)-nitrate gel (F:O = 1.0) in flowing oxygen atmosphere**

DSC results shown in Fig. 6.12 provide further insight into citrate-nitrate combustion synthesis of ThO<sub>2</sub>. Profile of auto-ignition exothermic peak can be seen along with that of high temperature exothermic peaks (600 K – 700 K). For fuel-deficient gels ( $0.75 \leq \text{F:O} < 1.0$ ), a weak auto-ignition spans over large temperature interval (20-25 K) and is followed by broad exothermic peak at ~ 660 K. On the other hand, fuel-rich gels ( $1.00 \leq \text{F:O} \leq 1.25$ ) undergo rapid auto-ignition with intense exothermic peak followed by two high temperature exotherms (~ 620 K and ~ 660 K). Variation of peak temperatures for these exothermic peaks with fuel to oxidant ratio (F:O) is shown in Fig. 6.14. It can be seen that with increasing F:O values, while autoignition temperature systematically decreases, the temperature of higher exothermic events show marginal increase.

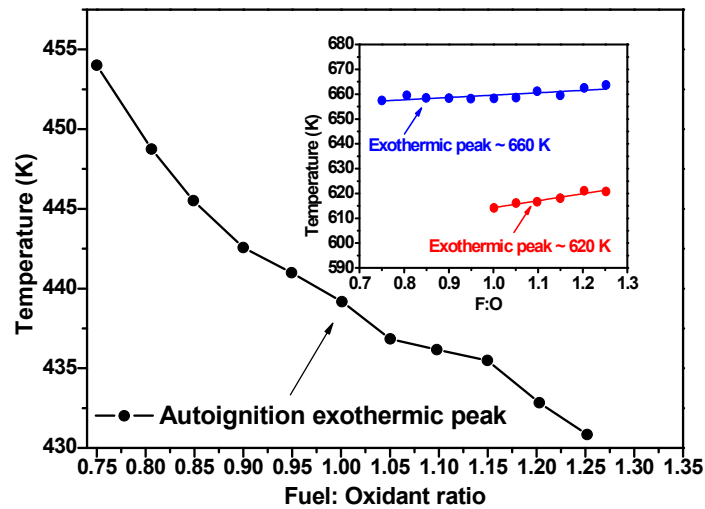


**Fig. 6.14. Variation of autoignition temperature with fuel to oxidant ratio.**

**Corresponding variation for high temperature exothermic peaks (620 K – 660 K) is shown in the inset**

Nature of DSC baseline over the temperature range from 450 K to 600 K (Fig. 6.12) is quite different for fuel-deficient and fuel-rich gels. This region shows the thermal behavior of auto-

ignited precursors up to the onset of exothermic oxidation of residual carbonaceous species. Fuel-deficient precursors ( $F:O < 1.0$ ) show a baseline shift around 575 K; typically like a weak glass transition event, which suggests glassy (or amorphous) nature of fuel-deficient auto-ignited precursors. Fuel-rich gels ( $F:O \geq 1.0$ ) on the other hand, show flat baseline, which is followed by two high temperature exothermic peaks ( $\sim 620$  K and  $\sim 660$  K).

Enthalpies associated with exothermic DSC peaks were evaluated from normalized DSC curves. These values are plotted as a function of F:O values in Fig. 6.15. For fuel-rich compositions, enthalpy values were obtained by adding the area associated with both high temperature exothermic peaks ( $\sim 620$  K and  $\sim 660$  K). Enthalpy associated with high temperature exotherm(s) increases linearly with F:O while that of the autoignition event decreases, as shown in the inset of Fig. 6.15. It must be mentioned that enthalpies associated with low temperature endothermic peak ( $\sim 410$  K) were nearly constant for all F:O values.

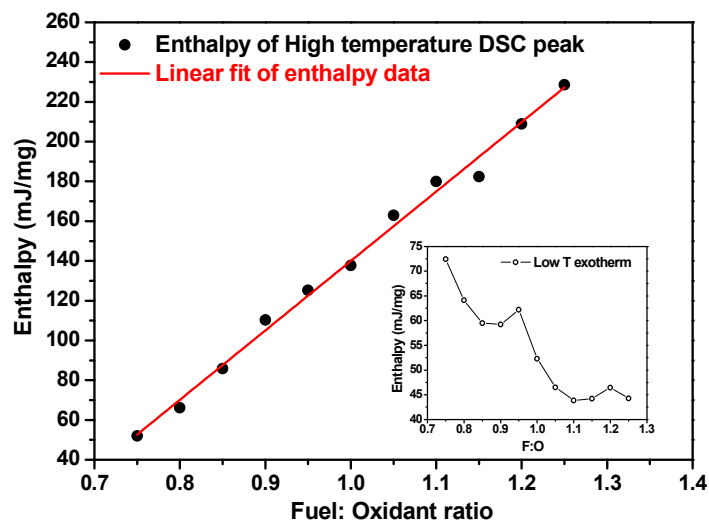


**Fig. 6.15.** Enthalpy associated with high temperature DSC exotherm(s) in citrate-Th(IV)-nitrate gels as a function of F:O. Corresponding variation in enthalpy of autoignition process is shown in the inset

### 6.3.2.2. X-ray diffraction studies on citrate-Th(IV)-nitrate gel and ThO<sub>2</sub> powders

Figure 6.16 shows XRD patterns recorded on as-prepared stoichiometric citrate-Th(IV)-nitrate gel, as-combusted powder and powder calcined to 723 K in air. While as-prepared gel is amorphous in nature, a broad diffraction hump ( $2\theta \sim 18^\circ$ ) indicates short-range ordering existing in the gel. Broad diffraction hump around  $27.5^\circ$  for as-combusted powder shows highly disordered combustion product. Diffraction peaks corresponding to cubic fluorite ThO<sub>2</sub> (space group: Fm3m) in air calcined powder confirm its nanocrystalline nature. Average crystallite size calculated from diffraction peak broadening using Scherrer formula was  $\sim 4$  nm. Average crystallite remains nearly same (3-5 nm) for studied F:O values ( $0.75 \leq F:O \leq 1.25$ ). Estimated lattice parameter is 5.609(3) Å, which is larger than bulk ThO<sub>2</sub> by  $\sim 0.5\%$  [181] and is expected due to nanocrystalline nature of powders. Upon calcination (973 K; static air), average crystallite size increases to  $\sim 15$  nm due to grain coarsening.

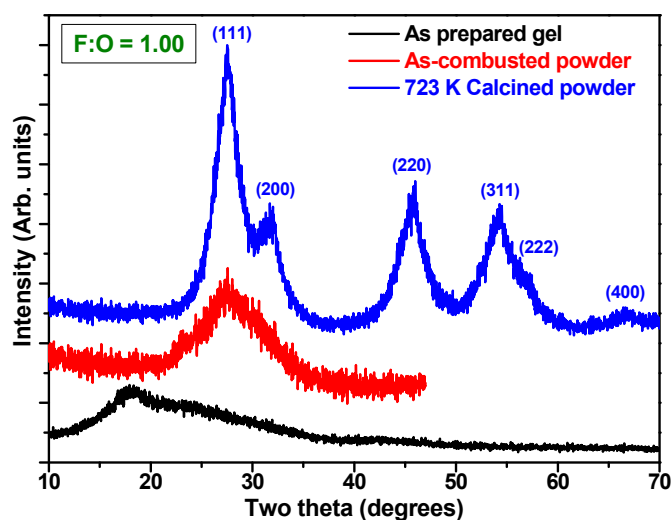


**Fig. 6.16.** Powder XRD patterns corresponding to as-prepared stoichiometric (F:O = 1.0) citrate-Th(IV)-nitrate gel, as-combusted ThO<sub>2</sub> powder and 723 K calcined powder

### 6.3.2.3. Raman Spectroscopic studies on citrate-Th(IV)-nitrate system

Ambient temperature Raman Spectra of thorium nitrate (solid), citric acid (solid) and stoichiometric citrate-Th(IV)-nitrate aqueous solutions are shown in Fig. 6.17. Raman spectra of pure components match with those reported earlier [248, 249]. However, Raman spectrum of citrate-Th(IV)-nitrate aqueous solution shows only one broad peak ( $\sim 1047 \text{ cm}^{-1}$ ), which resembles with vibration of free nitrate ion ( $\nu_1(A_1')$   $\sim 1052 \text{ cm}^{-1}$ ) and complexed nitrate ion ( $\sim 1038 \text{ cm}^{-1}$ ) as reported for aqueous solution of thorium nitrate [248]. It is different from the Raman band observed for solid thorium nitrate in the form of three overlapping peaks ( $\sim 1032 \text{ cm}^{-1}$ ,  $\sim 1036 \text{ cm}^{-1}$ ,  $\sim 1040 \text{ cm}^{-1}$ ) as shown in Fig. 6.17. Low energy Raman bands ( $700 \text{ cm}^{-1}$  -  $760 \text{ cm}^{-1}$ ) corresponding to free nitrate ( $\nu_4(E')$ ) as well as complexed nitrate species, which are observed in solid thorium nitrate and are reported for its aqueous solutions [248], are also absent in citrate-Th(IV)-nitrate solutions.

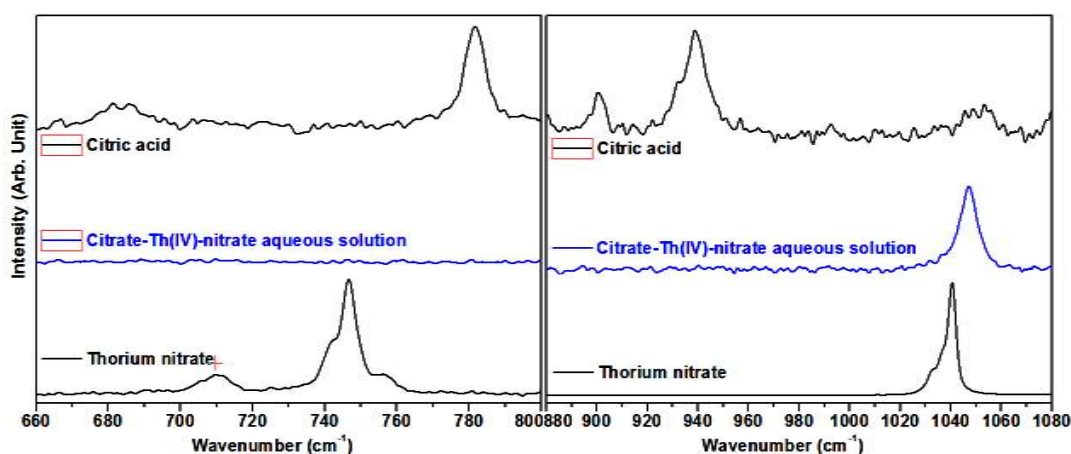


**Fig. 6.17. Ambient temperature Raman Spectra of thorium nitrate (solid), citric acid (solid) and stoichiometric citrate-Th(IV)-nitrate aqueous solution**

No Raman peak due to citric acid (or citrate ions) is observed in citrate-Th(IV)-nitrate aqueous solution. It must be mentioned that Raman spectra of citrate-Th(IV)-nitrate solutions

appeared similar for all F:O values studied here. These results confirm the presence of free nitrate species in as-prepared citrate-Th(IV)-nitrate solutions. Absence of Raman peaks due to citric acid (or citrate) indicates the formation of Th(IV)-citrate complexes in the aqueous solution. Ideally, free nitrate vibrational band in aqueous solution should result into band narrowing. Contrarily, broadening of Raman peak  $\sim 1047 \text{ cm}^{-1}$  in citrate-Th(IV)-nitrate solution indicates constrained motion of nitrate species brought about by the formation of Th(IV)-citrate-nitrate molecular complexes.

Figure 6.18 shows Raman Spectra of as-combusted powder obtained from stoichiometric citrate-Th(IV)-nitrate gel, Powder calcined at 723 K in air and ThO<sub>2</sub> sintered at 1773 K in argon atmosphere.

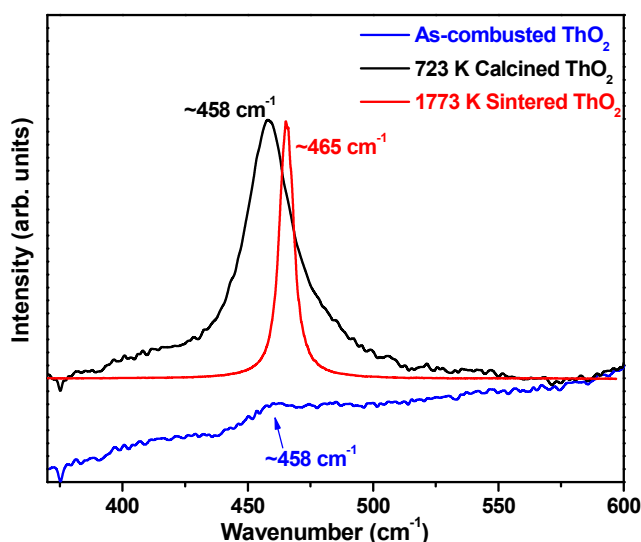


**Fig. 6.18. Ambient temperature Raman spectra of as-combusted citrate-Th(IV)-nitrate gel (F:O = 1.0), calcined ThO<sub>2</sub> powder and sintered ThO<sub>2</sub>**

As-combusted powder gives poorly resolved Raman spectrum with a broad hump around 458 cm<sup>-1</sup>, which indicate highly disordered ThO<sub>2</sub> phase. Upon calcination at 723 K in air, a well resolved broad Raman peak ( $\sim 458 \text{ cm}^{-1}$ ) corresponding to the first order Raman mode of

fluorite ThO<sub>2</sub> [250] is observed. As compared to bulk ThO<sub>2</sub> ( $\sim 465 \text{ cm}^{-1}$ , FWHM  $\sim 6.5 \text{ cm}^{-1}$ ) obtained by sintering of calcined powder at 1773 K, red shift in peak position (by  $\sim 7 \text{ cm}^{-1}$ ) with significant band broadening (FWHM  $\sim 23 \text{ cm}^{-1}$ ) observed in calcined ThO<sub>2</sub> powder confirm its nanocrystalline nature. The Raman peak shift can be attributed to unsaturated bonds at the surface of nano-sized ThO<sub>2</sub> crystallites.

#### 6.3.2.4. Citrate-nitrate solution combustion synthesis of ThO<sub>2</sub>: mechanistic aspects

Based on results presented above, following mechanism is proposed for citrate-nitrate combustion synthesis of ThO<sub>2</sub>. It is known that Th(IV) undergoes extensive hydrolysis in aqueous solution of thorium nitrate to form several mono- and poly-nuclear Th(IV)-OH complexes [241]. Nature and concentration of these complexes depend upon Th(IV) content, pH and temperature. Solutions used in present study ( $\sim 0.8$  molal Th(IV)) are highly acidic ( $\text{pH} \leq 1$ ) and Th(IV) predominantly exists in free ionic form ( $\text{Th}^{4+}$ ) with very little contribution of  $(\text{ThOH})^{3+}$  [251]. When citric acid is added to such solutions, Th(IV)-citrate complexes are formed, which are more stable ( $\log K_{\text{Th}(\text{C}_6\text{H}_5\text{O}_7)^+} = 13.0$ ) than Th(IV)-OH complexes ( $\log K_{(\text{ThOH})^{3+}} = 10.8$ ) or Th(IV)-nitrate complex ( $\log K_{(\text{Th-NO}_3)^{3+}} = 0.94$ ). Here, (Log K) refers to cumulative formation constant for such complexes. Similar trends in stability constants are reported for higher complexes ( $\text{ML}_2$ ,  $\text{ML}_3$ , etc.) also [251]. It is also reported that complexes with general composition  $\text{ML}$ ,  $\text{MHL}$ ,  $\text{ML}_2$ ,  $\text{MH}_2\text{L}_2$ ,  $\text{M}(\text{OH})_2\text{L}_2$ ,  $\text{ML}_3$ ,  $\text{MHL}_3$ ,  $\text{M}_2\text{L}_3$ ,  $(\text{ML})_n$ , etc. could be formed in Th(IV)-citrate aqueous solutions, where  $\text{M} = \text{Th(IV)}$  and  $\text{L} = \text{citrate ligand}$  [252-254]. However, there are no reports on isolation, characterization and thermal decomposition of any Th(IV)-citrate complex in solid form. In highly acidic aqueous solutions ( $\text{pH} \leq 1$ ), wherein citric acid is more likely to remain in protonated form, predominance of a complex species would depend upon pH, temperature, Th(IV):citrate molar ratio and solution's ionic strength. For solutions used in present study,

citric acid (fuel) to thorium nitrate (oxidant) molar ratio varies from 1.00 (F:O = 0.90) to 1.39 (F:O = 1.25). Taking into account the water of crystallization from Th(NO<sub>3</sub>)<sub>4</sub>·5H<sub>2</sub>O and citric acid (C<sub>6</sub>H<sub>8</sub>O<sub>7</sub>·H<sub>2</sub>O) along with solvent water used for preparation of starting solutions, the molal concentrations varied over (i) 0.80 to 1.108 for citric acid, (ii) 0.80 to 0.796 for Th(IV) and (iii) 3.204 to 3.186 for nitrate (NO<sub>3</sub><sup>-</sup>) for F:O = 0.90 to F:O = 1.25, respectively. Under highly acidic medium (pH ≤ 1) with citric acid to Th(IV) molar ratio varying over 1.00 to 1.39, Th(C<sub>6</sub>H<sub>5</sub>O<sub>7</sub>)<sup>+</sup> complexes are likely to exist along with Th(C<sub>6</sub>H<sub>5</sub>O<sub>7</sub>)<sub>2</sub><sup>2-</sup> in order to accommodate excess citric acid beyond M + L ⇌ ML equilibrium. These solutions also contain excess free nitrate (NO<sub>3</sub><sup>-</sup>) ions, as confirmed by Raman spectroscopy. Absence of Raman peaks due to citrate species and notable variation in profile of nitrate peak further support the formation of Th(IV)-citrate molecular complexes in aqueous solutions (Fig. 6.17). Heating these solutions result into loss of acidic water vapours. It must be noted here that few reports on citrate-nitrate combustion synthesis of ThO<sub>2</sub> mention appearance of white precipitate (attributed to thorium citrate) during initial heating of aqueous solution, which disappears upon further heating [123, 125]. In present studies, when as-prepared solutions (F:O = 0.90, 1.00, 1.10) were diluted with equal volume of water and heated up to 373 K over a boiling water bath, a white precipitate was obtained. This precipitate disappeared upon continued evaporation of excess water at 373 K. With loss of acidic vapours, effective concentrations of Th(IV), citrate and nitrate species increase and a highly viscous, transparent gel is obtained. Upon further heating, yellow-brown coloured bubbles could be seen appearing inside these gels, which indicated decomposition of free nitrate (nitric acid) along with removal of water that helps in gel network formation. This has been observed in DSC experiments in the form of broad endothermic peak ~ 410 K (Fig. 6.11). Similar results of release of H<sub>2</sub>O and NO<sub>2</sub> gases from citrate-Th(IV)-nitrate aqueous solutions have been reported by Kumar et al., [125] using evolved gas analysis (EGA) technique. Residue

obtained at this stage would contain Th(IV)-citrate-nitrate complexes, free citric acid (if any) and water of hydration. Absence of endothermic melting peak for citric acid (Fig. 6.13) in DSC thermogram of citrate-Th(IV)-nitrate gels (Fig. 6.12) suggest that citric acid is completely utilized in complex formation by forming higher complexes (such as ML<sub>2</sub>) apart from Th(C<sub>6</sub>H<sub>5</sub>O<sub>7</sub>)<sup>+</sup> (ML). Unlike glycine-Th(IV)-nitrate system (Section 6.3.1), ordering / crystallization of complex molecules is not observed in citrate-Th(IV)-nitrate precursors prior to autoignition due to multi-denticity of citric acid ligand as compared to glycine. These precursors therefore remain predominantly as random mixture (amorphous like) of complex molecules and residual species. Further heating of precursor leads to auto-ignition, initiated by the oxidative decomposition of nitrates as observed in terms of burst release of brown vapours during auto-ignition. For fuel-deficient compositions (F:O < 1.0), where nitrate has higher relative concentration than citric acid, auto-ignition wave spreads through the combusting mass and results into broad and weak exothermic peak in DSC experiments and a part of the citrate moieties is only oxidized. For fuel-rich compositions (F:O ≥ 1.0), since relative concentration of nitrate is lower than that of citric acid, nitrate species are more surrounded by Th(IV)-citrate complexes and the auto-ignition wave is not able to sustain through the dry gel-precursor. As a result, it appears as sharp exothermic peak, leaving behind mostly un-burnt amorphous precursor. In other words, the auto-ignition wave is not able to sustain itself in fuel-rich precursors. This was visibly observed when combustion was carried out in open DSC pans over a hot plate. Wherein fuel-deficient precursors converted to greyish-black coloured residue immediately after autoignition, all fuel-rich precursors remained yellowish solid. As a result of this, further heating of fuel-rich combustion residues show up two high temperature exotherms (~ 620 K and ~660 K) in contrast to single exotherm (~ 660 K) for all fuel-deficient residues. The lower temperature exotherm (~ 620 K) corresponds to oxidation of the partially burnt precursor, left during the rapid auto-ignition

event. Due to spread of autoignition wave all through the fuel deficient precursors, the product consists of highly disordered residual citrate moieties with ThO<sub>2</sub> crystallites. Due to this, heat flow behavior of auto-ignited product in fuel-deficient composition exhibit a baseline shift just before the onset of high temperature oxidation (as shown in inset of Fig. 6.12). The high temperature exotherm (~ 660 K) results from oxidative decomposition of residual citrate moieties [255, 256]. Powders obtained from glycine-Th(IV)-nitrate combustion showed better crystallinity as compared to those obtained through citrate-Th(IV)-nitrate combustion. Near-amorphous XRD patterns of citrate-nitrate combustion products are due to very small crystallite size (< 4 nm) and presence of large amounts of disordered carbonaceous residue as confirmed by FT-IR measurements. Raman studies also indicate highly disordered nature of as-combusted powders (Fig. 6.18). For a highly disordered precursor consisting of mixture of Th(IV)-citrate complexes and residual species (water, nitrate, etc.), autoignition temperature is likely to be governed by total fuel content. Autoignition is expected to occur at lower temperature with higher fuel availability. Systematically decreasing autoignition temperature with F:O value supports the above reasoning (Fig. 6.14). On the other hand, oxidation of residual carbonaceous species or partially burnt fuel would occur at same temperature irrespective of F:O ratio, which has also been observed (inset in Fig. 6.14).

It is known that thermal decomposition of citric acid [255] as well as metal citrates [256-259] is a complex multistep process passing through citrate dehydration to produce aconitic acid (or corresponding carboxyllates), which further undergoes decarboxylation to produce a cyclic compound, 'citraconic anhydride'. The anhydride thermally oxidizes to form CO<sub>2</sub> and H<sub>2</sub>O at higher temperatures [256]. Overall citrate decomposition is therefore a sluggish process, which also depends on heating rate and heating atmosphere (oxidizing / inert). While

there is no literature report on thermal decomposition behavior of isolated pure thorium citrates, it is clear from the studies that citrate-nitrate combustion synthesis of ThO<sub>2</sub> involves decomposition of thorium-citrate complexes along with free nitrate species. Combustion would therefore proceed in a sluggish manner and as-combusted powders would contain residual intermediate products of citrate decomposition. This would reduce the instantaneous exothermicity of combustion wave and lead to lesser pre-sintering of as-formed ThO<sub>2</sub> particles. Also, as-synthesized ThO<sub>2</sub> particles would be embedded in a matrix of un-burnt citrate residues (and nitrate, if any) and would not get the opportunity to grow in size during propagation of combustion wave, therefore resulting into smaller crystallites. XRD derived average crystallite size (3-5 nm) of as-combusted powders confirm the same.

Present studies on citrate-nitrate solution combustion synthesis of nanocrystalline ThO<sub>2</sub> powders have shown that citrate-Th(IV)-nitrate gels auto-ignite at low temperatures (430 K – 450 K) but overall combustion process is sluggish, primarily due to multi-step decomposition of citrate moieties. Thermal analysis and XRD studies confirm that presence of carbonaceous residue after auto-ignition in citrate-nitrate method act as an inert matrix and significantly prevent the aggregation of nanocrystalline ThO<sub>2</sub>, leading to formation of very small sized (3-5 nm) ThO<sub>2</sub> crystallites. These results are useful for preparation of nanocrystalline ThO<sub>2</sub> with control on powder properties.

### **6.3.3. Role of fuel to oxidant ratio on the mechanism of glycine-Th(IV)-nitrate combustion synthesis of ThO<sub>2</sub>**

#### **6.3.3.1. Powder properties of combustion synthesized nanocrystalline ThO<sub>2</sub>**

Figure 6.19 shows the variation in average crystallite size of as-combusted ThO<sub>2</sub> powders with fuel to oxidant ratio. Inset shows XRD patterns recorded on few representative samples

(F:O = 0.75, 0.90, 1.00, 1.25). These powders were synthesized by glycine-Th(IV)-nitrate and citrate-Th(IV)-nitrate solution combustion methods. Crystallite sizes were evaluated from line broadening of powder XRD patterns recorded on as-combusted powders. It can be seen that citrate-nitrate combustion synthesized ThO<sub>2</sub> powders have smaller crystallites (3-5 nm) as compared to those prepared by glycine-nitrate route (5-15 nm). Further, for the studied fuel to oxidant ratios, crystallite size does not vary much for citrate-nitrate derived powders. On the other hand, crystallite size of glycine-nitrate combustion synthesized ThO<sub>2</sub> powders abruptly drops from ~ 14-15 nm to ~ 5-6 nm at F:O ratio exceeding unity, i.e., for all fuel-rich precursors (F:O > 1.0). A sharp drop in average crystallite size upon variation of F:O from fuel-deficient to fuel-rich regime is quite interesting. Detailed experimental investigations have been performed to identify the origin of this variation in context of mechanism of combustion. These results are presented as follows:

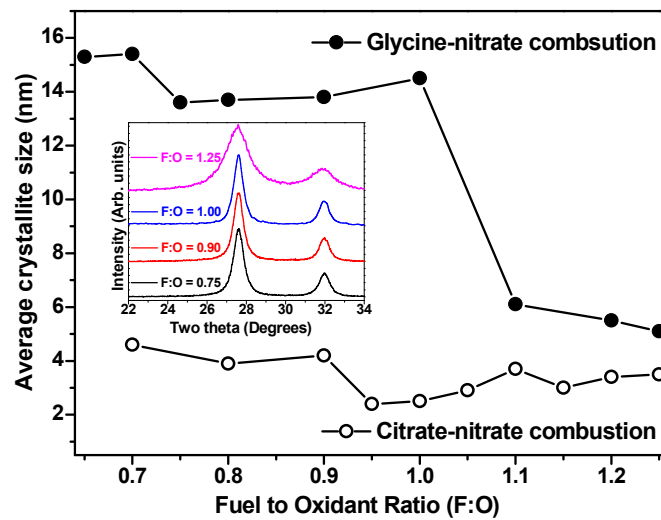


**Fig. 6.19.** Variation of average crystallite size with fuel to oxidant ratio for nanocrystalline ThO<sub>2</sub> synthesized from glycine-Th(IV)-nitrate and citrate-Th(IV)-nitrate combustion. Inset shows XRD patterns recorded on few representative samples (F:O = 0.75, 0.90, 1.00, 1.25)

Figure 6.20 shows F:O dependence of peak width (FWHM) of Raman spectra (first order Raman peak  $\sim 458\text{ cm}^{-1}$ ) recorded on citrate-nitrate and glycine-nitrate combustion products calcined at 723 K in air. Again in line with XRD results, citrate-nitrate combusted ThO<sub>2</sub> powders have larger peak width, which indicate their smaller crystallite size as well as higher structural disorder as compared to ThO<sub>2</sub> powders obtained from glycine-nitrate combustion. Here again, in case of glycine-nitrate combustion, Raman peak width abruptly increases for powders prepared by fuel-excess stoichiometries. These results provided further motivation to look into molecular level interactions in glycine-nitrate systems in more detail.

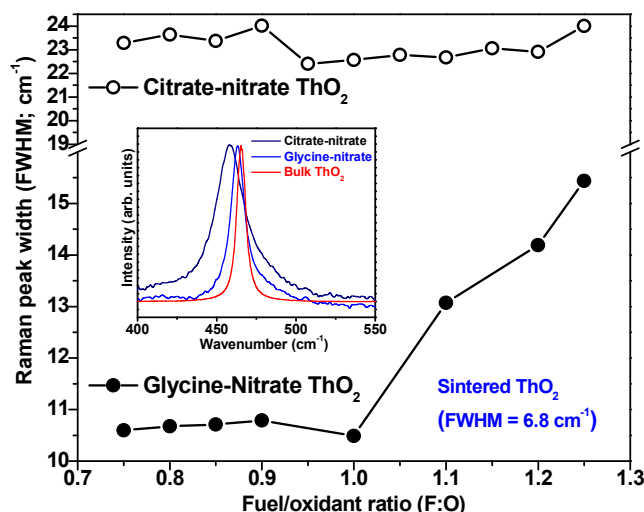


**Fig. 6.20.** Width (FWHM) of the first order Raman peak ( $\sim 458\text{ cm}^{-1}$ ) recorded on ThO<sub>2</sub> powders (calcined at 723 K) prepared by citrate-nitrate and glycine-nitrate combustion.

**Inset shows representative Raman spectra**

### 6.3.3.2. Thermal analysis of glycine-Th(IV)-nitrate gels with different F:O values

Figure 6.21 shows DSC thermograms for glycine-Th(IV)-nitrate gels for F:O = 0.75, 0.90, 1.00 and 1.25. Each thermogram shows a broad exothermic peak (470 K - 505 K) and, intense high temperature peak (507 K - 544 K) corresponding to crystallization / ordering of Th(IV)-glycine molecular complexes and, combustion of dehydrated gel-precursor,

respectively. Apart from molecular complexes, these gels may also contain free NO<sub>3</sub><sup>-</sup> ions and glycine (OOC-CH<sub>2</sub>-NH<sub>3</sub><sup>+</sup>) zwitterionic species, depending upon overall fuel to oxidant ratio.

It can be seen that there is notable change in (i) peak temperatures for both exotherms, (ii) line shape of low temperature exothermic peak and (iii) exothermicity of combustion peak with increasing F:O value. Table 6.1 presents the peak temperatures and enthalpy values as evaluated from DSC thermograms. Total enthalpy was evaluated for combination of both exotherms using a common baseline starting from the onset of low temperature exotherm and extending up to the end of combustion peak. No effort was made to evaluate the enthalpy associated with low temperature exotherms due to their overlapping nature with combustion exotherms; particularly for fuel-deficient precursors.

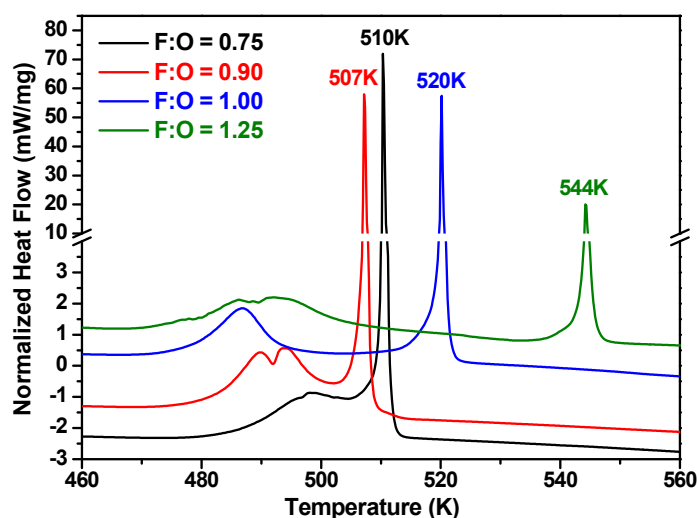


**Fig. 6.21. DSC thermograms of glycine-Th(IV)-nitrate gels with different fuel-to-oxidant ratios**

Observation of both exothermic peaks in DSC curves of the studied solutions (F:O= 0.75, 0.90, 1.00, 1.25) confirm that combustion is always preceded by crystallization / ordering of molecular complexes / aggregates present in these gels. With increasing glycine

concentration, crystallization / ordering shifts towards lower temperature (Table 6.1), which indicate that crystallization is facilitated by glycine.

Glycine concentration therefore plays an important role in the formation of Th<sup>4+</sup>-glycine-NO<sub>3</sub><sup>-</sup> complexes. With increasing F:O, combustion temperature reduces for fuel deficient gels (F:O < 1.0) and increases for fuel-rich gels (F:O > 1.0) as shown in Fig. 6.21 (See also Fig. 6.3). Higher combustion temperatures for fuel-rich gels indicate enhanced thermal stability of precursor, which arises due to enhanced stability of Th<sup>4+</sup>-glycine-NO<sub>3</sub><sup>-</sup> complexes (having higher glycine content) and due to the presence of more and more glycine moieties around the molecular complexes / aggregates.

**Table 6.1. Peak temperatures and enthalpy values obtained from analysis of DSC thermograms recorded on glycine-thorium nitrate aqueous gels**

Fuel to oxidant ratio (F:O)	0.75	0.90	1.00	1.25
Glycine: Th molar ratio	1.67	2.00	2.22	2.78
<b>A. Low temperature exotherm</b>				
Onset temperature (K)	483	481	477	469
Peak temperature (K)	498 <i>(Overlapped with 510 K peak)</i>	490, 494 <i>(Two overlapping peaks)</i>	487	478, 486, 493 <i>(Three overlapping peaks)</i>
<b>B. High temperature exotherm</b>				
Onset temperature (K)	510	507	520	544
Peak temperature (K)	510	507	520	544
Total enthalpy (A+B) (J/g)	~ 456	~ 526	~ 388	~ 427
Enthalpy of combustion (J/g)	~ 185	~ 154	~ 139	~ 82

Figure 6.21 also indicate variation in the shape of low temperature exothermic peak with increasing F:O. The peak broadens with increasing F:O and shows overlapping multi-peak features (Table 6.1). This suggests that more than one type of Th<sup>4+</sup>-glycine-NO<sub>3</sub><sup>-</sup> complexes

with varying number of glycine and NO<sub>3</sub><sup>-</sup> species are formed inside the gel with increasing glycine content. Crystallization kinetics can change with the change in the number of glycine and nitrate species. It may be noted that existence of both mono- and polynuclear complexes of glycine with tetravalent metal ions (Ce<sup>4+</sup>, Th<sup>4+</sup>, Zr<sup>4+</sup>) in aqueous solutions as well as in solid-state has been reported [240, 244, 245].

DSC results also show that exothermicity of combustion decreases with increasing F:O as indicated from combustion peak intensity as well as enthalpy of combustion (Table 6.1). This is understandable as under high glycine concentrations, combustion enthalpy is progressively compensated by the energy required for decomposition of excess residual fuel. This may also result into incomplete fuel burnout in gels containing higher fuel concentration. Fig. 6.22 shows photograph of as-combusted powders indicating progressively darker colour with increasing F:O value.



**Fig. 6.22. Photograph of as-combusted powders with varying F:O ( $0.65 \leq \text{F:O} \leq 1.25$ )**

Incomplete fuel burnout was also supported by weight loss measurements on powders calcined at 973 K in static air for 2 h, which showed 0.76 %, 1.22 %, 2.32 %, 3.56 % loss for F:O = 0.75, 0.90, 1.00 and 1.25, respectively. Notably, calcined powders were apparently identical in color for all values of F:O.

### 6.3.3.3. Small angle X-ray scattering (SAXS) on aqueous gels and as-combusted ThO<sub>2</sub>

For characterizing the microstructure of gels and as-combusted powders, SAXS measurements were performed. Fig. 6.23 shows normalized SAXS profiles of gels (F:O = 0.75, 0.90, 1.0) and crystals grown within the gel (F:O = 1.25) displayed on log-log scale. For gels, SAXS curves are nearly identical in low- $q$  region but differ in high- $q$  region whereas SAXS curve of crystals grown in glycine-rich solution (F:O = 1.25) deviates from other three gels in the whole  $q$ -range. Similarity of SAXS profiles for gels in low- $q$  region indicates identical nature of structural units (network) on large length scale existing in these gels, which can be viewed as clusters of Th<sup>4+</sup>-glycine-NO<sub>3</sub><sup>-</sup> molecular complexes along with free glycine and NO<sub>3</sub><sup>-</sup> ions in a network containing excess water molecules. Deviations observed in high- $q$  region of SAXS curves suggest presence of smaller crystallites / clusters of Th<sup>4+</sup>-glycine-NO<sub>3</sub><sup>-</sup> complexes in these gels and their average size vary with glycine concentration. This indicates that increasing glycine concentration influences both the nature and relative proportion of Th<sup>4+</sup>-glycine-NO<sub>3</sub><sup>-</sup> complexes in the gel.

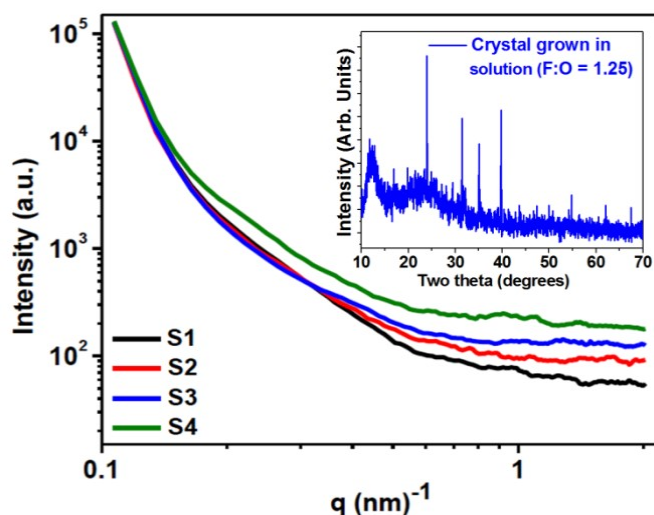


**Fig. 6.23.** Small angle X-ray scattering (SAXS) profiles of three gel samples (S1-S3; F:O = 0.75, 0.90, 1.00) and solid crystals obtained from glycine-rich gel (S4; F:O = 1.25). Inset shows powder XRD pattern of crystal grown in fuel-rich solution (F:O = 1.25)

SAXS profile of crystals obtained from glycine-rich solution (F:O = 1.25) differs over wider- $q$  region ( $q > 0.15 \text{ nm}^{-1}$ ) indicating a change in the structural morphology on larger length scale for this sample. Powder XRD pattern of this sample also showed sharp diffraction peaks, indicating its crystalline nature as shown in inset of Fig. 6.23. These crystals were highly moisture sensitive, which was observed during sample preparation for XRD experiments. Also, exact phase of the crystals could not be identified as it did not match with standard patterns available in JCPDF database. To understand the variation in the structural environment around Th<sup>4+</sup> ions in the precursor gel on the powder characteristics of as-combusted ThO<sub>2</sub>, all the four gel samples were subjected to combustion and the products obtained were characterized by SAXS analysis. Fig. 6.24 shows SAXS profiles of as-combusted ThO<sub>2</sub> powders plotted on log-log scale. SAXS data were unable to fit using a model with structure on a single length scale, indicating existence of multi-modal distribution of crystallites present in as-combusted powders. Hence, assuming the crystallites to be of spherical in shape and have bimodal size distribution, measured SAXS intensities  $I(q)$  were fit to sum of two expressions (equation-6.1); each for spherical particles with a specific radius.

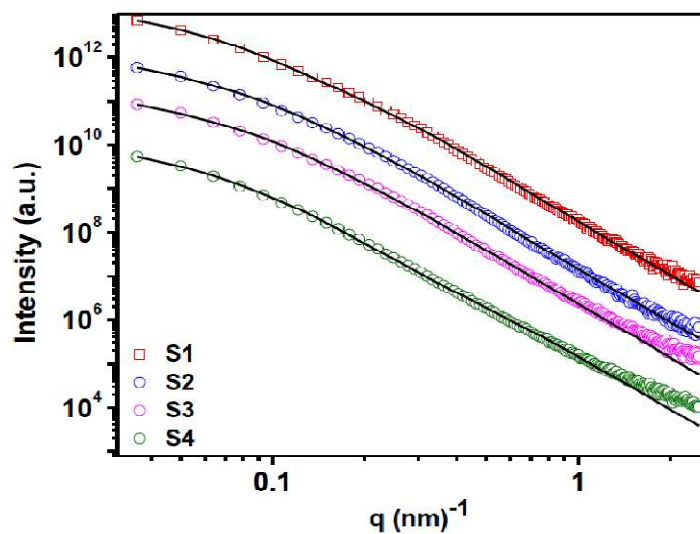


Fig. 6.24. SAXS profiles of as-combusted ThO<sub>2</sub> powders (S1-S4; F:O = 0.75, 0.90, 1.00, 1.25). Symbols are experimental data whereas solid lines are fits

$$I(q) = a1 \int_{R_{\min}}^{R_{\max}} P(q,r)D_1(r, \mu_1, \sigma_1)(V(r))^2 dr + a2 \int_{R_{\min}}^{R_{\max}} P(q,r)D_2(r, \mu_2, \sigma_2)(V(r))^2 dr \quad (6.1)$$

The first term in equation-6.11 represents scattering contribution from large size crystallites and the second term is for contribution from smaller crystallites. The parameters ‘a1’, ‘a2’ are scaling parameters and ‘V(r)’ denotes volume of the spherical crystallites. ‘P(q, r)’ is the square of the form factor and is given by following relation [260, 261]:

$$P(q,r) = \left[ \frac{3(\sin(qr) - qr \cos(qr))}{(qr)^3} \right]^2 \quad (6.2)$$

‘D1’ and ‘D2’ are size distribution functions with log-normal distribution given as [262].

$$D(r, \mu, \sigma) = \frac{1}{r \cdot \sigma \cdot \sqrt{2\pi}} \cdot \exp\left(-\frac{(\ln r - \mu)^2}{2 \cdot \sigma^2}\right) \quad (6.3)$$

Here, ‘r’ is the crystallite radius while ‘μ’ and ‘σ’ are the parameters of the distribution. ‘μ’ is related to mean value of crystallite radius by  $\langle r \rangle = \mu \exp(\sigma^2/2)$ .

It must be mentioned here that calculation of average ThO<sub>2</sub> crystallite sizes assuming spherical shape and cubic symmetry can introduce certain extent of uncertainty in the values. Yet, comparison of values from different samples must be reasonably acceptable. Experimental data have been fit to above expressions and results are shown in Fig. 6.24. Corresponding crystallite size distributions (small and large) are plotted in Fig. 6.25 (a) and (b). Results obtained from fitting the data are summarized in Table 6.2.

It can be noted that the average sizes of larger and smaller crystallites are in the range 14 - 9 nm and 3.2 - 0.6 nm, respectively. The average sizes and peak positions of distribution shifts toward lower values with increasing glycine concentration, indicating gradual reduction in crystallites size as the fuel content in gel-precursor increases. This can be explained as follows: Glycine-rich gels contain excess fuel that is freely present in the gel precursor. During combustion, this excess fuel would also undergo decomposition, thereby utilizing a part of combustion enthalpy.

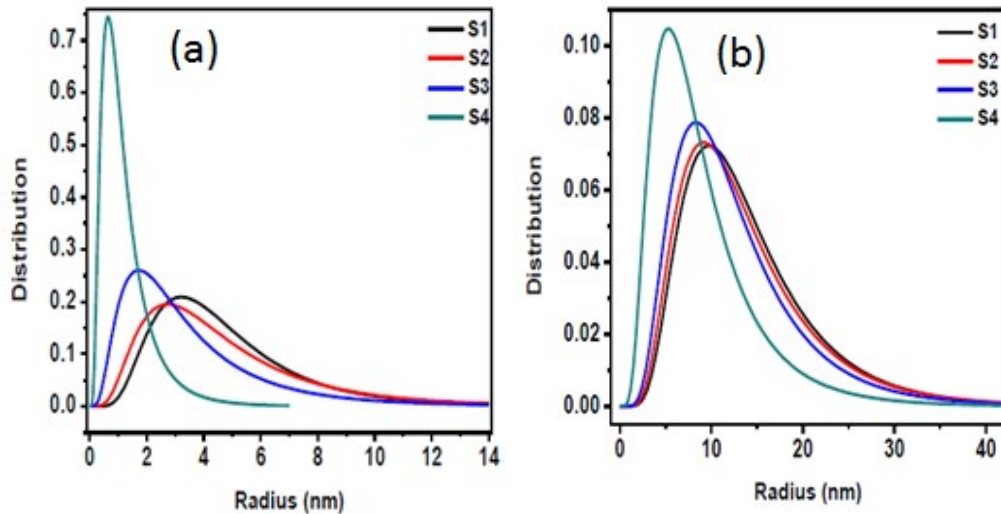


**Fig. 6.25. Crystallite size distribution for as-combusted ThO<sub>2</sub> powders (a) smaller crystallites and (b) larger crystallites. (S1-S4; F:O = 0.75, 0.90, 1.00, 1.25)**

This is indicated by a decreasing trend of combustion enthalpy with increasing F:O value (Table 6.1). Decomposition of gel-precursor having higher fuel concentration would also produce higher amounts of gaseous by-products. These gaseous species would cause local cooling of ThO<sub>2</sub> crystallites produced during combustion and therefore inhibit their local sintering / grain growth phenomenon. As a result, powders with smaller crystallites are likely to be formed. Both these effects tend to retard local sintering of ThO<sub>2</sub> crystallites formed by combustion and prevent their grain growth [263]. The excess gaseous byproducts also cool

down the un-burnt fuel, which thereafter remains as residual carbonaceous species in as-combusted product.

**Table 6.2. Crystallite size of as-combusted ThO<sub>2</sub> powders evaluated from SAXS data.**

Symbol ‘r’ and ‘R’ represent radius of smaller and larger crystallites, respectively

Fuel to oxidant ratio (F:O)	Smaller crystallites		Larger crystallites	
	Crystallite size at distribution maxima $r_p$ (nm)	Average crystallite size $\langle r \rangle$ (nm)	Crystallite size at distribution maxima $R_p$ (nm)	Average crystallite size $\langle R \rangle$ (nm)
0.75	3.2	4.8	9.7	14.2
0.90	2.7	4.8	9.1	13.7
1.00	1.7	3.6	8.3	12.6
1.25	0.6	1.2	5.3	9.1

#### 6.3.3.4. Role of F:O on mechanism of glycine-Th(IV)-nitrate combustion

Corroborating the results obtained from powder XRD, SAXS results also show that the crystallite size distribution is significantly narrower for powders obtained from glycine-rich gel (F:O = 1.25); particularly in the case of smaller particles. This can be explained as follows: The molar ratios between glycine and Th(VI) in studied solutions with F:O = 0.75, 0.90, 1.00 and 1.25 are 1.67, 2.0, 2.22 and 2.78, respectively (Table 6.1). Corresponding molar ratios of NO<sub>3</sub><sup>-</sup> ions to glycine; assuming that NO<sub>3</sub><sup>-</sup> ions are not lost from the gel during solvent evaporation under ambient conditions, are 2.4, 2.0, 1.8 and 1.44, respectively. This means that fuel-rich solution (F:O = 1.25) has ~2.78 glycine molecules per Th<sup>4+</sup> ion. Also, there exist ~ 1.44 NO<sub>3</sub><sup>-</sup> ions per glycine molecule. Regarding the formation of Th<sup>4+</sup>-glycine-NO<sub>3</sub><sup>-</sup> complexes, literature reports indicate that two types of complexes exists in solution as well as in solid-state. These are (i) mononuclear complexes  $\{\text{Th}(\text{H}_2\text{O})_3(\text{HGly})_3\}^{4+}$  where glycine to Th<sup>4+</sup> molar ratio is ~ 3 (or higher) and (ii) hexanuclear complexes  $\{(\text{Th}_6(\mu_3\text{-O})_4(\mu_3\text{-$

OH)<sub>4</sub>(H<sub>2</sub>O)<sub>6</sub>(Gly)<sub>6</sub>(HGly)<sub>6</sub>}<sup>6+</sup>, with glycine to Th<sup>4+</sup> molar ratio being 2 [244]. Similar hexanuclear complexes of glycine have also been reported for Ce<sup>4+</sup> ions [240]. It is also reported that in case of aqueous solutions, apart from relative concentration of metal ion (Th<sup>4+</sup>), ligand (glycine) and counter anion (NO<sub>3</sub><sup>-</sup>), stability of these complexes depends upon solution pH. With higher acidity (lower pH), stability of hexanuclear complex decreases and mononuclear complexes are predominantly formed [244]. In addition to the complexes mentioned above, other type of Th<sup>4+</sup>-glycine (1:1 molar ratio) complexes [247] have also been proposed. However, their accurate spectroscopic / crystal structure data is not available. Based on the literature information and observations made in present study, the following can be inferred regarding the nature of complexes formed in the gels. As mentioned earlier, Th<sup>4+</sup> undergoes severe hydrolysis in aqueous medium to produce mono- as well as poly-nuclear hydroxy species [237], which undergo competitive complexation in presence of strong ligand like glycine. When Th(NO<sub>3</sub>)<sub>4</sub>.5H<sub>2</sub>O is dissolved in water, Th<sup>4+</sup> hydrolysis occurs, which results into a decrease in solution pH. When glycine is introduced, formation of Th<sup>4+</sup>-glycine-NO<sub>3</sub><sup>-</sup> complex species takes place via carboxylate end of glycine zwitterions (<sup>+</sup>NH<sub>3</sub>-CH<sub>2</sub>-COO<sup>-</sup>). As a result of this, there is increased availability of free NO<sub>3</sub><sup>-</sup> ions in the solution. Further, presence of quaternary nitrogen in bonded glycinate moiety also contributes towards increasing the acidity of solution. As a result, solution becomes more and more acidic with progressive complexation. Acidic nature of aqueous solutions containing Th<sup>4+</sup>-NO<sub>3</sub><sup>-</sup> and Th<sup>4+</sup>-glycine-NO<sub>3</sub><sup>-</sup> species has also been experimentally verified.

From the above discussion, it can be inferred that under highly acidic conditions and increasing glycine to Th<sup>4+</sup> molar ratio, brought about by increase in F:O, both mononuclear and hexanuclear complexes are formed in aqueous solution containing thorium nitrate and glycine. Their relative fractions would however be governed by (i) availability of glycine and

(ii) relative stability of complexes. For fuel deficient systems (F:O = 0.75, 0.90), where glycine to Th<sup>4+</sup> molar ratio is 1.67 and 2.0, respectively, we suggest a larger fraction of hexanuclear complexes (glycine to Th<sup>4+</sup> molar ratio ~2) due to limited availability of glycine as well as higher stability of hexanuclear complexes in relatively lesser acidic solution. For stoichiometric as well as fuel-rich solutions (F:O = 1.00, 1.25); not only higher amounts of glycine (glycine to Th<sup>4+</sup> molar ratio = 2.22, 2.78, respectively) is present, but solution has further increased acidity. As a result, more and more fraction of mononuclear complexes (Glycine to Th<sup>4+</sup> molar ratio ~3) would be present in solution phase and the glycine-rich solution (F:O = 1.25) would have maximum fraction of mononuclear complexes. When such solutions are heated, excess solvent evaporates along with acidic vapours and effective concentration of complexes increases leading to their aggregation, which would be governed by their crystallization kinetics. One should therefore observe separate crystallization exotherms for different complex species during thermal analysis of such gels. DSC results (Fig. 6.21) also support this inference, wherein multiple overlapping crystallization exotherms are observed for gels containing higher amount of glycine (F:O = 1.0, 1.25). Each individual peak-like feature in DSC thermogram can therefore be attributed to crystallization of a particular type of complex.

Such aggregation would result into formation of a mixture of small crystallites of both mononuclear as well as hexanuclear Th<sup>4+</sup>-glycine-NO<sub>3</sub><sup>-</sup> complexes along with water of crystallization and residual glycine, if any. Further heating of gel precursor leads to combustion with rapid decomposition of the precursor. It is expected that decomposition of aggregates of hexanuclear complex would give rise to larger ThO<sub>2</sub> crystallites while that of mononuclear complex would result into smaller crystallites. This is because the hexanuclear complexes have smaller Th<sup>4+</sup>--Th<sup>4+</sup> distances compared to mononuclear complexes, and

hence more tendency for aggregation (Th<sup>4+</sup>-O-Th<sup>4+</sup> clustering). As a result, combustion of fuel-rich precursors (F:O = 1.25), which is likely to contain higher fraction of mononuclear complexes would give higher fraction of smaller ThO<sub>2</sub> crystallites while that of fuel-lean precursors (F:O = 0.75, 0.90) containing hexanuclear complexes as dominating species, would combust to give higher fraction of large ThO<sub>2</sub> crystallites. This explanation matches well with bimodal distribution of crystallites, estimated from SAXS results obtained on as-combusted powders. The distribution indeed shifts towards lower crystallite size with increasing fuel content along with higher fraction of smaller crystallites. Further, mononuclear Th<sup>4+</sup>-glycine-NO<sub>3</sub><sup>-</sup> complexes are more likely to be surrounded by higher numbers of glycine species as compared to hexanuclear complexes, which would be surrounded by more number of NO<sub>3</sub><sup>-</sup> ions. As a result, thermal decomposition of mononuclear complexes is likely to occur at relatively higher temperature, which indeed is observed in our DSC results where combustion shifts towards higher temperature with increasing F:O for fuel-rich gels. In case of fuel-deficient gels (F:O < 1.0), since hexanuclear complex is dominant species, more and more glycine available in aqueous solution with increasing F:O value is utilized for complex formation. Combustion of such precursor would be governed by decomposition of oxidizing nitrate ions surrounding these complexes. With higher availability of nitrate ions surrounding the hexanuclear complexes, combustion temperature is shifted downwards with increasing F:O for fuel-deficient gels.

#### **6.3.3.5. Supporting evidence for mechanism of glycine-nitrate combustion (FT-IR)**

Formation of mono- and hexanuclear Th<sup>4+</sup>-glycine-NO<sub>3</sub><sup>-</sup> complexes, as inferred from SAXS results, explain the observed bimodal distribution of ThO<sub>2</sub> crystallites and formation of higher fraction of smaller crystallite with increasing F:O. To further substantiate these inferences

and to monitor the structural changes in glycine-Th(IV)-nitrate aqueous gels, FT-IR studies were carried out. These results are discussed now.

Fig. 6.26 (a) shows the FT-IR patterns of aqueous gels having different F:O values over 1200-1800 cm<sup>-1</sup> region. FT-IR pattern of pure Th(NO<sub>3</sub>)<sub>4</sub>·5H<sub>2</sub>O is also plotted for comparison. All the patterns are characterized by peaks with maximum around 1383, 1458 and 1604 cm<sup>-1</sup>. Each spectrum in Fig. 6.26 (a) has been normalized with respect to most intense IR band (~1383 cm<sup>-1</sup>). Spectrum of Th(NO<sub>3</sub>)<sub>4</sub>·5H<sub>2</sub>O has been shown displaced in intensity scale for clarity in presentation. Among the above three peaks, the one at 1604 cm<sup>-1</sup> is more symmetric as compared to the other two peaks. The peak at 1383 cm<sup>-1</sup> is having two shoulder peaks, one at low energy side (1342 cm<sup>-1</sup>) and the other at high energy side (1413 cm<sup>-1</sup>).

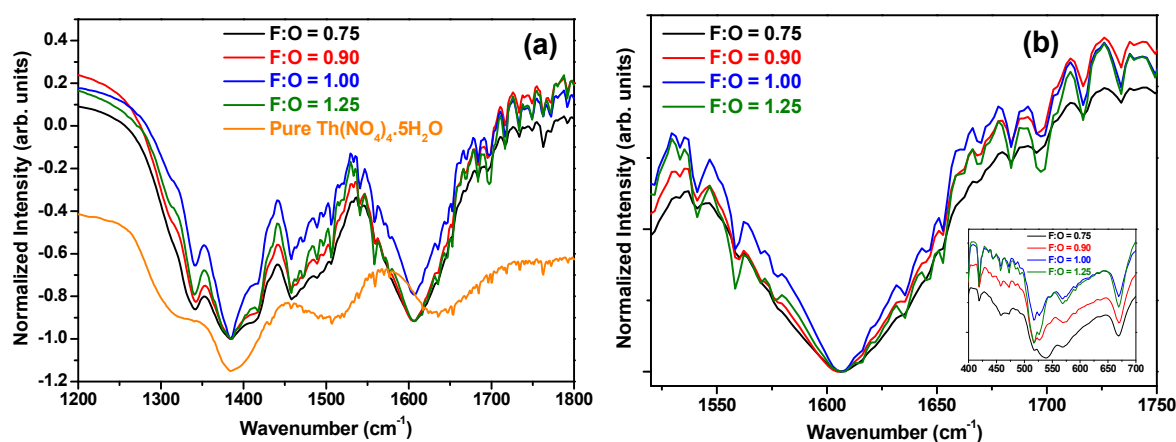


**Fig. 6.26. FT-IR spectra of glycine-Th(IV)-nitrate aqueous gels for different F:O values:**  
**(a) higher wave number range and (b) lower wave number range**

Based on earlier studies [239], the peaks at 1383 cm<sup>-1</sup>, 1458 cm<sup>-1</sup> and 1604 cm<sup>-1</sup> have been attributed to asymmetric stretching mode of NO<sub>3</sub><sup>-</sup> ions, symmetric and asymmetric stretching modes of COO<sup>-</sup> moiety, respectively. The symmetric shoulder peaks (1342 cm<sup>-1</sup> and 1413 cm<sup>-1</sup>) appearing along with 1383 cm<sup>-1</sup> peak have been assigned to different bending modes ( $\omega$

and  $\delta$ ) of -CH<sub>2</sub> linkages. With increase in fuel to oxidant ratio (F:O), peak maximum of all the peaks remains unaffected. However, line width of 1383 cm<sup>-1</sup> peak decreases with increasing F:O up to 1.0, beyond which, it again increases. Decrease in the line width corresponding to NO<sub>3</sub><sup>-</sup> groups indicates that the extent of free rotation of NO<sub>3</sub><sup>-</sup> group increases with F:O ratio. This can be explained in terms of progressive complexation of Th<sup>4+</sup> with carboxylate group of glycine in the first coordination sphere, which results into nitrate groups being replaced by glycine and therefore available in relatively free form. This is supported by the observation that the line width of 1383 cm<sup>-1</sup> peak for fuel-deficient gel (F:O = 0.75) is significantly lower than that of pure Th(NO<sub>3</sub>)<sub>4</sub>.5H<sub>2</sub>O. A progressive decrease in line width with increase in glycine concentration (up to F:O = 1.0) also indicate increase in glycine species in the local environment around Th<sup>4+</sup> species.

As mentioned earlier, glycine to Th<sup>4+</sup> molar ratio for F:O = 0.75, 0.90, 1.00 and 1.25 is 1.67, 2.00, 2.22 and 2.78, respectively. For mono- and hexanuclear Th<sup>4+</sup>-glycine-NO<sub>3</sub><sup>-</sup> complexes, ideal value of this ratio is 3 and 2, respectively [244]. Therefore, one would expect higher fraction of hexanuclear complexes in fuel-lean gels (F:O = 0.75, 0.90). For higher F:O (1.0, 1.25), both, stoichiometry and solution conditions favour higher fraction of mononuclear complexes, as mentioned while discussing SAXS results earlier. Hexanuclear complexes would have higher fraction of NO<sub>3</sub><sup>-</sup> ions surrounding the hexanuclear core while mononuclear complexes would be surrounded by higher fraction of glycine species. A net effect of increasing complexation would therefore be higher release of free NO<sub>3</sub><sup>-</sup> ions in the gel, thereby decreasing the line broadening for 1383 cm<sup>-1</sup> peak. As compared to stoichiometric gel (F:O = 1.00), a relatively broader peak for fuel-rich gel (F:O = 1.25) can be attributed to presence of mixed local environment of NO<sub>3</sub><sup>-</sup> species in a mixture of mononuclear and hexanuclear complexes. The line shape of COO<sup>-</sup> moiety is also marginally affected with

increase in F:O as can be seen from the line shape of peak at 1458 cm<sup>-1</sup> in Fig. 6.26 (a). These results confirm that local environment around Th<sup>4+</sup> species changes with increasing F:O.

A close look at peak due to -COO<sup>-</sup> stretching vibrations also reveal change in line broadening as a function of F:O ratio. This is clearly shown in Fig. 6.26 (b), where asymmetric stretching mode of -COO- group (1604 cm<sup>-1</sup>) is plotted as normalized signal. Again, line broadening decreases with increasing glycine concentration up to F:O = 1.0 and shows slight increase thereafter. Ordering of carboxylate groups around Th<sup>4+</sup> is the reason for observed decrease in the line width. Beyond F:O = 1.0, glycine species must be existing both as complex and as well as free ligand (multiple environments) which leads to slight increase in the line width. Similar reduction in line broadening is seen for low energy -COO- bending vibrations, as shown in inset of Fig. 6.26 (b).

#### 6.4. Conclusions

In this chapter, mechanism of solution combustion synthesis of nanocrystalline ThO<sub>2</sub> from glycine-nitrate and citrate-nitrate routes has been investigated using thermal analysis as the primary tool. Combustion has been carried out with varying fuel to oxidant ratios ( $0.75 \leq \text{F:O} \leq 1.25$ ) covering both fuel-deficient as well as fuel-rich stoichiometries. It has been concluded that combustion precursors have distinct chemistry as compared to their individual starting reactants. In the case of glycine-nitrate combustion of ThO<sub>2</sub>, formation of glycine-Th(IV)-nitrate molecular complexes and their crystallization / ordered aggregation prior to precursor's autoignition has been identified in terms of exothermic DSC peak observed before combustion. Formation of molecular complexes has been confirmed by XRD, FT-IR and Raman spectroscopic analysis. Unlike glycine-Th(IV)-nitrate complexes, citrate-Th(IV)-nitrate complexes do not undergo crystallization / ordered aggregation, as indicated by

thermal analysis. Instead, low temperature auto-ignition of amorphous citrate-nitrate precursors consisting of citrate-Th(IV)-nitrate molecular complexes, followed by sluggish thermal decomposition of citrate moieties is identified as the process mechanism to obtain relatively small, nanocrystalline (< 5 nm) ThO<sub>2</sub> powders. Based on detailed DSC studies it is concluded that, exothermicity of combustion reaction is higher with glycine-nitrate method compared to citrate-nitrate method even though Th(IV)-citrate-nitrate gels auto-ignite at lower temperatures than Th(IV)-glycine-nitrate gels. A bimodal crystallite size distribution has been observed for as-combusted nanocrystalline ThO<sub>2</sub> powders prepared by glycine-nitrate combustion using different fuel to oxidant ratios. Based on detailed SAXS and FT-IR analysis results, this has been explained in terms of formation of mono- and hexanuclear complexes of Th<sup>4+</sup> with glycine and varying number of water and nitrate species, wherein the relative fraction of these complexes determine the average crystallite size distribution of as-combusted ThO<sub>2</sub> powders. Mononuclear complexes in the precursor gel lead to the formation of smaller ThO<sub>2</sub> crystallites whereas the hexanuclear Th<sup>4+</sup> complexes lead to relatively larger size crystallites upon gel combustion. Multiple exothermic peaks observed prior to combustion in DSC patterns also confirm the formation of more than one type of complexes in the precursor gel.

Based on these studies, it is possible to select appropriate combustion route for preparation of nanocrystalline ThO<sub>2</sub> powders of desired properties. It is also possible to fine tune glycine-nitrate combustion method to obtain ThO<sub>2</sub> powders of predominantly smaller or larger crystallite sizes. Presented findings will also be useful to select appropriate fuel to oxidant stoichiometry (F:O) to synthesize ThO<sub>2</sub> and ThO<sub>2</sub>-based ceramics for applications in nuclear fuel fabrication.

Oxide-based nuclear fuels are fabricated by sintering oxide powder compacts at high temperatures. Motivation of using nanocrystalline oxide powders for fuel fabrication comes from their sinter-active properties due to high surface of volume ratio and reactive surface sites. These attributes facilitate sintering at relatively lower temperatures (compared to bulk oxide powders) and high density pellets suitable for use as nuclear fuel can be obtained. Another attribute of sintering of nanocrystalline powder compacts is rapid shrinkage, which may sometimes lead to loss of bulk density during final stage of sintering; a phenomenon known as desintering. Desintering of thoria is mentioned in literature but detailed studies to identify its origin for powders prepared by different synthesis routes are not reported. Understanding desintering behavior is essential to assess the potential of nanocrystalline thoria powder for nuclear fuel fabrication. With this objective, sintering of powder compacts prepared from thoria synthesized by glycine-nitrate and citrate-nitrate combustion has been investigated. These results are discussed in next chapter (chapter-7).

## References:

- [1] C. Degueudre, M.J. Joyce, “Evidence and uncertainty for uranium and thorium abundance: a review”, *Prog. Nucl. Energy* 124 (2020) 103299.
- [2] L.S. Keith, O.M. Faroon, B.A. Fowler, “Uranium (book chapter); handbook on the toxicology of metals: fourth edition (Eds: G.F. Nordberg, B.A. Fowler, M. Nordberg)”, Elsevier (2015) 1307-1345 (DOI: <https://doi.org/10.1016/C2011-0-07884-5>).
- [3] G. Sadagopan, K.S.V. Nambi, G. Venkataraman, V.K. Shukla, S. Kayasth, “Estimation of thorium in gas mantles to ascertain regulatory compliance”, *Radiat. Prot. Dosim.* 71(1) (1997) 53-56.
- [4] T.E. Leontis, “Properties of magnesium-thorium and magnesium-thorium-cerium alloys”, *J. Min. Metals Mater. Soc.* 4 (3) (1952) 287-294.
- [5] R.A. Glenner, P. Willey, P.S. Sledzik, E.P. Junger, “Dental fillings in civil war skulls: What do they tell us?”, *J. Am. Dent. Assoc.* 127(11) (1996) 1671-1677.
- [6] O. Hahn, F. Strassmann, “Über den nachweis und das verhalten der bei der bestrahlung des urans mittels neutronen entstehenden erdalkalimetalle (English translation: Concerning the existence of alkaline earth metals resulting from neutron irradiation of uranium)”, *Die Naturwissenschaften* 27 (1939) 11-15.
- [7] “The first reactor” The US department of energy report: DOE/NE-0046 (1982) 1-40 (Web-link: <https://www.energy.gov/ne/downloads/first-reactor>).
- [8] R.L. Crowther, “Use of thorium in boiling water reactors”, *J. Nucl. Energy AB* 16(4) (1962) 181-194.
- [9] J.R. Dietrich, “The physics of advanced reactors”, *Brit. J. Appl. Phys.* 7(S5) 302 (1956) S9-S23.
- [10] H.N. Sethna, “India’s atomic energy program: past and future”, *International Atomic Energy Agency (IAEA) Bulletin* 21 (5) (1979) 2-11.

## References

- [11] S. Banerjee, H.P. Gupta, “The evolution of the Indian nuclear power programme”, Prog. Nucl. Energy 101 (2017) 4-18.
- [12] International Atomic Energy Agency “Thorium fuel cycles - potential benefits and challenges”, IAEA-TECDOC-1450, IAEA, Vienna (2005) 1-105.
- [13] P.K. Wattal, “Back end of Indian nuclear fuel cycle - A road to sustainability”, Prog. Nucl. Energy 101 (2017) 133-145.
- [14] R. Natarajan, “Reprocessing of spent nuclear fuel in India: Present challenges and future programme”, Prog. Nucl. Energy 101 (2017) 118-132.
- [15] S.A. Ansari, P. Pathak, P.K. Mohapatra, V.K. Manchanda, “Aqueous partitioning of minor actinides by different processes” Sep. Purif. Rev. 40(1) (2011) 43-76.
- [16] M. Salvatores, “Nuclear fuel cycle strategies including partitioning and transmutation”, Nucl. Eng. Des. 235(7) (2005) 805-816.
- [17] Press Information Bureau, Government of India, “Setting up of ten indigenous nuclear power reactors” (Web-link: <http://pib.nic.in>)
- [18] S.C. Chetal, P. Chellapandi, P. Puthiyavinayagam, S. Raghupathy, V. Balasubramanian, P. Selvaraj, P. Mohanakrishnan, B. Raj, “Current status of fast reactors and future plans in India” Energy. Proced. 7 (2011) 64-73.
- [19] P. Puthiyavinayagam, P. Selvaraj, V. Balasubramanian, S. Raghupathy, K. Velusamy, K. Devan, B.K. Nashine, G.P. Kumar, K.V.S. Kumar, S. Varatharajan, P. Mohanakrishnan, G. Srinivasan, A.K. Bhaduri, “Development of fast breeder reactor technology in India”, Prog. Nucl. Energy 101 (Part A) (2017) 19-42.
- [20] Bharatiya Nabhikiya Vidyut Nigam Limited, Department of Atomic Energy “Present status of 500 MWe Prototype Fast Breeder Reactor (PFBR)”, (Web-link: <http://www.bhavini.nic.in>).

- [21] P. Rodriguez, C.V. Sundaram, "Nuclear and materials aspects of the thorium fuel cycle", *J. Nucl. Mater.* 100 (1981) 227-249.
- [22] R. Ramanna, S.M. Lee, "The thorium cycle for fast breeder reactors", *Pramana* 27(1-2) (1986) 129-137.
- [23] R. Chidambaram, C. Ganguly, "Plutonium and thorium in the Indian nuclear programme", *Curr. Sci. India* 70(1) (1996) 21-35.
- [24] P.K. Vijayan, V. Shivakumar, S. Basu, R.K. Sinha, "Role of thorium in the Indian nuclear power programme", *Prog. Nucl. Energy* 101 (2017) 43-52.
- [25] "Thoria-based nuclear fuels: thermophysical and thermodynamic properties, fabrication, reprocessing, and waste management", (Eds.: D. Das, S.R. Bharadwaj) Springer (2013) (DOI: 10.1007/978-1-4471-5589-8).
- [26] "Thorium-energy for the future", (Eds.: A.K. Nayak, B.R. Sehgal), Springer (2019) (DOI: 10.1007/978-981-13-2658-5).
- [27] S. Mukherji, B.K. Mohan, P.D. Krishnani, V. Jagannathan, S. Ganesan, "Thorium irradiation in Indian PHWRs - applications and limitations of origin code", *Proceedings of First National Conference in Nuclear Reactor Technology* (2002) (Web-link: [https://inis.iaea.org/search/search.aspx?orig\\_q=RN:34011468](https://inis.iaea.org/search/search.aspx?orig_q=RN:34011468)).
- [28] M. Das, "Design and irradiated experience with thorium based fuels in PHWRs" *Annual International Conference - Canadian Nuclear Association* (1992) 10.1-10.
- [29] P.S. Dhama, J.S. Yadav, K. Agarwal, "Power reactor thoria reprocessing facility (PRTRF), Trombay", *Proceedings of the Theme Meeting on the Journey of BARC Safety Council for Strengthening Safety Culture in BARC Facilities* (Eds: V.M. Jolly) (2017) (Web-link: [https://inis.iaea.org/search/search.aspx?orig\\_q=RN:48089837](https://inis.iaea.org/search/search.aspx?orig_q=RN:48089837)).
- [30] R.K. Sinha, A. Kakodkar, "Design and development of the AHWR - the Indian thorium fuelled innovative nuclear reactor" *Nucl. Eng. Des.* 236 (7-8) (2006) 683-700.

- [31] R. Sinha, A. Kakodkar, "India's passive breeder", Nucl. Eng. Int. 55(668) (2010) 30-31.
- [32] A. Kakodkar, "Evolution of nuclear reactor containments in India: Addressing the present day challenges", Nucl. Eng. Des. 269 (2014) 3-22.
- [33] S. Sengupta, S.B. Chafle, S. Mammen, K. Sasidharan, V.K. Raina, "Critical facility for AHWR and PHWRs", Proceedings of International Conference on Peaceful uses of Atomic Energy (2009). V. 1. [33a] C. Ronchi, J.-P. Hiernaut, Experimental measurement of pre-melting and melting of thorium dioxide, J. Alloys Comp. 240 (1-2) (1996) 179-185. [33b] R. Böhler, A. Quaini, L. Capriotti, P. Cakir, O. Beneš, K. Boboridis, A. Guiot, L. Luzzi, R.J.M. Konings, D. Manara, "The solidification behavior of the UO<sub>2</sub>-ThO<sub>2</sub> system in a laser heating study" J. Alloys. Comp. 616 (2014) 5-13.
- [34] D. Greneche, W.J. Szymczak, J.M. Buchheit, M. Delpech, A. Vasile, H. Golfier, "Rethinking the thorium fuel cycle: An industrial point of view", Proceedings of ICAPP (Nice, France), (2007) Paper-7367. [34a] S.F. Ashley, G.T. Park, W.J. Nuttall, C. Boxall, R.W. Grimes, "Thorium fuel has risks", Nature 492 (2012) 31-33.
- [35] D. Jain, V. Sudarsan, A.K. Tyagi, "Thorium-based metallic alloys as nuclear fuels: Present status, potential advantages and challenges", SMC Bulletin (Society for Materials Chemistry, India) 4 (1) (2013) pp. 27-40 (Web-link: <https://www.smcindia.org/smc-bulletin.php>).
- [36] P.K. Vijayan, A. Basak, I.V. Dulera, K.K. Vaze, S. Basu, "Conceptual design of Indian molten salt breeder reactor", Pramana - J. Phys. 85 (2015) 539–554.
- [37] T. Yamamoto, H. Suwarno, H. Kayano, M. Yamawaki, "Development of new reactor fuel materials: Hydrogen absorption properties of U-Th, U-Th-Zr and U-Th-Ti-Zr alloys", J. Nucl. Sci. Tech. 32(3) (1995) 260-262.

## References

- [38] K.A. Terrani, G.W.C. Silva, C.B. Yeamans, "Fabrication and characterization of uranium thorium zirconium hydride fuels", *Trans. Am. Nucl. Soc.* 98 (2008) 1060-1061.
- [39] S.M. McDeavitt, T.J. Downar, A.A. Solomon, S.T. Revankar, M.C. Hash, A.S. Hebden, "Thoria-based cermet nuclear fuel: Cermet fabrication and behavior estimates", *Proc. Int. Conf. Nucl. Eng. (ICONE 4)* (2002) 59-67.
- [40] C. Lombardi, L. Luzzi, E. Padovani, F. Vettrano, "Thoria and inert matrix fuels for a sustainable nuclear power", *Prog. Nucl. Energy* 50(8) (2008) 944-953.
- [41] J. Spino, H.S. Cruz, R. Jovani-Abril, R. Birtcher, C. Ferrero, "Bulk-nanocrystalline oxide nuclear fuels - An innovative material option for increasing fission gas retention, plasticity and radiation-tolerance", *J. Nucl. Mater.* 422 (1-3) (2012) 27-44.
- [42] H. György, S. Czifrus, "The utilization of thorium in generation IV reactors", *Prog. Nucl. Energy* 93 (2016) 306-317.
- [43] D. Heuer, E. Merle-Lucotte, M. Allibert, M. Brovchenko, V. Ghetta, P. Rubiolo, "Towards the thorium fuel cycle with molten salt fast reactors", *Ann. Nucl. Energy* 64 (2014) 421-429.
- [44] G.L. Hofman, L.C. Walters, T.H. Bauer, "Metallic fast reactor fuels", *Prog. Nucl. Energy* 31(1-2) (1997) 83-110.
- [45] W.J. Carmack, D.L. Porter, Y.I. Chang, S.L. Hayes, M.K. Meyer, D.E. Burkes, C.B. Lee, T. Mizuno, F. Delage, J. Somers, "Metallic fuels for advanced reactors", *J. Nucl. Mater.* 392 (2) (2009) 139-150.
- [46] Idaho National Laboratory, "Experimental breeder reactor-I (EBR-I) (Web-link: <https://inl.gov/experimental-breeder-reactor-i/>).
- [47] L.C. Walters, "Thirty years of fuels and materials information from EBR-II", *J. Nucl. Mater.* 270(1) (1999) 39-48.

- [48] K. D. Weaver, J. Gilleland, C. Whitmer, G. Zimmerman, “High burn-up fuels for fast reactors: past experience and novel applications”, International Congress on Advances in Nuclear Power Plants (ICAPP 2009) (2009) 795.
- [49] G. Locatelli, M. Mancini, N. Todeschini, “Generation IV nuclear reactors: Current status and future prospects”, *Energ. Policy* 61 (2013) 1503-1520.
- [50] Z.S. Takibaev, “Fast homogeneous nuclear reactor”, *Atom. Energy* 100 (2006) 154-156.
- [51] T. Jayakumar, M.D. Mathew, K. Laha, R. Sandhya, “Materials development for fast reactor applications”, *Nucl. Eng. Des.* 265 (2013) 1175-1180.
- [52] A. Riyas, P. Mohanakrishnan, “Studies on physics parameters of metal (U-Pu-Zr) fuelled FBR cores”, *Ann. Nucl. Energy* 35(1) (2008) 87-92.
- [53] P. Chellapandi, V. Balasubramaniyan, P. Puthiyavinayagam, R. Sundararajan, M. Kanakkil, P. Selvaraj, P.R. Vasudeva Rao, “Design of 500 MWe metal fuel demonstration fast reactor”, *Proc. Int. Conf. Nucl. Eng.* (2014) (DOI: <https://doi.org/10.1115/ICONE22-30727>).
- [54] Indira Gandhi Centre for Atomic Research, “Fast Breeder Test Reactor”, (Web-link: <http://www.igcar.gov.in/rfg/fbtrhist.html>).
- [55] B. Blumenthal, J.E. Sanecki, D.E. Busch, D.R. O’Boyle, “Thorium-uranium-plutonium alloys as potential fast power reactor fuels; part-II: Properties and irradiation behavior of thorium-uranium-plutonium alloys”, ANL-7259, Argonne National laboratory, Illinois (October 1969).
- [56] S.Z. Ghayeb, “Investigations of thorium-based fuels to improve actinide burning rate in S-PRISM reactor”, M.Sc. Thesis, The Pennsylvania State University (2008) (Web-link: <https://etda.libraries.psu.edu/catalog/9160>).

## References

- [57] R.G. Wymer, D.A. Douglas Jr., “Status and progress report for thorium fuel cycle development for period ending December 31, 1964”, Report no.: ORNL-3831, Oak Ridge National laboratory, Tennessee (May 1966).
- [58] “Fast spectrum reactors”, (Eds.: A.E. Waltar, D. Todd, P.V. Tsvetkov) Springer (2011) (ISBN 978-1-4419-9572-8).
- [59] D.E. Peterson, “The (Th-U) Thorium-uranium system”, Bull. Alloy Phase Diagr. 6 (5) (1985) 443-445.
- [60] S. Peterson, R.E. Adams, D.A. Douglas Jr., “Properties of thorium, its alloys and its compounds”, Report no.: ORNL-TM-1144, Oak Ridge National laboratory, Tennessee (June 1965).
- [61] D.R. Marr, D.A. Cantley, J.C. Chandler, D.C. McCurry, R.P. Omberg, “Performance of thorium fuelled fast breeders”, Report no.: HEDL-SA-1327-FP, Hanford Engineering Development Laboratory, Richland, USA (October 1977).
- [62] G.L. Copeland, “Evaluation of thorium-uranium alloys for the unclad metal breeder reactor”, Report no.: ORNL-4557, Oak Ridge National Laboratory, Tennessee (June 1970).
- [63] B. Blumenthal, J.E. Sanecki, D.E. Busch, “Thorium-uranium-plutonium alloys as potential fast power reactor fuels; part-I: Thorium-uranium-plutonium phase diagram”, Report no.: ANL-7258, Argonne National Laboratory, Illinois (September 1968).
- [64] C.S. Holden, “Rapid computational path for sustainable and renewable nuclear energy using metallic thorium fuels”, Proceedings of 2<sup>nd</sup> Thorium energy conference (ThEC-2010), Mountain View CA (2010).
- [65] R.M. Carroll, “The effects of reactor irradiation on thorium-uranium alloy fuel plates”, Report no.: ORNL-1938, Oak Ridge National Laboratory, Tennessee (August 1955).

## References

- [66] B.R. Hayward, P. Corzine, "Thorium uranium fuel elements for SRE", Proc. 2<sup>nd</sup> UN Int. Conf. Peaceful uses of Atom. Energy, Geneva (October 1958).
- [67] J.L. Ballif, B.R. Hayward, J.W. Walter, "Engineering evaluation of a mixed alloy fuel element irradiated at elevated temperatures in SRE", Technical report no.: NAA-SR-3888, Atomics International Division, North American Aviation Incorporation, California, USA (June 1960).
- [68] A.R. Olsen, "Thorium and thorium alloys: Preliminary corrosion tests", Report no.: ORNL-1066, Oak Ridge National Laboratory, Tennessee (November 1951).
- [69] M.S. Farkas, A.A. Bauer, R.F. Dickerson, "Development of thorium-uranium-base fuel alloys," Report no.: BMI-1428, Battelle Memorial Institute, Columbus, Ohio (March 1960).
- [70] R.H. Cole, L.E. Wilkinson, "Development of high strength ternary and quaternary thorium-uranium base alloys", Technical report no.: ATL-A-128, Advanced Technology Laboratory, California (1961).
- [71] J.H. Kittel, J.A. Horak, W.F. Murphy, S.H. Paine, "Effect of irradiation on thorium and thorium-uranium alloys", Technical report no.: ANL-5674, Argonne National laboratory, Illinois, USA (April 1963).
- [72] A.L. Bement, "Burn-up and specific power calculations for the thermal neutron irradiation on thorium-uranium alloys", Technical report no: HW-56631, General Electric Co. Hanford Atomic Products Operation, Richland, Washington (1958).
- [73] F.W. Dodge, E.W. Murbach, L.A. Hanson, "Low decontamination reprocessing of thorium-uranium alloys by induction drip melting", Nucl. Sci. Eng. 6 (6) (1959) 533-536.
- [74] P. Chiotti, A.F. Voigt, "Pyrometallurgical processing", Technical report: A/CONF.15/P/517; ISC-1018, Ames Laboratory, Iowa (October 1958).

- [75] W.N. Hensen, "Electrolysis of thorium and uranium", US-Patent no.: US 2951793 (1960).
- [76] S. Jiang, K. Liu, Y. Liu, T. Yin, Z. Chai, W. Shi, "Electrochemical behavior of Th(IV) on the bismuth electrode in LiCl–KCl eutectic", *J. Nucl. Mater.* 523 (2019) 268-275.
- [77] G.B. Zorzoli, "Use of metallic thorium for LWBRs and LWRs", *Nucl. Tech.* 20 (1973) 109-113.
- [78] F. Correa, D.J. Driscoll, D.D. Lanning, "An evaluation of tight pitch PWR cores", technical report no.: MIT-EL-79-022, Massachusetts Institute of Technology, Cambridge, Massachusetts (1979).
- [79] Z.S. Li, X.J. Liu, C.P. Wang, "Thermodynamic modelling of the Th-U, Th-Zr and Th-U-Zr systems", *J. Alloy Compd.* 473 (2009) 193-198.
- [80] S.Z. Ghrayeb, K.N. Ivanov, S.H. Levine, E.P. Loewen, "Burn-up performance of sodium-cooled fast reactors utilizing thorium-based fuels", *Nucl. Tech.* 176 (2011) 188-194.
- [81] T. Okawa, H. Sekimoto, S. Nakayama, "Design study on power flattening to sodium cooled large scale CANDLE burning reactor with using thorium fuel", *Proc. 18<sup>th</sup> Int. Conf. Nucl. Eng., ICON18, China, (2010).*
- [82] M.T. Simnad, "The U-ZrH<sub>x</sub> alloy: Its properties and use in TRIGA fuel", *Nucl. Engg. Des.* 64 (1981) 403-422.
- [83] K. Konashi, B.A. Pudjanto, T. Terai, M. Yamawaki, "Thermodynamic stability of ThZr<sub>2</sub>H<sub>x</sub> at high temperature", *J. Phys. Chem. Solids* 66 (2–4) (2005) 625-628.
- [84] T. Yamamoto, H. Suwarno, F. Ono, H. Kayano, M. Yamawaki, "Preparation, analysis and irradiation of hydride Th-U-Zr alloy samples for a new fuel", *J. Alloy Compd.* 271-273 (1998) 702-706.

- [85] S. Das, R. Kumar, S.B. Roy, A.K. Suri, "Development study on metallic thorium and uranium-thorium alloy", BARC Newsletter-Founder's Day Special issue (2011) 72-76.
- [86] S. Das, R. Kumar, S. Kaity, S. Neogy, K.N. Hareendran, S.B. Roy, G.K. Dey, B.S.S. Daniel, G.P. Chaudhari, "Characterization of microstructural, mechanical and thermal properties and ageing study of Th-3 wt.% U alloy" Nucl. Eng. Des. 282 (2015) 116-125.
- [87] S. Das, S. Kaity, R. Kumar, J. Banerjee, S.B. Roy, G.P. Chaudhari, B.S.S. Daniel, "Characterization of microstructural, mechanical and thermophysical properties of Th-52 U alloy", J. Nucl. Mater. 480 (2016) 223-234.
- [88] S. Das, S.B. Roy, G.P. Chaudhari, B.S.S. Daniel, "Microstructural evolution of as-cast Th-U alloys", Prog. Nucl. Energy 88 (2016) 285-296.
- [89] R. Kumar, S. Das, S.B. Roy, R. Agarwal, J. Banerjee, S.K. Satpati, "Effect of Mo addition on the microstructural evolution and  $\gamma$ -U stability in Th-U alloys", J. Nucl. Mater. 539 (2020) 152317.
- [90] S. Vaidyanathan, "Thorium utilization in pressurized water reactors using bimetallic thorium-zirconium alloy cladding", Nucl. Tech. (2020) (DOI: <https://doi.org/10.1080/00295450.2019.1706377>).
- [91] D. Escorcia-Ortiz, J. François, C. Martín-del-Campo, "Comparative study of the neutronic performance of thorium-based metallic fuel and MOX fuel in an ASTRID-like fast reactor core", Nucl. Eng. Des. 347 (2019) 122-131.
- [92] J.K. Startt, C.S. Deo, "First principles study of the structure and elastic properties of thorium metal", MRS Adv. 1 (35) (2016) 2447-2452.
- [93] A. Karahan, J. Buongiorno, "A new code for predicting the thermo-mechanical and irradiation behavior of metallic fuels in sodium fast reactors", J. Nucl. Mater. 396 (2010) 283-293.

## References

- [94] K. Lassmann, "TRANSURANUS: a fuel rod analysis code ready for use", *J. Nucl. Mater.* 188 (1992) 295-302.
- [95] J.P. Hamond, "Physical, mechanical and irradiation properties of thorium and thorium alloys", ORNL-4218, Oak Ridge National Laboratory, USA (1968) 29-30.
- [96] J.K. Fink, M.G. Chasanov, L. Leibowitz, "Thermophysical properties of thorium and uranium systems for use in reactor safety analysis", Report no.: ANL-CEN-RSD-77-1, Argonne National Laboratory (1977) 11-12.
- [97] M. Lung, "A present review of the thorium nuclear fuel cycles", European commission report no.: EUR-17771-EN, (1997).
- [98] S. Kolay, S. Phapale, R. Dawar, M. Jafar, S. N. Achary, A. K. Tyagi, R. Mishra, M. Basu, "Phase characterization and thermal study of SrF<sub>2</sub> and NdF<sub>3</sub> doped fluoride salt containing 78 mol % LiF - 20 mol % ThF<sub>4</sub> - 2 mol % UF<sub>4</sub>", *J. Radioanal. Nucl. Chem.* 314 (2) (2017) 1267-1271.
- [99] M. Verwerft, B. Boer, "Thorium oxide nuclear fuels", *Comprehensive nuclear materials* (Second edition) 5 (2020) 139-168 (DOI: <https://doi.org/10.1016/B978-0-12-803581-8.11770-9>).
- [100] S. Usha, R.R. Ramanarayanan, P. Mohanakrishnan, R.P. Kapoor, "Research reactor KAMINI", *Nucl. Eng. Des.* 236 (7-8) (2006) 872-880.
- [101] T.K. Mukherjee, "Processing of Indian monazite for the recovery of thorium and uranium values", *Proceedings of International Conference on Characterisation and Quality Control of Nuclear Fuels* (Eds.: C. Ganguly, R.N. Jayaraj) Allied Publishers Pvt. Ltd. (2002) 187-195.
- [102] J.R. Johnson, C.E. Curtis, "Note on sintering of ThO<sub>2</sub>", *J. Am. Ceram. Soc.* 37(12) (1954) 611.

## References

- [103] T.R.G. Kutty, K.B. Khan, P.V. Hegde, J. Banerjee, A.K. Sengupta, S. Majumdar, H.S. Kamath, "Development of a master sintering curve for ThO<sub>2</sub>", *J. Nucl. Mater.* 327(2-3) (2004) 211-219.
- [104] P. Balakrishna, B.P. Varma, T.S. Krishnan, T.R.R. Mohan, P. Ramakrishnan, "Thorium oxide: Calcination, compaction and sintering", *J. Nucl. Mater.* 160(1) (1988) 88-94.
- [105] N. Clavier, R. Podor, L. Deliere, J. Ravoux, N. Dacheux, "Combining in situ HT-ESEM observations and dilatometry: An original and fast way to the sintering map of ThO<sub>2</sub>", *Mater. Chem. Phys.* 137(3) (2013) 742-749.
- [106] K. Ananthasivan, S. Balakrishnan, S. Anthonysamy, R. Divakar, E. Mohandas, V. Ganesan, "Synthesis and sintering of nanocrystalline thoria doped with CaO and MgO derived through oxalate-deagglomeration", *J. Nucl. Mater.* 434 (1-3) (2013) 223-229.
- [107] G.P. Halbfinger, M. Kolodney, "Activated Sintering of ThO<sub>2</sub> and ThO<sub>2</sub>-Y<sub>2</sub>O<sub>3</sub> with NiO", *J. Am. Ceram. Soc.* 55(10) (1972) 519-524.
- [108] A. Baena, T. Cardinaels, J. Vleugels, K. Binnemans, M. Verwerft, "Activated sintering of ThO<sub>2</sub> with Al<sub>2</sub>O<sub>3</sub> under reducing and oxidizing conditions", *J. Nucl. Mater.* 470 (2016) 34-43.
- [109] K. Ananthasivan, S. Anthonysamy, C. Sudha, A.L.E. Terrance, P.R. Vasudeva Rao, "Thoria doped with cations of group VB-synthesis and sintering", *J. Nucl. Mater.* 300(2-3) (2002) 217-229.
- [110] T.R.G. Kutty, P.V. Hegde, K.B. Khan, T. Jarvis, A.K. Sengupta, S. Majumdar, H.S. Kamath, "Characterization and densification studies on ThO<sub>2</sub>-UO<sub>2</sub> pellets derived from ThO<sub>2</sub> and U<sub>3</sub>O<sub>8</sub> powders", *J. Nucl. Mater.* 335 (3) (2004) 462-470.
- [111] V. Tyrpekl, M. Cologna, D. Robba, J. Somers, "Sintering behaviour of nanocrystalline ThO<sub>2</sub> powder using spark plasma sintering", *J. Eur. Ceram. Soc.* 36(3) (2016) 767-772.

- [112] W. Straka, S. Amoah, J. Schwartz, “Densification of thoria through flash sintering”, *MRS Commun.* 7(3) (2017) 677-682.
- [113] D. Sanjay Kumar, K. Ananthasivan, R.V. Krishnan, S. Amirthapandian, A. Dasgupta, “Studies on the synthesis of nanocrystalline  $Y_2O_3$  and  $ThO_2$  through volume combustion and their sintering”, *J. Nucl. Mater.* 479 (2016) 585-592.
- [114] R.D. Purohit, S. Saha, A.K. Tyagi, “Nanocrystalline thoria powders via glycine-nitrate combustion” *J. Nucl. Mater.* 288 (1) (2001) 7-10. [114a] F. Cappia, D. Hudry, E. Courtois, A. Janßen, L. Luzzi, R.J.M. Konings, D. Manara, High-temperature and melting behavior of nanocrystalline refractory compounds: an experimental approach applied to thorium dioxide, *Mater. Res. Express* 1 (2014) 0250341-12.
- [115] J. Spino, K. Vennix, M. Coquerelle, “Detailed characterisation of the rim microstructure in PWR fuels in the burn-up range 40–67 GWd/tM”, *J. Nucl. Mater.* 231 (3) (1996) 179-190.
- [116] L. Bonato, M. Viot, X. Le Goff, P. Moisy, S.I. Nikitenko, “Sonochemical dissolution of nanoscale  $ThO_2$  and partial conversion into a thorium peroxo sulphate”, *Ultrason. Sonochem.* 69 (2020) 105235.
- [117] S. Dash, A. Singh, P.K. Ajikumar, H. Subramanian, M. Rajalakshmi, A.K. Tyagi, A.K. Arora, S.V. Narasimhan, B. Raj, “Synthesis and characterization of nanocrystalline thoria obtained from thermally decomposed thorium carbonate”, *J. Nucl. Mater.* 303 (2–3) (2002) 156-168.
- [118] S. Dash, R. Krishnan, M. Kamruddin, A.K. Tyagi, B. Raj, “Temperature programmed decomposition of thorium oxalate hexahydrate”, *J. Nucl. Mater.* 295(2-3) (2001) 281-289.

## References

- [119] S. Dash, M. Kamruddin, P.K. Ajikumar, A.K. Tyagi, B. Raj, S. Bera, S.V. Narasimhan, “Temperature programmed decomposition of thorium nitrate pentahydrate”, *J. Nucl. Mater.* 278 (2–3) (2000) 173-185.
- [120] T.V. Plakhova, A.Y. Romanchuk, D.V. Likhosherstova, A.E. Baranchikov, P.V. Dorovatovskii, R.D. Svetogorov, T.B. Shatalova, T.B. Egorova, A.L. Trigub, K.O. Kvashnina, V.K. Ivanov, S.N. Kalmykov, “Size effects in nanocrystalline thoria”, *J. Phys. Chem. C* 123 (37) (2019) 23167-23176. [120a] D. Hudry, C. Apostolidis, O. Walter, T. Gouder, E. Courtois, C. Kübel, D. Meyer, Controlled Synthesis of Thorium and Uranium Oxide Nanocrystals, *Chem. Eur. J.*, 19 (2013) 5297-5305.
- [121] F. Deganello, A.K. Tyagi, “Solution combustion synthesis, energy and environment: Best parameters for better materials”, *Prog. Cryst. Growth Char.* 64 (2018) 23-61.
- [122] A. Varma, A.S. Mukasyan, A.S. Rogachev, K.V. Manukyan, “Solution combustion synthesis of nanoscale materials”, *Chem. Rev.* 116 (2016) 14493-14586.
- [123] V. Chandramouli, S. Anthonysamy, P.R. Vasudeva Rao, “Combustion synthesis of thoria - A feasibility study”, *J. Nucl. Mater.* 265(3) (1999) 255-261.
- [124] S. Anthonysamy, K. Ananthasivan, V. Chandramouli, I. Kaliappan, P.R. Vasudeva Rao, “Combustion synthesis of urania-thoria solid solutions”, *J. Nucl. Mater.* 278(2) (2000) 346-357.
- [125] D. Sanjay Kumar, K. Ananthasivan, S. Amirthapandian, A. Dasgupta, G. Jogeswara Rao, “Citrate gel-combustion synthesis and sintering of nanocrystalline ThO<sub>2</sub> powders”, *J. Nucl. Mater.* 497 (2017) 16-29.
- [126] R.D. Purohit, S. Saha, A.K. Tyagi, “Combustion synthesis of 5 and 10 mol% YO<sub>1.5</sub> doped ThO<sub>2</sub> powders”, *J. Nucl. Mater.* 323 (1) (2003) 36-40.

- [127] K.C. Patil, M.S. Hegde, T. Rattan, S.T. Aruna, "Chemistry of nanocrystalline oxide materials combustion synthesis, properties and applications", World Scientific Publications (2008) (DOI: <https://doi.org/10.1142/6754>).
- [128] F.-T Li, J. Ran, M. Jaroniec, S.Z. Qiao, "Solution combustion synthesis of metal oxide nanomaterials for energy storage and conversion", *Nanoscale* 7(42) (2015) 17590-17610.
- [129] A. Kumar, E.E. Wolf, A.S. Mukasyan, "Solution combustion synthesis of metal nanopowders: nickel-reaction pathways", *AIChE J.* 57(8) (2011) 2207-2214.
- [130] A. Kumar, E.E. Wolf, A.S. Mukasyan, "Solution combustion synthesis of metal nanopowders: Copper and copper / nickel alloys", *AIChE J.* 57(12) (2011) 3473-3479.
- [131] S. Zhang, Z.A. Munir, "The combustion synthesis of refractory nitrides: Part II the synthesis of niobium nitride", *J. Mater. Sci.* 26 (1991) 3380–3385.
- [132] "Nitride ceramics: Combustion synthesis, properties, and applications", (Eds.: A.A. Gromov, L.N. Chukhlomina) Wiley-VCH Verlag GmbH (2015) (DOI:10.1002/9783527684533).
- [133] H.V. Kirakosyan, K.T. Nazaretyan, R.A. Mnatsakanyan, S.V. Aydinyan, S.L. Kharatyan, "Solution combustion synthesis of nanostructured molybdenum carbide", *J. Nanopart. Res.* 20 (2018) 214.
- [134] N.A. Marand, S.M. Masoudpanah, M. Sh. Bafghi, "Solution combustion synthesis of nickel sulfide composite powders", *Ceram. Int.* 44 (14) (2018) 17277-17282.
- [135] K. Rajeshwar, N.R. De Tacconi, "Solution combustion synthesis of oxide semiconductors for solar energy conversion and environmental remediation", *Chem. Soc. Rev.* 38 (7) (2009) 1984-1998.

- [136] K.C. Thomas, J.R. Kale, R.G. Dalavi, K. Venkatesh, R. Kameswaran, A.V.R. Reddy  
"Development of an IR-based carbon analyser for uranium metal", BARC Newsletter  
311 (2009) 2-6 (Web-link: <http://barc.gov.in/publications/nl/2009/200912.pdf/>)
- [137] B.D. Cullity, "Elements of X-ray diffraction", Addison-Wesley Publishing Company  
Inc. (1956).
- [138] R. Tilley, "Crystals and crystal structures", John Wiley & Sons, Ltd. (2006) (ISBN-13  
978-0-470-01820-0).
- [139] E. Smith, G. Dent, "Modern Raman spectroscopy - A practical approach", John Wiley  
& Sons, Ltd. (2006) (ISBN 0-471-49794-0).
- [140] M. Roessle, D.I. Svergun, "Small angle X-ray scattering", In "Encyclopaedia of  
biophysics" (Eds.: G.C.K. Roberts) Springer, Berlin, Heidelberg (2013) (DOI:  
[https://doi.org/10.1007/978-3-642-16712-6\\_284](https://doi.org/10.1007/978-3-642-16712-6_284)).
- [141] P.W. Schmidt, R. Height, "Slit height corrections in small angle X-ray scattering", Acta  
Crystallogr. 13 (1960) 480-483.
- [142] G. Höhne, W.F. Hemminger, H.J. Flammersheim, "Differential scanning calorimetry",  
Springer-Verlag. (2003) (ISBN 978-3-540-00467-7).
- [143] M. Reading, A. Luget, R. Wilson, "Modulated differential scanning calorimetry",  
Thermochim. Acta 238(C) (1994) 295-307.
- [144] J.E.K. Schawe, T. Hutter, C. Heitz, I. Alig, D. Lellinger, "Stochastic temperature  
modulation: A new technique in temperature-modulated DSC", Thermochim. Acta 446  
(2006) 147-155.
- [145] N. Manoj, D. Jain, J.K. Gautam, K.C. Thomas, V. Sudarsan, C.G.S. Pillai, R.K. Vatsa,  
A.K. Tyagi, "A simple, reliable and cost-effective, high temperature dilatometer for  
bulk thermal expansion studies on solids", Measurement 92 (2016) 318-325.

- [146] W.J. Parker, R.J. Jenkins, C.P. Butler, G.L. Abbott, “Flash method of determining thermal diffusivity, heat capacity, and thermal conductivity”, *J. Appl. Phys.* 32 (1961) 1679-1684.
- [147] H.S. Carslaw, J.C. Jaeger, “Conduction of heat in solids”, 2nd edition, Oxford University Press, New York, (1959).
- [148] D. Jain, D. Das, B.N. Jagatap, “Thorium-based fuels for advanced nuclear reactors: Thermophysical, thermochemical and thermodynamic properties”, in A.K. Nayak, B.R. Sehgal (Eds.), *Thorium—Energy for the Future*, Springer (2019) (ISBN 978-981-13-2658-5) 257-275.
- [149] Y.S. Touloukian, R.W. Powell, C.Y. Ho, P.G. Klemens, “Thermophysical properties of matter - The TPRC data series. Volume 1. Thermal conductivity - metallic elements and alloys”, (1970) 429-440; 381-384.
- [150] Y.S. Touloukian, R.W. Powell, C.Y. Ho, M.C. Nicolaou, “Thermophysical properties of matter - The TPRC data series. Volume 10. Thermal diffusivity”, (1974) 205-208.
- [151] Y.S. Touloukian, E.H. Buyco, “Thermophysical properties of matter - The TPRC data series. Volume 4. Specific heat - metallic elements and alloys”, (1971) 268-270.
- [152] Y.S. Touloukian, R.K. Kirby, R.E. Taylor, P.D. Desai, “Thermophysical properties of matter - The TPRC data series. Volume 12. Thermal expansion metallic elements and alloys”, (1975) 365-372.
- [153] H.G. Schettler, J.J. Martin, F.A. Schmidt, G.C. Danielson, “Thermal conductivity of high purity thorium”, *Phys. Rev.* 187 (3) (1969) 801-804.
- [154] T.A. Sandenaw, “Thermal conductivity of uranium: Effects of purity and microstructure”, Report no.: LA-6092-MS, United States (1975) 1-8.
- [155] Y. Takahashi, M. Yamawaki, K. Yamamoto, “Thermophysical properties of uranium-zirconium alloys”, *J. Nucl. Mater.* 154 (1988) 141-144.

## References

- [156] R.W. Logan, D.H. Wood, "Thermal expansion of rolled and extruded uranium", *J. Less-Common Met.* 90 (1983) 233-241.
- [157] J. Nakamura, Y. Takahashi, S. Izumi, M. Kanno, "Heat capacity of metallic uranium and thorium from 80 to 1000 K", *J. Nucl. Mater.* 88 (1980) 64-72.
- [158] M. Boivineau, H. Colin, J.M. Vermeulen, Th. Thévenin, "Thermophysical properties of solid and liquid thorium", *Int. J. Thermophys.* 17(5) (1996) 1001-1010.
- [159] S. Zhou, R. Jacobs, W. Xie, E. Tea, C. Hin, D. Morgan, "Combined ab-initio and empirical model of the thermal conductivity of uranium, uranium-zirconium, and uranium-molybdenum", *Phys. Rev. Mater.* 2 (2018) 083401-1-21.
- [160] Y. Li, A. Chernatynskiy, J.R. Kennedy, S.B. Sinnott, S.R. Phillpot, Lattice expansion by intrinsic defects in uranium by molecular dynamics simulation, *J. Nucl. Mater.* 475 (2016) 6-18.
- [161] K.D. Joshi, S.C. Gupta, S. Banerjee, "Ab-initio theoretical analysis of thermal expansivity, thermal vibrations and melting of thorium", *Phil. Mag.* 88 (27) (2008) 3145-3152.
- [162] S. Jaroszewicz, H.O. Mosca, J.E. Garcés, "The temperature behaviour of the elastic and thermodynamic properties of fcc thorium", *J. Nucl. Mater.* 429(1-3) (2012) 136-142.
- [163] L. Kývala, D. Legut, "Lattice dynamics and thermal properties of thorium metal and thorium monocarbide" *Phys. Rev. B* 101 (2020) 075117.
- [164] P.L. Vijay, J.C. Sehra, C.V. Sundaram, K.R. Gurumurthy, R.V. Raghavan, "Studies on the preparation of thorium metal sponge from thorium oxalate", *BARC Report no.:* 969 (1978) 1-11.
- [165] M.D. Smith, R.W.K. Honeycombe, "The effect of oxygen, carbon and nitrogen on the properties of sintered thorium", *J. Nucl. Mater.* 4 (1959) 345-355.

- [166] Inorganic Crystal Structure Database (ICSD FIZ Karlsruhe GmbH, Version 4.4.0 (2020); collection code: 653236); from: J. Bohet, W. Müller, “Preparation and structure studies of “Van Arkel” protactinium”, *J. Less-Common Met.* 57 (2) (1978) 185-1995.
- [167] International Centre for Diffraction Data (ICDD Database; JCPDF card no.: 720659).
- [168] Inorganic Crystal Structure Database (ICSD FIZ Karlsruhe GmbH, Version 4.4.0 (2020) collection code: 253564) from: V.K. Tripathi, R. Nagarajan, “Sol–gel synthesis of high-purity actinide oxide ThO<sub>2</sub> and its solid solutions with technologically important tin and zinc ions” *Inorg. Chem.* 55 (24) (2016) 12798-12806.
- [169] Inorganic Crystal Structure Database (ICSD FIZ Karlsruhe GmbH, Version 4.4.0 (2020) collection code: 35204); from: S.A. Barrett, A.J. Jacobson, B.C. Tofield, B.E.F. Fender, “The preparation and structure of barium uranium oxide BaUO<sub>3+x</sub>”, *Acta Crystallogr. B* 38 (1982) 2775-2781. [169a] S. Ellison, A. Williams, *Eurachem / CITAC guide: Quantifying Uncertainty in Analytical Measurement* (2012) ISBN 978-0-948926-30-3 (Web-link: [www.eurachem.org](http://www.eurachem.org)).
- [170] Inorganic Crystal Structure Database (ICSD FIZ Karlsruhe GmbH, Version 4.4.0 (2020) collection code: 24223); from: R.E. Rundle, N.C. Baenziger, A.S. Wilson, R.A. McDonald, “The structures of the carbides, nitrides and oxides of uranium”, *J. Am. Chem. Soc.* 70 (1948) 99-105.
- [171] Inorganic Crystal Structure Database (ICSD FIZ Karlsruhe GmbH, Version 4.4.0 (2020) collection code: 26476); from: A.E. Austin, “Carbon positions in uranium carbides”, *Acta Crystallogr.* 12 (1959) 159-161.
- [172] “Augmented uranium metal production facility”, *BARC Newsletter* 200 (2000) 15-18 (Web-link: <http://barc.gov.in/publications/nl/2000/200009.pdf>).
- [173] G.C. Allen, P.M. Tucker, “Surface oxidation of uranium metal as studied by X-ray photoelectron spectroscopy”, *J. Chem. Soc. Dalton* 5 (1973) 470-474.

- [174] R. Rao, R.K. Bhagat, N.P. Salke, A. Kumar, "Raman spectroscopic investigation of thorium dioxide-uranium dioxide ( $\text{ThO}_2\text{-UO}_2$ ) fuel materials", *Appl. Spectrosc.* 68(1) (2014) 44-48.
- [175] "Thermophysical properties of materials for nuclear engineering: A tutorial and collection of data", (IAEA-THPH), International Atomic Energy Agency, Vienna (2008).
- [176] I.F. Barwood, B.R. Butcher, "The  $\alpha \rightarrow \beta$  phase transformation in uranium", *J. Nucl. Mater.* 8 (1963) 232-240.
- [177] C. Yoo, H. Cynn, P. Söderlind, "Phase diagram of uranium at high pressures and temperatures", *Phys. Rev. B* 57 (1998) 10359-10362.
- [178] P. Zhou, X. Wang, H. Yang, X. Fu, "Effect of vacuum heat treatment on oxidation of uranium surfaces", *Rare Metal Mat. Eng.* 37 (2008) 94-97.
- [179] G. Erez, U. Even, "The Wiedemann-Franz ratio of metallic uranium at elevated temperatures", *J. Appl. Phys.* 37 (1966) 4633-4644.
- [180] S. Nasu, S. Fukushima, T. Ohmichi, T. Kikuchi, "Thermal diffusivity of uranium by laser pulse method from 20° to 850°C", *Jap. J. Appl. Phys.* 7 (1968) 682.
- [181] D. Jain, C.G.S. Pillai, B.S. Rao, R.V. Kulkarni, E. Ramdasan and K.C. Sahoo, "Thermal diffusivity and thermal conductivity studies on thoria-lanthana solid solutions up to 10 mol. %  $\text{LaO}_{1.5}$ ", *J. Nucl. Mater.* 353 (2006) 35-41.
- [182] S.S. Parker, J.T. White, P. Hosemann, A.T. Nelson, "Thermophysical properties of thorium mononitride from 298 to 1700 K", *J. Nucl. Mater.* 526 (2019) 151760.
- [183] H. He, J. Majewski, D.D. Allred, P. Wang, X. Wen, K.D. Rector, "Formation of solid thorium monoxide at near-ambient conditions as observed by neutron reflectometry and interpreted by screened hybrid functional calculations", *J. Nucl. Mater.* 487 (2017) 288-296.

## References

- [184] B.R. Butcher, A.H. Rowe, "Phase transformation in uranium", *Nature* (1953) 817.
- [185] H.H. Klpefer, P. Chiotti, "Characteristics of the solid state transformations in uranium", USAEC Report no.: ISC-893 (1957) 1-113.
- [186] W.S. Blackburn, " $\alpha$ - $\beta$  Thermal cycling of uranium", *J. Nucl. Mater.* 2 (1960) 191.
- [187] J.J. Stobo, "Alpha beta cycling of uranium", *J. Nucl. Mater.* 2 (1960) 97-109.
- [188] L.T. Lloyd, "Thermal expansion of alpha-uranium single crystals", *J. Nucl. Mater.* 3 (1961) 67-71.
- [189] L.T. Lloyd, C.S. Barrett, "Thermal expansion of alpha uranium", *J. Nucl. Mater.* 18 (1966) 55-59.
- [190] E.S. Fisher, "Preparation of alpha uranium single crystals by a grain-coarsening method", *J. Metals* 9 (1957) 882-888.
- [191] D.C. Wallace, "Specific heat of thorium at high temperatures", *Phys. Rev.* 120 (1) (1960) 84-88.
- [192] E.A. Mit'kina, "Experimental determination of the true specific heats of uranium, thorium, and other metals", *Sov. Atom Energy* 7 (2) (1959) 163-165.
- [193] F.L. Oetting, D.T. Peterson, "Heat capacity of well characterized thorium metal from 298 to 700 K", *J. Less-Common Met.* 128 (1987) 231-239.
- [194] D.C. Ginnings, R.J. Corruccini, "Heat capacities at high temperatures of uranium, uranium trichloride, and uranium tetrachloride, *J. Res. Nat. Bur. Stand.* 39 (1947) 309-316.
- [195] F.K. Oetting, M.H. Rand, R.J. Ackermann, "The chemical thermodynamics of actinide elements and compounds, Part 1, The actinide elements", International Atomic Energy Agency (IAEA), Vienna (1976).
- [196] A.L. Loeb, "Thermal conductivity: VIII, A theory of thermal conductivity of porous materials", *J. Am. Ceram. Soc.* 37 (1954) 96-99.

## References

- [197] S. Kaity, J. Banerjee, M.R. Nair, K. Ravi, S. Dash, T.R.G. Kutty, A. Kumar, R.P. Singh, "Microstructural and thermophysical properties of U-6 wt.% Zr alloy for fast reactor application", *J. Nucl. Mater.* 427 (2012) 1-11.
- [198] C. Hin, "Thermal conductivity of metallic uranium", NEUP 14-6767 (2018) (Web-link: <https://www.osti.gov/servlets/purl/1433931>).
- [199] M. Floyd, B. Bromley, J. Pencer, "A Canadian perspective on progress in thorium fuel science and technology", *CNL Nucl. Rev.* 6 (1) (2017) 1-17.
- [200] S. Thakur, P.S.R. Krishna, A.B. Shinde, R. Kumar, S.B. Roy, "Quantitative analysis of thorium phase in Th-U alloys using diffraction studies", *AIP Conf. Proc.* 1832 (2017) 060012.
- [201] P. Chiotti, "High temperature crystal structure of thorium", *J. Electrochem. Soc.* (1955) 567-570.
- [202] G.G. Bente, "A Physical Metallurgical Study of Thorium-Rich Thorium-Uranium Alloys", Report no.: NAA-SR-2069 (1958).
- [203] G.H. Bannister, R.C. Burnett, J.R. Murray, "Ageing and hot hardness characteristics of certain thorium alloys", *J. Nucl. Mater.* 2(1) (1960) 51-61.
- [204] "Chemical technology division annual technical report for 1986," ANL-87-19, Argonne National Laboratory (1987) 122.
- [205] V. Crewe, S. Lawroski, "Reactor development program progress report", Argonne National Laboratory, ANL-7230, Lemont, IL, USA (1966).
- [206] O. Beneš D. Manara R.J.M. Konings, "Thermodynamic assessment of the Th-U-Pu system", *J. Nucl. Mater.* 449 (1-3) (2014) 15-22.
- [207] S. Kneppel, "Aqueous corrosion of thorium alloys and zircaloy-clad thorium alloys", NMI-1226, United States Atomic Energy Commission (1960) 1-49 (Web-link: <https://play.google.com/books/reader?id=OGCWvHY4xRwC&hl=en&pg=GBS.PA1>)

- [208] D.S. Evans, G.V. Raynor, "The solubility of zirconium in  $\alpha$ -thorium", *J. Nucl. Mater.* 4 (1) (1961) 66-69.
- [209] R.I. Sheldon, D.E. Peterson, "The (U-Zr) Uranium-zirconium system", *Bull. Alloy Phase Diagr.* 10 (2) (1989) 165-171.
- [210] O.N. Carlson, "Some studies on the uranium-thorium-zirconium ternary alloy system", AECD-3206, United States Atomic Energy Commission (1950) 1-72.
- [211] J.W. Goffard, R.K. Marshall, "Irradiation behavior of Zircaloy-2 clad thorium-uranium-zirconium alloy fuel elements Interim report 1", BNWL-479, Pacific Northwest Laboratory, United States Atomic Energy Commission (1967).
- [212] T. Okawa, S. Nakayama, H. Sekimoto, "Design study on power flattening to sodium cooled large-scale CANDLE burning reactor with using thorium fuel", *Energ. Convers. Manage.* 53 (1) (2012) 182-188.
- [213] Inorganic crystal Structure Database (ICSD FIZ Karlsruhe GmbH, Version 4.4.0 (2020) collection code: 164572) from: A.I. Kolesnikov, A.M. Balagurov, I.O. Bashkin, A.V. Belushkin, E.G. Ponyatovsky, M. Prager, "Neutron scattering studies of ordered gamma -ZrD", *J. Phys. Condens-Mat.* 6 (43) (1994) 8977-8988.
- [214] Inorganic crystal Structure Database (ICSD FIZ Karlsruhe GmbH, Version 4.4.0 (2020) collection code: 16559) from: B.O. Loopstra, "Neutron diffraction investigation of  $U_3O_8$ ", *Acta Crystallogr.* 17 (1964) 651-654.
- [215] Inorganic crystal Structure Database (ICSD FIZ Karlsruhe GmbH, Version 4.4.0 (2020) collection code: 246035) from: S.K. Sali, N.K. Kulkarni, K. Krishnan, S.N. Achary, A.K. Tyagi, "Oxidation / reduction studies on  $Zr_yU_{1-y}O_{2+x}$  and delineation of a new orthorhombic phase in U-Zr-O system", *J. Solid-State Chem.* 181 (8) (2008) 1859-1866.

## References

- [216] Inorganic crystal Structure Database (ICSD FIZ Karlsruhe GmbH, Version 4.4.0 (2020) collection code: 108756) from: H.L. Luo, J.G. Huber, “Superconductivity in Th-Zr alloys”, *J. Less-Common Met.* 65 (1) (1979) 13-17.
- [217] J.M. Elorrieta, L.J. Bonales, M. Naji, D. Manara, V.G. Baonza, J. Cobos, “Laser-induced oxidation of  $\text{UO}_2$ : A Raman study”, *J. Raman Spectrosc.* 49 (5) (2018) 878-884.
- [218] H. He, D. Shoesmith, “Raman spectroscopic studies of defect structures and phase transition in hyper-stoichiometric  $\text{UO}_{2+x}$ ”, *Phys. Chem. Chem. Phys.* 12 (2010) 8109-8118.
- [219] X. Zhao, D. Vanderbilt, “Phonons and lattice dielectric properties of zirconia”, *Phys. Rev. B* 65 (2002) 075105.
- [220] E. Hashem, A. Seibert, J-F. Vigier, M. Naji, S. Mastromarino, A. Ciccioli, D. Manara, “Solid-liquid equilibria in the  $\text{ThO}_2$ - $\text{ZrO}_2$  system: An experimental study” *J. Nucl. Mater.* 521 (2019) 99-108.
- [221] O.N. Carlson, E.R. Stevens, “A compilation of thorium binary phase diagrams”, USAEC Report (1968) (Web-link: <https://www.osti.gov/servlets/purl/4529064>).
- [222] G.B. Skinner, H.L. Johnston, “Thermal Expansion of zirconium between 298°K and 1600°K”, *J. Chem Phys.* 21 (1953) 1383.
- [223] P.L. Brown, E. Curti, B. Grambow, C. Ekberg, “Chemical thermodynamics of zirconium”, OECD Nuclear energy agency, data bank (Eds.: F.J. Mompean, J. Perrone, M. Illemassene) (2005) (Web-link: <https://www.oecd-nea.org/dbtdb/pubs/vol8-zirconium.pdf>).
- [224] C.G.S. Pillai, P. Raj, “Thermal Conductivity of  $\text{ThO}_2$  and  $\text{Th}_{0.98}\text{U}_{0.02}\text{O}_2$ ”, *J. Nucl. Mater.* 277 (2000) 116-119.

- [225] S.S. Manoharan, K.C. Patil, "Combustion synthesis of metal chromite powders", *J. Am. Ceram. Soc.* 75 (1992) 1012-1015.
- [226] S.R. Jain, K.C. Adiga, V.R. Pai Verneker, "A new approach to thermochemical calculations of condensed fuel-oxidizer mixtures," *Combust. Flame* 40 (6) (1981) 71-79.
- [227] S. Roy, A. Das Sharma, S.N. Roy, H.S. Maiti, "Synthesis of  $\text{YBa}_2\text{Cu}_3\text{O}_{7-x}$  Powder by Autoignition of Citrate-Nitrate Gel", *J. Mater. Res.* 8(11) (1993) 2761-2766.
- [228] M. Gizowska, I. Kobus, K. Perkowski, M. Piatek, G. Konopka, I. Witosławska, M. Osuchowski, "Size and morphology of yttria nanopowders obtained by solution combustion synthesis" *Arch. Metall. Mater.* 63(2) (2018) 743-748.
- [229] G.A.M. Hussein, H.M. Ismail, "Texture assessment of thoria as a final decomposition product of hydrated thorium nitrate and oxycarbonate", *Colloids Surf. A*: 99 (1995) 129-139.
- [230] I.M. Weiss, C. Muth, R. Drumm, H.O.K. Kirchner, "Thermal decomposition of the amino acids glycine, cysteine, aspartic acid, asparagine, glutamic acid, glutamine, arginine and histidine", *BMC Biophys.* 11 (2018) 1-15.
- [231] N. Raje, A.V.R. Reddy, "Mechanistic aspects of thermal decomposition of thorium oxalate hexahydrate: A review", *Thermochim. Acta* 505 (2010) 53-58.
- [232] H. Hayashi, T. Watanabe, "Properties of thoria obtained by thermal decomposition of thorium salts", *Nippon Kagaku Kaishi* 4 (1973) 858-860.
- [233] Y. Saito, "Thermal decomposition of thorium oxalate", *J. Jpn. Soc. Powder Metall.* 17(1971) 235-242.
- [234] M.T. Aybers, "Kinetic study of the thermal decomposition of thorium oxalate dehydrate", *J. Nucl. Mater.* 252 (1998) 28-33.
- [235] D.Y. Chung, E. H. Lee, "Microwave-induced combustion synthesis of  $\text{Ce}_{1-x}\text{Sm}_x\text{O}_{2-x/2}$  powder and its characterization", *J. Alloys Compd.* 374 (2004) 69-73.

- [236] “The Aldrich Library of FT-IR Spectra, Edition-II, Volume-1”, 1 898 A 897-898.
- [237] S. Kumar, A.K. Rai, V.B. Singh, S.B. Rai, “Vibrational spectrum of glycine molecule”, *Spectrochim. Acta A* 61 (2005) 2741-2746.
- [238] J. R. Ferraro, A. Walker, “Comparison of the infrared spectra of the hydrates and anhydrous salts in the systems  $\text{UO}_2(\text{NO}_3)_2$  and  $\text{Th}(\text{NO}_3)_4$ ”, *J. Chem. Phys.* 45 (1966) 550-552.
- [239] J.H-Paredes, D.G-Mitnik, H.E. E-Ponce, M.E. A-Ramos, A.D-Moller, “Band structure, optical properties and infrared spectrum of glycine–sodium nitrate crystal”, *J. Mole. Str.* 875 (2008) 295-301.
- [240] S.L. Estes, M.R. Antonio, L. Soderholm, “Tetravalent Ce in the nitrate-decorated hexanuclear cluster  $[\text{Ce}_6(\mu_3\text{-O})_4(\mu_3\text{-OH})_4]^{12+}$ : A structural end point for ceria nanoparticles, *J. Phys. Chem. C* 120 (2016) 5810-5818.
- [241] M. Rand, L. Fuger, I. Grenthe, V. Neck, D. Rai, “Chemical thermodynamics: Chemical thermodynamics of thorium”, (OECD, NEA-TDB) Vol. 11, Elsevier, Amsterdam (2007).
- [242] C. Hennig, K. Schmeide, V. Brendler, H. Moll, S. Tsushima, A.C. Scheinost, “EXAFS Investigation of U(VI), U(IV), and Th(IV) sulfato complexes in aqueous solution”, *Inorg. Chem.* 46 (2007) 5882-5892.
- [243] J. Rothe, M.A. Denecke, V. Neck, R. Muller, J.I. Kim, XAFS “Investigation of the structure of aqueous thorium(IV) species, colloids, and solid thorium(IV) oxide / hydroxide”, *Inorg. Chem.* 41 (2002) 249-258.
- [244] C. Hennig, S. Takao, K. Takao, S. Weiss, W. Kraus, F. Emmerling, A.C. Scheinosta, “Structure and stability range of a hexanuclear Th(IV)-glycine complex”, *Dalton Trans.* 41 (2012) 12818-12823.

## References

- [245] Y. Hu, K.E. Knope, S. Skanthakumar, L. Soderholm, "Understanding the ligand-directed assembly of a hexanuclear Th<sup>IV</sup> molecular cluster in aqueous solution", *Eur. J. Inorg. Chem.* 24 (2013) 4159-4163.
- [246] M. Nourmand, N. Meissami, "Complex formation between uranium(VI) and thorium (IV) ions with some  $\alpha$ -amino-acids", *J. Chem. Soc. Dalton* 8 (1983) 1529-1533.
- [247] Bismondo, L. Rizzo, G. Tomat, "Thermodynamic properties of actinide complexes. uranyl (VI)- and thorium (IV)-glycine systems", *Inorg. Chim. Acta* 74 (1983) 21-24.
- [248] B.G. Oliver, A.R. Davis, "The structure of aqueous thorium nitrate solution by laser Raman spectroscopy", *J. Inorg. Nucl. Chem.* 34 (1972) 2851-2860.
- [249] Z. Huang, X. Chen, Y. Li, J. Chen, J. Lin, J. Wang, J. Lei, R. Chen, "Quantitative determination of citric acid in seminal plasma by using Raman spectroscopy", *Appl. Spectrosc.* 67 (7) (2013) 757-760.
- [250] A.K. Arora, M. Rajalakshmi, T.R. Ravindran, V. Sivasubramanian, "Raman spectroscopy of optical phonon confinement in nanostructured materials", *J. Raman Spectrosc.* 38 (2007) 604-617.
- [251] D. Langmuir, J.S. Herman, "The mobility of thorium in natural waters at low temperatures", *Geochim. Cosmochim. Ac.* 44 (1980) 1753-1766.
- [252] M. Bobtelsky, B. Graus, "Thorium citrate complexes, their composition, structure and behavior", *J. Am. Chem. Soc.* 76 (6) (1954,) 1536-1539.
- [253] G.R. Choppin, H.N. Erten, Y. Xia, "Variation of stability constants of thorium citrate complexes with ionic strength", *Radiochim. Acta* 74 (1996) 123-127.
- [254] D.P. Raymond, J.R. Duffield, D.R. Williams, "Complexation of plutonium and thorium in aqueous environments", *Inorg. Chim. Acta* 140 (1987) 309-313.
- [255] M.M. Barbooti, D.A. Al-Sammerrai, "Thermal decomposition of citric acid", *Thermochim. Acta* 98 (1986) 119-126.

- [256] D. Hennings, W. Mayr, "Thermal decomposition of (BaTi) citrates into barium titanate", *J. Solid State Chem.* 26 (1978) 329-338.
- [257] N.S. Gajbhiye, S. Prasad, "Thermal decomposition of hexahydrated nickel iron citrate", *Thermochim. Acta* 285 (1996) 325-336.
- [258] J. Tsay, T. Fang, "Effects of molar ratio of citric acid to cations and of pH value on the formation and thermal-decomposition behavior of barium titanium citrate", *J. Am. Ceram. Soc.* 82(6) (1999) 1409-1415.
- [259] A. Marcilla, A. Gómez-Siurana, M. Beltrán, I. Martínez-Castellanos, I. Blasco, D. Berenguer, "TGA-FTIR study of the pyrolysis of sodium citrate and its effect on the pyrolysis of tobacco and tobacco/SBA-15 mixtures under N<sub>2</sub> and air atmospheres", *J. Sci. Food Agr.* 98 (15) (2018) 5916-5931.
- [260] O. Glatter, O. Kratky, "Small angle X-ray scattering", Academic, London (1982).
- [261] A. Guinier, G. Fournet, "Small angle scattering of X-rays", Wiley, New York (1955).
- [262] J. Aitchison, J.A.C. Brown, "The log normal distribution", Cambridge University Press, Cambridge (1957).
- [263] R.D. Purohit, B.P. Sharma, K.T. Pillai, A.K. Tyagi, "Ultrafine ceria powders via glycine-nitrate combustion", *Mater. Res. Bull.* 36 (15) (2001) 2711-2721.
- [264] V.R. Choudhary, A.M. Rajput, B. Prabhakar, A.S. Mamman, "Partial oxidation of methane to CO and H<sub>2</sub> over nickel and/or cobalt containing ZrO<sub>2</sub>, ThO<sub>2</sub>, UO<sub>2</sub>, TiO<sub>2</sub> and SiO<sub>2</sub> catalysts", *Fuel* 77 (15) (1998) 1803-1807.
- [265] V. Múčka, J. Podlaha, R. Silber, "NiO-ThO<sub>2</sub> mixed catalysts in hydrogen peroxide decomposition and influence of ionizing radiation", *Radiat. Phys. Chem.* 59 (5-6) (2000) 467-475.

## References

- [266] P. Balakrishna, B.N. Murty, K.P. Chakraborty, R.N. Jayaraj, C. Ganguly, “Special features in powder preparation, pressing, and sintering of uranium dioxide”, *Mater. Manuf. Process.* 15(5) (2000) 679-693.
- [267] C.S. Morgan, K.H. McCorkle, G.L. Powell, “Sintering and desintering of thoria”, In: Kuczynski G.C. (Eds.) *Sintering and Related Phenomena*. Materials Science Research, Vol. 6, Springer, Boston, MA (1973).
- [268] J.M. Pope, K.C. Radford, “Physical properties of some thoria powders and their influence on sinterability”, *J. Nucl. Mater.* 52 (1974) 241-254.
- [269] Z. Chen, J. Mabon, J. Wen, R. Trice, “Degradation of plasma-sprayed yttria-stabilized zirconia coatings via ingress of vanadium oxide”, *J. Eur. Ceram. Soc.* 29(9) (2009) 1647-1656.
- [270] M.A. Delfrate, J. Lemaitre, V. Buscaglia, M. Leoni, P. Nanni, “Slip casting of submicron BaTiO<sub>3</sub> produced by low-temperature aqueous synthesis”, *J. Eur. Ceram. Soc.* 16(9) (1996) 975-984.
- [271] T.K. Gupta, R.L. Coble, “Sintering of ZnO: II, density decrease and pore growth during the final stage of the process”, *J. Am. Ceram. Soc.* 51 (9) (1968) 525-528.
- [272] C.-H. Chang, J.F. Rufner, K.V. Benthem, R.H.R. Castro, “Design of desintering in tin dioxide nanoparticles”, *Chem. Mater.* 25(21) (2013) 4262-4268.
- [273] P. Duran, J. Tartaj, C. Moure, “Sintering behaviour and microstructural evolution of agglomerated spherical particles of high-purity barium titanate”, *Ceram. Int.* 29(4) (2003) 419-425.
- [274] C.-Y. Tsao, W.-H. Tuan, K.-C. Feng, “De-sintering of Ba<sub>5</sub>Nb<sub>4</sub>O<sub>15</sub> ceramic and its influence on microwave characteristics”, *J. Eur. Ceram. Soc.* 37(4) (2017) 1517-1521.
- [275] Cs. Balázs, F.S. Cinar, O. Addemir, F. Wéber, P. Arató, “Manufacture and examination of C/Si<sub>3</sub>N<sub>4</sub> nanocomposites” *J. Eur. Ceram. Soc.* 24(12) (2004) 3287-3294.

- [276] R. Besler, M.R. da Silva, J.J. do Rosario, M. Dosta, S. Heinrich, R. Janssen, “Sintering simulation of periodic macro porous alumina”, *J. Am. Ceram. Soc.* 98(11) (2015) 3496-3502.
- [277] K. Ananthasivan, S. Anthonysamy, A. Singh, P.R. Vasudeva Rao, “De-agglomeration of thorium oxalate - A method for the synthesis of sinter active thoria”, *J. Nucl. Mater.* 306 (1) (2002) 1-9.
- [278] R.H.R. Castro, “Controlling sintering and grain growth of nanoceramics”, *Cerâmica* 65 (373) (2019) 122-129. **[278a]** Thermodynamics of sintering, R.M. German, *Sintering of advanced materials: Fundamentals and processes* (Ed.: Z.Z. Fang) Woodhead Publishing Ltd. (2010), ISBN 978-1-84569-562-0. **[278b]** G.S. Upadhyaya, *Sintered metallic and ceramic Materials*, John Wiley & Sons Ltd. (1999) ISBN 0-471-98155-9.
- [279] O. Sudre, F.F. Lange, “The effect of inclusions on densification; III, The desintering phenomenon”, *J. Am. Ceram. Soc.* 75 (12) (1992) 3241-3251.
- [280] F. Li, J. Pan, A. Cocks, “Defect healing and cracking in ceramic films during constrained sintering” *J. Am. Ceram. Soc.* 95(12) (2012) 3743-3749.
- [281] S. Knight, R. Korlacki, C. Dugan, J.C. Petrosky, A. Mock, P.A. Dowben, J. Matthew Mann, M.M. Kimani, M. Schubert, “Infrared-active phonon modes in single-crystal thorium dioxide and uranium dioxide”, *J. Appl. Phys.* 127 (2020) 125103.

## CHAPTER 7

### Desintering in combustion synthesized ThO<sub>2</sub>:

#### A comparison of glycine-nitrate and citrate-nitrate route

---

##### 7.1. Introduction

In chapter-6, mechanisms of formation for nanocrystalline ThO<sub>2</sub> by solution combustion synthesis based on, glycine-nitrate and citrate-nitrate routes have been discussed in detail. Role of molecular interactions on the nature of combustion process and powder characteristics of as-combusted ThO<sub>2</sub> obtained from these two routes have been identified. Effect of fuel to oxidant ratio (F:O) on the nature and mechanism of combustion has also been identified for both, fuel-deficient (F:O < 1.0) as well as fuel-rich (F:O > 1.0) stoichiometries of starting aqueous solutions. As-combusted ThO<sub>2</sub> is obtained in the form of nanocrystalline powders and may also have residual carbonaceous contents in it, which can be removed by calcination. Nanocrystalline ThO<sub>2</sub> powders can be directly employed as such or in the form of slurry in suitable fluids for their applications as support matrix for catalysis [264, 265]. For other applications such as ceramic oxide nuclear fuel, high-temperature refractory oxide, high temperature oxide-ion conductor, transparent oxide ceramics, etc., it is required in the form of dense ceramic. In India, dense ThO<sub>2</sub> pellets are used in (i) pressurized heavy water reactors (PHWRs) for neutron flux flattening, (ii) Fast Breeder Test Reactor (FBTR) for <sup>233</sup>U breeding and (iii) research reactors (Dhruva) for irradiation studies. These pellets are prepared by high temperature sintering ( $\geq 2000$  K) of powder compacts prepared from bulk ThO<sub>2</sub> powders. Sintering of bulk ThO<sub>2</sub> has been widely investigated [102-104]. Microstructure of ThO<sub>2</sub> ceramics obtained from sintering of bulk powders comprise of large grains and wide grain size distribution.

Such microstructure degrades pellet's mechanical strength, which is undesired for nuclear fuel application. Coarse microstructure also makes it difficult to dissolve irradiated ThO<sub>2</sub> pellets for fuel reprocessing and necessitate addition of highly corrosive fluoride ions for fuel dissolution. An alternative approach is use of nanocrystalline ThO<sub>2</sub> powders for nuclear fuel fabrication, which can be efficiently sintered to obtain high density pellets with uniform microstructure consisting of sub-micron or nano-sized grains. As compared to conventional ceramic fuels, bulk nanocrystalline ceramics offer many advantages such as (i) better fission gas retention capability in small sized isolated closed pores, (ii) better resistance to fuel-clad interactions by efficiently relaxing the interaction stresses (super-plasticity behavior) and (iii) improved tolerance to irradiation induced amorphisation due to nanostructure morphology [41]. Apart from their use as nuclear fuels, dense ThO<sub>2</sub> ceramics obtained from nanocrystalline powders are advantageous for other applications, as mentioned above. Reported studies on combustion synthesized nanocrystalline ThO<sub>2</sub> have focused on its synthesis and powder properties [109, 114, 123, 124] as well as sintering of compacts made from such powders [113, 125]. One limiting issue usually observed with nanocrystalline (or sub-micron sized) ThO<sub>2</sub> powders is undesired loss of bulk density during high temperature processing, a phenomenon known as desintering (also referred as runaway / break away sintering). From the point of view of nuclear fuel pellets fabrication, sintering conditions must be optimized to completely avoid the occurrence of desintering / bloating [266]. While occurrence of desintering has been reported for fine ThO<sub>2</sub> powders [106, 113, 267], a systematic study with different combustion routes and fuel to oxidant stoichiometries is not available. The present study addresses this aspect wherein powder properties and sintering behavior of nanocrystalline ThO<sub>2</sub> powders obtained from glycine-nitrate and citrate-nitrate solution combustion methods, over a range of fuel to oxidant ratios have been investigated. In

particular, nature and extent of desintering effect and its origin in nanocrystalline ThO<sub>2</sub> compacts prepared from two synthesis routes have been discussed in this chapter.

## 7.2. Experimental

Throughout this chapter, **glycine-nitrate derived ThO<sub>2</sub>** and **citrate-nitrate derived ThO<sub>2</sub>** have been referred as **gn-ThO<sub>2</sub>** and **cn-ThO<sub>2</sub>**, respectively. Nanocrystalline ThO<sub>2</sub> was prepared from solution combustion synthesis method using two routes namely, glycine-nitrate combustion and citrate-nitrate combustion as detailed in chapter-6 (section 6.2.). Fuel to oxidant ratios (F:O) were varied over 0.65 – 1.20 and 0.90 – 1.25 for glycine-nitrate and citrate-nitrate routes, respectively. Combustion reactions were performed inside a fume-hood with due care to minimize air-borne (aerosol-borne) powder spillage / loss during combustion. Combustion was more intense / vigorous and visibly rapid for glycine-Th(IV)-nitrate gels as compared to citrate-Th(IV)-nitrate gels.

As-combusted powders were calcined at 973 K for 5 h in static air atmosphere and weight loss upon calcination was measured. Based on studies reported by Pope et al., [268], wherein grain coarsening was observed in the form of narrowing of powder X-ray diffraction lines for ThO<sub>2</sub> powders calcined at 1023 K, calcination temperature in present investigations was restricted to 973 K to minimize changes in nanocrystalline powder morphology while eliminating carbonaceous residues. Tap density of calcined powders were measured by filling the powder into a volume calibrated test tube (internal diameter ~7 mm) and tapped vertically against a wooden platform till the volume reading (~ 1 cm<sup>3</sup>) became invariant with successive tapping. From the weight of the filled powder and volume reading, tap-density was calculated. Phase identification of as-combusted and calcined ThO<sub>2</sub> powders was carried out using powder XRD. Average crystallite size was estimated using (i) Scherrer formula ( $t =$

$0.9\lambda / B.\cos(\theta)$ ) and (ii) Williamson-Hall Plot ( $B.\cos(\theta) = \epsilon.\sin(\theta) + k\lambda / t$ ). Average lattice strain ( $\epsilon$ ) was estimated from the slope of Williamson-Hall Plot.

Sintering experiments on calcined ThO<sub>2</sub> powder compacts were performed by following the process flow-sheet shown in Fig. 7.1. This flow sheet was adopted keeping in mind the conventional process adopted for preparation of oxide ceramic nuclear fuel pellets. Calcined ThO<sub>2</sub> powders were ground in an agate mortar-pestle with intermittent scratching of powder from mortar walls. Gn-ThO<sub>2</sub> powders were sticky to mortar-pestle surface during grinding. As-ground powders were pre-compacted into cylindrical pellets using a 12 mm diameter tungsten carbide (WC) die at ~ 150 MPa pressure. These compacts were crushed and ground again (granulation) for 30 minutes and finally compacted into 6 mm diameter green pellets using WC die at ~ 500 MPa pressure. Green densities of pellets were calculated by measured weight and geometric volume. These green pellets were used for sintering studies. Sintering experiments were carried out in a vertical thermo mechanical analyzer (TMA). Linear shrinkage curves were recorded by heating the green pellets from 308 K to 1773 K (heating rate = 10 K / min.) followed by isothermal heating at the highest temperature for 1 h. Cooling up to 473 K was controlled (20 K / min.) followed by furnace cooling up to ambient temperature. Load over the sample was kept minimum (~ 1 g) to enable shrinkage measurement in dilatometry mode. All sintering experiments were performed in flowing helium atmosphere (He, 99.9%, flow rate = 60 ml / min.). Sintered pellets were weighed to calculate the weight change during sintering. Sintered density was evaluated geometrically. Morphology of calcined powders and sintered thoria pellets were measured using scanning electron microscope (SEM). Few ThO<sub>2</sub> samples were characterized by FT-IR spectroscopy using disc shaped thin semi-transparent pellets made in IR-grade KBr matrix.

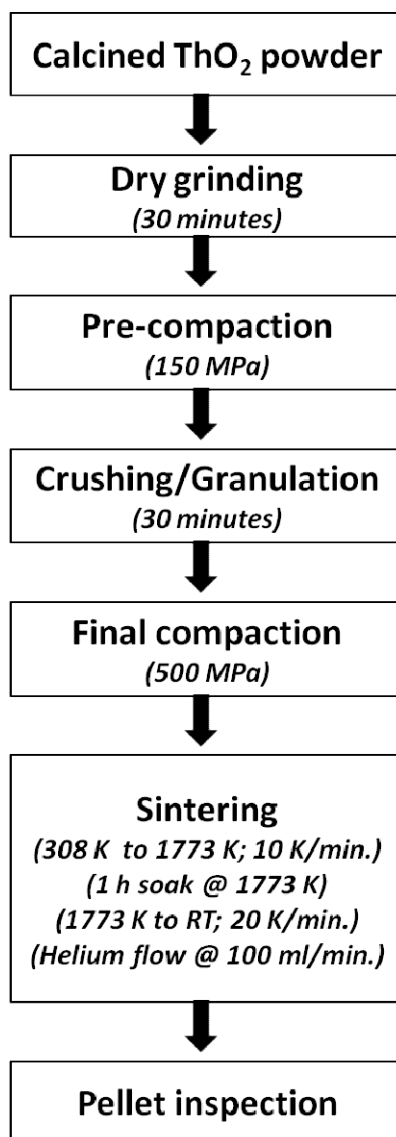
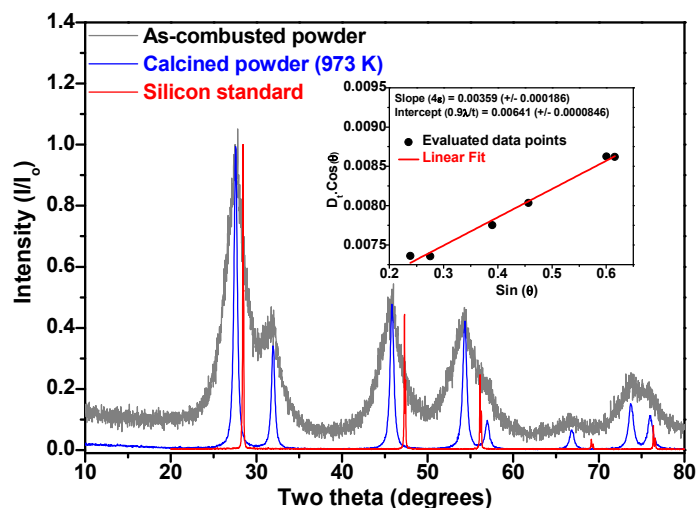


Fig. 7.1. Flow sheet for ThO<sub>2</sub> pellet processing

### 7.3. Results and discussion

#### 7.3.1. Powder properties of gn-ThO<sub>2</sub> and cn-ThO<sub>2</sub> powders

Figure 7.2 shows a representative XRD pattern for as-combusted and calcined ThO<sub>2</sub> powder obtained from citrate-Th(IV)-nitrate route (F:O = 1.10). Powder pattern of silicon standard is also plotted in the same figure. Inset shows the evaluated Williamson-Hall plot for the calcined sample. XRD patterns of all as-combusted and calcined samples obtained through glycine-nitrate and citrate-nitrate routes are shown in Fig. 7.3(a) and Fig. 7.3(b), respectively.



**Fig. 7.2. Powder XRD pattern of citrate-Th(IV)-nitrate as-combusted product (F:O = 1.10), calcined ThO<sub>2</sub> powder and silicon standard. Inset shows the Williamson-Hall plot for calcined ThO<sub>2</sub> powder**

XRD patterns indicated cubic fluorite structure of ThO<sub>2</sub> (space group: Fm3m) for both, as-combusted as well as calcined powders. Compared to calcined powders, diffraction patterns of as-combusted powders showed broader peaks, which indicated the presence of smaller crystallites in the later (Fig. 7.3 (a) and (b)). Powders obtained through glycine-nitrate route showed better crystallinity as compared to those obtained through citrate-nitrate route, which was indicated by higher signal to noise ratio (S/N) and narrow line widths of normalized XRD patterns as shown in insets of Fig. 7.3(a) and (b). Lattice parameter evaluated for as-combusted and calcined powders for stoichiometric combustion (F:O = 1.00) were 5.595(3) Å and 5.594(2) Å for gn-ThO<sub>2</sub> and, 5.610(5) Å and 5.594(3) Å for cn-ThO<sub>2</sub>, respectively. As-combusted cn-ThO<sub>2</sub> powders show relatively larger lattice parameter as compared to gn-ThO<sub>2</sub>, which suggest smaller size and greater structural disorder. As-combusted cn-ThO<sub>2</sub> powders show XRD pattern close to amorphous materials due to very small crystallite size as well as presence of large amounts of carbonaceous residues. Calcination of powders in air at

973 K resulted into grain coarsening, which is apparent from improved crystallinity as well as narrowing of the diffraction peaks (Fig. 7.3 (a) and (b)).

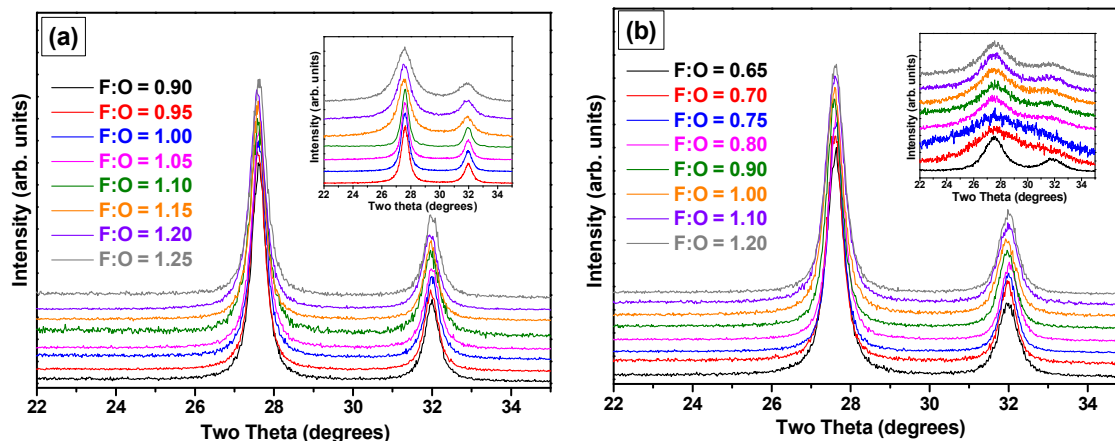


**Fig. 7.3. Section of powder XRD patterns recorded on (a) calcined gn- $\text{ThO}_2$  and (b) calcined cn- $\text{ThO}_2$  for studied fuel to oxidant ratios. Inset in each figure shows XRD trace of as-combusted powders**

Average crystallite size and lattice strain were calculated for all calcined samples. These results are presented in Table 7.1 and Table 7.2 along with other powder properties. It can be seen that for as-combusted gn- $\text{ThO}_2$  powders, with increasing F:O values, average crystallite size abruptly reduced for fuel-rich gel compositions (F:O > 1.0). This has been explained in chapter-6 (Section 6.3) in terms of preferential abundance of mono-nuclear glycine-Th(IV)-nitrate molecular complexes over hexanuclear glycine-Th(IV)-nitrate complexes in aqueous gels for fuel-rich stoichiometries. On the other hand, average crystallite size of as-combusted cn- $\text{ThO}_2$  powders remained within 3-5 nm for all F:O values and did not systematically vary with it. Average crystallite sizes evaluated from the Scherrer formula were smaller (~ 15-20 nm) than those evaluated from the Williamson-Hall plot (~ 20-25 nm). Calcined powders of both gn- $\text{ThO}_2$  and cn- $\text{ThO}_2$  showed positive values of average lattice strain, indicating the

presence of expansive strain. Upon calcination, average crystallite size increased mainly due to grain coarsening and attained similar size range for both, gn-ThO<sub>2</sub> and cn-ThO<sub>2</sub> powders.

**Table 7.1. Powder properties of gn-ThO<sub>2</sub> powders (973 K calcined samples)**

F:O	Average crystallite size (nm)			Average lattice strain ( $\times 10^{-3}$ ) From W-H plot	Weight loss during air calcination (%)	Powder tap density at 298 K (kg.m <sup>-3</sup> )
	Calcined powders (W-H plot)	Calcined powders (Scherrer formula)	As-combusted powders (Scherrer formula)			
<b>0.65</b>	20.4 ( $\pm 1.8$ )	15.3 ( $\pm 0.2$ )	15.3 ( $\pm 0.3$ )	2.37 ( $\pm 0.31$ )	0.98	144
<b>0.70</b>	20.7 ( $\pm 1.7$ )	16.7 ( $\pm 0.3$ )	15.4 ( $\pm 0.4$ )	1.52 ( $\pm 0.29$ )	1.03	135
<b>0.75</b>	23.8 ( $\pm 2.5$ )	18.9 ( $\pm 0.3$ )	13.6 ( $\pm 0.5$ )	1.76 ( $\pm 0.29$ )	0.76	141
<b>0.80</b>	23.6 ( $\pm 5.1$ )	17.6 ( $\pm 0.3$ )	13.6 ( $\pm 0.3$ )	2.12 ( $\pm 0.62$ )	0.05	112
<b>0.90</b>	22.6 ( $\pm 4.8$ )	17.4 ( $\pm 0.3$ )	13.8 ( $\pm 0.4$ )	2.15 ( $\pm 0.65$ )	0.22	131
<b>1.00</b>	24.9 ( $\pm 8.7$ )	15.3 ( $\pm 0.1$ )	14.5 ( $\pm 0.5$ )	3.75 ( $\pm 1.06$ )	0.56	123
<b>1.10</b>	18.3 ( $\pm 3.8$ )	14.3 ( $\pm 0.1$ )	6.1 ( $\pm 0.6$ )	2.51 ( $\pm 0.91$ )	2.32	140
<b>1.20</b>	19.1 ( $\pm 2.2$ )	15.4 ( $\pm 0.2$ )	5.5 ( $\pm 0.5$ )	1.83 ( $\pm 0.50$ )	3.61	158

**Table 7.2. Powder properties of cn-ThO<sub>2</sub> powders (973 K calcined samples)**

F:O	Average crystallite size (nm)			Average lattice strain ( $\times 10^{-3}$ ) From W-H plot	Weight loss during air calcination (%)	Powder tap density at 298 K (kg.m <sup>-3</sup> )
	Calcined powders (W-H plot)	Calcined powders (Scherrer formula)	As-combusted powders (Scherrer formula)			
<b>0.90</b>	22.9 ( $\pm 1.5$ )	18.7 ( $\pm 0.4$ )	5.2 ( $\pm 0.5$ )	1.49 ( $\pm 0.25$ )	8.93	1040
<b>0.95</b>	24.3 ( $\pm 1.4$ )	20.1 ( $\pm 0.4$ )	2.4 ( $\pm 1.1$ )	1.33 ( $\pm 0.19$ )	10.04	1090
<b>1.00</b>	22.7 ( $\pm 2.1$ )	18.3 ( $\pm 0.3$ )	2.5 ( $\pm 1.0$ )	1.27 ( $\pm 0.33$ )	6.49	890
<b>1.05</b>	21.2 ( $\pm 2.3$ )	18.0 ( $\pm 0.4$ )	2.9 ( $\pm 1.2$ )	1.24 ( $\pm 0.42$ )	11.07	1010
<b>1.10</b>	21.0 ( $\pm 4.4$ )	15.5 ( $\pm 0.2$ )	3.7 ( $\pm 1.0$ )	2.08 ( $\pm 0.80$ )	11.97	967
<b>1.15</b>	26.0 ( $\pm 1.5$ )	20.6 ( $\pm 0.1$ )	3.0 ( $\pm 0.7$ )	1.49 ( $\pm 0.16$ )	8.60	870
<b>1.20</b>	22.4 ( $\pm 1.2$ )	18.0 ( $\pm 0.3$ )	3.4 ( $\pm 0.6$ )	1.67 ( $\pm 0.18$ )	8.85	920
<b>1.25</b>	21.7 ( $\pm 0.8$ )	20.7 ( $\pm 0.4$ )	3.5 ( $\pm 0.4$ )	1.59 ( $\pm 0.22$ )	9.57	960

These results are among the very few reports wherein very small ThO<sub>2</sub> crystallites ( $\leq 5$  nm) could be prepared by a simple one step solution combustion method either by selecting optimum F:O value or by selecting appropriate fuel. Yet, retaining small size crystallites without appreciable grain coarsening is challenging during calcination. One possible approach could be mixing as-combusted powders with a suitable inert matrix, followed by calcination and finally, selective removal of matrix without any contamination of ThO<sub>2</sub> powders. Such approach may help in preparation of large quantities of ThO<sub>2</sub> powders having 5 nm to 10 nm average crystallite size.

Table 7.1 and Table 7.2 also show that weight loss upon calcination is higher in cn-ThO<sub>2</sub> powders (6.5 - 12 wt. %) as compared to gn-ThO<sub>2</sub> powders (0 - 3.6 wt. %). Gn-ThO<sub>2</sub> powders prepared from fuel-deficient combustions (F:O = 0.80 - 0.90) showed minimum weight loss. Higher weight loss for F:O < 0.80 and F:O > 1 for gn-ThO<sub>2</sub> indicated decomposition of excess nitrate and carbonaceous residues, respectively. This was supported by the color of as-combusted gn-ThO<sub>2</sub> powders, which became progressively darker with increasing F:O (Fig. 6.22; Chapter-6). All calcined powders (gn-ThO<sub>2</sub> and cn-ThO<sub>2</sub>) appeared white in color. A fraction of total weight loss during calcination can also be attributed to loss of moisture adsorbed on the surface of these nano-sized powders. Higher weight loss for cn-ThO<sub>2</sub> powders during calcination (6.5 - 12 wt. %) indicated significant amounts of partially oxidized citrate fuel moieties (or intermediates formed during citric acid / citrate-nitrate decomposition) in as-combusted powders. This has been explained in chapter-6 (Section 6.3.2.4) in terms of a complex multistep process of citric acid / metal citrate decomposition to produce various intermediates, whose complete oxidation is a sluggish process, strongly dependent on heating rate as well as atmosphere in which decomposition is carried out. citrate-Th(IV)-nitrate combustion products therefore usually contain residual intermediate

products due to incomplete citrate decomposition during propagation of combustion flame. These residual carbonaceous species are oxidized into gaseous end products (CO, CO<sub>2</sub>, H<sub>2</sub>O, etc.) upon steady-state heat treatment during calcination in air and a higher extent of weight loss is observed. Sluggish nature of citrate-nitrate combustion is also one of the reasons for obtaining highly disordered and very small sized (< 5 nm) ThO<sub>2</sub> crystallites in as-combusted products (Table 7.2).

In case of glycine-Th(IV)-nitrate combustion, thermal decomposition of glycine is a relatively rapid process with burst release of large amounts of H<sub>2</sub>O and NH<sub>3</sub> gases as decomposition products along with residual carbon and CHNO moieties [230], which further oxidizes to give gaseous products. Glycine-nitrate combustion is also associated with higher temperatures due to large enthalpy of combustion as compared to citrate-nitrate decomposition [121]. As a result of this, combustion wave propagates fast through the gel precursor leaving behind highly fluffy and porous product with high surface area. All gn-ThO<sub>2</sub> powders prepared in present investigation were highly fluffy than cn-ThO<sub>2</sub> powders. Tap densities of calcined powders are given in Table 7.1 and Table 7.2. gn-ThO<sub>2</sub> powders show 6 to 7 times lower tap density than cn-ThO<sub>2</sub> powders, which indicates stark difference in powder morphologies between gn-ThO<sub>2</sub> and cn-ThO<sub>2</sub>. Gn-ThO<sub>2</sub> powders were highly fluffy in nature while cn-ThO<sub>2</sub> powders settled easily. Fig. 7.4 shows a representative photograph of equal masses of as-combusted gn-ThO<sub>2</sub> and cn-ThO<sub>2</sub> powders, before and after calcination. These observations along with tap densities indicated higher surface area of gn-ThO<sub>2</sub> powders in comparison to cn-ThO<sub>2</sub>.

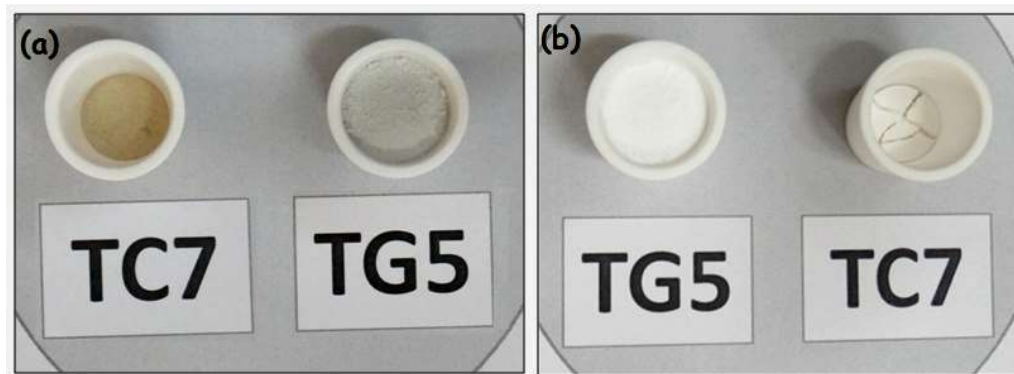


**Fig. 7.4. (a) Equal amounts of as-combusted cn-ThO<sub>2</sub> (TC7; F:O = 1.05) and gn-ThO<sub>2</sub> (TG5; F:O = 1.00); (b) corresponding powders after air calcination at 973 K for 5 h**

### 7.3.2. Sintering behavior of gn-ThO<sub>2</sub> and cn-ThO<sub>2</sub> powder compacts

Fig. 7.5 (a) and (b) show the baseline corrected linear shrinkage profiles for gn-ThO<sub>2</sub> and cn-ThO<sub>2</sub> powder compacts, respectively, measured from dilatometry experiments. Fractional shrinkage ( $dL/L_0$ ) is plotted as a function of temperature for non-isothermal heating cycle (308 K to 1773 K; heating rate = 10 K / min.). Here ‘dL’ is the change in sample length and ‘L<sub>0</sub>’ is the length of starting powder compact (green compact). Shrinkage behavior for ThO<sub>2</sub> prepared with different F:O values are plotted together.

It can be seen that linear shrinkage behavior of gn-ThO<sub>2</sub> compacts is continuous over the studied temperature range whereas two distinct shrinkage stages, spanning from ~ 1100 K to ~ 1650 K and ~ 1650 K to 1773 K can be noted for cn-ThO<sub>2</sub> compacts. During high temperature sintering, various diffusion mechanisms such as grain boundary diffusion, lattice diffusion, plastic flow, etc. operate simultaneously and are responsible for continuous and rapid densification of gn-ThO<sub>2</sub> compacts. Two distinct regions observed in shrinkage curves of cn-ThO<sub>2</sub> compacts suggest predominance of grain boundary diffusion at lower

temperatures followed by lattice diffusion and other mechanisms such as mass transport through defects at higher temperatures.

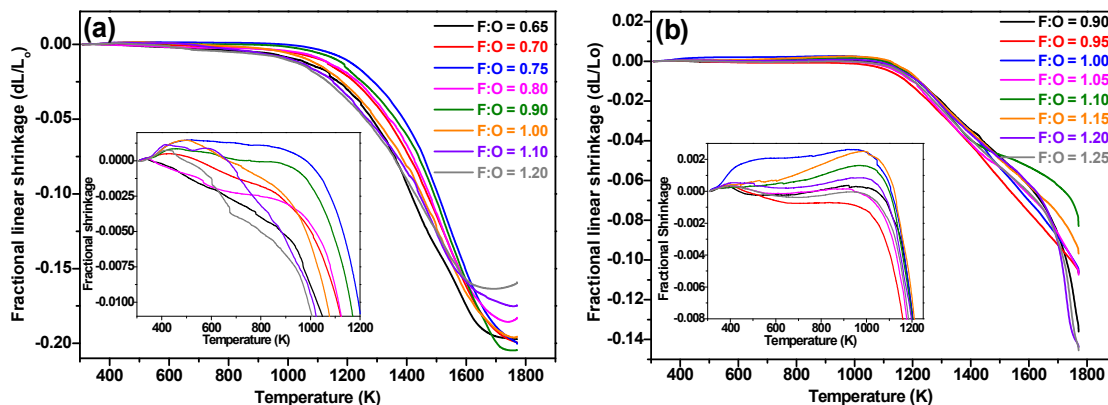


**Fig. 7.5. Linear shrinkage behavior of (a) gn- $\text{ThO}_2$  and (b) cn- $\text{ThO}_2$  compacts under non-isothermal constant rate heating program. Inset shows the nature of curve before the onset of rapid sintering**

For uniformity in the analysis of shrinkage curves, onset temperature of shrinkage was taken as temperature corresponding to completion of 1% fractional shrinkage. Green densities as well as other important parameters evaluated from analysis of measured shrinkage curves are presented in Table 7.3 and Table 7.4 for gn- $\text{ThO}_2$  and cn- $\text{ThO}_2$ , respectively.

From these tables, it is clear that gn- $\text{ThO}_2$  compacts have lower green densities (46% - 48% of theoretical density (TD)) compared to cn- $\text{ThO}_2$  compacts (55% - 56% TD). This is attributed to highly fluffy and porous morphology of gn- $\text{ThO}_2$  powders as compared to cn- $\text{ThO}_2$ , which results in less efficient packing for the former. For gn- $\text{ThO}_2$ , green density increases for fuel-rich stoichiometries (F:O > 1.0) while no such trend was observed for green densities of cn- $\text{ThO}_2$  with F:O value. An increase in green densities of for gn- $\text{ThO}_2$  compacts (> 51% TD) obtained from combustion of fuel-rich gels is attributed to smaller  $\text{ThO}_2$

crystallites (average crystallite size ~ 5-6 nm) in as-combusted powders (F:O = 1.10, 1.20; Table 1). Even though calcination results into grain coarsening, the calcined powders would contain both larger and smaller crystallites. A powder containing a mixture of large (~ 15-20 nm) and small (< 10 nm), randomly shaped crystallites is expected to show higher packing efficiency. Higher green densities of cn-ThO<sub>2</sub> compacts (~ 55% TD) can be interpreted in terms of smaller crystallites (3-5 nm) in as-combusted powders (for all values of F:O). It can also be seen that sintered ThO<sub>2</sub> pellets up to ~ 94% and ~ 92% theoretical densities were obtained from gn-ThO<sub>2</sub> and cn-ThO<sub>2</sub> powder compacts, respectively under the sintering protocol adopted in present investigations.

**Table 7.3. Details of sintering parameters for gn-ThO<sub>2</sub> compacts**

F:O	Green density (kg.m <sup>-3</sup> )	T <sub>onset</sub> (K)	Weight change during sintering (%)	Sintered density (kg.m <sup>-3</sup> )	Theoretical Density (% TD)	Linear shrinkage (%)	Radial shrinkage (%)	Desintering (%)	Pellet status ( <i>visible to eyes</i> )
0.65	4620	1026	-3.3	8960	89.5	21.1	21.5	0.14	cracks
0.70	4810	1108	-2.5	9430	94.2	21.0	20.8	0.40	good
0.75	4610	1193	-1.9	9120	91.0	21.4	21.3	0.47	good
0.80	4780	1113	-1.7	8580	85.7	18.1	19.3	1.91	cracks
0.90	4590	1161	-2.1	8640	86.3	20.3	20.8	1.55	cracks
1.00	4770	1066	-2.4	8660	86.5	19.5	19.2	1.67	cracks
1.10	5110	1010	-2.2	8950	89.4	17.3	19.2	1.75	cracks
1.20	5120	990	-2.3	8860	88.5	15.9	17.8	1.95	cracks

**Table 7.4. Details of sintering parameters for cn-ThO<sub>2</sub> compacts**

<b>F:O</b>	<b>Green density (kg.m<sup>-3</sup>)</b>	<b>T<sub>onset</sub> (K)</b>	<b>Weight change during sintering (%)</b>	<b>Sintered density (kg.m<sup>-3</sup>)</b>	<b>Theoretic al Density (% TD)</b>	<b>Linear shrinkage (%)</b>	<b>Radial shrinkage (%)</b>	<b>Desinte ring (%)</b>	<b>Pellet status (visible to eyes)</b>
<b>0.90</b>	5410	948	-1.7	9030	90.2	16.2	16.0	Nil	good
<b>0.95</b>	5650	905	-1.6	9060	90.5	15.5	15.2	Nil	good
<b>1.00</b>	5540	949	-2.1	8950	89.4	17.4	16.7	Nil	good
<b>1.05</b>	5550	925	-1.6	8720	87.1	16.7	15.3	Nil	good
<b>1.10</b>	5530	944	-1.7	8520	85.1	16.1	15.0	Nil	good
<b>1.15</b>	5270	950	-1.9	8820	88.1	16.9	16.0	Nil	good
<b>1.20</b>	5530	947	-1.9	9250	92.4	16.9	16.2	Nil	good
<b>1.25</b>	5530	930	-2.2	9200	91.9	17.0	16.8	Nil	good

Another important observation is onset temperature of shrinkage ( $T_{\text{onset}}$ ; taken as temperature at which  $dL/L_0 > 1\%$ ). For cn-ThO<sub>2</sub> compacts, shrinkage starts quite early (905 K to 950 K; varying over a span of 45 K with different F:O values) as compared to gn-ThO<sub>2</sub> (990 K to 1193 K; varying over a span of 203 K with different F:O values). Higher  $T_{\text{onset}}$  for gn-ThO<sub>2</sub> can be attributed to presence of pre-sintered grains in as-combusted powders due to highly exothermic and rapid combustion, which results into formation of hard agglomerates that have lesser reactive surfaces. On the other hand, lower exothermicity and sluggish nature of combustion in citrate-nitrate gels produce softer agglomerates with relatively high reactive surface structure. Such agglomerates would enable grain to grain neck formation followed by diffusion-driven shrinkage to commence at lower temperatures. For cn-ThO<sub>2</sub>,  $T_{\text{onset}}$  does not show any systematic variation with F:O value. For gn-ThO<sub>2</sub> on the contrary,  $T_{\text{onset}}$  initially increases with increasing F:O ( $0.65 \leq \text{F:O} \leq 0.90$ ) and thereafter shows a decrease for higher

F:O values ( $F:O > 0.9$ ). Initial increase in ' $T_{\text{onset}}$ ' for gn-ThO<sub>2</sub> (up to  $F:O \leq 0.9$ ) can be attributed to nearly complete combustion (higher exothermicity) with lesser carbonaceous residues (un-burnt fuel moieties) present in as-combusted powders (see weight change column in Table 7.1), which causes as-prepared ThO<sub>2</sub> grains to experience higher heat treatment and therefore hard agglomerates are formed. Such agglomerates would tend to undergo densification at higher temperatures. Decrease in ' $T_{\text{onset}}$ ' for fuel-rich gn-ThO<sub>2</sub> compacts ( $F:O \geq 1.00$ ) can be attributed to (i) presence of larger fraction of smaller crystallites and (ii) lesser grain hardening during combustion as the heat evolved during combustion (exothermicity) is also partially utilized for excess fuel oxidation. Such compacts would show densification at lower temperatures. Fig. 7.5(a) and (b) also confirm higher fractional shrinkage for gn-ThO<sub>2</sub> compacts (16.3 - 20.4%) as compared to cn-ThO<sub>2</sub> compacts (8.3 - 14.3%) during non-isothermal heating. Rapid shrinkage of gn-ThO<sub>2</sub> compacts, where most of the shrinkage is completed during non-isothermal heating, as compared to two-step shrinkage of cn-ThO<sub>2</sub> compacts, which is not complete during non-isothermal heating, is the reason for this difference. Origin of such a distinct behavior can be attributed to different morphologies of gn-ThO<sub>2</sub> and cn-ThO<sub>2</sub> powders, which influence the properties (packing density and packing morphology) of green compacts, and their sintering behavior.

Nature of shrinkage curves in high temperature region during non-isothermal heating is quite interesting. For most of gn-ThO<sub>2</sub> compacts, shrinkage is completed well before the highest temperature (1773 K) is reached. It is seen in terms of change in slope of shrinkage curves from negative to positive (Fig. 7.5(a)). On the other hand, cn-ThO<sub>2</sub> compacts continue to show rapid shrinkage up to 1773 K (Fig. 7.5(b)). It becomes clearer from the nature of shrinkage curves recorded during isothermal heating segment (1773 K for 1 h) that immediately followed the non-isothermal heating zone. This is shown in Fig. 7.6(a) and (b)

for gn-ThO<sub>2</sub> and cn-ThO<sub>2</sub> compacts, respectively. For ease of observation, shrinkage value at the beginning of isothermal zone (time = 0) has been marked as ‘zero’ as shown in Fig. 7.6(a) and (b). Most gn-ThO<sub>2</sub> compacts show expansion rather than shrinkage during isothermal heating. Extent of expansion increases with increasing F:O. Except for highly fuel-deficient gn-ThO<sub>2</sub> (F:O = 0.65), all other compacts show reversal of shrinkage or desintering. These results also indicate that for gn-ThO<sub>2</sub> compacts, peak sintering temperature of 1773 K was rather detrimental (except for F:O = 0.65, 0.70, 0.75) as the shrinkage curves had already reversed direction before 1773 K (Fig. 7.5(a)).

On the other hand, for cn-ThO<sub>2</sub>, no expansion is observed during isothermal heating and all compacts continue to shrink, as seen in Fig. 7.6(b). It is apparent that further shrinkage was possible by extending the duration of isothermal heating. Therefore, in complete contrast to gn-ThO<sub>2</sub>, cn-ThO<sub>2</sub> compacts did not show any desintering effect for powders studied here. Extent of desintering in gn-ThO<sub>2</sub> was evaluated from the point of slope change in shrinkage curve up to the end of isothermal heating zone.

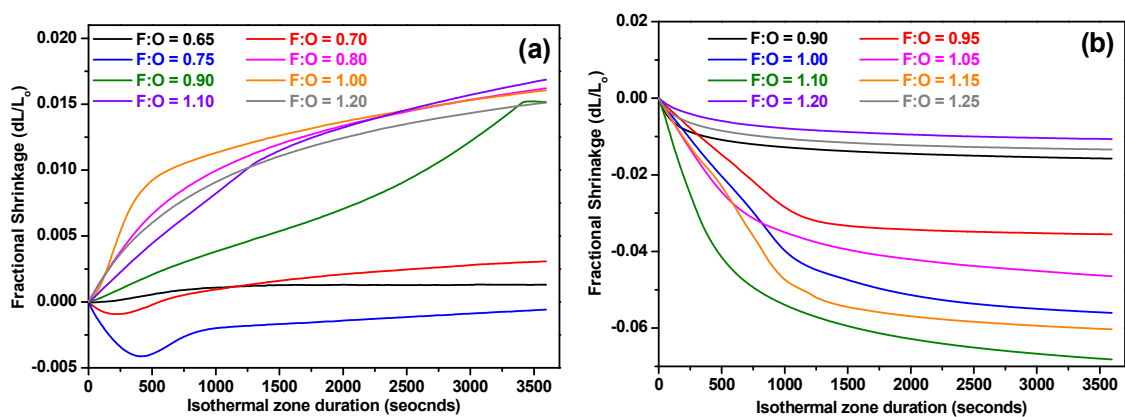


**Fig. 7.6. Linear shrinkage behavior of (a) gn-ThO<sub>2</sub> and (b) cn-ThO<sub>2</sub> compacts during isothermal heating cycle (1773 K for 1 h)**

These values are presented in terms of percentage desintering in Table 7.3 and Table 7.4 for gn-ThO<sub>2</sub> and cn-ThO<sub>2</sub> compacts, respectively. It can be seen that extent of desintering in gn-ThO<sub>2</sub> compacts increased with increasing F:O value. It must be noted that most of the gn-ThO<sub>2</sub> compacts which showed desintering, also resulted into sintered pellets with visible cracks. All sintered cn-ThO<sub>2</sub> pellets were obtained without any visible crack and showed good pellet quality, typically required for nuclear fuel pellets.

### 7.3.3. Morphology of gn-ThO<sub>2</sub> and cn-ThO<sub>2</sub> powders and sintered pellets

Morphology analysis of sintered pellets can be useful to understand the origin of observed desintering phenomenon. With this view, detailed microstructural characterization was carried out. Fig. 7.7 shows a representative set of SEM micrographs recorded on gn-ThO<sub>2</sub> and cn-ThO<sub>2</sub> samples (calcined powders, sintered pellet surface and fractured surface of sintered pellet). The micrographs recorded on calcined powders (Fig. 7.7 (a)) reveal fluffy and porous morphology of gn-ThO<sub>2</sub> powders while cn-ThO<sub>2</sub> shows distinct isolated agglomerates (Fig. 7.7 (b)). These powder morphologies support the powder characteristics shown in Table 1 and Table 2 wherein highly fluffy and porous gn-ThO<sub>2</sub> powders have 6-7 times lower tap densities than cn-ThO<sub>2</sub> powders (also see Fig. 7.4). Sintered surfaces of both gn-ThO<sub>2</sub> and cn-ThO<sub>2</sub> pellets as shown in Fig. 7.7 (c) and 7.7 (d), respectively, appear similar with uniform microstructure consisting of sub-micron to micron (< 3 μm) sized grains with well defined grain boundaries. Cn-ThO<sub>2</sub> pellet shows relatively higher number of small isolated intra- as well as inter-grain pores as compared to gn-ThO<sub>2</sub> pellet. Fractured surface micrographs (Fig. 7.7 (e) and 7.7 (f)) on the other hand show quite distinct morphologies. While gn-ThO<sub>2</sub> fracture surface shows uniform distribution of large number of closed pores predominantly located at grain boundary junctions and fewer intra-grain pores (Fig. 7.7(e)),

cn-ThO<sub>2</sub> fractured surface shows relatively larger pores (as compared to gn-ThO<sub>2</sub>) located at the grain boundary interfaces as well as several smaller intra-grain pores (Fig. 7.7 (f)).

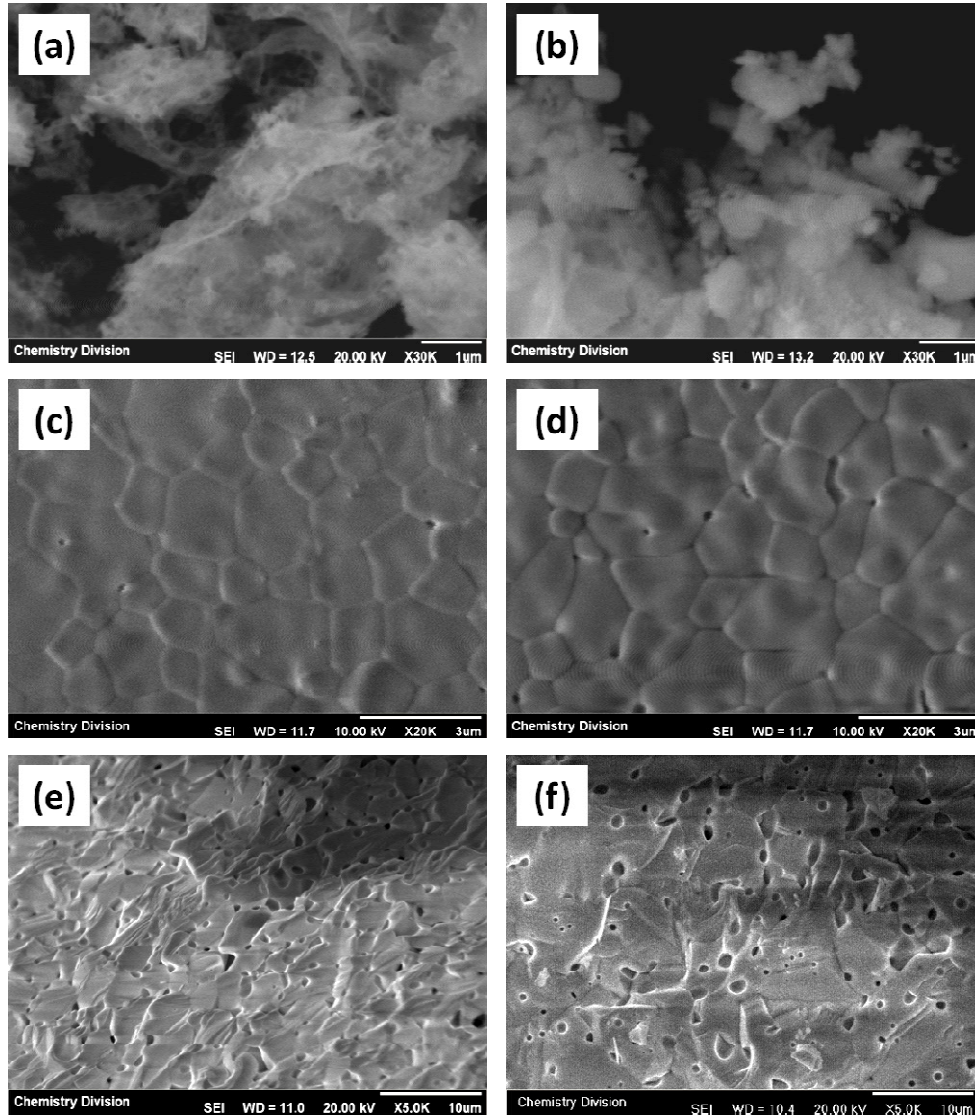


**Fig. 7.7. SEM micrographs recorded on (i) calcined powders (a) gn-ThO<sub>2</sub> (F:O = 0.9) (b) cn-ThO<sub>2</sub> (F:O = 0.9) (ii) sintered pellet surface (c) gn-ThO<sub>2</sub>, (d) cn-ThO<sub>2</sub>, (iii) fractured pellet surface (e) gn-ThO<sub>2</sub>, (f) cn-ThO<sub>2</sub>**

Fig. 7.8(a) and (b) shows SEM micrographs recorded on fractured surface of sintered gn-ThO<sub>2</sub> and cn-ThO<sub>2</sub> at higher magnification with pore sizes as estimated using SEM unit's image analysis software.

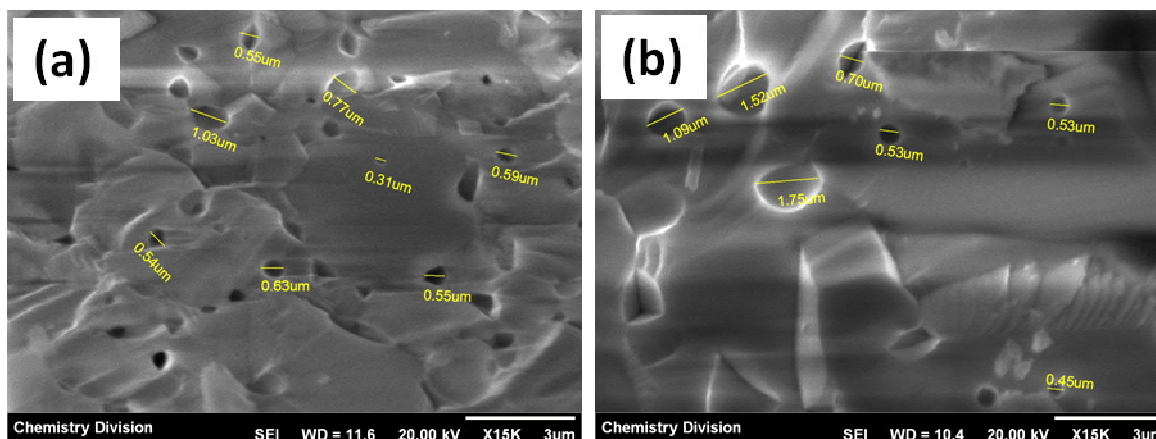


**Fig. 7.8. SEM micrographs recorded on fractured pellet surface of (a) gn-ThO<sub>2</sub> and (b) cn-ThO<sub>2</sub> at higher magnification. Pore sizes are also indicated in the micrographs**

It can be seen from Fig. 7.8 (a) and (b) that while most of the inter-grain pores in gn-ThO<sub>2</sub> are sub-micron sized while those in cn-ThO<sub>2</sub> are relatively larger. Also, cn-ThO<sub>2</sub> shows sub-micron sized intra-grain pores in addition of inter-grain porosity. Dark lines / shades seen in micrographs (Fig. 7.8) are due to charging effect observed in highly insulating ThO<sub>2</sub> samples. It will be interesting to know the origin of desintering in nanocrystalline gn-ThO<sub>2</sub> compacts and its complete absence in compacts made from cn-ThO<sub>2</sub> powders; both processed under identical conditions. This aspect is studied in the following section.

#### 7.3.4. Discussion (Desintering of nanocrystalline ThO<sub>2</sub>)

The phenomenon of desintering refers to decrease in bulk density of a material (usually ceramic) upon firing at elevated temperatures for prolonged duration. For a wide range of ceramics such as stabilized zirconia [269], BaTiO<sub>3</sub> [270], ThO<sub>2</sub> [106, 267], yttria doped ThO<sub>2</sub> [113], etc., reduction in bulk densities even up to 10% has been reported. Desintering is usually observed for compacts made from very fine powders (sub-micron or nano-sized) with high surface to volume ratio and higher specific surface area. Desintering can lead to the formation of micro-cracks or large blister defects in ceramics, which deteriorate their

mechanical strength. It is less prevalent during sintering of micron-sized bulk ceramics. Occurrence of desintering in ceramic materials has been explained in different ways. One of the reasons given for desintering effect relates to pore volume expansion due to gas pressure inside the closed isolated pores of highly dense (density > 95% TD) ceramics during grain growth stage [271]. Desintering has also been attributed to redox changes in one or more of the constituent ions in a given ceramic; brought about by thermal treatment [272], high temperature decomposition of metal carbonates surface layer over oxide particles [273], formation of abnormal grains or abnormal grain growth during densification [274], release of carbon in the form of CO/CO<sub>2</sub> during processing of nanocomposites [275] and, variation in particle to particle coordination due to random packing of particles / crystallites in the green compact [276]. Few reports have mentioned desintering effect in powder compacts of ThO<sub>2</sub> and ThO<sub>2</sub>-based oxides prepared from de-agglomerated oxalates [106, 273, 277]. However, so far no dilatometry study has come to our notice that highlights desintering effect in combustion synthesized nanocrystalline ThO<sub>2</sub>. Morgan et al., [267] studied desintering of ThO<sub>2</sub> powder compacts obtained via oxalate decomposition with detailed analysis of gases trapped inside the sintered pellets. Their results indicated that gases trapped inside closed isolated pores may not be the prime reason for desintering. Similarly, carbonate decomposition is also unlikely to be responsible for observed desintering in ThO<sub>2</sub> as thermal decomposition of thorium carbonate (as well as oxy-carbonate) is reported at much lower temperatures (< 750 K) [231]. Further, if present, carbonate / oxy-carbonate phase is more likely in cn-ThO<sub>2</sub> than in gn-ThO<sub>2</sub> samples since the former contains more residual carbonaceous contents in as-combusted powders. Hence it is expected than desintering must be more favourable in cn-ThO<sub>2</sub>, which is contrary to the experimental observation in the present study. Redox inertness of Th(IV) over the studied temperature range under both, inert

and oxidizing atmospheres rules out desintering to be caused by change in the oxidation state of Th<sup>4+</sup> or O<sup>2-</sup> in the case of ThO<sub>2</sub>.

Micrographs recorded on fractured surface of gn-ThO<sub>2</sub> and cn-ThO<sub>2</sub> (Fig. 7.7e, 7.7f and Fig. 7.8), show larger inter-grain pores in cn-ThO<sub>2</sub> but higher inter-grain pore density in gn-ThO<sub>2</sub>. From these results, it is not possible to unequivocally attribute observed desintering to the release of gaseous by-products from the pores during final stage of sintering. Also, weight losses recorded in all studied samples (Table 7.3 and Table 7.4) are comparable for most of the gn-ThO<sub>2</sub> and cn-ThO<sub>2</sub> compacts, suggesting that gas release cannot be the reason for difference in sintering behavior. It is inferred from these results that desintering observed exclusively in gn-ThO<sub>2</sub> compacts is due to powder properties. This is now described in detail as follows.

It is known that solid-state sintering is governed by thermally activated, diffusion controlled mass transport across both solid-solid and solid-vapour interface regions of participating grains, and sintering atmosphere (gas). Dihedral angle between two individual grains therefore is a major driving force for mass transport. For two grains, which are touching each other, dihedral angle is defined as the angle made by tangents drawn from the triple junction point on two solid-gas interfaces of participating grains. Triple junction point is defined as point at which (solid<sub>grain-1</sub> - solid<sub>grain-2</sub>), (solid<sub>grain-1</sub> - gas) and (solid<sub>grain-2</sub> - gas) interfaces meet. Higher value of dihedral angle facilitates mass transfer across the solid-vapour interface, which leads to both densification as well as grain growth with pore elimination [278]. On the other hand, if dihedral angle reduces at certain stage of sintering (particularly during rapid shrinkage / densification), it becomes a driving force for mass flow against the surface curvature potential and results into pore volume increase; also known as de-

densification or desintering. Figure 7.8 (c) schematically illustrate various mass transport mechanisms that take place during sintering process. Dihedral angle between coexisting phases (solid-solid interface and solid-vapour interface) that govern the mass transport phenomenon is also shown [278a, 278b].

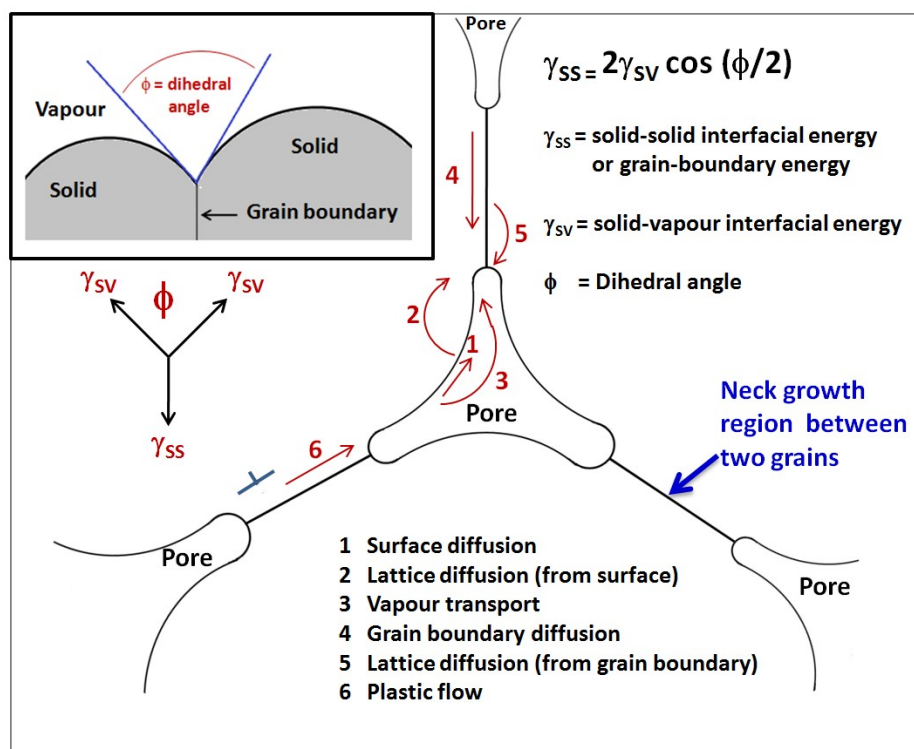


**Fig. 7.8 (c). Schematic illustration of various mass transport mechanisms that take place during sintering process. Inset shows the dihedral angle ( $\phi$ ) between coexisting phases (solid-solid interface and solid-vapour interface) that govern the mass transport**

In this case, depending upon the exact value of dihedral angle, densification may be limited by inhibited grain growth and large numbers of inter-grain pores are formed. This interfacial chemical diffusion mechanism is strongly dependent on starting particle / grain morphology as well as its evolution during rapid densification stage. From above discussion, it is clear that desintering could be observed at different extents in nanocrystalline materials of different

particle / grain morphologies even though the individual average grain sizes are comparable. Thus desintering is notably related to particle / crystallite / agglomerate shape as well as their relative packing and temperature dependent evolution. Green compacts of gn-ThO<sub>2</sub> and cn-ThO<sub>2</sub> studied in present investigation are also formed by agglomerates of primary crystallites with nano-sized substructures. However, their agglomerate morphologies are likely to be different since the powder morphologies (Fig 7.7a and b) are quite distinct. As a result their sintering would also depend upon the microstructure of green compacts formed by them.

Sudre et al. [279] have explained the occurrence of desintering phenomenon in terms of breakup of inter-grain bridges within a polycrystalline solid due to the presence of inclusions and reported that such breakup can lead to cracks in sintered body. Driving force for such breakup is suggested to be stress within the polycrystalline grain network due to high rate of densification. In light of this model and looking at the shrinkage curves of gn-ThO<sub>2</sub> compacts (Fig. 7.5a), it can be seen than gn-ThO<sub>2</sub> compacts undergo very rapid shrinkage during non-isothermal heating. Rapid densification of green compacts consisting of nano-sized grains results into a microstructure that shows continuous interconnected porosity and negligible grain growth. Further heating allows rapid grain growth and interconnected pore structure transformed to a uniform distribution of isolated pores, which is observed in SEM micrographs (Fig. 7.7e). This could have also caused higher inter-grain strain brought about by decrease in dihedral angle during the shrinkage and led to crack formation resulting from desintering.

Alternatively, observed difference in sintering behavior of gn-ThO<sub>2</sub> and cn-ThO<sub>2</sub> can be explained based on the distribution in average crystallite size and associated density variations in the pellets prepared from the powder samples. For gn-ThO<sub>2</sub> samples, average

crystallite sizes evaluated using Scherrer equation vary over the range of 5-15 nm as F:O increases from 0.65 to 1.20. Unlike this, for cn-ThO<sub>2</sub> samples, it varies over a narrow range (3-5 nm) (Table 7.1 and Table 7.2) for as-combusted powders ( $0.90 \leq \text{F:O} \leq 1.25$ ). Further, with increasing F:O, gn-ThO<sub>2</sub> shows increasing fraction of smaller crystallites resulting from decomposition of mono-nuclear Th(IV)-glycine-nitrate complexes, as detailed in chapter-6 (Section 6.3.3). Variation in crystallite size also leads to particle size variation. Although calcination leads to grain coarsening in gn-ThO<sub>2</sub> and cn-ThO<sub>2</sub>, the overall size distribution in former would be relatively wider with bi-modal size distribution than the later. Further, due to highly exothermic nature of glycine-nitrate combustion relative to citrate-nitrate combustion, crystallites formed in the former route are pre-sintered and therefore form hard agglomerates. On the other hand cn-ThO<sub>2</sub> powders consist of softer agglomerates due to relatively lower combustion temperatures. Larger particle size distribution leads to packing inhomogeneities and associated density variation in the green pellets, which means that green pellets of gn-ThO<sub>2</sub> would have randomly distributed distinct regions of variable densities. Density inhomogeneities in green pellets also get reflected in sintered samples, which evolve in terms of a network having regions having density gradients (regions with lower and higher densities) connected by inter-grain regions [279]. This result into structural strain in material undergoing densification and prevent uniform mass transport (diffusion of atoms / structural units) within the pellet during heating, leading to material segregation and eventually to cracks which appear on the pellet surface. Li et al., have also reported [280] local variation in the density of green compact to be the major reason for desintering and proposed that uniform distribution of powder density in the starting green compacts is the most effective way to avoid crack formation due to desintering in high density ceramics.

### 7.3.5. Supporting evidence to proposed origin of desintering in ThO<sub>2</sub> (FT-IR results)

Heating a powder compact at high temperatures generally leads to grain growth, reduction in grain boundary regions and decrease in extent of strain in the lattice. However, density inhomogeneities present in a powder compacts can prevent uniform grain growth during sintering, leading to segregated regions (desintered regions) and generation of lattice strain. Line shapes corresponding to different vibrational modes of a lattice are expected to change with nature and extent of lattice strain. In view of this, FT-IR studies were performed on calcined and sintered ThO<sub>2</sub> samples obtained from fuel-rich (F:O = 1.20) stoichiometry in both glycine-nitrate and citrate-nitrate synthesis routes. Fuel-excess stoichiometry was chosen since gn-ThO<sub>2</sub> obtained from it showed maximum desintering (~ 2%), while no desintering was observed for cn-ThO<sub>2</sub> (F:O = 1.20). FT-IR results are discussed as follows:

Fig. 7.9 (a) and (b) show the ambient temperature FT-IR spectra of calcined (973 K; air) and sintered (1773 K, inert atmosphere) samples, respectively for both gn-ThO<sub>2</sub> and cn-ThO<sub>2</sub>. Insets show spectra over the region of 2500-3300 cm<sup>-1</sup> with peaks corresponding to C-H stretching vibrations ~ 2900 cm<sup>-1</sup>, confirming the presence of carbonaceous impurities in both the samples.

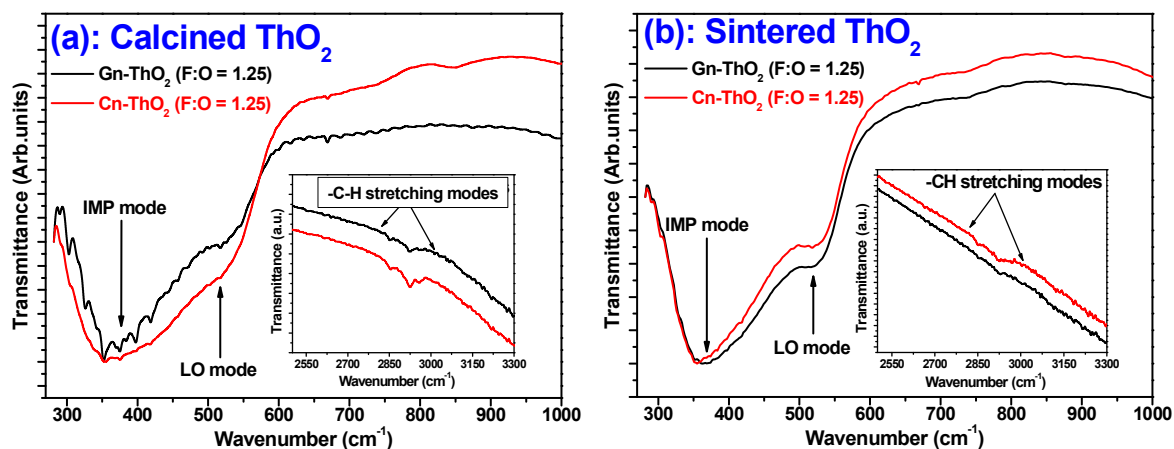


**Fig. 7.9.** FT-IR Spectra of gn-ThO<sub>2</sub> and cn-ThO<sub>2</sub> powders: (a) air calcined at 973 K and (b) sintered at 1773K. For both samples F:O ratio is 1.20

Based on experimental results from spectroscopic ellipsometry on single crystal ThO<sub>2</sub> as well as density functional theory (DFT) calculations, Knight et al., [281] recently elaborated three IR active modes of cubic ThO<sub>2</sub> namely, transverse optical mode (TO), longitudinal optical mode (LO) and impurity-like phonon mode (IMP), positioned over the wave number regions 260-280 cm<sup>-1</sup>, 555-587 cm<sup>-1</sup> and 410-430 cm<sup>-1</sup>, respectively. Due to limitation of spectrometer, TO mode could not be observed in the present experiments; while both IMP and LO modes appeared as broad overlapping bands centred around ~ 380 cm<sup>-1</sup> and ~ 525 cm<sup>-1</sup>, respectively with a red shift in both modes as compared to single crystal ThO<sub>2</sub>. For calcined samples (Fig. 7.9(a)), cn-ThO<sub>2</sub> shows notable band broadening relative to gn-ThO<sub>2</sub>, which is understandable in terms of higher structural disorder in relatively smaller cn-ThO<sub>2</sub> grains (see Table 7.1 and Table 7.2) as well as presence of soft agglomerates with dangling surface bonds brought about by sluggish nature of citrate-nitrate combustion. On the other hand, gn-ThO<sub>2</sub> grains; having seen higher temperature during rapid and intense glycine-nitrate combustion process, have less disorder and thereby giving rise to narrower IR-bands. It may be noted that relative intensities of IR bands corresponding to C-H stretching vibrations (~ 2900 cm<sup>-1</sup>) are higher in cn-ThO<sub>2</sub> compared to gn-ThO<sub>2</sub>, confirming that higher extent of residual carbon is present in former sample compared to latter (Fig. 7.9(a)). This is in line with the citrate-nitrate decomposition mechanism discussed in chapter-6 (Section 6.3.2) paper. In contrast to calcined samples, IR-spectra of sintered samples (Fig. 7.9(b)) show that sintered cn-ThO<sub>2</sub> has narrower IR bands with a marginal red shift in peak position as compared to sintered gn-ThO<sub>2</sub>. Relative increase in broadening of IR-bands in sintered gn-ThO<sub>2</sub> can be explained based on non-uniform grain growth brought about by inhomogeneous density distribution, associated strain generation and desintering. Similar to calcined samples, inset in Fig. 7.9 (b) confirms relatively higher residual carbon content in cn-ThO<sub>2</sub> as compared to gn-ThO<sub>2</sub>, after heat treatment up to 1773 K in inert atmosphere, although extent

of carbon content is much lower in 1773 K heated samples. The marginal red shift in IR peak position of cn-ThO<sub>2</sub> could be attributed to the lattice expansion caused by carbon residue in ThO<sub>2</sub> lattice at interstitial sites, thereby weakening the Th-O bonds (red shift could not be clearly seen for samples calcined at 973 K, probably due to significant changes in line shapes). Presence of carbon residue in sintered samples of both gn-ThO<sub>2</sub> and cn-ThO<sub>2</sub> and exclusive desintering in gn-ThO<sub>2</sub>, support the inference that presence of carbon or release of carbonaceous gases / vapours during sintering is not the dominating cause of desintering.

#### 7.4. Conclusions

Nanocrystalline ThO<sub>2</sub> powders prepared by two different solution combustion methods using fuels such as glycine and citric acid under a wide range of fuel to oxidant ratios (0.65 to 1.25) have been characterized for their powder properties such as average crystallite size, powder tap density, lattice strain, etc. Detailed sintering studies by dilatometry revealed that desintering at high temperature occur only in ThO<sub>2</sub> samples prepared by glycine-nitrate method and not with that prepared by citrate-nitrate method. This has been explained based on inhomogeneous variation in packing densities (density gradients) occurring with the sample pellets obtained from glycine-nitrate method due to relatively broad crystallite/particle size distribution, which resulted into higher lattice strain in sintered gn-ThO<sub>2</sub> pellets. Presence of higher lattice strain has been confirmed by FT-IR studies. Over all studies conclude that citrate-nitrate method offer better powder properties compared to glycine-nitrate method for ThO<sub>2</sub> and these results are quite relevant for ThO<sub>2</sub> based nuclear fuel fabrication as well as selecting a protocol for preparation of ThO<sub>2</sub>-based dense ceramics.

## References:

- [1] C. Degueudre, M.J. Joyce, “Evidence and uncertainty for uranium and thorium abundance: a review”, *Prog. Nucl. Energy* 124 (2020) 103299.
- [2] L.S. Keith, O.M. Faroon, B.A. Fowler, “Uranium (book chapter); handbook on the toxicology of metals: fourth edition (Eds: G.F. Nordberg, B.A. Fowler, M. Nordberg)”, Elsevier (2015) 1307-1345 (DOI: <https://doi.org/10.1016/C2011-0-07884-5>).
- [3] G. Sadagopan, K.S.V. Nambi, G. Venkataraman, V.K. Shukla, S. Kayasth, “Estimation of thorium in gas mantles to ascertain regulatory compliance”, *Radiat. Prot. Dosim.* 71(1) (1997) 53-56.
- [4] T.E. Leontis, “Properties of magnesium-thorium and magnesium-thorium-cerium alloys”, *J. Min. Metals Mater. Soc.* 4 (3) (1952) 287-294.
- [5] R.A. Glenner, P. Willey, P.S. Sledzik, E.P. Junger, “Dental fillings in civil war skulls: What do they tell us?”, *J. Am. Dent. Assoc.* 127(11) (1996) 1671-1677.
- [6] O. Hahn, F. Strassmann, “Über den nachweis und das verhalten der bei der bestrahlung des urans mittels neutronen entstehenden erdalkalimetalle (English translation: Concerning the existence of alkaline earth metals resulting from neutron irradiation of uranium)”, *Die Naturwissenschaften* 27 (1939) 11-15.
- [7] “The first reactor” The US department of energy report: DOE/NE-0046 (1982) 1-40 (Web-link: <https://www.energy.gov/ne/downloads/first-reactor>).
- [8] R.L. Crowther, “Use of thorium in boiling water reactors”, *J. Nucl. Energy AB* 16(4) (1962) 181-194.
- [9] J.R. Dietrich, “The physics of advanced reactors”, *Brit. J. Appl. Phys.* 7(S5) 302 (1956) S9-S23.
- [10] H.N. Sethna, “India’s atomic energy program: past and future”, *International Atomic Energy Agency (IAEA) Bulletin* 21 (5) (1979) 2-11.

## References

- [11] S. Banerjee, H.P. Gupta, “The evolution of the Indian nuclear power programme”, Prog. Nucl. Energy 101 (2017) 4-18.
- [12] International Atomic Energy Agency “Thorium fuel cycles - potential benefits and challenges”, IAEA-TECDOC-1450, IAEA, Vienna (2005) 1-105.
- [13] P.K. Wattal, “Back end of Indian nuclear fuel cycle - A road to sustainability”, Prog. Nucl. Energy 101 (2017) 133-145.
- [14] R. Natarajan, “Reprocessing of spent nuclear fuel in India: Present challenges and future programme”, Prog. Nucl. Energy 101 (2017) 118-132.
- [15] S.A. Ansari, P. Pathak, P.K. Mohapatra, V.K. Manchanda, “Aqueous partitioning of minor actinides by different processes” Sep. Purif. Rev. 40(1) (2011) 43-76.
- [16] M. Salvatores, “Nuclear fuel cycle strategies including partitioning and transmutation”, Nucl. Eng. Des. 235(7) (2005) 805-816.
- [17] Press Information Bureau, Government of India, “Setting up of ten indigenous nuclear power reactors” (Web-link: <http://pib.nic.in>)
- [18] S.C. Chetal, P. Chellapandi, P. Puthiyavinayagam, S. Raghupathy, V. Balasubramanian, P. Selvaraj, P. Mohanakrishnan, B. Raj, “Current status of fast reactors and future plans in India” Energy. Proced. 7 (2011) 64-73.
- [19] P. Puthiyavinayagam, P. Selvaraj, V. Balasubramanian, S. Raghupathy, K. Velusamy, K. Devan, B.K. Nashine, G.P. Kumar, K.V.S. Kumar, S. Varatharajan, P. Mohanakrishnan, G. Srinivasan, A.K. Bhaduri, “Development of fast breeder reactor technology in India”, Prog. Nucl. Energy 101 (Part A) (2017) 19-42.
- [20] Bharatiya Nabhikiya Vidyut Nigam Limited, Department of Atomic Energy “Present status of 500 MWe Prototype Fast Breeder Reactor (PFBR)”, (Web-link: <http://www.bhavini.nic.in>).

- [21] P. Rodriguez, C.V. Sundaram, “Nuclear and materials aspects of the thorium fuel cycle”, *J. Nucl. Mater.* 100 (1981) 227-249.
- [22] R. Ramanna, S.M. Lee, “The thorium cycle for fast breeder reactors”, *Pramana* 27(1-2) (1986) 129-137.
- [23] R. Chidambaram, C. Ganguly, “Plutonium and thorium in the Indian nuclear programme”, *Curr. Sci. India* 70(1) (1996) 21-35.
- [24] P.K. Vijayan, V. Shivakumar, S. Basu, R.K. Sinha, “Role of thorium in the Indian nuclear power programme”, *Prog. Nucl. Energy* 101 (2017) 43-52.
- [25] “Thoria-based nuclear fuels: thermophysical and thermodynamic properties, fabrication, reprocessing, and waste management”, (Eds.: D. Das, S.R. Bharadwaj) Springer (2013) (DOI: 10.1007/978-1-4471-5589-8).
- [26] “Thorium-energy for the future”, (Eds.: A.K. Nayak, B.R. Sehgal), Springer (2019) (DOI: 10.1007/978-981-13-2658-5).
- [27] S. Mukherji, B.K. Mohan, P.D. Krishnani, V. Jagannathan, S. Ganesan, “Thorium irradiation in Indian PHWRs - applications and limitations of origin code”, *Proceedings of First National Conference in Nuclear Reactor Technology* (2002) (Web-link: [https://inis.iaea.org/search/search.aspx?orig\\_q=RN:34011468](https://inis.iaea.org/search/search.aspx?orig_q=RN:34011468)).
- [28] M. Das, “Design and irradiated experience with thorium based fuels in PHWRs” *Annual International Conference - Canadian Nuclear Association* (1992) 10.1-10.
- [29] P.S. Dharmi, J.S. Yadav, K. Agarwal, “Power reactor thoria reprocessing facility (PRTRF), Trombay”, *Proceedings of the Theme Meeting on the Journey of BARC Safety Council for Strengthening Safety Culture in BARC Facilities* (Eds: V.M. Jolly) (2017) (Web-link: [https://inis.iaea.org/search/search.aspx?orig\\_q=RN:48089837](https://inis.iaea.org/search/search.aspx?orig_q=RN:48089837)).
- [30] R.K. Sinha, A. Kakodkar, “Design and development of the AHWR - the Indian thorium fuelled innovative nuclear reactor” *Nucl. Eng. Des.* 236 (7-8) (2006) 683-700.

- [31] R. Sinha, A. Kakodkar, "India's passive breeder", Nucl. Eng. Int. 55(668) (2010) 30-31.
- [32] A. Kakodkar, "Evolution of nuclear reactor containments in India: Addressing the present day challenges", Nucl. Eng. Des. 269 (2014) 3-22.
- [33] S. Sengupta, S.B. Chafle, S. Mammen, K. Sasidharan, V.K. Raina, "Critical facility for AHWR and PHWRs", Proceedings of International Conference on Peaceful uses of Atomic Energy (2009). V. 1. **[33a]** C. Ronchi, J.-P. Hiernaut, Experimental measurement of pre-melting and melting of thorium dioxide, J. Alloys Comp. 240 (1-2) (1996) 179-185. **[33b]** R. Böhler, A. Quaini, L. Capriotti, P. Cakir, O. Beneš, K. Boboridis, A. Guiot, L. Luzzi, R.J.M. Konings, D. Manara, "The solidification behavior of the UO<sub>2</sub>-ThO<sub>2</sub> system in a laser heating study" J. Alloys. Comp. 616 (2014) 5-13.
- [34] D. Greneche, W.J. Szymczak, J.M. Buchheit, M. Delpech, A. Vasile, H. Golfier, "Rethinking the thorium fuel cycle: An industrial point of view", Proceedings of ICAPP (Nice, France), (2007) Paper-7367. **[34a]** S.F. Ashley, G.T. Park, W.J. Nuttall, C. Boxall, R.W. Grimes, "Thorium fuel has risks", Nature 492 (2012) 31-33.
- [35] D. Jain, V. Sudarsan, A.K. Tyagi, "Thorium-based metallic alloys as nuclear fuels: Present status, potential advantages and challenges", SMC Bulletin (Society for Materials Chemistry, India) 4 (1) (2013) pp. 27-40 (Web-link: <https://www.smcindia.org/smc-bulletin.php>).
- [36] P.K. Vijayan, A. Basak, I.V. Dulera, K.K. Vaze, S. Basu, "Conceptual design of Indian molten salt breeder reactor", Pramana - J. Phys. 85 (2015) 539-554.
- [37] T. Yamamoto, H. Suwarno, H. Kayano, M. Yamawaki, "Development of new reactor fuel materials: Hydrogen absorption properties of U-Th, U-Th-Zr and U-Th-Ti-Zr alloys", J. Nucl. Sci. Tech. 32(3) (1995) 260-262.

## References

- [38] K.A. Terrani, G.W.C. Silva, C.B. Yeamans, “Fabrication and characterization of uranium thorium zirconium hydride fuels”, *Trans. Am. Nucl. Soc.* 98 (2008) 1060-1061.
- [39] S.M. McDeavitt, T.J. Downar, A.A. Solomon, S.T. Revankar, M.C. Hash, A.S. Hebden, “Thoria-based cermet nuclear fuel: Cermet fabrication and behavior estimates”, *Proc. Int. Conf. Nucl. Eng. (ICONE 4)* (2002) 59-67.
- [40] C. Lombardi, L. Luzzi, E. Padovani, F. Vettrano, “Thoria and inert matrix fuels for a sustainable nuclear power”, *Prog. Nucl. Energy* 50(8) (2008) 944-953.
- [41] J. Spino, H.S. Cruz, R. Jovani-Abril, R. Birtcher, C. Ferrero, “Bulk-nanocrystalline oxide nuclear fuels - An innovative material option for increasing fission gas retention, plasticity and radiation-tolerance”, *J. Nucl. Mater.* 422 (1-3) (2012) 27-44.
- [42] H. György, S. Czifrus, “The utilization of thorium in generation IV reactors”, *Prog. Nucl. Energy* 93 (2016) 306-317.
- [43] D. Heuer, E. Merle-Lucotte, M. Allibert, M. Brovchenko, V. Ghetta, P. Rubiolo, “Towards the thorium fuel cycle with molten salt fast reactors”, *Ann. Nucl. Energy* 64 (2014) 421-429.
- [44] G.L. Hofman, L.C. Walters, T.H. Bauer, “Metallic fast reactor fuels”, *Prog. Nucl. Energy* 31(1-2) (1997) 83-110.
- [45] W.J. Carmack, D.L. Porter, Y.I. Chang, S.L. Hayes, M.K. Meyer, D.E. Burkes, C.B. Lee, T. Mizuno, F. Delage, J. Somers, “Metallic fuels for advanced reactors”, *J. Nucl. Mater.* 392 (2) (2009) 139-150.
- [46] Idaho National Laboratory, “Experimental breeder reactor-I (EBR-I) (Web-link: <https://inl.gov/experimental-breeder-reactor-i/>).
- [47] L.C. Walters, “Thirty years of fuels and materials information from EBR-II”, *J. Nucl. Mater.* 270(1) (1999) 39-48.

- [48] K. D. Weaver, J. Gilleland, C. Whitmer, G. Zimmerman, “High burn-up fuels for fast reactors: past experience and novel applications”, International Congress on Advances in Nuclear Power Plants (ICAPP 2009) (2009) 795.
- [49] G. Locatelli, M. Mancini, N. Todeschini, “Generation IV nuclear reactors: Current status and future prospects”, *Energ. Policy* 61 (2013) 1503-1520.
- [50] Z.S. Takibaev, “Fast homogeneous nuclear reactor”, *Atom. Energy* 100 (2006) 154-156.
- [51] T. Jayakumar, M.D. Mathew, K. Laha, R. Sandhya, “Materials development for fast reactor applications”, *Nucl. Eng. Des.* 265 (2013) 1175-1180.
- [52] A. Riyas, P. Mohanakrishnan, “Studies on physics parameters of metal (U-Pu-Zr) fuelled FBR cores”, *Ann. Nucl. Energy* 35(1) (2008) 87-92.
- [53] P. Chellapandi, V. Balasubramaniyan, P. Puthiyavinayagam, R. Sundararajan, M. Kanakkil, P. Selvaraj, P.R. Vasudeva Rao, “Design of 500 MWe metal fuel demonstration fast reactor”, *Proc. Int. Conf. Nucl. Eng.* (2014) (DOI: <https://doi.org/10.1115/ICONE22-30727>).
- [54] Indira Gandhi Centre for Atomic Research, “Fast Breeder Test Reactor”, (Web-link: <http://www.igcar.gov.in/rfg/fbtrhist.html>).
- [55] B. Blumenthal, J.E. Sanecki, D.E. Busch, D.R. O’Boyle, “Thorium-uranium-plutonium alloys as potential fast power reactor fuels; part-II: Properties and irradiation behavior of thorium-uranium-plutonium alloys”, ANL-7259, Argonne National laboratory, Illinois (October 1969).
- [56] S.Z. Ghayeb, “Investigations of thorium-based fuels to improve actinide burning rate in S-PRISM reactor”, M.Sc. Thesis, The Pennsylvania State University (2008) (Web-link: <https://etda.libraries.psu.edu/catalog/9160>).

## References

- [57] R.G. Wymer, D.A. Douglas Jr., "Status and progress report for thorium fuel cycle development for period ending December 31, 1964", Report no.: ORNL-3831, Oak Ridge National laboratory, Tennessee (May 1966).
- [58] "Fast spectrum reactors", (Eds.: A.E. Waltar, D. Todd, P.V. Tsvetkov) Springer (2011) (ISBN 978-1-4419-9572-8).
- [59] D.E. Peterson, "The (Th-U) Thorium-uranium system", Bull. Alloy Phase Diagr. 6 (5) (1985) 443-445.
- [60] S. Peterson, R.E. Adams, D.A. Douglas Jr., "Properties of thorium, its alloys and its compounds", Report no.: ORNL-TM-1144, Oak Ridge National laboratory, Tennessee (June 1965).
- [61] D.R. Marr, D.A. Cantley, J.C. Chandler, D.C. McCurry, R.P. Omberg, "Performance of thorium fuelled fast breeders", Report no.: HEDL-SA-1327-FP, Hanford Engineering Development Laboratory, Richland, USA (October 1977).
- [62] G.L. Copeland, "Evaluation of thorium-uranium alloys for the unclad metal breeder reactor", Report no.: ORNL-4557, Oak Ridge National Laboratory, Tennessee (June 1970).
- [63] B. Blumenthal, J.E. Sanecki, D.E. Busch, "Thorium-uranium-plutonium alloys as potential fast power reactor fuels; part-I: Thorium-uranium-plutonium phase diagram", Report no.: ANL-7258, Argonne National Laboratory, Illinois (September 1968).
- [64] C.S. Holden, "Rapid computational path for sustainable and renewable nuclear energy using metallic thorium fuels", Proceedings of 2<sup>nd</sup> Thorium energy conference (ThEC-2010), Mountain View CA (2010).
- [65] R.M. Carroll, "The effects of reactor irradiation on thorium-uranium alloy fuel plates", Report no.: ORNL-1938, Oak Ridge National Laboratory, Tennessee (August 1955).

## References

- [66] B.R. Hayward, P. Corzine, "Thorium uranium fuel elements for SRE", Proc. 2<sup>nd</sup> UN Int. Conf. Peaceful uses of Atom. Energy, Geneva (October 1958).
- [67] J.L. Ballif, B.R. Hayward, J.W. Walter, "Engineering evaluation of a mixed alloy fuel element irradiated at elevated temperatures in SRE", Technical report no.: NAA-SR-3888, Atomics International Division, North American Aviation Incorporation, California, USA (June 1960).
- [68] A.R. Olsen, "Thorium and thorium alloys: Preliminary corrosion tests", Report no.: ORNL-1066, Oak Ridge National Laboratory, Tennessee (November 1951).
- [69] M.S. Farkas, A.A. Bauer, R.F. Dickerson, "Development of thorium-uranium-base fuel alloys," Report no.: BMI-1428, Battelle Memorial Institute, Columbus, Ohio (March 1960).
- [70] R.H. Cole, L.E. Wilkinson, "Development of high strength ternary and quaternary thorium-uranium base alloys", Technical report no.: ATL-A-128, Advanced Technology Laboratory, California (1961).
- [71] J.H. Kittel, J.A. Horak, W.F. Murphy, S.H. Paine, "Effect of irradiation on thorium and thorium-uranium alloys", Technical report no.: ANL-5674, Argonne National laboratory, Illinois, USA (April 1963).
- [72] A.L. Bement, "Burn-up and specific power calculations for the thermal neutron irradiation on thorium-uranium alloys", Technical report no: HW-56631, General Electric Co. Hanford Atomic Products Operation, Richland, Washington (1958).
- [73] F.W. Dodge, E.W. Murbach, L.A. Hanson, "Low decontamination reprocessing of thorium-uranium alloys by induction drip melting", Nucl. Sci. Eng. 6 (6) (1959) 533-536.
- [74] P. Chiotti, A.F. Voigt, "Pyrometallurgical processing", Technical report: A/CONF.15/P/517; ISC-1018, Ames Laboratory, Iowa (October 1958).

- [75] W.N. Hensen, "Electrolysis of thorium and uranium", US-Patent no.: US 2951793 (1960).
- [76] S. Jiang, K. Liu, Y. Liu, T. Yin, Z. Chai, W. Shi, "Electrochemical behavior of Th(IV) on the bismuth electrode in LiCl–KCl eutectic", *J. Nucl. Mater.* 523 (2019) 268-275.
- [77] G.B. Zorzoli, "Use of metallic thorium for LWBRs and LWRs", *Nucl. Tech.* 20 (1973) 109-113.
- [78] F. Correa, D.J. Driscoll, D.D. Lanning, "An evaluation of tight pitch PWR cores", technical report no.: MIT-EL-79-022, Massachusetts Institute of Technology, Cambridge, Massachusetts (1979).
- [79] Z.S. Li, X.J. Liu, C.P. Wang, "Thermodynamic modelling of the Th-U, Th-Zr and Th-U-Zr systems", *J. Alloy Compd.* 473 (2009) 193-198.
- [80] S.Z. Ghrayeb, K.N. Ivanov, S.H. Levine, E.P. Loewen, "Burn-up performance of sodium-cooled fast reactors utilizing thorium-based fuels", *Nucl. Tech.* 176 (2011) 188-194.
- [81] T. Okawa, H. Sekimoto, S. Nakayama, "Design study on power flattening to sodium cooled large scale CANDLE burning reactor with using thorium fuel", *Proc. 18<sup>th</sup> Int. Conf. Nucl. Eng., ICON18, China, (2010).*
- [82] M.T. Simnad, "The U-ZrH<sub>x</sub> alloy: Its properties and use in TRIGA fuel", *Nucl. Engg. Des.* 64 (1981) 403-422.
- [83] K. Konashi, B.A. Pudjanto, T. Terai, M. Yamawaki, "Thermodynamic stability of ThZr<sub>2</sub>H<sub>x</sub> at high temperature", *J. Phys. Chem. Solids* 66 (2–4) (2005) 625-628.
- [84] T. Yamamoto, H. Suwarno, F. Ono, H. Kayano, M. Yamawaki, "Preparation, analysis and irradiation of hydride Th-U-Zr alloy samples for a new fuel", *J. Alloy Compd.* 271-273 (1998) 702-706.

- [85] S. Das, R. Kumar, S.B. Roy, A.K. Suri, "Development study on metallic thorium and uranium-thorium alloy", BARC Newsletter-Founder's Day Special issue (2011) 72-76.
- [86] S. Das, R. Kumar, S. Kaity, S. Neogy, K.N. Hareendran, S.B. Roy, G.K. Dey, B.S.S. Daniel, G.P. Chaudhari, "Characterization of microstructural, mechanical and thermal properties and ageing study of Th-3 wt.% U alloy" Nucl. Eng. Des. 282 (2015) 116-125.
- [87] S. Das, S. Kaity, R. Kumar, J. Banerjee, S.B. Roy, G.P. Chaudhari, B.S.S. Daniel, "Characterization of microstructural, mechanical and thermophysical properties of Th-52 U alloy", J. Nucl. Mater. 480 (2016) 223-234.
- [88] S. Das, S.B. Roy, G.P. Chaudhari, B.S.S. Daniel, "Microstructural evolution of as-cast Th-U alloys", Prog. Nucl. Energy 88 (2016) 285-296.
- [89] R. Kumar, S. Das, S.B. Roy, R. Agarwal, J. Banerjee, S.K. Satpati, "Effect of Mo addition on the microstructural evolution and  $\gamma$ -U stability in Th-U alloys", J. Nucl. Mater. 539 (2020) 152317.
- [90] S. Vaidyanathan, "Thorium utilization in pressurized water reactors using bimetallic thorium-zirconium alloy cladding", Nucl. Tech. (2020) (DOI: <https://doi.org/10.1080/00295450.2019.1706377>).
- [91] D. Escorcia-Ortiz, J. François, C. Martín-del-Campo, "Comparative study of the neutronic performance of thorium-based metallic fuel and MOX fuel in an ASTRID-like fast reactor core", Nucl. Eng. Des. 347 (2019) 122-131.
- [92] J.K. Startt, C.S. Deo, "First principles study of the structure and elastic properties of thorium metal", MRS Adv. 1 (35) (2016) 2447-2452.
- [93] A. Karahan, J. Buongiorno, "A new code for predicting the thermo-mechanical and irradiation behavior of metallic fuels in sodium fast reactors", J. Nucl. Mater. 396 (2010) 283-293.

## References

- [94] K. Lassmann, "TRANSURANUS: a fuel rod analysis code ready for use", *J. Nucl. Mater.* 188 (1992) 295-302.
- [95] J.P. Hamond, "Physical, mechanical and irradiation properties of thorium and thorium alloys", ORNL-4218, Oak Ridge National Laboratory, USA (1968) 29-30.
- [96] J.K. Fink, M.G. Chasanov, L. Leibowitz, "Thermophysical properties of thorium and uranium systems for use in reactor safety analysis", Report no.: ANL-CEN-RSD-77-1, Argonne National Laboratory (1977) 11-12.
- [97] M. Lung, "A present review of the thorium nuclear fuel cycles", European commission report no.: EUR-17771-EN, (1997).
- [98] S. Kolay, S. Phapale, R. Dawar, M. Jafar, S. N. Achary, A. K. Tyagi, R. Mishra, M. Basu, "Phase characterization and thermal study of SrF<sub>2</sub> and NdF<sub>3</sub> doped fluoride salt containing 78 mol % LiF - 20 mol % ThF<sub>4</sub> - 2 mol % UF<sub>4</sub>", *J. Radioanal. Nucl. Chem.* 314 (2) (2017) 1267-1271.
- [99] M. Verwerft, B. Boer, "Thorium oxide nuclear fuels", *Comprehensive nuclear materials* (Second edition) 5 (2020) 139-168 (DOI: <https://doi.org/10.1016/B978-0-12-803581-8.11770-9>).
- [100] S. Usha, R.R. Ramanarayanan, P. Mohanakrishnan, R.P. Kapoor, "Research reactor KAMINI", *Nucl. Eng. Des.* 236 (7-8) (2006) 872-880.
- [101] T.K. Mukherjee, "Processing of Indian monazite for the recovery of thorium and uranium values", *Proceedings of International Conference on Characterisation and Quality Control of Nuclear Fuels* (Eds.: C. Ganguly, R.N. Jayaraj) Allied Publishers Pvt. Ltd. (2002) 187-195.
- [102] J.R. Johnson, C.E. Curtis, "Note on sintering of ThO<sub>2</sub>", *J. Am. Ceram. Soc.* 37(12) (1954) 611.

## References

- [103] T.R.G. Kutty, K.B. Khan, P.V. Hegde, J. Banerjee, A.K. Sengupta, S. Majumdar, H.S. Kamath, "Development of a master sintering curve for ThO<sub>2</sub>", *J. Nucl. Mater.* 327(2-3) (2004) 211-219.
- [104] P. Balakrishna, B.P. Varma, T.S. Krishnan, T.R.R. Mohan, P. Ramakrishnan, "Thorium oxide: Calcination, compaction and sintering", *J. Nucl. Mater.* 160(1) (1988) 88-94.
- [105] N. Clavier, R. Podor, L. Deliere, J. Ravoux, N. Dacheux, "Combining in situ HT-ESEM observations and dilatometry: An original and fast way to the sintering map of ThO<sub>2</sub>", *Mater. Chem. Phys.* 137(3) (2013) 742-749.
- [106] K. Ananthasivan, S. Balakrishnan, S. Anthonysamy, R. Divakar, E. Mohandas, V. Ganesan, "Synthesis and sintering of nanocrystalline thoria doped with CaO and MgO derived through oxalate-deagglomeration", *J. Nucl. Mater.* 434 (1-3) (2013) 223-229.
- [107] G.P. Halbfinger, M. Kolodney, "Activated Sintering of ThO<sub>2</sub> and ThO<sub>2</sub>-Y<sub>2</sub>O<sub>3</sub> with NiO", *J. Am. Ceram. Soc.* 55(10) (1972) 519-524.
- [108] A. Baena, T. Cardinaels, J. Vleugels, K. Binnemans, M. Verwerft, "Activated sintering of ThO<sub>2</sub> with Al<sub>2</sub>O<sub>3</sub> under reducing and oxidizing conditions", *J. Nucl. Mater.* 470 (2016) 34-43.
- [109] K. Ananthasivan, S. Anthonysamy, C. Sudha, A.L.E. Terrance, P.R. Vasudeva Rao, "Thoria doped with cations of group VB-synthesis and sintering", *J. Nucl. Mater.* 300(2-3) (2002) 217-229.
- [110] T.R.G. Kutty, P.V. Hegde, K.B. Khan, T. Jarvis, A.K. Sengupta, S. Majumdar, H.S. Kamath, "Characterization and densification studies on ThO<sub>2</sub>-UO<sub>2</sub> pellets derived from ThO<sub>2</sub> and U<sub>3</sub>O<sub>8</sub> powders", *J. Nucl. Mater.* 335 (3) (2004) 462-470.
- [111] V. Tyrpekl, M. Cologna, D. Robba, J. Somers, "Sintering behaviour of nanocrystalline ThO<sub>2</sub> powder using spark plasma sintering", *J. Eur. Ceram. Soc.* 36(3) (2016) 767-772.

- [112] W. Straka, S. Amoah, J. Schwartz, “Densification of thoria through flash sintering”, *MRS Commun.* 7(3) (2017) 677-682.
- [113] D. Sanjay Kumar, K. Ananthasivan, R.V. Krishnan, S. Amirthapandian, A. Dasgupta, “Studies on the synthesis of nanocrystalline  $Y_2O_3$  and  $ThO_2$  through volume combustion and their sintering”, *J. Nucl. Mater.* 479 (2016) 585-592.
- [114] R.D. Purohit, S. Saha, A.K. Tyagi, “Nanocrystalline thoria powders via glycine-nitrate combustion” *J. Nucl. Mater.* 288 (1) (2001) 7-10. [114a] F. Cappia, D. Hudry, E. Courtois, A. Janßen, L. Luzzi, R.J.M. Konings, D. Manara, High-temperature and melting behavior of nanocrystalline refractory compounds: an experimental approach applied to thorium dioxide, *Mater. Res. Express* 1 (2014) 0250341-12.
- [115] J. Spino, K. Vennix, M. Coquerelle, “Detailed characterisation of the rim microstructure in PWR fuels in the burn-up range 40–67 GWd/tM”, *J. Nucl. Mater.* 231 (3) (1996) 179-190.
- [116] L. Bonato, M. Viot, X. Le Goff, P. Moisy, S.I. Nikitenko, “Sonochemical dissolution of nanoscale  $ThO_2$  and partial conversion into a thorium peroxo sulphate”, *Ultrason. Sonochem.* 69 (2020) 105235.
- [117] S. Dash, A. Singh, P.K. Ajikumar, H. Subramanian, M. Rajalakshmi, A.K. Tyagi, A.K. Arora, S.V. Narasimhan, B. Raj, “Synthesis and characterization of nanocrystalline thoria obtained from thermally decomposed thorium carbonate”, *J. Nucl. Mater.* 303 (2–3) (2002) 156-168.
- [118] S. Dash, R. Krishnan, M. Kamruddin, A.K. Tyagi, B. Raj, “Temperature programmed decomposition of thorium oxalate hexahydrate”, *J. Nucl. Mater.* 295(2-3) (2001) 281-289.

## References

- [119] S. Dash, M. Kamruddin, P.K. Ajikumar, A.K. Tyagi, B. Raj, S. Bera, S.V. Narasimhan, “Temperature programmed decomposition of thorium nitrate pentahydrate”, *J. Nucl. Mater.* 278 (2–3) (2000) 173-185.
- [120] T.V. Plakhova, A.Y. Romanchuk, D.V. Likhosherstova, A.E. Baranchikov, P.V. Dorovatovskii, R.D. Svetogorov, T.B. Shatalova, T.B. Egorova, A.L. Trigub, K.O. Kvashnina, V.K. Ivanov, S.N. Kalmykov, “Size effects in nanocrystalline thoria”, *J. Phys. Chem. C* 123 (37) (2019) 23167-23176. [120a] D. Hudry, C. Apostolidis, O. Walter, T. Gouder, E. Courtois, C. Kübel, D. Meyer, Controlled Synthesis of Thorium and Uranium Oxide Nanocrystals, *Chem. Eur. J.*, 19 (2013) 5297-5305.
- [121] F. Deganello, A.K. Tyagi, “Solution combustion synthesis, energy and environment: Best parameters for better materials”, *Prog. Cryst. Growth Char.* 64 (2018) 23-61.
- [122] A. Varma, A.S. Mukasyan, A.S. Rogachev, K.V. Manukyan, “Solution combustion synthesis of nanoscale materials”, *Chem. Rev.* 116 (2016) 14493-14586.
- [123] V. Chandramouli, S. Anthonysamy, P.R. Vasudeva Rao, “Combustion synthesis of thoria - A feasibility study”, *J. Nucl. Mater.* 265(3) (1999) 255-261.
- [124] S. Anthonysamy, K. Ananthasivan, V. Chandramouli, I. Kaliappan, P.R. Vasudeva Rao, “Combustion synthesis of urania-thoria solid solutions”, *J. Nucl. Mater.* 278(2) (2000) 346-357.
- [125] D. Sanjay Kumar, K. Ananthasivan, S. Amirthapandian, A. Dasgupta, G. Jogeswara Rao, “Citrate gel-combustion synthesis and sintering of nanocrystalline ThO<sub>2</sub> powders”, *J. Nucl. Mater.* 497 (2017) 16-29.
- [126] R.D. Purohit, S. Saha, A.K. Tyagi, “Combustion synthesis of 5 and 10 mol% YO<sub>1.5</sub> doped ThO<sub>2</sub> powders”, *J. Nucl. Mater.* 323 (1) (2003) 36-40.

- [127] K.C. Patil, M.S. Hegde, T. Rattan, S.T. Aruna, "Chemistry of nanocrystalline oxide materials combustion synthesis, properties and applications", World Scientific Publications (2008) (DOI: <https://doi.org/10.1142/6754>).
- [128] F.-T Li, J. Ran, M. Jaroniec, S.Z. Qiao, "Solution combustion synthesis of metal oxide nanomaterials for energy storage and conversion", *Nanoscale* 7(42) (2015) 17590-17610.
- [129] A. Kumar, E.E. Wolf, A.S. Mukasyan, "Solution combustion synthesis of metal nanopowders: nickel-reaction pathways", *AIChE J.* 57(8) (2011) 2207-2214.
- [130] A. Kumar, E.E. Wolf, A.S. Mukasyan, "Solution combustion synthesis of metal nanopowders: Copper and copper / nickel alloys", *AIChE J.* 57(12) (2011) 3473-3479.
- [131] S. Zhang, Z.A. Munir, "The combustion synthesis of refractory nitrides: Part II the synthesis of niobium nitride", *J. Mater. Sci.* 26 (1991) 3380–3385.
- [132] "Nitride ceramics: Combustion synthesis, properties, and applications", (Eds.: A.A. Gromov, L.N. Chukhlomina) Wiley-VCH Verlag GmbH (2015) (DOI:10.1002/9783527684533).
- [133] H.V. Kirakosyan, K.T. Nazaretyan, R.A. Mnatsakanyan, S.V. Aydinyan, S.L. Kharatyan, "Solution combustion synthesis of nanostructured molybdenum carbide", *J. Nanopart. Res.* 20 (2018) 214.
- [134] N.A. Marand, S.M. Masoudpanah, M. Sh. Bafghi, "Solution combustion synthesis of nickel sulfide composite powders", *Ceram. Int.* 44 (14) (2018) 17277-17282.
- [135] K. Rajeshwar, N.R. De Tacconi, "Solution combustion synthesis of oxide semiconductors for solar energy conversion and environmental remediation", *Chem. Soc. Rev.* 38 (7) (2009) 1984-1998.

- [136] K.C. Thomas, J.R. Kale, R.G. Dalavi, K. Venkatesh, R. Kameswaran, A.V.R. Reddy  
"Development of an IR-based carbon analyser for uranium metal", BARC Newsletter  
311 (2009) 2-6 (Web-link: <http://barc.gov.in/publications/nl/2009/200912.pdf/>)
- [137] B.D. Cullity, "Elements of X-ray diffraction", Addison-Wesley Publishing Company  
Inc. (1956).
- [138] R. Tilley, "Crystals and crystal structures", John Wiley & Sons, Ltd. (2006) (ISBN-13  
978-0-470-01820-0).
- [139] E. Smith, G. Dent, "Modern Raman spectroscopy - A practical approach", John Wiley  
& Sons, Ltd. (2006) (ISBN 0-471-49794-0).
- [140] M. Roessle, D.I. Svergun, "Small angle X-ray scattering", In "Encyclopaedia of  
biophysics" (Eds.: G.C.K. Roberts) Springer, Berlin, Heidelberg (2013) (DOI:  
[https://doi.org/10.1007/978-3-642-16712-6\\_284](https://doi.org/10.1007/978-3-642-16712-6_284)).
- [141] P.W. Schmidt, R. Height, "Slit height corrections in small angle X-ray scattering", Acta  
Crystallogr. 13 (1960) 480-483.
- [142] G. Höhne, W.F. Hemminger, H.J. Flammersheim, "Differential scanning calorimetry",  
Springer-Verlag. (2003) (ISBN 978-3-540-00467-7).
- [143] M. Reading, A. Luget, R. Wilson, "Modulated differential scanning calorimetry",  
Thermochim. Acta 238(C) (1994) 295-307.
- [144] J.E.K. Schawe, T. Hutter, C. Heitz, I. Alig, D. Lellinger, "Stochastic temperature  
modulation: A new technique in temperature-modulated DSC", Thermochim. Acta 446  
(2006) 147-155.
- [145] N. Manoj, D. Jain, J.K. Gautam, K.C. Thomas, V. Sudarsan, C.G.S. Pillai, R.K. Vatsa,  
A.K. Tyagi, "A simple, reliable and cost-effective, high temperature dilatometer for  
bulk thermal expansion studies on solids", Measurement 92 (2016) 318-325.

- [146] W.J. Parker, R.J. Jenkins, C.P. Butler, G.L. Abbott, “Flash method of determining thermal diffusivity, heat capacity, and thermal conductivity”, *J. Appl. Phys.* 32 (1961) 1679-1684.
- [147] H.S. Carslaw, J.C. Jaeger, “Conduction of heat in solids”, 2nd edition, Oxford University Press, New York, (1959).
- [148] D. Jain, D. Das, B.N. Jagatap, “Thorium-based fuels for advanced nuclear reactors: Thermophysical, thermochemical and thermodynamic properties”, in A.K. Nayak, B.R. Sehgal (Eds.), *Thorium—Energy for the Future*, Springer (2019) (ISBN 978-981-13-2658-5) 257-275.
- [149] Y.S. Touloukian, R.W. Powell, C.Y. Ho, P.G. Klemens, “Thermophysical properties of matter - The TPRC data series. Volume 1. Thermal conductivity - metallic elements and alloys”, (1970) 429-440; 381-384.
- [150] Y.S. Touloukian, R.W. Powell, C.Y. Ho, M.C. Nicolaou, “Thermophysical properties of matter - The TPRC data series. Volume 10. Thermal diffusivity”, (1974) 205-208.
- [151] Y.S. Touloukian, E.H. Buyco, “Thermophysical properties of matter - The TPRC data series. Volume 4. Specific heat - metallic elements and alloys”, (1971) 268-270.
- [152] Y.S. Touloukian, R.K. Kirby, R.E. Taylor, P.D. Desai, “Thermophysical properties of matter - The TPRC data series. Volume 12. Thermal expansion metallic elements and alloys”, (1975) 365-372.
- [153] H.G. Schettler, J.J. Martin, F.A. Schmidt, G.C. Danielson, “Thermal conductivity of high purity thorium”, *Phys. Rev.* 187 (3) (1969) 801-804.
- [154] T.A. Sandenaw, “Thermal conductivity of uranium: Effects of purity and microstructure”, Report no.: LA-6092-MS, United States (1975) 1-8.
- [155] Y. Takahashi, M. Yamawaki, K. Yamamoto, “Thermophysical properties of uranium-zirconium alloys”, *J. Nucl. Mater.* 154 (1988) 141-144.

- [156] R.W. Logan, D.H. Wood, "Thermal expansion of rolled and extruded uranium", *J. Less-Common Met.* 90 (1983) 233-241.
- [157] J. Nakamura, Y. Takahashi, S. Izumi, M. Kanno, "Heat capacity of metallic uranium and thorium from 80 to 1000 K", *J. Nucl. Mater.* 88 (1980) 64-72.
- [158] M. Boivineau, H. Colin, J.M. Vermeulen, Th. Thévenin, "Thermophysical properties of solid and liquid thorium", *Int. J. Thermophys.* 17(5) (1996) 1001-1010.
- [159] S. Zhou, R. Jacobs, W. Xie, E. Tea, C. Hin, D. Morgan, "Combined ab-initio and empirical model of the thermal conductivity of uranium, uranium-zirconium, and uranium-molybdenum", *Phys. Rev. Mater.* 2 (2018) 083401-1-21.
- [160] Y. Li, A. Chernatynskiy, J.R. Kennedy, S.B. Sinnott, S.R. Phillpot, Lattice expansion by intrinsic defects in uranium by molecular dynamics simulation, *J. Nucl. Mater.* 475 (2016) 6-18.
- [161] K.D. Joshi, S.C. Gupta, S. Banerjee, "Ab-initio theoretical analysis of thermal expansivity, thermal vibrations and melting of thorium", *Phil. Mag.* 88 (27) (2008) 3145-3152.
- [162] S. Jaroszewicz, H.O. Mosca, J.E. Garcés, "The temperature behaviour of the elastic and thermodynamic properties of fcc thorium", *J. Nucl. Mater.* 429(1-3) (2012) 136-142.
- [163] L. Kývala, D. Legut, "Lattice dynamics and thermal properties of thorium metal and thorium monocarbide" *Phys. Rev. B* 101 (2020) 075117.
- [164] P.L. Vijay, J.C. Sehra, C.V. Sundaram, K.R. Gurumurthy, R.V. Raghavan, "Studies on the preparation of thorium metal sponge from thorium oxalate", *BARC Report no.:* 969 (1978) 1-11.
- [165] M.D. Smith, R.W.K. Honeycombe, "The effect of oxygen, carbon and nitrogen on the properties of sintered thorium", *J. Nucl. Mater.* 4 (1959) 345-355.

- [166] Inorganic Crystal Structure Database (ICSD FIZ Karlsruhe GmbH, Version 4.4.0 (2020); collection code: 653236); from: J. Bohet, W. Müller, “Preparation and structure studies of “Van Arkel” protactinium”, *J. Less-Common Met.* 57 (2) (1978) 185-1995.
- [167] International Centre for Diffraction Data (ICDD Database; JCPDF card no.: 720659).
- [168] Inorganic Crystal Structure Database (ICSD FIZ Karlsruhe GmbH, Version 4.4.0 (2020) collection code: 253564) from: V.K. Tripathi, R. Nagarajan, “Sol–gel synthesis of high-purity actinide oxide ThO<sub>2</sub> and its solid solutions with technologically important tin and zinc ions” *Inorg. Chem.* 55 (24) (2016) 12798-12806.
- [169] Inorganic Crystal Structure Database (ICSD FIZ Karlsruhe GmbH, Version 4.4.0 (2020) collection code: 35204); from: S.A. Barrett, A.J. Jacobson, B.C. Tofield, B.E.F. Fender, “The preparation and structure of barium uranium oxide BaUO<sub>3+x</sub>”, *Acta Crystallogr. B* 38 (1982) 2775-2781. [169a] S. Ellison, A. Williams, Eurachem / CITAC guide: Quantifying Uncertainty in Analytical Measurement (2012) ISBN 978-0-948926-30-3 (Web-link: [www.eurachem.org](http://www.eurachem.org)).
- [170] Inorganic Crystal Structure Database (ICSD FIZ Karlsruhe GmbH, Version 4.4.0 (2020) collection code: 24223); from: R.E. Rundle, N.C. Baenziger, A.S. Wilson, R.A. McDonald, “The structures of the carbides, nitrides and oxides of uranium”, *J. Am. Chem. Soc.* 70 (1948) 99-105.
- [171] Inorganic Crystal Structure Database (ICSD FIZ Karlsruhe GmbH, Version 4.4.0 (2020) collection code: 26476); from: A.E. Austin, “Carbon positions in uranium carbides”, *Acta Crystallogr.* 12 (1959) 159-161.
- [172] “Augmented uranium metal production facility”, BARC Newsletter 200 (2000) 15-18 (Web-link: <http://barc.gov.in/publications/nl/2000/200009.pdf>).
- [173] G.C. Allen, P.M. Tucker, “Surface oxidation of uranium metal as studied by X-ray photoelectron spectroscopy”, *J. Chem. Soc. Dalton* 5 (1973) 470-474.

- [174] R. Rao, R.K. Bhagat, N.P. Salke, A. Kumar, "Raman spectroscopic investigation of thorium dioxide-uranium dioxide ( $\text{ThO}_2\text{-UO}_2$ ) fuel materials", *Appl. Spectrosc.* 68(1) (2014) 44-48.
- [175] "Thermophysical properties of materials for nuclear engineering: A tutorial and collection of data", (IAEA-THPH), International Atomic Energy Agency, Vienna (2008).
- [176] I.F. Barwood, B.R. Butcher, "The  $\alpha \rightarrow \beta$  phase transformation in uranium", *J. Nucl. Mater.* 8 (1963) 232-240.
- [177] C. Yoo, H. Cynn, P. Söderlind, "Phase diagram of uranium at high pressures and temperatures", *Phys. Rev. B* 57 (1998) 10359-10362.
- [178] P. Zhou, X. Wang, H. Yang, X. Fu, "Effect of vacuum heat treatment on oxidation of uranium surfaces", *Rare Metal Mat. Eng.* 37 (2008) 94-97.
- [179] G. Erez, U. Even, "The Wiedemann-Franz ratio of metallic uranium at elevated temperatures", *J. Appl. Phys.* 37 (1966) 4633-4644.
- [180] S. Nasu, S. Fukushima, T. Ohmichi, T. Kikuchi, "Thermal diffusivity of uranium by laser pulse method from 20° to 850°C", *Jap. J. Appl. Phys.* 7 (1968) 682.
- [181] D. Jain, C.G.S. Pillai, B.S. Rao, R.V. Kulkarni, E. Ramdasan and K.C. Sahoo, "Thermal diffusivity and thermal conductivity studies on thoria-lanthana solid solutions up to 10 mol. %  $\text{LaO}_{1.5}$ ", *J. Nucl. Mater.* 353 (2006) 35-41.
- [182] S.S. Parker, J.T. White, P. Hosemann, A.T. Nelson, "Thermophysical properties of thorium mononitride from 298 to 1700 K", *J. Nucl. Mater.* 526 (2019) 151760.
- [183] H. He, J. Majewski, D.D. Allred, P. Wang, X. Wen, K.D. Rector, "Formation of solid thorium monoxide at near-ambient conditions as observed by neutron reflectometry and interpreted by screened hybrid functional calculations", *J. Nucl. Mater.* 487 (2017) 288-296.

## References

- [184] B.R. Butcher, A.H. Rowe, "Phase transformation in uranium", *Nature* (1953) 817.
- [185] H.H. Klpefer, P. Chiotti, "Characteristics of the solid state transformations in uranium", USAEC Report no.: ISC-893 (1957) 1-113.
- [186] W.S. Blackburn, " $\alpha$ - $\beta$  Thermal cycling of uranium", *J. Nucl. Mater.* 2 (1960) 191.
- [187] J.J. Stobo, "Alpha beta cycling of uranium", *J. Nucl. Mater.* 2 (1960) 97-109.
- [188] L.T. Lloyd, "Thermal expansion of alpha-uranium single crystals", *J. Nucl. Mater.* 3 (1961) 67-71.
- [189] L.T. Lloyd, C.S. Barrett, "Thermal expansion of alpha uranium", *J. Nucl. Mater.* 18 (1966) 55-59.
- [190] E.S. Fisher, "Preparation of alpha uranium single crystals by a grain-coarsening method", *J. Metals* 9 (1957) 882-888.
- [191] D.C. Wallace, "Specific heat of thorium at high temperatures", *Phys. Rev.* 120 (1) (1960) 84-88.
- [192] E.A. Mit'kina, "Experimental determination of the true specific heats of uranium, thorium, and other metals", *Sov. Atom Energy* 7 (2) (1959) 163-165.
- [193] F.L. Oetting, D.T. Peterson, "Heat capacity of well characterized thorium metal from 298 to 700 K", *J. Less-Common Met.* 128 (1987) 231-239.
- [194] D.C. Ginnings, R.J. Corruccini, "Heat capacities at high temperatures of uranium, uranium trichloride, and uranium tetrachloride, *J. Res. Nat. Bur. Stand.* 39 (1947) 309-316.
- [195] F.K. Oetting, M.H. Rand, R.J. Ackermann, "The chemical thermodynamics of actinide elements and compounds, Part 1, The actinide elements", International Atomic Energy Agency (IAEA), Vienna (1976).
- [196] A.L. Loeb, "Thermal conductivity: VIII, A theory of thermal conductivity of porous materials", *J. Am. Ceram. Soc.* 37 (1954) 96-99.

## References

- [197] S. Kaity, J. Banerjee, M.R. Nair, K. Ravi, S. Dash, T.R.G. Kutty, A. Kumar, R.P. Singh, "Microstructural and thermophysical properties of U-6 wt.% Zr alloy for fast reactor application", *J. Nucl. Mater.* 427 (2012) 1-11.
- [198] C. Hin, "Thermal conductivity of metallic uranium", NEUP 14-6767 (2018) (Web-link: <https://www.osti.gov/servlets/purl/1433931>).
- [199] M. Floyd, B. Bromley, J. Pencer, "A Canadian perspective on progress in thorium fuel science and technology", *CNL Nucl. Rev.* 6 (1) (2017) 1-17.
- [200] S. Thakur, P.S.R. Krishna, A.B. Shinde, R. Kumar, S.B. Roy, "Quantitative analysis of thorium phase in Th-U alloys using diffraction studies", *AIP Conf. Proc.* 1832 (2017) 060012.
- [201] P. Chiotti, "High temperature crystal structure of thorium", *J. Electrochem. Soc.* (1955) 567-570.
- [202] G.G. Bente, "A Physical Metallurgical Study of Thorium-Rich Thorium-Uranium Alloys", Report no.: NAA-SR-2069 (1958).
- [203] G.H. Bannister, R.C. Burnett, J.R. Murray, "Ageing and hot hardness characteristics of certain thorium alloys", *J. Nucl. Mater.* 2(1) (1960) 51-61.
- [204] "Chemical technology division annual technical report for 1986," ANL-87-19, Argonne National Laboratory (1987) 122.
- [205] V. Crewe, S. Lawroski, "Reactor development program progress report", Argonne National Laboratory, ANL-7230, Lemont, IL, USA (1966).
- [206] O. Beneš D. Manara R.J.M. Konings, "Thermodynamic assessment of the Th-U-Pu system", *J. Nucl. Mater.* 449 (1-3) (2014) 15-22.
- [207] S. Kneppel, "Aqueous corrosion of thorium alloys and zircaloy-clad thorium alloys", NMI-1226, United States Atomic Energy Commission (1960) 1-49 (Web-link: <https://play.google.com/books/reader?id=OGCWvHY4xRwC&hl=en&pg=GBS.PA1>)

- [208] D.S. Evans, G.V. Raynor, "The solubility of zirconium in  $\alpha$ -thorium", *J. Nucl. Mater.* 4 (1) (1961) 66-69.
- [209] R.I. Sheldon, D.E. Peterson, "The (U-Zr) Uranium-zirconium system", *Bull. Alloy Phase Diagr.* 10 (2) (1989) 165-171.
- [210] O.N. Carlson, "Some studies on the uranium-thorium-zirconium ternary alloy system", AECD-3206, United States Atomic Energy Commission (1950) 1-72.
- [211] J.W. Goffard, R.K. Marshall, "Irradiation behavior of Zircaloy-2 clad thorium-uranium-zirconium alloy fuel elements Interim report 1", BNWL-479, Pacific Northwest Laboratory, United States Atomic Energy Commission (1967).
- [212] T. Okawa, S. Nakayama, H. Sekimoto, "Design study on power flattening to sodium cooled large-scale CANDLE burning reactor with using thorium fuel", *Energ. Convers. Manage.* 53 (1) (2012) 182-188.
- [213] Inorganic crystal Structure Database (ICSD FIZ Karlsruhe GmbH, Version 4.4.0 (2020) collection code: 164572) from: A.I. Kolesnikov, A.M. Balagurov, I.O. Bashkin, A.V. Belushkin, E.G. Ponyatovsky, M. Prager, "Neutron scattering studies of ordered gamma -ZrD", *J. Phys. Condens-Mat.* 6 (43) (1994) 8977-8988.
- [214] Inorganic crystal Structure Database (ICSD FIZ Karlsruhe GmbH, Version 4.4.0 (2020) collection code: 16559) from: B.O. Loopstra, "Neutron diffraction investigation of  $U_3O_8$ ", *Acta Crystallogr.* 17 (1964) 651-654.
- [215] Inorganic crystal Structure Database (ICSD FIZ Karlsruhe GmbH, Version 4.4.0 (2020) collection code: 246035) from: S.K. Sali, N.K. Kulkarni, K. Krishnan, S.N. Achary, A.K. Tyagi, "Oxidation / reduction studies on  $Zr_yU_{1-y}O_{2+x}$  and delineation of a new orthorhombic phase in U-Zr-O system", *J. Solid-State Chem.* 181 (8) (2008) 1859-1866.

- [216] Inorganic crystal Structure Database (ICSD FIZ Karlsruhe GmbH, Version 4.4.0 (2020) collection code: 108756) from: H.L. Luo, J.G. Huber, “Superconductivity in Th-Zr alloys”, *J. Less-Common Met.* 65 (1) (1979) 13-17.
- [217] J.M. Elorrieta, L.J. Bonales, M. Naji, D. Manara, V.G. Baonza, J. Cobos, “Laser-induced oxidation of  $\text{UO}_2$ : A Raman study”, *J. Raman Spectrosc.* 49 (5) (2018) 878-884.
- [218] H. He, D. Shoesmith, “Raman spectroscopic studies of defect structures and phase transition in hyper-stoichiometric  $\text{UO}_{2+x}$ ”, *Phys. Chem. Chem. Phys.* 12 (2010) 8109-8118.
- [219] X. Zhao, D. Vanderbilt, “Phonons and lattice dielectric properties of zirconia”, *Phys. Rev. B* 65 (2002) 075105.
- [220] E. Hashem, A. Seibert, J-F. Vigier, M. Naji, S. Mastromarino, A. Ciccioli, D. Manara, “Solid-liquid equilibria in the  $\text{ThO}_2$ - $\text{ZrO}_2$  system: An experimental study” *J. Nucl. Mater.* 521 (2019) 99-108.
- [221] O.N. Carlson, E.R. Stevens, “A compilation of thorium binary phase diagrams”, USAEC Report (1968) (Web-link: <https://www.osti.gov/servlets/purl/4529064>).
- [222] G.B. Skinner, H.L. Johnston, “Thermal Expansion of zirconium between 298°K and 1600°K”, *J. Chem Phys.* 21 (1953) 1383.
- [223] P.L. Brown, E. Curti, B. Grambow, C. Ekberg, “Chemical thermodynamics of zirconium”, OECD Nuclear energy agency, data bank (Eds.: F.J. Mompean, J. Perrone, M. Illemassene) (2005) (Web-link: <https://www.oecd-nea.org/dbtdb/pubs/vol8-zirconium.pdf>).
- [224] C.G.S. Pillai, P. Raj, “Thermal Conductivity of  $\text{ThO}_2$  and  $\text{Th}_{0.98}\text{U}_{0.02}\text{O}_2$ ”, *J. Nucl. Mater.* 277 (2000) 116-119.

- [225] S.S. Manoharan, K.C. Patil, "Combustion synthesis of metal chromite powders", *J. Am. Ceram. Soc.* 75 (1992) 1012-1015.
- [226] S.R. Jain, K.C. Adiga, V.R. Pai Verneker, "A new approach to thermochemical calculations of condensed fuel-oxidizer mixtures," *Combust. Flame* 40 (6) (1981) 71-79.
- [227] S. Roy, A. Das Sharma, S.N. Roy, H.S. Maiti, "Synthesis of  $\text{YBa}_2\text{Cu}_3\text{O}_{7-x}$  Powder by Autoignition of Citrate-Nitrate Gel", *J. Mater. Res.* 8(11) (1993) 2761-2766.
- [228] M. Gizowska, I. Kobus, K. Perkowski, M. Piatek, G. Konopka, I. Witosławska, M. Osuchowski, "Size and morphology of yttria nanopowders obtained by solution combustion synthesis" *Arch. Metall. Mater.* 63(2) (2018) 743-748.
- [229] G.A.M. Hussein, H.M. Ismail, "Texture assessment of thoria as a final decomposition product of hydrated thorium nitrate and oxycarbonate", *Colloids Surf. A*: 99 (1995) 129-139.
- [230] I.M. Weiss, C. Muth, R. Drumm, H.O.K. Kirchner, "Thermal decomposition of the amino acids glycine, cysteine, aspartic acid, asparagine, glutamic acid, glutamine, arginine and histidine", *BMC Biophys.* 11 (2018) 1-15.
- [231] N. Raje, A.V.R. Reddy, "Mechanistic aspects of thermal decomposition of thorium oxalate hexahydrate: A review", *Thermochim. Acta* 505 (2010) 53-58.
- [232] H. Hayashi, T. Watanabe, "Properties of thoria obtained by thermal decomposition of thorium salts", *Nippon Kagaku Kaishi* 4 (1973) 858-860.
- [233] Y. Saito, "Thermal decomposition of thorium oxalate", *J. Jpn. Soc. Powder Metall.* 17(1971) 235-242.
- [234] M.T. Aybers, "Kinetic study of the thermal decomposition of thorium oxalate dehydrate", *J. Nucl. Mater.* 252 (1998) 28-33.
- [235] D.Y. Chung, E. H. Lee, "Microwave-induced combustion synthesis of  $\text{Ce}_{1-x}\text{Sm}_x\text{O}_{2-x/2}$  powder and its characterization", *J. Alloys Compd.* 374 (2004) 69-73.

- [236] "The Aldrich Library of FT-IR Spectra, Edition-II, Volume-1", 1 898 A 897-898.
- [237] S. Kumar, A.K. Rai, V.B. Singh, S.B. Rai, "Vibrational spectrum of glycine molecule", *Spectrochim. Acta A* 61 (2005) 2741-2746.
- [238] J. R. Ferraro, A. Walker, "Comparison of the infrared spectra of the hydrates and anhydrous salts in the systems  $\text{UO}_2(\text{NO}_3)_2$  and  $\text{Th}(\text{NO}_3)_4$ ", *J. Chem. Phys.* 45 (1966) 550-552.
- [239] J.H-Paredes, D.G-Mitnik, H.E. E-Ponce, M.E. A-Ramos, A.D-Moller, "Band structure, optical properties and infrared spectrum of glycine-sodium nitrate crystal", *J. Mole. Str.* 875 (2008) 295-301.
- [240] S.L. Estes, M.R. Antonio, L. Soderholm, "Tetravalent Ce in the nitrate-decorated hexanuclear cluster  $[\text{Ce}_6(\mu_3\text{-O})_4(\mu_3\text{-OH})_4]^{12+}$ : A structural end point for ceria nanoparticles, *J. Phys. Chem. C* 120 (2016) 5810-5818.
- [241] M. Rand, L. Fuger, I. Grenthe, V. Neck, D. Rai, "Chemical thermodynamics: Chemical thermodynamics of thorium", (OECD, NEA-TDB) Vol. 11, Elsevier, Amsterdam (2007).
- [242] C. Hennig, K. Schmeide, V. Brendler, H. Moll, S. Tsushima, A.C. Scheinost, "EXAFS Investigation of U(VI), U(IV), and Th(IV) sulfato complexes in aqueous solution", *Inorg. Chem.* 46 (2007) 5882-5892.
- [243] J. Rothe, M.A. Denecke, V. Neck, R. Muller, J.I. Kim, XAFS "Investigation of the structure of aqueous thorium(IV) species, colloids, and solid thorium(IV) oxide / hydroxide", *Inorg. Chem.* 41 (2002) 249-258.
- [244] C. Hennig, S. Takao, K. Takao, S. Weiss, W. Kraus, F. Emmerling, A.C. Scheinosta, "Structure and stability range of a hexanuclear Th(IV)-glycine complex", *Dalton Trans.* 41 (2012) 12818-12823.

## References

- [245] Y. Hu, K.E. Knope, S. Skanthakumar, L. Soderholm, "Understanding the ligand-directed assembly of a hexanuclear Th<sup>IV</sup> molecular cluster in aqueous solution", *Eur. J. Inorg. Chem.* 24 (2013) 4159-4163.
- [246] M. Nourmand, N. Meissami, "Complex formation between uranium(VI) and thorium (IV) ions with some  $\alpha$ -amino-acids", *J. Chem. Soc. Dalton* 8 (1983) 1529-1533.
- [247] Bismondo, L. Rizzo, G. Tomat, "Thermodynamic properties of actinide complexes. uranyl (VI)- and thorium (IV)-glycine systems", *Inorg. Chim. Acta* 74 (1983) 21-24.
- [248] B.G. Oliver, A.R. Davis, "The structure of aqueous thorium nitrate solution by laser Raman spectroscopy", *J. Inorg. Nucl. Chem.* 34 (1972) 2851-2860.
- [249] Z. Huang, X. Chen, Y. Li, J. Chen, J. Lin, J. Wang, J. Lei, R. Chen, "Quantitative determination of citric acid in seminal plasma by using Raman spectroscopy", *Appl. Spectrosc.* 67 (7) (2013) 757-760.
- [250] A.K. Arora, M. Rajalakshmi, T.R. Ravindran, V. Sivasubramanian, "Raman spectroscopy of optical phonon confinement in nanostructured materials", *J. Raman Spectrosc.* 38 (2007) 604-617.
- [251] D. Langmuir, J.S. Herman, "The mobility of thorium in natural waters at low temperatures", *Geochim. Cosmochim. Ac.* 44 (1980) 1753-1766.
- [252] M. Bobtelsky, B. Graus, "Thorium citrate complexes, their composition, structure and behavior", *J. Am. Chem. Soc.* 76 (6) (1954,) 1536-1539.
- [253] G.R. Choppin, H.N. Erten, Y. Xia, "Variation of stability constants of thorium citrate complexes with ionic strength", *Radiochim. Acta* 74 (1996) 123-127.
- [254] D.P. Raymond, J.R. Duffield, D.R. Williams, "Complexation of plutonium and thorium in aqueous environments", *Inorg. Chim. Acta* 140 (1987) 309-313.
- [255] M.M. Barbooti, D.A. Al-Sammerrai, "Thermal decomposition of citric acid", *Thermochim. Acta* 98 (1986) 119-126.

- [256] D. Hennings, W. Mayr, "Thermal decomposition of (BaTi) citrates into barium titanate", *J. Solid State Chem.* 26 (1978) 329-338.
- [257] N.S. Gajbhiye, S. Prasad, "Thermal decomposition of hexahydrated nickel iron citrate", *Thermochim. Acta* 285 (1996) 325-336.
- [258] J. Tsay, T. Fang, "Effects of molar ratio of citric acid to cations and of pH value on the formation and thermal-decomposition behavior of barium titanium citrate", *J. Am. Ceram. Soc.* 82(6) (1999) 1409-1415.
- [259] A. Marcilla, A. Gómez-Siurana, M. Beltrán, I. Martínez-Castellanos, I. Blasco, D. Berenguer, "TGA-FTIR study of the pyrolysis of sodium citrate and its effect on the pyrolysis of tobacco and tobacco/SBA-15 mixtures under N<sub>2</sub> and air atmospheres", *J. Sci. Food Agr.* 98 (15) (2018) 5916-5931.
- [260] O. Glatter, O. Kratky, "Small angle X-ray scattering", Academic, London (1982).
- [261] A. Guinier, G. Fournet, "Small angle scattering of X-rays", Wiley, New York (1955).
- [262] J. Aitchison, J.A.C. Brown, "The log normal distribution", Cambridge University Press, Cambridge (1957).
- [263] R.D. Purohit, B.P. Sharma, K.T. Pillai, A.K. Tyagi, "Ultrafine ceria powders via glycine-nitrate combustion", *Mater. Res. Bull.* 36 (15) (2001) 2711-2721.
- [264] V.R. Choudhary, A.M. Rajput, B. Prabhakar, A.S. Mamman, "Partial oxidation of methane to CO and H<sub>2</sub> over nickel and/or cobalt containing ZrO<sub>2</sub>, ThO<sub>2</sub>, UO<sub>2</sub>, TiO<sub>2</sub> and SiO<sub>2</sub> catalysts", *Fuel* 77 (15) (1998) 1803-1807.
- [265] V. Múčka, J. Podlaha, R. Silber, "NiO-ThO<sub>2</sub> mixed catalysts in hydrogen peroxide decomposition and influence of ionizing radiation", *Radiat. Phys. Chem.* 59 (5-6) (2000) 467-475.

## References

- [266] P. Balakrishna, B.N. Murty, K.P. Chakraborty, R.N. Jayaraj, C. Ganguly, "Special features in powder preparation, pressing, and sintering of uranium dioxide", *Mater. Manuf. Process.* 15(5) (2000) 679-693.
- [267] C.S. Morgan, K.H. McCorkle, G.L. Powell, "Sintering and desintering of thoria", In: Kuczynski G.C. (Eds.) *Sintering and Related Phenomena*. Materials Science Research, Vol. 6, Springer, Boston, MA (1973).
- [268] J.M. Pope, K.C. Radford, "Physical properties of some thoria powders and their influence on sinterability", *J. Nucl. Mater.* 52 (1974) 241-254.
- [269] Z. Chen, J. Mabon, J. Wen, R. Trice, "Degradation of plasma-sprayed yttria-stabilized zirconia coatings via ingress of vanadium oxide", *J. Eur. Ceram. Soc.* 29(9) (2009) 1647-1656.
- [270] M.A. Delfrate, J. Lemaitre, V. Buscaglia, M. Leoni, P. Nanni, "Slip casting of submicron BaTiO<sub>3</sub> produced by low-temperature aqueous synthesis", *J. Eur. Ceram. Soc.* 16(9) (1996) 975-984.
- [271] T.K. Gupta, R.L. Coble, "Sintering of ZnO: II, density decrease and pore growth during the final stage of the process", *J. Am. Ceram. Soc.* 51 (9) (1968) 525-528.
- [272] C.-H. Chang, J.F. Rufner, K.V. Benthem, R.H.R. Castro, "Design of desintering in tin dioxide nanoparticles", *Chem. Mater.* 25(21) (2013) 4262-4268.
- [273] P. Duran, J. Tartaj, C. Moure, "Sintering behaviour and microstructural evolution of agglomerated spherical particles of high-purity barium titanate", *Ceram. Int.* 29(4) (2003) 419-425.
- [274] C.-Y. Tsao, W.-H. Tuan, K.-C. Feng, "De-sintering of Ba<sub>5</sub>Nb<sub>4</sub>O<sub>15</sub> ceramic and its influence on microwave characteristics", *J. Eur. Ceram. Soc.* 37(4) (2017) 1517-1521.
- [275] Cs. Balázsi, F.S. Cinar, O. Addemir, F. Wéber, P. Arató, "Manufacture and examination of C/Si<sub>3</sub>N<sub>4</sub> nanocomposites" *J. Eur. Ceram. Soc.* 24(12) (2004) 3287-3294.

- [276] R. Besler, M.R. da Silva, J.J. do Rosario, M. Dosta, S. Heinrich, R. Janssen, “Sintering simulation of periodic macro porous alumina”, *J. Am. Ceram. Soc.* 98(11) (2015) 3496-3502.
- [277] K. Ananthasivan, S. Anthonysamy, A. Singh, P.R. Vasudeva Rao, “De-agglomeration of thorium oxalate - A method for the synthesis of sinter active thoria”, *J. Nucl. Mater.* 306 (1) (2002) 1-9.
- [278] R.H.R. Castro, “Controlling sintering and grain growth of nanoceramics”, *Cerâmica* 65 (373) (2019) 122-129. **[278a]** Thermodynamics of sintering, R.M. German, *Sintering of advanced materials: Fundamentals and processes* (Ed.: Z.Z. Fang) Woodhead Publishing Ltd. (2010), ISBN 978-1-84569-562-0. **[278b]** G.S. Upadhyaya, *Sintered metallic and ceramic Materials*, John Wiley & Sons Ltd. (1999) ISBN 0-471-98155-9.
- [279] O. Sudre, F.F. Lange, “The effect of inclusions on densification; III, The desintering phenomenon”, *J. Am. Ceram. Soc.* 75 (12) (1992) 3241-3251.
- [280] F. Li, J. Pan, A. Cocks, “Defect healing and cracking in ceramic films during constrained sintering” *J. Am. Ceram. Soc.* 95(12) (2012) 3743-3749.
- [281] S. Knight, R. Korlacki, C. Dugan, J.C. Petrosky, A. Mock, P.A. Dowben, J. Matthew Mann, M.M. Kimani, M. Schubert, “Infrared-active phonon modes in single-crystal thorium dioxide and uranium dioxide”, *J. Appl. Phys.* 127 (2020) 125103.

## CHAPTER 8

### Summary and future scope

---

The thesis presents experimental results on two different categories of thorium-based materials namely, thorium-based metallic alloys (chapter 3, 4 and 5) and nanocrystalline thorium-based ceramics (chapter 6 and 7), which are being developed for their applications as nuclear fuels for Indian nuclear power program.

In the case of metallic alloy fuels, literature survey indicates that thorium-based metallic alloys can be excellent nuclear fuels for both thermal and fast spectrum nuclear reactors. At the same time, limited information is available on their thermophysical properties, which is essential to assess their fuel performance potential. Generation of indigenous database on their thermophysical properties as a function of temperature and composition is needed in the first phase of their development as nuclear fuels. With this objective, preparation, characterization and high temperature thermophysical properties evaluation of Th-U binary alloys, Th-U-Zr ternary alloys and their constituent metals (Th, U and Zr) have been carried out in the present work. Major outcome of studies on metallic alloys and future perspective in this direction are summarized as follows:

- High temperature thermophysical properties database generated on nuclear-grade thorium and uranium metals during present work would serve as reference dataset for future studies on metallic alloy fuels.
- In terms of thermophysical behavior, thorium metal has the best performance attributes with highest thermal conductivity ( $\sim 48 \text{ W.m}^{-1}\text{K}^{-1}$  ( $\pm 4\%$ ) at 298 K) that increases with temperature ( $\lambda_T = 0.0105 \times T + 44.53$ ; 298 K – 1373 K), isotropic thermal expansion ( $\text{CTE}_{\text{Th metal}} \sim 12.76 \times 10^{-6} \text{ K}^{-1}$  ( $\pm 2\%$ ); 298 K - 1373 K) that is comparable to ceramic

- fuels ( $CTE_{ThO_2} \sim 9.7 \times 10^{-6} K^{-1}$ ;  $CTE_{UO_2} \sim 10.0 \times 10^{-6} K^{-1}$ ;  $CTE_{PuO_2} \sim 11.4 \times 10^{-6} K^{-1}$ ; 298 K – 1273 K) and low stored energy in terms of lower specific heat ( $C_{P(Th)} @ 298 K \sim 26.5 J.mol^{-1}K^{-1}$ ;  $C_{P(U)} @ 298 K \sim 28.1 J.mol^{-1}K^{-1}$ ;  $\pm 3\%$ ). Results obtained on thorium metal further motivate to explore its utilization as fertile matrix alloyed with U and / or Pu in the form of dispersion alloys.
- Thermophysical properties of uranium confirm its excellent performance potential in high temperature cubic (BCC  $\gamma$ -phase) allotrope (phase transition temperatures:  $\sim 948 K$  ( $\alpha-U \rightarrow \beta-U$ );  $\sim 1051 K$  ( $\beta-U \rightarrow \gamma-U$ )), which has isotropic expansion ( $CTE_{\gamma-U} \sim 22.1 \times 10^{-6} K^{-1}$ ; 1060 K – 1273 K) and high thermal conductivity ( $\sim 43.5 W.m^{-1}K^{-1}$ ; 1076 K – 1273 K). These results motivate to explore uranium-based cubic alloy fuels, which can exhibit isotropic expansion behavior from ambient temperatures up to melting.
- Effect of allotropic phase transformation on thermophysical properties of polycrystalline uranium metal has been established over a wide temperature range (298 K – 1273 K) for the first time.
- Results obtained on Th-U binary (Th-10U, Th-20U) and Th-U-Zr ternary (90Th-7U-3Zr, 90Th-3U-7Zr) alloys have established that both these alloys have dispersion fuel microstructure, which is suitable for safe irradiation in thermal and fast neutron spectrum conditions. Thermophysical properties of these alloys are superior ( $\lambda_{Th-10U}: \sim 31 W.m^{-1}K^{-1}$ ,  $\lambda_{Th-20U}: \sim 30.5 W.m^{-1}K^{-1}$  at 298 K and  $\lambda_{Th-10U}: \sim 41 W.m^{-1}K^{-1}$ ,  $\lambda_{Th-20U}: \sim 42 W.m^{-1}K^{-1}$  at 1273 K) to most of the uranium-based metallic alloy fuels such as U-Zr binary alloys ( $(\lambda_{U-14Zr}: \sim 18.5 W.m^{-1}K^{-1}$  at 298 K and  $\sim 35 W.m^{-1}K^{-1}$  at 900 K), U-Pu-Zr ternary alloys, etc.
- Present results also confirm that preparation of thorium-based alloy fuels with minimum non-metallic impurities (C, N, O, H, etc.) as well as phase homogenized microstructures (i.e., high temperature annealed alloys) is essential to obtain superior fuel performance in

terms of lower fuel swelling, better heat transfer behavior, etc. While preparation of high purity uranium (total non metallic impurities within 1000 to 1500 ppm) is routinely practiced, that of high purity thorium metal requires to be optimized; particularly with respect to oxygen to maintain below 1000 ppm.

- Estimation of the extent of oxide phase inclusions as fine precipitates; as is the case with Th/U metals, or dissolved oxygen (observed for zirconium-rich phases) should be carried out by micro-analysis techniques such as electron probe micro analysis (EPMA).
- Future activities towards development of thorium-based metallic alloys are aimed to prepare new Th-U binary alloys (Th-5U, Th-15U, etc.) with compositions intermediate to those reported here (Th-10U, Th-20U). It is planned to carry out detailed microstructural investigation and evaluation of their thermophysical properties in correlation with as-cast and phase homogenized alloy microstructure. Since Th-Zr binary system shows large solubility region, it is planned to characterize the solubility limits in ternary alloys and their effect on thermophysical properties.
- Studies on metallic alloy SIMFUELS are very limited. Future scope of work on metallic alloy fuels is to prepare such SIMFUEL compositions corresponding to different burn-ups (1-10 atom %) and investigate their phase behavior and thermophysical properties as a function of temperature and composition.
- While results obtained during present work have provided the first of its kind information on high temperature thermophysical behavior of few Th-U and Th-U-Zr alloy compositions, further studies (as mentioned above) will help in identifying the alloys, which can be taken for test irradiation in research reactors for assessment of their in-pile behavior.

In the later part of work (chapter 6 and 7), mechanism of solution combustion synthesis of nanocrystalline thoria has been investigated in detail for glycine-nitrate and citrate-nitrate

systems. Powder properties of nanocrystalline thoria and their sintering behavior have been investigated. A summary of the outcome of these studies and future plans in this direction are given below.

- In a first of its kind of investigation, usefulness of thermal analysis to probe the molecular mechanism of solution combustion process has been established.
- Present studies have confirmed that molecular interactions among the species present in aqueous solution of metal nitrates and fuels, which are governed by the metal-ligand complexation chemistry, influence the nature of combustion and properties of as-combusted oxide powders.
- It has been established that very small ( $< 5$  nm)  $\text{ThO}_2$  particles can be prepared by citrate-Th(IV)-nitrate solution combustion at low temperatures ( $< 550$  K) and powder properties do not vary significantly with fuel-to-oxidant ratio (F:O). On the other hand, F:O significantly affects the nature of complexes in glycine-Th(IV)-nitrate gels. Therefore synthesis of nanocrystalline  $\text{ThO}_2$  by glycine-nitrate route can be effectively tailored to obtain predominantly larger ( $> 15$  nm) or smaller ( $< 5$  nm) crystallites.
- Results obtained from sintering studies on nanocrystalline  $\text{ThO}_2$  powders have established the conditions to obtain high density  $\text{ThO}_2$  pellets (up to 94 % TD) by sintering at readily achievable temperatures ( $< 1773$  K) for short duration ( $< 1$  h).
- Another important outcome of the present work is desintering behavior observed in nanocrystalline  $\text{ThO}_2$ . It has been observed that desintering exclusively occurs in  $\text{ThO}_2$  powders synthesized by glycine-nitrate combustion and is related to powder properties that results into non-uniform density distribution in green compacts. Absence of desintering in citrate-nitrate combustion derived  $\text{ThO}_2$  is an important result that will be useful for preparation of thoria-based ceramics including nuclear fuel pellets.

- Present results on mechanism of solution combustion synthesis of nanocrystalline ThO<sub>2</sub> motivate for similar studies on oxides of uranium and Th-U, both of which are candidate starting materials to develop oxide fuels with superior irradiation performance.
- Another scope of the future investigation stems from the need to structurally characterize various complexes formed in thorium / uranium-based aqueous gel environment by spectroscopic techniques. Such studies will provide evidence to the suggestion that combustion is strongly influenced by metal-ligand complexation chemistry and properties of combustion synthesized oxide powders can be pre-designed, if complex chemistry in gel is well understood. Such studies will be taken up in future on oxides of actinides and lanthanides.

## CHAPTER 8

### Summary and future scope

---

The thesis presents experimental results on two different categories of thorium-based materials namely, thorium-based metallic alloys (chapter 3, 4 and 5) and nanocrystalline thorium-based ceramics (chapter 6 and 7), which are being developed for their applications as nuclear fuels for Indian nuclear power program.

In the case of metallic alloy fuels, literature survey indicates that thorium-based metallic alloys can be excellent nuclear fuels for both thermal and fast spectrum nuclear reactors. At the same time, limited information is available on their thermophysical properties, which is essential to assess their fuel performance potential. Generation of indigenous database on their thermophysical properties as a function of temperature and composition is needed in the first phase of their development as nuclear fuels. With this objective, preparation, characterization and high temperature thermophysical properties evaluation of Th-U binary alloys, Th-U-Zr ternary alloys and their constituent metals (Th, U and Zr) have been carried out in the present work. Major outcome of studies on metallic alloys and future perspective in this direction are summarized as follows:

- High temperature thermophysical properties database generated on nuclear-grade thorium and uranium metals during present work would serve as reference dataset for future studies on metallic alloy fuels.
- In terms of thermophysical behavior, thorium metal has the best performance attributes with highest thermal conductivity ( $\sim 48 \text{ W.m}^{-1}\text{K}^{-1}$  ( $\pm 4\%$ ) at 298 K) that increases with temperature ( $\lambda_T = 0.0105 \times T + 44.53$ ; 298 K – 1373 K), isotropic thermal expansion ( $\text{CTE}_{\text{Th metal}} \sim 12.76 \times 10^{-6} \text{ K}^{-1}$  ( $\pm 2\%$ ); 298 K - 1373 K) that is comparable to ceramic

- fuels ( $CTE_{ThO_2} \sim 9.7 \times 10^{-6} K^{-1}$ ;  $CTE_{UO_2} \sim 10.0 \times 10^{-6} K^{-1}$ ;  $CTE_{PuO_2} \sim 11.4 \times 10^{-6} K^{-1}$ ; 298 K – 1273 K) and low stored energy in terms of lower specific heat ( $C_{P(Th)} @ 298 K \sim 26.5 J.mol^{-1}K^{-1}$ ;  $C_{P(U)} @ 298 K \sim 28.1 J.mol^{-1}K^{-1}$ ;  $\pm 3\%$ ). Results obtained on thorium metal further motivate to explore its utilization as fertile matrix alloyed with U and / or Pu in the form of dispersion alloys.
- Thermophysical properties of uranium confirm its excellent performance potential in high temperature cubic (BCC  $\gamma$ -phase) allotrope (phase transition temperatures:  $\sim 948 K$  ( $\alpha$ -U  $\rightarrow$   $\beta$ -U);  $\sim 1051 K$  ( $\beta$ -U  $\rightarrow$   $\gamma$ -U)), which has isotropic expansion ( $CTE_{\gamma-U} \sim 22.1 \times 10^{-6} K^{-1}$ ; 1060 K – 1273 K) and high thermal conductivity ( $\sim 43.5 W.m^{-1}K^{-1}$ ; 1076 K – 1273 K). These results motivate to explore uranium-based cubic alloy fuels, which can exhibit isotropic expansion behavior from ambient temperatures up to melting.
- Effect of allotropic phase transformation on thermophysical properties of polycrystalline uranium metal has been established over a wide temperature range (298 K – 1273 K) for the first time.
- Results obtained on Th-U binary (Th-10U, Th-20U) and Th-U-Zr ternary (90Th-7U-3Zr, 90Th-3U-7Zr) alloys have established that both these alloys have dispersion fuel microstructure, which is suitable for safe irradiation in thermal and fast neutron spectrum conditions. Thermophysical properties of these alloys are superior ( $\lambda_{Th-10U}: \sim 31 W.m^{-1}K^{-1}$ ,  $\lambda_{Th-20U}: \sim 30.5 W.m^{-1}K^{-1}$  at 298 K and  $\lambda_{Th-10U}: \sim 41 W.m^{-1}K^{-1}$ ,  $\lambda_{Th-20U}: \sim 42 W.m^{-1}K^{-1}$  at 1273 K) to most of the uranium-based metallic alloy fuels such as U-Zr binary alloys ( $(\lambda_{U-14Zr}: \sim 18.5 W.m^{-1}K^{-1}$  at 298 K and  $\sim 35 W.m^{-1}K^{-1}$  at 900 K), U-Pu-Zr ternary alloys, etc.
- Present results also confirm that preparation of thorium-based alloy fuels with minimum non-metallic impurities (C, N, O, H, etc.) as well as phase homogenized microstructures (i.e., high temperature annealed alloys) is essential to obtain superior fuel performance in

terms of lower fuel swelling, better heat transfer behavior, etc. While preparation of high purity uranium (total non metallic impurities within 1000 to 1500 ppm) is routinely practiced, that of high purity thorium metal requires to be optimized; particularly with respect to oxygen to maintain below 1000 ppm.

- Estimation of the extent of oxide phase inclusions as fine precipitates; as is the case with Th/U metals, or dissolved oxygen (observed for zirconium-rich phases) should be carried out by micro-analysis techniques such as electron probe micro analysis (EPMA).
- Future activities towards development of thorium-based metallic alloys are aimed to prepare new Th-U binary alloys (Th-5U, Th-15U, etc.) with compositions intermediate to those reported here (Th-10U, Th-20U). It is planned to carry out detailed microstructural investigation and evaluation of their thermophysical properties in correlation with as-cast and phase homogenized alloy microstructure. Since Th-Zr binary system shows large solubility region, it is planned to characterize the solubility limits in ternary alloys and their effect on thermophysical properties.
- Studies on metallic alloy SIMFUELS are very limited. Future scope of work on metallic alloy fuels is to prepare such SIMFUEL compositions corresponding to different burn-ups (1-10 atom %) and investigate their phase behavior and thermophysical properties as a function of temperature and composition.
- While results obtained during present work have provided the first of its kind information on high temperature thermophysical behavior of few Th-U and Th-U-Zr alloy compositions, further studies (as mentioned above) will help in identifying the alloys, which can be taken for test irradiation in research reactors for assessment of their in-pile behavior.

In the later part of work (chapter 6 and 7), mechanism of solution combustion synthesis of nanocrystalline thoria has been investigated in detail for glycine-nitrate and citrate-nitrate

systems. Powder properties of nanocrystalline thoria and their sintering behavior have been investigated. A summary of the outcome of these studies and future plans in this direction are given below.

- In a first of its kind of investigation, usefulness of thermal analysis to probe the molecular mechanism of solution combustion process has been established.
- Present studies have confirmed that molecular interactions among the species present in aqueous solution of metal nitrates and fuels, which are governed by the metal-ligand complexation chemistry, influence the nature of combustion and properties of as-combusted oxide powders.
- It has been established that very small ( $< 5$  nm)  $\text{ThO}_2$  particles can be prepared by citrate-Th(IV)-nitrate solution combustion at low temperatures ( $< 550$  K) and powder properties do not vary significantly with fuel-to-oxidant ratio (F:O). On the other hand, F:O significantly affects the nature of complexes in glycine-Th(IV)-nitrate gels. Therefore synthesis of nanocrystalline  $\text{ThO}_2$  by glycine-nitrate route can be effectively tailored to obtain predominantly larger ( $> 15$  nm) or smaller ( $< 5$  nm) crystallites.
- Results obtained from sintering studies on nanocrystalline  $\text{ThO}_2$  powders have established the conditions to obtain high density  $\text{ThO}_2$  pellets (up to 94 % TD) by sintering at readily achievable temperatures ( $< 1773$  K) for short duration ( $< 1$  h).
- Another important outcome of the present work is desintering behavior observed in nanocrystalline  $\text{ThO}_2$ . It has been observed that desintering exclusively occurs in  $\text{ThO}_2$  powders synthesized by glycine-nitrate combustion and is related to powder properties that results into non-uniform density distribution in green compacts. Absence of desintering in citrate-nitrate combustion derived  $\text{ThO}_2$  is an important result that will be useful for preparation of thoria-based ceramics including nuclear fuel pellets.

- Present results on mechanism of solution combustion synthesis of nanocrystalline ThO<sub>2</sub> motivate for similar studies on oxides of uranium and Th-U, both of which are candidate starting materials to develop oxide fuels with superior irradiation performance.
- Another scope of the future investigation stems from the need to structurally characterize various complexes formed in thorium / uranium-based aqueous gel environment by spectroscopic techniques. Such studies will provide evidence to the suggestion that combustion is strongly influenced by metal-ligand complexation chemistry and properties of combustion synthesized oxide powders can be pre-designed, if complex chemistry in gel is well understood. Such studies will be taken up in future on oxides of actinides and lanthanides.

## SYNOPSIS

Energy is the key driver of life on our planet. Enormous energy received from the sun maintains ecological and environmental balance on the earth. In the era of industrial development, growing global population and rapid globalization, the human life index is directly linked with energy consumption. A notable fraction of this energy is required as electricity, which is presently being produced on an enormous scale mainly by combusting exhaustible fossil fuels (coal, oil, gas, etc.). This has resulted into adverse climate changes and the global efforts are being re-focused on strategies that can minimize climate damage and provide energy in a sustained manner. Renewable energy resources (solar, hydro, wind, nuclear, biomass, tidal, etc.) therefore have taken centre stage in current energy policy across the world. Among them, nuclear energy option fulfills all major attributes such as high energy density, base-load capacity, clean & green energy source, renewability (by fuel reprocessing), sustainability, etc. Energy obtained from the sun is also of nuclear origin. With more than six decades of industrial maturity on nuclear energy systems, its contribution to global energy mix is steadily increasing. Advanced fission-based nuclear energy systems presently under development stage consist of generation-IV reactors [1], which aim for improved economics with higher safety and proliferation resistant reactors with minimum waste generation. These goals are more likely to be met with large-scale utilization of thorium, which is an excellent nuclear material but less utilized for its potential. Th-based ceramics, alloys and fluoride-salts are among the potential fuel options for advanced reactors [2, 3]. In India, rapid expansion of nuclear energy capacity is taking place. India's three-stage nuclear power program aims for large-scale utilization of country's vast thorium reserves for electricity production. In coherence with India's future plans to build oxide and metal-fuelled fast reactors [4], it is important that Th-based fuel options are timely developed. For assessment of such fuels, research on their preparative aspects and thermophysical

characterization is essential. These data are primary input parameters for development and assessment of fuel performance codes in reactor physics studies and safety analyses. While understanding of Th-based oxide fuels has reached some maturity; mostly contributed by Indian researchers [5], very limited literature is available on Th-based metallic alloy fuels. These alloys have promising physico-chemical properties along with neutronic advantages of thorium. Understanding their thermophysical behavior is therefore essential. A major portion of the work carried out in the present study covers preparation, characterization and thermophysical assessment of thorium-based metallic alloys.

In the area of ceramic/oxide fuels, development of high burn-up fuels with maximum energy extraction potential and minimum proliferation risk is desired. High density actinide oxides that have uniform and fine-grained microstructure (nano or sub-micron) have such potential. These oxides offer better thermal conductivity, high mechanical strength, higher fission gas retention capability and improved tolerance to radiation damage during reactor irradiation [6]. Such fuels can be prepared using nanocrystalline powders. Recent literature highlights methodologies for synthesis and processing of nanocrystalline actinide oxides [7, 8]. From the point of view of nuclear fuel production, synthesis of these oxides should involve simple precursors with minimum steps. Synthesis should also be energy efficient process with high product yield and minimum waste generation. With these considerations, synthesis routes such as precipitation and solution combustion are promising options. Literature on combustion synthesized nanocrystalline ThO<sub>2</sub> indicates that while precursor to ThO<sub>2</sub> conversion and ThO<sub>2</sub> powder properties are well reported, mechanism of combustion is less understood, which is crucial for understanding the origin of powder properties of the combustion product. To address this gap-area, solution combustion synthesis of nanocrystalline ThO<sub>2</sub> has been investigated via glycine-nitrate and citrate-nitrate routes,

primarily utilizing thermal analysis. Important insights into combustion process have been identified.

The thesis consists of eight chapters. Chapter-1 presents the importance and relevance of Th-based metallic alloys and nanocrystalline ThO<sub>2</sub>-based oxides for nuclear energy applications. Chapter-2 briefly summarizes the materials used to carry out the reported research work, synthesis methods to prepare metallic alloys and ceramic oxides and experimental techniques for characterization of these samples. Techniques used for measurement of thermal and thermophysical properties are also summarized. Chapter-3 to 7 detail the results of work carried out. Chapter-8 presents summary of results and outlines the future scope of work. A brief summary of each chapter is presented as follows:

### **Chapter-1: Introduction**

This chapter describes how thorium, which is 2 to 3 times more abundant than natural uranium; is easily extractable from earth's resources and has superior nuclear properties, is likely to play an increasingly important role in advanced nuclear energy technologies. The chapter is divided into two sections, which summarize the relevance of Th-based metallic alloys and ThO<sub>2</sub>-based nanocrystalline ceramics.

Section-A presents the basis upon which potential of Th-based metallic alloys as candidate fuels for advanced reactors is conceived. Nuclear / neutronic properties of Th-based fuels in general and advantages offered by its metallic alloys are compared with conventional U/Pu-based fuels. It has been suggested that Th metal alloyed with suitable fissile element(s) (<sup>233</sup>U/<sup>235</sup>U/Pu) would have promising fuel performance potential. Literature information on preparation, characterization and irradiation behavior of these alloy fuels is summarized. Need for indigenous database on thermophysical properties of these alloys is explained.

Section-B covers the importance of nanocrystalline actinide oxides for fabrication of advanced ceramic nuclear fuels, which have improved performance potential as compared to oxide fuels derived from bulk powders. Advantages and limitations of fuel pellets obtained from nanocrystalline powders have been discussed. A brief review of literature on synthesis of nanocrystalline ThO<sub>2</sub> is presented and gap areas, which are addressed in the present studies, are outlined. Methods used to process nanocrystalline oxide powders into fuel-grade dense ceramics are discussed. These include powder to pellet method, microwave processing, spark-plasma sintering, etc. Importance of detailed understanding of synthesis mechanism of nanocrystalline actinide oxides has been mentioned. Finally, desintering phenomenon and its influence on ceramic nuclear fuel processing have been explained to conclude this chapter.

## **Chapter-2: Experimental**

This chapter summarizes synthesis methods and characterization techniques used during the course of work. Two methods, namely (i) DC-arc melting for preparation of metallic alloys and (ii) solution combustion for synthesis of nanocrystalline oxides are described in detail. Experimental care required for handling/processing of air sensitive metals/alloys under ambient/inert atmosphere has been mentioned. Brief information on characterization techniques such as elemental (C, N, O) analysis, powder X-ray diffraction (PXRD), scanning electron microscopy (SEM), energy-dispersive spectroscopy (EDS), optical microscopy, Raman spectroscopy, Fourier transform infra red (FT-IR) spectroscopy, small angle X-ray spectroscopy (SAXS), thermo gravimetry (TG), etc., which were used during the course of work, is presented. Theory and application of thermophysical property measurement techniques used in the present study are detailed. These include thermo-mechanical analysis (TMA) and dilatometry for evaluation of thermal expansion and sintering behavior, differential scanning calorimetry (DSC) for heat capacity measurements and characterization

of thermal effects and laser flash technique for thermal diffusivity measurement. Calibration aspects and source of errors while using these techniques have been mentioned.

### **Chapter-3: Thermophysical studies on reactor-grade uranium and thorium metals**

Uranium (U) and thorium (Th) are main constituents of thorium-based metallic alloy fuels. Plutonium (Pu) is added as an alternate fissile additive. Zirconium (Zr) or molybdenum (Mo) can be used for phase stabilization and/or improving alloy properties. To understand thermophysical behavior of alloys made from these elements, it is essential to generate reliable and reproducible database on constituent elements. Literature information on U and Th is insufficient and scattered [9]. To address this, thermophysical properties of reactor-grade Th and U metals have been evaluated. These results are reported in chapter-3. Th and U metals were characterized for their elemental and structural purity and suitably processed to obtain specimens in required shape and dimension. Experimental results on bulk thermal expansion (298 K – 1373 K), thermal diffusivity (298 K – 1373 K) and specific heat capacity (273 K – 773 K) have been reported. Quality of these results has been discussed in terms of extent of oxidation during measurements and reproducibility of results. Thermal conductivity of U and Th metals (298 K – 1373 K) has been evaluated from experimental data on diffusivity, density and heat capacity. Effect of structural phase transformations on thermophysical properties of U metal has been described in detail. Both thermal conductivity and thermal diffusivity abruptly increase when orthorhombic U (stable up to ~948 K) transforms to tetragonal phase (stable over ~948 K to ~1051 K), and thereafter to body centered cubic (BCC) phase (stable from ~1051 K to melting temperature). On the other hand, Th metal remains stable in face centered cubic (FCC) structure over the studied temperature range (298 K to 1373 K). Thermal expansion behavior of U indicated notable influence of expansion anisotropy during thermal cycling, resulting from the structural phase

transformations and microstructural changes. As expected, both U and Th showed significantly higher thermal conductivity as compared to their dioxides (ThO<sub>2</sub> and UO<sub>2</sub>). At ambient temperature, thermal conductivity of Th (~48 W m<sup>-1</sup> K<sup>-1</sup>) is twice than that of U (~24 W m<sup>-1</sup> K<sup>-1</sup>). Thermal conductivities of Th and U increase with temperature. Also, Th shows significantly lower thermal expansion (~12.4 x 10<sup>-6</sup> / K) than U (~19.6 x 10<sup>-6</sup> / K) over 300 K to 950 K. Results obtained during these investigations have been critically compared with those reported in literature [9] and merits of present results in the context of their usefulness for reactor physics and fuel performance analysis have been discussed.

#### **Chapter-4: Thermophysical studies on thorium-uranium binary metallic alloys**

Thorium-uranium binary alloys are potential fuels for sodium-cooled fast reactors [10]. (1-x)Th-(x)U (x = 5 to 20 wt.%) are representative compositions considered for fuel application and hence estimation of their thermophysical properties is a primary requirement. Chapter-4 details the preparation and characterization of Th-10U, Th-20U and U-10Zr alloys (wt. %) and their thermophysical properties over a temperature range from 298 K to 1273 K. These alloys were prepared by DC-arc melting technique; phase homogenized by vacuum annealing and characterized by elemental analysis, XRD, SEM and EDS techniques. Vacuum annealed Th-U alloys are bi-phasic in nature and contained uniformly distributed Th- and U-rich phases. U-10Zr alloy also showed Zr-rich phases distributed in U-rich base alloy. Elemental analysis confirmed the alloy preparation and processing without any additional oxidation and ascertained their quality for evaluation of thermophysical properties. Experimental results on thermal diffusivity (298 K - 1273 K), thermal expansion (298 K - 1373 K) and specific heat (273 K - 773 K) have been reported. Temperature dependence of thermal conductivity of binary alloys; as evaluated from temperature dependent density, thermal diffusivity and specific heat has been discussed. Thermal diffusivity of Th-U alloys

drops significantly ( $\sim 22\text{-}24 \text{ cm}^2.\text{s}^{-1}$  at 298 K) as compared to Th ( $\sim 36 \text{ cm}^2.\text{s}^{-1}$  at 298 K), which has been explained in terms of impeding heat transport from (i) phase boundaries in composite alloys and (ii) residual strain. Thermal expansion behavior of Th-10U alloy remains almost similar to that of Th metal while thermal expansivity of Th-20U is higher and exhibits the occurrence of structural phase transitions of U. These results have been explained in terms of lower bulk density of Th ( $\sim 11400 \text{ kg.m}^{-3}$ ; 300 K) as compared to U ( $\sim 18900 \text{ kg.m}^{-3}$ ; 300 K), which masks the observation of higher thermal expansion U phase in Th-rich (Th  $\geq 90$  wt. %) alloys. Partial solubility of U in Th at high temperatures, which may remain to some extent in alloy phase and therefore affect the thermal expansion behavior, has been suggested. Thermal expansion of U-10Zr alloy is also discussed. Results shows only one phase transition ( $\alpha \rightarrow \beta$ ) at  $\sim 970$  K, beyond which the alloy acquires isotropic cubic phase ( $\gamma\text{-U}, \beta\text{-Zr}$ ) and  $\beta \rightarrow \gamma$  transition is not observed. Thermal conductivity of binary alloys has been found to be lower than pure metals. Higher conductivity of Th-U alloys as compared to U-Zr is a significant advantage for their use as nuclear fuels. All these results are discussed in details in chapter-4.

## **Chapter-5: Thermophysical studies on thorium-uranium-zirconium ternary alloys**

It is known that alloying actinides with zirconium improves alloy's mechanical properties as well as resistance towards fuel-clad interaction. For this reason, Th-U-Zr ternary alloys can be potential fuel for high burn-up irradiations. This chapter describes the preparation and characterization of ternary alloys namely Th-3U-7Zr and Th-7U-3Zr (wt. %) and their thermophysical assessment. Alloys prepared by DC-arc melting were characterized for their structure, morphology and composition using XRD, SEM and EDS techniques, respectively. Phase analysis indicated composite nature of these alloys consisting of U-rich precipitates dispersed in matrix of Th-Zr solid solution and Th-rich phase. Occasional occurrence of  $\text{ThO}_2$

(dendrites) and  $ZrO_2$  inclusions were also observed. Bulk thermal expansion and thermal diffusivity were measured over 298 K to 1373 K. Thermal conductivity was evaluated from measured diffusivity and expansivity along with specific heat evaluated from the law of weighted fractions. Results showed that heat transport behavior of ternary alloys further deteriorated (as compared to Th-U binary alloys) upon Zr-incorporation. Thermal diffusivity of both ternary alloys was lower than that of Th-20U alloys. Thermal expansion did not vary significantly from that of Th metal. Th-7U-3Zr alloy showed expansion anomaly associated with orthorhombic ( $\alpha$ ) to tetragonal ( $\beta$ ) phase transition of U. Results of the effect of thermal cycling (298 K - 1273 K) on thermal diffusivity of Th-U-Zr ternary alloys have been discussed in details. Thermal diffusivity of as-cast alloys varies with successive thermal cycles and reproducible results are obtained only after six thermal cycles. Since as-cast metallic fuel is proposed to be used in Indian fast reactors, these results are discussed from the perspective of variation in thermophysical properties of alloy fuels from as-cast state to high temperature phase homogenized state.

#### **Chapter-6: Combustion synthesis of nanocrystalline $ThO_2$ : Probing synthesis mechanism by thermal analysis**

Nanocrystalline actinide oxides are used to produce high density ceramic fuels with better physico-chemical properties. Among the methods available for synthesis of these oxides, solution combustion is a simple, scalable and high efficiency process [11]. Literature reports are available on powder synthesis, characterization and its conversion into dense ceramics. However, mechanism of combustion, which governs the properties of synthesized powders, is not well understood. This chapter presents our results on glycine-nitrate and citrate-nitrate combustion synthesis of nanocrystalline  $ThO_2$ , wherein combustion mechanism has been investigated using thermal analysis. Combustion process was studied by varying the fuel-to-

oxidant ratio (F:O;  $0.65 \leq \text{F:O} \leq 1.25$ ). Results show that glycine-nitrate gels contain mono- and poly-nuclear  $\text{Th}^{4+}$ -glycine- $\text{NO}_3^-$  complexes, fraction of which depends upon F:O. These complexes show distinct ordering in gel phase. Upon heating, these complexes undergo exothermic crystallization (ordered aggregation) to form amorphous or crystalline molecular solids. Powder characteristics of as-combusted  $\text{ThO}_2$ , such as average crystallite size, surface roughness, etc., depends upon the nature and relative fraction of these complexes. At low F:O values hexanuclear  $\text{Th}^{4+}$ -glycine- $\text{NO}_3^-$  complexes dominate in gel phase while higher F:O values favour mononuclear complexes. Combustion of gel consisting of mononuclear complexes leads to smaller  $\text{ThO}_2$  crystallites as compared to hexanuclear complexes. Results obtained on citrate-nitrate combustion on the other hand suggest no such ordering of  $\text{Th}^{4+}$ -citrate- $\text{NO}_3^-$  complexes. Low temperature auto-ignition ( $\sim 430$  K) of amorphous citrate-nitrate gels consisting of  $\text{Th}^{4+}$ -citrate- $\text{NO}_3^-$  complexes, followed by sluggish thermal decomposition of citrate moieties is suggested to be the main reason for obtaining very fine ( $< 5$  nm) nanocrystalline  $\text{ThO}_2$  powders in contrast to glycine-nitrate combustion, wherein highly fluffy and porous nanocrystalline  $\text{ThO}_2$  powders with relatively large grain size ( $\sim 15$  nm) are obtained. These results are discussed in detail in this chapter.

### **Chapter-7: Desintering in combustion synthesized $\text{ThO}_2$ : A comparison of glycine-nitrate and citrate-nitrate route**

Sintering is an important stage in nuclear fuel fabrication by which powdered oxides are converted into dense fuel pellets. Nanocrystalline oxides usually sinter to high density ceramics at relatively low temperatures as compared to bulk powders. A limiting issue observed with nanocrystalline  $\text{ThO}_2$  powders is undesired loss of bulk density during high temperature processing, a phenomenon known as desintering. This chapter presents the results of sintering studies carried out on nanocrystalline  $\text{ThO}_2$  compacts synthesized by

glycine-nitrate and citrate-nitrate routes. Sintering experiments were performed on calcined ThO<sub>2</sub> powder compacts using dilatometry. Results showed that glycine-nitrate derived ThO<sub>2</sub> showed varying extent of desintering effect with different F:O values, while no desintering was observed for citrate-nitrate derived ThO<sub>2</sub>. This has been explained in terms of powder properties that cause breakup of inter-grain bridges during rapid densification due to tensile stress in presence of inclusions. Results have been discussed in light of microstructural characterization of sintered pellets. These findings are useful to select synthesis method and F:O value for solution combustion synthesis of ThO<sub>2</sub> and ThO<sub>2</sub>-based powders, which can be consolidated to high density, uniform microstructure ceramics without any desintering.

### **Chapter-8: Conclusion and future scope**

In this chapter, major findings and highlights of our studies on Th-based metallic alloys and nanocrystalline ThO<sub>2</sub> ceramics have been summarized. The database generated on thermophysical properties of Th-U, U-Zr and Th-U-Zr alloys as well as constituent metals would serve as first hand reference for further investigations on alloys with variable compositions and alloys formed with inclusion of simulated fission product metals. The studies have opened up an interesting area to investigate the thermophysical behavior of alloy nuclear fuels with detailed microstructural evolution occurring during thermal cycling of alloys with high chemical diffusion and phase/microstructure reorganization. Presented results on mechanism of combustion synthesis of nanocrystalline ThO<sub>2</sub> have given relevant new information and opened a complete area of understanding the mechanism of synthesis of ceramics by wet-chemical methods using thermal analysis. Results of desintering studies will serve as guide for further process optimization to minimize the undesired loss of bulk density during high temperature processing of ceramics.

## References:

- [1] "A Technology Roadmap for Generation IV Nuclear Energy Systems, Issued by the US DOE Nuclear Energy Research Advisory committee and the Generation IV International Forum", December 2002. (DOI: 10.2172/859105).
- [2] H. György, S. Czifrus, "The utilization of thorium in Generation IV reactors", *Prog. Nucl. Energy* 93 (2016) 306-317.
- [3] P. Rodriguez, C. V. Sundaram, "Nuclear and materials aspects of the thorium fuel cycle", *J. Nucl. Mater.* 100 (1981) 227-249.
- [4] S.C. Chetal, P. Chellapandi, P. Puthiyavinayagam, S. Raghupathy, V. Balasubramanian, P. Selvaraj, P. Mohanakrishnan, B. Raj, "Current Status of Fast Reactors and Future Plans in India", *Energy Procedia* 7 (2011) 64-73.
- [5] "Thoria-based Nuclear Fuels: Thermophysical and Thermodynamic Properties, Fabrication, Reprocessing, and Waste Management" (Eds.: D. Das, S.R. Bharadwaj) Springer (2013) (DOI: 10.1007/978-1-4471-5589-8)
- [6] J. Spino, H.S. Cruz, R. Jovani-Abril, R. Birtcher, C. Ferrero, "Bulk-nanocrystalline oxide nuclear fuels - An innovative material option for increasing fission gas retention, plasticity and radiation-tolerance", *J. Nucl. Mater.*, 422 (2012) 27-44.
- [7] R.D. Purohit, S. Saha, A. K. Tyagi, "Nanocrystalline thoria powders via glycine-nitrate combustion", *J. Nucl. Mater.* 288 (2001) 7-10.
- [8] V. Tyrpekl, M. Cologna, J.-F. Vigier, A. Cambriani, W. Weerd, J. Somers, "Preparation of bulk-nanostructured UO<sub>2</sub> pellets using high-pressure spark plasma sintering for LWR fuel safety assessment", *J. Am. Ceram. Soc.*, 100 (2017) 1269-1274.
- [9] Y. S. Touloukian, R. W. Powell, C. Y. Ho, P. G. Klemens, "Thermophysical Properties of Matter - The TPRC Data Series. Volume 1. Thermal Conductivity - Metallic Elements & Alloys", (1970).

- [10] B. Blumenthal, J. E. Sanecki, D. E. Busch, D. R. O'Boyle, "Thorium-uranium-plutonium alloys as potential fast power reactor fuels; part-II: Properties and irradiation behavior of thorium-uranium-plutonium alloys", Report no.: ANL-7259, Argonne National laboratory, Illinois (1969).
- [11] F. Deganello, A. K. Tyagi, "Solution combustion synthesis, energy and environment: Best parameters for better materials", *Prog. Cryst. Growth Char.* 64 (2018) 23-61.

## References:

- [1] C. Degueudre, M.J. Joyce, “Evidence and uncertainty for uranium and thorium abundance: a review”, *Prog. Nucl. Energy* 124 (2020) 103299.
- [2] L.S. Keith, O.M. Faroon, B.A. Fowler, “Uranium (book chapter); handbook on the toxicology of metals: fourth edition (Eds: G.F. Nordberg, B.A. Fowler, M. Nordberg)”, Elsevier (2015) 1307-1345 (DOI: <https://doi.org/10.1016/C2011-0-07884-5>).
- [3] G. Sadagopan, K.S.V. Nambi, G. Venkataraman, V.K. Shukla, S. Kayasth, “Estimation of thorium in gas mantles to ascertain regulatory compliance”, *Radiat. Prot. Dosim.* 71(1) (1997) 53-56.
- [4] T.E. Leontis, “Properties of magnesium-thorium and magnesium-thorium-cerium alloys”, *J. Min. Metals Mater. Soc.* 4 (3) (1952) 287-294.
- [5] R.A. Glenner, P. Willey, P.S. Sledzik, E.P. Junger, “Dental fillings in civil war skulls: What do they tell us?”, *J. Am. Dent. Assoc.* 127(11) (1996) 1671-1677.
- [6] O. Hahn, F. Strassmann, “Über den nachweis und das verhalten der bei der bestrahlung des urans mittels neutronen entstehenden erdalkalimetalle (English translation: Concerning the existence of alkaline earth metals resulting from neutron irradiation of uranium)”, *Die Naturwissenschaften* 27 (1939) 11-15.
- [7] “The first reactor” The US department of energy report: DOE/NE-0046 (1982) 1-40 (Web-link: <https://www.energy.gov/ne/downloads/first-reactor>).
- [8] R.L. Crowther, “Use of thorium in boiling water reactors”, *J. Nucl. Energy AB* 16(4) (1962) 181-194.
- [9] J.R. Dietrich, “The physics of advanced reactors”, *Brit. J. Appl. Phys.* 7(S5) 302 (1956) S9-S23.
- [10] H.N. Sethna, “India’s atomic energy program: past and future”, *International Atomic Energy Agency (IAEA) Bulletin* 21 (5) (1979) 2-11.

## References

- [11] S. Banerjee, H.P. Gupta, “The evolution of the Indian nuclear power programme”, Prog. Nucl. Energy 101 (2017) 4-18.
- [12] International Atomic Energy Agency “Thorium fuel cycles - potential benefits and challenges”, IAEA-TECDOC-1450, IAEA, Vienna (2005) 1-105.
- [13] P.K. Wattal, “Back end of Indian nuclear fuel cycle - A road to sustainability”, Prog. Nucl. Energy 101 (2017) 133-145.
- [14] R. Natarajan, “Reprocessing of spent nuclear fuel in India: Present challenges and future programme”, Prog. Nucl. Energy 101 (2017) 118-132.
- [15] S.A. Ansari, P. Pathak, P.K. Mohapatra, V.K. Manchanda, “Aqueous partitioning of minor actinides by different processes” Sep. Purif. Rev. 40(1) (2011) 43-76.
- [16] M. Salvatores, “Nuclear fuel cycle strategies including partitioning and transmutation”, Nucl. Eng. Des. 235(7) (2005) 805-816.
- [17] Press Information Bureau, Government of India, “Setting up of ten indigenous nuclear power reactors” (Web-link: <http://pib.nic.in>)
- [18] S.C. Chetal, P. Chellapandi, P. Puthiyavinayagam, S. Raghupathy, V. Balasubramanian, P. Selvaraj, P. Mohanakrishnan, B. Raj, “Current status of fast reactors and future plans in India” Energy. Proced. 7 (2011) 64-73.
- [19] P. Puthiyavinayagam, P. Selvaraj, V. Balasubramanian, S. Raghupathy, K. Velusamy, K. Devan, B.K. Nashine, G.P. Kumar, K.V.S. Kumar, S. Varatharajan, P. Mohanakrishnan, G. Srinivasan, A.K. Bhaduri, “Development of fast breeder reactor technology in India”, Prog. Nucl. Energy 101 (Part A) (2017) 19-42.
- [20] Bharatiya Nabhikiya Vidyut Nigam Limited, Department of Atomic Energy “Present status of 500 MWe Prototype Fast Breeder Reactor (PFBR)”, (Web-link: <http://www.bhavini.nic.in>).

## References

- [21] P. Rodriguez, C.V. Sundaram, "Nuclear and materials aspects of the thorium fuel cycle", *J. Nucl. Mater.* 100 (1981) 227-249.
- [22] R. Ramanna, S.M. Lee, "The thorium cycle for fast breeder reactors", *Pramana* 27(1-2) (1986) 129-137.
- [23] R. Chidambaram, C. Ganguly, "Plutonium and thorium in the Indian nuclear programme", *Curr. Sci. India* 70(1) (1996) 21-35.
- [24] P.K. Vijayan, V. Shivakumar, S. Basu, R.K. Sinha, "Role of thorium in the Indian nuclear power programme", *Prog. Nucl. Energy* 101 (2017) 43-52.
- [25] "Thoria-based nuclear fuels: thermophysical and thermodynamic properties, fabrication, reprocessing, and waste management", (Eds.: D. Das, S.R. Bharadwaj) Springer (2013) (DOI: 10.1007/978-1-4471-5589-8).
- [26] "Thorium-energy for the future", (Eds.: A.K. Nayak, B.R. Sehgal), Springer (2019) (DOI: 10.1007/978-981-13-2658-5).
- [27] S. Mukherji, B.K. Mohan, P.D. Krishnani, V. Jagannathan, S. Ganesan, "Thorium irradiation in Indian PHWRs - applications and limitations of origin code", *Proceedings of First National Conference in Nuclear Reactor Technology* (2002) (Web-link: [https://inis.iaea.org/search/search.aspx?orig\\_q=RN:34011468](https://inis.iaea.org/search/search.aspx?orig_q=RN:34011468)).
- [28] M. Das, "Design and irradiated experience with thorium based fuels in PHWRs" *Annual International Conference - Canadian Nuclear Association* (1992) 10.1-10.
- [29] P.S. Dharmi, J.S. Yadav, K. Agarwal, "Power reactor thoria reprocessing facility (PRTRF), Trombay", *Proceedings of the Theme Meeting on the Journey of BARC Safety Council for Strengthening Safety Culture in BARC Facilities* (Eds: V.M. Jolly) (2017) (Web-link: [https://inis.iaea.org/search/search.aspx?orig\\_q=RN:48089837](https://inis.iaea.org/search/search.aspx?orig_q=RN:48089837)).
- [30] R.K. Sinha, A. Kakodkar, "Design and development of the AHWR - the Indian thorium fuelled innovative nuclear reactor" *Nucl. Eng. Des.* 236 (7-8) (2006) 683-700.

- [31] R. Sinha, A. Kakodkar, "India's passive breeder", Nucl. Eng. Int. 55(668) (2010) 30-31.
- [32] A. Kakodkar, "Evolution of nuclear reactor containments in India: Addressing the present day challenges", Nucl. Eng. Des. 269 (2014) 3-22.
- [33] S. Sengupta, S.B. Chafle, S. Mammen, K. Sasidharan, V.K. Raina, "Critical facility for AHWR and PHWRs", Proceedings of International Conference on Peaceful uses of Atomic Energy (2009). V. 1. [33a] C. Ronchi, J.-P. Hiernaut, Experimental measurement of pre-melting and melting of thorium dioxide, J. Alloys Comp. 240 (1-2) (1996) 179-185. [33b] R. Böhler, A. Quaini, L. Capriotti, P. Cakir, O. Beneš, K. Boboridis, A. Guiot, L. Luzzi, R.J.M. Konings, D. Manara, "The solidification behavior of the UO<sub>2</sub>-ThO<sub>2</sub> system in a laser heating study" J. Alloys. Comp. 616 (2014) 5-13.
- [34] D. Greneche, W.J. Szymczak, J.M. Buchheit, M. Delpech, A. Vasile, H. Golfier, "Rethinking the thorium fuel cycle: An industrial point of view", Proceedings of ICAPP (Nice, France), (2007) Paper-7367. [34a] S.F. Ashley, G.T. Park, W.J. Nuttall, C. Boxall, R.W. Grimes, "Thorium fuel has risks", Nature 492 (2012) 31-33.
- [35] D. Jain, V. Sudarsan, A.K. Tyagi, "Thorium-based metallic alloys as nuclear fuels: Present status, potential advantages and challenges", SMC Bulletin (Society for Materials Chemistry, India) 4 (1) (2013) pp. 27-40 (Web-link: <https://www.smcindia.org/smc-bulletin.php>).
- [36] P.K. Vijayan, A. Basak, I.V. Dulera, K.K. Vaze, S. Basu, "Conceptual design of Indian molten salt breeder reactor", Pramana - J. Phys. 85 (2015) 539-554.
- [37] T. Yamamoto, H. Suwarno, H. Kayano, M. Yamawaki, "Development of new reactor fuel materials: Hydrogen absorption properties of U-Th, U-Th-Zr and U-Th-Ti-Zr alloys", J. Nucl. Sci. Tech. 32(3) (1995) 260-262.

## References

- [38] K.A. Terrani, G.W.C. Silva, C.B. Yeamans, “Fabrication and characterization of uranium thorium zirconium hydride fuels”, *Trans. Am. Nucl. Soc.* 98 (2008) 1060-1061.
- [39] S.M. McDevitt, T.J. Downar, A.A. Solomon, S.T. Revankar, M.C. Hash, A.S. Hebden, “Thoria-based cermet nuclear fuel: Cermet fabrication and behavior estimates”, *Proc. Int. Conf. Nucl. Eng. (ICONE 4)* (2002) 59-67.
- [40] C. Lombardi, L. Luzzi, E. Padovani, F. Vettrano, “Thoria and inert matrix fuels for a sustainable nuclear power”, *Prog. Nucl. Energy* 50(8) (2008) 944-953.
- [41] J. Spino, H.S. Cruz, R. Jovani-Abril, R. Birtcher, C. Ferrero, “Bulk-nanocrystalline oxide nuclear fuels - An innovative material option for increasing fission gas retention, plasticity and radiation-tolerance”, *J. Nucl. Mater.* 422 (1-3) (2012) 27-44.
- [42] H. György, S. Czifrus, “The utilization of thorium in generation IV reactors”, *Prog. Nucl. Energy* 93 (2016) 306-317.
- [43] D. Heuer, E. Merle-Lucotte, M. Allibert, M. Brovchenko, V. Ghetta, P. Rubiolo, “Towards the thorium fuel cycle with molten salt fast reactors”, *Ann. Nucl. Energy* 64 (2014) 421-429.
- [44] G.L. Hofman, L.C. Walters, T.H. Bauer, “Metallic fast reactor fuels”, *Prog. Nucl. Energy* 31(1-2) (1997) 83-110.
- [45] W.J. Carmack, D.L. Porter, Y.I. Chang, S.L. Hayes, M.K. Meyer, D.E. Burkes, C.B. Lee, T. Mizuno, F. Delage, J. Somers, “Metallic fuels for advanced reactors”, *J. Nucl. Mater.* 392 (2) (2009) 139-150.
- [46] Idaho National Laboratory, “Experimental breeder reactor-I (EBR-I) (Web-link: <https://inl.gov/experimental-breeder-reactor-i/>).
- [47] L.C. Walters, “Thirty years of fuels and materials information from EBR-II”, *J. Nucl. Mater.* 270(1) (1999) 39-48.

- [48] K. D. Weaver, J. Gilleland, C. Whitmer, G. Zimmerman, “High burn-up fuels for fast reactors: past experience and novel applications”, International Congress on Advances in Nuclear Power Plants (ICAPP 2009) (2009) 795.
- [49] G. Locatelli, M. Mancini, N. Todeschini, “Generation IV nuclear reactors: Current status and future prospects”, *Energ. Policy* 61 (2013) 1503-1520.
- [50] Z.S. Takibaev, “Fast homogeneous nuclear reactor”, *Atom. Energy* 100 (2006) 154-156.
- [51] T. Jayakumar, M.D. Mathew, K. Laha, R. Sandhya, “Materials development for fast reactor applications”, *Nucl. Eng. Des.* 265 (2013) 1175-1180.
- [52] A. Riyas, P. Mohanakrishnan, “Studies on physics parameters of metal (U-Pu-Zr) fuelled FBR cores”, *Ann. Nucl. Energy* 35(1) (2008) 87-92.
- [53] P. Chellapandi, V. Balasubramaniyan, P. Puthiyavinayagam, R. Sundararajan, M. Kanakkil, P. Selvaraj, P.R. Vasudeva Rao, “Design of 500 MWe metal fuel demonstration fast reactor”, *Proc. Int. Conf. Nucl. Eng.* (2014) (DOI: <https://doi.org/10.1115/ICONE22-30727>).
- [54] Indira Gandhi Centre for Atomic Research, “Fast Breeder Test Reactor”, (Web-link: <http://www.igcar.gov.in/rfg/fbtrhist.html>).
- [55] B. Blumenthal, J.E. Sanecki, D.E. Busch, D.R. O’Boyle, “Thorium-uranium-plutonium alloys as potential fast power reactor fuels; part-II: Properties and irradiation behavior of thorium-uranium-plutonium alloys”, ANL-7259, Argonne National laboratory, Illinois (October 1969).
- [56] S.Z. Ghayeb, “Investigations of thorium-based fuels to improve actinide burning rate in S-PRISM reactor”, M.Sc. Thesis, The Pennsylvania State University (2008) (Web-link: <https://etda.libraries.psu.edu/catalog/9160>).

## References

- [57] R.G. Wymer, D.A. Douglas Jr., "Status and progress report for thorium fuel cycle development for period ending December 31, 1964", Report no.: ORNL-3831, Oak Ridge National laboratory, Tennessee (May 1966).
- [58] "Fast spectrum reactors", (Eds.: A.E. Waltar, D. Todd, P.V. Tsvetkov) Springer (2011) (ISBN 978-1-4419-9572-8).
- [59] D.E. Peterson, "The (Th-U) Thorium-uranium system", Bull. Alloy Phase Diagr. 6 (5) (1985) 443-445.
- [60] S. Peterson, R.E. Adams, D.A. Douglas Jr., "Properties of thorium, its alloys and its compounds", Report no.: ORNL-TM-1144, Oak Ridge National laboratory, Tennessee (June 1965).
- [61] D.R. Marr, D.A. Cantley, J.C. Chandler, D.C. McCurry, R.P. Omberg, "Performance of thorium fuelled fast breeders", Report no.: HEDL-SA-1327-FP, Hanford Engineering Development Laboratory, Richland, USA (October 1977).
- [62] G.L. Copeland, "Evaluation of thorium-uranium alloys for the unclad metal breeder reactor", Report no.: ORNL-4557, Oak Ridge National Laboratory, Tennessee (June 1970).
- [63] B. Blumenthal, J.E. Sanecki, D.E. Busch, "Thorium-uranium-plutonium alloys as potential fast power reactor fuels; part-I: Thorium-uranium-plutonium phase diagram", Report no.: ANL-7258, Argonne National Laboratory, Illinois (September 1968).
- [64] C.S. Holden, "Rapid computational path for sustainable and renewable nuclear energy using metallic thorium fuels", Proceedings of 2<sup>nd</sup> Thorium energy conference (ThEC-2010), Mountain View CA (2010).
- [65] R.M. Carroll, "The effects of reactor irradiation on thorium-uranium alloy fuel plates", Report no.: ORNL-1938, Oak Ridge National Laboratory, Tennessee (August 1955).

## References

- [66] B.R. Hayward, P. Corzine, "Thorium uranium fuel elements for SRE", Proc. 2<sup>nd</sup> UN Int. Conf. Peaceful uses of Atom. Energy, Geneva (October 1958).
- [67] J.L. Ballif, B.R. Hayward, J.W. Walter, "Engineering evaluation of a mixed alloy fuel element irradiated at elevated temperatures in SRE", Technical report no.: NAA-SR-3888, Atomics International Division, North American Aviation Incorporation, California, USA (June 1960).
- [68] A.R. Olsen, "Thorium and thorium alloys: Preliminary corrosion tests", Report no.: ORNL-1066, Oak Ridge National Laboratory, Tennessee (November 1951).
- [69] M.S. Farkas, A.A. Bauer, R.F. Dickerson, "Development of thorium-uranium-base fuel alloys," Report no.: BMI-1428, Battelle Memorial Institute, Columbus, Ohio (March 1960).
- [70] R.H. Cole, L.E. Wilkinson, "Development of high strength ternary and quaternary thorium-uranium base alloys", Technical report no.: ATL-A-128, Advanced Technology Laboratory, California (1961).
- [71] J.H. Kittel, J.A. Horak, W.F. Murphy, S.H. Paine, "Effect of irradiation on thorium and thorium-uranium alloys", Technical report no.: ANL-5674, Argonne National laboratory, Illinois, USA (April 1963).
- [72] A.L. Bement, "Burn-up and specific power calculations for the thermal neutron irradiation on thorium-uranium alloys", Technical report no: HW-56631, General Electric Co. Hanford Atomic Products Operation, Richland, Washington (1958).
- [73] F.W. Dodge, E.W. Murbach, L.A. Hanson, "Low decontamination reprocessing of thorium-uranium alloys by induction drip melting", Nucl. Sci. Eng. 6 (6) (1959) 533-536.
- [74] P. Chiotti, A.F. Voigt, "Pyrometallurgical processing", Technical report: A/CONF.15/P/517; ISC-1018, Ames Laboratory, Iowa (October 1958).

- [75] W.N. Hensen, "Electrolysis of thorium and uranium", US-Patent no.: US 2951793 (1960).
- [76] S. Jiang, K. Liu, Y. Liu, T. Yin, Z. Chai, W. Shi, "Electrochemical behavior of Th(IV) on the bismuth electrode in LiCl–KCl eutectic", *J. Nucl. Mater.* 523 (2019) 268-275.
- [77] G.B. Zorzoli, "Use of metallic thorium for LWBRs and LWRs", *Nucl. Tech.* 20 (1973) 109-113.
- [78] F. Correa, D.J. Driscoll, D.D. Lanning, "An evaluation of tight pitch PWR cores", technical report no.: MIT-EL-79-022, Massachusetts Institute of Technology, Cambridge, Massachusetts (1979).
- [79] Z.S. Li, X.J. Liu, C.P. Wang, "Thermodynamic modelling of the Th-U, Th-Zr and Th-U-Zr systems", *J. Alloy Compd.* 473 (2009) 193-198.
- [80] S.Z. Ghrayeb, K.N. Ivanov, S.H. Levine, E.P. Loewen, "Burn-up performance of sodium-cooled fast reactors utilizing thorium-based fuels", *Nucl. Tech.* 176 (2011) 188-194.
- [81] T. Okawa, H. Sekimoto, S. Nakayama, "Design study on power flattening to sodium cooled large scale CANDLE burning reactor with using thorium fuel", *Proc. 18<sup>th</sup> Int. Conf. Nucl. Eng., ICON18, China, (2010).*
- [82] M.T. Simnad, "The U-ZrH<sub>x</sub> alloy: Its properties and use in TRIGA fuel", *Nucl. Engg. Des.* 64 (1981) 403-422.
- [83] K. Konashi, B.A. Pudjanto, T. Terai, M. Yamawaki, "Thermodynamic stability of ThZr<sub>2</sub>H<sub>x</sub> at high temperature", *J. Phys. Chem. Solids* 66 (2–4) (2005) 625-628.
- [84] T. Yamamoto, H. Suwarno, F. Ono, H. Kayano, M. Yamawaki, "Preparation, analysis and irradiation of hydride Th-U-Zr alloy samples for a new fuel", *J. Alloy Compd.* 271-273 (1998) 702-706.

- [85] S. Das, R. Kumar, S.B. Roy, A.K. Suri, "Development study on metallic thorium and uranium-thorium alloy", BARC Newsletter-Founder's Day Special issue (2011) 72-76.
- [86] S. Das, R. Kumar, S. Kaity, S. Neogy, K.N. Hareendran, S.B. Roy, G.K. Dey, B.S.S. Daniel, G.P. Chaudhari, "Characterization of microstructural, mechanical and thermal properties and ageing study of Th-3 wt.% U alloy" Nucl. Eng. Des. 282 (2015) 116-125.
- [87] S. Das, S. Kaity, R. Kumar, J. Banerjee, S.B. Roy, G.P. Chaudhari, B.S.S. Daniel, "Characterization of microstructural, mechanical and thermophysical properties of Th-52 U alloy", J. Nucl. Mater. 480 (2016) 223-234.
- [88] S. Das, S.B. Roy, G.P. Chaudhari, B.S.S. Daniel, "Microstructural evolution of as-cast Th-U alloys", Prog. Nucl. Energy 88 (2016) 285-296.
- [89] R. Kumar, S. Das, S.B. Roy, R. Agarwal, J. Banerjee, S.K. Satpati, "Effect of Mo addition on the microstructural evolution and  $\gamma$ -U stability in Th-U alloys", J. Nucl. Mater. 539 (2020) 152317.
- [90] S. Vaidyanathan, "Thorium utilization in pressurized water reactors using bimetallic thorium-zirconium alloy cladding", Nucl. Tech. (2020) (DOI: <https://doi.org/10.1080/00295450.2019.1706377>).
- [91] D. Escorcia-Ortiz, J. François, C. Martín-del-Campo, "Comparative study of the neutronic performance of thorium-based metallic fuel and MOX fuel in an ASTRID-like fast reactor core", Nucl. Eng. Des. 347 (2019) 122-131.
- [92] J.K. Startt, C.S. Deo, "First principles study of the structure and elastic properties of thorium metal", MRS Adv. 1 (35) (2016) 2447-2452.
- [93] A. Karahan, J. Buongiorno, "A new code for predicting the thermo-mechanical and irradiation behavior of metallic fuels in sodium fast reactors", J. Nucl. Mater. 396 (2010) 283-293.

## References

- [94] K. Lassmann, "TRANSURANUS: a fuel rod analysis code ready for use", *J. Nucl. Mater.* 188 (1992) 295-302.
- [95] J.P. Hamond, "Physical, mechanical and irradiation properties of thorium and thorium alloys", ORNL-4218, Oak Ridge National Laboratory, USA (1968) 29-30.
- [96] J.K. Fink, M.G. Chasanov, L. Leibowitz, "Thermophysical properties of thorium and uranium systems for use in reactor safety analysis", Report no.: ANL-CEN-RSD-77-1, Argonne National Laboratory (1977) 11-12.
- [97] M. Lung, "A present review of the thorium nuclear fuel cycles", European commission report no.: EUR-17771-EN, (1997).
- [98] S. Kolay, S. Phapale, R. Dawar, M. Jafar, S. N. Achary, A. K. Tyagi, R. Mishra, M. Basu, "Phase characterization and thermal study of SrF<sub>2</sub> and NdF<sub>3</sub> doped fluoride salt containing 78 mol % LiF - 20 mol % ThF<sub>4</sub> - 2 mol % UF<sub>4</sub>", *J. Radioanal. Nucl. Chem.* 314 (2) (2017) 1267-1271.
- [99] M. Verwerft, B. Boer, "Thorium oxide nuclear fuels", *Comprehensive nuclear materials* (Second edition) 5 (2020) 139-168 (DOI: <https://doi.org/10.1016/B978-0-12-803581-8.11770-9>).
- [100] S. Usha, R.R. Ramanarayanan, P. Mohanakrishnan, R.P. Kapoor, "Research reactor KAMINI", *Nucl. Eng. Des.* 236 (7-8) (2006) 872-880.
- [101] T.K. Mukherjee, "Processing of Indian monazite for the recovery of thorium and uranium values", *Proceedings of International Conference on Characterisation and Quality Control of Nuclear Fuels* (Eds.: C. Ganguly, R.N. Jayaraj) Allied Publishers Pvt. Ltd. (2002) 187-195.
- [102] J.R. Johnson, C.E. Curtis, "Note on sintering of ThO<sub>2</sub>", *J. Am. Ceram. Soc.* 37(12) (1954) 611.

## References

- [103] T.R.G. Kutty, K.B. Khan, P.V. Hegde, J. Banerjee, A.K. Sengupta, S. Majumdar, H.S. Kamath, "Development of a master sintering curve for ThO<sub>2</sub>", *J. Nucl. Mater.* 327(2-3) (2004) 211-219.
- [104] P. Balakrishna, B.P. Varma, T.S. Krishnan, T.R.R. Mohan, P. Ramakrishnan, "Thorium oxide: Calcination, compaction and sintering", *J. Nucl. Mater.* 160(1) (1988) 88-94.
- [105] N. Clavier, R. Podor, L. Deliere, J. Ravoux, N. Dacheux, "Combining in situ HT-ESEM observations and dilatometry: An original and fast way to the sintering map of ThO<sub>2</sub>", *Mater. Chem. Phys.* 137(3) (2013) 742-749.
- [106] K. Ananthasivan, S. Balakrishnan, S. Anthonysamy, R. Divakar, E. Mohandas, V. Ganesan, "Synthesis and sintering of nanocrystalline thoria doped with CaO and MgO derived through oxalate-deagglomeration", *J. Nucl. Mater.* 434 (1-3) (2013) 223-229.
- [107] G.P. Halbfinger, M. Kolodney, "Activated Sintering of ThO<sub>2</sub> and ThO<sub>2</sub>-Y<sub>2</sub>O<sub>3</sub> with NiO", *J. Am. Ceram. Soc.* 55(10) (1972) 519-524.
- [108] A. Baena, T. Cardinaels, J. Vleugels, K. Binnemans, M. Verwerft, "Activated sintering of ThO<sub>2</sub> with Al<sub>2</sub>O<sub>3</sub> under reducing and oxidizing conditions", *J. Nucl. Mater.* 470 (2016) 34-43.
- [109] K. Ananthasivan, S. Anthonysamy, C. Sudha, A.L.E. Terrance, P.R. Vasudeva Rao, "Thoria doped with cations of group VB-synthesis and sintering", *J. Nucl. Mater.* 300(2-3) (2002) 217-229.
- [110] T.R.G. Kutty, P.V. Hegde, K.B. Khan, T. Jarvis, A.K. Sengupta, S. Majumdar, H.S. Kamath, "Characterization and densification studies on ThO<sub>2</sub>-UO<sub>2</sub> pellets derived from ThO<sub>2</sub> and U<sub>3</sub>O<sub>8</sub> powders", *J. Nucl. Mater.* 335 (3) (2004) 462-470.
- [111] V. Tyrpekl, M. Cologna, D. Robba, J. Somers, "Sintering behaviour of nanocrystalline ThO<sub>2</sub> powder using spark plasma sintering", *J. Eur. Ceram. Soc.* 36(3) (2016) 767-772.

- [112] W. Straka, S. Amoah, J. Schwartz, “Densification of thoria through flash sintering”, *MRS Commun.* 7(3) (2017) 677-682.
- [113] D. Sanjay Kumar, K. Ananthasivan, R.V. Krishnan, S. Amirthapandian, A. Dasgupta, “Studies on the synthesis of nanocrystalline  $Y_2O_3$  and  $ThO_2$  through volume combustion and their sintering”, *J. Nucl. Mater.* 479 (2016) 585-592.
- [114] R.D. Purohit, S. Saha, A.K. Tyagi, “Nanocrystalline thoria powders via glycine-nitrate combustion” *J. Nucl. Mater.* 288 (1) (2001) 7-10. [114a] F. Cappia, D. Hudry, E. Courtois, A. Janßen, L. Luzzi, R.J.M. Konings, D. Manara, High-temperature and melting behavior of nanocrystalline refractory compounds: an experimental approach applied to thorium dioxide, *Mater. Res. Express* 1 (2014) 0250341-12.
- [115] J. Spino, K. Vennix, M. Coquerelle, “Detailed characterisation of the rim microstructure in PWR fuels in the burn-up range 40–67 GWd/tM”, *J. Nucl. Mater.* 231 (3) (1996) 179-190.
- [116] L. Bonato, M. Viot, X. Le Goff, P. Moisy, S.I. Nikitenko, “Sonochemical dissolution of nanoscale  $ThO_2$  and partial conversion into a thorium peroxo sulphate”, *Ultrason. Sonochem.* 69 (2020) 105235.
- [117] S. Dash, A. Singh, P.K. Ajikumar, H. Subramanian, M. Rajalakshmi, A.K. Tyagi, A.K. Arora, S.V. Narasimhan, B. Raj, “Synthesis and characterization of nanocrystalline thoria obtained from thermally decomposed thorium carbonate”, *J. Nucl. Mater.* 303 (2–3) (2002) 156-168.
- [118] S. Dash, R. Krishnan, M. Kamruddin, A.K. Tyagi, B. Raj, “Temperature programmed decomposition of thorium oxalate hexahydrate”, *J. Nucl. Mater.* 295(2-3) (2001) 281-289.

## References

- [119] S. Dash, M. Kamruddin, P.K. Ajikumar, A.K. Tyagi, B. Raj, S. Bera, S.V. Narasimhan, “Temperature programmed decomposition of thorium nitrate pentahydrate”, *J. Nucl. Mater.* 278 (2–3) (2000) 173-185.
- [120] T.V. Plakhova, A.Y. Romanchuk, D.V. Likhosherstova, A.E. Baranchikov, P.V. Dorovatovskii, R.D. Svetogorov, T.B. Shatalova, T.B. Egorova, A.L. Trigub, K.O. Kvashnina, V.K. Ivanov, S.N. Kalmykov, “Size effects in nanocrystalline thoria”, *J. Phys. Chem. C* 123 (37) (2019) 23167-23176. [120a] D. Hudry, C. Apostolidis, O. Walter, T. Gouder, E. Courtois, C. Kübel, D. Meyer, Controlled Synthesis of Thorium and Uranium Oxide Nanocrystals, *Chem. Eur. J.*, 19 (2013) 5297-5305.
- [121] F. Deganello, A.K. Tyagi, “Solution combustion synthesis, energy and environment: Best parameters for better materials”, *Prog. Cryst. Growth Char.* 64 (2018) 23-61.
- [122] A. Varma, A.S. Mukasyan, A.S. Rogachev, K.V. Manukyan, “Solution combustion synthesis of nanoscale materials”, *Chem. Rev.* 116 (2016) 14493-14586.
- [123] V. Chandramouli, S. Anthonysamy, P.R. Vasudeva Rao, “Combustion synthesis of thoria - A feasibility study”, *J. Nucl. Mater.* 265(3) (1999) 255-261.
- [124] S. Anthonysamy, K. Ananthasivan, V. Chandramouli, I. Kaliappan, P.R. Vasudeva Rao, “Combustion synthesis of urania-thoria solid solutions”, *J. Nucl. Mater.* 278(2) (2000) 346-357.
- [125] D. Sanjay Kumar, K. Ananthasivan, S. Amirthapandian, A. Dasgupta, G. Jogeswara Rao, “Citrate gel-combustion synthesis and sintering of nanocrystalline ThO<sub>2</sub> powders”, *J. Nucl. Mater.* 497 (2017) 16-29.
- [126] R.D. Purohit, S. Saha, A.K. Tyagi, “Combustion synthesis of 5 and 10 mol% YO<sub>1.5</sub> doped ThO<sub>2</sub> powders”, *J. Nucl. Mater.* 323 (1) (2003) 36-40.

- [127] K.C. Patil, M.S. Hegde, T. Rattan, S.T. Aruna, "Chemistry of nanocrystalline oxide materials combustion synthesis, properties and applications", World Scientific Publications (2008) (DOI: <https://doi.org/10.1142/6754>).
- [128] F.-T Li, J. Ran, M. Jaroniec, S.Z. Qiao, "Solution combustion synthesis of metal oxide nanomaterials for energy storage and conversion", *Nanoscale* 7(42) (2015) 17590-17610.
- [129] A. Kumar, E.E. Wolf, A.S. Mukasyan, "Solution combustion synthesis of metal nanopowders: nickel-reaction pathways", *AIChE J.* 57(8) (2011) 2207-2214.
- [130] A. Kumar, E.E. Wolf, A.S. Mukasyan, "Solution combustion synthesis of metal nanopowders: Copper and copper / nickel alloys", *AIChE J.* 57(12) (2011) 3473-3479.
- [131] S. Zhang, Z.A. Munir, "The combustion synthesis of refractory nitrides: Part II the synthesis of niobium nitride", *J. Mater. Sci.* 26 (1991) 3380–3385.
- [132] "Nitride ceramics: Combustion synthesis, properties, and applications", (Eds.: A.A. Gromov, L.N. Chukhlomina) Wiley-VCH Verlag GmbH (2015) (DOI:10.1002/9783527684533).
- [133] H.V. Kirakosyan, K.T. Nazaretyan, R.A. Mnatsakanyan, S.V. Aydinyan, S.L. Kharatyan, "Solution combustion synthesis of nanostructured molybdenum carbide", *J. Nanopart. Res.* 20 (2018) 214.
- [134] N.A. Marand, S.M. Masoudpanah, M. Sh. Bafghi, "Solution combustion synthesis of nickel sulfide composite powders", *Ceram. Int.* 44 (14) (2018) 17277-17282.
- [135] K. Rajeshwar, N.R. De Tacconi, "Solution combustion synthesis of oxide semiconductors for solar energy conversion and environmental remediation", *Chem. Soc. Rev.* 38 (7) (2009) 1984-1998.

- [136] K.C. Thomas, J.R. Kale, R.G. Dalavi, K. Venkatesh, R. Kameswaran, A.V.R. Reddy  
"Development of an IR-based carbon analyser for uranium metal", BARC Newsletter  
311 (2009) 2-6 (Web-link: <http://barc.gov.in/publications/nl/2009/200912.pdf/>)
- [137] B.D. Cullity, "Elements of X-ray diffraction", Addison-Wesley Publishing Company  
Inc. (1956).
- [138] R. Tilley, "Crystals and crystal structures", John Wiley & Sons, Ltd. (2006) (ISBN-13  
978-0-470-01820-0).
- [139] E. Smith, G. Dent, "Modern Raman spectroscopy - A practical approach", John Wiley  
& Sons, Ltd. (2006) (ISBN 0-471-49794-0).
- [140] M. Roessle, D.I. Svergun, "Small angle X-ray scattering", In "Encyclopaedia of  
biophysics" (Eds.: G.C.K. Roberts) Springer, Berlin, Heidelberg (2013) (DOI:  
[https://doi.org/10.1007/978-3-642-16712-6\\_284](https://doi.org/10.1007/978-3-642-16712-6_284)).
- [141] P.W. Schmidt, R. Height, "Slit height corrections in small angle X-ray scattering", Acta  
Crystallogr. 13 (1960) 480-483.
- [142] G. Höhne, W.F. Hemminger, H.J. Flammersheim, "Differential scanning calorimetry",  
Springer-Verlag. (2003) (ISBN 978-3-540-00467-7).
- [143] M. Reading, A. Luget, R. Wilson, "Modulated differential scanning calorimetry",  
Thermochim. Acta 238(C) (1994) 295-307.
- [144] J.E.K. Schawe, T. Hutter, C. Heitz, I. Alig, D. Lellinger, "Stochastic temperature  
modulation: A new technique in temperature-modulated DSC", Thermochim. Acta 446  
(2006) 147-155.
- [145] N. Manoj, D. Jain, J.K. Gautam, K.C. Thomas, V. Sudarsan, C.G.S. Pillai, R.K. Vatsa,  
A.K. Tyagi, "A simple, reliable and cost-effective, high temperature dilatometer for  
bulk thermal expansion studies on solids", Measurement 92 (2016) 318-325.

- [146] W.J. Parker, R.J. Jenkins, C.P. Butler, G.L. Abbott, “Flash method of determining thermal diffusivity, heat capacity, and thermal conductivity”, *J. Appl. Phys.* 32 (1961) 1679-1684.
- [147] H.S. Carslaw, J.C. Jaeger, “Conduction of heat in solids”, 2nd edition, Oxford University Press, New York, (1959).
- [148] D. Jain, D. Das, B.N. Jagatap, “Thorium-based fuels for advanced nuclear reactors: Thermophysical, thermochemical and thermodynamic properties”, in A.K. Nayak, B.R. Sehgal (Eds.), *Thorium—Energy for the Future*, Springer (2019) (ISBN 978-981-13-2658-5) 257-275.
- [149] Y.S. Touloukian, R.W. Powell, C.Y. Ho, P.G. Klemens, “Thermophysical properties of matter - The TPRC data series. Volume 1. Thermal conductivity - metallic elements and alloys”, (1970) 429-440; 381-384.
- [150] Y.S. Touloukian, R.W. Powell, C.Y. Ho, M.C. Nicolaou, “Thermophysical properties of matter - The TPRC data series. Volume 10. Thermal diffusivity”, (1974) 205-208.
- [151] Y.S. Touloukian, E.H. Buyco, “Thermophysical properties of matter - The TPRC data series. Volume 4. Specific heat - metallic elements and alloys”, (1971) 268-270.
- [152] Y.S. Touloukian, R.K. Kirby, R.E. Taylor, P.D. Desai, “Thermophysical properties of matter - The TPRC data series. Volume 12. Thermal expansion metallic elements and alloys”, (1975) 365-372.
- [153] H.G. Schettler, J.J. Martin, F.A. Schmidt, G.C. Danielson, “Thermal conductivity of high purity thorium”, *Phys. Rev.* 187 (3) (1969) 801-804.
- [154] T.A. Sandenaw, “Thermal conductivity of uranium: Effects of purity and microstructure”, Report no.: LA-6092-MS, United States (1975) 1-8.
- [155] Y. Takahashi, M. Yamawaki, K. Yamamoto, “Thermophysical properties of uranium-zirconium alloys”, *J. Nucl. Mater.* 154 (1988) 141-144.

- [156] R.W. Logan, D.H. Wood, "Thermal expansion of rolled and extruded uranium", *J. Less-Common Met.* 90 (1983) 233-241.
- [157] J. Nakamura, Y. Takahashi, S. Izumi, M. Kanno, "Heat capacity of metallic uranium and thorium from 80 to 1000 K", *J. Nucl. Mater.* 88 (1980) 64-72.
- [158] M. Boivineau, H. Colin, J.M. Vermeulen, Th. Thévenin, "Thermophysical properties of solid and liquid thorium", *Int. J. Thermophys.* 17(5) (1996) 1001-1010.
- [159] S. Zhou, R. Jacobs, W. Xie, E. Tea, C. Hin, D. Morgan, "Combined ab-initio and empirical model of the thermal conductivity of uranium, uranium-zirconium, and uranium-molybdenum", *Phys. Rev. Mater.* 2 (2018) 083401-1-21.
- [160] Y. Li, A. Chernatynskiy, J.R. Kennedy, S.B. Sinnott, S.R. Phillpot, Lattice expansion by intrinsic defects in uranium by molecular dynamics simulation, *J. Nucl. Mater.* 475 (2016) 6-18.
- [161] K.D. Joshi, S.C. Gupta, S. Banerjee, "Ab-initio theoretical analysis of thermal expansivity, thermal vibrations and melting of thorium", *Phil. Mag.* 88 (27) (2008) 3145-3152.
- [162] S. Jaroszewicz, H.O. Mosca, J.E. Garcés, "The temperature behaviour of the elastic and thermodynamic properties of fcc thorium", *J. Nucl. Mater.* 429(1-3) (2012) 136-142.
- [163] L. Kývala, D. Legut, "Lattice dynamics and thermal properties of thorium metal and thorium monocarbide" *Phys. Rev. B* 101 (2020) 075117.
- [164] P.L. Vijay, J.C. Sehra, C.V. Sundaram, K.R. Gurumurthy, R.V. Raghavan, "Studies on the preparation of thorium metal sponge from thorium oxalate", *BARC Report no.:* 969 (1978) 1-11.
- [165] M.D. Smith, R.W.K. Honeycombe, "The effect of oxygen, carbon and nitrogen on the properties of sintered thorium", *J. Nucl. Mater.* 4 (1959) 345-355.

- [166] Inorganic Crystal Structure Database (ICSD FIZ Karlsruhe GmbH, Version 4.4.0 (2020); collection code: 653236); from: J. Bohet, W. Müller, “Preparation and structure studies of “Van Arkel” protactinium”, *J. Less-Common Met.* 57 (2) (1978) 185-1995.
- [167] International Centre for Diffraction Data (ICDD Database; JCPDF card no.: 720659).
- [168] Inorganic Crystal Structure Database (ICSD FIZ Karlsruhe GmbH, Version 4.4.0 (2020) collection code: 253564) from: V.K. Tripathi, R. Nagarajan, “Sol–gel synthesis of high-purity actinide oxide ThO<sub>2</sub> and its solid solutions with technologically important tin and zinc ions” *Inorg. Chem.* 55 (24) (2016) 12798-12806.
- [169] Inorganic Crystal Structure Database (ICSD FIZ Karlsruhe GmbH, Version 4.4.0 (2020) collection code: 35204); from: S.A. Barrett, A.J. Jacobson, B.C. Tofield, B.E.F. Fender, “The preparation and structure of barium uranium oxide BaUO<sub>3+x</sub>”, *Acta Crystallogr. B* 38 (1982) 2775-2781. [169a] S. Ellison, A. Williams, *Eurachem / CITAC guide: Quantifying Uncertainty in Analytical Measurement* (2012) ISBN 978-0-948926-30-3 (Web-link: [www.eurachem.org](http://www.eurachem.org)).
- [170] Inorganic Crystal Structure Database (ICSD FIZ Karlsruhe GmbH, Version 4.4.0 (2020) collection code: 24223); from: R.E. Rundle, N.C. Baenziger, A.S. Wilson, R.A. McDonald, “The structures of the carbides, nitrides and oxides of uranium”, *J. Am. Chem. Soc.* 70 (1948) 99-105.
- [171] Inorganic Crystal Structure Database (ICSD FIZ Karlsruhe GmbH, Version 4.4.0 (2020) collection code: 26476); from: A.E. Austin, “Carbon positions in uranium carbides”, *Acta Crystallogr.* 12 (1959) 159-161.
- [172] “Augmented uranium metal production facility”, *BARC Newsletter* 200 (2000) 15-18 (Web-link: <http://barc.gov.in/publications/nl/2000/200009.pdf>).
- [173] G.C. Allen, P.M. Tucker, “Surface oxidation of uranium metal as studied by X-ray photoelectron spectroscopy”, *J. Chem. Soc. Dalton* 5 (1973) 470-474.

- [174] R. Rao, R.K. Bhagat, N.P. Salke, A. Kumar, "Raman spectroscopic investigation of thorium dioxide-uranium dioxide ( $\text{ThO}_2\text{-UO}_2$ ) fuel materials", *Appl. Spectrosc.* 68(1) (2014) 44-48.
- [175] "Thermophysical properties of materials for nuclear engineering: A tutorial and collection of data", (IAEA-THPH), International Atomic Energy Agency, Vienna (2008).
- [176] I.F. Barwood, B.R. Butcher, "The  $\alpha \rightarrow \beta$  phase transformation in uranium", *J. Nucl. Mater.* 8 (1963) 232-240.
- [177] C. Yoo, H. Cynn, P. Söderlind, "Phase diagram of uranium at high pressures and temperatures", *Phys. Rev. B* 57 (1998) 10359-10362.
- [178] P. Zhou, X. Wang, H. Yang, X. Fu, "Effect of vacuum heat treatment on oxidation of uranium surfaces", *Rare Metal Mat. Eng.* 37 (2008) 94-97.
- [179] G. Erez, U. Even, "The Wiedemann-Franz ratio of metallic uranium at elevated temperatures", *J. Appl. Phys.* 37 (1966) 4633-4644.
- [180] S. Nasu, S. Fukushima, T. Ohmichi, T. Kikuchi, "Thermal diffusivity of uranium by laser pulse method from 20° to 850°C", *Jap. J. Appl. Phys.* 7 (1968) 682.
- [181] D. Jain, C.G.S. Pillai, B.S. Rao, R.V. Kulkarni, E. Ramdasan and K.C. Sahoo, "Thermal diffusivity and thermal conductivity studies on thoria-lanthana solid solutions up to 10 mol. %  $\text{LaO}_{1.5}$ ", *J. Nucl. Mater.* 353 (2006) 35-41.
- [182] S.S. Parker, J.T. White, P. Hosemann, A.T. Nelson, "Thermophysical properties of thorium mononitride from 298 to 1700 K", *J. Nucl. Mater.* 526 (2019) 151760.
- [183] H. He, J. Majewski, D.D. Allred, P. Wang, X. Wen, K.D. Rector, "Formation of solid thorium monoxide at near-ambient conditions as observed by neutron reflectometry and interpreted by screened hybrid functional calculations", *J. Nucl. Mater.* 487 (2017) 288-296.

## References

- [184] B.R. Butcher, A.H. Rowe, "Phase transformation in uranium", *Nature* (1953) 817.
- [185] H.H. Klpefer, P. Chiotti, "Characteristics of the solid state transformations in uranium", USAEC Report no.: ISC-893 (1957) 1-113.
- [186] W.S. Blackburn, " $\alpha$ - $\beta$  Thermal cycling of uranium", *J. Nucl. Mater.* 2 (1960) 191.
- [187] J.J. Stobo, "Alpha beta cycling of uranium", *J. Nucl. Mater.* 2 (1960) 97-109.
- [188] L.T. Lloyd, "Thermal expansion of alpha-uranium single crystals", *J. Nucl. Mater.* 3 (1961) 67-71.
- [189] L.T. Lloyd, C.S. Barrett, "Thermal expansion of alpha uranium", *J. Nucl. Mater.* 18 (1966) 55-59.
- [190] E.S. Fisher, "Preparation of alpha uranium single crystals by a grain-coarsening method", *J. Metals* 9 (1957) 882-888.
- [191] D.C. Wallace, "Specific heat of thorium at high temperatures", *Phys. Rev.* 120 (1) (1960) 84-88.
- [192] E.A. Mit'kina, "Experimental determination of the true specific heats of uranium, thorium, and other metals", *Sov. Atom Energy* 7 (2) (1959) 163-165.
- [193] F.L. Oetting, D.T. Peterson, "Heat capacity of well characterized thorium metal from 298 to 700 K", *J. Less-Common Met.* 128 (1987) 231-239.
- [194] D.C. Ginnings, R.J. Corruccini, "Heat capacities at high temperatures of uranium, uranium trichloride, and uranium tetrachloride, *J. Res. Nat. Bur. Stand.* 39 (1947) 309-316.
- [195] F.K. Oetting, M.H. Rand, R.J. Ackermann, "The chemical thermodynamics of actinide elements and compounds, Part 1, The actinide elements", International Atomic Energy Agency (IAEA), Vienna (1976).
- [196] A.L. Loeb, "Thermal conductivity: VIII, A theory of thermal conductivity of porous materials", *J. Am. Ceram. Soc.* 37 (1954) 96-99.

## References

- [197] S. Kaity, J. Banerjee, M.R. Nair, K. Ravi, S. Dash, T.R.G. Kutty, A. Kumar, R.P. Singh, "Microstructural and thermophysical properties of U-6 wt.% Zr alloy for fast reactor application", *J. Nucl. Mater.* 427 (2012) 1-11.
- [198] C. Hin, "Thermal conductivity of metallic uranium", NEUP 14-6767 (2018) (Web-link: <https://www.osti.gov/servlets/purl/1433931>).
- [199] M. Floyd, B. Bromley, J. Pencer, "A Canadian perspective on progress in thorium fuel science and technology", *CNL Nucl. Rev.* 6 (1) (2017) 1-17.
- [200] S. Thakur, P.S.R. Krishna, A.B. Shinde, R. Kumar, S.B. Roy, "Quantitative analysis of thorium phase in Th-U alloys using diffraction studies", *AIP Conf. Proc.* 1832 (2017) 060012.
- [201] P. Chiotti, "High temperature crystal structure of thorium", *J. Electrochem. Soc.* (1955) 567-570.
- [202] G.G. Bente, "A Physical Metallurgical Study of Thorium-Rich Thorium-Uranium Alloys", Report no.: NAA-SR-2069 (1958).
- [203] G.H. Bannister, R.C. Burnett, J.R. Murray, "Ageing and hot hardness characteristics of certain thorium alloys", *J. Nucl. Mater.* 2(1) (1960) 51-61.
- [204] "Chemical technology division annual technical report for 1986," ANL-87-19, Argonne National Laboratory (1987) 122.
- [205] V. Crewe, S. Lawroski, "Reactor development program progress report", Argonne National Laboratory, ANL-7230, Lemont, IL, USA (1966).
- [206] O. Beneš D. Manara R.J.M. Konings, "Thermodynamic assessment of the Th-U-Pu system", *J. Nucl. Mater.* 449 (1-3) (2014) 15-22.
- [207] S. Kneppel, "Aqueous corrosion of thorium alloys and zircaloy-clad thorium alloys", NMI-1226, United States Atomic Energy Commission (1960) 1-49 (Web-link: <https://play.google.com/books/reader?id=OGCWvHY4xRwC&hl=en&pg=GBS.PA1>)

- [208] D.S. Evans, G.V. Raynor, "The solubility of zirconium in  $\alpha$ -thorium", *J. Nucl. Mater.* 4 (1) (1961) 66-69.
- [209] R.I. Sheldon, D.E. Peterson, "The (U-Zr) Uranium-zirconium system", *Bull. Alloy Phase Diagr.* 10 (2) (1989) 165-171.
- [210] O.N. Carlson, "Some studies on the uranium-thorium-zirconium ternary alloy system", AECD-3206, United States Atomic Energy Commission (1950) 1-72.
- [211] J.W. Goffard, R.K. Marshall, "Irradiation behavior of Zircaloy-2 clad thorium-uranium-zirconium alloy fuel elements Interim report 1", BNWL-479, Pacific Northwest Laboratory, United States Atomic Energy Commission (1967).
- [212] T. Okawa, S. Nakayama, H. Sekimoto, "Design study on power flattening to sodium cooled large-scale CANDLE burning reactor with using thorium fuel", *Energ. Convers. Manage.* 53 (1) (2012) 182-188.
- [213] Inorganic crystal Structure Database (ICSD FIZ Karlsruhe GmbH, Version 4.4.0 (2020) collection code: 164572) from: A.I. Kolesnikov, A.M. Balagurov, I.O. Bashkin, A.V. Belushkin, E.G. Ponyatovsky, M. Prager, "Neutron scattering studies of ordered gamma -ZrD", *J. Phys. Condens-Mat.* 6 (43) (1994) 8977-8988.
- [214] Inorganic crystal Structure Database (ICSD FIZ Karlsruhe GmbH, Version 4.4.0 (2020) collection code: 16559) from: B.O. Loopstra, "Neutron diffraction investigation of  $U_3O_8$ ", *Acta Crystallogr.* 17 (1964) 651-654.
- [215] Inorganic crystal Structure Database (ICSD FIZ Karlsruhe GmbH, Version 4.4.0 (2020) collection code: 246035) from: S.K. Sali, N.K. Kulkarni, K. Krishnan, S.N. Achary, A.K. Tyagi, "Oxidation / reduction studies on  $Zr_yU_{1-y}O_{2+x}$  and delineation of a new orthorhombic phase in U-Zr-O system", *J. Solid-State Chem.* 181 (8) (2008) 1859-1866.

## References

- [216] Inorganic crystal Structure Database (ICSD FIZ Karlsruhe GmbH, Version 4.4.0 (2020) collection code: 108756) from: H.L. Luo, J.G. Huber, “Superconductivity in Th-Zr alloys”, *J. Less-Common Met.* 65 (1) (1979) 13-17.
- [217] J.M. Elorrieta, L.J. Bonales, M. Naji, D. Manara, V.G. Baonza, J. Cobos, “Laser-induced oxidation of  $\text{UO}_2$ : A Raman study”, *J. Raman Spectrosc.* 49 (5) (2018) 878-884.
- [218] H. He, D. Shoesmith, “Raman spectroscopic studies of defect structures and phase transition in hyper-stoichiometric  $\text{UO}_{2+x}$ ”, *Phys. Chem. Chem. Phys.* 12 (2010) 8109-8118.
- [219] X. Zhao, D. Vanderbilt, “Phonons and lattice dielectric properties of zirconia”, *Phys. Rev. B* 65 (2002) 075105.
- [220] E. Hashem, A. Seibert, J-F. Vigier, M. Naji, S. Mastromarino, A. Ciccioli, D. Manara, “Solid-liquid equilibria in the  $\text{ThO}_2$ - $\text{ZrO}_2$  system: An experimental study” *J. Nucl. Mater.* 521 (2019) 99-108.
- [221] O.N. Carlson, E.R. Stevens, “A compilation of thorium binary phase diagrams”, USAEC Report (1968) (Web-link: <https://www.osti.gov/servlets/purl/4529064>).
- [222] G.B. Skinner, H.L. Johnston, “Thermal Expansion of zirconium between 298°K and 1600°K”, *J. Chem Phys.* 21 (1953) 1383.
- [223] P.L. Brown, E. Curti, B. Grambow, C. Ekberg, “Chemical thermodynamics of zirconium”, OECD Nuclear energy agency, data bank (Eds.: F.J. Mompean, J. Perrone, M. Illemassene) (2005) (Web-link: <https://www.oecd-nea.org/dbtdb/pubs/vol8-zirconium.pdf>).
- [224] C.G.S. Pillai, P. Raj, “Thermal Conductivity of  $\text{ThO}_2$  and  $\text{Th}_{0.98}\text{U}_{0.02}\text{O}_2$ ”, *J. Nucl. Mater.* 277 (2000) 116-119.

- [225] S.S. Manoharan, K.C. Patil, "Combustion synthesis of metal chromite powders", *J. Am. Ceram. Soc.* 75 (1992) 1012-1015.
- [226] S.R. Jain, K.C. Adiga, V.R. Pai Verneker, "A new approach to thermochemical calculations of condensed fuel-oxidizer mixtures," *Combust. Flame* 40 (6) (1981) 71-79.
- [227] S. Roy, A. Das Sharma, S.N. Roy, H.S. Maiti, "Synthesis of  $\text{YBa}_2\text{Cu}_3\text{O}_{7-x}$  Powder by Autoignition of Citrate-Nitrate Gel", *J. Mater. Res.* 8(11) (1993) 2761-2766.
- [228] M. Gizowska, I. Kobus, K. Perkowski, M. Piatek, G. Konopka, I. Witosławska, M. Osuchowski, "Size and morphology of yttria nanopowders obtained by solution combustion synthesis" *Arch. Metall. Mater.* 63(2) (2018) 743-748.
- [229] G.A.M. Hussein, H.M. Ismail, "Texture assessment of thoria as a final decomposition product of hydrated thorium nitrate and oxycarbonate", *Colloids Surf. A*: 99 (1995) 129-139.
- [230] I.M. Weiss, C. Muth, R. Drumm, H.O.K. Kirchner, "Thermal decomposition of the amino acids glycine, cysteine, aspartic acid, asparagine, glutamic acid, glutamine, arginine and histidine", *BMC Biophys.* 11 (2018) 1-15.
- [231] N. Raje, A.V.R. Reddy, "Mechanistic aspects of thermal decomposition of thorium oxalate hexahydrate: A review", *Thermochim. Acta* 505 (2010) 53-58.
- [232] H. Hayashi, T. Watanabe, "Properties of thoria obtained by thermal decomposition of thorium salts", *Nippon Kagaku Kaishi* 4 (1973) 858-860.
- [233] Y. Saito, "Thermal decomposition of thorium oxalate", *J. Jpn. Soc. Powder Metall.* 17(1971) 235-242.
- [234] M.T. Aybers, "Kinetic study of the thermal decomposition of thorium oxalate dehydrate", *J. Nucl. Mater.* 252 (1998) 28-33.
- [235] D.Y. Chung, E. H. Lee, "Microwave-induced combustion synthesis of  $\text{Ce}_{1-x}\text{Sm}_x\text{O}_{2-x/2}$  powder and its characterization", *J. Alloys Compd.* 374 (2004) 69-73.

## References

- [236] “The Aldrich Library of FT-IR Spectra, Edition-II, Volume-1”, 1 898 A 897-898.
- [237] S. Kumar, A.K. Rai, V.B. Singh, S.B. Rai, “Vibrational spectrum of glycine molecule”, *Spectrochim. Acta A* 61 (2005) 2741-2746.
- [238] J. R. Ferraro, A. Walker, “Comparison of the infrared spectra of the hydrates and anhydrous salts in the systems  $\text{UO}_2(\text{NO}_3)_2$  and  $\text{Th}(\text{NO}_3)_4$ ”, *J. Chem. Phys.* 45 (1966) 550-552.
- [239] J.H-Paredes, D.G-Mitnik, H.E. E-Ponce, M.E. A-Ramos, A.D-Moller, “Band structure, optical properties and infrared spectrum of glycine–sodium nitrate crystal”, *J. Mole. Str.* 875 (2008) 295-301.
- [240] S.L. Estes, M.R. Antonio, L. Soderholm, “Tetravalent Ce in the nitrate-decorated hexanuclear cluster  $[\text{Ce}_6(\mu_3\text{-O})_4(\mu_3\text{-OH})_4]^{12+}$ : A structural end point for ceria nanoparticles, *J. Phys. Chem. C* 120 (2016) 5810-5818.
- [241] M. Rand, L. Fuger, I. Grenthe, V. Neck, D. Rai, “Chemical thermodynamics: Chemical thermodynamics of thorium”, (OECD, NEA-TDB) Vol. 11, Elsevier, Amsterdam (2007).
- [242] C. Hennig, K. Schmeide, V. Brendler, H. Moll, S. Tsushima, A.C. Scheinost, “EXAFS Investigation of U(VI), U(IV), and Th(IV) sulfato complexes in aqueous solution”, *Inorg. Chem.* 46 (2007) 5882-5892.
- [243] J. Rothe, M.A. Denecke, V. Neck, R. Muller, J.I. Kim, XAFS “Investigation of the structure of aqueous thorium(IV) species, colloids, and solid thorium(IV) oxide / hydroxide”, *Inorg. Chem.* 41 (2002) 249-258.
- [244] C. Hennig, S. Takao, K. Takao, S. Weiss, W. Kraus, F. Emmerling, A.C. Scheinosta, “Structure and stability range of a hexanuclear Th(IV)-glycine complex”, *Dalton Trans.* 41 (2012) 12818-12823.

## References

- [245] Y. Hu, K.E. Knope, S. Skanthakumar, L. Soderholm, "Understanding the ligand-directed assembly of a hexanuclear Th<sup>IV</sup> molecular cluster in aqueous solution", *Eur. J. Inorg. Chem.* 24 (2013) 4159-4163.
- [246] M. Nourmand, N. Meissami, "Complex formation between uranium(VI) and thorium (IV) ions with some  $\alpha$ -amino-acids", *J. Chem. Soc. Dalton* 8 (1983) 1529-1533.
- [247] Bismondo, L. Rizzo, G. Tomat, "Thermodynamic properties of actinide complexes. uranyl (VI)- and thorium (IV)-glycine systems", *Inorg. Chim. Acta* 74 (1983) 21-24.
- [248] B.G. Oliver, A.R. Davis, "The structure of aqueous thorium nitrate solution by laser Raman spectroscopy", *J. Inorg. Nucl. Chem.* 34 (1972) 2851-2860.
- [249] Z. Huang, X. Chen, Y. Li, J. Chen, J. Lin, J. Wang, J. Lei, R. Chen, "Quantitative determination of citric acid in seminal plasma by using Raman spectroscopy", *Appl. Spectrosc.* 67 (7) (2013) 757-760.
- [250] A.K. Arora, M. Rajalakshmi, T.R. Ravindran, V. Sivasubramanian, "Raman spectroscopy of optical phonon confinement in nanostructured materials", *J. Raman Spectrosc.* 38 (2007) 604-617.
- [251] D. Langmuir, J.S. Herman, "The mobility of thorium in natural waters at low temperatures", *Geochim. Cosmochim. Ac.* 44 (1980) 1753-1766.
- [252] M. Bobtelsky, B. Graus, "Thorium citrate complexes, their composition, structure and behavior", *J. Am. Chem. Soc.* 76 (6) (1954,) 1536-1539.
- [253] G.R. Choppin, H.N. Erten, Y. Xia, "Variation of stability constants of thorium citrate complexes with ionic strength", *Radiochim. Acta* 74 (1996) 123-127.
- [254] D.P. Raymond, J.R. Duffield, D.R. Williams, "Complexation of plutonium and thorium in aqueous environments", *Inorg. Chim. Acta* 140 (1987) 309-313.
- [255] M.M. Barbooti, D.A. Al-Sammerrai, "Thermal decomposition of citric acid", *Thermochim. Acta* 98 (1986) 119-126.

- [256] D. Hennings, W. Mayr, "Thermal decomposition of (BaTi) citrates into barium titanate", *J. Solid State Chem.* 26 (1978) 329-338.
- [257] N.S. Gajbhiye, S. Prasad, "Thermal decomposition of hexahydrated nickel iron citrate", *Thermochim. Acta* 285 (1996) 325-336.
- [258] J. Tsay, T. Fang, "Effects of molar ratio of citric acid to cations and of pH value on the formation and thermal-decomposition behavior of barium titanium citrate", *J. Am. Ceram. Soc.* 82(6) (1999) 1409-1415.
- [259] A. Marcilla, A. Gómez-Siurana, M. Beltrán, I. Martínez-Castellanos, I. Blasco, D. Berenguer, "TGA-FTIR study of the pyrolysis of sodium citrate and its effect on the pyrolysis of tobacco and tobacco/SBA-15 mixtures under N<sub>2</sub> and air atmospheres", *J. Sci. Food Agr.* 98 (15) (2018) 5916-5931.
- [260] O. Glatter, O. Kratky, "Small angle X-ray scattering", Academic, London (1982).
- [261] A. Guinier, G. Fournet, "Small angle scattering of X-rays", Wiley, New York (1955).
- [262] J. Aitchison, J.A.C. Brown, "The log normal distribution", Cambridge University Press, Cambridge (1957).
- [263] R.D. Purohit, B.P. Sharma, K.T. Pillai, A.K. Tyagi, "Ultrafine ceria powders via glycine-nitrate combustion", *Mater. Res. Bull.* 36 (15) (2001) 2711-2721.
- [264] V.R. Choudhary, A.M. Rajput, B. Prabhakar, A.S. Mamman, "Partial oxidation of methane to CO and H<sub>2</sub> over nickel and/or cobalt containing ZrO<sub>2</sub>, ThO<sub>2</sub>, UO<sub>2</sub>, TiO<sub>2</sub> and SiO<sub>2</sub> catalysts", *Fuel* 77 (15) (1998) 1803-1807.
- [265] V. Múčka, J. Podlaha, R. Silber, "NiO-ThO<sub>2</sub> mixed catalysts in hydrogen peroxide decomposition and influence of ionizing radiation", *Radiat. Phys. Chem.* 59 (5-6) (2000) 467-475.

## References

- [266] P. Balakrishna, B.N. Murty, K.P. Chakraborty, R.N. Jayaraj, C. Ganguly, "Special features in powder preparation, pressing, and sintering of uranium dioxide", *Mater. Manuf. Process.* 15(5) (2000) 679-693.
- [267] C.S. Morgan, K.H. McCorkle, G.L. Powell, "Sintering and desintering of thoria", In: Kuczynski G.C. (Eds.) *Sintering and Related Phenomena*. Materials Science Research, Vol. 6, Springer, Boston, MA (1973).
- [268] J.M. Pope, K.C. Radford, "Physical properties of some thoria powders and their influence on sinterability", *J. Nucl. Mater.* 52 (1974) 241-254.
- [269] Z. Chen, J. Mabon, J. Wen, R. Trice, "Degradation of plasma-sprayed yttria-stabilized zirconia coatings via ingress of vanadium oxide", *J. Eur. Ceram. Soc.* 29(9) (2009) 1647-1656.
- [270] M.A. Delfrate, J. Lemaitre, V. Buscaglia, M. Leoni, P. Nanni, "Slip casting of submicron BaTiO<sub>3</sub> produced by low-temperature aqueous synthesis", *J. Eur. Ceram. Soc.* 16(9) (1996) 975-984.
- [271] T.K. Gupta, R.L. Coble, "Sintering of ZnO: II, density decrease and pore growth during the final stage of the process", *J. Am. Ceram. Soc.* 51 (9) (1968) 525-528.
- [272] C.-H. Chang, J.F. Rufner, K.V. Benthem, R.H.R. Castro, "Design of desintering in tin dioxide nanoparticles", *Chem. Mater.* 25(21) (2013) 4262-4268.
- [273] P. Duran, J. Tartaj, C. Moure, "Sintering behaviour and microstructural evolution of agglomerated spherical particles of high-purity barium titanate", *Ceram. Int.* 29(4) (2003) 419-425.
- [274] C.-Y. Tsao, W.-H. Tuan, K.-C. Feng, "De-sintering of Ba<sub>5</sub>Nb<sub>4</sub>O<sub>15</sub> ceramic and its influence on microwave characteristics", *J. Eur. Ceram. Soc.* 37(4) (2017) 1517-1521.
- [275] Cs. Balázsi, F.S. Cinar, O. Addemir, F. Wéber, P. Arató, "Manufacture and examination of C/Si<sub>3</sub>N<sub>4</sub> nanocomposites" *J. Eur. Ceram. Soc.* 24(12) (2004) 3287-3294.

- [276] R. Besler, M.R. da Silva, J.J. do Rosario, M. Dosta, S. Heinrich, R. Janssen, “Sintering simulation of periodic macro porous alumina”, *J. Am. Ceram. Soc.* 98(11) (2015) 3496-3502.
- [277] K. Ananthasivan, S. Anthonysamy, A. Singh, P.R. Vasudeva Rao, “De-agglomeration of thorium oxalate - A method for the synthesis of sinter active thoria”, *J. Nucl. Mater.* 306 (1) (2002) 1-9.
- [278] R.H.R. Castro, “Controlling sintering and grain growth of nanoceramics”, *Cerâmica* 65 (373) (2019) 122-129. **[278a]** Thermodynamics of sintering, R.M. German, *Sintering of advanced materials: Fundamentals and processes* (Ed.: Z.Z. Fang) Woodhead Publishing Ltd. (2010), ISBN 978-1-84569-562-0. **[278b]** G.S. Upadhyaya, *Sintered metallic and ceramic Materials*, John Wiley & Sons Ltd. (1999) ISBN 0-471-98155-9.
- [279] O. Sudre, F.F. Lange, “The effect of inclusions on densification; III, The desintering phenomenon”, *J. Am. Ceram. Soc.* 75 (12) (1992) 3241-3251.
- [280] F. Li, J. Pan, A. Cocks, “Defect healing and cracking in ceramic films during constrained sintering” *J. Am. Ceram. Soc.* 95(12) (2012) 3743-3749.
- [281] S. Knight, R. Korlacki, C. Dugan, J.C. Petrosky, A. Mock, P.A. Dowben, J. Matthew Mann, M.M. Kimani, M. Schubert, “Infrared-active phonon modes in single-crystal thorium dioxide and uranium dioxide”, *J. Appl. Phys.* 127 (2020) 125103.

## Thesis Highlight

**Name of the Student:** Dheeraj Jain  
(Enrolment no.: CHEM 01201204014 dated 01.09.2012)

**Name of the CI/OCC:** BARC, Mumbai

**Thesis Title:** Preparation, characterization and thermophysical investigations on thorium-based nuclear fuels and related systems

**Discipline:** Chemical Sciences      **Sub-Area of Discipline:** Nuclear Materials

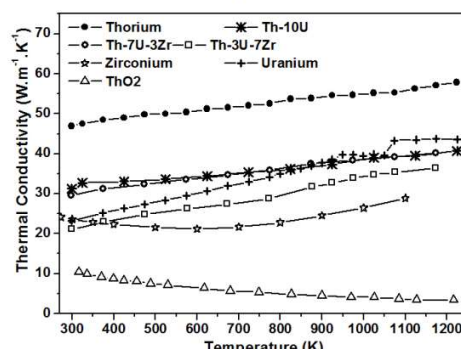
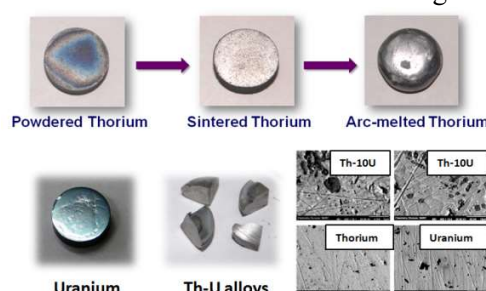
**Date of viva voce:** 28 January 2021

Thorium-based nuclear fuels are being developed in India in line with the three-stage nuclear energy program spearheaded by Department of Atomic Energy. Development of advanced fuels that can be utilized in thermal and fast neutron spectrum is essential. Bulk metallic alloys and oxides with nano / sub-micron grain structure are potential fuels. For development of new fuels, reliable data on their physico-chemical properties are needed, which are scarcely available for thorium-based metallic alloys.

To address this, Th-U binary alloys (Th-10U, Th-20U), Th-U-Zr ternary alloys (Th-7U-3Zr, Th-3U-7Zr) and their constituent metals have been investigated during the doctoral research presented in this thesis. Reliable experimental database on high temperature thermophysical properties of these alloys has been established over 298 K to 1373 K. Effect of structural phase transformations in uranium (orthorhombic  $\rightarrow$  tetragonal  $\rightarrow$  cubic) on its thermophysical properties has been established. Obtained results demonstrate that studied alloys are excellent dispersion-fuel options consisting of uranium-rich phase(s) uniformly dispersed in thorium-rich matrix, which result into isotropic swelling behavior and superior heat transport properties as compared to U-Zr / U-Pu-Zr alloys. Effect of impurities on thermophysical properties of alloys has been

discussed, which would enable development of better fuel performance and safety analysis codes. Effect of thermal cycling on thermophysical properties of as-cast ternary alloys has also been established.

For development of nanocrystalline oxide nuclear fuels, solution combustion synthesis of nanocrystalline ThO<sub>2</sub> has been investigated using thermal analysis and spectroscopic techniques and mechanisms of combustion proceeding via thermal evolution of Th(IV)-glycine-nitrate and Th(IV)-citrate-nitrate molecular complexes have been proposed. Role of fuel-to-oxidant ratio on the nature of molecular interaction in aqueous gel precursors and their effect on the powder properties of nanocrystalline ThO<sub>2</sub> has also been identified. These results have opened up a new area of research wherein for preparation of nanocrystalline metal oxides, wet-chemical synthesis methods can be investigated from the perspective of progressive evolution of solution structure of metal ions (complexes) during the synthesis protocol. Sintering studies on synthesized nanocrystalline thoria ceramics have shown exclusive desintering in glycine-nitrate combustion products, which has been attributed to powder morphology and structural strain originating during the rapid shrinkage of green compacts. These results are expected to be useful in selecting suitable protocol for synthesis of nanocrystalline actinide oxide powders for fuel development purpose.



**Thorium-based alloys and their thermal conductivity variation with temperature**